PERMIAN BASIN CORE WORKSHOP - DOE FUNDED RESERVOIR CHARACTERIZATION PROJECTS

PERMIAN BASIN SECTION – SEPM

PREPARED BY THE EXHIBITORS AND
ORGANIZED, COMPILED AND EDITED BY

Emily L. Stoudt
Dennis W. Dull
Michael R. Raines
Texaco Exploration & Production Inc.

Permian Basin Section – SEPM Publication No. 98-40

Reprinted with permission of the Permain Basin Section - SEPM © SEPM 1999

PERMIAN BASIN PALEOGEOGRAPHY & CORE STUDY LOCATIONS

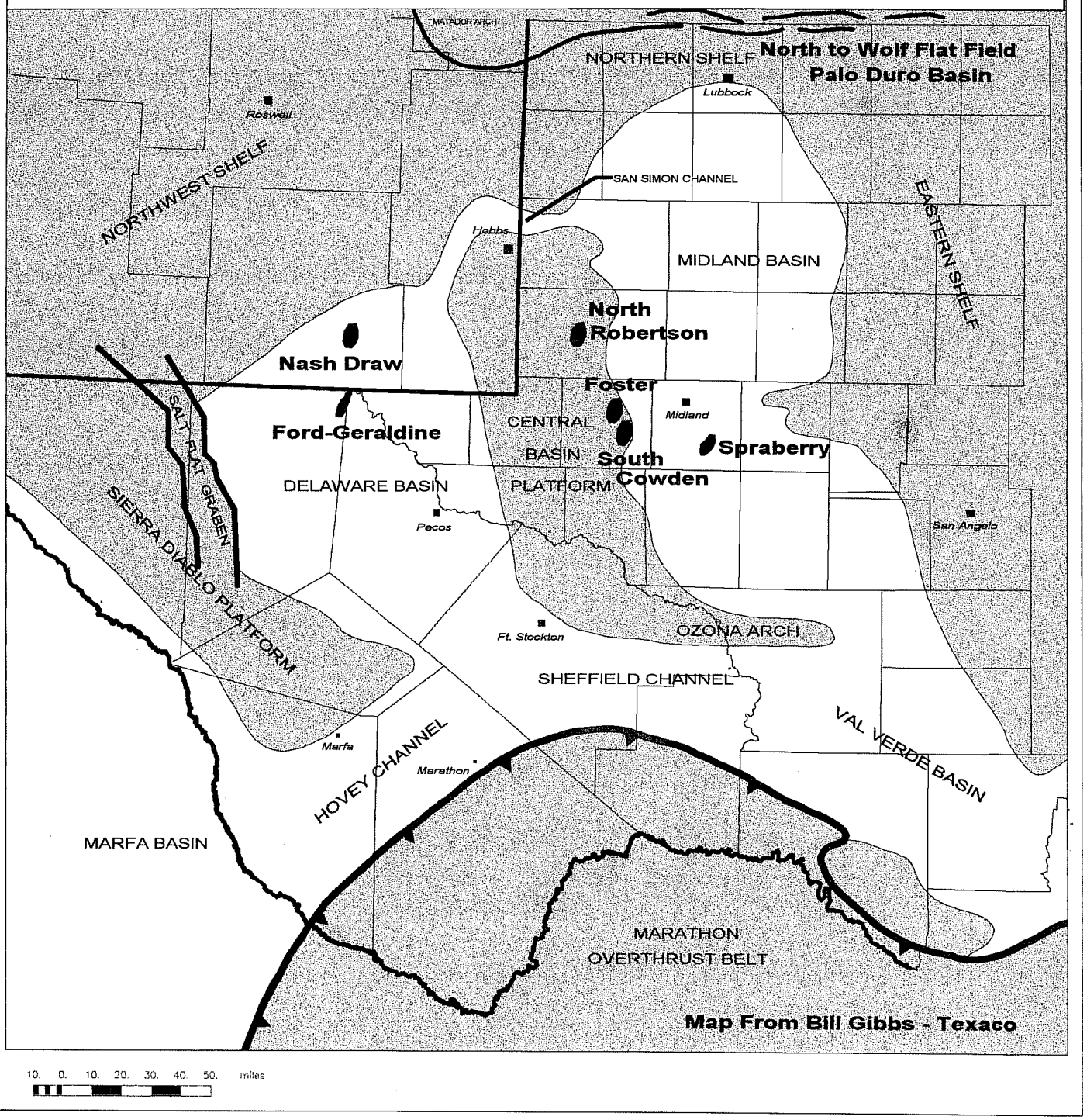

TABLE OF CONTENTS

Chairperson/Editor's Preface.....
PBS-SEPM Officers .....

CORE WORKSHOP TECHNICAL PAPERS

CARBONATE RESERVOIRS

LOWER CISCO FORMATION (PENNSYLVANIAN-VIRGILIAN) PALEOKARST, WOLF FLAT FIELD, NORTHEAST SHELF PALO DURO BASIN, TEXAS. Robert C. Trentham, Muskoka Consultants; Robert Lindsey & Rex C. Price, Chevron U.S.A. Production Co., Midland Texas; Don D. Pack, Consultant, Houston, Texas.

DEPOSITIONAL ENVIRONMENTS FROM CORE, NORTH ROBERTSON (CLEAR FORK) UNIT, GAINES COUNTY, TEXAS. Brian H. Pregger and William H. Dixon, Fina Oil and Chemical Company, Houston, Texas.

THE USE OF CORE IN AN INTEGRATED 3D SEISMIC, GEOLOGICAL AND ENGINEERING STUDY OF THE GRAYBURG/SAN ANDRES OF FOSTER AND SOUTH COWDEN FIELDS, ECTOR COUNTY, TEXAS. Robert C. Trentham, Muskoka Consultants; William C. Robinson, Seismic Decisions; Richard E. Weinbrandt, Consultant, Midland, Texas.

RESERVOIR CHARACTERIZATION OF THE UPPER PERMIAN GRAYBURG FORMATION IN PREPARATION FOR A HORIZONTAL-WELL CO2 FLOOD, SOUTH COWDEN UNIT, WEST TEXAS. Craig D. Caldwell, Ken J. Harpole, and Matt G. Gerard, Phillips Petroleum Co., Bartlesville, Oklahoma.

CYCLE STRATIGRAPHY AND DIAGENESIS OF THE GRAYBURG FORMATION: SOUTH COWDEN FIELD, ECTOR COUNTY, TEXAS. Stephen C. Ruppel & F. Jerry Lucia, Bureau of Economic Geology, The University of Texas At Austin, Austin, Texas

CLASTIC RESERVOIRS

FRACTURE CHARACTERIZATION BASED ON ORIENTED HORIZONTAL CORE FROM THE SPRABERRY TREND RESERVOIR: A CASE STUDY. Paul McDonald, Parker & Parsley; John C. Lorenz, Sandia National Labs; Charlie Sizemore, Parker & Parsley; David S. Schechter, New Mexico PRRC, Tom Sheffield, Parker & Parsley.

ADVANCED OIL RECOVERY TECHNOLOGIES FOR IMPROVED RECOVERY FROM SLOPE BASIN CLASTIC RESERVOIRS, NASH DRAW BRUSHY CANYON POOL, EDDY COUNTY, NEW MEXICO. Bruce Uzynski, Consulting Geolgist; Bruce A. Stubbs, Consulting Engineer; Mark B. Murphy, Strata Production Co., Roswell, NM.

RAMSEY SANDSTONE DEEP-WATER CHANNEL-LEVEE AND LOBE DEPOSITS, FORD GERALDINE UNIT, REEVES AND CULBERSON COUNTIES, TEXAS. Shirley P. Dutton, Mark D. Barton, Sigrid J. Clift, and Jose I. Guzman, Bureau of Economic Geology, The University of Texas At Austin, Austin, Texas.

CHAIRPERSON/EDITOR'S PREFACE

Since the early 1990's, the U.S. Department of Energy has supplied co-funding with the oil industry for a number of projects designed to develop better ways of recovering the vast amount of oil and gas that are presently left behind in mature reservoirs. In many cases, the amount of movable, but unrecovered, hydrocarbons far exceeds the amount produced. This is particularly true for older (Paleozoic), tighter rock units that display dramatic porosity and permeability variations, such as the producing units in the Permian Basin. In particular, the multiple hundred million-barrel fields found in carbonate shelfal deposits of the Clear Fork, Glorieta, San Andres and Grayburg formations have been targeted. So too have the tight basinal sandstone reservoirs of the Spraberry formation and the Delaware Mountain Group. In most cases, fields that exist in these formations have yielded less than 35% of their original oil in place, even after CO2 flooding. Clearly both the oil industry and the U.S. government would like to discover better ways of increasing production from such reservoirs. Techniques developed during funded projects in particular fields are to be shared with all producers, in the hope that they will benefit everyone and not just the fields and operators for whom the research was undertaken.

Virtually every operator makes use of the log, seismic, and engineering data available in producing fields. Unfortunately, "hard" rock data (cores) are much less readily available than other types of data. Even where cores exist, they are often used only to obtain accurate porosity and permeability measurements; not to generate better reservoir models. Thus many of the DOE funded projects involved core examination and the incorporation of "real" rock data into modeling of producing reservoirs. The resulting reservoir characterization studies virtually always displayed more accurate pictures of the variations in the "containers" (reservoir rocks) that hold the oil and gas.

The purpose of this core workshop is to give geologists, geophysicists and engineers the opportunity to view cores from some of the major producing horizons in the Permian Basin. More importantly, the modeling value of the core derived reservoir characterization studies may encourage a wider use of this important data set. We will all benefit if we can develop better reservoir models and recover a larger percentage of the reserves we have already discovered.

Emily L. Stoudt
General Chairman/Editor

1997-1998 PERMIAN BASIN SECTION – SEPM OFFICERS

President..... William L. Basham
President-Elect .....Douglas B. Swift
First Vice President .....Timothy J. Hunt
Second Vice President .....Charles Kerans
Secretary .....Thomas J. Tinney
Treasurer .....Fred H. Behken
Executive Director .....Paula L. Mitchell

LOWER CISCO FORMATION (PENNSYLVANIAN-VIRGILIAN) PALEOKARST, WOLF FLAT FIELD, NORTHEAST SHELF PALO DURO BASIN, TEXAS

Robert C. Trentham
Muskoka Consultants
Midland, Texas

Robert F. Lindsay
Chevron U.S.A. Production Co.
Midland, Texas

Rex C. Price
Chevron U.S.A. Production Co.
Midland, Texas

Don D. Pack
Consultant
Houston, Texas

ABSTRACT

Wolf Flat field is productive from karstified Lower Cisco Formation. The field is positioned at the edge of the rimmed northeast shelf margin. Mounds, peripheral- and back-mound skeletal debri, and oolitic facies form the vertical and lateral succession. Mounds are composed of crinoids, bryozoans, corals and algae. Skeletal packstone/grainstones surround mounds, with back-mound wackestone. Ooid grainstone formed in high-energy passages onto the shelf and cap shallowing-upward cycles.

Karstification resulted from two 100+ ft. (30+ m) sea level drops. Sea level dropped in a step-by-step manner to form numerous (~20) porous intervals at the vadose/phreatic contact. Aragonitic mound and skeletal grainstone/packstone/wackestones experienced intense dissolution. Calcitic ooid grainstones experienced less dissolution and form cave roofs and floors. Carbonate dissolution was in two phases. First, small vertically oriented pipes formed, resembling a "swiss cheese" texture. Second, was intense dissolution that created a "sponge" texture, with porosities up to 60-70%. Eventually, collapse breccias formed, with some clasts transported and rounded in the karst system.

Porosity was reduced by vadose silt, breccia clasts, banded speleothem cements, transgressive shale infilling, and burial saddle dolomite. Portions of the field nearest the rimmed margin are dolomitized. Areas further away from the rim are limestone.

Stable isotope analysis of $\delta^{18}O$ fall within the range of early meteoric diagenesis and $\delta^{13}C$ values are all negative and become more negative closer to the exposure surface. All porous intervals have been correlated and found to extend through all facies and lithologies within the field.

DEPOSITIONAL ENVIRONMENTS FROM CORE, NORTH ROBERTSON (CLEAR FORK) UNIT, GAINES COUNTY, TEXAS

BRIAN H. PREGGER and WILLIAM H. DIXON
Fina Oil and Chemical Company
Houston, Texas

INTRODUCTION

Large, low-permeability shallow-shelf carbonate reservoirs in the Permian (Leonard) Clear Fork and Glorieta Formations on the Central Basin Platform and Northwest Shelf of the Midland Basin have producibility problems directly related to the characteristics of the reservoir rock. Thick, cyclic sections of widely varying carbonate facies result in complex, heterogeneous, and compartmentalized reservoirs, contributing to low lateral and vertical sweep efficiencies during secondary recovery operations. To optimize the economics of large secondary (and tertiary) projects, it becomes imperative for their design to be based on an understanding of the geologic framework responsible for the inherent reservoir characteristics. Recognizing this, Fina Oil and Chemical Company cored four North Robertson (Clear Fork) Unit wells in 1995 and 1996 as part of the DOE Class II program in an effort to help characterize the reservoir. Examples of the depositional environments present in these cores are described below.

DISCUSSION

The Fina-operated North Robertson (Clear Fork) Unit (NRU) is located on the northern edge of the Central Basin Platform in southwestern Gaines County, Texas (Figure 1). The unit is situated on the crest of a large, doubly-plunging anticline oriented northwest-southeast, on trend with the deep-seated structural grain of the area. NRU is one of several large secondary recovery units producing from this feature, including the Exxon Robertson Unit to the southeast and the Spirit Energy North Riley Unit to the northwest. Production at NRU is from the Permian Clear Fork (Upper and Lower) and Glorieta Formations. The productive interval has a total thickness of approximately 1500 feet (Figure 2), with an average of 250 feet of net porosity > 4%. The entire section with the exception of the lowest 50-100 feet of the reservoir has been pervasively dolomitized. The non-dolomitized part of the Lower Clear Fork is a limestone. The reservoir is extremely heterogeneous; porosity is scattered throughout the 1500 feet of unitized section. Porosities, permeabilities, and pay continuity vary considerably across the unit, but are generally low. Porosity within the pay intervals averages 7%, and permeability averages 1.5 md.

Production in the NRU area began in 1956 with 40-acre primary development. A total of 17 MMBO was produced from 141 wells in the NRU area during primary production. NRU was formed in 1987 to waterflood the Clear Fork and Glorieta interval. To date, 117 20-acre and 17 10-acre infill wells have been drilled in the unit (Figure 3), which has a cumulative production of 10.6 MMBO since unitization. Present production is approximately 3,000 BOPD.

The trapping mechanism for hydrocarbons at NRU is a combination of structure and stratigraphy. The large, anticlinal structure is the primary reason for the localization of hydrocarbons in the unit area, but the heterogeneous nature of the carbonate facies in the reservoir section introduces a stratigraphic component to the trap. In most of the unit the relative structural position of any individual well is not as significant as the relative abundance of good reservoir at that location. For example, production from the northeast flank of the structure (Figure 3) is better than that from the structurally higher southwest flank

Reservoir heterogeneity within the Clear Fork/Glorieta section at NRU is a result of the cyclic nature of the carbonate deposition within the unit area during the Permian, and the subsequent diagenetic alteration overprinting the rocks. The section at NRU is composed of a complex sequence of shallowing-upwards carbonate cycles, with shallower water facies capping deeper water facies. This occurs at several different scales, but the result is a gradual shift from predominantly open shelf and shelf-margin rocks (reefs and shoals) in the Lower Clear Fork, to predominantly lagoonal and tidal flat rocks in the Upper Clear Fork and Glorieta.

The cyclicity of deposition within the Permian section produced an intimate interlayering of porous and nonporous carbonate depositional facies throughout the 1500 feet of unitized interval. This has resulted in the presence of many thin porosity zones, few of which exceed 20 feet in thickness (Figure 2). These porosity zones also tend to be limited in lateral extent, rarely extending on an individual basis across the entire unit. The Clear Fork/Glorieta reservoir interval as a result is thick and laterally extensive, but exceedingly compartmentalized.

Good reservoir (porosity > 4%, permeability > 0.5md) at NRU is present throughout the unitized interval, although it is much more prevalent in the lower and middle parts of the section. Several of the original carbonate depositional facies tend to have the best present day reservoir characteristics. These include grainstone shoals common in the eastern and northern parts of the unit, reef debris aprons scattered across the unit, and burrowed lagoonal wackestones and packstones common in the central, western, and southern parts of the unit. Porosities and permeabilities are higher in the grainstone and reef debris facies, but the lagoonal facies are volumetrically more abundant.

Diagenetic alteration, including post-depositional dissolution, dolomitization, and cementation by calcite, dolomite, and anhydrite, has both enhanced and occluded porosity

and permeability within the reservoir, although not in a strictly systematic fashion relative to original depositional facies. One diagenetic "facies" in particular, a solution collapse breccia that appears to play an important part in localizing production in the unit, developed without regard to original depositional facies.

As part of the DOE Class II project at NRU, 4 wells were cored, with a total of 2,730 feet of core recovered. This core has provided an opportunity to examine the varied depositional facies in the Clear Fork/Glorieta section, and to relate their distribution to production in the unit. The major depositional facies seen in the cores are described below. The relative positions of these facies are illustrated in Figure 4, a generalized depositional model of the Clear Fork and Glorieta in the NRU area. The photographs illustrating these facies were taken from cores from two wells, NRU Nos. 1509 and 3533 (Figure 3). These two wells have the most extensive cored sections within the unit.

DEPOSITIONAL FACIES

Fusulinid Shoal (Figure 5)

Packstones to grainstones composed predominantly of fusulinids, either as preserved tests or dissolution molds. A strongly bimodal porosity distribution is typical of this facies, as fusulinid molds and dolomite intercrystalline porosity are often both present. As a consequence, this facies can have good porosity and permeability. The fusulinid shoals are most common in the Lower Clear Fork, where the depositional environment was less restricted and of higher energy than the bulk of the Upper Clear Fork and Glorieta. Two types of fusulinids have been identified: larger, 4 - 5 mm *Parafusulina* spp.-types, and smaller, 0.5 - 1.5 mm *Schubertella* spp.-types. Commonly the *Schubertella*-type fusulinids are found as discrete accumulations, suggesting either a mechanical sorting by current action, or the possibility that the *Schubertella*-types preferred a different environment, perhaps on the lagoonal side of reefs and bioherms, rather than on the seaward side.

Grainstone Shoal (Figure 6)

Grainstones containing fusulinids, bryozoans, skeletal fragments, peloids, crinoids, ooids, and dascycladacean algae. These rocks commonly display cross-bedding, scour-and-fill features, burrows, and rip-up clasts. This along with the relative lack of lime mud suggests a higher-energy environment. This facies was probably deposited in current and/or wave effected areas of the shelf, between the lagoon and the open shelf. Grainstone shoal rocks commonly have both biomoldic and intercrystalline porosity, and are typically the best reservoir rocks in the section. They are present most abundantly in the Lower Clear Fork.

Reef (Figure7)

Rocks composed of frame-building bryozoans in growth position encased in mud are present in several parts of the section. These bryozoans are massive, unilaminate, and bilaminate cyclostome types. They have erect, laminar, and bifoliate growth forms which

acted as effective baffles for fine-grained sediment during deposition. Associated with these bryozoans are pelecypods, brachiopods, gastropods, rugose corals, crinoids, and fusulinids. These species are larger and more abundant than elsewhere in the section. The bryozoans acted as a wave and current resistant framework in a high-energy setting, and are therefore considered to be reefs. These reefs are best developed in the Lower Clear Fork, and are rare in the middle and upper portions of the section. They do not extend more than ten feet vertically in any of the cores. The reservoir potential of these rocks is negligible, as they contain extremely low porosities and permeabilities.

Reef Debris Apron / Reef Talus (Figure 8)
Immediately adjacent to the reefs are grainstones and packstones consisting of reworked skeletal fragments and fusulinids indicative of deposition in a high-to-moderate energy environment. These deposits are interpreted as reef debris aprons. High-angle bedding of up to 30 degrees is observed in this facies, and burrowing is absent. Commonly, large (2 - 4 inch diameter) rounded cobbles of consolidated reef debris are incorporated into these rocks. These clasts have undergone several periods of movement, based on the number of laminar carbonate coatings they exhibit, and represent reef talus, eroded and redeposited during storms. The reef debris aprons are not extensive vertically in the section, but in the Lower Clear Fork separate debris aprons appear to have coalesced into laterally extensive deposits. High porosities and permeabilities are present in these rocks, and they normally make good reservoirs.

Bioherm (Figure 9)
Packstones to grainstones containing fenestrate bryozoans, fusulinids, algae, and crinoids are present intermittently throughout the section. These rocks represent biologic assemblages that are not as wave resistant as the reef assemblage, and would have developed in lower-energy, probably lagoonal environments. These rocks can have good porosities and permeabilities, but as they are scattered sparsely throughout the section, they do not make a significant contribution to production.

Lagoon (Figure 10)
Wackestones to packstones containing peloids and skeletal fragments are interpreted to have been deposited in a back-reef, lagoonal environment. These rocks are characteristically bioturbated and burrowed, with varying percentages of finely disseminated to nodular anhydrite. These rocks are thick and areally extensive, making up a large percentage of the Clear Fork and Glorieta section. They have only moderate porosity and permeability values, and so are not the best reservoir rock in the section. However, because of their total volume, they are a significant contributor to production.

Tidal Flat Algal (Figure 11)
Mudstones to packstones that are light in color, thinnly bedded and exhibit fenestral fabric are identified as tidal flat algal rocks. These rocks are common in the Upper Clear Fork and Glorieta. They can have high porosity values, but they contain extremely low permeabilities, and are prime contributors to the overestimation of porosity log-based pay in the reservoir.

Island Complex (Figure12)
Common in the Upper Clear Fork are thinly-interbedded sequences of intertidal to supratidal facies which are interpreted to represent deposition as an island complex. These facies include beaches consisting of packstones to grainstones of rounded skeletal fragments with inclined bedding, a lack of burrowing, and fine plant debris. Interbedded with these are tidal flat algal mat rocks, wackestones and packstones with root casts, dessication features, and abundant whole plant fragments. Massive to burrowed dense, light gray intervals are interpreted as having been deposited in saline ponds in the island centers. Coal beds, up to two inches thick, are also interbedded. The relative abundance of organic matter in these sequences suggests that the climate at the time of deposition was humid rather than arid. The island complexes can develop porosity in certain facies, but permeability is minimal, and they are not considered reservoir.

Solution Collapse Breccia (Figure13)
Various zones throughout the cores exhibit disruption and brecciation of original bedding, possibly due to solution collapse. Large, rotated clasts of dolomite have been fractured and infilled with dolomite and anhydrite. Diagenesis has obliterated most of the original texture in these rocks, although it is apparent that the brecciation was not facies-selective. Several of these solution-collapse breccias are found directly below island complexes and exposure surfaces, lending credence to the idea that the climate was probably humid. They are up to 40 feet thick in the cores, but do not appear to be laterally continuous for any distance. Porosity and permeability are usually high in these zones, and they appear to make a major contribution to oil production from the section (as well as acting as thief zones during water injection).

Figure 1. Location map of the Fina North Robertson Unit, showing the unit's position relative to other secondary recovery units on the Central Basin Platform and Northwest Shelf of the Midland Basin.

Figure 2. Logs of the two cored wells used to illustrate the described depositional environments. The depth of each core photo is represented by the numbers between the porosity and permeability curves. Numbers represent figure numbers.

Figure 3. Structure map of the top of the Upper Clear Fork in the North Robertson Unit. The two referenced cored wells are highlighted.

Figure 4. Generalized depositional model of the Clear Fork and Glorieta in the North Robertson Unit area. Stacked prograding carbonate cycles containing these varied facies create the complexity of the Clear Fork reservoirs.

Figure 5. Fusulinid shoal. A grainstone of large *Parafusulina*-type fusulinids is present from 7240.7' to 7249'. Above this is a wackestone highlighting individual fusulinid tests. NRU 1509, 7239.4-7249'.

Figure 6. Grainstone shoal. A grainstone of peloids and fossil fragments. Faint cross-bedding is present at 6177.5' NRU 1509, 6169.3-6179'.

Figure 7. Reef. A large cyclostome bryozoans in growth position is seen from 7282' to 7283'. It is encased in mud, with grainier facies representing reworked reef debris both above and below. NRU 1509, 7278-7287'.

Figure 8. Reef Debris Apron / Reef Talus. Interbedded with grainstones of the reef debris apron are large rounded cobbles of reworked reef material. NRU 1509, 7210.2-7219.9'

Figure 9. Bioherm. Grainstones and packstones containing a mixed assemblage of fusulinids, skeletal fragments, and bryozoans. NRU 1509, 7229.6-7239.4'.

Figure 10. Lagoon. Bioturbated wackestones and packstones of peloids and skeletal fragments. One large, anhydrite-filled burrow can be seen between 6807.5' and 6809.5'. NRU 3533, 6807.5-6817.5'.

Figure 11. Tidal Flat Algal. Light colored, thinly-bedded dolomite with incipient fenestral fabric (6246') and dessication features. NRU 1509, 6238.5-6248.4'.

Figure 12. Island Complex. An intimate association of intratidal to supratidal dolomites containing root traces (6631.5'), high-angle bedding, fenestral fabric (6624'), and coal beds (6624.5'). NRU 3533, 6622.5-6632.5'.

Figure 13. Solution Collapse Breccia. Chaotic assemblage of fractured, rotated clasts of dolomite of various original facies. Original depositional fabrics are harder to discern in these rocks than in most of the other rocks in the reservoir. Light-colored alteration rims around anhydrite nodules contain higher permeabilities than does the non-altered groundmass. NRU 3533, 6826.7-6836.2'.

LOCATION MAP

FINA
NORTH ROBERTSON UNIT

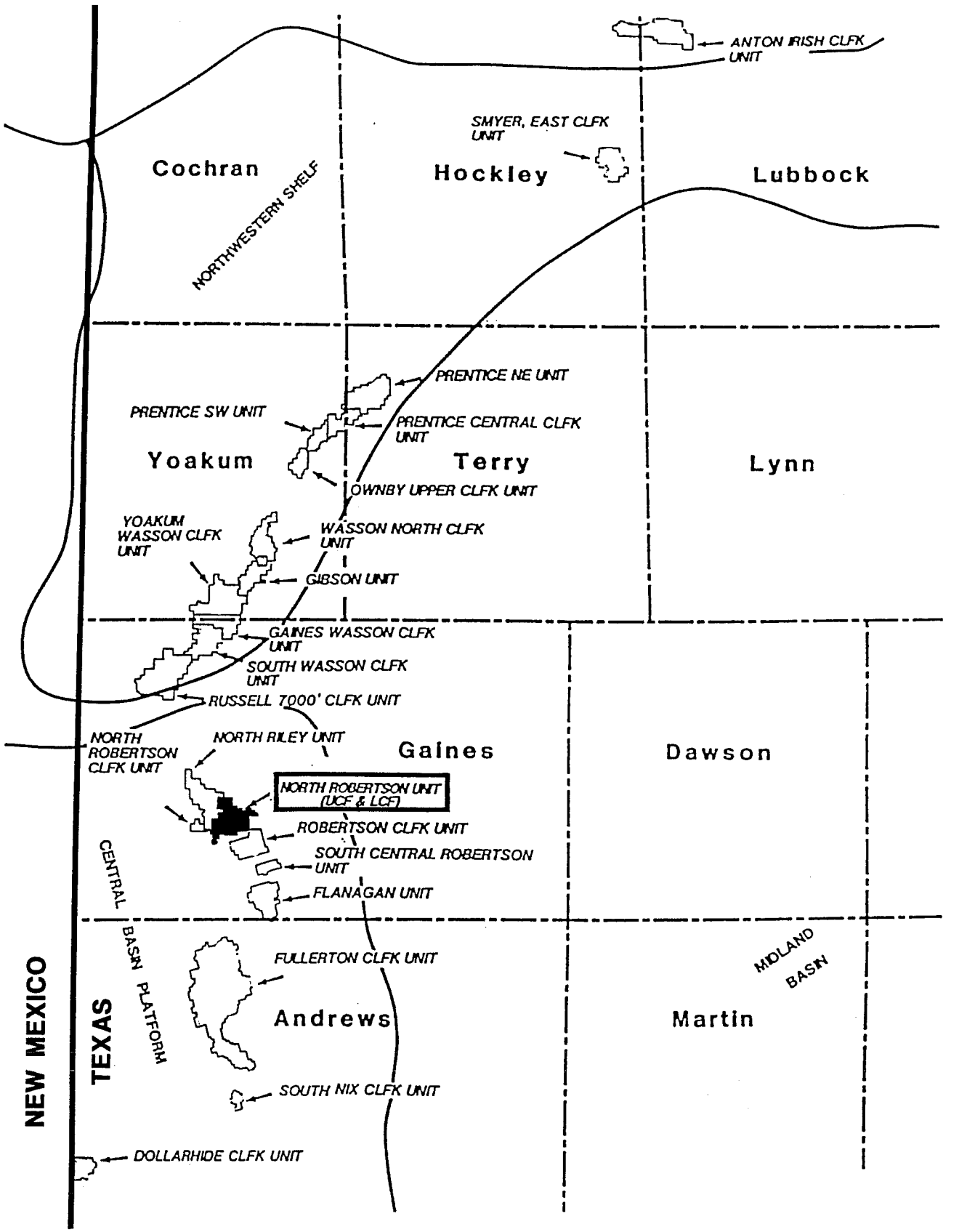

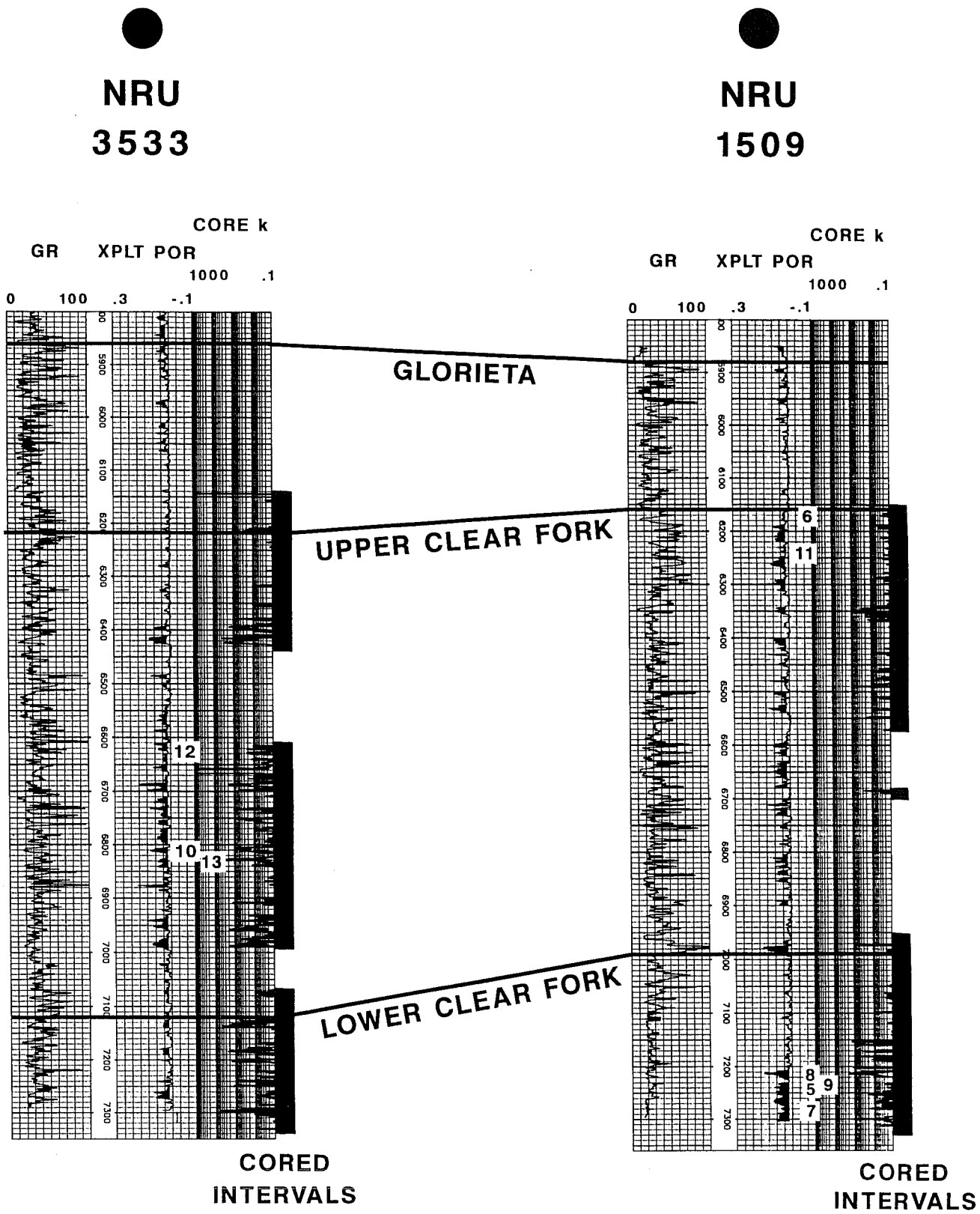
NRU
3533
NRU
1509
CORE k
GR
XPLT POR
1000
0
100
.3
-.1
.1
GLORIETA
UPPER CLEAR FORK
LOWER CLEAR FORK
12
10
13
6
11
8
5
9
7
CORED
INTERVALS
CORED
INTERVALS

NORTH ROBERTSON UNIT

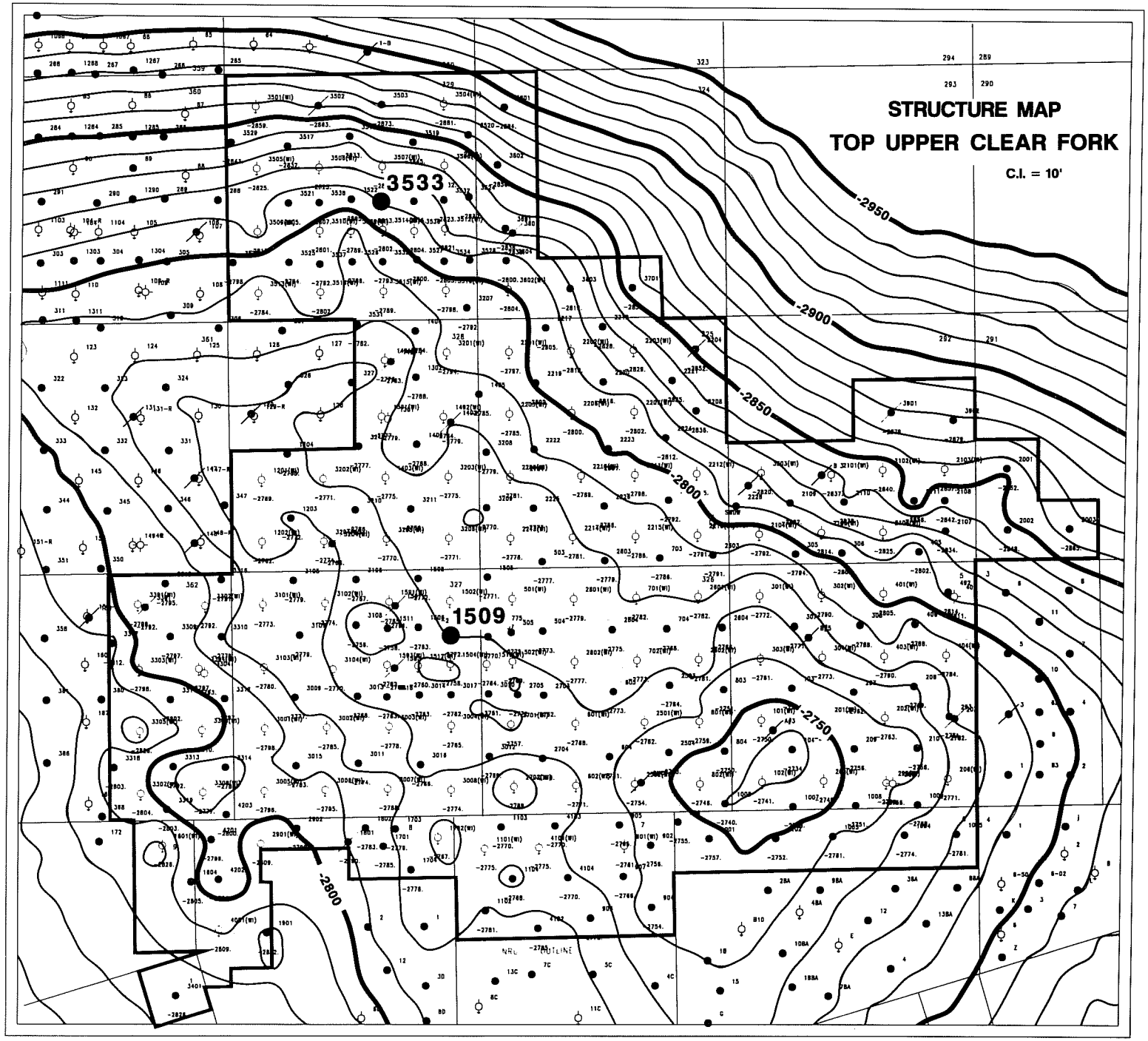

GENERALIZED DEPOSITIONAL MODEL
NRU CLEAR FORK AND GLORIETA FORMATIONS

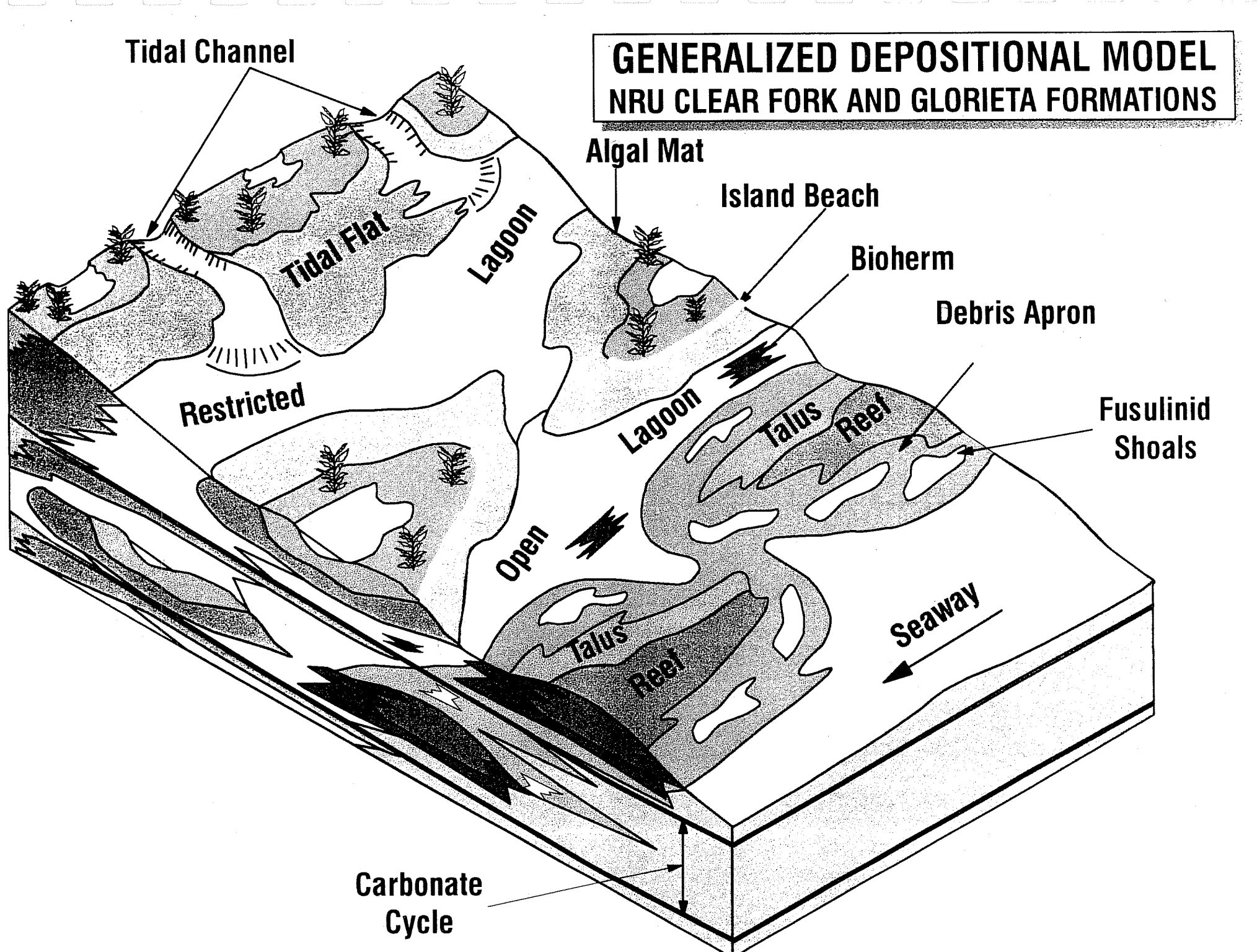

7243
7245
7247
76

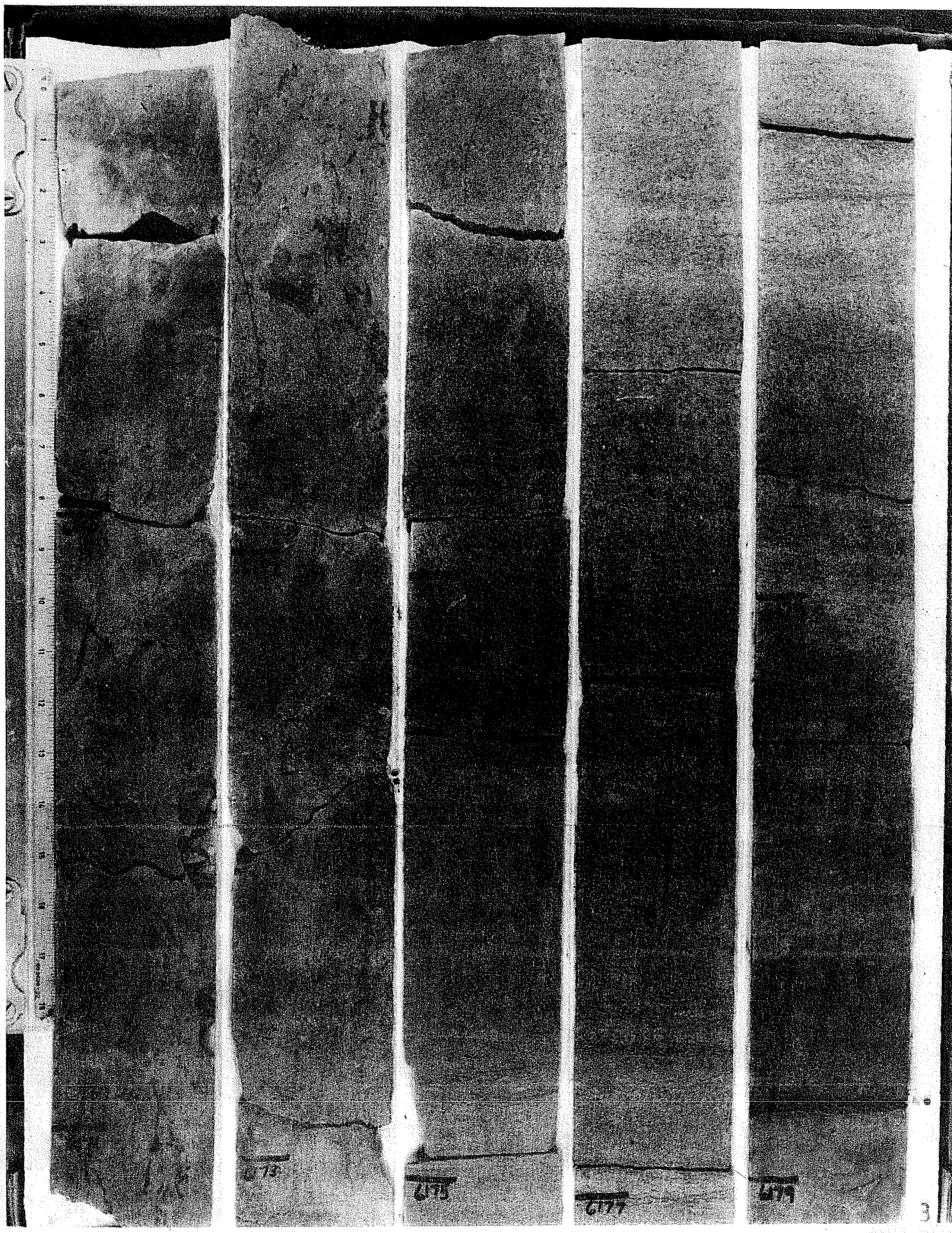
6173
6175
6177
6179

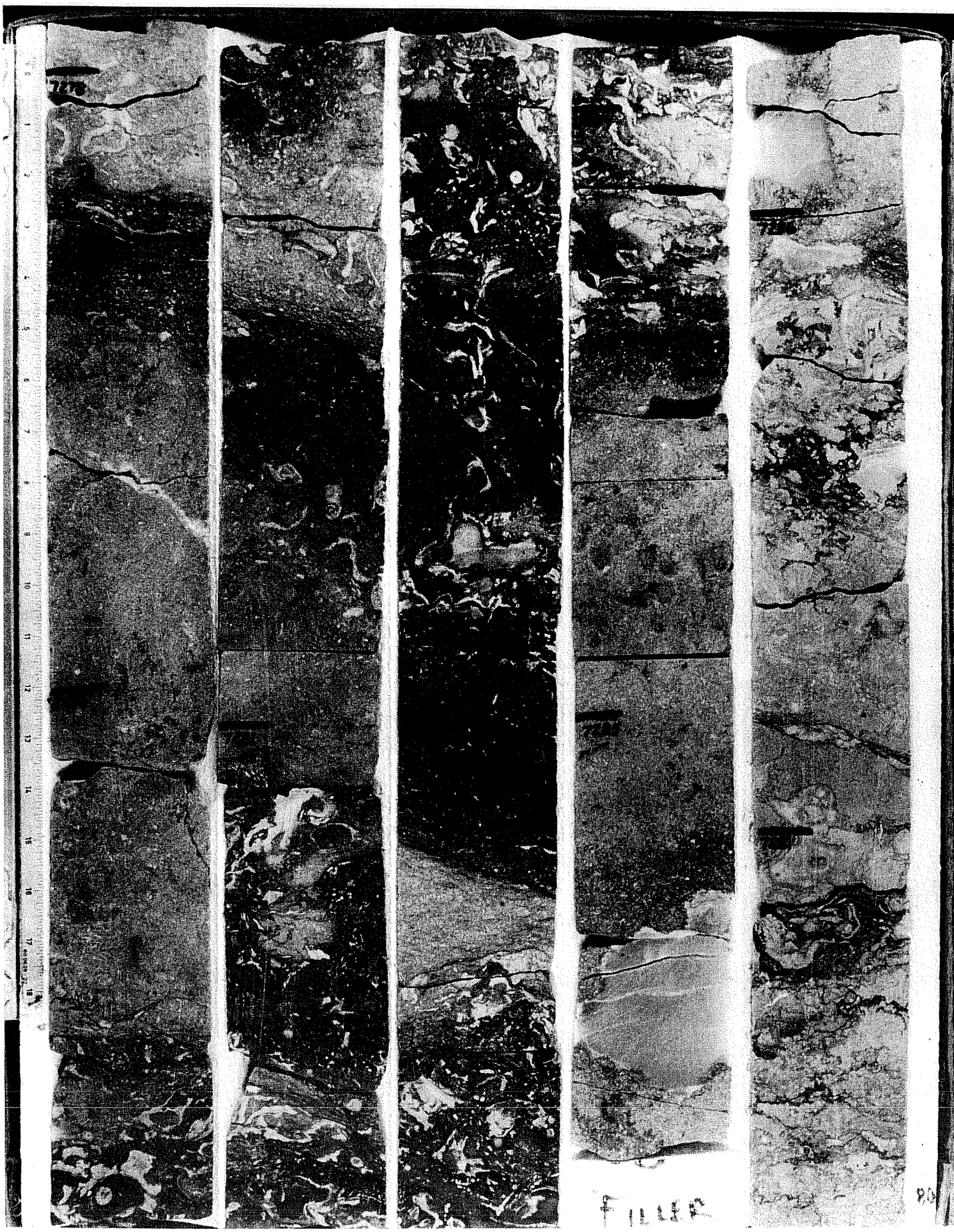
7276
FILLER

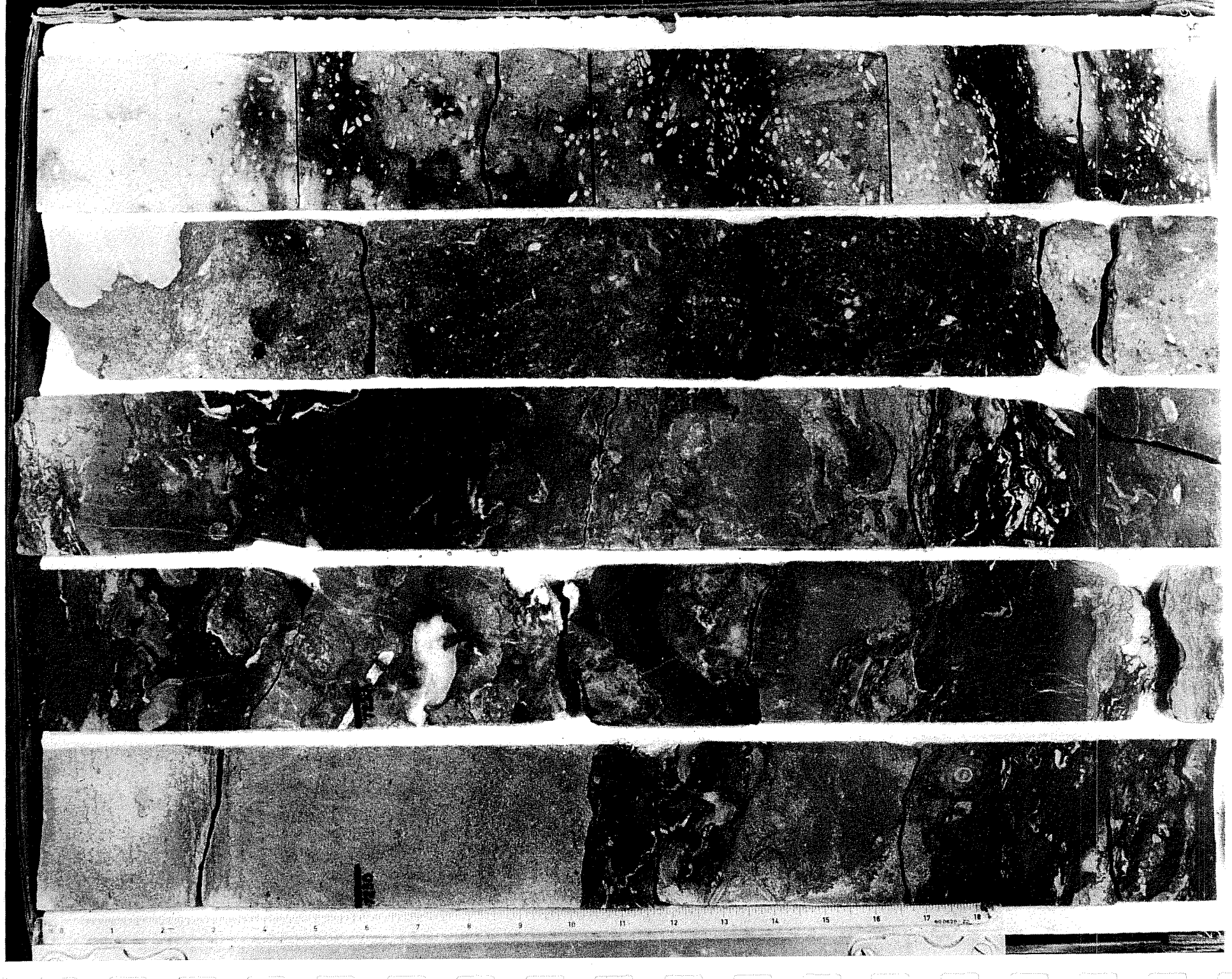

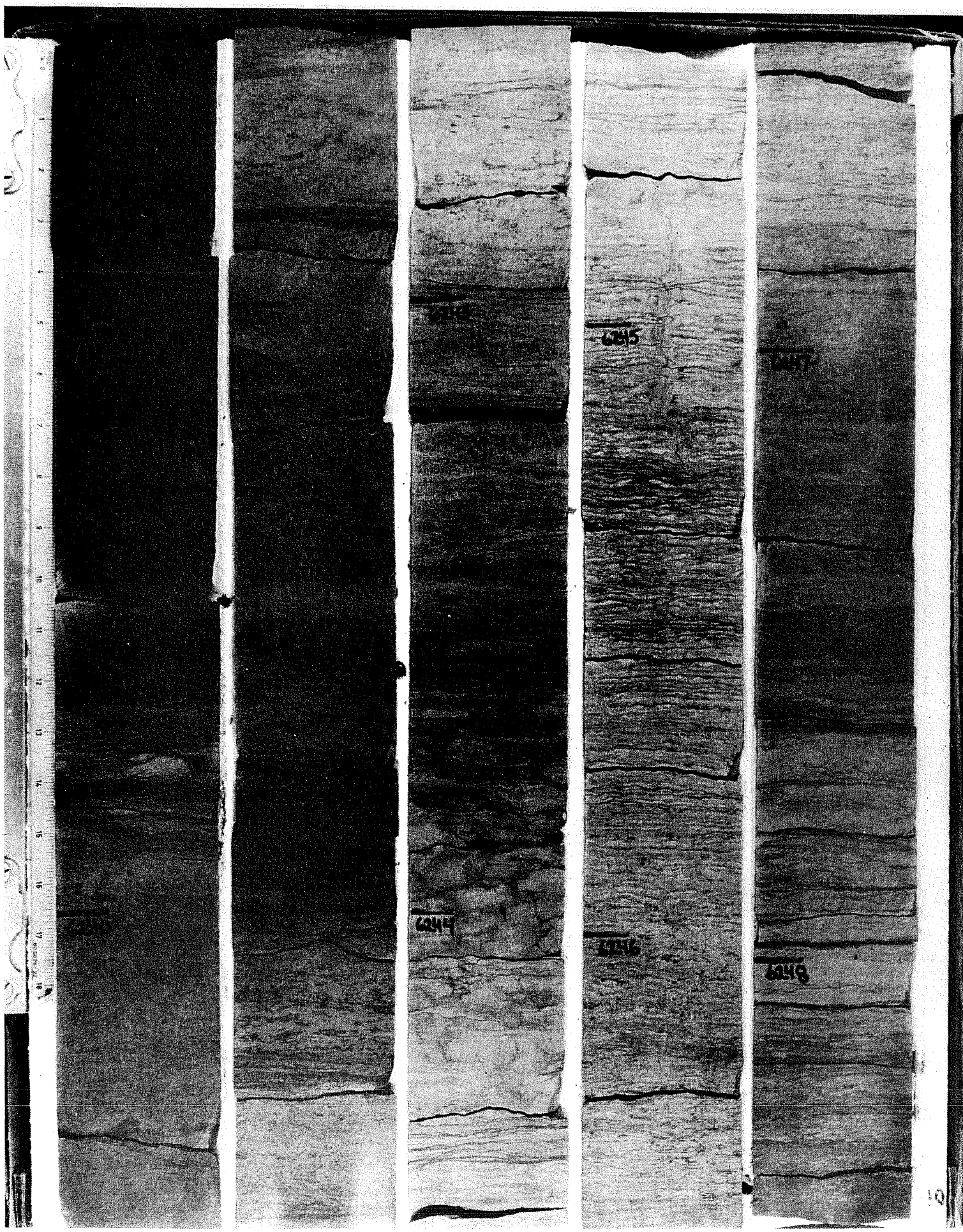
6245
6247
6249

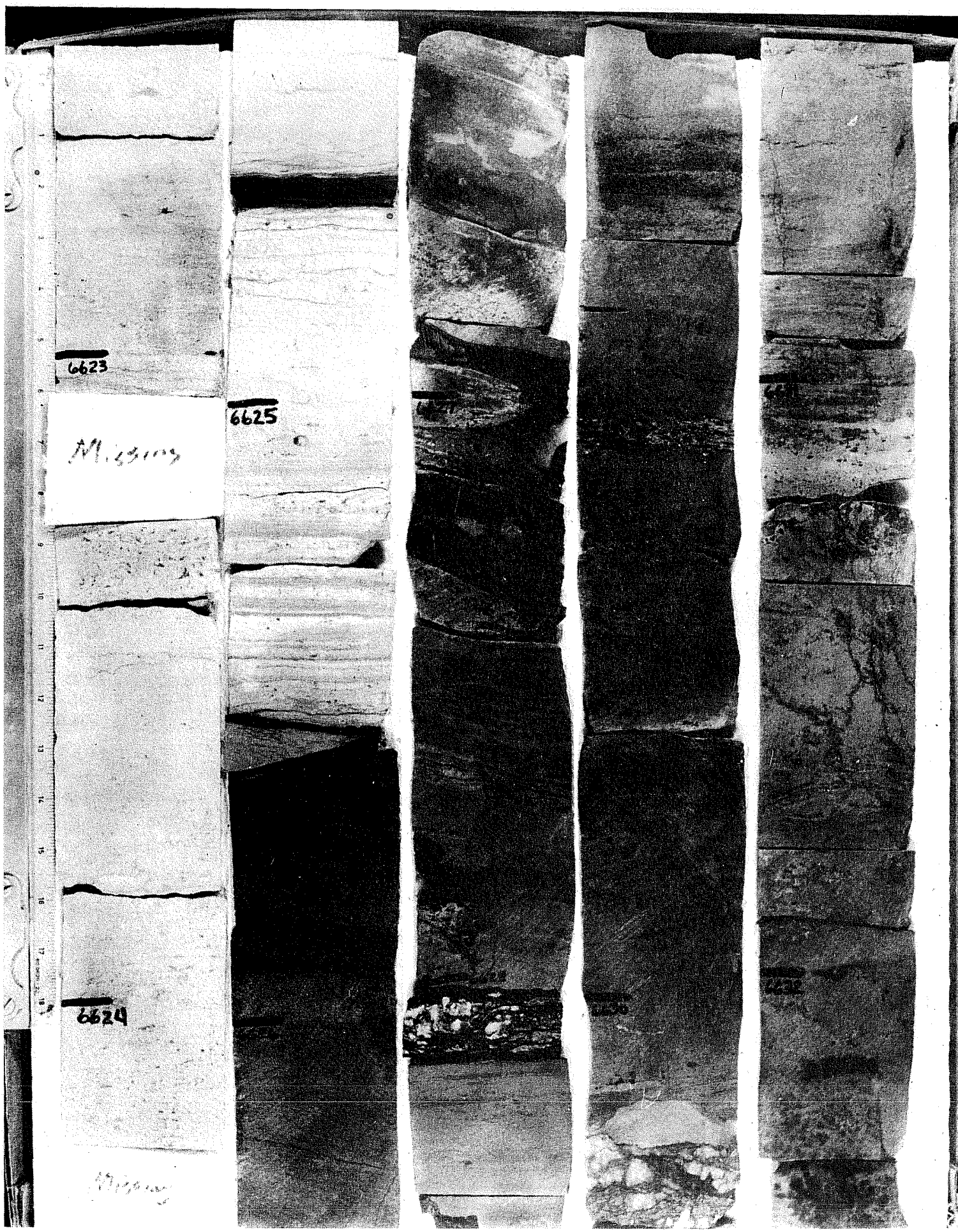
6623
6625
6624

THE USE OF CORE IN AN INTEGRATED 3D SEISMIC, GEOLOGICAL AND ENGINEERING STUDY OF THE GRAYBURG/SAN ANDRES OF FOSTER AND SOUTH COWDEN FIELDS, ECTOR COUNTY, TEXAS.

ROBERT C. TRENTHAM, MUSKOKA CONSULTANTS, WILLIAM C. ROBINSON, SEISMIC DECISIONS, RICHARD E. WEINBRANDT, CONSULTANT.

ABSTRACT

A project to recover economic amounts of oil from a very mature oil field is being conducted by Laguna Petroleum Corporation of Midland, Texas, with partial funding from a U. S. Department of Energy grant to study shallow carbonate rock reservoirs. The objectives of the project are to use modern engineering methods to optimize oil field management and to use geological and geophysical data to discover untapped potential within the petroleum reservoirs. The integration of data and techniques from these disciplines has yielded results greater than those achievable without their cooperation. The cost of successfully accomplishing these goals is to be low enough for even small independent operators to afford.

During the Phase 1 period of this project, field management was influenced by preliminary geological work done to define the distribution of porosity within the upper and lower parts of the Grayburg Formation and within the upper part of the San Andres Formation. Implementation of the field development recommendations made at the end of Phase 1 were based on an engineering simulation run using production history and geologic models. Oil production was doubled as a result of that work. Several wells were worked over and newly drilled wells contributed additional high quality subsurface core and log data. A "pipeline" fracturing technique, designed to double the induced fracture length over other methods, was used to improve fluid production by more effectively contacting the reservoir. Water chemistry analyses, noting the difference of salinity of Grayburg fluids versus San Andres fluids, have been used to determine the reservoir origin of produced water, implicating San Andres water contamination of Grayburg production

Melding new core and log data (products of Phase 1 recommendations) with pre-existing data lead to the development of a better understanding of the depositional and diagenetic history of the Grayburg and San Andres Formations. Geologic log markers within the Grayburg represent low permeability zones that act as vertical barriers to fluid movement during oil production. Areas of reservoir with low porosity dolomite or anhydrite-filled dolomite result in poor production qualities and reduced water injection capacity. Also, core and log evaluation associate the top of the San Andres with a major karst event, and provide insight for a methodology to identify potential water producing intervals. Thus, the San Andres has been downgraded as a potential waterflood target.

The analyses of the seismic data have become a major factor in defining productive properties of the Grayburg reservoir. Seismic inversion is used to convert the seismic data to velocity traces, a form from which a quantitative evaluation of reservoir properties is extracted. Calibration of seismic-derived interval velocity attributes, using well log porosity information, enable mapping the distribution of porosity of the individual upper Grayburg zones comparable to production fluid flow zones. These detailed maps have modified the earlier reservoir description made from sparse subsurface data. This revised picture discloses reservoir compartments not recognized before, serves as a vital parameter in the revised engineering model of the reservoir, and modifies the influence of the production history and the original oil in place values. Future drilling will be guided by the new engineering model.

Initial seismic analyses targeted an understanding of the correlation basic geology and reservoir factors to seismic wiggle-trace data. Stratigraphy specific to a thick carbonate sequence with few internal seismic reflectors was examined, including a hands-on review of core to establish seismic-to-rock relationships. Consideration of the effect of rock properties, particularly porosity, on seismic data response, focused on those most important factors for continued study. Forward modeling was employed to visualize aspects of the geology with seismic reflection response, to exactly identify key geologic levels in the seismic data.

Observations were made of the various seismic waveform attributes, but no strong correlations with important rock properties have been recognized

The initial simulation model results, using seismic-derived porosity maps, fit within expectations, although some porosity modifications are being made. Continued well testing will provide data necessary for a more complete simulation. Team members worked closely to develop methodologies to bridge the distances among historically diverse scientific disciplines.

Introduction

The objective of this two-phase study is to demonstrate an integrated methodology for reservoir characterization of shallow shelf carbonate reservoir that is feasible, and cost effective for the independent operator. Furthermore, it will provide one of the first public demonstrations of the enhancement of reservoir characterization using high-resolution three dimensional (3D) seismic data.

This particular project is evaluating the Grayburg and San Andres reservoirs in the Foster and South Cowden Fields, Ector County, Texas (Fig. A). This sixty eight (68) years old field was approaching its economic limit and the leases evaluated would have been abandoned in ten (10) years. A multi-disciplinary approach to waterflood design and implementation, along with the addition of reserves by selective infill drilling and deepening, is being applied to this field. This approach in reservoir development will be applicable to a wide range of shallow shelf carbonate reservoirs throughout the United States.

The first phase of the project included the design, acquisition, and interpretation of the 3D seismic survey, the collection and evaluation of geologic (core and log) data, and engineering (historical production, well test, injection) data from a variety of sources. From this work, a geologically based production history model was simulated. Based on the recommendations made at the end of Phase One, three new wells were drilled, one existing well was deepened, two wells were worked over, one TA'd well was re-entered, and one well was converted to injection. In addition, the quality of the injection water was greatly improved, a step necessary prior to increasing injection in the project area. The realignment of the waterflood and all additional well work await the completion of the seismic based history match and engineering simulation.

GEOPHYSICS

A 3D seismic survey was acquired over three and one half square miles of this mature oil field for the ultimate purpose of mapping subsurface geologic parameters that affect oil production. The major guideline for interpretation is to establish a methodology for analyzing data and mapping significant criteria using state-of-the-art computer tools economically available to any company or individual.

Conceptually, two key ideas have been developed which guide the use of seismic data to assist production planning. First, determining quantitative map products based on seismic factors is necessary for input to engineering models, and second, the exact positions of thin geologic flow units must be determined in order to accurately relate seismic data to well and production data. These two interpretation requirements are complex, and are discussed throughout this report. The maps, which are of real use in this project, are not achieved by using conventional interpretation methods.

Seismic Project Status

The project underwent a change of geophysical interpreters in July 1996. William C. Robinson, geophysical consultant of Midland, Texas, joined the project.

The seismic project is being analyzed using the PC-based Vest 3DSEIS interpretation system. This software is most appropriate for stratigraphic interpretation of seismic data because the extensive set of

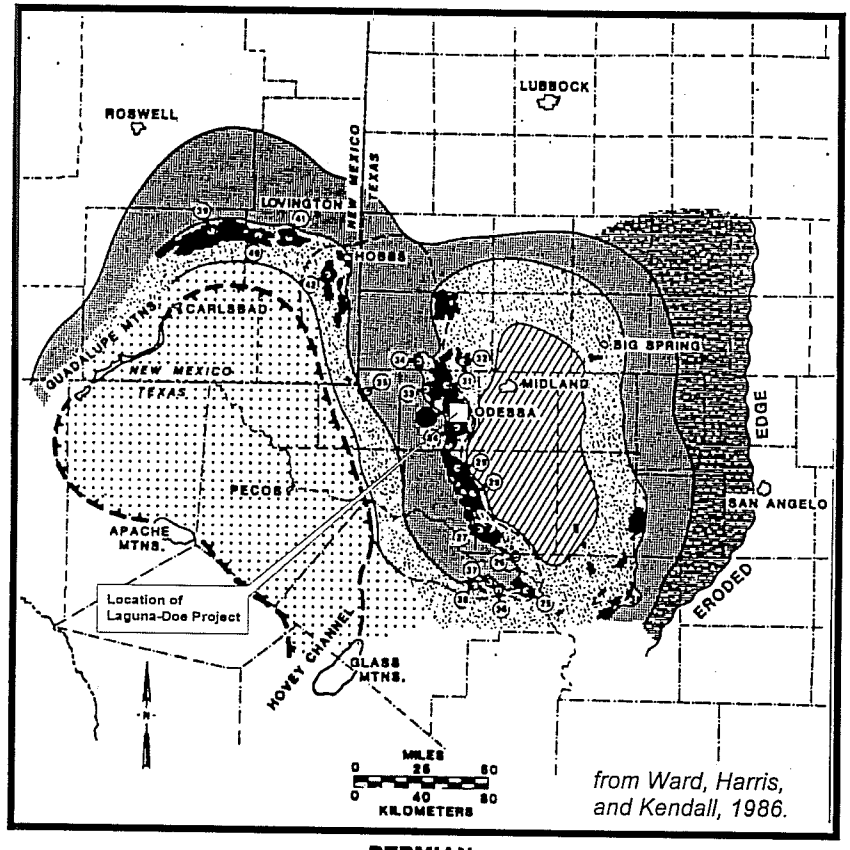

PERMIAN
MIDDLE GUADALUPE SERIES
GRAYBURG FORMATION

- CAPITAN "REEF" FRONT (SUBSURFACE)
- DELAWARE BASIN-CHERRY CANYON FORMATION BASINAL SANDSTONE, SILT, SHALE AND LIMESTONE
- DOLOMITE
- OUTLINE CENTRAL BASIN PLATFORM
- (H) OILFIELDS LISTED IN TABLES
- EVAPORITIC FACIES-DOLOMITE. POROSITY PLUGGED BY EVAPORITES.
- LIMESTONE
- ANHYDRITE AND HALITE RED SANDSTONE, RED SILTS, RED SHALES AND BEDDED ANHYDRITE
- OIL OR GAS FIELD

SIMPLIFIED GEOLOGIC MAP OF THE GRAYBURG FORMATION, PERMIAN BASIN, SHOWING THE LOCATIONS OF PRODUCING FIELDS. SEE TABLE 2 IN APPENDIX FOR DETAILED DESCRIPTIONS OF THE NUMBERED FIELDS.

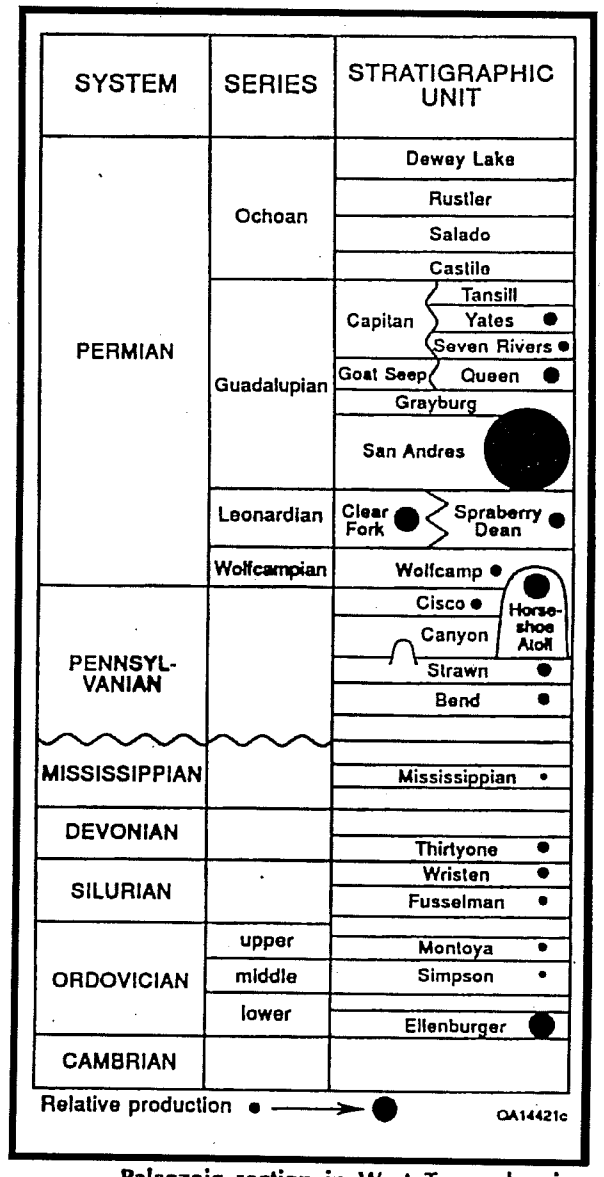

Paleozoic section in West Texas showing relative importance of oil producing unit (from Galloway and others, 1983).

Figure A. Location Map for the Laguna-DOE Project and Stratigraphic Column.

tools within that package uniquely fit one project criterion of being economically available to independent oil companies and individuals. Supplementing the Vest system is the PC-based mapping and display software SURFER version 6.xx by Golden Software. This program is used to create superior quality maps of any geological and geophysical parameter and provides complete base map capabilities. The Workbench software can also import these maps.

Base map construction was accomplished by editing pre-existing spreadsheet and CAD-type digital files using SURFER (Fig. 1). A master spreadsheet, recording surveyed well locations and extensive well top data, is used to post wells, including deviated holes. This file has been updated and added-to over time with new wells and new data columns. Culture data such as lease lines and roads reside in another spreadsheet. The spreadsheet definition here is basically that a row (across) of numbers or characters (representing a single well) consists of data values of location, well name, horizon depths, porosity values, production, etc., so that many wells create many rows and, thus, columns of values (Fig. 2). Geophysical spreadsheets contain three columns: two surface location coordinates and any other mappable parameter, such as depth, time, amplitude, velocity, etc. The master base map serves as a common base for all subsequent maps of geology, geophysics, and engineering.

In July 1996, the status of seismic interpretations was reviewed to determine steps to be taken for moving ahead. The seismic data (Fig. 3b) were reviewed to determine characteristics of bandwidth and phase. Using the Fourier analysis built into 3DSEIS, the bandwidth of the migrated stack data volume was determined to be sharply contained between 20-80 Hz. Because the vibroseis sweep was 10-110 Hz, the data process sequence was reviewed. Although the processes were generally appropriate and adequate, one filter parameter within the surface-consistent deconvolution steps had band limited the data initially to 20-80 Hz. Tests indicated that the excluded amplitudes could not be recovered by additional spectral balancing of the data. The process sequence was re-run by Dawson Geophysical, except for the first deconvolution routine. The reprocessed data volume now contains a full-bandwidth wavelet which maximizes resolution, as a comparison of examples of both data sets indicates (Fig. 3a). The application of the spectral balancing process at critical places within the processing sequence is necessary to recover waveform amplitudes correctly and optimize the useful bandwidth. Monitoring bandwidth throughout the processing effort is essential.

Data phase was determined by comparing reflections at well tie locations with synthetic seismograms made using available sonic log digits. Digital log files in various formats were standardized to the GMA binary format for the master log library. Synthetic seismograms were made using zero-phase and "quadrant" phase-shifted wavelets of several bandwidths. Other displays using "octant" shifts (45 degrees) refine the matching process. Direct comparisons of zero-phase synthetic seismograms with sets of phase-shifted traces (Fig. 4) indicated that the data from the processor required a phase lead (between 90 and 180 degrees) to tie the zero-phase synthetic seismogram. Subsequently, optimum results from inversion modeling comparisons were achieved using data phase-shifted 135 degrees. Thus, the data volume was phase shifted, using the 3DSEIS phase shift routine, to produce a new data volume of zero phase data which has been used in subsequent analyses.

Synthetic seismograms were incorporated into a cross section and a 2D forward model was created to show ties of log correlations with seismic (and synthetic) reflections and demonstrate visual changes across the interpolated model. The results of this and other models are discussed later.

Project Orientation

A critical need for the re-development of basic relationships, both personal and data-associated, was met twenty-one months after the project began, when the new geophysicist joined the staff. Familiarization with the project included a review of project location, various data available, existing previous work, association with team members and equipment, and project objectives. The importance of the meetings of team members is stressed since the integration of disciplines is essential to project success. Early discussions took place with team members, exposing their study objectives of relating geology, production

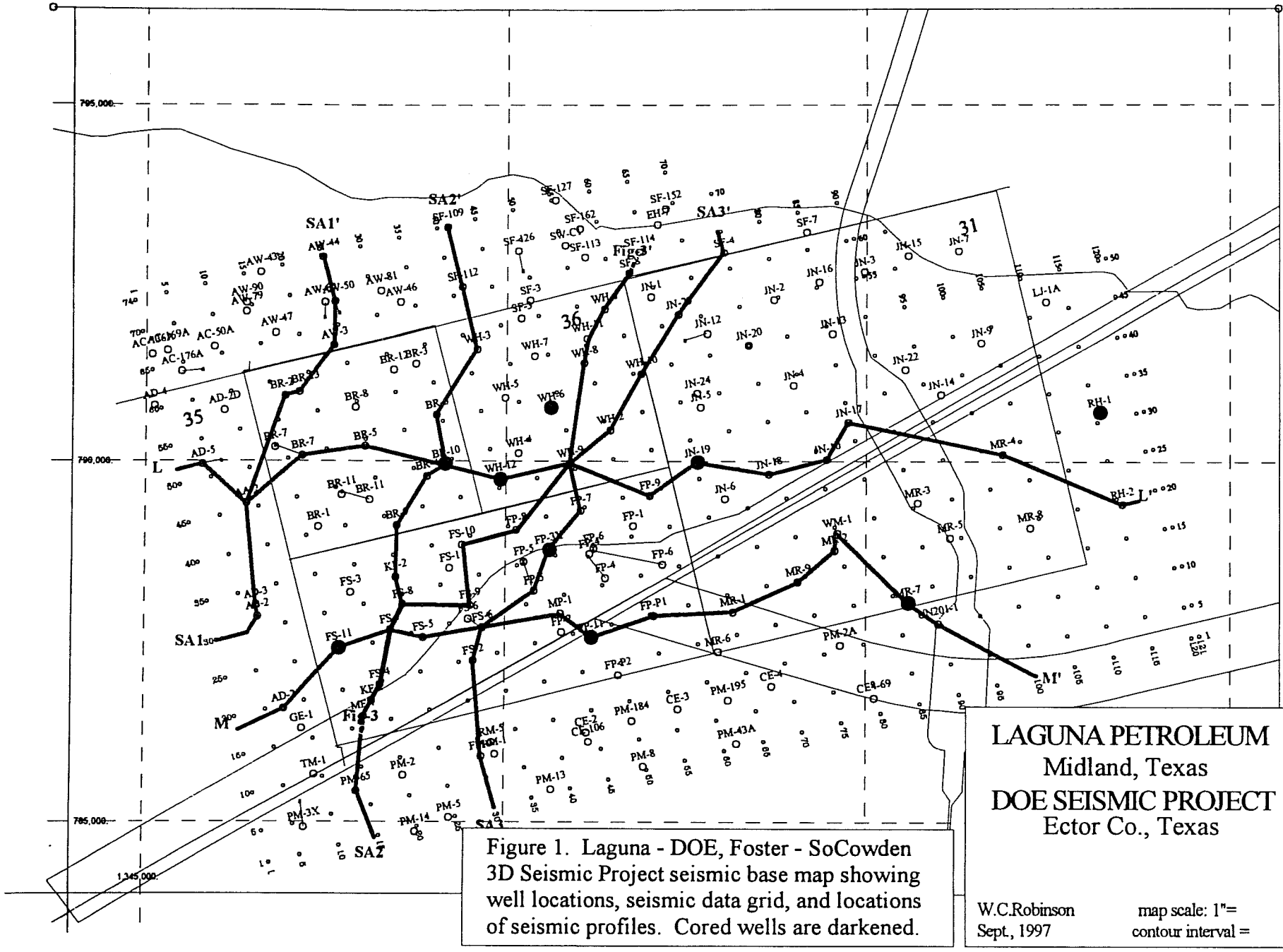

Figure 1. Laguna - DOE, Foster - SoCowden 3D Seismic Project seismic base map showing well locations, seismic data grid, and locations of seismic profiles. Cored wells are darkened.

LAGUNA PETROLEUM
Midland, Texas
DOE SEISMIC PROJECT
Ector Co., Texas

W.C.Robinson
Sept., 1997

map scale: 1"=
contour interval =

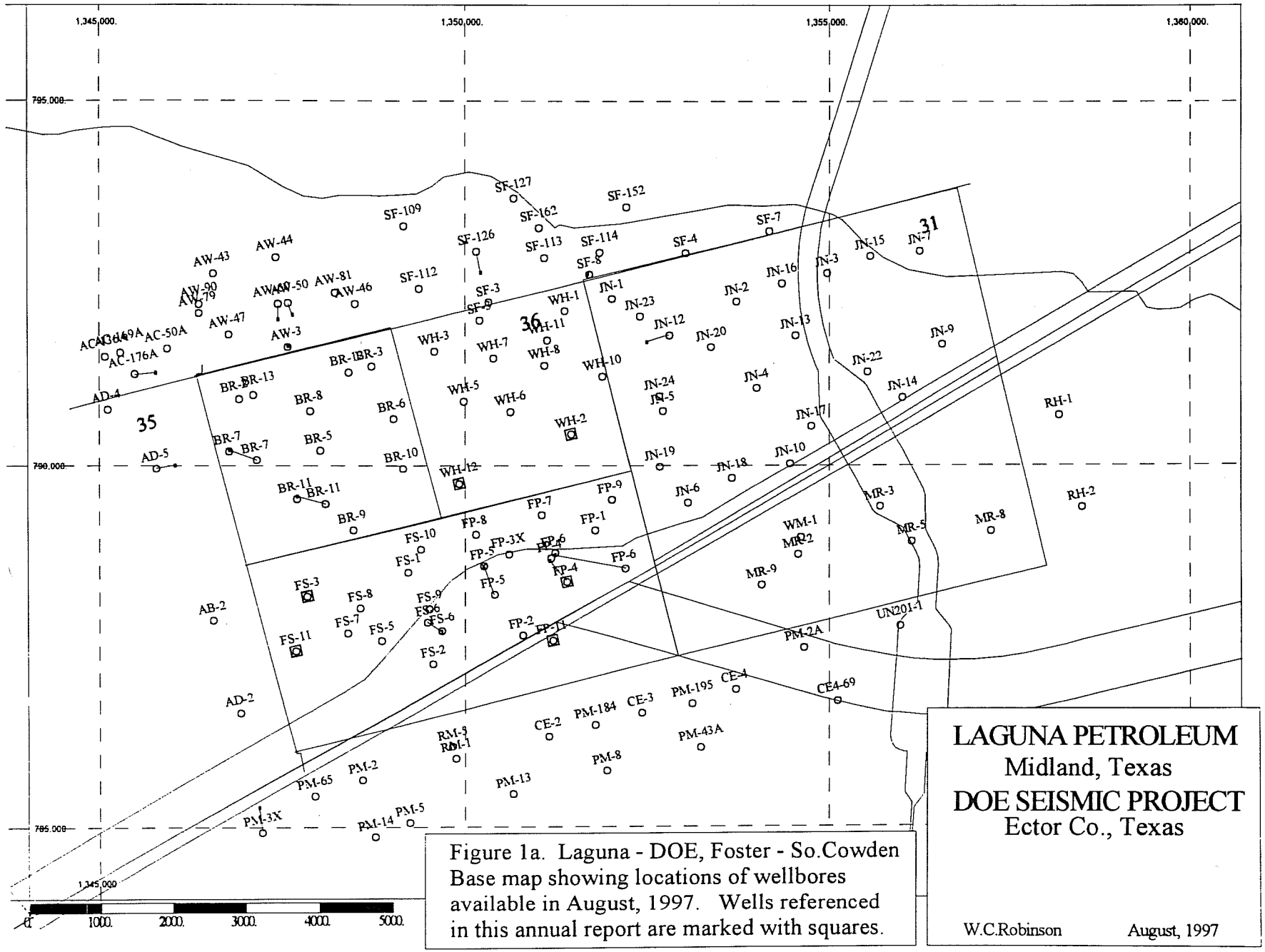

Figure 1a. Laguna - DOE, Foster - So.Cowden Base map showing locations of wellbores available in August, 1997. Wells referenced in this annual report are marked with squares.

LAGUNA PETROLEUM

Midland, Texas

DOE SEISMIC PROJECT

Ector Co., Texas

W.C.Robinson August, 1997

DOEWLL4

X-DOE	Y	##	elev	Oper	fee	wll#	API #	LogDatu	Yates	7River	Queen	l.Qn	Grbg	GrbgSS	GbA1	GbA1A
1347123	790974	BR-1	2927	L.E.	BROCK	13	4.214E+11	2942	2694	2907	3236	3743.5	3816	-874	3820.5	3848.5
1347599	792231	AW-5(	2936	AMOCO	WITCHER	50	4.214E+11	2937	2707	2920	3250	3764.5	3837	-900	3837.5	3872.6
1346402	789419	AA-2	2938	F.V.	ADDIS	A-2										
1346572	787863	AB-2	0	F.V.	ADDIS	B-2										
1345084	791492	AC-136	2955	AMOCO	COWDEN	136-A	4.214E+11	2955	2720.5	2932	3267.5	3794.5	3864	-909	3865	3898.5
1345293	791550	AC-169	0	AMOCO	COWDEN	169-A										
1345489	791258	AC-176	0	AMOCO	COWDEN	176-A										
1345939	791604	AC-50A	0	AMOCO	COWDEN	50-A										
1346945	786591	AD-2	2940	F.V.	ADDIS	2	4.214E+11	2954	2657.5	2871.5	3195.5	3696.5	3763	-809	3765.5	3788.9
1346084	790712	AD-2D	2941	F.V.	ADDIS	2						3727	3794		3796	3826
1346550	788020	AD-3	2936	F.V.	ADDIS	3	4.214E+11	2948	2656	2866	3194	3691	3753	-805	3753.5	3777.3
1345118	790775	AD-4	2931	F.V.	ADDIS	4	4.214E+11	2953	2681	2892	3228.5	3755	3813.5	-860.5	3818.5	3846.5
1345790	789959	AD-5	2943	F.V.	ADDIS	5										
1347593	791631	AW-3	2925	AMOCO	WITCHER	3	4.214E+11	2948	2698.5	2911.5	3241	3765	3828.5	-880.5	3830	3865.7
1346579	792634	AW-43	2926	AMOCO	WITCHER	43										
1347433	792851	AW-44	2927	AMOCO	WITCHER	44										
1348502	792216	AW-46	2922	AMOCO	WITCHER	46										
1346788	791797	AW-47	2928	AMOCO	WITCHER	47										
1347459	792217	AW-60	2925	AMOCO	WITCHER	60	4.214E+11	2934	2704.5	2919.5	3250.5	3771	3841	-907	3842	3870
1346376	792087	AW-79	0	AMOCO	WITCHER	79										
1348232	792376	AW-81	0	AMOCO	WITCHER	81										
1346375	792213	AW-90	2943	AMOCO	WITCHER	90										
1347400	789095	BR-1	2938	L.E.	BROCK	1										
1349153	789961	BR-10	2924	L.E.	BROCK	10	4.214E+11	2934	2677	2886	3217	3718	3797	-863	3801.5	3827.5
1348099	789473	BR-11	2938	L.E.	BROCK	11		2936	2647	2863	3201	3729	3803	-867	3805.5	3834.5
1347714	789535	BR-11	2929	surfaceLoc		sfcloc	4.214E+11									
1348413	791285	BR-12	2923	L.E.	BROCK	12	4.214E+11	2938	2694	2905	3236	3746	3819	-881	3820.5	3850.5
1346926	790922	BR-2	2934	L.E.	BROCK	2										
1348722	791362	BR-3	2920	L.E.	BROCK	3	4.214E+11	2938				3736	3818	-880	3822	3846
1348889	789795	BR-4	2931	L.E.	BROCK	4										
1348029	790212	BR-5	2927	L.E.	BROCK	5	4.214E+11	2941				3725.5	3800	-859	3803	3833
1349019	790653	BR-6	2923	L.E.	BROCK	6	4.214E+11	2933	2684	2900	3232.5	3740	3819.5	-886.5	3821	3850.5
1347171	790085	BR-7	2939	L.E.	BROCK	7		2939	2661	2880	3222	3739	3808	-869	3810	3839.5
1346791	790200	BR-7	2929	surfaceLoc		sfcloc	4.214E+11									
1347898	790758	BR-8	2925	L.E.	BROCK	8	4.214E+11	2935	2688	2900	3230	3741	3816	-881	3819.5	3848
1348478	789113	BR-9	2927	L.E.	BROCK	9	4.214E+11	2937	2657	2873	3205	3697.5	3770	-833	3774.5	3796.5

Figure 2. Example from the well data spreadsheet for the Foster - So. Cowden project.

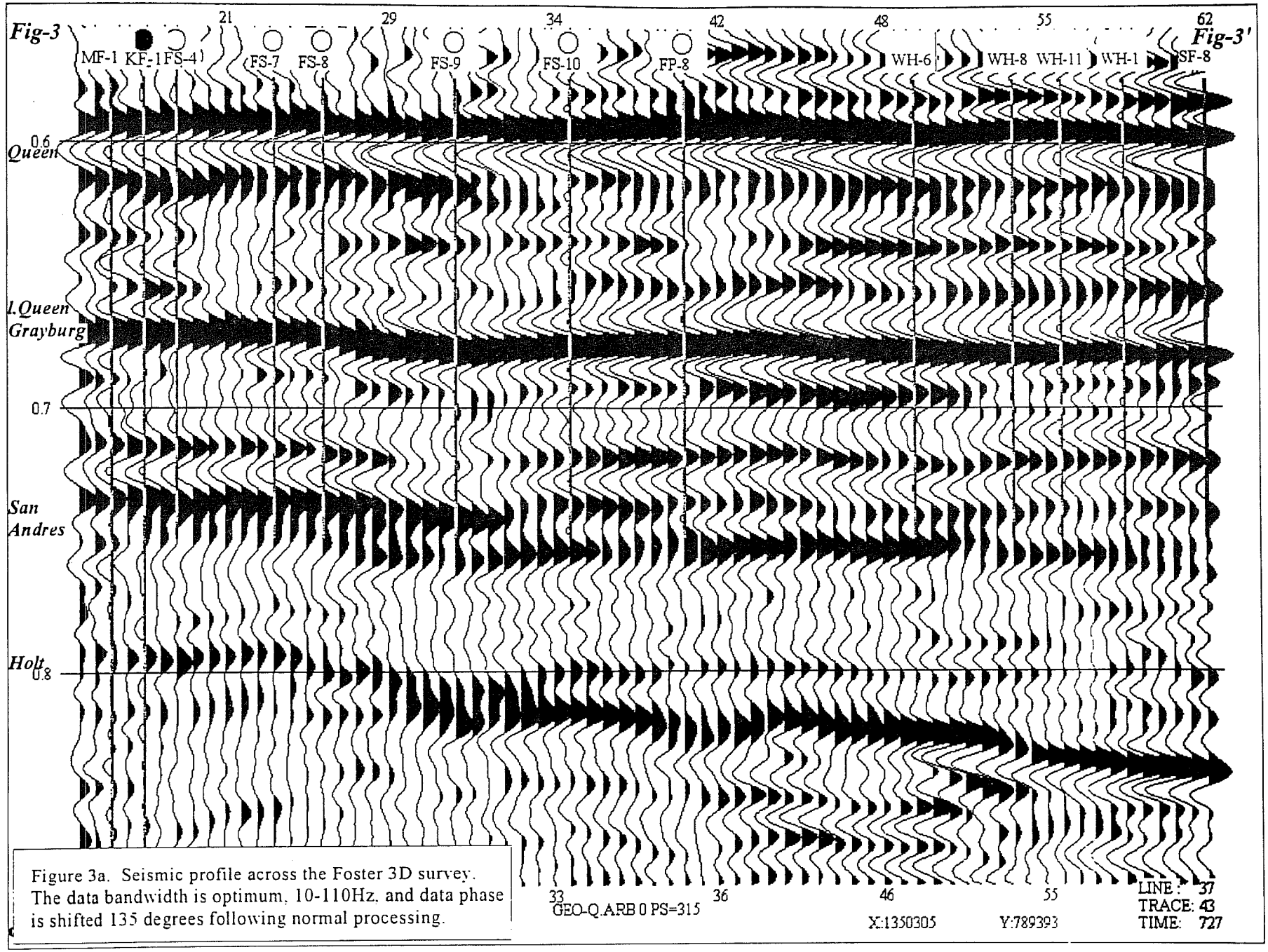

Figure 3a. Seismic profile across the Foster 3D survey. The data bandwidth is optimum, 10-110Hz, and data phase is shifted 135 degrees following normal processing.

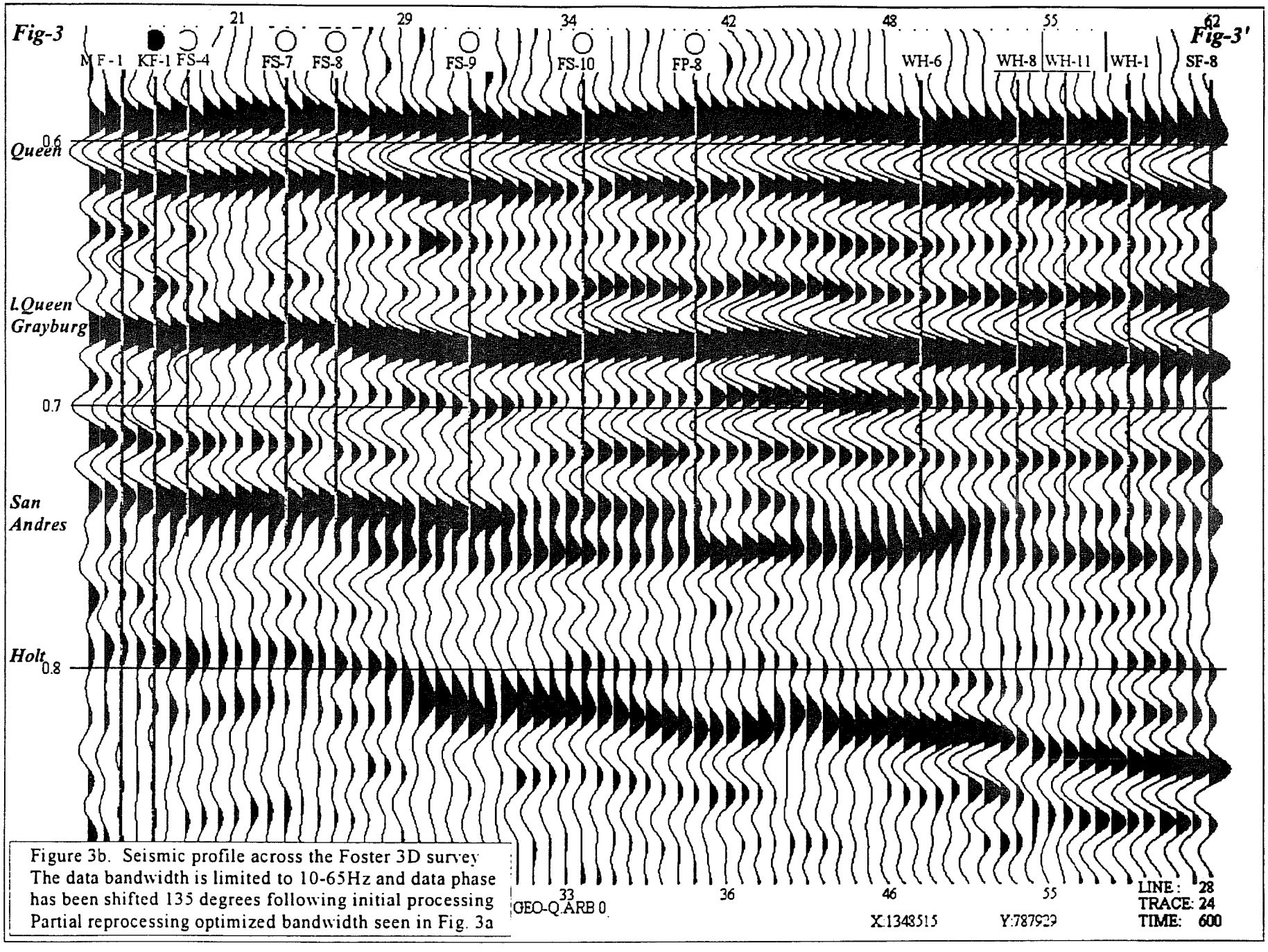

Figure 3b. Seismic profile across the Foster 3D survey
The data bandwidth is limited to 10-65Hz and data phase has been shifted 135 degrees following initial processing
Partial reprocessing optimized bandwidth seen in Fig. 3a

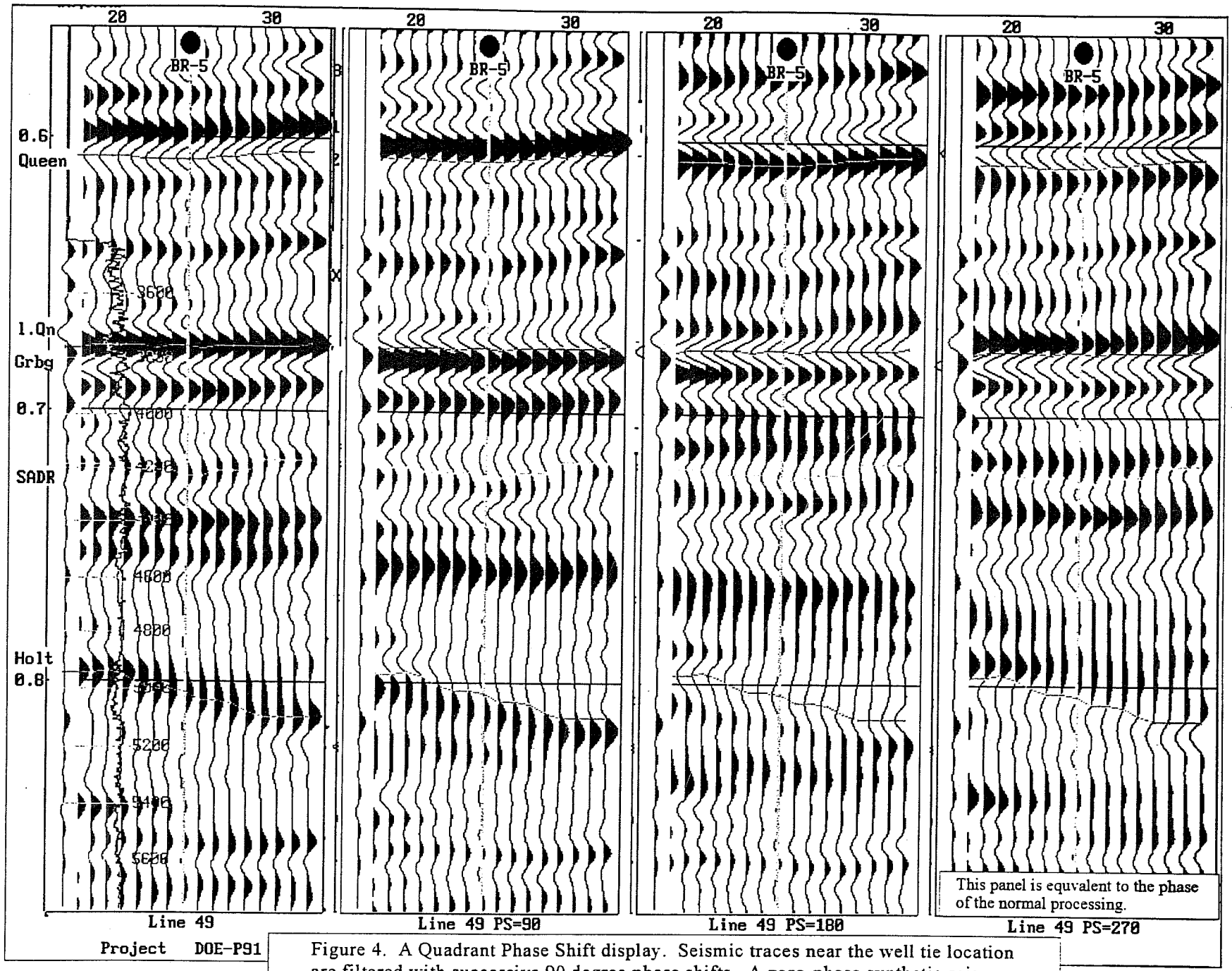

Figure 4. A Quadrant Phase Shift display. Seismic traces near the well tie location are filtered with successive 90 degree phase shifts. A zero-phase synthetic seismogram made from the well sonic log is at the right of each panel. It contains the data bandwidth and its similarity to data traces assists in determining data phase.

history, and waterflood realignment program characteristics and their interest in the ability of the seismic data to detail those relationships between well control points. Examples of topics discussed were 1) relating the resolution of seismic reflection intervals to log fine-sequence resolution, 2) preliminary map observations compared statistically to zone porosity measurements and a test of the mechanical interface between geophysical and engineering computer software packages, 3) data resolution optimization, and 4) project plans and timing. Preliminary correlations were made for seismic reflections, simple and complex geometries of the Grayburg and San Andres were discussed, and an approximate vertical resolution of the seismic wavelet was estimated at 100 ft.

Attendance at a seminar sponsored by the University of Texas Lands and the Bureau of Economic Geology (November 6, 1996) provided insight for this project from the presented methodology. Work by the Bureau relates fine-cycle sedimentation packages in the South Cowden field to the seismic sequence. Recognition of geometries of various facies (tidal channels, bars or banks) will be a mapping objective in the Laguna project since rock properties associated with those facies strongly affect internal permeability and production flow.

The starting point of this stratigraphic study of seismic data was to take a quick look at basic reflection data attributes to observe obvious characteristics. Reflection changes occur within the Grayburg across the survey, indicating the formation is not homogeneous.

An early concern was the choices of geologic data to be targeted for comparison to seismic data. Statistics support the use of any parameters that will correlate as potentially assisting oil production. These factors typically include structural trap, seal and reservoir mapping. Structure in section is probably not a trapping factor, but laterally extensive intra-formation seals exist as fluid flow boundaries. These boundaries are identified as well log correlations. Reservoir heterogeneity is a major factor controlling oil production and waterflood effectiveness. Mapping porosity satisfies theoretical, observable, and practical requirements of the integrated study. Porosity can be quantified in many ways (net, phi-h, GAP, cut-off, etc.), so consideration of the seismic response and the end need for engineering model parameters has determined the use of Gross Average Porosity as the key parameter in this project.

Following suggestions from articles regarding use of seismic data to guide log property estimation (Schultz, Ronen, Hattori, and Corbett, 1995) and (Watts, Hinterlong, and Taylor), initial relationships between the seismic data and well data were sought. An early exercise was to compare the preliminary Grayburg reflection waveform attributes (such as instantaneous frequency and amplitude) over a short interval with Grayburg A1 zone average porosity, established from porosity-type log measurements in wells. The results were colorful and interesting, but geologically were weakly related, and served only to test the compatibility of seismic and well-derived data files with the engineering software. Because of those weak results, little importance was attached to the maps. It is now realized that these early maps did not even relate geologic zone positions correctly. This fact is mentioned because it is important to recognize errors in analysis as well as successes.

The objective at the early stage of any project is to make many observations efficaciously, creating profiles, cross sections, and maps. Deeper, time-consuming evaluations come later, once a degree of understanding and priority is established. The current study is limited to the Grayburg and San Andres formations, although maps of shallower and deeper formations have been made in order to recognize any significant geologic relationships. A list of logical maps of seismic reflections was initially established, including the Yates, Queen, lower Queen, Grayburg, San Andres, and some event immediately below the San Andres. These reflections were subsequently tracked on the seismic data and were mapped as surfaces of time structure, isochrons, and reflection amplitude. Subsurface (well) data from the spreadsheet were used to generate a series of contoured structure and isopach maps. These maps are used in the inversion model analyses and the production volume models.

Initial observations of the seismic data were focused on reflection character across the estimated time interval containing the Grayburg Formation. Synthetic seismograms placed geologic correlations (ranging

from 40 - 140 ft apart) at various positions within the sequence of reflections, falling near peaks, troughs, and zero-crossings (see synthetic models in Fig. 7). No consistent correlation criteria could be established because none exist. No reliable map of any geologic correlation within the Grayburg could be made using the seismic data because of the absence of those criteria.

A strong amplitude anomaly was noticed on the map of the amplitude of the seismic reflection initially attributed to the top of the San Andres. It was somewhat related to the presence of porosity (within the first 100 ft of the San Andres sequence) in wells. The relationship compelled investigation as a useful indicator of porosity distribution. The initial reaction (from general experience) was that the existence of porosity near the top of San Andres should result in weaker reflection amplitude. However, utilizing the recent cores, the project geologist points out that there are no strong lithologic changes separating the Grayburg from the San Andres, so that only a weak San Andres reflection should exist normally. The reflectivity would potentially *increase* with porosity development. A forward model was made to test the effects of various amounts of upper San Andres porosity situations on seismic reflectivity, and the result compared well with the observed seismic amplitude increase.

Important Realizations

The seismic data do not respond as mappable reflection events to log correlations, not as peaks, not as troughs, and certainly not as zero-crossings. Peaks and troughs are the compound seismic response to impedance boundaries, but the zero crossing has no geological significance whatsoever. The fact is that seismic wiggle trace resolution, even optimized, is not adequate to map the detail of geology required for production model simulations. In fact, the rock characteristics are expected to vary so that any unique seismic criteria for a geologic marker would fail across the project. In addition, the quantitative (as opposed to qualitative or relative relationships) results needed to describe rock properties in absolute terms are not possible using reflection data. The course of study was set away from the wiggle trace data volume.

Seismic Correlation with Geology

Project personnel met to discuss the geology in general, to review well data, and to discuss well cores for the Foster-Pegues-11, the Foster-11, and the Witcher-12, wells drilled during Phase II of this project. This orientation with the laid out cores was of great benefit. Two-wall display, dip-oriented well log cross sections (L-L' and M-M') were constructed to demonstrate Grayburg and San Andres zone characteristics (Fig. 1). Two normal scale (10in/second) seismic profiles connecting the same well locations, several with sonic logs, show the seismic response across the zones and deep structural relationships not shown on logs (Fig. 5 and Fig. 6). These profiles, enlarged to 40in/second vertical scale ("zoomed" in), better show details of reflections associated with the Grayburg and San Andres. A companion cross section of synthetic seismograms enlarged to well log scale (2.5in/100 ft) helps to visualize vertical resolution relationships. A 2D forward interpolation model of the synthetic seismograms across the Grayburg sequence demonstrates some expected seismic changes across section L-L' (Fig. 7). Notably, the reflection tracked as the top of the Grayburg is closely associated with the A1 correlation in section 36, but diverges to tie to a lower Queen carbonate bed (separated from the Grayburg A1) in section 31. The strongest, most consistent seismic event cannot be used to locate the boundary of the first Grayburg fluid flow zone. Seismic profile M-M' duplicates the southern well log cross section map trace, also showing the seismic sequence from the Queen formation downward to the Pennsylvanian. Three strike-oriented seismic profiles have been built as arbitrary lines, but well log cross sections were not built to match them.

Synthetic models were created (Fig. 8) to demonstrate possible variations of porosity in the A1 and A2 zones within the top 120 ft of the Grayburg formation. Except for basal quartz sand deposits less than 10 ft thick at major inter-formation boundaries, the Grayburg lithology is dolomite and anhydrite. Reflections within the Grayburg most likely emanate from porosity contrasts. Model limits range from no porosity to extreme porosity. The responses likely to be observed in project well data are between 0% and 18%.

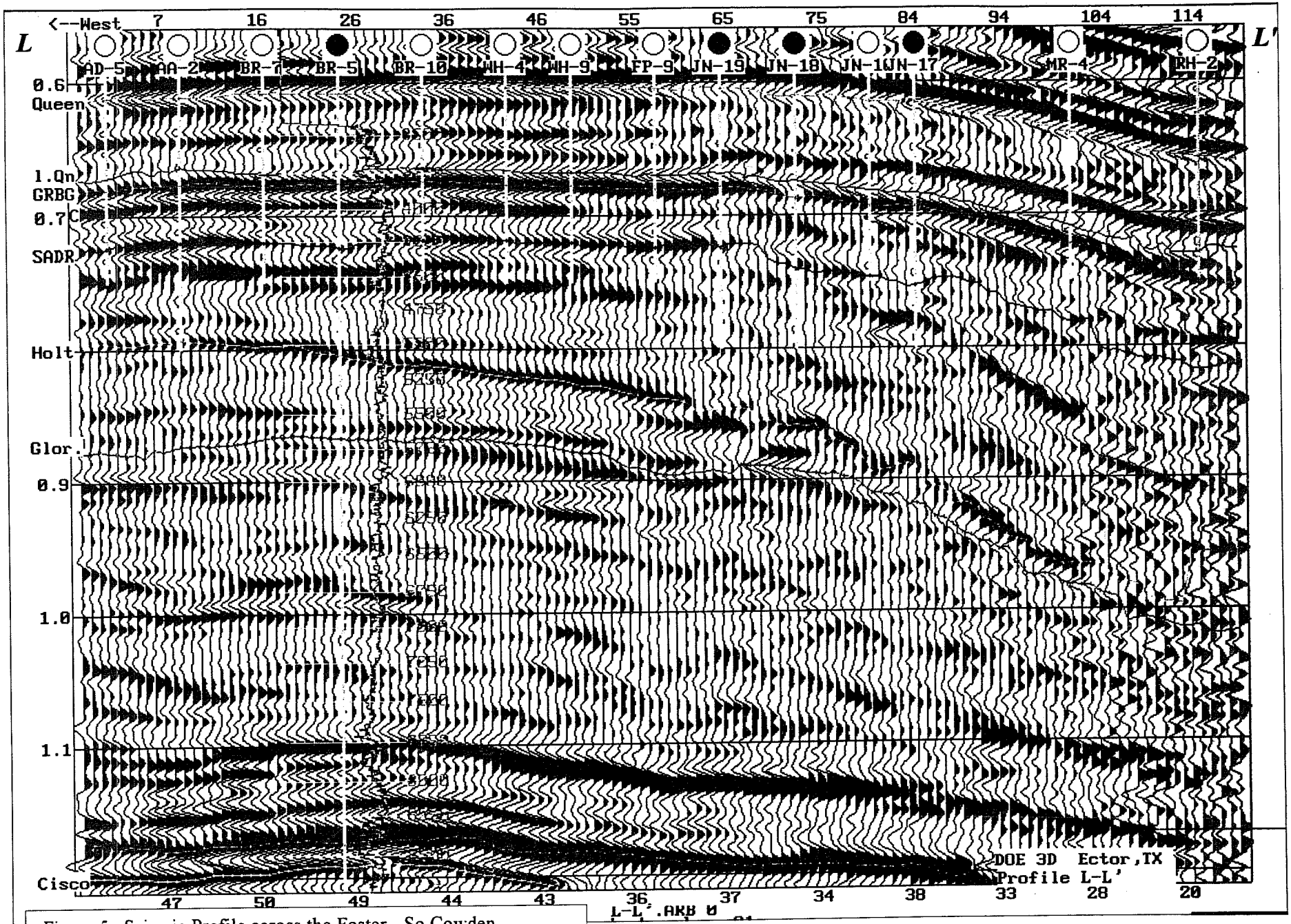

Figure 5. Seismic Profile across the Foster - So.Cowden 3D seismic survey, showing some structural and stratigraphic features of the project.

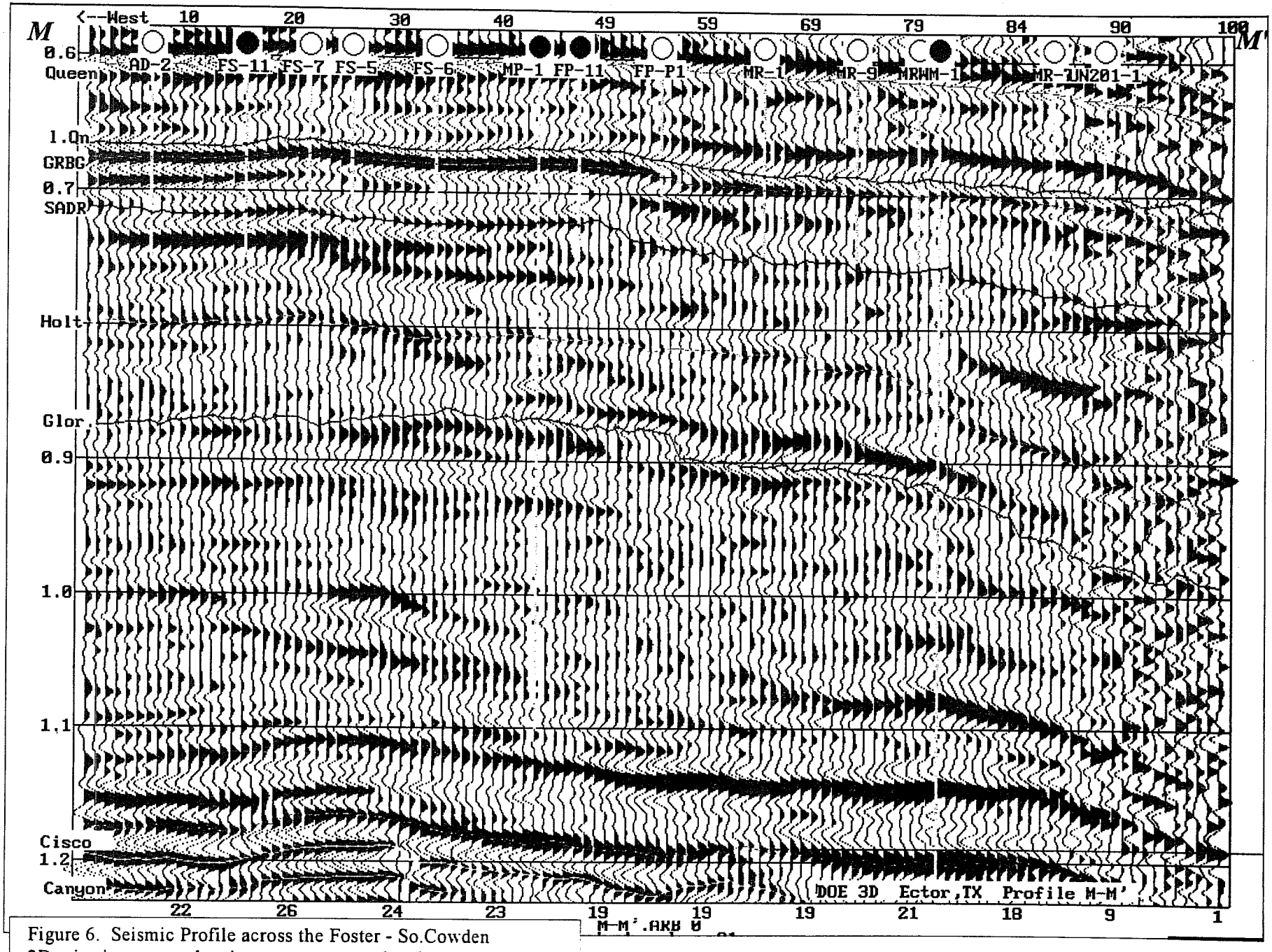

Figure 6. Seismic Profile across the Foster - So.Cowden 3D seismic survey, showing some structural and stratigraphic features of the project.

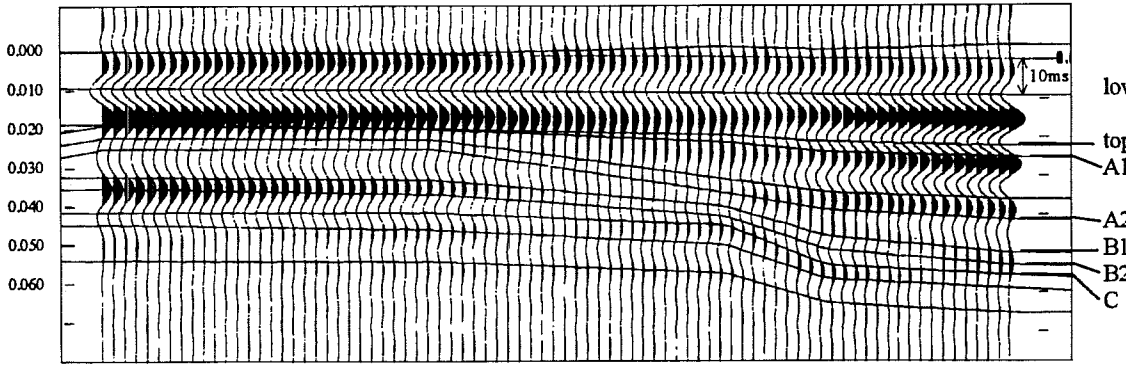

Figure 7 . A seismic forward model made of synthetic seismograms generated from well sonic logs and interpolated logs. These traces represent the expected changes of seismic data character due to geologic variations across the survey discussed in this report.

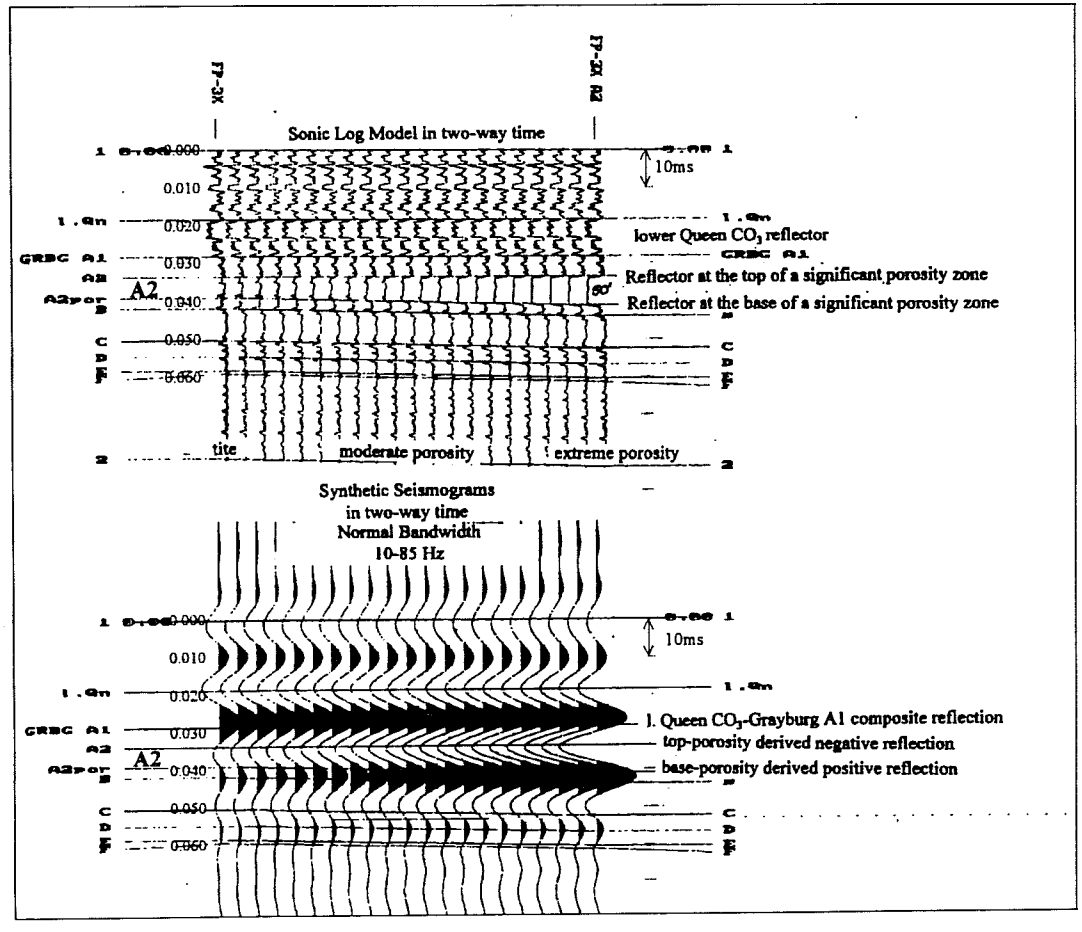

Figure 8 . A seismic forward model similar to Fig. 7, but changes are made to only a single sonic log. The amount of porosity in the A2 zone is varied from very low (left) to very high (right). The purpose is to create a significant pair of impedance contrasts, at the top and the base of the modeled porous unit. The seismic response is a trough, then peak reflection having increased strength with increased porosity.

Synthetic models were also created to demonstrate possible variations of porosity in the associated with the lower Grayburg and upper San Andres formations. Nine models varying the velocity of the lower 60 ft of the Grayburg (G and H), and the first and second 50 ft of the San Andres are arranged in panels of a wall display as a sort of matrix. The reflection responses of the models are compared to the reflections on the seismic wiggle-trace data to formulate an interpretation. It is important to recognize that the cause of a reflection associated with the top of the San Andres may take on different forms, depending on the rock properties above and below that horizon.

The first series of maps, discussed previously, includes subsurface and seismic reflection maps of main correlation horizons. All Grayburg internal correlations (log calls) were mapped as isopach intervals, both for quality control purposes and for their information value. The seismic reflection from near the top of the Grayburg (Fig. 9) was mapped, showing the features of the relatively flat shelf area in section 36 and the structural break to the outer shelf in section 31.

Reflections from the lower Permian (Fig. 10), Pennsylvanian and Devonian were mapped to relate buried structure and (perhaps) faulting to the structural boundaries observed in the Grayburg sequence. Faults were tracked and may extend upward to the Grayburg; structure-associated paleotopography possibly affected some Grayburg and San Andres facies and diagenetic distributions.

Seismic Inversion Modeling

To satisfy the objective of mapping quantitative values related to reservoir porosity, derived from seismic data, seismic inversion modeling is used. Seismic inversion modeling is a method of converting processed seismic amplitude trace data (wiggle traces) into traces which resemble sonic log curves. In practice, it is a process of converting seismic amplitude data from sinusoidal traces containing a seismic wavelet to blocky, log-like traces with wavelet complexity removed. The ambiguities of the seismic wavelet (inadequate resolution and reflection interference) are removed from observations. The inverted traces are still represented in time, not depth. Density is not considered in the inversion process used in this study. The inversion model is computed using software within the Vest 3DSEIS system.

Where forward synthetic modeling attempts to predict seismic effect from a defined geology, inversion modeling attempts to calculate seismic (sonic?) velocity from seismic data. A human interpreter mentally incorporates knowledge from wells of the rocks and their distribution into a larger picture assisted by seismic data, essentially constraining the interpretation to the facts or reasonable fiction. Inversion modeling incorporates the facts of lithology-influenced data to create a more easily interpreted data set. Constrained inversion modeling input parameters consider: (1) tracked reflection horizons, (2) sonic log-derived velocity values, and (3) the interpreter's experience with the project geology to extend log-defined velocity limits. A range of velocity values is defined for each tracked reflection (an approximate lithology boundary) and for the total interval between tracked reflections. Provisions are made for other geological situations that may also occur. Seismic amplitude data to be modeled must be zero phase to provide geologically correct results. The inversion model result is very sensitive to data phase and can also be used effectively as a tool to refine phase correction. Model testing is an essential precursor to model building. Testing constraint parameters, amplitude factors, and comparing test models to well logs requires (well-spent) time.

A preliminary model was calculated for this project to specifically analyze the Grayburg and San Andres sequences. The model input parameters have been refined and expanded in the current model, but the results of the preliminary model are remarkable in the presentation of velocity-related characteristics of the seismic data. The inversion model is effective for the shelf area of section 36 of the seismic project, but the outer shelf geology in section 36 was not included in the following analyses because of inadequate constraint control in the preliminary model.

The seismic inversion model created in December 1996 produced a high correlation relationship of the inversion-derived average interval velocity cross-plotted with gross average porosity of the Grayburg A

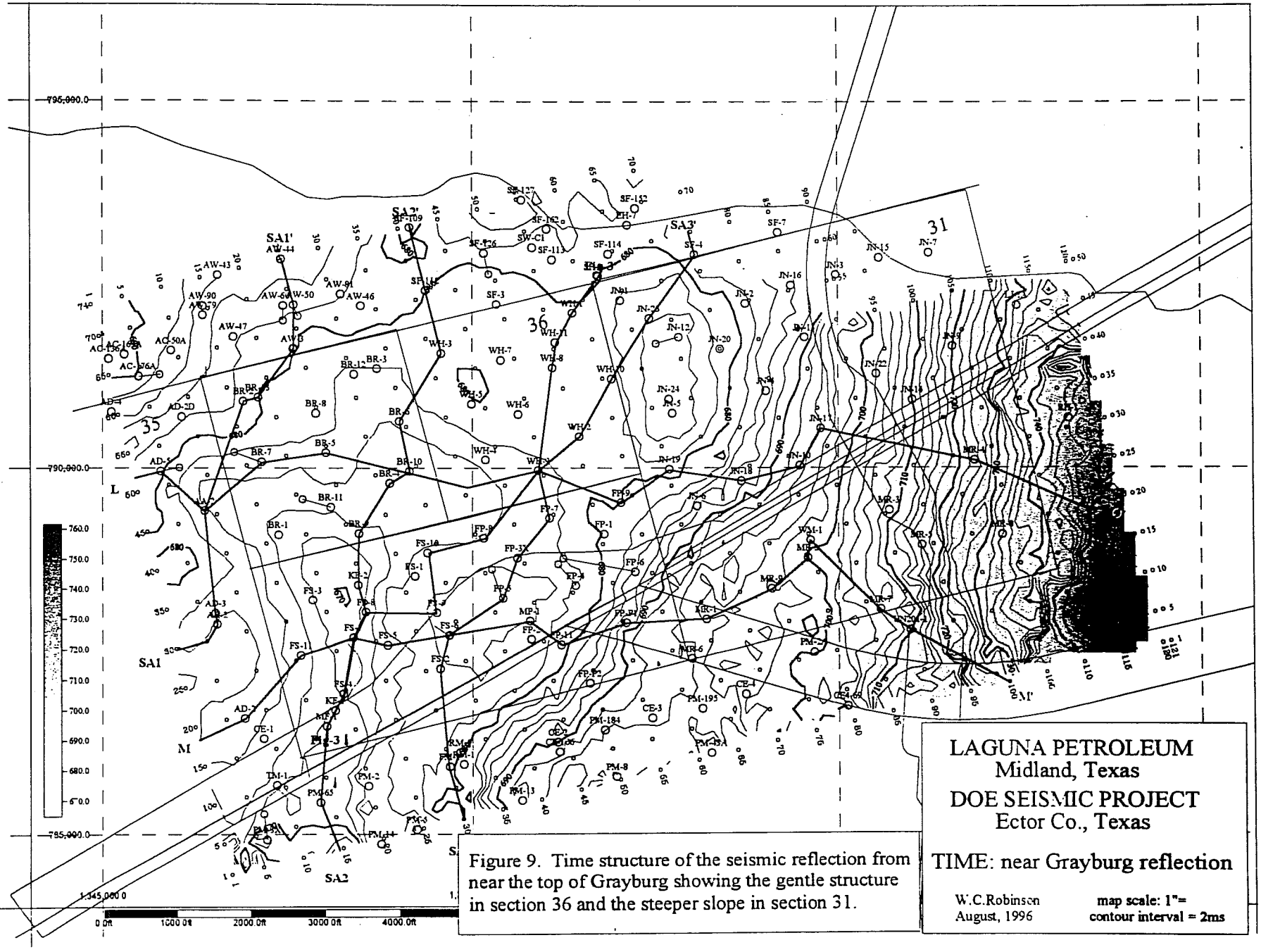

Figure 9. Time structure of the seismic reflection from near the top of Grayburg showing the gentle structure in section 36 and the steeper slope in section 31.

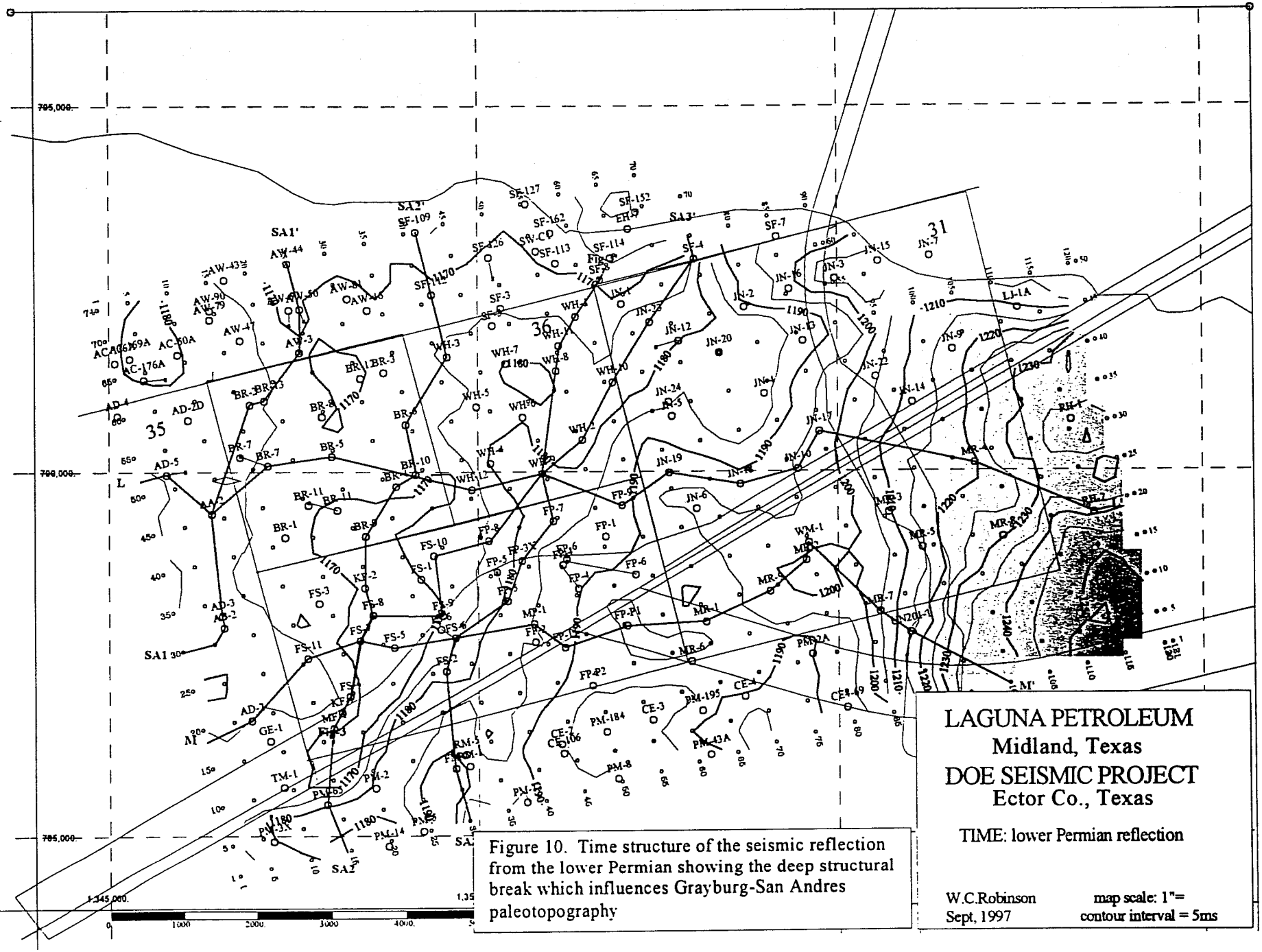

Figure 10. Time structure of the seismic reflection from the lower Permian showing the deep structural break which influences Grayburg-San Andres paleotopography

zone. The top of the A zone was defined by revising the reflection surface mapped as the Grayburg. The re-picking was done using the profile view of the inversion data, placing the pick at the low-to-high velocity interface (lower Queen - Grayburg). The 3DSEIS program allows tracking of non-amplitude data. The pick coincides with the top of the A in section 36, where the wells with rock property data are located. However, in section 31, the A1 is not the first carbonate below the lower Queen marker and does not coincide with top of the Grayburg. The study was not carried far into section 31. The bottom of the A interval was picked universally 10 ms below the A horizon, since the improved method had not then been developed.

Improving the inversion model itself involved testing other seismic parameter choices and more precisely identifying wavelet phase. Listed here are the user-input parameters that affect the inversion model and have been extensively tested:

Horizons - are located by tracking a peak or trough reflection associated with an impedance contrast definable in geologic terms to position velocity constraint values; modeling results show that the reflections may not coincide with lithologic boundaries

Velocity Constraints - are values of velocity determined from sonic logs, used to control inversion model trace values; minimum and maximum values set a range that represents geologic possibilities within each stratigraphic sequence being modeled

Amplitude - is a relationship of the processed seismic data with a synthetic seismogram

Bandwidth - is an approximation of wavelet bandwidth across the volume (X, Y, & Time) of amplitude data to be inverted

Phase - is a variable that strongly affects the velocity values of the inversion trace and is a function of the input data rather than being a test parameter (see example on the preceding page)

Modifications to the preliminary inversion model input parameters involved varying the constraints of horizon position and velocity values. The lower Queen reflection is a consistent lithologic boundary and was retained. The "Grayburg" reflection is a composite reflection that does not resolve the top of the A zone, but is used to set the velocity at the top of the Grayburg sequence. The reflection near the San Andres may result from rock property changes near the interface since no continuous lithologic boundaries exist between the lower Grayburg and the San Andres. For this reason, the San Andres constraint is not handled as a lithologic boundary. Below the top of the San Andres constraint, values are needed, but reflections are discontinuous because of structural and stratigraphic complexity. The Holt, a carbonate unit in the lower San Andres, has been picked to constrain velocities within the San Andres.

Extensive testing preceded the calculation of a workable inversion model of section 36, the area of virtually all well log-derived porosity control, and the area of the production history model. Constraint parameters were tested, varying a range of input items. The parameters used in the current model include basic reflection horizons of the lower Queen (-), the "near" top of Grayburg (+), the "near" top of San Andres (+), and the Holt lime. The original seismic wiggle data traces were phase-shifted 135 degrees to become zero-phase. The bandwidth defined for the model was 8-12-85-100 Hz, slightly less than the optimum band but inclusive of traces in noisier areas.

Successful test model traces made in the testing have visually (qualitatively) good similarity to sonic logs in relative velocity curve shape and display resolution on the order of 50 ft (Fig. 11). Progressive, small changes in successive model parameters were made to preserve the success of the preliminary model and to improve upon it. The objective of the optimized model is to have high cross-plot correlations of inversion-derived velocity and wellbore-derived porosity for all productive zones.

Inversion Model Analysis

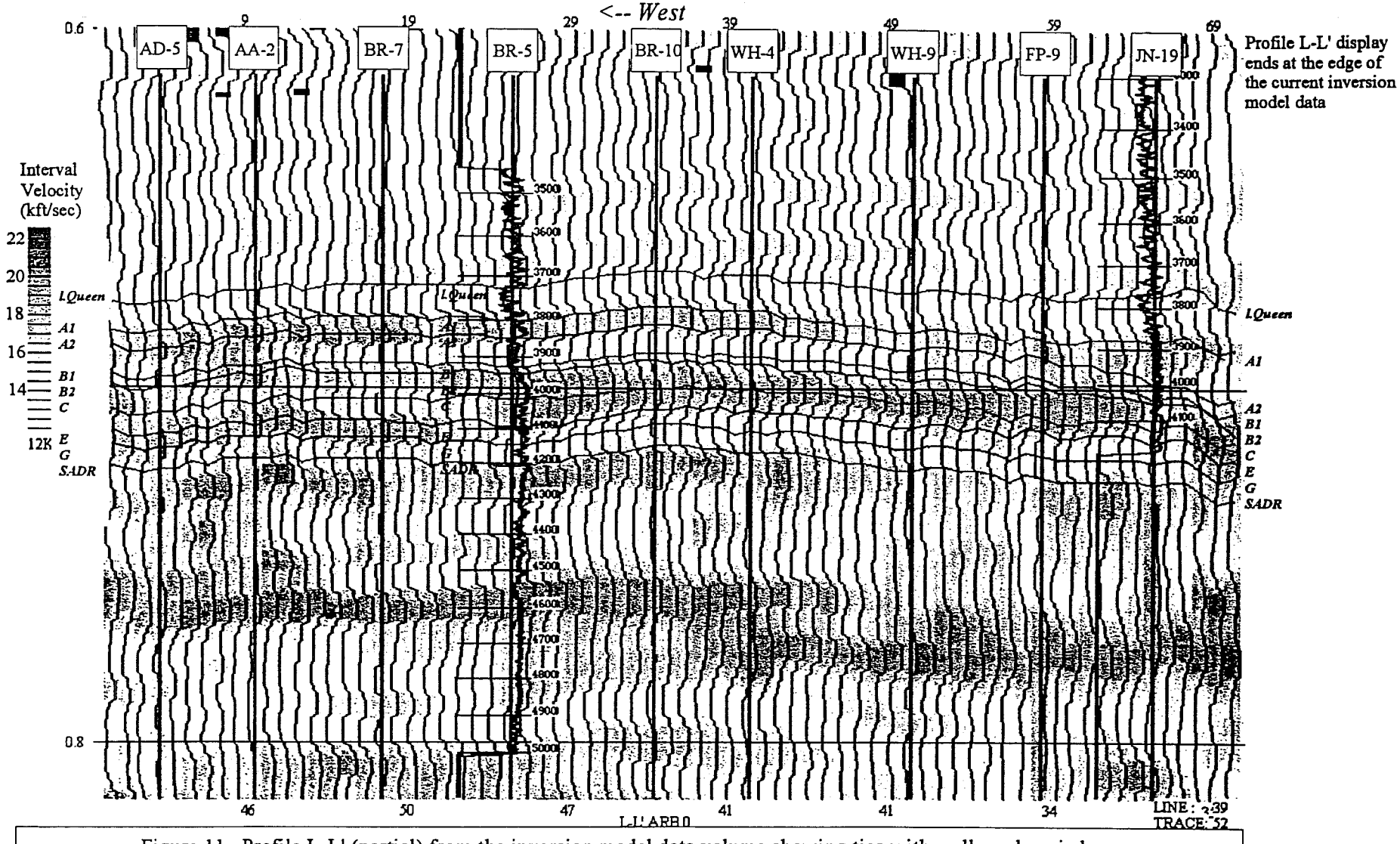

Figure 11. Profile L-L' (partial) from the inversion model data volume showing ties with wells and sonic logs.

Definitions used in this report:

analysis boundaries - surfaces defined by log correlations, which may or may not be seismic reflection horizons, positioned in seismic time in order to isolate seismic characteristics for a very specific zone; they commonly cross changes in rock properties

zone - the rock volume, bounded by log correlations, to be compared to a volume of seismic data

cross-plot - a graph showing the relationship of some seismic data property and a rock property (for example, seismic velocity vs. gross average porosity); a line of best fit is determined, the slope of which can be used to convert data from seismic property values into log property values

The primary geologic objective is to map the distribution of particular rock properties which can be used to describe fluid volume and fluid movement between wells over the long production history of the oil field, and to help predict future fluid behavior as a factor in engineering models for fluid flow simulation. Further objectives of the analysis are to find relationships of seismic data characteristics with rock properties, and to map the distribution of those properties for the studied geologic sequences. In order for these relationships to be meaningful, several factors must be resolved: (1) seismic characteristics of velocity must be accurately portrayed, (2) zones must be accurately defined, and (3) geologic properties under consideration must be represented in the seismic data. Seismic waveform attributes which are commonly discussed in the literature and are easy to produce were examined initially, but it has been concluded that their uses do not specifically meet the above criteria and provide only vague, empirical observations.

Qualification of test case inversion models for sonic velocity (geologic) accuracy addressed profile and map presentations. The profile views of inversion model traces (Fig. 11) are comparable with sonic logs (in time); where the inversion traces look like the sonic logs, the model is deemed successful. The map view of the average interval velocity within geologic zones is comparable with well log-derived rock property data, specifically, gross average porosity of those zones. The map analysis is more subjective than the profile analysis, but is ultimately the more important data product. The model used to create the current porosity distribution maps has good trace character and is associated with optimum velocity vs. porosity cross-plots for the A zone.

Accurate analysis of an inversion model for very specific geologic zones requires accurate positioning of zone boundaries in time in the seismic data. For this project, only the first of several zones of interest, the Grayburg A1, is defined by a seismic reflection event, and then only approximately because of limited resolution. The engineering model requirements demand the thinnest intervals possible to be measured and mapped. The thinnest mapped intervals of production are the Grayburg A, subdivided into A1 (~70 ft) and the A2 (~50 ft), the Grayburg B, subdivided into B1 (~50 ft) and the B2 (~50 ft), and the Grayburg C (~30 ft). The lower Grayburg and the San Andres are also defined by zones of similar thickness. The inversion model describes vertical sequence intervals on the order of 5 ms (40-50 ft) thick, which might represent the true seismic resolution. If this conclusion is correct, analyses of those thin intervals are meaningful when applied to the flow unit thicknesses.

Establishment of analysis boundaries for the preliminary analysis was based on an interval of Grayburg A zone assumed to be 10 ms thick. This is a reasonable, but general estimate, which works in section 36, but is not adequate just off structure in section 31 where that sequence thickens. In addition the B and C and the San Andres boundaries are not defined in any way by mappable seismic events and must be set some other way. A series of isopach maps (Figs. 12) was made from well data showing the thickness of the subdivided Grayburg zones. These maps have been used to predict an accurate position for each log correlation by converting thickness in feet to time in milliseconds. Summing the four Grayburg intervals that were calculated leads to creation of a San Andres time surface that is close to the reflection initially picked as the San Andres.

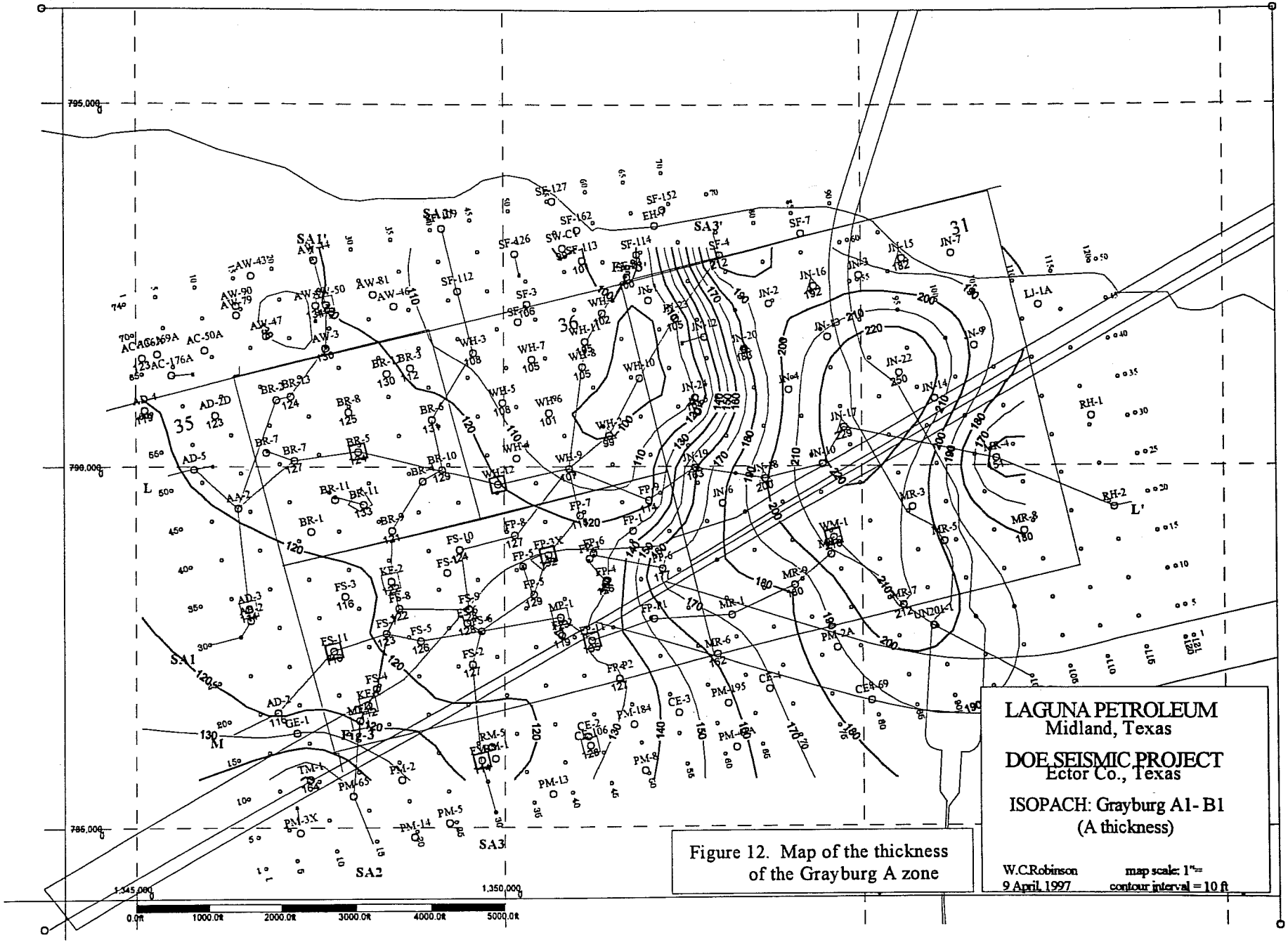

Figure 12. Map of the thickness of the Grayburg A zone

The development of analysis zone boundaries as seismic horizons also enabled an evaluation of several waveform attributes regarding their usefulness in responding to reservoir properties. Interval average slices were made for zones measuring instantaneous amplitude, instantaneous frequency, and instantaneous phase. Porosity data were cross-plotted with the interval average values for the A, B, C, and E zones. No clear relationships have been recognized in the cross-plots. The solution to analyzing the Grayburg geology does not lie in mapping the waveform attributes, at least not to the degree required for the engineering model.

A library of logs was compiled for easy access and review of zone boundaries and characteristics. Neutron source logs used for calibration of seismic maps show wellbore porosity characteristics, the manipulated values of which are listed on a spreadsheet. Sonic logs are also included with correlations marked. The integrated (in time) sonic logs are the source of interval velocity values used to convert the isopach maps to isochron maps.

Conversion of Seismic Data to Rock Property Data

Zones of the Grayburg (A, B, and C) were measured for average interval velocity from the inversion model. The interval averaging technique considers all samples (spaced one ms apart) between boundary horizon surfaces. The boundaries follow the time structure of the tracked horizons and are not time slices.

For carbonate rocks, rock velocity and rock porosity are related inversely; as porosity increases, interval velocity decreases. In this project seismic-derived average interval velocity is strongly related in the Grayburg A zone, moderately related in the B zone, and weakly related in the C zone, given the values of porosity calculated from calibration-quality well logs. No usable relationships are yet seen for the lower Grayburg or the San Andres, to be discussed later.

The values of porosity or any other rock property are in some sort of manipulated form. In order to relate to seismic data, these values must represent an adequately thick zone and the porosity parameter that is sensed as an acoustic impedance. Gross Average Porosity is an average of porosity for each foot of zone, no matter how thick the zone is. Clearly, thin zones will affect seismic response differently than thick zones having similar Gross Average Porosity. Data sets considering net feet of porosity commonly are subject to some minimum porosity cutoff value, and, again, total thickness can affect the seismic response. Porosity times height (phiH) values consider thickness and are likely to affect seismic response in a consistent way. The upper Grayburg zones do not vary radically in thickness in section 36, so that thickness-induced problems are minimal.

Quantitative comparison of inversion-derived velocity versus log-derived porosity is accomplished for each zone by cross plotting. The geologic parameter most useful to explaining historical production and advancing future development is rock porosity. The form of porosity most likely to be imaged by the seismic data in this project is Gross Average Porosity of a defined interval. The relationship of velocity and porosity is handled as a linear function, although, according to Schlumberger (Schlumberger Log Interpretation Charts) the relationship is slightly non-linear (Fig. 13). Porosity values used for calibration of maps are chosen strictly from neutron density logs. For several wells, values of porosity derived from a sonic tool and a neutron source tool were compared to show a difference in calculated porosity in dolomite, particularly where anhydrite is also present (Fig. 22). The difference in porosity determined from different log types, up to several porosity percent, is significant. Since the seismic data are being calibrated using log data, it is important to be consistent with log type. Continuing attention is also being paid to the possibility of detecting an anhydrite effect where converted porosity values are negative.

The cross-plot points determine the statistical best-fit relationship used to convert velocity to porosity (Fig. 13). The cross-plot graph displays the total Grayburg A zone, and, individually, the A1 and A2 zones. Velocity values for the A1 are higher than for the total A interval, and velocity values for the A2 are lower. Theoretically, the seismic velocity value trend should be comparable for all zones, the difference in the

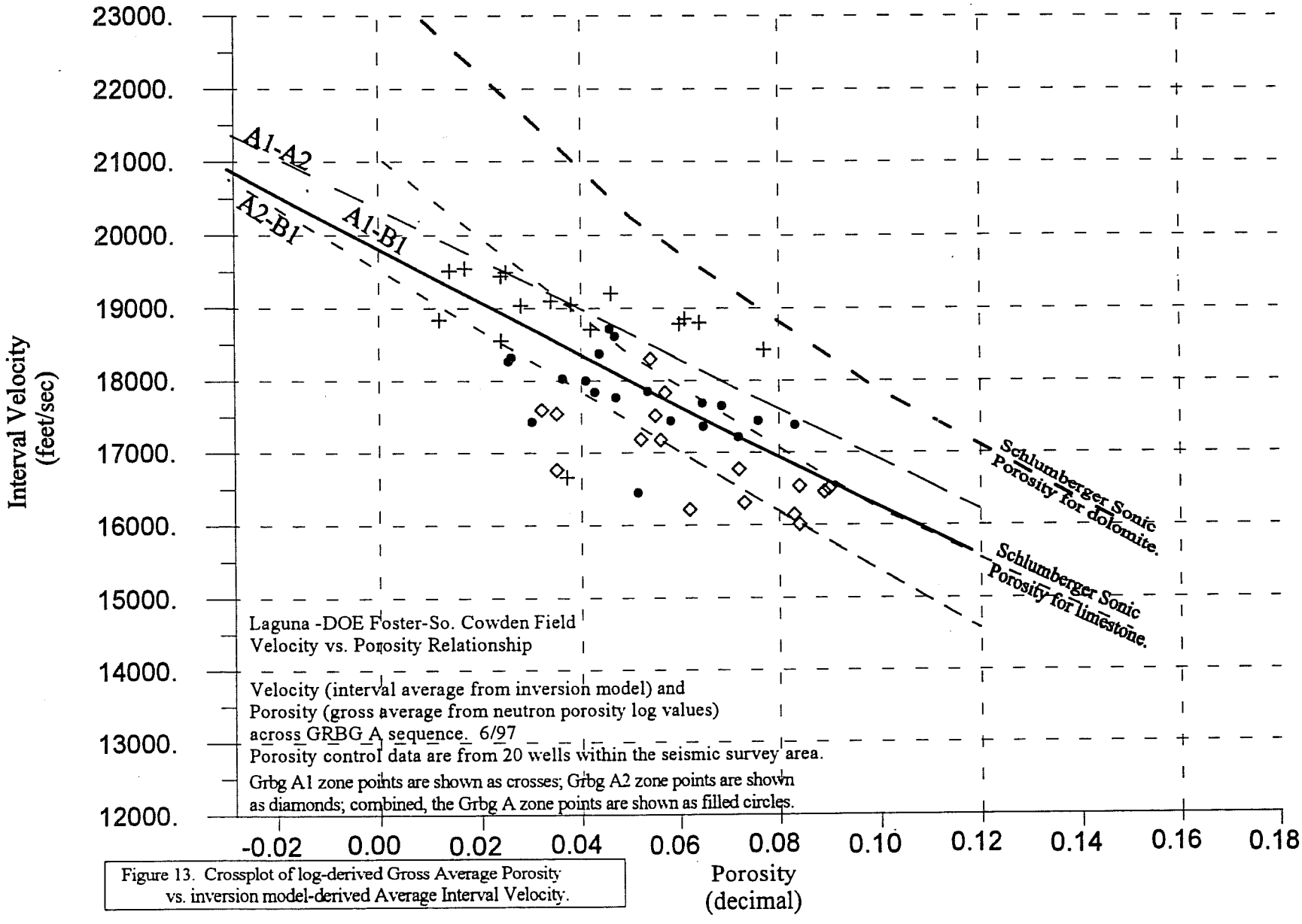

Figure 13. Crossplot of log-derived Gross Average Porosity vs. inversion model-derived Average Interval Velocity.

distribution of points being related to porosity. Because the calculation of porosity is handled empirically, that is, the conversion relationship fits the data being used and may differ for each geologic zone, the conversion function is calibrated independently for each set of velocity vs. porosity points. A perfect seismic model should require only one curve - preferably similar to the Schlumberger curve - to convert velocity data for any geologic zone.

The alignment of cross-plot points is of importance in determining the most reasonable linear fit. Determination of the slope function has been influenced by the slope of the Schlumberger relationship and knowledge of log data quality, weighing higher the better quality data. Thus, the statistical best-fit line calculated by the analysis program was not used. The expectations of converting interval velocity to porosity have been a point of lengthy discussion. Ultimately the successful comparison of two forms of data depends on the correctness and consistency of *both*.

The interval velocity was compared to the Gross Average Porosity values at included well points using the seismic-guided log analysis software in the Vest interpretation system. The comparison for *all wells available* with gross average porosity estimate has a poor relationship (Fig. 14a). It was recognized that the neutron-type logs, ranging in age from the 1950's to 1970's, lack the calibration consistency needed to measure porosity accurately and should not be used to calibrate seismic data as porosity data. When only wells with recent, calibrated neutron density logs were considered, the correlation of inversion-derived average interval velocity with Gross Average Porosity is reasonably good (Fig. 14b). Spreadsheet values of Gross Average Porosity in qualified wells range from less than 3% to more than 8%, but the porosity in other, non-calibration wells likely exceed these limits. The "error", or scatter, of the points from the line that they determine, is within 1.5% typically with only a few points falling intolerably (> 2%) away from the line. The area around these wells may not be imaged perfectly by the seismic data or the calculated porosity values may have unrealized problems. Difference maps, commonly used to reduce mistie values inherent in the conversion process, are not used (so far) for this project.

The final step in mapping is to convert the inversion model-derived average interval velocity values (Fig. 15a) to porosity values (Fig. 15b) using the cross-plot line relationship. The conversion is handled automatically by the Vest 3DSEIS program, which uses either a linear recursion method to determine the fit of the line or, in the case here, a line determined by the user. Multiple curve (non-linear) relationships have been used for conversion, although the process is not so automatic. The calculated values of calibrated Gross Average Porosity are exported from the 3DSEIS program as a spreadsheet for plotting in Surfer as a map and as a spreadsheet for the production model. The process of incorporating the porosity distribution into the production model is under way and will be discussed in a future report. From initial observations, however, the porosity maps relate well to cumulative production in section 36. High seismic-derived porosity in the northeast part of section 36 relates to the highest cumulative production in the section.

Seismic Conclusions

The values of porosity calculated for various zones in section 36 exceed the range of values in calibration wells, indicating that drilled wells do not represent the full range of porosity possibilities. Some seismic velocities convert to porosities of 14% (porous dolomite and possibly sandstone) while some convert to negative 2% (anhydrite?), using a single line relationship. A multi-slope conversion curve will be used for future conversions to limit high porosity conversions to the range observed in wells in the high-porosity area. The alignment of cross-plot points for the A1 and A2 zones is very organized; points in the B1 and B2 are less organized but still predict a reasonable porosity distribution. Cross-plots from the C zone and lower Grayburg do not graph reasonably and the reason for this poor result is not obvious. Results for the lower Grayburg and San Andres currently seem poor as cross-plots, a combination of unexpected inversion model character and limited calibration control. Further evaluation of the effectiveness of seismic-derived porosity maps will be made from qualifying production history models and, eventually, field operation choices.

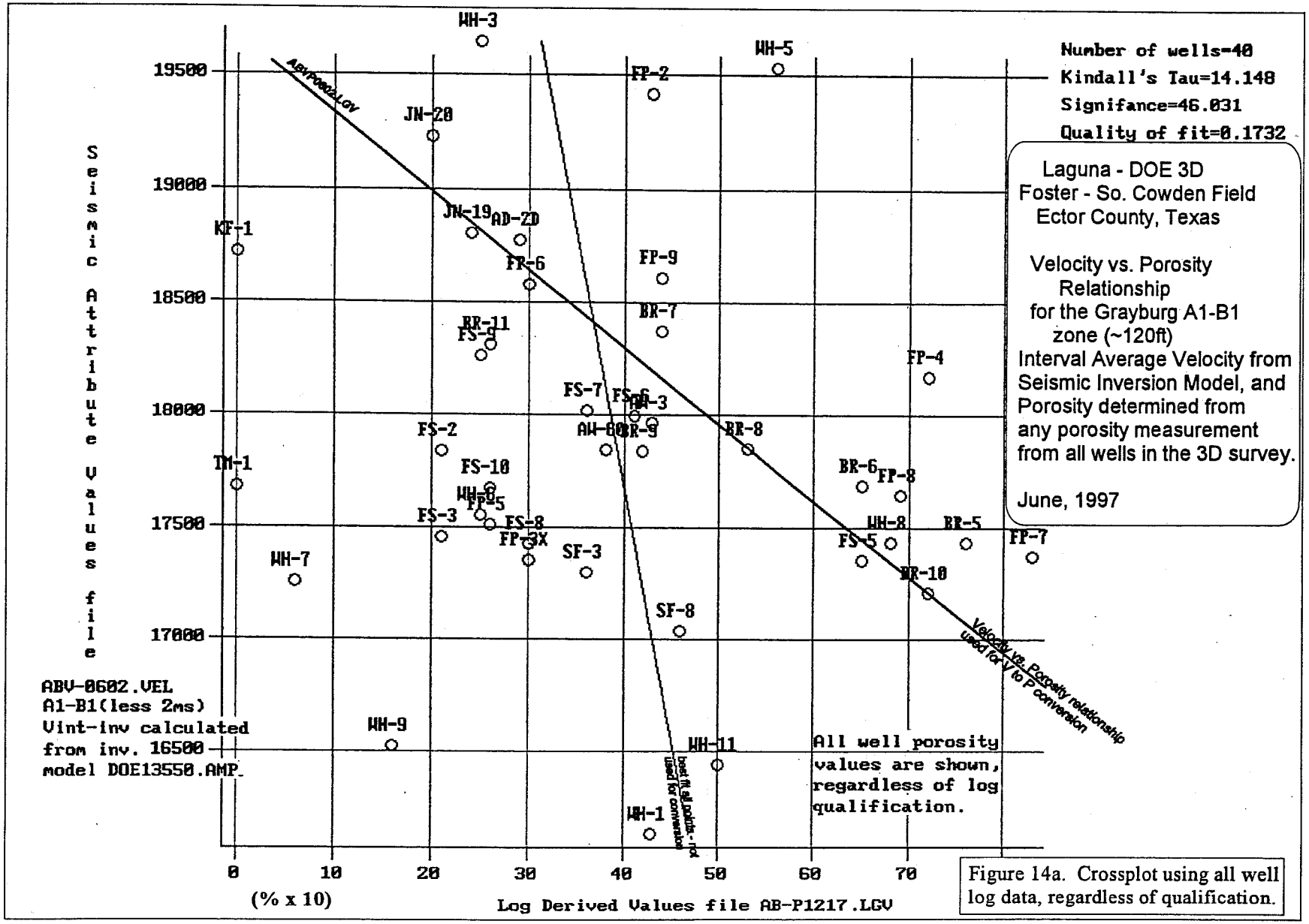

Figure 14a. Crossplot using all well log data, regardless of qualification.

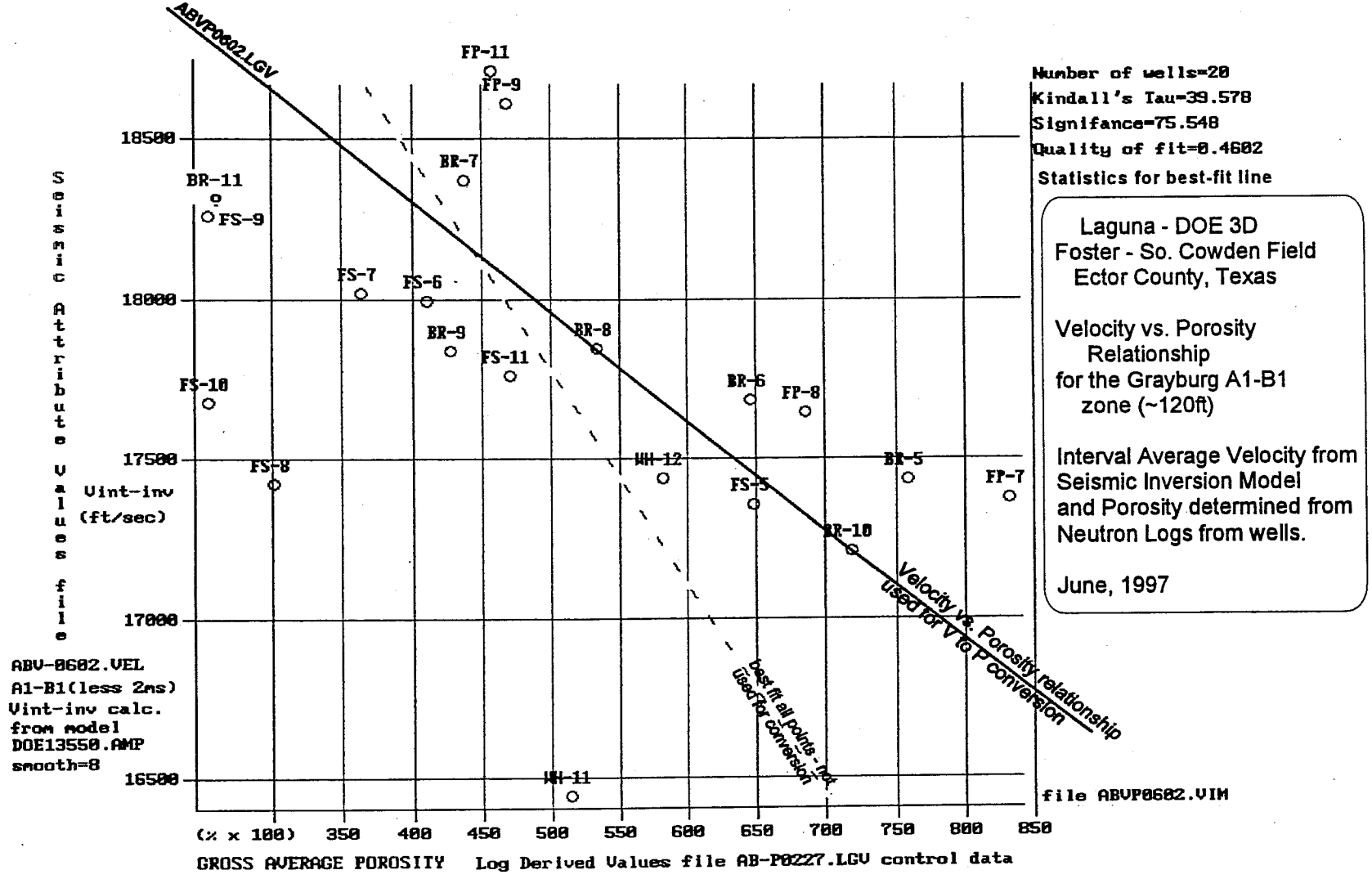

Figure 14b. Crossplot using only modern Neutron Density log data.

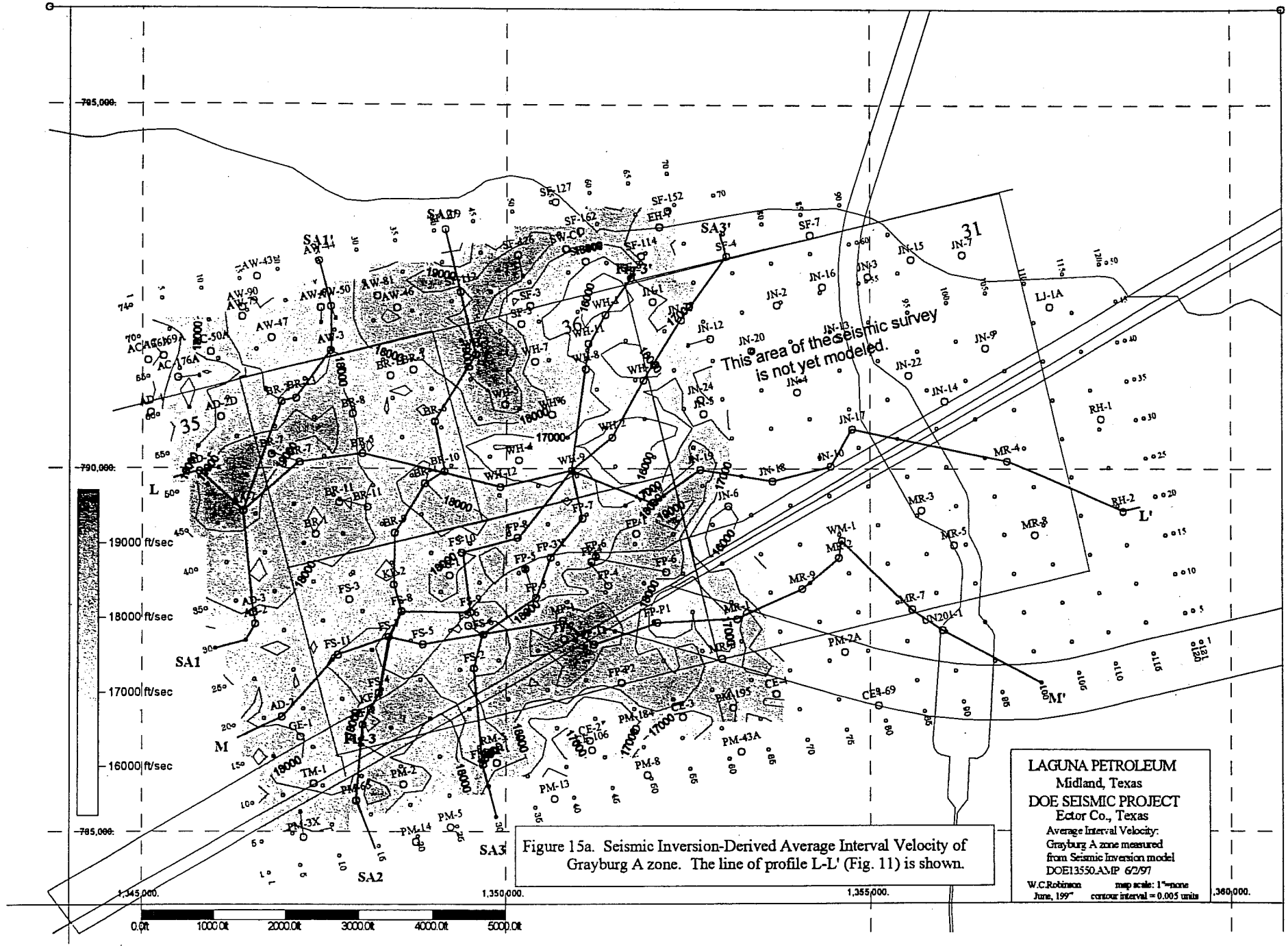

Figure 15a. Seismic Inversion-Derived Average Interval Velocity of Grayburg A zone. The line of profile L-L' (Fig. 11) is shown.

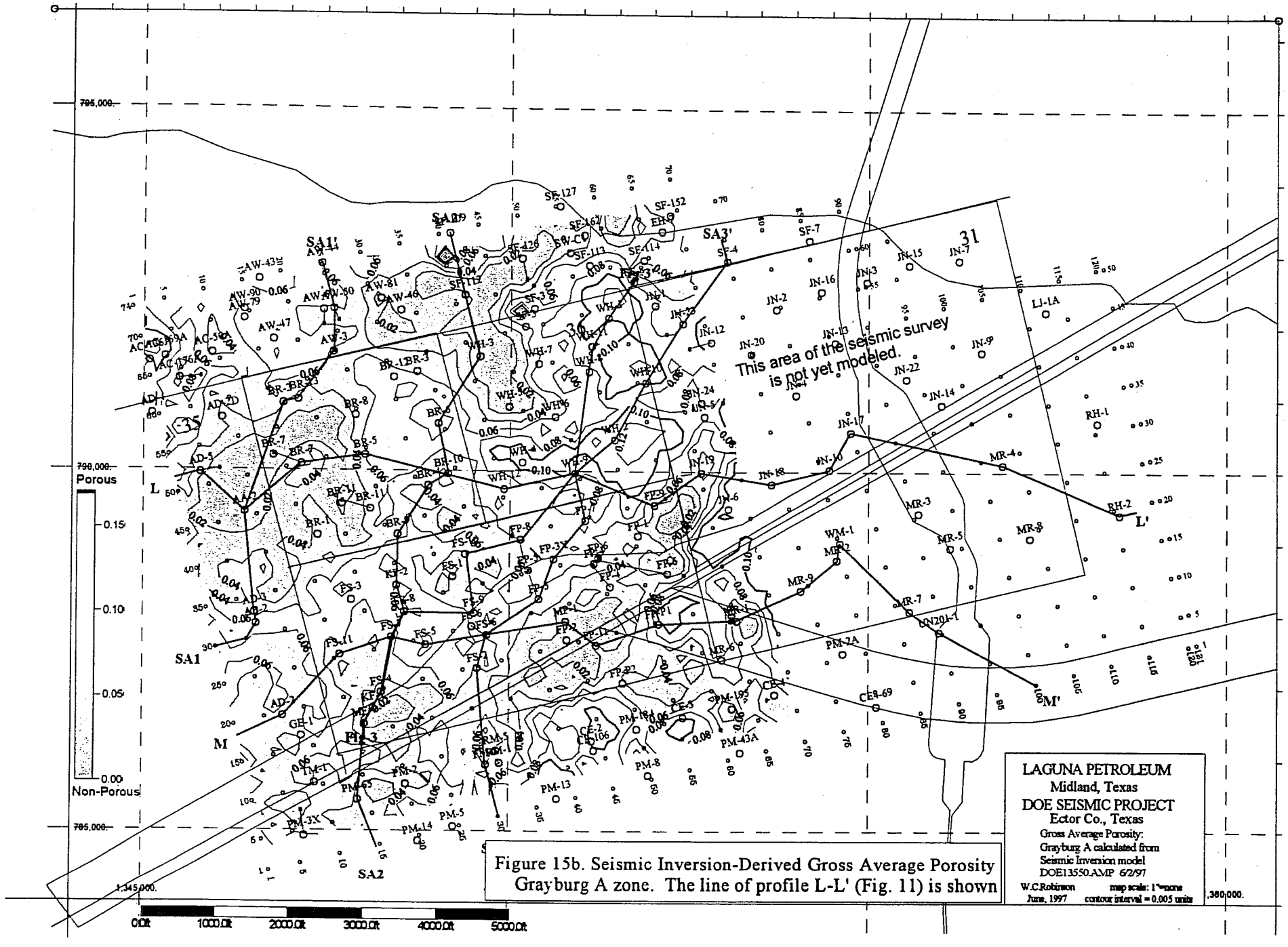

Figure 15b. Seismic Inversion-Derived Gross Average Porosity Grayburg A zone. The line of profile L-L' (Fig. 11) is shown

Seismic Inversion Modeling is an effective process to convert seismic data from an ambiguous, non-unique form to a quasi-unique form controlled with lithologic constraints. The modeling itself is sensitive to reflection data variables, including processing, particularly stacking alignment, bandwidth-related scaling, and phase correction. The analysis of the model and its relation to rock property data are sensitive to the correct positioning of geologic zones in the seismic data volume and to the form that the subsurface data take. Although well data seem to set the standard for qualifying the accuracy of seismic results, the form that well data may take can be subjective and the quality of well data certainly can vary. Well data, on the near wellbore scale, may not be directly comparable to seismic data on its scale.

Geologic Objectives

Reservoir Description

The reservoir description is an integration of the 3-D seismic interpretation with the geologic model derived from the core description, thin section study and cross section work. The presence of clinoforms, in both the reservoir portion of the Grayburg and the San Andres is significant. These clinoforms correlate to facies changes (the presence of the grainstone shoal) seen in the core and on the cross sections. The extent seems to be influenced by the presence of paleostructures identified by both seismic and geologic mapping. These facies changes have lateral continuity, as identified in the 3-D seismic volume, which would have been difficult to predict from well control alone. Identification of the facies belts will impact the design of the waterflood.

Grayburg. The Grayburg was deposited as a carbonate ramp on the eastern margin of the Central Basin Platform. The carbonate ramp slowly deepened across the study area from west to east into the Midland Basin. The Grayburg within the project area was deposited as numerous packages of sediments (parasequences) ranging from 5 to 30 ft thick that act as flow units in the reservoir. These shallowing-upward units are composed of siliciclastic bases and carbonate tops. The siliciclastics range from dolomitic to highly dolomitic and were deposited only as part of some parasequences. The carbonate portion of each unit has been heavily dolomitized.

On the deeper portion of the ramp (most eastern part) the Grayburg dolostones are composed of deeper water fusulinid wackestones. Higher on the ramp, the dolostones are composed of thicker bedded, higher energy grainstones and packstones. Landward, in a quiet lagoon behind the grainstone shoals, the dolostones are composed of thinner bedded, muddier packstones and wackestones with significant amounts of primary anhydrite. In between, the thicker and thinner units interfinger. The individual flow units are, therefore, thicker down dip and thinner and more numerous up dip.

The siliciclastic basal beds are thicker and more numerous in the upper third of the Grayburg which corresponds to the main pay interval. The fine grained siliciclastics were originally transported from the sabka onto the shelves during sea level lowstands. Once the sea level rose and flooded the shelf, the sands were reworked along with the dolomitic rubble and any soil which formed during the lowstand.

Porosity distribution within the Grayburg is controlled by both depositional facies and diagenesis. The thicker bedded grain-rich facies, most often seen in the high energy shoal portion of each sequence, have the best porosity; whereas, the thinner bedded mud-rich facies both up dip in the lagoon and down dip in the fusulinid wackestones have the poorest. Subaerial exposure of the individual units, though short lived, created additional secondary dissolution porosity. Deep burial diagenesis both enhanced and reduced interparticle porosity and permeability. Anhydrite has been mobile during both the depositional (and early burial) and during the burial diagenetic phase.

San Andres. The San Andres was deposited in a similar environment as the Grayburg. There is,

however, a lack of siliciclastics in the San Andres and the distinctive basal beds are absent. Consequently, the "shaley" gamma ray signature is also absent. Much of the San Andres in core was composed of higher energy packstones and grainstones. Unlike the Grayburg, there are capping intertidal and supratidal facies in the San Andres.

Although the San Andres and Grayburg reservoirs have a similar depositional history they have very dissimilar diagenetic histories. This resulted in the subsequent hydrocarbon accumulations being quite different. At the end of San Andres time there was a major (+/- 250 ft), long term sea level drop which subaerially exposed the porous intervals and caused extensive dissolution, reprecipitation, and infilling with debris (karstification). The upper San Andres in the study area was above the water table and undergoing major dissolution and collapse. The blocky character of the porous zones in the upper San Andres is believed to be a result of this process. Erosion of the San Andres also resulted in an angular unconformity with truncation of the porous intervals against the unconformity. This may have resulted in the development of separate oil/water contacts within the different porous zones, a possibility which is under review.

Core and Log Developed Depositional and Diagenetic History of the Grayburg and San Andres

The existing core data available at the inception of the project was almost entirely from the upper Grayburg. The only cores still available were taken in the Witcher-6 (see Fig. 1 for well and core locations) and are 177 ft from the upper Grayburg and 60 ft from the San Andres. As a result of the preliminary simulation completed at the end of Phase One of the study, however, it was realized that the lower Grayburg is a virtually undeveloped reservoir and the San Andres had significant remaining untapped oil in place. These two reservoirs were the least understood. The drilling program implemented in Phase Two included the recovery of core from both the lower Grayburg and the San Andres in order to better understand these reservoirs.

Foster-11 (FS-11) Core

The Foster-11 was cored in the lower Grayburg from 4045 - 4148 ft and the San Andres cored from 4149 - 4220 ft (see Note[1]). The core analysis indicates that the lowermost Grayburg is relatively tight. The San Andres core analyses from the Foster-11, are consistent with the two San Andres cores (Witcher-6, and Brock-10) taken prior to the study.

The lower Grayburg dolomite was found to consist of a series of shallowing upward cycles composed primarily of shallow subtidal to intertidal to supratidal facies. The visible porosity is primarily fenestral with little if any secondary porosity. There are some small, 2-4 ft long vertical fractures with oil staining. The deepest water facies (Maximum Flooding Surface), a fusulinacean wackestone, are found within 30 ft of the transgressive base of the Grayburg. There are some fine grained siliciclastic which have percolated down into the karst associated with terminal San Andres event and at the base of the Grayburg. A number of exposure surfaces with associated minor karstification are seen in this section.

The San Andres is composed of very porous and permeable cross-bedded ooid and skeletal packstones and grainstones separated by intervals of massive anhydrite with collapsed mudstone and wackestone rubble. These anhydritic intervals are interpreted to be cavern fill sediments as they are featureless and lack the classic "chicken wire texture" of sabkha anhydrite. The terminal event of the San Andres is a

---

[1] Note: Because of a driller's error, the core depths were 45 ft off from the electric log depths. Thus 4200 ft in the core equals 4155 ft in the electric log. Core depths referred to in this report are adjusted. The core analyses report, however, reflects the depths as recorded at the well site.

major subaerial exposure surface with an associated drop in the water table of at least 60 ft at the Foster-11 location (Fig.16), and 50 ft at the Witcher-2 location (the Witcher-2 is structurally lower and basinward of the Foster-11). During subaerial exposure a sequence of mudstones and wackestones, originally interbedded with the grainstones and packstones, underwent intense dissolution. The aragonitic mudstones and wackestones were prone to dissolution by fresh water in the vadose environment, whereas the calcite rich grainstones and packstones were resistant and acted as cave roofs and floors. There is crackle breccia, indicative of incipient cave roof collapse, in the core near the base of the grainstone at 4198 ft (4153 ft on logs) above one of the anhydrite infill intervals.

Foster-11 (FS-11) Logs

There are no area-wide log correlations in the upper 150 ft of the San Andres. From the core/log relationships, the lithology ranges from 100% anhydrite: to 50% wackestone/ mudstone or anhydrite and 50% grainstone/packstone: to almost 100% grainstone/packstone (Fig.17). Beginning 50 - 75 ft below the top of the San Andres, and extending down at least 150 ft, there is a to be a series of 30 - 70 ft thick shallowing upward sequences, which shallow into thick, highly porous units (interpreted to be grainstone shoals), capped by less porous units (interpreted to be lower energy packstone/wackestone). These units are identified by a porous log signature, as there is little gamma log character. When these facies were plotted on a map of seismic reflection amplitudes at the top of the San Andres, a good correlation was seen. Anhydrite-rich log character is correlated with low reflection amplitude, and grainstone/packstone (>8% porosity) log character with high reflection amplitude.

Witcher-12 (WH-12) Core

The Witcher-12 (Fig.17) was cored in the lower Grayburg from 4190 - 4225 ft and the San Andres cored from 4226 - 4369 ft, with full recovery. A review of the core indicated the San Andres interval has excellent oil shows and fluorescence. There are three main intervals with porosity and shows. The deepest zone (4341- 4355 ft) is an interval of leached fusulinacean wackestone to packstone with bleeding oil. The interval has 9 ft of greater than 9.5% porosity, with permeabilities ranging from 0.67 to 5.01mD. This zone also appears to have excellent porosity (12% to 16%) on the neutron/density cross-plot. The middle zone (4316-4332 ft) is a fine-grained skeletal packstone to grainstone with excellent oil stain; it has 18 ft of greater than 8.4% porosity, with permeabilities ranging from 0.78 to 14.74mD with most in the range of 2.5mD - 5.0mD. The upper porous zone in the San Andres (4268-4302 ft) is an oil-stained, mottled, cross-bedded, skeletal packstone with fractures bleeding oil. Within the upper porosity zone (4273-4312 ft) there is 11 ft of greater than 7.7% porosity. The permeabilities, however, range from only 0.7 - 1.3mD.

The lower Grayburg, as in the FS-11, is a series of shallowing upward cycles composed primarily of shallow subtidal to intertidal to supratidal facies. The visible porosity is primarily fenestral with little if any secondary porosity. The deepest water facies (associated with Maximum Flooding Surface), a fusulinacean wackestone, are also found within 30 ft of the transgressive base of the Grayburg. There are only minor, fine-grained siliciclastics at the base of the Grayburg. A number of exposure surfaces with associated minor karstification are seen in this section.

Foster-Pegues-11(FP-11)

The full description of the core was discussed in the 1995-1996 annual report. One hundred and twenty feet (120 ft) of core were recovered from the lower Grayburg in the Foster-Pegues-11 (FP-11). The cored interval began in the lower "B" zone (basal upper Grayburg) and included the "C", "D", "E", and part of the "F" zones of the lower Grayburg. The purpose of coring this interval was to gain information on the lower Grayburg, which the reservoir simulation had identified as having significant untapped reserves.

The interval is composed primarily of shallow subtidal to supratidal shallowing upward carbonate sequences with minor anhydrite. There is a significant interval with tidal flat "Teepee Structures" in the "D" zone, and evidence of at least 34 ft of subaerial exposure in the "C" zone. Capping the "C" zone is a red to gray

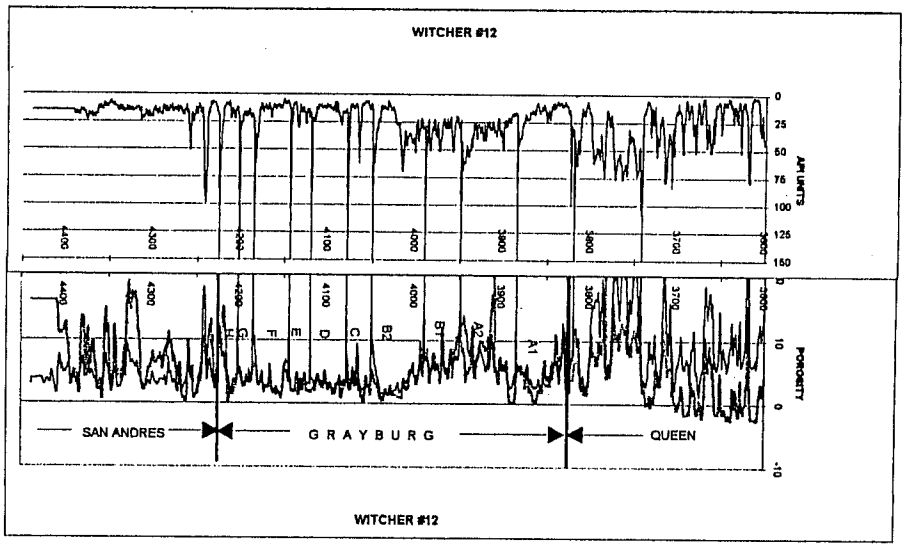

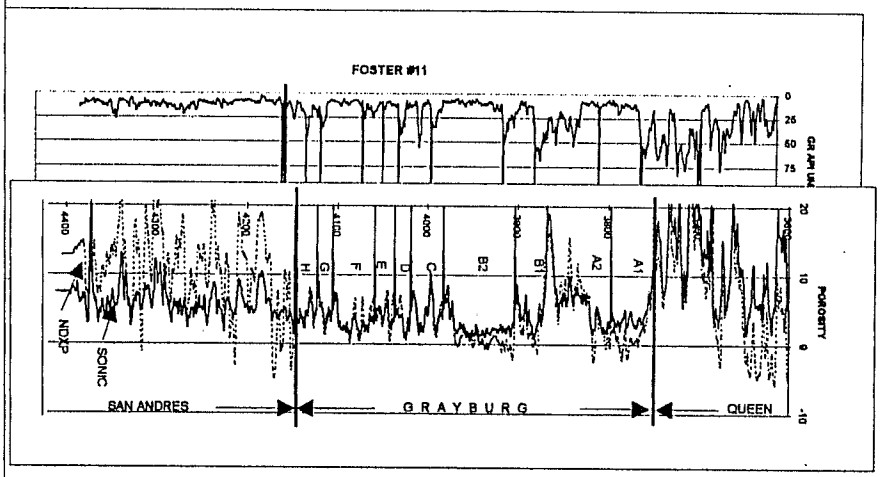

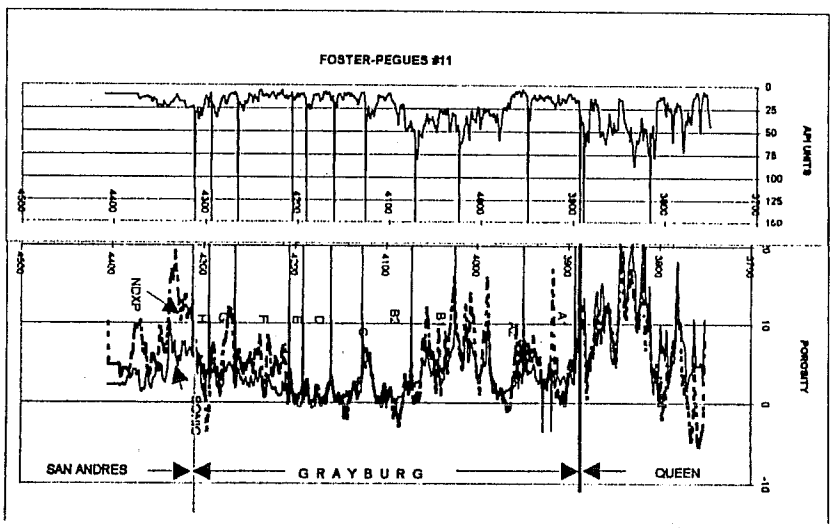

Figure 16. Gamma Ray, Neutron/Density crossplot and Sonic logs for Witcher #12, Foster #11, and Foster-Pegues #11. Wells hung on top of Grayburg.

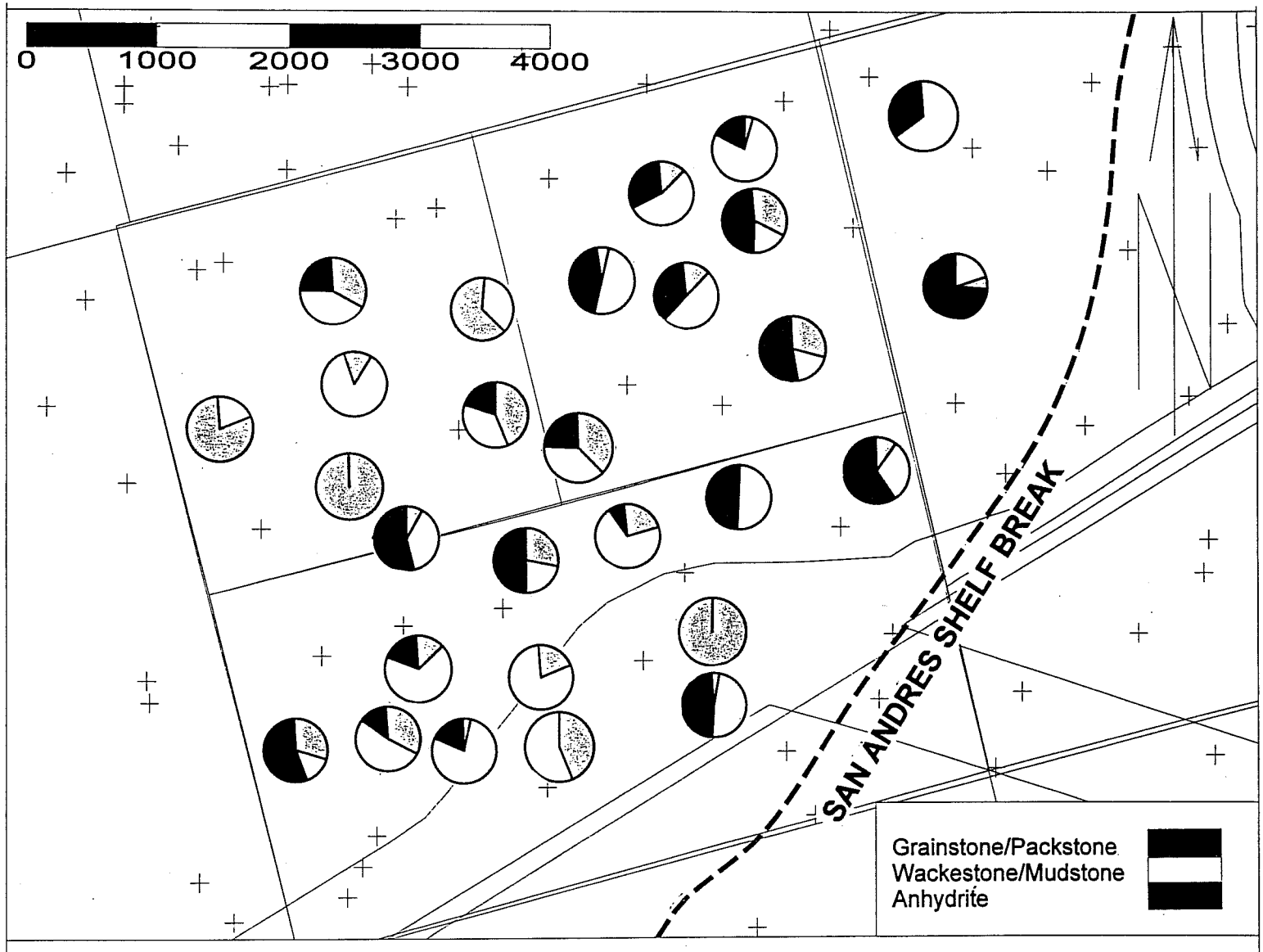

Figure 17. Distribution of Grainstone/Packstone, Wackestone/Mudstone, and Anyhdrite facies in upper 50 feet of San Andres showing possible karst (Anhydrite) and Shoal (Grainstone/Packstone) development. From log analysis.

terrigenous sand that transgressed the top of the lower Grayburg subaerial exposure surface. This surface and the associated karstification have also been identified, over 60 miles to the northwest, in the Eunice Monument South (Grayburg) Field on the west side of the Central Basin platform in Lea County, New Mexico, where it also represents the boundary between the upper and lower Grayburg (R. Lindsay, personal communication).

One of the main questions raised in reviewing the initial simulation results was "why is the San Andres not as productive as expected?" The San Andres is productive in both the Foster and South Cowden Fields where it has had a variable production history. Two wells, the Foster-11 and Witcher-12, were cored across the San Andres/ Grayburg in order to provide a better understanding of the stratigraphic boundary and how it controls production. The upper San Andres in the study area is composed of a series of cross-bedded ooid, fusulinacean, and skeletal grainstone and packstone shoals capped by thin-bedded wackestone and mudstone intervals. The cores reveal a terminal San Andres subaerial exposure event that created facies specific cavernous porosity which was later the site of massive anhydrite and/or shale filling. The mudstone and wackestone intervals appear to have been prone to dissolution, while the grainstone and packstone rich intervals were resistant to dissolution and formed cave floors and roofs. The paleo water table in the study area appears to be 50 - 70 ft below the top of San Andres based on the change from vertical vadose to horizontal phreatic features. There is no correlatable clastic unit at the top of the San Andres, nor are there internal markers to aid correlations.

Based on the core description, the San Andres on logs was divided into three facies packages: high-energy grainstone/packstone, low energy mudstone/ wackestone, and anhydrite dominated diagenetic. The San Andres was then divided into 50 ft thick intervals based on the recognition of the paleo water table 50 ft below the top of San Andres, and a thin, discontinuous marker at +/-100 ft below the San Andres top, which coincides with the base of observed fresh water diagenesis. In the uppermost 50 ft, a grainstone to packstone shoal, was developed at a break in slope on the shelf, and on the windward flanks of low relief paleo-highs (Fig.17). The low energy mudstone/wackestone facies and areas of anhydrite diagenesis were found in the more protected lagoonal area. The interval 50 - 100 ft below the top of San Andres also shows depositional facies distributed relative to paleo-structure. There is significantly less anhydrite, however, as the bulk of this interval was below the water table during exposure.

The San Andres/Grayburg boundary is both a barrier to oil migration and associated with a seismic reflector despite its lack of a paleosol or clastic rubble. Total dissolved solids in the San Andres waters are 50% higher than in Grayburg waters, and reservoir pressures are significantly different. Core analyses from the San Andres indicate a high percentage of secondary porosity, which is confirmed by sonic/neutron-density cross-plot log analysis. The down dip extent of this exposure surface is unknown. Log correlation of the vadose interval as a depositional sequence would result in misinterpreting the truncated San Andres in tectonically active areas. An understanding of the importance of diagenesis in the San Andres reservoir is critical in successful well completions.

Witcher-2 (WH-2) Deepening

Based on log character (Fig. 18), the upper 21 ft of the San Andres is composed of a 2 ft thick massive anhydrite, an 11 ft thick shale rich cave infill and a 7 ft thick massive anhydrite, above a porous (16% cross-plot porosity) interval with possible fractures (crackle breccia?). At the base of the porous unit, and just above the interpreted water table, is another anhydrite interval. As in the Foster-11, the porous interval is believed to be calcite rich grainstone/packstone. This diagenetic overprint on the uppermost San Andres has a major impact on reservoir distribution and behavior. Without a proper understanding of this diagenetic history, successful completions in the San Andres are "hit or miss". The Witcher-2 was completed flowing from acidized perfs in the upper 60 ft of the San Andres in an area with high seismic reflection amplitude.

Integration of Geologic Results Derived from Modern Logs, Core Descriptions, Core Analyses and

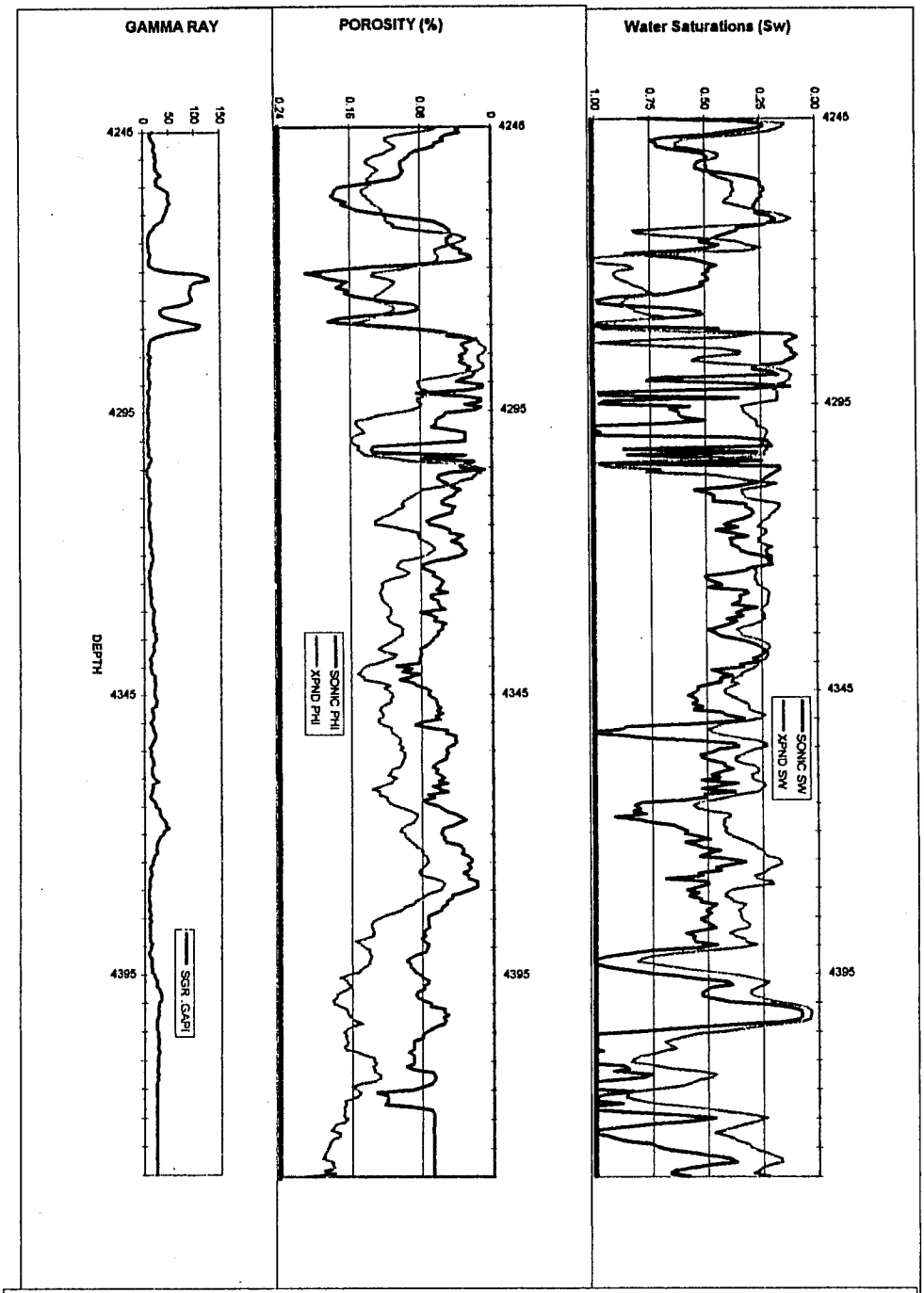

Figure18. Witcher #2 water saturation calculations for San Andres. Calculated using both Sonic and Neutron/Density porosity.

Seismic into A Reservoir Model to be input into the Simulator

Core K and F for All Cores

During the simulation, a question arose regarding the permeability and porosity of the different layers used in the model. Although six wells were cored (Fig. 1) in sections 36, 31, and 32 (just to the east of section 31), only the cores taken in the Sun Witcher-6 still exist. The Sun Witcher-6 was cored in the upper Grayburg and San Andres. The Arco Brock-10 was cored in the San Andres. The Arco Foster-Pegues-3-X was cored in the upper Grayburg. The General American Maurice-7 was cored in the upper Grayburg. The Great Western Johnson-19 was cored in the upper and lower Grayburg. The Richmond Drilling Maurice-3-A was cored in the upper Grayburg. Recovered was a total of 950 ft of upper Grayburg, 40 ft of lower Grayburg, and 115 ft of San Andres. Unfortunately, the Witcher-6 core only covers upper Grayburg and a portion of the San Andres and does not adequately describe the entire reservoir. The recovery of cores in three new drills, the Foster-Pegues-11 (lower Grayburg), Foster-11 (lower Grayburg and San Andres), and the Witcher-12 (lower Grayburg and San Andres) provides a framework to better describe the entire reservoir.

A closer examination of the **F** vs. **K** was undertaken and a series of plots was generated using the core reports from the existing, and recently recovered cores. The "All Wells All " plot (Fig. 19) of **F** vs. **K** contains analyses from all the cored wells. The wide scatter of data initially appears to show no distinct trend. However, there are three distinct populations: a high permeability/low porosity "fracture field", a low permeability/high porosity "secondary" or "vugular field", and a permeability/porosity field which exhibits a "normal" distribution for shallow shelf carbonates.

The fracture field is present in the Grayburg Formation in the Witcher-6, Johnson-19, Maurice-7, and Foster-Pegues-3X. In each well, there are a limited number of values (2-3) indicating that fractures make only a minor contribution. In addition, there are two 4 - 5 ft thick intervals in the core taken from the Foster-Pegues-11 with oil staining in fractures. The log analysis indicates that these zones have less than 3% porosity and would not have been perforated without the core data. "Chatter" on the sonic log is evident in those intervals with fracture porosity in core, and can be used to predict fractured intervals on logs.

The "secondary" porosity field is composed of San Andres in the Brock-10 and Witcher-6, and some upper Grayburg in the Maurice-7. The San Andres in the Witcher-6 core is composed of clean, high-energy grainstones and packstones with secondary interparticle porosity.

Analyses from the Brock-10, Foster-11, Witcher-12, and Witcher-6 indicate that the San Andres reservoir is a poor water flood candidate. Although the logs and cores indicate zones with 18 - 20% porosity, the low permeability (averaging 1 mD at 10% **F**) would preclude successful waterflooding on 20 acre spacing, and raise the risk of successfully waterflooding on 10 acres. This conclusion is supported by the marginal results in a San Andres water flood project west of the study area.

Few Grayburg analyses fall in the secondary porosity range, leading to the conclusion that most of the upper Grayburg reservoir is composed of connected interparticle (primary) porosity with good permeability. Those analyses that do plot in the secondary field are believed to represent leached grainstone shoals. The analysis of the Foster-Pegues-11, the first lower Grayburg new drill, shows the cored, lower Grayburg in this well to have a large component of primarily tight dolomite with less than 4% porosity and less than 0.2 mD of permeability, and a small component of "Secondary Porosity" with porosity 3 - 6% and permeabilities of 0.3 mD. The best log porosity, however, in the "G" and "H" zones was entirely below the cored interval (The "G" and "H" zones were cored in the WH-12 and FS-11). There is a significant component of fracture porosity (less than 3% porosity but up to 20 mD of permeability) in the "C" and "E" intervals. The fractures in the "C" are proposed as the explanation for the behavior of the Foster-1WI after clean out. The well had been injecting into the "A" zones only and was cleaned out through the lower Grayburg. When injection resumed, the well took up to 200 BWPD, initially on vacuum, with 85% of the injection water entering the "C" zone.

Work With Other Team Members to Implement A Completion Technique Designed to Double the

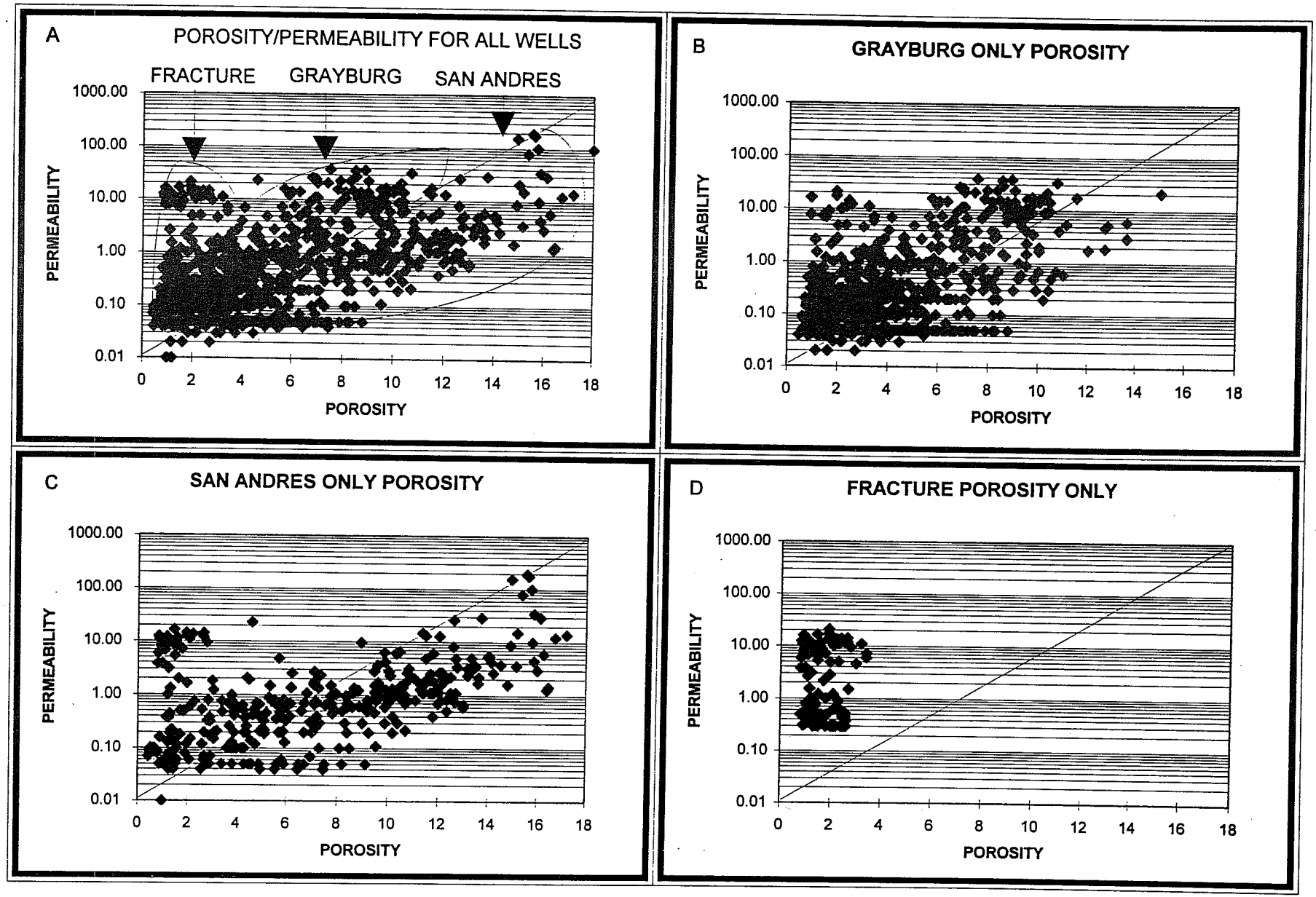

Figure 19. All core data in study area. (A) Primary, Secondary, and Fracture porosity fields. (B) Grayburg only porosity/permeabilities. (C) San Andres only porosity/permeabilities. (D) Fracture porosity.

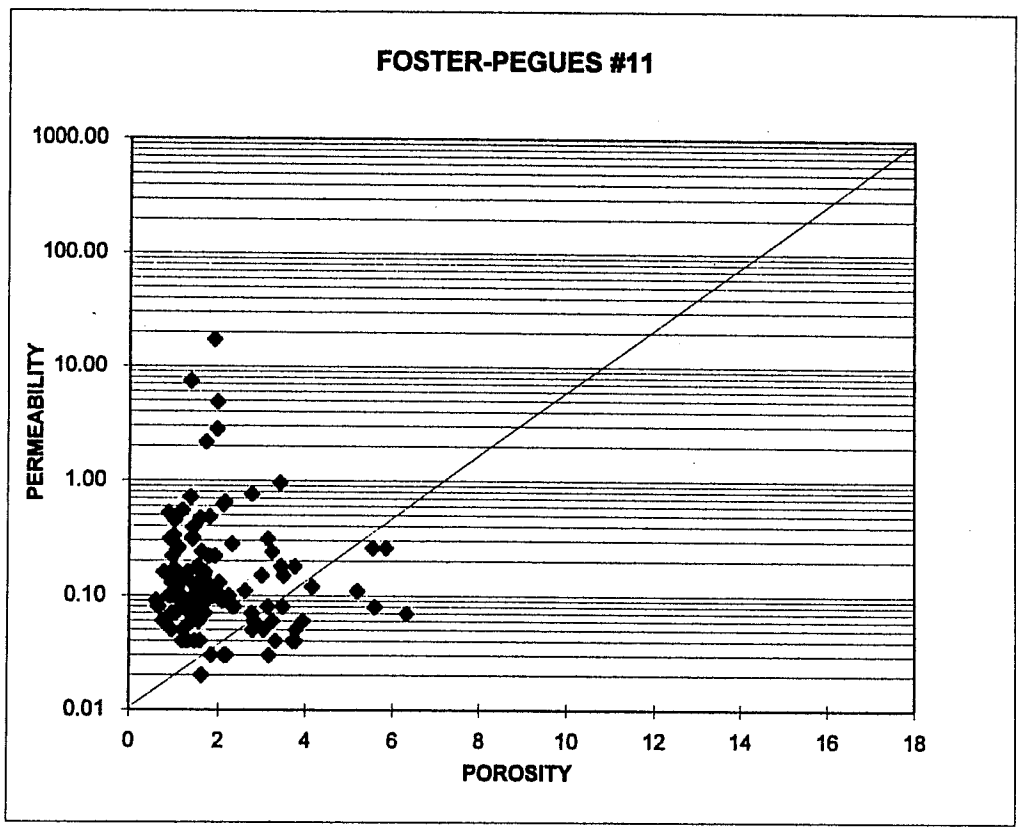

Figure 20. Core analyses for Foster-Pegues #11, demonstrating low porosity and permeability in C, D, E, and F Zones.

Fracture Length in the lower Grayburg and San Andres

The San Andres in the Witcher-12 (Fig. 16) was evaluated and tested during the first quarter 1997. Because of the time required to complete whole core analysis, it was decided to perforate and acidize the upper two zones in the San Andres to determine their potential producibility based on visual inspection of the core and log analysis. Initially, the upper two porous zones in the San Andres were perforated and acid spotted. On swab test the zones had very slow fluid entry and only about 10% oil cut (see ENGINEERING).

The results of the acid stimulation of these two zones were later confirmed by the core analyses. The upper zone has very low permeabilities due to anhydrite infilling and would require additional stimulation. Although the middle zone has better permeabilities, the geologic model proposed for the upper San Andres assumes significant areal variability and, therefore, the core permeabilities may not be representative of the zone away from the well bore. The hypothesis is that subaerial exposure and fresh water diagenesis has significantly altered the San Andres reservoir. Evaluation of the slabbed core indicated the presence of fresh water diagenesis as deep as 95 ft below the top of San Andres. There are intervals with mudstone and wackestone collapse breccias encased in cavern-fill, massive anhydrite. These are interbedded with porous grainstone and packstone intervals (the tested intervals), with only minor dissolution but variable anhydrite infill. Other cavernous intervals are filled with very fine sand and silt that percolated down, and partially filled, solution enlarged vertical fractures in the vadose zone.

Log analysis would typically lead to the conclusion that both of the tested intervals should be productive. Since neither zone is commercially productive without fracture stimulation, the large amount of secondary porosity cannot be contacted without significant effort following the development of a better understanding of the reservoir. Although the porous grainstone and packstone intervals locally have excellent porosity and permeability, they have become compartmentalized during fresh water diagenesis, shale infiltration during exposure, and later anhydrite pore-infilling during burial, which reduced overall permeability.

Water Saturations

Water saturations (Sw's) for the San Andres, in the Foster-11 (Fig. 21), calculated using neutron/density cross-plot porosity appear to be too optimistic (9-20% Sw) when compared with visual inspection of the core and the production history of other wells in the area. When water saturations for the same interval are calculated using sonic porosity, some zones calculate to have higher, and more realistic, saturations (34 - 46% Sw), while other zones calculate "wet" (50 - 100% Sw). When two zones with cross-plot porosities of 14-18% and low Sw's (calculated by both methods) were perforated and acidized, pumping production rates of only 4-5 BO and 6-8 BWPD were obtained.

A possible explanation for these results is found in the porosity/permeability cross-plots of the core data. Although many analyzed intervals have permeabilities of >1 mD for porosities of 14-18%, other highly porous zones have permeabilities of <1 mD. A comparison of the cross-plot neutron/density porosity (which match well with the core analyses), to the sonic porosity is revealing. There appears to be 8 - 10% secondary porosity above the sonic porosity (Fig. 22). Zones with up to 18% total porosity may have only 5 - 7% sonic (primary interconnected) porosity and low permeabilities (<1mD). This observation coupled with the production test results indicates that there is a dual porosity system in the San Andres. One system is porous but not very permeable (vuggy), and the other is permeable and porous (interparticle connected). The San Andres had been fractured and tested in the FS-11 but because the frac treatment was below the oil/water contact, the large volume of water produced precluded an accurate assessment of the San Andres production capacity.

The Witcher-2 was deepened from the upper Grayburg through the lower Grayburg and the San Andres to contact reservoir not previously productive at this area. Again, as in the Foster-11, Sw calculations using neutron-density cross-plot porosities are overly optimistic (Fig. 18). Water saturations calculated using sonic porosities were more variable and more realistic. A lower zone, 4388-4398 ft, was perfed and

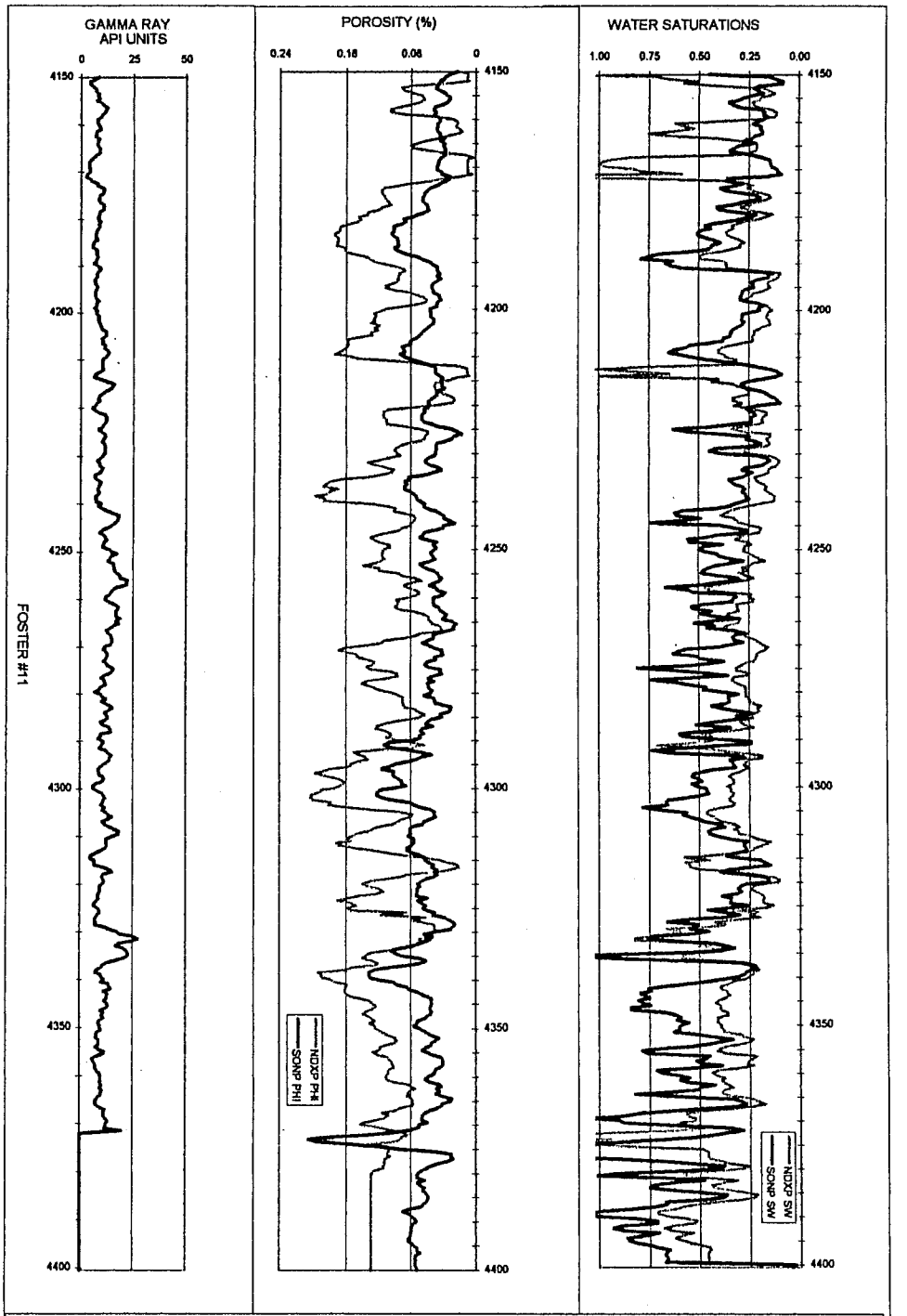

Figure 21. Foster #11 water saturation calculations for San Andres interval. Sw's calculated using Sonic porosity and Neutron/Density cross plot porosity to approximate interparticle and vuggy saturations.

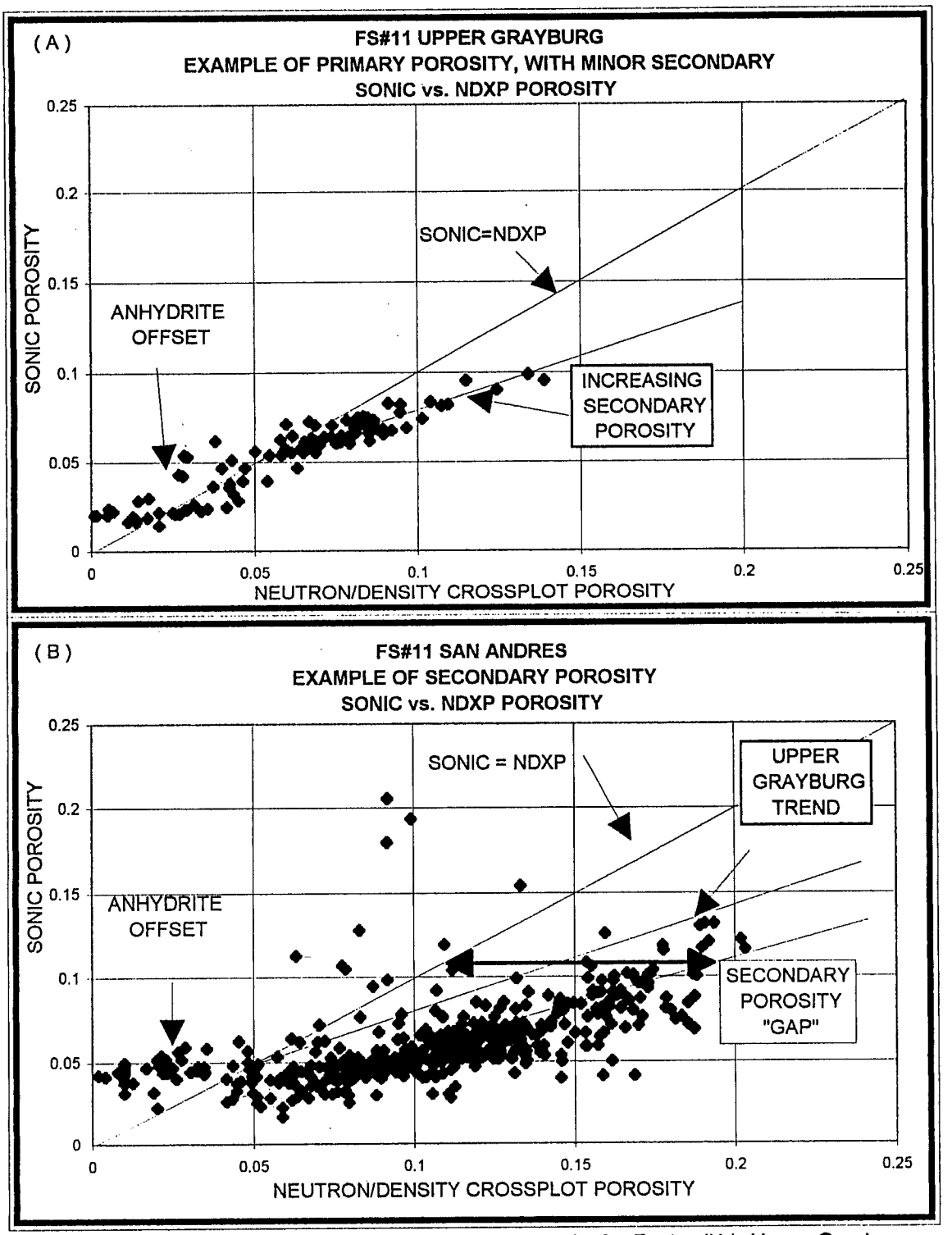

Figure 22. Cross plot of Sonic vs. Neutron/Density porosity for Foster #11. Upper Grayburg (A) showing primary porosity with little secondary porosity, andxSan Andres (A) with mostly secondary porosity.

acidized based on fair mud log shows and marginal cross-plot water saturations (16-45%). This zone flowed 100% water, confirming the sonic derived water saturations (55-100%) were correct. The zone from 4290 - 4315 ft had cross-plot porosities of 9-13% and sonic derived water saturations of from 12 - 45%. Upon completion, the San Andres produced 3500 BO and 13500 BW in less than 6 months. There appears to be the dual porosity system present in this interval as the water production initially dropped at a faster rate than the oil production. The oil production declined at a rapid rate to 4 - 5 BO and 30 BW and the San Andres was abandoned after producing for only 6 months. The WH-2 well was recompleted in the lower Grayburg and has produced, through the end of August 1997, 11,850 BO, and 1,777 MCF in 6 months.

Development of A Usable Seismic Velocity/Log Porosity Transform

Geological/Geophysical Integration

A considerable amount of time has been spent working closely with the Project Geophysicist, in an effort to combine the geologic model with the seismic interpretation. The geologic model consists of a high-energy packstone/grainstone-dominated San Andres with an exposed, eroded and karsted top, a tidal flat dominated lower Grayburg with multiple small exposure surfaces, and a high stand dominated upper Grayburg with laterally extensive grainstone/packstone shoals. This triad also reflects the variable production history with the upper Grayburg being a mature field with a poorly designed waterflood, an undeveloped lower Grayburg with essentially virgin pressures, and the San Andres with a varied production history and multiple oil/water relationships.

For the seismic inversion model to be successful, it is essential that the geological zones be properly identified within the seismic data. The first "problem" was identifying the A1 Zone top, as well as the Grayburg top, and delineating the "Lowstand Wedge" of sediments that is present between the A1 and Grayburg in the east part of the survey. If the wedge zone, which is predominantly low velocity, were included in the A1 zone, the inversion would be incorrectly interpreted. This error would then have been carried down through the section. This "wedge zone", which appears to thicken to the east and south, may equate to part of the Grayburg 4 sequence identified in the South Cowden Field Study (Ruppel and Lucia, 1996).

A second problem is on the cross-plot of the "total gross porosity" from logs and the seismic velocity (Fig. 14a). It was noted that the smallest error bars were associated with the most modern logs. Those wells where both neutron and density are the best fit to the velocity in the A1 and A2 zones. Although there is less secondary porosity in the Grayburg than in the San Andres, where the cross-plot neutron/density porosity is typically twice the sonic porosity, sonic or density logs alone under-report the gross interval porosity.

The integrated geological/geophysical effort developed a usable seismic velocity/log porosity transform for each Grayburg producing interval. To develop confidence in the porosity log/seismic velocity transform, however, it is necessary to understand how the mineralogical and textural variations in the reservoir impact the transform. As noted previously, in the core analyses there are different porosity/permeability (Ø/k) transforms for intervals with "primary" porosity only and predominantly "secondary" porosity, (Fig. 19). In intervals where sonic and neutron/density cross-plot (NDXP) porosity exhibit little separation, core F/k plot within the "primary" porosity field. This relationship exists in the lower Grayburg and in the upper Grayburg where grainstone shoals are not present. For intervals where sonic and NDXP porosity show significant (>2%) separation, core F/k plot within the "secondary" porosity field. This relationship exists in the San Andres and in the grainstone shoals in the upper Grayburg.

Visual inspection of the porosity suite, plotted on a single log, and the equivalent core F/k, led to the belief that the primary and secondary "porosity regions" have different slope relationships. In intervals with significant secondary porosity, an estimated 2/3% increase in secondary porosity for every 1% increase in

total log porosity seemed to fit, above 6% porosity, (Fig. 22). For example, at 18% total porosity (from the NDXP), an estimate of 8% secondary (2/3 X (18-6)) and 10% primary ((1/3 X (18-6))+ 6) porosity fit log derived values. For intervals with 0 - 6% porosity, little secondary (vuggy) porosity is present, and anhydrite is a major mineralogical component, causing the density tool to register abnormally low values. In intervals with only minor amounts of secondary porosity, the Sonic vs. NDXP cross-plot exhibits little deviation from a 1:1 relationship regardless of the total porosity. This data set matches the "Primary Porosity" data set from core data.

Evaluation Of The Effectiveness Of Recent Completions Utilizing Water Analyses

Analyses of produced water have become a standard method to determine if water production is from the San Andres or the lower Grayburg in the study area. Enough isolated water samples have been recovered to distinguish waters by their Sodium (Na+), Chloride (Cl-), and Total Dissolved Solids (TDS). Waters with TDS's of 60,000 - 64,000 PPM are San Andres in origin and waters with TDS's from 36,000 - 42,000 PPM are lower Grayburg in origin (Fig. 23).

The Witcher-12 (WH-12) produced water sampled two weeks after the lower Grayburg completion, indicated the water is almost entirely from the San Andres (60,000 PPM TDS). As the fracture completion was designed to frac the lower Grayburg and frac down into the San Andres, this was expected.

The Foster-11 (FS-11) produced water was sampled a number of times after completion in the lower Grayburg and the analyses indicate a steady increase in the San Andres component in the water. This was not anticipated, as the perforations and fracture treatment were designed to stay in the lower Grayburg only.

During the first quarter of 1997, the Witcher-2 (WH-2), was plugged back from the San Andres and recompleted in the lower Grayburg. A different type of fracture treatment, a "Pipeline Frac" (see ENGINEERING), was utilized in an attempt to stay "in zone" in the lower Grayburg and not fracture down into the San Andres (see first quarter 1997 report for details). At the end the first quarter 1997, the WH-2 well had just begun pumping and had not stabilized. During the second quarter 1997, the well IP'd pumping at a rate of 110 BO, 210 BW, 12 MCFGPD, dropping to 66 BO, 140 BW, 16 MCFGPD at the end of the quarter. In contrast the WH-12 had IP'd pumping 60 BO, 400 BW, 10 MCFGPD, falling to 25 BO, 180 BW, 8 MCFGPD over a similar time period. Produced water analyses indicated that the "Pipeline Frac" had indeed stayed in zone as the produced water from the WH-2 contained 37,000 PPM total dissolved solids (TDS), indicative of uncontaminated lower Grayburg water. The produced water samples collected from the WH-2 San Andres interval consistently tested at 62,000 PPM TDS.

In contrast, the produced water from the WH-12, completed with a conventional frac, initially contained 48,000 PPM TDS, rising to 64,000 PPM TDS after 3 months. This indicated that the initial production was a mix of lower Grayburg and San Andres, increasing to 100% San Andres water within three months.

Evaluation of the effectiveness of recent completions, plug backs and injector conversions by monitoring produced water composition continues. The Foster-Pegues-4 (FP-4), was converted to injection during the first quarter 1997. The Foster-Pegues-5 (FP-5), the offset well to the west, experienced an increase in production beginning in April. At the end of the 2nd quarter 1997, however, the FP-5 had experienced flood water break through and injection into the FP-4 well had been reduced. Both the FP-4 and FP-5 are being closely monitored.

From discussions with Robert Lindsay, Senior Petrographer of Chevron, this type of break through response is not unusual in Grayburg shallow shelf carbonates. Thin (from 1 - 6 ft thick), transgressive grainstones at the base of thick (30 - 50 ft) sequences can exhibit normal porosity (6 - 12%), but very high permeabilities (R. Lindsay reports values as high as 1 Darcy in these intervals at Eunice Monument South Unit). The interval suspected of causing the break through in the FP-5 is correlated with an ooid grainstone in the core in the Witcher-6 1/2 mile to the north.

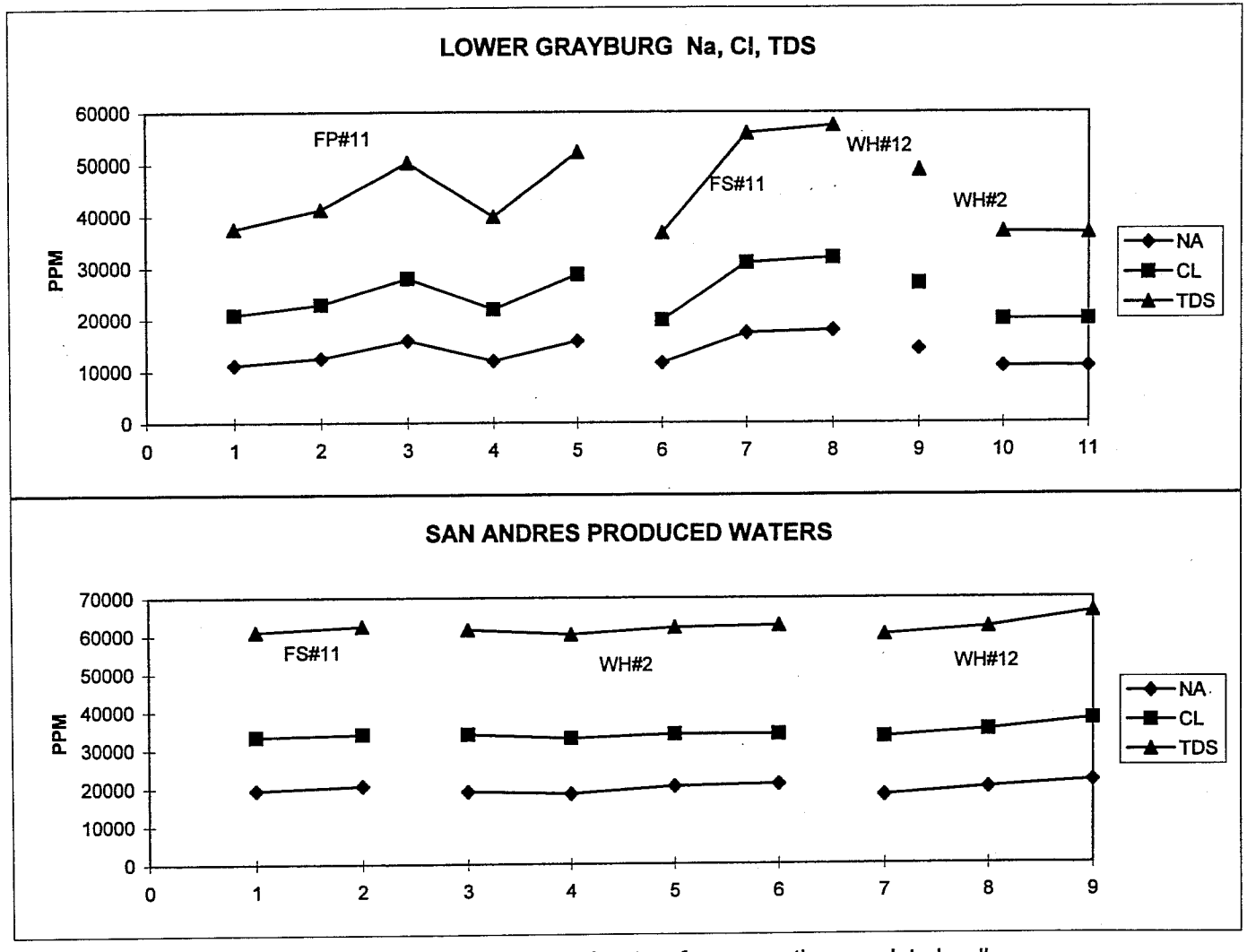

Figure 23. Analyses of produced waters from recently completed wells.
(A) lower Grayburg or mixed producers, (B) San Andres producers.

Water sampling and analyses on both producing and injection wells will continue. All producing wells and injection water stations were sampled in May 1996. All the wells and injection stations will be resampled yearly to provide a base line.

ENGINEERING

The FS-11 was initially completed in the San Andres formation based on log calculations and core recoveries. The interval from 4238 (-1311) - 4323 ft (-1396) was perforated and acidized with 1500 gallons 15% NeFe acid. Following the acid treatment production rates of 3 - 4 BOPD and 6 - 8 BWPD were established. The well had to be fracture treated to increase production, but because water bearing zones were indicated both above and below the perforated interval, a fracture treatment had to be designed to minimize frac height growth in an attempt to stay out of these zones. A "Mini Frac" consisted of a first stage of pumping 3500 gallons of cross-linked gel and 6000 pounds of 100 mesh sand into the perforations. This stage was immediately followed with 2000 gallons of nitrified cross-linked gel and 6000 pounds of sand. The small stimulation failed to achieve economic levels of production as the well was producing at rates of 3 BOPD, 15 BWPD and 2 MCFPD after being on production for less than three months. A bottom hole pressure test indicated the frac wing length to be less than 30 ft, which confirmed the belief that the fracture treatment was too small to be successful. Therefore, a larger fracture treatment would be necessary on the San Andres to achieve economic production.

However a larger stimulation was not attempted because it was felt the frac height growth could not be controlled enough to stay out of water bearing zones above and below the perforated interval. Thus the well was plugged back and perforated in the lower Grayburg from 4030 (-1103) - 4035 ft (-1108). The lower Grayburg was perforated in this manner in order to coincide with a frac design of treating the interval from midpoint and allowing the fracture treatment to grow vertically throughout the gross producing interval. Again, in an attempt to limit frac height growth, a small fracture treatment was designed for the interval. It was attempted to frac the zone utilizing a small pre-frac pad of crossed-linked gel followed by a sand laden cross-linked gel. However, the small pre-frac pad caused the treatment to prematurely screen out resulting in very little propant being pumped into the formation. Again low producing rates were achieved.

To obtain a commercially productive well it was decided a much larger fracture treatment had to be utilized although a larger treatment would produce frac heights of much greater lengths than desired. In January of 1997, an additional 10 ft of interval was perforated increasing the interval to 4020 (-1093) - 4035 ft (-1108). The interval was fracture treated with 30,000 gallons of 50 lbs linear gel and 85,420 lbs of 20/40 Ottawa sand. After achieving producing rates of up to 35 BOPD, the well potentialed for 27 BO, 240 BW and 20 MCF. A build up test on the lower Grayburg indicated near virgin reservoir pressure (2037 psi) as predicted by the simulation.

Witcher-2 (WH-2)

During the third quarter of 1996, the first deepening of an existing well was completed. The Witcher-2 (Fig.1) is one of the original 40-acre wells drilled in the 1940's. It was originally completed open hole and shot with nitro in the upper Grayburg with TD being 20 ft above the top of lower Grayburg. The well was deepened through the San Andres down to 4450 ft. No cores were taken during the deepening of this well but a full suite of logs: Compensated Neutron, Three Detector Density, Long Spacing Sonic, Dual Laterolog, Micro-CFL, and Spectral Gamma Log and Mud Log were run. Located in the northwest quarter of section 36, the purpose of the well was to test the lower Grayburg and determine if the San Andres was below the "historic" oil/water contact. Simulation results indicated untapped reserves in the lower Grayburg at this location and the "historic" oil/water contact of -1340 in the San Andres is coincident with the top of San Andres (-1334) at this location. There has been production in other wells deeper than 1340 and this location was chosen to test the paradigm.

The well was initially perforated in the San Andres from 4389 (-1462) - 4398 ft (-1471) and acidized with 1000 gallons 15% NeFe acid. The well flowed 100% water at rates of 240 BWPD. A CIBP was set at 4360 ft and the well was re-perforated at 4291 ft (-1364), 4301 ft (-1374) and 4325 ft (-1398). The intervals were acidized with 1500 gallons 15% NeFe and tested at rates of 200 BFPD with a high water cut. Production logs indicated the interval of 4325 ft (-1398) was producing 100% water, thus a CIBP was set at 4318 ft. The well was put on pump and produced at rates of 60 BOPD, 120 BWPD and 10 MCFPD from perforations at 4291 ft and 4301 ft. The production declined to 5 BOPD, 60 BWPD and 2 MCFPD in three months. This is believed to be a result of the low permeability associated with the San Andres (see GEOLOGY). This proves however, that the "historic" oil/water contact needs revision. Based on core and log evaluations, It is now believed that the San Andres has multiple oil/water contacts. This will be tested in future new drills and deepenings.

In March of 1997 the well was plugged back due to low producing rates. A CIBP was set at 4280 ft and the lower Grayburg was perforated from 4190 (-1263) - 4240 ft (-1313). The zone was acidized with 2500 gallons 15% NeFe acid. As in the past there was a need to fracture treat an interval yet limit the frac height growth to the productive zone. A relatively new frac technique called "Pipeline Frac" was employed. A "Pipeline Frac" consist of pumping a very large cross-linked gel pad followed by a small volume of sand laden Linear gel. The theory behind the "Pipeline Frac", is that the technique utilizes the differential viscosity's of two fluids to cause viscous fingering while pumping the fluids. This allows the selective placement of propant across the perforated interval when no stress barriers are present above and below the producing horizon.

The lower Grayburg was "Pipeline" fraced with 36,000 gallons of 35 lb cross-linked gel, 17,500 gallons of linear gel and 53,640 lbs of 16/30 Ottawa sand. The well was put on pump and three days after recovering the frac load was producing 106 BOPD, 216 BWPD and 11 MCFPD. The well potentialed for 87 BOPD, 168 BWPD and 12 MCFPD.

The initial bottom hole pressure buildup test for the lower Grayburg in this new completion was conducted 45 days after the workover. When this test was conducted, the well was producing 85 BOPD, 170 BWPD and 11 MCFPD. Foam in the annulus dominated early time data, making the analysis uncertain. However, qualitative analysis indicates a skin of about -5 and a 200 ft frac wing length. This frac wing length is far greater than the 30 - 50 ft frac wing length achieved in wells utilizing more conventional fracture techniques. It is apparent the "Pipeline" fracture treatment demonstrated to be successful at creating greater depths of penetration of the sand laden fluid into the formation without producing large fracture height growth. The produced water chemistry (see GEOLOGY) also supports the fact that the fracture treatment stayed within the lower Grayburg.

Through the first six months of production, the well has produced 11,850 BO and 1,777 MCF from the lower Grayburg. The well is currently producing 47 BO, 102 BW and 10 MCF per day.

Witcher-12 (WH-12)

During the fourth quarter 1996, the Witcher-12 (WH-12) was drilled to test the simulation and contact additional reserves in the San Andres and the lower Grayburg. It located in the southwest corner of the northeast quarter of section 36 to take advantage of the lack of producing there. The well is 330 ft southwest of the Witcher-4 WIW (WH-4), a well drilled on 40 acre spacing in 1941, converted to injection in 1961, and plugged in 1991. It is 690 ft north of the Foster-Pegues-8.

The well was drilled to 4435 ft. A full suite of logs: Compensated Neutron, Three Detector Density, Long Spacing Sonic, Dual Laterolog, Micro-CFL, Spectral Gamma Log and Mud Log were run (Fig. 16). Additionally, a Repeat Formation Tester was employed in an effort to obtain reservoir pressure data. Twelve unsuccessful tests were attempted, with two different pad configurations before the effort was abandoned. A Core was cut in the lower Grayburg and San Andres to provide rock property information for these two intervals. Production casing was set through the San Andres to 4432 ft. Initially the two

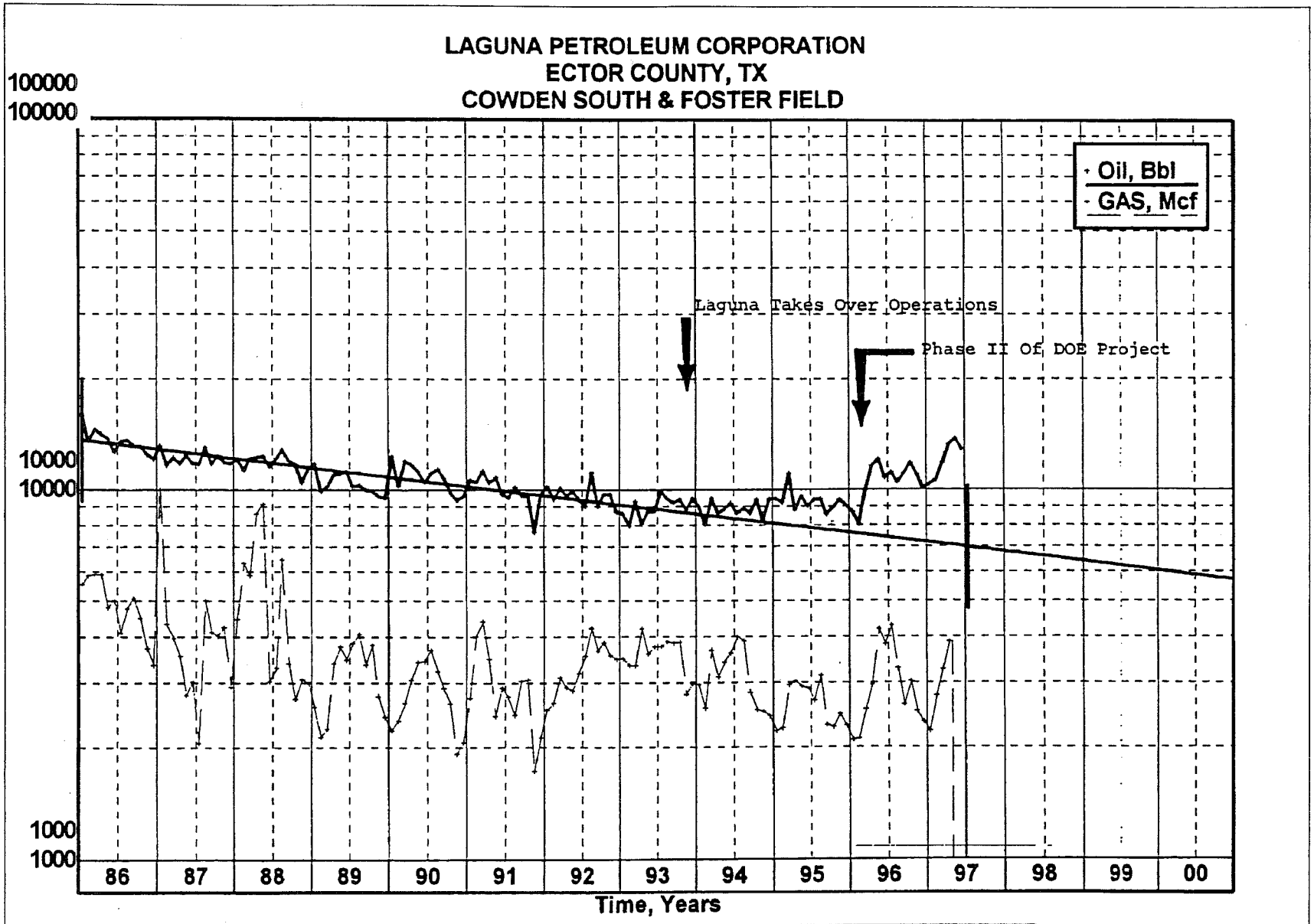

Figure 24. Section 36 production from 1986 to present, showing decline and impact of project recommendations.

uppermost of three porosity zones in the San Andres were tested (see GEOLOGY). The middle zone was tested first; perforated from 4318 (-1379) - 4330 ft (-1391) and acidized with 1200 gals 15% NEFE acid. The zone swabbed dry in two hours, with entry rates thereafter of 400 ft of fluid per hour with 15% oil cut. A CIBP was set at 4310 ft and the uppermost zone was perforated from 4275 (-1336) - 4287 (-1348) ft, and acidized with 1850 gals 15% NEFE acid. This zone swabbed dry in 1 1/4 hours, and had entry rates of 500 ft of fluid per hour with a 10% oil cut thereafter. These entry rates would not have resulted in a commercially successful well without additional stimulation. Because of the potential for water encroachment from the zone below 4375 ft, it was decided not to fracture stimulate the San Andres zones.

Because of previous failures to successfully fracture stimulate the San Andres without producing large volumes of water, a different methodology had to be applied. It was decided to fracture stimulate a porous interval in the lower Grayburg, with the anticipation that the frac height of a "conventional" frac would be sufficient to grow down to the productive intervals in the San Andres but not enough to communicate with the water bearing interval below 4375 (-1336) ft. The lower Grayburg was perforated from 4166 (-1227) - 4182 ft (-1243) and acidized with 1250 gallons of 15% NEFE acid. The interval was then fracture treated with 23,520 gallons of 35 lbs cross-linked gel and 125,500 lbs 16/30 Brady sand.

The well potentialed pumping 55 BOPD, 372 BWPD and 16 MCFPD. The water analyses (see GEOLOGY) indicates the majority of the produced water is from the San Andres formation that indicates that the attempt to frac down into the San Andres was accomplished. At the end of the second quarter 1997, production was 28 BO, 180 BW, and 10 MCFGPD.

Completions and Production

Analysis of buildup and falloff tests continued on a routine basis. The results of these tests have been incorporated into the design of the fracture treatments. The main problem has been how to fracture the low permeability oil zones without communicating with the high permeability and high-pressure water zones. Well testing continues, reinforcing the preliminary conclusion that the water flood, as designed and implemented, is ineffective. One positive outcome of the well work has been the arrest of the decline for section 36 seen in the years prior to the implementation of study recommendations. Since June of 1993, the production has risen to 14,000 BOPM from 8700 BOPM (Fig. 24).

REFERENCES

Editor not credited, *Porosity and Lithology Determination from Sonic Log and CNL* Compensated Log,* Schlumberger Log Interpretation Charts, page 35, figure CP-2C, 1989.

Galloway, W.E., Ewing, T.E., Garrett, C.M., Jr., Tyler, N., and Bebout, D.G., 1983, Atlas of Major Texas Oil Reservoirs: the University of Texas at Austin, Bureau of Economic Geology Special Publication, 139 p.

Schultz, P.S., S.Ronen, M.Hattori, and C. Corbett, Seismic-guided estimation of log properties (in three parts), *The Leading Edge*, 305-310 (May), 674-678 (June), and 770-776 (July), 1994.

Ruppel, S.C., and Lucia, F.J., 1996, Diagenetic Control of Permeability Development in a Highly Cyclic, Shallow-Water Carbonate Reservoir: South Cowden Grayburg Field, Ector County, Texas, in Permian Basin Oil and Gas Fields: Keys to Success That Unlock Future Reserves, WTGS Symposium, Oct. 31-Nov. 1,1996, Publication 96-101, R.L.Martin, editor, p. 7-23.

Ward, R.F., Kendall, C.G., and Harris, P.M.,1986, Upper Permian (Guadalupian) Facies and Their Association with Hydrocarbons – Permian Basin, West Texas and New Mexico: American Association of Petroleum Geologists Bulletin, v.70, no. 3, p.239-262.

Watts, G.P., G.D. Hinterlong, A.R. Taylor, 3-D Seismic evaluation for Reservoir Description, West Welch Unit, Dawson County, Texas, *Oxy/DOE Class II Project Technical Report,* 60 pages (plus figures), date

presented: September 27, 1995.

ACKNOWLEDGMENTS

We would like to thank:

The United States Department of Energy, Laguna Petroleum, and Phillips Petroleum for their funding of this cost shared project, Cooperative Agreement No. DE-FC22-94BC14982

Paul Laverty, Computer consultant

Dawson Geophysical, Schlumberger GeoQuest, and Scientific Softwatre Intercorp for software and technical support.

We would like to acknowledge James J. Reeves and Hoxie W. Smith for conceiving and managing the DOE study and for being responsible for the geophysical study. We would like to acknowledge that, since April 1996, William C. Robinson has been responsible for the reprocessing and reinterpreting the seismic data and for the geophysical study. Also, since that date, Robert C. Trentham has been responsible for project management.

RESERVOIR CHARACTERIZATION OF THE UPPER PERMIAN GRAYBURG FORMATION IN PREPARATION FOR A HORIZONTAL-WELL CO2 FLOOD, SOUTH COWDEN UNIT, WEST TEXAS

Craig D. Caldwell, Ken J. Harpole, and Matt G. Gerard

Phillips Petroleum Co., Bartlesville, OK 74004

ABSTRACT

Since initial development in the late 1940s, South Cowden Unit (SCU), located on the eastern margin of the Central Basin Platform, has produced 35 million barrels of oil from the Upper Permian Grayburg Formation. Under waterflood since 1965, SCU is approaching the economic limit of waterflood operation, and a CO_2 flood employing horizontal injection wells has been proposed. A detailed geologic description of the reservoir interval was prepared for integration into a reservoir simulation model used to predict CO_2 flood performance.

The reservoir interval at SCU has a gross thickness of approximately 150 ft and is composed mainly of burrow–mottled dolopackstones. These dolostones are characterized by a distinctive gray/tan mottling reflecting variations in porosity and oil staining. Tan oil–stained areas, interpreted to be carbonate–sand–filled burrows, are dolograinstones, dolopackstones, and washed dolopackstones. Porosity in these areas typically ranges from 10 to 32% and is intergranular, intercrystalline, and moldic. Permeability generally varies from 2 to 400 md. Gray interburrow areas, lacking oil staining, are dolopackstones and dolowackestones with 2 to 9% moldic and intercrystalline porosity and 0.002 to 2 md permeability. The relative amounts of tan and gray dolomite, determined by the degree of bioturbation, can profoundly affect reservoir porosity and permeability.

Reservoir porosity and permeability are also a function of anhydrite content. An inverse relationship exists between porosity and permeability and the amount of poikilotopic anhydrite cement in the tan dolomite areas. Limited core data suggest that the decrease in porosity in the northwestern (paleolandward) part of SCU is related, at least in part, to an increase in anhydrite content.

Reservoir permeability is a function of bioturbation, anhydrite content, and pore size in the tan dolomite areas. Pore size is related to depositional texture, diagenesis, and consequent crystal size. Very finely to finely crystalline tan dolomites, most likely reflecting dolomitization of muddy burrow–filling sediments, are characterized by very small intercrystalline pores and permeabilities generally ranging from less than 1 md to 16 md. Finely to medium-crystalline tan dolograinstones and washed dolopackstones, reflecting dolomitization of carbonate-sand-filled burrows with relatively minor mud–size material, are characterized by larger intergranular pores

and significantly better permeabilities typically ranging from 100 to 500 md. Tan dolomites with similar porosities may have markedly different permeabilities due to differences in pore size, thus more than one porosity/permeability transform is necessary to characterize rocks of the SCU reservoir interval.

The vertically oriented character of the porous and permeable, tan, dolomite burrow structures, characterizing rocks of the SCU reservoir interval, provides a favorable condition for the application of horizontal injection wells. The vertical movement of fluids and gases through the reservoir interval may be partially restricted, however, by rare, laterally continuous, relatively low–permeability, sandy dolopackstone layers. It is critical to determine the stratigraphic position of these low–permeability layers relative to those of the proposed, horizontal, CO_2-injection wells.

INTRODUCTION

Over ten billion barrels of oil have been produced from the San Andres and Grayburg Formations of the Permian Basin, west Texas and southeast New Mexico (Bebout and others, 1987). San Andres and Grayburg fields, discovered mainly in the 1920s, 30s, and 40s, have cumulative productions ranging from less than one million to greater than 750 million barrels of oil (Ward and others, 1986). Major, Permian Basin San Andres and Grayburg fields, including South Cowden Unit the focus of this study, are shown in Figure 1.

San Andres and Grayburg reservoirs exhibit low recovery efficiencies, generally less than 30%, in response to conventional primary and secondary recovery practices. Galloway and others (1983), Tyler and others (1984), Ruppel and Cander (1988), and Fogg and Lucia (1990) stated that the low recovery efficiencies of these reservoirs are a function of inefficient sweep of the reservoirs related to an incomplete understanding of reservoir heterogeneities. The aforementioned authors suggested that a significant amount of the remaining mobile oil can be produced through a better understanding of the reservoir architecture and the integration of geologic and engineering data to develop and improve infill drilling programs, CO_2 and waterflood programs, and selective completion procedures. This study provides a detailed petrographic description of the South Cowden Unit reservoir interval for integration into a reservoir simulation model for a proposed CO_2 flood using horizontal injection wells.

FIELD/UNIT HISTORY

South Cowden field, discovered in 1932, is located in Ector County, Texas on the eastern margin of the Central Basin Platform (Fig. 1). The field is part of a nearly continuous trend of Upper Permian Grayburg production extending northward into Foster and Johnson fields. As of January 1994, South Cowden field had produced 154 million barrels of oil from the Grayburg Formation (Ruppel and Bebout, 1995). The number of producing wells in the field reached 516 in 1980 (Ward and others, 1986).

South Cowden field is divided into several units. The most productive units are, from north to south: the Unocal Moss Unit, the Fina Emmons Unit, and the Phillips Petroleum South Cowden Unit (Fig. 2). South Cowden Unit (SCU), the focus of this study, produces from an anticlinal structure formed by the drape of Grayburg strata over a lobe-shaped, San Andres depositional thick (Ruppel and Bebout, 1995). The gross thickness of the Grayburg reservoir interval at SCU is approximately 150 ft, with the top of the interval occurring at a drilling depth of approximately 4,500' to 4,700'.

Hydrocarbon production from the area that is now South Cowden Unit began in 1948. Since 1948 approximately 100 producing wells were drilled in the area on 20-acre spacing. The area was unitized for secondary waterflood operations in 1965 with initial water injection from peripheral wells around the edge of the anticlinal structure. Leaseline cooperative water injection along the northern unit boundary was added in the early 1970s, and several additional water injection wells were drilled in the interior of the unit in the late 1970s and early 1980s. In early 1995 SCU, nearing its economic limit for waterflood operations, was producing just over 400 BOPD at a watercut in excess of 95% from 39 producers and 11 water injectors (Fig. 3). The cumulative primary and secondary recovery from SCU is estimated to be 35 million STB of oil or approximately 20% of the original oil in place.

CO_2 feasibility studies conducted in the early 1990s indicated that SCU was a good technical candidate for a conventional CO_2 flood, but the project did not meet economic criteria. Harpole and others (1996) suggested that most of the wells in the unit were not suited for conversion to a CO_2 WAG injection because of mechanical or completion problems, and the cost for new injection wells and related facilities for a conventional CO_2 flood was too high relative to the recoverable oil. Thus, a CO_2 flood was proposed using two horizontal injection wells drilled from a centralized facility, thereby reducing upfront capital costs. Engineering studies and a detailed reservoir description, the later of which is summarized in this paper, will be integrated into a reservoir simulation model for a CO_2 flood using horizontal injection wells. This project was selected as a demonstration project under the DOE Class II Oil Program for shallow-shelf carbonate reservoirs and is financially supported in part by the DOE.

METHODS OF INVESTIGATION

Approximately 1,300 ft of core were described from five SCU wells (SCU 8-19--470 ft; SCU 7-10--249 ft; SCU 8-11--170 ft; SCU 6-23--237 ft; and SCU 6-24--180 ft). An additional 120 ft of core were reviewed from the Unocal Moss Unit 16-14 well. Locations of the cored study wells are shown in Figure 2. Cored intervals are primarily from the Grayburg Formation; the lower 120 ft and 35 ft of the overlying Queen Formation were cored in the SCU 8-19 and 6-23. In addition to macroscopic descriptions, 211 thin sections were described and point counted (SCU 8-19--97 t.s.; 7-10--63 t.s.; 8-11--12 t.s.; 6-23--15 t.s.; 6-24--13 t.s.; and Moss Unit 16-14--11 t.s.). Most of these thin sections are from the Grayburg reservoir interval. A total of fifty-three samples from the SCU 8-19, 7-10, and 8-11 were analyzed using x-ray diffraction. The most complete Grayburg/Queen section was recovered from the SCU 8-19, thus this well serves as the type well for much of the following discussion (Fig. 4). The Grayburg Formation at South Cowden Unit is divided into seven stratigraphic intervals designated Zones A - G (Fig. 4). The basis for this division is discussed later

in this report.

LITHOFACIES DESCRIPTIONS

Eleven rock types defined from the SCU Grayburg and Queen core studies are grouped into five dolostone lithofacies (Fig. 4, Key). These lithofacies are:

1. Fusulinid dolowackestone,
2. Ooid peloid dolograinstone,
3. Sandy dolopackstone,
4. Burrow–mottled dolopackstone, and
5. Fenestral dolopackstone.

Fusulinid dolowackestones and ooid peloid dolograinstones make up the lower part of the cored Grayburg Formation at SCU (Zone A, Fig. 4). The middle part of the Grayburg (Zones B, C, and the lower part of Zone D, Fig. 4) is interbedded sandy dolopackstone, ooid peloid dolograinstone, fusulinid dolowackestone, and burrow–mottled dolopackstone. The upper Grayburg (Zones E, F, G, and the upper part of Zone D) is dominated by burrow–mottled dolopackstone. Sandy dolopackstones and fenestral dolopackstones make up the cored portion of the Queen Formation. The SCU reservoir interval, Zones C through F, is composed mainly of burrow-mottled dolopackstones.

Although most Grayburg dolostones at SCU contain less than 2% anhydrite, some Grayburg intervals contain as much as 15 to 20% anhydrite. Anhydrite occurs as replacement nodules and cements intercrystalline, intergranular, moldic, and fracture porosity. In the SCU 8-19 the lower 50 ft of the Queen Formation is 1 to 10% anhydrite, and the overlying 70 ft of cored Queen is 15 to 45% anhydrite. Gypsum is very rare in the Grayburg/Queen cored interval and is generally restricted to white alteration rims on anhydrite nodules.

Siliciclastics, mainly very fine– to fine–grained detrital quartz and feldspar, are less than 5% in all Grayburg/Queen lithofacies with the exception of the sandy dolopackstone lithofacies. Sandy dolopackstones of the Grayburg and Queen Formations are 10 to 20% and 10 to 40% siliciclastics, respectively. Gypsum and calcite are generally absent or occur in trace amounts in the Grayburg and Queen Formations. Depositional textures are difficult to distinguish in all lithofacies due to diagenesis, in particular dolomitization.

Fusulinid Dolowackestone Lithofacies

Much of the lower Grayburg Formation at South Cowden Unit is composed of fusulinid dolowackestones and dolopackstones (Figs. 4 and 5A). Fusulinid dolostones are rare in the middle part of the Grayburg Formation and absent in the upper Grayburg and overlying lower part of the Queen Formation. Fusulinids are scarce to common, and echinoderm debris is rare in rocks of this lithofacies; no other bioclasts are distinguishable. Intergranular areas are generally dolomitized

carbonate mud which in places appears pelleted. Very fine– to fine–sand–size detrital quartz is less than 3%, and coarsely to very coarsely crystalline anhydrite, typically cementing or partially cementing biomoldic pores, varies from 3 to 14%. Small anhydrite nodules are rare.

Carbonaceous and argillaceous stylolitic seams and laminae are numerous in some fusulinid dolowackestone/dolopackstone intervals, e.g., core units 4 and 5, SCU 8-19, resulting in slightly higher gamma-ray log values for these intervals (Fig. 4). The "hotter", gamma–ray log signature associated with core units 4 and 5 is observed at this stratigraphic level throughout SCU.

Burrow mottling significantly affects porosity and permeability in rocks of this lithofacies. Fusulinid dolostones lacking burrow mottling have core analysis porosities of 5 to 17% and Kmax values of 0.4 to 2.5 md. Burrow–mottled, oil–stained fusulinid dolostones have core analysis porosities ranging from 15 to 20% and Kmax values from 280 to 880 md. The better porosity and permeability in burrow-mottled dolostones is related to the presence of intergranular porosity within bioturbated areas. In areas lacking bioturbation porosity is mainly biomoldic and intercrystalline (Fig. 6A). Biomolds are typically leached or partially leached fusulinids. As stated above, biomolds are commonly cemented or partially cemented by anhydrite.

The normal-marine biota, bioturbation, and generally muddy character of fusulinid dolowackestones and dolopackstones suggest deposition in an open–marine outer-platform setting in waters generally below normal wave base, perhaps 10 to 20 meters or less in depth. Rare fusulinid intraclast dolograinstones and washed dolopackstones interbedded with the muddy fusulinid rocks suggest times or areas of higher-energy traction deposition. Numerous authors have proposed a similar outer-platform or outer-ramp depositional setting for San Andres and Grayburg fusulinid wackestones and packstones of the Permian Basin (Bebout and others, 1987; Ruppel and Cander, 1988; Tyler and others, 1991; Kerans and others, 1994). Sonnenfeld's (1991) study of San Andres-age rocks of the Permian Basin suggests that the optimal depth for fusulinids was approximately 10 m. Fusulinids may have been transported downslope, however, to depths of 60 m (Kerans and others, 1994).

Ooid Peloid Dolograinstone Lithofacies

Ooid peloid dolograinstones and washed dolopackstones occur mainly in the lower and middle parts of the Grayburg Formation (Zone B and the upper part of Zone A, Fig. 4). Rocks of this lithofacies are mottled or display small– to medium–scale, trough cross stratification. In places, mottling appears to be related to bioturbation. Burrowed areas are commonly oil stained. Framework grains are mainly medium- to coarse-sand-size ooids and peloids. Echinoderm debris, peloidal intraclasts, and grapestone grains are rare. Detrital quartz is generally absent. Due to dolomitization ooid nuclei and oolitic coats (cortices) are difficult to distinguish (Fig. 6B).

Porosity in rocks of this lithofacies is intergranular and relatively rare moldic (Fig. 6B). Core analysis porosity is typically 6 to 16%, and Kmax generally varies from 3 to 40 md with some dolograinstone intervals having permeabilities of 100 to 300 md. Intergranular porosity has been partially occluded by finely to medium-crystalline dolomite cement and small amounts (<1% to

3%) of coarsely crystalline calcite cement. The ooid dolograinstone interval which occurs at the top of the Grayburg Formation throughout SCU (core unit 18, Fig. 4) is partially cemented by coarsely to very coarsely crystalline anhydrite. Cored dolograinstones elsewhere in the Grayburg Formation are generally less than 1% anhydrite.

Cross–stratified and bioturbated, ooid peloid dolograinstones and washed dolopackstones record deposition on moderate- to high–energy shoals and in near–shoal areas. Water depths in this setting were a few meters or less. Wave and current energy on shoal crests winnowed mud–size material and produced oolitically coated grains. Carbonate sands washed into off-shoal areas were bioturbated in places.

Sandy Dolopackstone Lithofacies

Thin, areally extensive, sandy dolopackstone and dolomitic sandstone beds are used to establish the internal stratigraphy of the Grayburg reservoir interval at SCU (see Stratigraphy and Depositional Cycles section). Sandy dolopackstones and dolomitic sandstones are relatively scarce in the Grayburg Formation but dominate the cored portion of the overlying Queen Formation (Fig. 4). Sandy dolopackstones in the two formations display some noteworthy differences addressed below.

Angular to subangular, very fine– to fine–sand-size siliciclastic material typically varies from 10 to 20% in sandy dolopackstones of the Grayburg Formation and from 10 to 40% in sandy dolopackstones/dolomitic sandstones of the Queen Formation. Siliciclastic material in both formations is approximately 85 to 90% quartz and 10 to 15% alkali feldspar, as determined by x-ray diffraction (XRD) analysis. Carbonaceous and argillaceous stylolitic seams and laminae are locally common in rocks of this lithofacies (Fig. 5B), and some beds contain small amounts of sand–size opaque material resembling detrital carbonaceous debris. Clay mineral content, determined by XRD analysis, varies from 1 to 7%. The relatively "hot", gamma–ray log character of sandy dolopackstones and dolomitic sandstones (Fig. 4) is related to the presence of clay minerals, carbonaceous debris, and detrital alkali (potassium-bearing) feldspars. Anhydrite is generally less than 1% in sandy dolopackstones of the Grayburg Formation and varies from 1 to 45% in sandy dolostones of the Queen Formation.

Carbonate grains in sandy dolopackstones of the Grayburg Formation are predominantly fine–sand–size peloids (Fig. 6C). These grains are most likely fecal pellets and micritized bioclasts. Medium– to coarse–sand–size ooids and less numerous peloidal intraclasts and grapestone grains are rare to common in Grayburg sandy dolopackstones (Fig. 6D), and fusulinids and echinoderm debris, though generally absent, are present in some beds. Sandy washed dolopackstones of the Queen Formation contain common peloids, ooids, and intraclasts (Fig. 7A).

Sandy dolostones of the Grayburg Formation are commonly mottled and display small burrows which are elliptical on the slabbed core surfaces. By contrast, sandy washed dolopackstones of the Queen Formation display horizontal and low–angle stratification, ripple cross stratification, and less

common burrows.

Porosity in these rocks is intergranular, intercrystalline, and leached grain (Fig. 6C). Carbonate grains and detrital feldspars display evidence of dissolution. Core analysis porosity is typically 10 to 13%, and Kmax is 0.1 to 9 md. The effect of relatively low–permeability sandy dolostones and dolomitic sandstone layers on Grayburg production is discussed in the Reservoir Character section.

Low–angle and ripple stratification and common ooids and intraclasts in sandy washed dolopackstones of the Queen Formation indicate deposition in moderate- to relatively high–energy marine waters a few meters or less in depth. The amount of siliciclastic sand, typically greater than 20%, suggests an inner-platform nearshore or shoreline setting and differentiates these oolitic rocks from ooid peloid dolograinstones of the lower and middle Grayburg. Sandy dolopackstones of the Grayburg Formation typically contain less than 20% siliciclastic sand, are burrow mottled, and have relatively scarce ooids, intraclasts, fusulinids, and echinoderms suggesting lower-energy deposition in a more seaward setting.

Ruppel and Bebout (1995) suggested that the well sorted, very fine- to fine-grained, Grayburg siliciclastics units at South Cowden field record the subaqueous reworking of lowstand eolian sediments during sea level rise and marine transgression. A similar depositional process was proposed by Fischer and Sarntheim (1988) for numerous Permian siliciclastic units in the Delaware Basin.

Burrow-mottled Dolopackstone Lithofacies

Rocks of the burrow-mottled dolopackstone lithofacies display a distinctive, vertically oriented gray/tan mottling reflecting variations in porosity and oil staining (Fig. 5C and 5D). Tan oil–stained areas are typically 2 to 8 cm in width, up to a few tens of centimeters in length, and are dolograinstones, dolopackstones, and washed dolopackstones. Gray, lower-porosity areas, lacking oil staining, are generally dolopackstones and dolowackestones and commonly display short (<2 cm) anhydrite–cemented fractures. These fractures do not extend into the adjacent tan dolomite areas.

Due to diagenesis, in particular dolomitization and dissolution, grains are generally difficult to distinguish in both the tan and gray dolomite areas. Distinguishable grains are typically classified as peloids. Coated grains are recognizable in some tan dolomites, and fusulinids and echinoderms are visible in burrow-mottled dolopackstones in the middle part of the Grayburg Formation, Zones C and D. Bryozoans, green algae, and intraclasts are very rare. Quartz sand is generally absent.

The distinctive gray/tan mottling which characterizes rocks of this lithofacies was observed at Rhodes Cowden Unit, just north of Johnson/Foster field, by C. D. Caldwell and described by numerous other authors working San Andres/Grayburg fields of the Permian Basin (e.g., Longacre, 1980; Bebout and others, 1987, Dune field; Ruppel and Cander, 1988, Emma field;

Major and others, 1990, East Penwell Unit; and Leary and Vogt, 1990, Seminole field). Most of these papers relate this mottling to bioturbation and consequent variations in porosity and oil staining. This lithofacies makes up the bulk of the reservoir interval at South Cowden Unit and is the major reservoir lithofacies at East Penwell and Rhodes Cowden Units.

Gray areas are a very finely to medium-crystalline, anhedral dolomite mosaic (Fig. 7B). Dolomite crystals in these areas are typically 0.01 to 0.1 mm in length, as determined from thin section study, with most crystals occurring in the coarser part of this size range, i.e., 0.03 to 0.1 mm.

Tan dolomite areas fall into one of three categories based on crystal size. Category I tan dolomites are very finely to medium-crystalline with crystals typically 0.01 to 0.1 mm in length (Figs. 7C,7D,8A, and 8C). Crystals are evenly distributed throughout this size range, or in some samples occur mainly in the coarser end of the size range (Fig. 8C). Category II dolomite crystals also range from 0.01 to 0.1 mm, but crystals in this category occur mainly in the finer part of the size range, i.e., 0.01 to 0.03 mm (Fig. 8D). Tan dolomites of category III are very finely to finely crystalline with crystals typically less than 0.01 mm to 0.03 mm in length (Fig. 8B). Pore size and permeability are directly related to crystal size in most tan dolomite samples. The relationship of crystal size to permeability is discussed in the Reservoir Character section.

Thin section study suggests that tan dolomites have significantly better porosity than gray dolomites in rocks of this lithofacies (compare Fig. 7B--gray dolomite and Fig. 7C, 7D--tan dolomite). In an effort to quantify this relationship, seventy-nine core plugs were taken specifically from the tan and gray areas to determine the petrophysical properties of these two dolomites. Plugs were taken from the SCU 8-19, 7-10, 6-23, and 8-11 cores.

Core plugs from the gray dolomite areas generally have 2 to 9% porosity and 0.002 to 2 md permeability (Fig. 9). Porosity in the gray areas is moldic and intercrystalline (Fig. 7B). By contrast, tan dolomite plugs have porosities typically ranging from 10 to 32% and permeabilities ranging from 2 to 400 md (Fig. 9). Porosity in the tan areas is intergranular, intercrystalline, and less common moldic. Intergranular porosity is significantly better in the tan dolomites than in the lower-porosity gray dolomites. This intergranular porosity may have acted as a conduit for the movement of diagenetic fluids, some of which may have partially leached carbonate grains and matrix enhancing porosity in the tan dolomites. Tan dolomite areas are interpreted to be carbonate-sand-filled burrows, and gray lower-porosity dolomites are muddy interburrow areas.

Core plug data indicate that the relative amounts of gray and tan dolomite, which are largely a function of bioturbation, can markedly affect porosity and permeability in rocks of the burrow–mottled dolopackstone lithofacies. Mottled dolopackstone porosity is also related to the amount of intergranular and intercrystalline anhydrite cement. An inverse relationship exists between porosity and anhydrite content (Table I). The possible role of late-stage anhydrite (or gypsum?) dissolution in porosity development is discussed later in this report.

An average porosity and permeability were calculated, in each of the five SCU study wells, for rocks of the burrow-mottled dolopackstone lithofacies. These calculations were derived from whole-core data. Thus, core pieces used in these analyses typically contain both tan and gray

dolomites. The average porosities from the five wells range from 12.8 to 15.5%, and the average maximum permeabilities vary from 4.9 to 30 md.

The variability of carbonate grain types, including fusulinids and coated grains; the presence of vertical, relatively large carbonate–sand–filled burrows; and the general absence of siliciclastics in rocks of this lithofacies suggest subtidal marine deposition generally below or near normal wave base in a mid-platform setting. Coated grains, formed on higher-energy shoals in this setting, were washed into quieter-water, muddy near-shoal areas. An open, subtidal platform setting has been proposed by numerous authors for similar, burrow-mottled peloid packstones and grainstones on the Central Basin Platform (Ruppel and Cander, 1988; Leary and Vogt, 1990; and Major and others, 1990).

Leary and Vogt (1986, 1990) studied the isotopic composition of gray/tan-mottled San Andres dolostones from five fields along the eastern margin of the Central Basin Platform (Seminole, Foster, Means, Hanford, and North Robertson). Gray and tan dolomites studied by Leary and Vogt have $\delta^{18}O$ values of 4.6 o/oo and 3.1 o/oo, respectively. In paired gray and tan samples, in which the tan and gray samples were taken within 10 cm of each other, tan dolomites were depleted by as much as 3.5 o/oo. Leary and Vogt suggested a diagenetic sequence for the mottled dolostones that consists of an early selective dolomitization of more permeable bioturbated areas by mixed marine/meteoric fluids; a large-scale replacement dolomitization by seawater evaporated to gypsum saturation, responsible for the gray dolomite of the interburrow areas; and a final phase of dolomitization or dolomite stabilization of the more permeable, bioturbated tan areas by an isotopically lighter fluid.

Major and others (1990) presented an alternative diagenetic model to explain similar isotopic compositions of gray and tan dolomites at East Penwell Unit. In their model, a late–stage leaching increased permeability in the tan areas by widening intercrystalline pore throats and preferentially removing the early isotopically enriched centers of dolomite rhombs, thus resulting in the depleted oxygen isotopic compositions of the tan areas.

Isotopic data are not available for gray and tan dolomites of the burrow–mottled dolopackstone lithofacies at SCU. It is speculated, however, that these dolostones are isotopically similar to those discussed in the aforementioned studies. It is noteworthy that the dissolution of the central parts of dolomite rhombs, described by Major and his co-authors, is relatively rare in the South Cowden Unit burrow–mottled dolopackstones, and in most samples this dissolution had very little effect on porosity, permeability, and presumably isotopic composition of the tan areas.

Fenestral Dolopackstone Lithofacies

Rocks of the fenestral dolopackstone lithofacies are restricted to the Queen Formation in the five SCU study wells. Anhydrite layers and lenses, a few millimeters to several centimeters thick, are associated with fenestral dolopackstones and dolowackestones composing this lithofacies (Fig. 5E). Bedding is rarely inclined with dips up to 30 degrees (Pl. 5E).

Carbonate grains in this lithofacies are fine–sand–size peloids; less numerous medium– to coarse–sand–size peloidal intraclasts and coated grains; and rare, granule–size broken and coated grains, some resembling vadose pisolites. Mollusk debris, though generally rare, is common in some beds. Quartz sand is less than 1%.

Anhydrite occludes most of the intergranular and fenestral porosity in dolopackstones and dolowackestones of this lithofacies and in places replaces grains and matrix. Fenestral dolopackstones are typically 20 to 25% anhydrite. Core analysis porosity and permeability data are not available for rocks of this lithofacies, but wireline–log studies indicate porosities are less than 4%.

Anhydrite layers and lenses described above record the cementation of dessication cracks by coarsely to very coarsely crystalline, blocky to bladed anhydrite. Finely textured internal sediment lines the floor of some of the larger dessication structures. These dessication structures, the aforementioned fenestral fabric, and the relatively rare and restricted marine biota which characterize this lithofacies suggest upper intertidal to supratidal deposition marked by periods of subareial exposure. The aforementioned inclined beds are most likely the limbs of teepee structures.

DEPOSITIONAL MODEL

Grayburg/Queen lithofacies defined in this study are very similar to San Andres and Grayburg lithofacies recognized by other authors working in the Permian Basin (Bebout and others, 1987; Rupple and Cander, 1988; Garber and Harris, 1990; Leary and Vogt, 1990; and Ruppel and Bebout, 1995). Fusulinid dolowackestones composing most of the lower Grayburg Formation at SCU record outer-platform open-marine deposition below normal wave base in waters 10 to 20 m or less in depth. Published reports suggest that fusulinid wackestones and packstones generally record maximum water depths in San Andres/Grayburg deposits of the Permian Basin. This outer-platform setting passed landward (westward) into high–energy carbonate shoals and intershoal areas characterized by cross–stratified and burrow-mottled, ooid peloid dolograinstones. Where high-energy carbonate shoals did not develop, outer-platform, muddy fusulinid-rich sediments pass westward into a mid- or inner-platform setting characterized by burrow-mottled dolopackstones. Ruppel and Bebout (1995) in their depositional model for South Cowden field placed peloid wackestones/packstones, analogous to rocks of the burrow-mottled dolopackstone lithofacies, in an inner-ramp setting behind high-energy, ramp-crest shoals, and Leary and Vogt (1990) showed burrow-mottled pellet grainstones on a shallow subtidal platform landward of open-marine fusulinid wackestones and packstones. The inner-platform setting at SCU is represented by sandy and fenestral dolopackstones of the Queen Formation. Sandy, oolitic and intraclastic washed dolopackstones record moderate- to high-energy shoreline deposition and interbedded fenestral dolopackstones and thin anhydrites record upper intertidal to supratidal deposition.

The Grayburg/Queen carbonate platform faced prevailing winds from the northeast (Walker and others, 1995) and open–marine waters of the Midland basin. Cyclicity of the outer-platform, mid-platform, and inner-platform deposits is discussed below.

STRATIGRAPHY AND DEPOSITIONAL CYCLES

Laterally extensive, sandy dolostone layers, characterized by relatively "hot", gamma–ray log signatures, were used to establish the Grayburg reservoir stratigraphy at South Cowden Unit. These sandy dolopackstones and dolomitic sandstones form the basal units of Zones C, D, and F of the Grayburg Formation (Fig. 4). The relatively "hot" gamma–ray interval at the base of Zone E reflects the concentration of carbonaceous and argillaceous material along locally common stylolites.

Bebout and others (1987) used similar, laterally extensive, dolomitic siltstone layers to establish the Grayburg stratigraphy at Dune field, and Ruppel and Cander (1988) stated that thin siliciclastic units form readily traceable marker beds at Emma San Andres field. Bebout and his co-authors wrote that the dolomitic siltstone beds at Dune field represent geologic time lines and thus can be used to establish a time stratigraphic framework.

As discussed in the lithofacies descriptions, sandy dolopackstones and dolomitic sandstones of the Grayburg Formation at SCU may record marine reworking of lowstand eolian sands during a sea level rise or marine transgression (Kerans and others, 1995; Ruppel and Bebout, 1995). In this model, thin, sandy dolomite beds are the initial deposits of high-frequency cycles (HFC) which make up the Grayburg Formation. Kerans and his co-workers stated that these cycles are equivalent to parasequences defined by Vail (1987) and Van Wagoner and others (1991).

Sandy dolopackstones and dolomitic sandstones composing core units 10K (base of C Zone), 12A (base of D Zone), and 15 (base of F Zone) in the SCU 8–19 (Fig. 4) correlate with the basal transgressive units of three HFC recognized by Ruppel and Bebout (1995) at South Cowden field. A typical Grayburg HFC at SCU consists of a basal, transgressive sandy dolopackstone/dolomitic sandstone, recording marine reworking of lowstand siliciclastics, overlain by outer-platform fusulinid dolowackestone and/or mid-platform burrow–mottled dolopackstone, and capping the cycle a regressive, ooid peloid dolograinstone. Tidal flat deposits, capping high-frequency Grayburg cycles in the updip platform interior of South Cowden field (Ruppel and Bebout, 1995), were not recognized in the five SCU study wells. Inner-platform, tidal flat deposits, represented by rocks of the fenestral dolopackstone lithofacies, are restricted to the Queen Formation in the study wells.

In an alternative depositional model, sandy dolopackstones and dolomitic sandstones of the Grayburg Formation may reflect deposition in subtidal marine waters landward of the platform–crest oolite shoals. In this model fusulinid dolowackestones and/or burrow–mottled dolopackstones record the initial phases of marine transgression. These rocks are overlain by regressive, ooid peloid dolograinstones, and capping the sequence are back-shoal sandy dolopackstones. This model lacks the regional insights of Kerans and Ruppel's work and at present is considered the least attractive of the two models.

RESERVOIR CHARACTER

Porosity and Bioturbation

Grayburg porosity and permeability at SCU are a function of original depositional texture and diagenesis, reflected in the lithofacies classification. Biomoldic and intercrystalline porosity, characterizing rocks of the fusulinid dolowackestone lithofacies, lower Grayburg, record secondary dissolution of carbonate grains and intergranular carbonate mud. Bioturbated areas in some fusulinid dolostones display intergranular porosity. By contrast, the main pore type associated with ooid peloid dolograinstones in the lower and middle parts of the Grayburg Formation is intergranular. Rocks of the fusulinid dolowackestone and ooid peloid dolograinstone lithofacies in places display good porosity and permeability, but in general, these rocks occur below the SCU oil/water contact (approx. -1800 ft) and thus are not hydrocarbon productive. Sandy dolopackstones are generally finely textured and have relatively poor permeabilities, and anhydrite cement occludes most of the primary and secondary porosity in sandy dolopackstones and fenestral dolopackstones of the Queen Formation.

Reservoir rocks at SCU are predominantly burrow–mottled dolopackstones. Porosity in these rocks is mainly a function of bioturbation and anhydrite cementation. As discussed in the lithofacies descriptions, tan carbonate–sand–filled burrows have porosities generally ranging from 10 to 32%, and gray, muddier interburrow areas have porosities ranging from 2 to 9%. Porosity in the tan areas is mainly intergranular and intercrystalline and less common moldic.

A clear mylar sheet with a 1–inch–square grid pattern was used to estimate the relative amounts of gray and tan dolomite and nodular anhydrite for each 1–foot interval of burrow–mottled dolopackstone in the five SCU study wells. Percentages of tan and gray dolomite and megascopic anhydrite were calculated and plotted on wireline–log/core graphs (Fig. 4). Those intervals dominated by gray dolomite typically have relatively low wireline–log porosities; intervals dominated by tan dolomite typically have relatively good wireline-log porosities. Comparison of the gray/tan plot and wireline–log porosity in the SCU 8–19 reservoir interval shows that porosity variation in this interval is largely a function of the varying amounts of gray and tan dolomite related to the extent of bioturbation.

Some of the low–porosity, gray dolomite layers appear to be correlative in the five SCU study wells. Laterally continuous, gray dolomite layers may reflect times or areas where conditions were less conducive to bioturbation. Some tan dolomite layers also appear to be correlative on a local scale.

Porosity and Anhydrite Cementation

An inverse relationship exists between anhydrite content and porosity in tan dolomites of the burrow–mottled dolopackstone lithofacies, i.e., as the amount of anhydrite increases porosity decreases (Table I). Poikilotopic anhydrite, the main form of anhydrite in the reservoir interval, is generally restricted to tan dolomite areas and is typically difficult to distinguish without the aid

of thin sections. Poikilotopic anhydrite cements intergranular, intercrystalline, and moldic pores and replaces dolomite (Fig. 8C,8D).

Though based on limited data, there appears to be a general increase in anhydrite, and corresponding decrease in reservoir porosity, in the northwestern part of the study area. For example, compare the anhydrite content and porosity in the SCU 8–19 and 6–23 to that in the more westward SCU 8–11 and Moss Unit 16–14 (Table I). This regional variation may be related to a northwestward (paleolandward) source of anhydrite–precipitating fluids. Alternatively, this variation may be related to regional variations in anhydrite dissolution discussed in the following paragraph. Contrary to this general trend are significant local variations in anhydrite content (e.g., tan dolomites in the SCU 6-24 contain significantly more anhydrite than tan dolomites in the nearby 8-19 or 6-23). The cause of these local variations requires additional study.

Sulfate dissolution and consequent porosity enhancement have been reported from numerous San Andres and Grayburg reservoirs in the Permian Basin (Bebout and others, 1987; Ruppel and Cander, 1988; Longacre, 1990; Siemers and others, 1995), and Ruppel and Bebout (1995) suggested that sulfate dissolution was critical to porosity development in mottled dolostones of South Cowden field. By contrast, anhydrite crystals showing evidence of dissolution are rare or absent in most burrow–mottled dolopackstone samples studied for this report. Additionally, anhydrite in the category II and III tan dolomites typically occurs in small patches a few tenths of a millimeter across, the dissolution of which would result in pores significantly larger than those observed in these rocks (Fig. 8D). By contrast, the dolomite fabric of some category I, anhydrite–cemented, tan dolomite areas is very similar to that of immediately adjacent porous areas lacking anhydrite cement (Fig. 8C). This similarity suggests that porosity development in some category I tan dolomites may be related in part to sulfate dissolution resulting in the relatively open dolomite framework which characterizes these rocks. Ruppel and Bebout wrote that the fluids responsible for sulfate dissolution at South Cowden field may have been derived from the basin during a pre-oil-migration phase of diagenesis. This basinal source of sulfate-leaching fluids would be consistent with the general westward increase in anhydrite observed at SCU.

Porosity/Permeability Relationships

Burrow–mottled dolopackstone permeability is a function of bioturbation and anhydrite content, as described above, and pore size. Pore size is related to depositional texture and diagenesis and consequent crystal size in the tan dolomite areas. As previously discussed, tan dolomites can be placed in one of three categories based on crystal size. Categories I, II, and III are characterized by progressively smaller crystal size. Decreases in crystal size are accompanied by decreases in pore-body and pore-throat size and lower permeabilities (Table III and Fig. 10).

Markedly different permeabilities characterizing tan dolomites of the burrow-mottled dolopackstone lithofacies are not necessarily related to significantly different porosities. For

example, the average porosity of tan dolomite plugs from the SCU 6–23 and 7–10 wells is 21%, but the average permeability of plugs from the 6-23 and 7-10 is 90 and 10 md, respectively (Table II). Whole core analysis data for burrow–mottled dolopackstones from the 6-23 and 7-10 also show this relationship, suggesting a single porosity/permeability transform does not adequately describe the varying porosity/permeability relationships at South Cowden Unit (Fig. 11).

Relatively low permeabilities characterizing tan dolomites of the SCU 7–10 are a function of comparatively small pore body and pore throat sizes (Table III). Tan dolomites of the 7-10 are predominantly category III (Fig. 8B), while tan dolomites of the SCU 6-23 are predominantly category I (Fig. 8A). The very finely to finely crystalline tan dolomites which characterize burrow-mottled dolopackstones of the 7-10 suggest burrowing–filling sediments in the area of the 7-10 were generally finer grained and muddier than burrow-filling sediments in the area of the 6-23. Tan dolomites in the 7–10 are mainly dolopackstones with intercrystalline porosity. By contrast, tan burrow-filling sediments in the 6–23 are dolopackstones, washed dolopackstones, and dolograinstones, and pores in these rocks are predominantly intergranular. Core data are limited, but muddier burrow-filling sediments resulting in category II and III tan dolomites, characterizing much of the SCU 7–10 and 8–11 reservoir intervals, may dominate burrow fillings in more protected, quieter-water interior parts of the platform. Category I dolograinstones and washed dolopackstones which characterize tan dolomites of the SCU 6-23 and 8-19 may reflect deposition and bioturbation in higher-energy, more seaward parts of the platform.

Low-permeability, Sandy Dolopackstone Layers

Areally extensive sandy dolopackstone/dolomitic sandstone layers, used to establish the internal stratigraphy of the Grayburg reservoir interval at SCU (Fig. 4, Zones C through F), may in some cases partially restrict the vertical movement of fluids and gases within the reservoir. For example, the sandy dolopackstone layer at the base of Zone D (core unit 12A, Figs. 4 and 6D), "separating" Zone D from the underlying Zone C, has an average Kmax of less than 0.1 md to 0.55 md and an average porosity of approximately 10% in the five SCU study wells. This low–permeability layer and a thin, anhydrite–cemented, fusulinid dolowackestone layer near the middle of Zone D (core unit 13A, Kmax 0.2 to 2.8 md in the SCU study wells) may partially restrict vertical flow between reservoir rocks in Zone C and the upper part of Zone D. RFT data from the SCU 8–19 and 6–23 suggest vertical communication between Zones C and D is partially restricted. By contrast, the relatively "hot" gamma–ray interval at the base of Zone E is not associated with a sandy dolostone layer, and the average Kmax over this interval varies from 0.37 to 15 md for the five study wells. Core analysis and RFT data suggest reservoir rocks of Zone E and the upper part of Zone D should be in communication in most wells. Finally, the average Kmax of the sandy dolostone layer at the base of Zone F (core unit 15, Fig. 4) "separating" Zones E and F, varies from 0.02 to 0.6 md in the SCU 8–19, 7–10, 6–23, and 6-24 but is significantly higher, 6.6 md, in the SCU 8–11. Average core analysis porosity for this layer is 5 to 13.5%. While petrographic and core analysis studies suggest this layer may in places act as a partial restriction to vertical flow, RFT data from the SCU 8–19 and 6–23 suggest Zones E and F are in

pressure communication.

Low–porosity, burrow-mottled dolopackstone layers dominated by gray dolomite should not form significant barriers to the vertical movement of reservoir fluids and gases. These layers, e.g., the low-porosity layer at the base of core unit 14C (Fig. 4, 4,730-4,733') contain a reduced, but still significant amount, 20–40%, of high–porosity and high-permeability tan dolomite typically occurring as vertically oriented burrow structures. These tan burrow structures should act as conduits for the vertical movement of fluids and gases. RFT data from Zone E in the SCU 8–19 and 6–23 indicate this zone is in vertical communication throughout despite the presence of low–porosity, gray dolomite layers.

SUMMARY

The Grayburg reservoir interval at South Cowden Unit has a gross thickness of approximately 150 ft and is composed mainly of burrow–mottled dolopackstones, recording subtidal mid-platform deposition. These dolomites are characterized by a distinctive, vertically oriented gray/tan mottling. Tan, oil-stained areas are carbonate–sand–filled burrows. These areas have core analysis porosities generally ranging from 10 to 32% and permeabilities ranging from 2 to 500 md. Porosity in the tan dolomite areas is mainly intergranular, intercrystalline, and moldic. Gray interburrow areas typically have porosities of 2 to 9% and permeabilities of 0.002 to 2 md.

Reservoir porosity is mainly a function of the degree of bioturbation i.e., the relative amounts of gray and tan dolomite, and the extent of poikilotopic anhydrite cementation in tan dolomite areas. An inverse relationship exists between anhydrite content and porosity. Limited core data suggest a general increase in anhydrite and corresponding decrease in porosity in the northwestern (paleolandward) part of SCU. On a well-to-well scale anhydrite distribution is quite variable, however, and can be difficult to predict. Anhydrite dissolution may have been an important porosity-forming process in some of the more coarsely textured tan dolomites, and the lower-anhydrite content in the east and southeast parts of SCU may reflect increased anhydrite dissolution by basin-derived fluids (Ruppel and Bebout, 1995) and/or decreased anhydrite precipitation from platform-interior-derived fluids.

Reservoir permeability is a function of bioturbation and anhydrite content, as described above, and pore size. Pore size in the tan dolomite areas is largely related to the original depositional texture of the burrow-filling sediment and diagenesis. Very finely to finely crystalline tan dolopackstones, most likely reflecting dolomitization of muddy burrow-filling sediments, are characterized by very small intercrystalline pores and low permeabilities typically ranging from less than 1 md to 16 md. Finely to medium-crystalline tan dolograinstones and washed dolopackstones are characterized by larger intergranular pores and significantly better permeabilities varying from 100 to 500 md. Limited core data suggest burrow–filling sediments may be muddier in the more western (landward) parts of SCU resulting in more finely crystalline tan dolomites with smaller pore throats and lower permeabilities. Due to differences in pore size, tan dolomites with similar porosities may have markedly different permeabilities. As a result, more than one porosity/permeability transform is needed to represent the SCU reservoir interval.

In general, the vertically oriented, permeable, tan, dolomite burrow structures in the SCU reservoir interval provide favorable conditions for the application of a CO_2 flood using horizontal injection wells. Rare, areally extensive, relatively thin, sandy dolomite/dolomitic sandstone layers may, however, act as partial barriers to the vertical migration of reservoir fluids and gases. Thus, it is critical to understand the stratigraphic position of these rare low-permeability layers relative to that of the horizontal CO2 injection wells.

ACKNOWLEDGMENTS

The authors would like to thank Phillips Petroleum Company for permission to publish this paper. This work was supported in part by a grant from the Department of Energy, Class II Oil Program for the study of shallow-shelf carbonate reservoirs. Special thanks to Kelly Curtis and Kathy Smith, Phillips Petroleum Co., for preparing the figures and plates. X-ray diffraction analyses were conducted by Dave Cowan, PPCo., and mercury injection data were analyzed by James Howard, PPCo. The Unocal Moss Unit 16-14 core was viewed courtesy of the Texas Bureau of Economic Geology, Austin, Texas.

FIGURES

Figure 1. Paleogeographic map of the Permian Basin, western Texas and southeastern New Mexico, and Leonardian and Guadalupian stratigraphic column for this region. The paleogeographic map shows those San Andres and Grayburg fields which have produced over 10 MMBO. Named fields are referred to in the text. The square shaded area on the map is Ector Co., Texas. (modified from Bebout and Harris, 1986).

Figure 2. Top of Grayburg Formation structure map. South Cowden Unit is shaded. Fina Emmons Unit is section 8, blk. 42, immediately to the north of SCU. The remaining area to the north and northwest is the Unocal Moss Unit. Wells from which cores were studied are shown.

Figure 3. Production history of South Cowden Unit, Ector Co., Texas.

Figure 4. Wireline log/core graph of the Phillips Petroleum Co. SCU 8-19 well, Section 18, Block 42, T-3-S, T. and P. RR. Co. Survey, Ector Co., Texas.

Figure 5. Core photographs of Grayburg and Queen lithofacies, South Cowden Unit. (A) Fusulinid dolowackestone with moldic porosity (SCU 8-19, core unit 5). (B) Sandy dolopackstone with common stylolites (SCU 8-19, core unit 15). (C and D) Burrow-mottled dolopackstone lithofacies showing characteristic, vertically oriented gray/tan mottling. Tan areas are oil stained and have significantly better porosity and permeability than adjacent gray dolomite areas (SCU 8-19, core units 14A and 16). (E) Fenestral dolopackstone lithofacies displaying inclined bedding typical of teepee structures. The large, anhydrite-cemented dessication structure (layer) in the upper part of the slab contains internal sediment visible along the right side of the core (SCU 8-19, unit 29).

Figure 6. Thin section photomicrographs of the Grayburg Formation, South Cowden Unit. (A) Moldic and intercrystalline porosity characteristic of the fusulinid dolowackestone lithofacies. Large molds are leached fusulinids (SCU 8-19, core unit 5, 30X). (B) Ooid peloid dolograinstone lithofacies displaying good intergranular porosity (SCU 8-19, core unit 9, 30X). (C-E) Sandy dolostone (C and D) and dolomitic sandstone (E) of the sandy dolopackstone lithofacies. Siliciclastics are very fine-sand. Fine- to medium-sand-size peloids of uncertain affinity are shown in photo C. Photo D shows a coarse-sand-size coated grain (grapestone). Pores in the photo C sample are intercrystallline, moldic (leached carbonate grains), and leached feldspars (C--SCU 8-19, core unit 10E, 30X; D--SCU 8-19, core unit 12A, 30X; E--SCU 8-19, core unit 15, 30X). All scale bars are 0.5 mm in length.

Figure 7. Thin section photomicrographs of the Queen and Grayburg Formations, South Cowden Unit. (A) Sandy dolopackstone lithofacies of the Queen Formation displaying common medium-sand-size ooids and abundant very fine-grained siliciclastic sand (SCU 8-19, core unit 26, 30X). (B) Gray dolomite of the burrow-mottled dolopackstone lithofacies. This sample displays moldic porosity and at left center an echinoderm fragment (SCU 8-19, core unit 14C, 30X). (C-D) Porous, category I tan dolomite of the burrow-mottled dolopackstone lithofacies. Porosity is mainly intergranular (C--SCU 8-19, core unit 14C, 30X; D--SCU 8-19, core unit 16, 80X). All scale bars are 0.5 mm in length.

Figure 8. Thin section photomicrographs of the burrow-mottled dolopackstone lithofacies, Grayburg Formation, South Cowden Unit. (A) Finely to medium crystalline, category I tan dolomite with 20% porosity and 190 md permeability. This sample appears to be a peloid dolograinstone or washed dolopackstone (SCU 6-23, 80X). (B) Very finely crystalline, category III tan dolomite, peloid dolopackstone, with 19% porosity and 4 md permeability (SCU 7-10, 80X). This sample and the photo A sample have similar porosities but markedly different permeabilities. (C) Category I tan dolomite with 23% porosity and 137 md permeability. The right half of the photomicrograph shows an area cemented by anhydrite. The left half of the photo shows an area where anhydrite cement was not precipitated or was precipitated and subsequently leached (SCU 8-19, core unit 14C, 80X). (D) Category II tan dolomite with 16% porosity and 6.9 md permeability. Anhydrite replaces dolomite and cements porosity. Anhydrite dissolution would create pores markedly larger than those characterizing this sample (SCU 8-11, 80X). All scale bars are 0.5 mm in length.

Figure 9. Crossplot of porosity and permeability data for gray and tan dolomites of the burrow-mottled dolopackstone lithofacies, SCU 8-19, 7-10, 6-23, and 8-11 cores.

Figure 10. Crossplot of porosity and permeability data for tan dolomites of the burrow-mottled dolopackstone lithofacies showing variations in permeabilities associated with tan dolomites of Categories I, II, and III.

Figure 11. Crossplot of whole-core analysis porosity and permeability data from rocks of the burrow-mottled dolopackstone lithofacies, SCU 7-10, 6-23, and Fina Emmons Unit 135.

REFERENCES CITED

Bebout, D. G.; Lucia, F. J.; Hocott, C. R.; Fogg, G. E.; and Vander Stoep, G. W., 1987, Characterization of the Grayburg Reservoir, University Lands Dune Field, Crane County, Texas: University Texas, Austin, Bureau of Economic Geology, Report of Investigations No. 168, 98 p.

Fischer, A. G.; and Sarntheim, M., 1988, Airborne silts and dune-derived sands in the Permian of the Delaware Basin: Journal of Sedimentary Petrology, v. 58, p. 637-643.

Fogg, G. E.; and Lucia, F. J., 1990, Reservoir modeling of restricted platform carbonates: geologic/geostatistical characterization of interwell-scale reservoir heterogeneity, Dune field, Crane County, Texas: Univ. Texas, Austin, Bureau of Economic Geology, Report of Investigations No. 190, 66p.

Galloway, W. E.; Ewing, T. E.; Garrett, C. M.; Tyler, N.; and Bebout, D. G., 1983, Atlas of major Texas oil reservoirs: University Texas, Austin, Bureau of Economic Geology, 139 p.

Garber, R. A.; and Harris, P. M., 1990, Depositional facies of Grayburg/San Andres dolostone reservoirs, Central Basin Platform, Permian Basin, in Bebout D. G. and Harris P. M. (eds.), Geologic and engineering approaches in evaluation of San Andres/Grayburg.

Harpole, K. J.; Gerard, M. G.; Snow, S. C.; and Caldwell, C. D., 1996, Use of production and well test data with predictive history matching to improve reservoir characterization for CO_2 flooding at the South Cowden Unit: Society of Petroleum Engineers Paper 35226, presented at 1996 Permian Basin Oil and Gas Recovery Conference, p. 633-641.

Kerans, C.; Lucia, F. J.; and Senger, R. K., 1994, Integrated characterization of carbonate ramp reservoirs using Permian San Andres Formation outcrop analogs: American Association of Petroleum Geologists Bulletin, v. 78, no. 2, p. 181-216.

, 1995, Use of one- and two-dimensional cycle analysis in establishing high-frequency sequence frameworks, in Read, J. F.; Kerans, C.; and Weber, L. J. (eds.), Milankovitch sea-level changes, cycles, and reservoirs on carbonate platforms in greenhouse and ice-house worlds: Society of Economic Paleontologists and Mineralogists, Short Course No. 35, Part 2, p. 1-20.

Leary, D. A.; and Vogt, J. N., 1986, Diagenesis of the Permian (Guadalupian) San Andres Formation, Central Basin Platform, West Texas in Bebout, D. G.; and Harris, P. M. (eds.), Hydrocarbon reservoir studies San Andres/Grayburg Formations, Permian Basin: Permian Basin Section— Society of Economic Paleontologists and Mineralogists Pub. No. 86-26.

; and Vogt, J. N., 1990, Diagenesis of the San Andres Formation (Guadalupian), Central Basin Platform, in Bebout, D. G.; and Harris, P. M. (eds.), Geologic and engineering approaches in evaluation of San Andres/Grayburg hydrocarbon reservoirs - Permian basin: University Texas, Austin, Bureau of Economic Geology, p. 21-48.

Longacre, S. A., 1980, Dolomite reservoirs from Permian biomicrites, in Halley, R. B.; and Loucks, R. G. (eds.), Carbonate reservoir rocks: Society of Economic Paleontologists and Mineralogists, Core Workshop No. 1, p. 105-117.

Major, R. P.; Vander Stoep, G. W.; and Holtz, M. H., 1990, Delineation of unrecovered mobile oil in a mature dolomite reservoir: East Penwell San Andres Unit, University Lands, West Texas: University Texas, Austin, Bureau of Economic Geology, Report of Investigations No. 194, 51 p.

Mitchum, R. M., Jr.; and Van Wagoner, J. C., 1991, High-frequency sequences and their stacking patterns: Sequence-stratigraphic evidence of high-frequency eustatic cycles, in Biddle, K. T.; and Schlager, W. (eds.), The record of sea-level fluctuations: Sedimentary Geology, v. 70, p. 131-160.

Siemers, W. T.; Prezbindowski, D. R.; Skinnider, V. L.; Maple, L. C.; Gerard, M. G.; Nagaty, M. E.; and Howard, J. J., 1995, Multidisciplinary study to optimize reservoir management of the North Penwell (San Andres) Unit, Ector County, Texas: American Association of Petroleum Geologists Bulletin, v. 79, no. 9, p. 1407.

Sonnenfeld, M. D., 1991, High frequency cyclicity within shelf margin and slope strata of the upper San Andres sequence, Last Chance Canyon, in Meader-Roberts, S.; Candelaria, M. P.; and Moore, G. E. (eds.), Sequence stratigraphy, facies, and reservoir geometries of the San Andres, Grayburg, and Queen Formations, Guadalupe Mountains, New Mexico and Texas: Permian Basin Section, Society Economic Paleontologists and Mineralogists Publication 91-32, p. 11-51.

Ruppel, S. C.; and H. S. Cander, 1988, Effects of facies and diagenesis on reservoir heterogeneity: Emma San Andres Field, West Texas: University Texas, Austin, Bureau of Economic Geology, Report of Investigations No. 178, 67 p.

; and Bebout, D. G., 1995, Effects of stratal architecture and diagenesis on reservoir development in the Grayburg Formation, South Cowden field, Ector County Texas: University Texas, Austin, Bureau of Economic Geology, Technical Report.

Tyler, N.; Galloway, W. E.; Garrett, C. M.; and Ewing, T. E., 1984, Oil accumulation, production characteristics, and targets for additional recovery in major oil reservoirs of Texas: University of Texas, Austin, Bureau of Economic Geology Geological Circular 84-2, 31 p.

; Bebout, D. G.; Garrett, C. M., Jr.; Guevara, E. H.; Hocott, C. R.; Holtz, M. H.; Hovorka,

S. D.; Kerans, C.; Lucia, F. J.; Major, R. P.; Ruppel, S. C.; and Vander Stoep, G. W., 1991, Integrated characterization of Permian Basin reservoirs, University Lands, West Texas: targeting the remaining resource for advanced oil recovery: University Texas, Austin, Bureau of Economic Geology, Report of Investigations No. 203, 136 p.

Vail, P. R., 1987, Seismic stratigraphy interpretation procedure, in Bally, A. W. (ed.), Atlas of seismic stratigraphy, vol. 1: American Association of Petroleum Geologists Studies in Geology, no. 27, p. 1-10.

Van Wagoner, J. C.; Posamentier, H. W.; Mitchum, R. M., Jr.; Vail, P. R.; Sarg, J. F.; Loutit, T. S.; and Hardenbol, J., 1988, An overview of the fundamentals of sequence stratigraphy and key definitions, in Wilgns, C. K.; Hastings, B. S.; Kendall, C. G. St. C.; Posamentier, H. W.; Ross, C. A.; and Van Wagoner, J. C. (eds.), Sea-level changes: An integrated approach: Society of Economic Paleontologists and Mineralogists Special Publication No. 42, p. 39-46.

Walker, D. A.; Golonka, J.; Reid, A.; and Reid, S., 1995, The effects of paleolatitude and paleogeography on Late Paleozoic carbonate sedimentation in West Texas; Part II: Permian: West Texas Geological Society, vol. 34, no. 6, p. 5-15.

Ward, R. F.; Kendall, C. G. St. C.; and Harris, P. M., 1986, Upper Permian (Guadalupian) facies and their association with hydrocarbons - Permian Basin, West Texas and New Mexico: American Association of Petroleum Geologists Bulletin, v. 70, no. 3, p. 239-262.

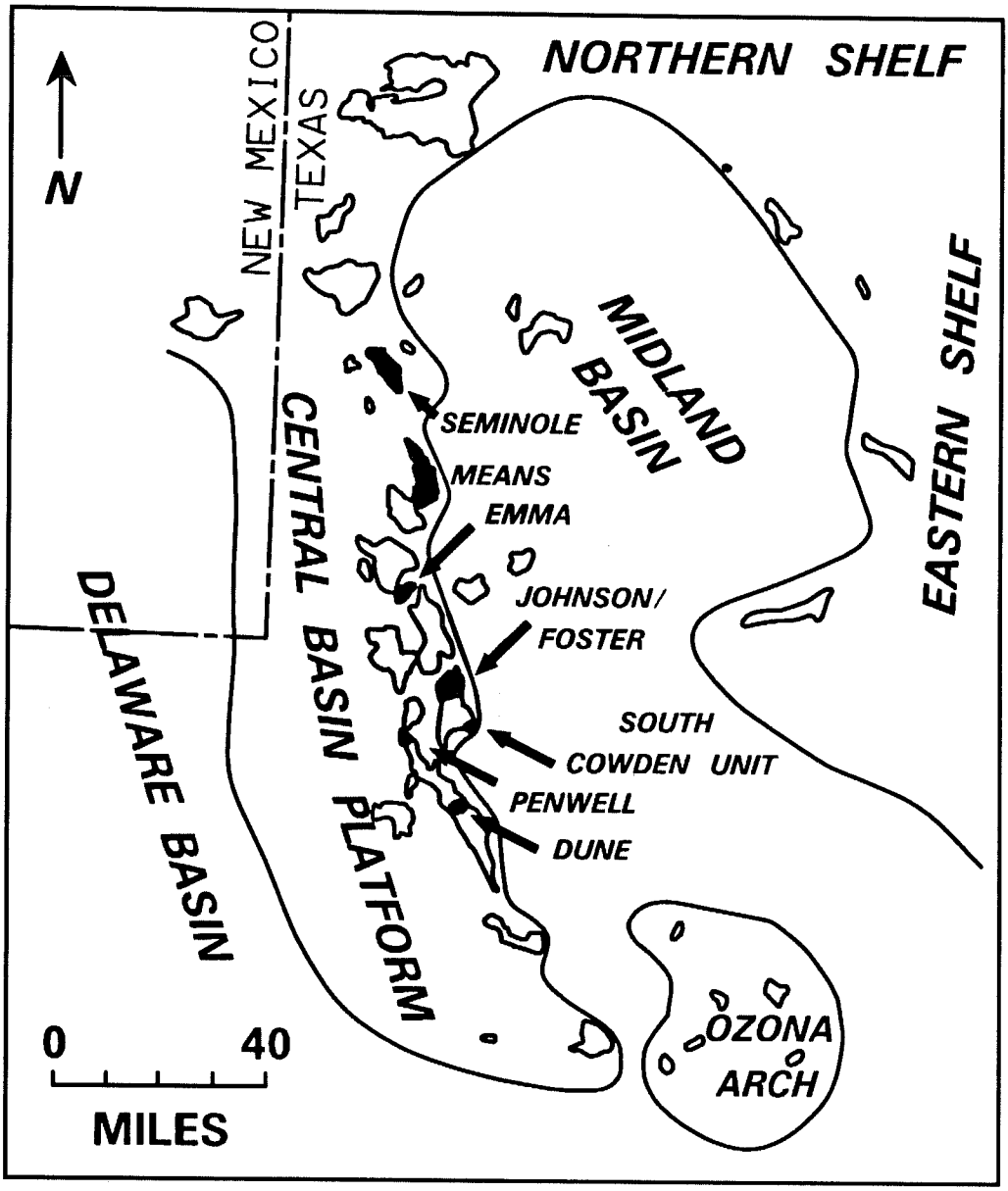

SYSTEM	SERIES	STRATIGRAPHIC UNIT
UPPER PERMIAN	GUADALUPIAN	CAPITAN FM. — TANSILL FM.
		CAPITAN FM. — YATES FM.
		CAPITAN FM. — SEVEN RIVERS FM.
		GOAT SEEP — QUEEN FM.
		GRAYBURG FM.
		SAN ANDRES FM.
LOWER PERMIAN	LEONARDIAN	GLORIETA FM.
		CLEAR FORK GP.

/ABC/CC091895A.DGN KRC

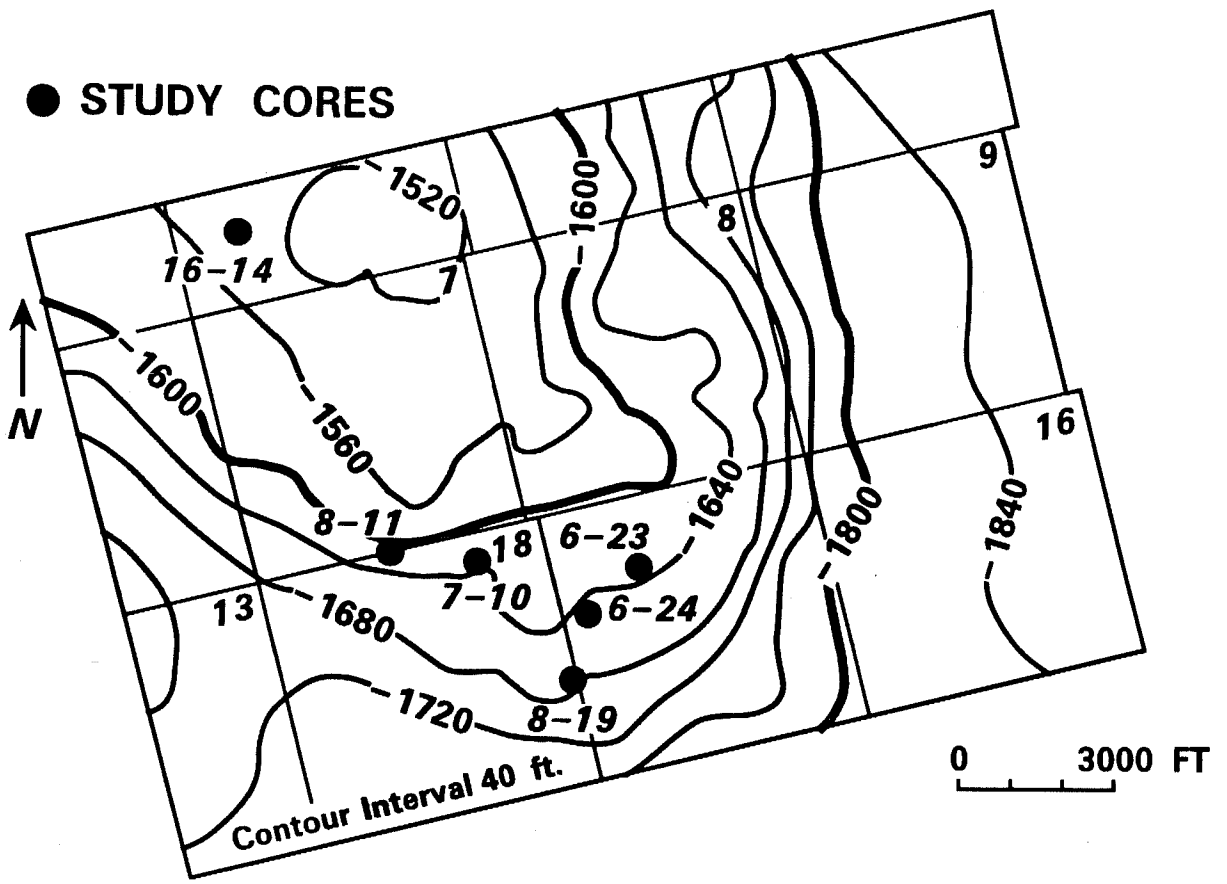

/ABC/CC091895A.DGN KRC

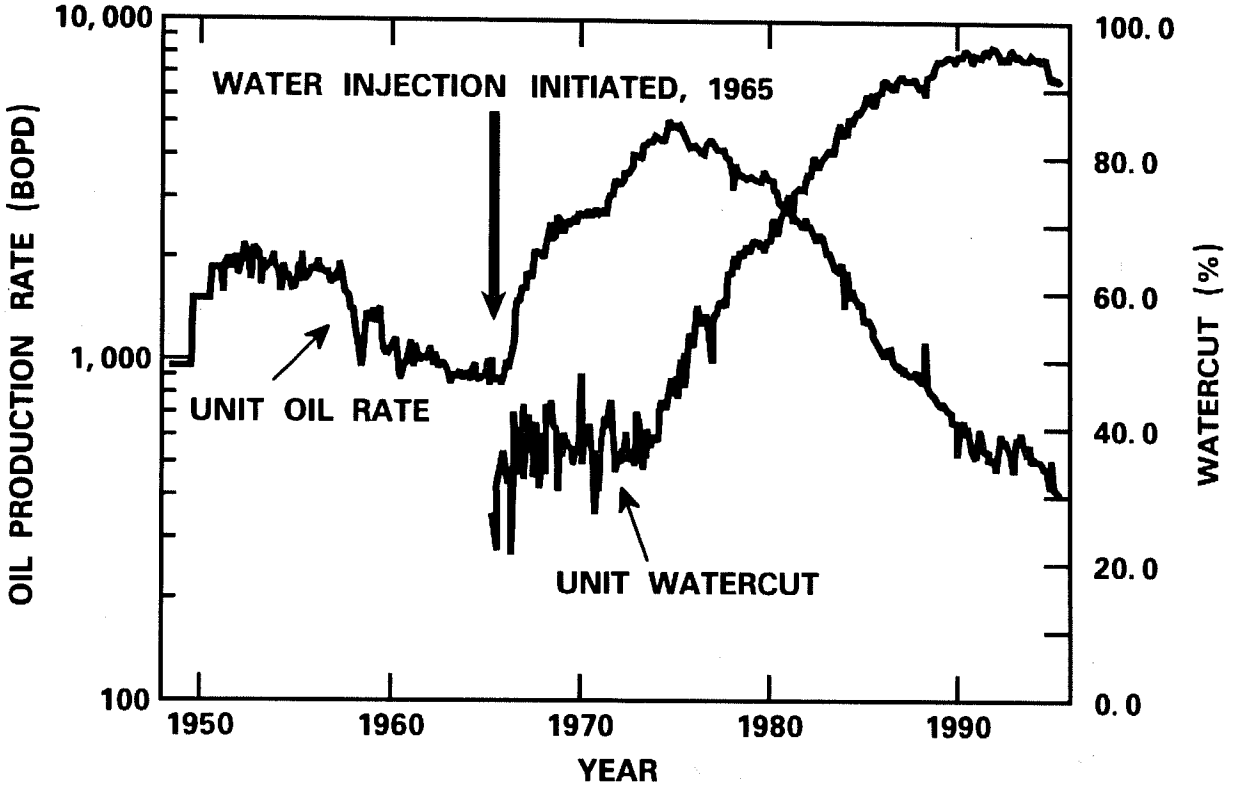

/ABC/CC091895A.DGN KRC

4908
S. COWDEN 8-19
A

S. COWDEN 8-19
4684
B

38A
S. COWDEN 8-19
4739
C

4664
D

4553

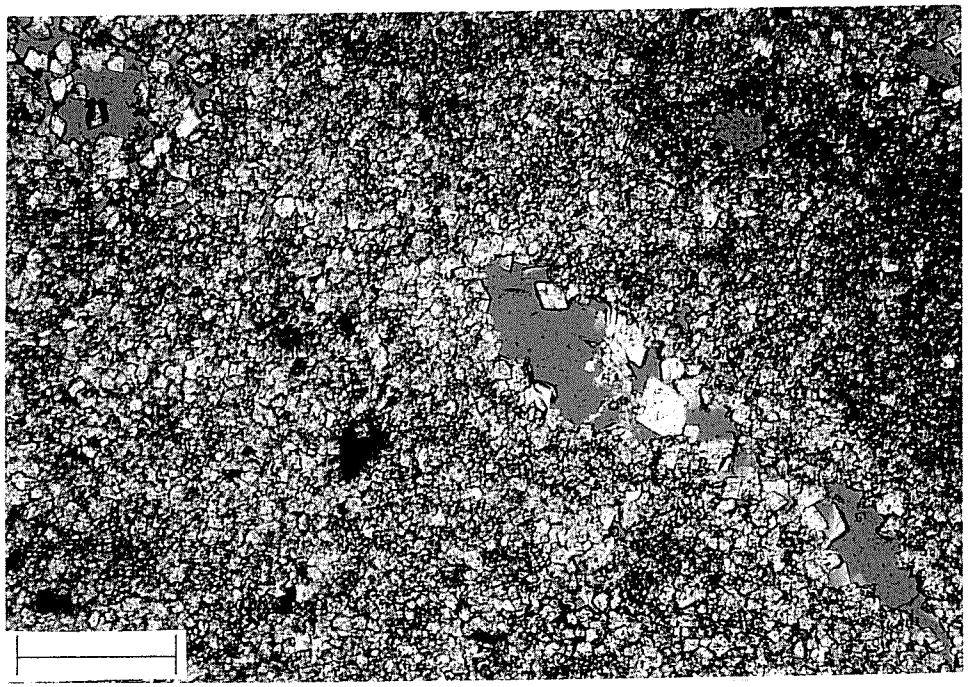

A

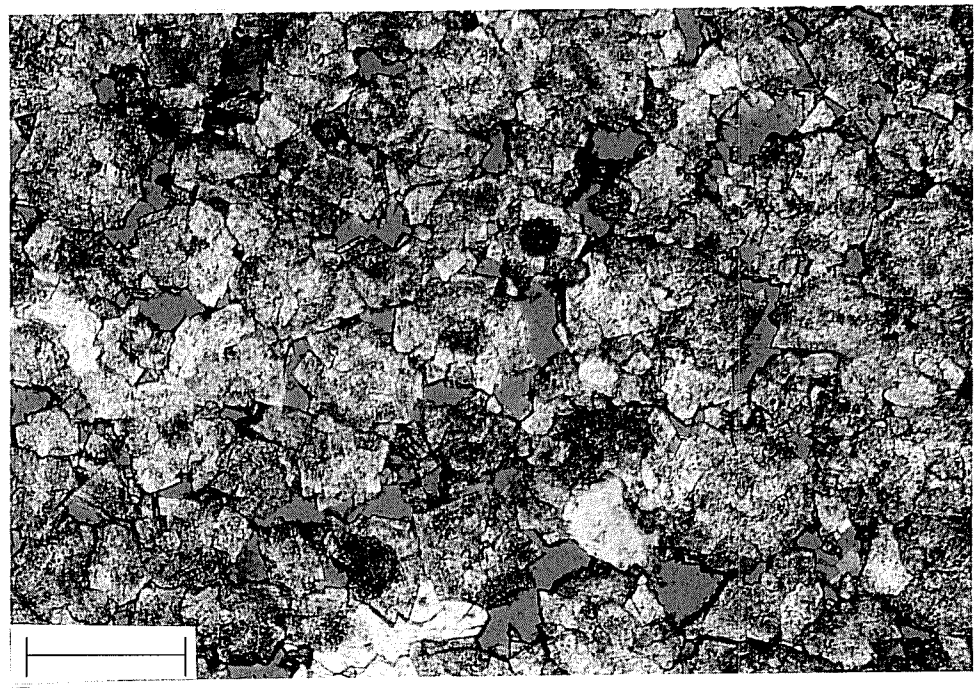

B

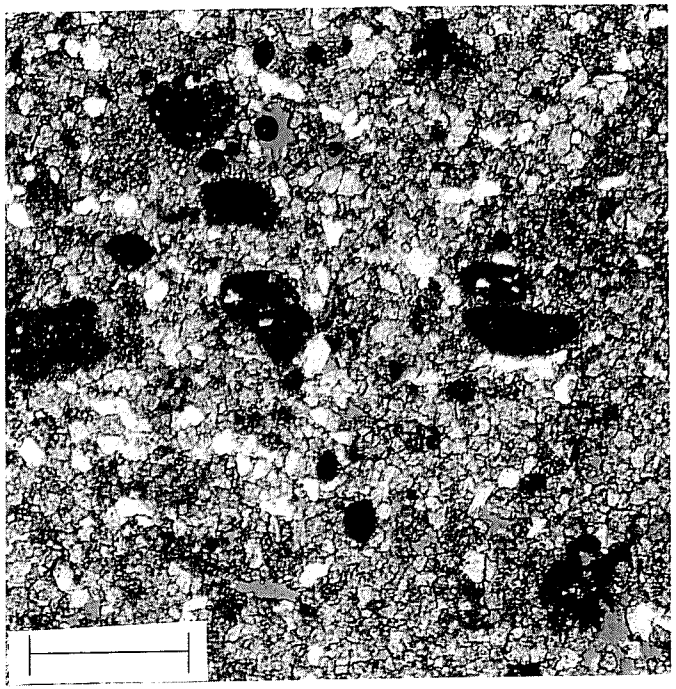

C

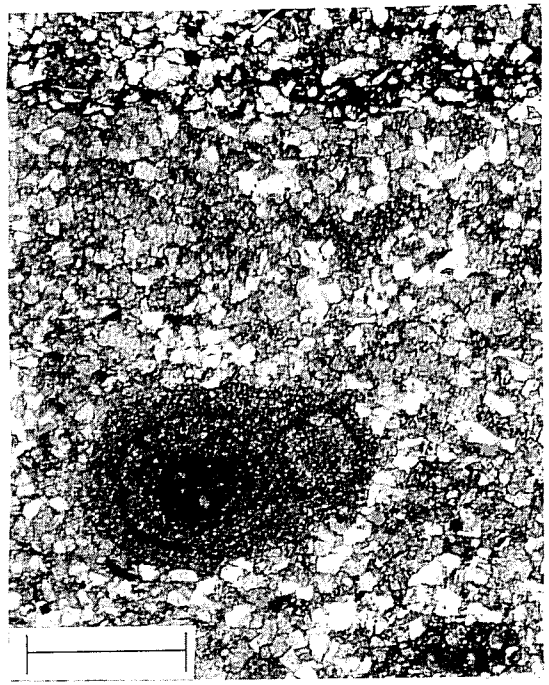

D

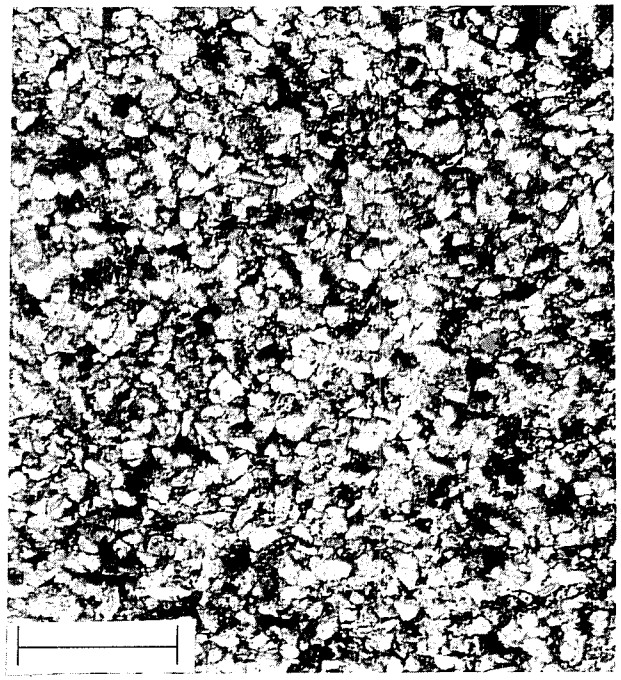

E

A
B
C
D

A
B
C
D

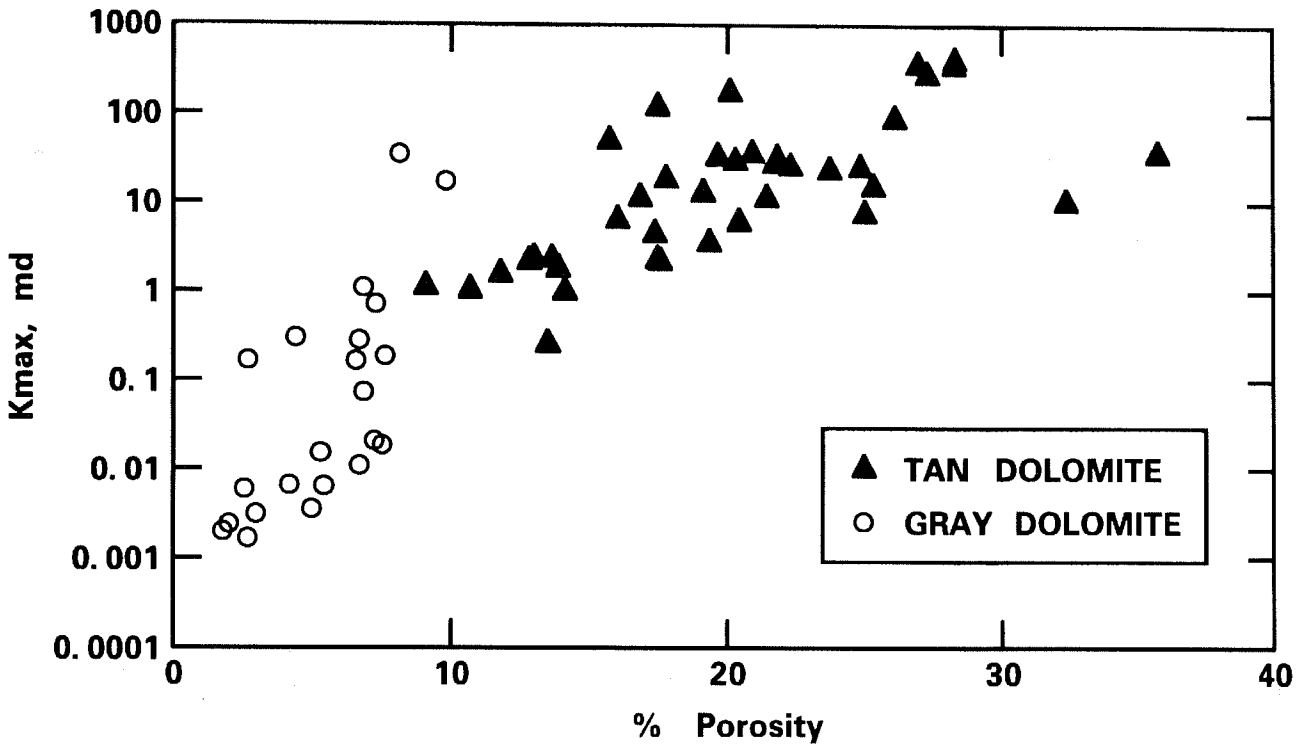

/ABC/CC091895A.DGN KRC

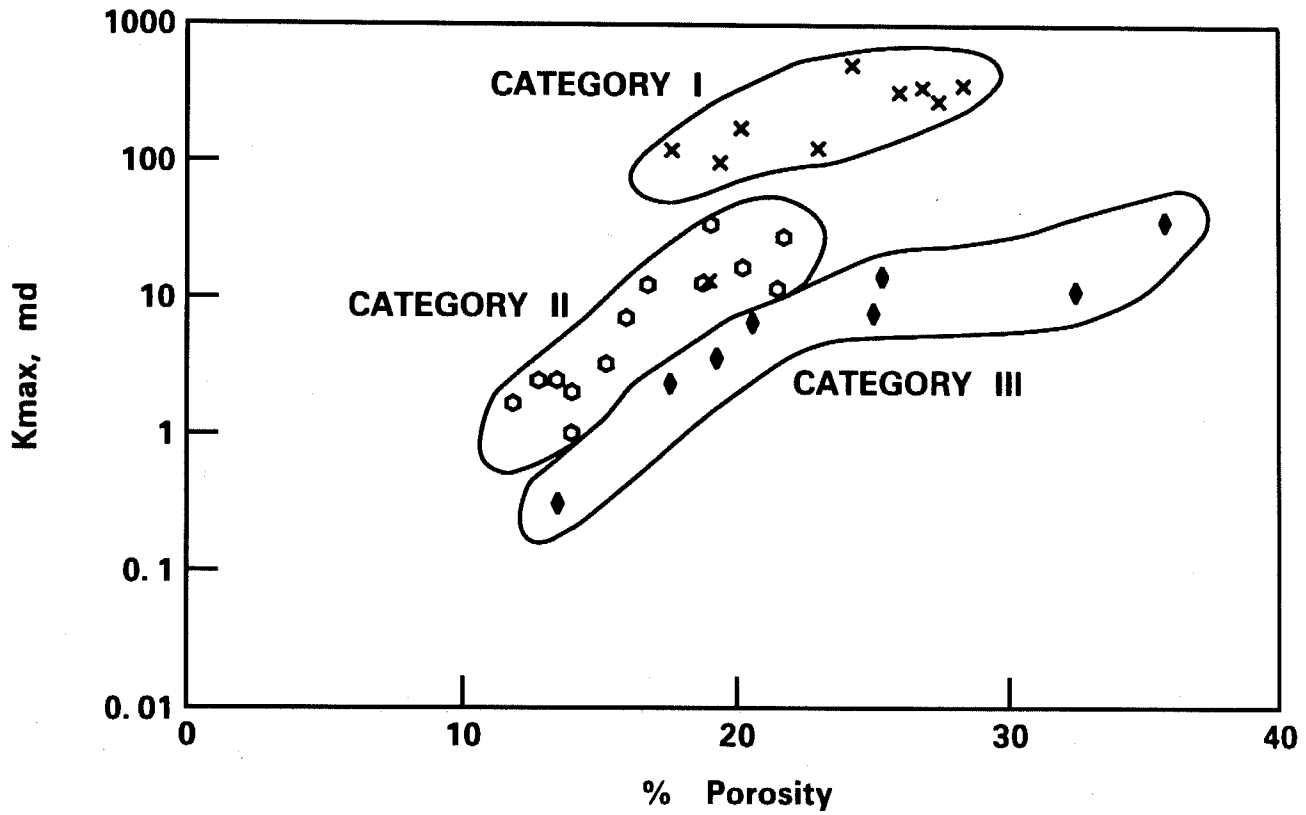

CC012098A /ABC/CC012098.DGN KRC

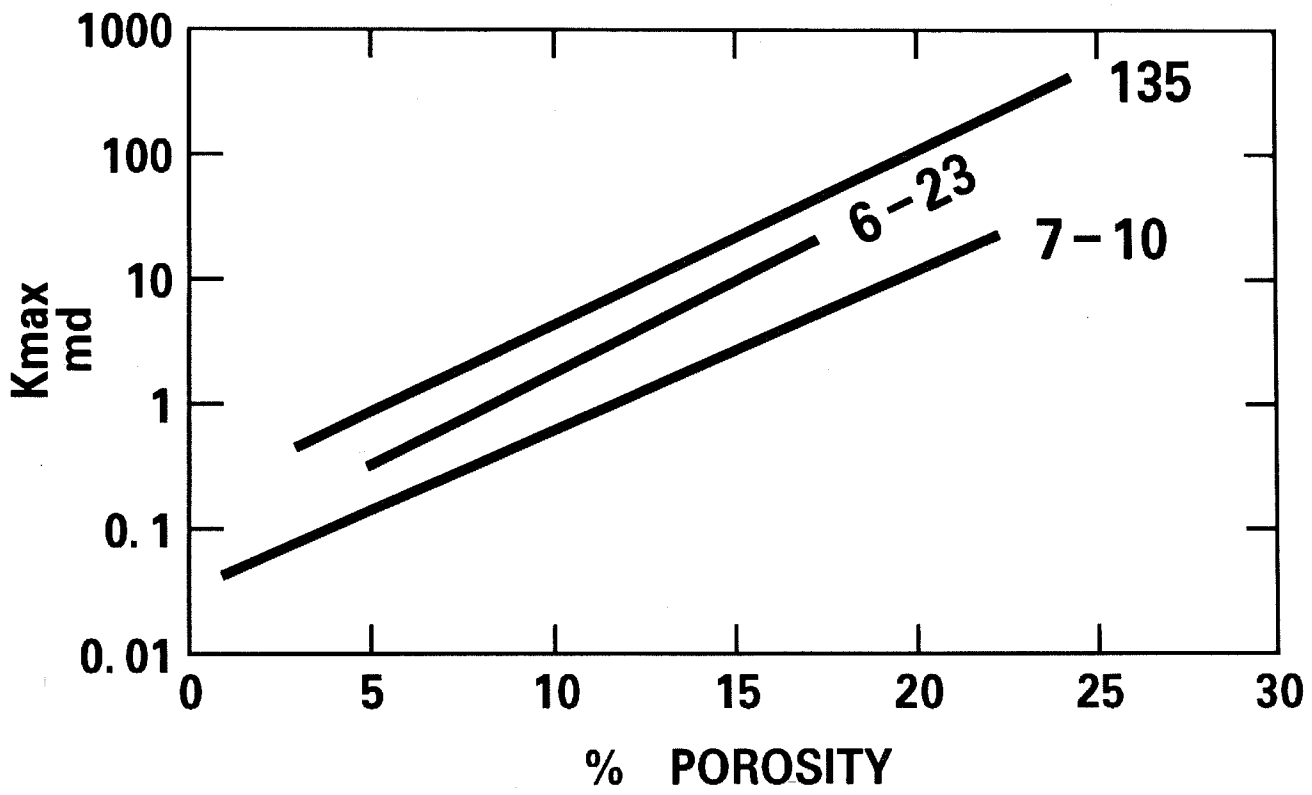

/ABC/CC091895A.DGN KRC

WELL	AVERAGE POROSITY TAN DOLO. (Core Analysis)	PERCENT ANHYDRITE TAN DOLO. (Thin Section)
6-23	21.0%	1.0%
7-10	21.0%	5.5%
8-19	24.0%	1.0%
6-24	N.A.	10.7%
8-11	14.5%	11.5%
16-14	~ 5.5-7%	15.5%

Table I. Average porosity and anhydrite content of tan dolomites, burrow-mottled dolopackstone lithofacies, by well.

/ABC/CC091895A.DGN KRC

WELL	AVERAGE POROSITY TAN DOLO.	AVERAGE PERMEABILITY TAN DOLO.	% SAMPLES TAN DOLO. CATEGORIES I	II	III
6-23	21.0%	90 md	50	30	20
7-10	21.0%	10 md	0	33	67
8-19	24.0%	175 md	83	17	0
8-11	14.5%	8 md	0	100	0

Table II. Average porosity and permeability of tan dolomites, burrow-mottled dolopackstone lithofacies, by well.

/ABC/CC091895A.DGN KRC

WELL	SAMPLE DEPTH (ft)	CORE POROSITY %	CORE PERMEABILITY (md)	PORE THROAT RADIUS*	TAN DOLO. CATEGORY
8-19	4709	26.1	338	6.80	I
	4723.6	26.7	374	6.03	I
	4724.3	19.4	100	6.80	I
	4736	24.3	514	8.50	I
7-10	4639.6	25.0	8.14	4.27	II
	4672	25.3	16.2	0.76	III
	4679	20.4	6.6	0.34	III
	4682.3	17.5	2.5	1.09	III
8-11	4613	21.6	29.1	1.69	II
	4670	16.8	12.3	0.43	II
6-23	4652.8	35.7	38.7	1.68	III
	4702.8	19.1	14	0.84	II
	4640.7	20.1	190	5.34	I

Table III. Porosities, permeabilities, and pore throat radii of tan dolomites (categories I, II, and III) of the burrow-mottled dolopackstone lithofacies (*James Howard, 1996, personal communication).

Attention Publisher – The following statement needs to be typed and placed at the top of this article, as it is copyrighted by SPE

"Copyright © The Society of Petroleum Engineers, 1997. Reprinted by permission. *Fracture Characterization Based on Oriented Horizontal Core From the Spraberry Trend Reservoir: A Case Study* – by Paul McDonald, John C. Lorenz, Charlie Sizemore, David S. Schechter, Tom Sheffield Originally presented at the 1997 SPE Annual Technical Conference and Exhibition in San Antonio, Texas, October 5-8, 1997.

Ω

SPE 38664

Fracture Characterization Based on Oriented Horizontal Core From the Spraberry Trend Reservoir: A Case Study

Paul McDonald, SPE, Parker & Parsley, John C. Lorenz, SPE, Sandia National Labs, Charlie Sizemore, SPE, Parker & Parsley, David S. Schechter, SPE, New Mexico PRRC, Tom Sheffield, SPE, Parker & Parsley

This paper was prepared for presentation at the 1997 SPE Annual Technical Conference and Exhibition held in San Antonio, Texas, 5–8 October 1997.

This paper was selected for presentation by an SPE Program Committee following review of information contained in an abstract submitted by the author(s). Contents of the paper, as presented, have not been reviewed by the Society of Petroleum Engineers and are subject to correction by the author(s). The material, as presented, does not necessarily reflect any position of the Society of Petroleum Engineers, its officers, or members. Papers presented at SPE meetings are subject to publication review by Editorial Committees of the Society of Petroleum Engineers. Electronic reproduction, distribution, or storage of any part of this paper for commercial purposes without the written consent of the Society of Petroleum Engineers is prohibited. Permission to reproduce in print is restricted to an abstract of not more than 300 words; illustrations may not be copied. The abstract must contain conspicuous acknowledgment of where and by whom the paper was presented. Write Librarian, SPE, P.O. Box 833836, Richardson, TX 75083-3836, U.S.A., fax 01-972-952-9435.

Abstract

As detailed fracture characterization of the Spraberry Trend continues, there exists an imbalance in the primary sources of fracture data. Measurements of spacing, density, permeability and orientation have traditionally been calculated or inferred from pulse and/or tracer type tests. To date, no direct measurement of Spraberry fracture properties from core in a horizontal plane are known. Approximately 400' of horizontal core was recently taken from the two main pay sections in the Upper Spraberry (1U and 5U) in Midland County, Texas. This paper will describe the acquisition, orientation, and subsequent analysis of the first ever horizontal core taken from the Spraberry Trend.

Introduction

Natural fractures existing over a regional area have long been known to dominate all aspects of performance in the Spraberry Trend Area[1]. However, there is little or no information on the actual fracture system other than: orientation, on a gross basis, from pulse and/or tracer tests in the 50's and 60's, and fracture spacing inferred from simulation and a few existing vertical cores. Previous descriptions and old core reports did not distinguish between natural and coring induced fractures, thus almost all information from the early years, when almost all Spraberry data was obtained, provides no detailed information on the natural fracture system. The first vertical core, taken as part of the current program in 1993 from the Shackelford Spraberry Unit #1-38A, intersected a vertical natural fracture with significant mineralization that had clearly grown into unoccupied space. This open, mineralized fracture was contained within a thin pay sand and was observed to terminate at a shale parting. This fracture was the first documented evidence of the existence of a mineralized natural fracture within the pay sand.

The orientation, containment within zone, degree of mineralization, fracture aperture and spacing are important questions when considering fluid flow in naturally fractured reservoirs. However, after considerable data gathering, it became apparent that only superficial characterization of the natural fracture system was available. Recent acquisition of the horizontal core has radically altered understanding of the natural fracture system in the Spraberry Trend Area. This well, the E.T. O' Daniel #28, was cored with the intent of intersecting natural fractures in the thin sand streaks where oil saturation is found in the Upper Spraberry. Over 100 natural fractures were intersected exhibiting an intriguing and diverse array of fracturing behavior.

Geology

The Spraberry formation was deposited during the Permian age within the Leonardian system in the Midland Basin, a part of the province known as the Permian Basin of West Texas and Southeast New Mexico. The depositional environment consisted of a combination of turbidity and density currents sourced from the northwestern shelf area. The Spraberry formation facies can be characterized as submarine fan and basin plane deposits and consists of very fine grained sandstones to coarse grained siltstones and mudstones. The various fan complexes can be traced to the north in Dawson and Lynn counties and are considered the source material for the fan lobe sequences within the area of study in eastern Midland County.

Since its discovery, the Spraberry has been subdivided into three principal intervals, the lower, middle and upper Spraberry formations. In the late 1980's, Tyler and Gholston further subdivided the Spraberry intervals to represent distinct episodes, or operational units, within each of the submarine fan complexes (Figure 1)[2]. Six of these operational units were found in the Upper Spraberry and two in the Lower Spraberry. Only two of the six operational units in the Upper Spraberry (1U and 5U) have been identified as containing reservoir quality rock capable of making significant production contributions.

The proposed target of the horizontal core was the natural fractures within the main pay intervals of the 1U and 5U sands. Net pay within each of these zones averages between 8 and 14 ft.

the hole to the KOP. Circulation was established with a fluid rate of 50 gallons per minute (gpm) and an air rate of 150 gallons per minute equivalent (gpm eq.) at the motor. The build section was drilled on an azimuth of 167 degrees from 6,838 ft. measured depth (MD) to 7,488 ft. MD resulting in a radius of curvature of 414 ft. with a DLS of 13.85 degrees/100 ft.

Upper Spraberry 5U Coring Summary. The first coring assembly was made up on the surface and run in the hole to the KOP. Circulation was established with the foamed air/brine mixture, the assembly was run to bottom, and coring operations were initiated.

The Upper Spraberry 5U sand was cored and drilled from 7,488 ft. MD to 7,931 ft. MD for a total of 443 ft. with a net core recovery of 169 ft. (Figure 3). Core run #1 resulted in zero recovery and an extremely low ROP of 35.3 min./ft. The bit design was changed from a standard diamond core bit to a 6-1/8" X 2-5/8" PDC design, increasing ROP tremendously. Core runs #2 and #3 resulted in 58 ft. of core recovery. Core run #4 was successful but the core was lost when the core catcher assembly failed at the surface during breakdown procedures. The catcher design was changed from a single slip dog catcher to a triple assembly consisting of a slip dog catcher, a basket catcher, and a split ring catcher. Core run #5 resulted in a 20 ft. recovery. Determining that the catcher assembly was too conservative, the basket catcher was dropped for subsequent core runs. Core run #6 resulted in only 6 in. of recovery due to rubble in the hole. After a clean up run, core runs #7 - #9 resulted in 89.5 ft. of recovery which terminated coring operations in the 5U.

Upper Spraberry 1U Casing Exit and Curve Summary. A 7-5/8" retrievable bridge plug (RBP) was run in the hole via electric wireline to a depth of 6,750 ft. but set unsuccessfully. The plug and setting tool were removed from the hole and a second plug was successfully set at 6,750 ft. with two sacks of sand on top of the plug. A 30 ft. section of the 7-5/8" casing from 6,609 ft. to 6,639 ft. was milled out using a 7-5/8" section mill. A caliper log was then run across the milled interval to verify the actual amount of casing removed. For the cement kick off plug, a slurry of class "C" w/1% $CaCl_2$ was pumped and allowed to set for 24 hours to attain sufficient compressive strength for kick off. The plug was then tagged with the drill string to locate the top of cement. Upon tagging the plug, the top was found below the proposed KOP, necessitating pumping a second plug. After another 24 hour curing period, the plug was tagged and dressed off to the KOP of 6,612 ft.

The curve build BHA was made up on the surface and run in the hole to the KOP. Circulation was established with a fluid rate of 50 gpm and an air rate of 140 gpm eq. at the motor. The build section was drilled on an azimuth of 157.7 degrees from 6,612 ft. MD to 7,330 ft. MD resulting in a radius of curvature of 457 ft. with a DLS of 12.53°/100 ft.

Upper Spraberry 1U Coring Summary. The coring assembly consisting of a 6-1/8" X 2-5/8" PDC bit, scribe shoe with slip dog and split ring catchers, 6-1/8" X 2-5/8" X 30' core barrel with aluminum inner barrel, 4-3/4" monel drill collar with EMS survey tool, 4-3/4" monel collar, and crossover sub was made up and run in the hole on 3-1/2" IF drill pipe to the KOP. Circulation was established with the foamed air/brine mixture, the assembly was run to bottom, and coring operations were initiated.

The Upper Spraberry 1U sand was cored and drilled from 7,330 ft. MD to 7,727 ft. MD for a total of 397 ft. with a net core recovery of 226 ft. (Figure 3). Core runs #1 and #2 resulted in net core recovery of 62 ft. Core run #3 resulted in net recovery of 8 ft. before the core barrel jammed with black shale, indicating that the well path was out of zone. After a clean out and TVD correction run, core runs #4 - #8 resulted in a net recovery of 153 ft. Core run #9 resulted in a net recovery of 3 ft. before the barrel jammed and coring operations were terminated.

Fracture Characterization[3]

Three distinct fracture sets, trending NNE, NE, and ENE, are present in cores from the 1U and 5U reservoirs. NE fractures are commonly mineralized with barite and are found only in the 1U reservoir. Unmineralized NNE and ENE fractures occur in the 5U reservoir. Unmineralized ENE fractures are also more widely distributed within the black shales overlying both the 1U and 5U reservoirs, and locally near the top of the 1U unit. However, no fractures are present in the black shales underlying either reservoir. Each fracture set has its own characteristic and distinct patterns of 1) spacing, 2) mineralization, 3) distribution with respect to lithology, 4) surface characteristics, and 5) distribution of strikes. Therefore each fracture set is most likely to have resulted from a separate stress event. Aspects of these fractures that are important to production are as follows: 1) fracture strikes are segregated by reservoir unit 2) NE fractures are typically partially mineralized, but mineralization is absent in this set at the base of the 1U reservoir 3) none of the NNE or ENE fractures are mineralized 4) no fractures are present in the shales underlying both reservoirs, but ENE fractures occur in shales overlying both reservoirs.

Orientation. Three distinct natural fracture orientations are present in these horizontal cores, trending approximately NNE, NE, and ENE (Table 1).

Although the total range of strikes for each fracture set is about 25 degrees, the distribution of those strikes varies by set (Figures 4 and 5). Most of the NE fractures occur within a narrow range (5 degrees) of distribution while most of the ENE fractures fall within a somewhat broader (20 degree) distribution of strikes. The ENE fracture strikes are relatively scattered within the total range of nearly 30 degrees.

Stratigraphic and Lithologic Controls. All 28 NNE fractures occur within the 5U reservoir, while the entire set of 46 NE-striking fractures is contained within the 1U reservoir.

intermediate relative age, and the NNE fractures youngest. If the stress orientations have not changed since the formation of the youngest fractures, the maximum horizontal in situ compressive stress should then, theoretically, parallel the youngest fracture set. While this interpretation seems uncomfortably complex for this deep basin area of minimal structure, it would seem to best explain the data as presently understood.

Correlation of Core Fractures to Wellbore Image Log. A wellbore image log was run in the horizontal hole along the upper 1U interval. Although the images seem to be of good quality, there is an unsettling ambiguity in the correlation of log and core fractures (Figure 7).

In order to analyze this ambiguity, a six inch tolerance was used (i.e., an imaged fracture is assumed to correlate to a fracture in core if it is within plus or minus six inches of the measured core depth), and only the intervals where both core and log data are available were considered. In this interval, there are 24 fractures in core that have no correlative fractures at the equivalent depth in the image log, and 36 fractures in the image log that have no equivalents in the core. A maximum of only 15 fractures are definitively present in both the core and the image log, no matter what depth shifts are applied. Fracture swarms and isolated fractures in core, which should have made easily recognizable patterns in the image log and thus provided good core-log tie points, have not left similarly-obvious patterns on the image log.

Nevertheless, the overall fracture strike trend indicated by the image log is nearly aligned with the average of the fracture orientations measured in core. The secondary trend of ENE fractures in the core is also present in the image log, within the approximately correct measured-depth intervals.

The reasons for agreement in strike without a one-to-one correlation of individual fractures are unclear. Stretch during conveyance of the imaging tool and the common depth ambiguity of cores make exact depth determinations difficult and may explain some of the discrepancy. However these factors can not account for the significant over count of fractures (133%) made by the image log relative to the natural fractures in core. It has been suggested that the log is seeing fractures that were missed by the naked eye during minute core examination (unlikely, and which moreover would be insignificant to production if present). However, the images on the log do not indicate that any of the fracture apertures are significantly less than others. Coring induced fractures that formed in the wellbore but not in the core might also explain the apparent over count, but with the present images it is not possible to distinguish these from natural fractures. Moreover, this would not account for the mineralized fractures that are present in the core but not apparent in the image log.

In general, the patterns of fracture positions and the numbers of fractures in the core and image log are not compatible, although the average fracture strikes are. This suggests that image logs should be calibrated with core wherever possible.

Conclusion

Acquisition of this core unequivocally documents numerous, closely spaced natural fractures in the reservoirs of the Spraberry formation and led to the following major conclusions: 1) Acquisition and orientation of the horizontal core was a mechanical success. Drilling procedures, in fact, proved to be not unlike that of coring a vertical well. 2) Three distinct fracture sets, trending NNE, NE, and ENE, are present in the cores from the 1U and 5U reservoirs. NE fractures are commonly mineralized with barite and are found only in the 1U reservoir. Unmineralized NNE and ENE fractures occur in the 5U reservoir. 3) Each fracture set has its distinct pattern of spacing, mineralization, distribution with respect to lithology, surface characteristics and distribution of strikes. Therefore each fracture set is most likely to have resulted from a separate stress event. 4) There was an unsettling ambiguity in the correlation of the fractures found in the core and the fractures found on the well bore image log. Orientation of the fracture sets from the core and logs were similar, however, there was a significant over count (133%) of fractures made by the image log relative to the natural fractures in the core.

Acknowledgments

This work was performed under DOE Contract No. DE-FC22-95BC14942. The authors of this paper would like to acknowledge Lynn Clayton and Charles Troxell for the excellent field work done during the course of this project. Doug Jeffers with Scientific Drilling was instrumental in providing the expertise for the orientation assembly. Lastly, the authors would like to thank John Sabby for his excellent work on the Midkiff Unit.

References

1. Schechter, D.S.: "Advanced Reservoir Characterization and Evaluation of CO_2 Gravity Drainage in the Naturally Fractured Spraberry Trend Area," First Annual Technical Progress Report, Contract No. DE-FC22-95BC14942, U.S. DOE (Dec 1996).
2. Tyler, N., and Gholston, J.C.: "Heterogeneous Deep-Sea Fan Reservoir, Shackelford and Preston Waterflood Units, Spraberry Trend, West Texas," Report of Investigation No. 171, Bureau of Economic Geology, The University of Texas, Austin, 1988.
3. Lorenz, John: "Summary of Observations and Interim Interpretations: Fractures in Horizontal Spraberry Cores, E.T. O'Daniel Well #28", Internal Memo to Project Team, December 12, 1996.

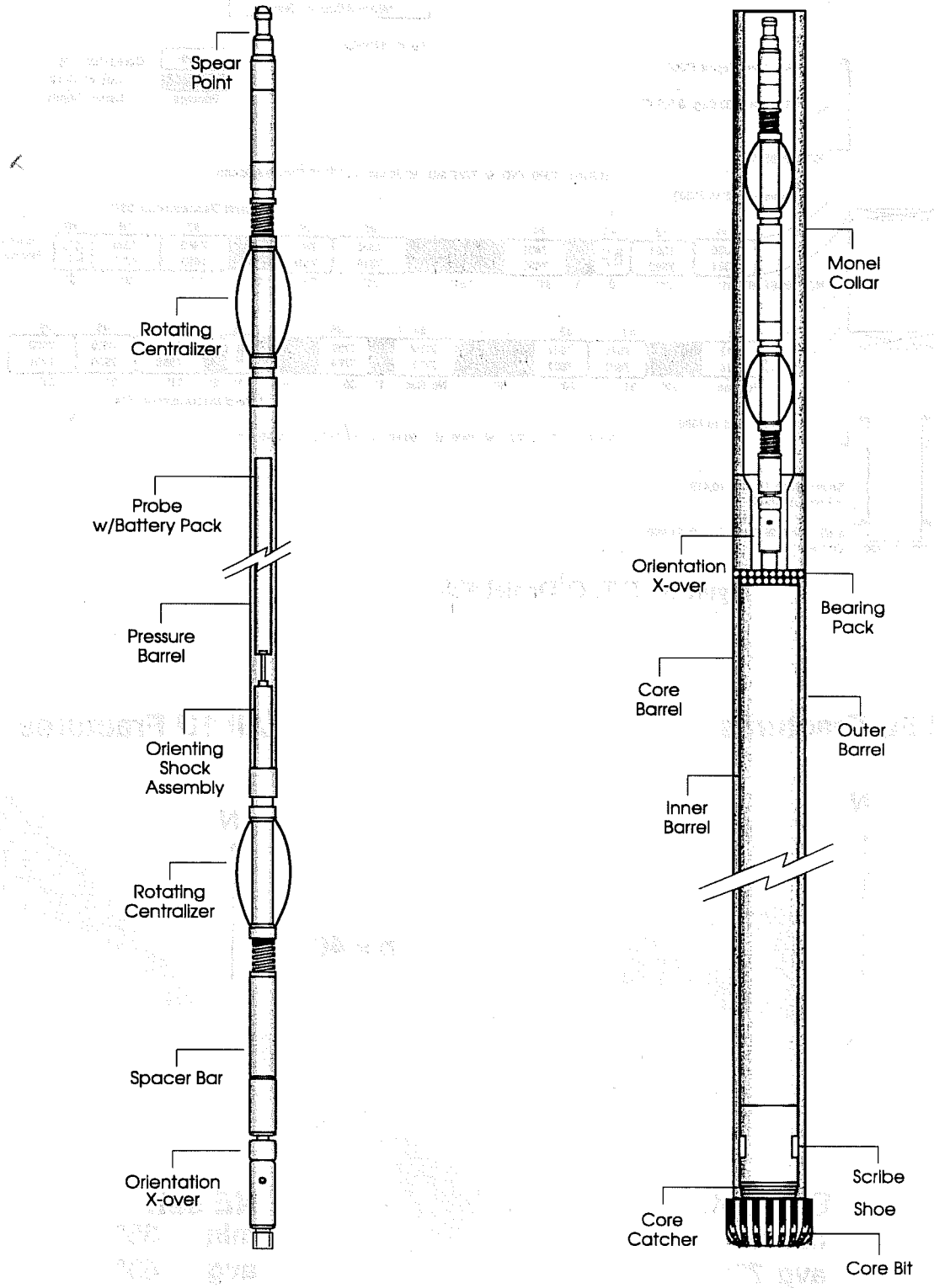

Figure 2 - Bottom Hole Coring and Orientation Assembly

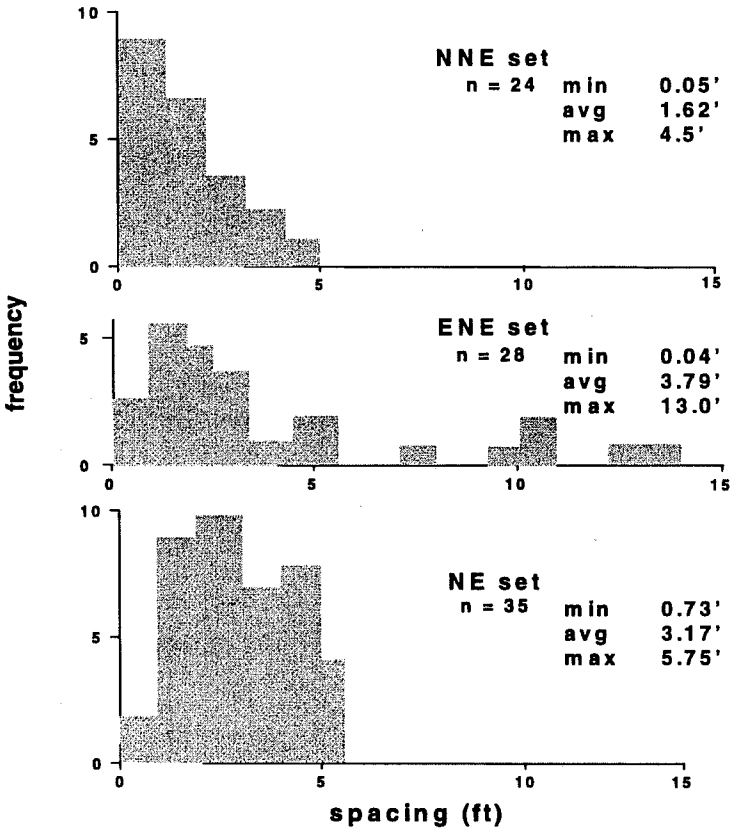

Figure 6

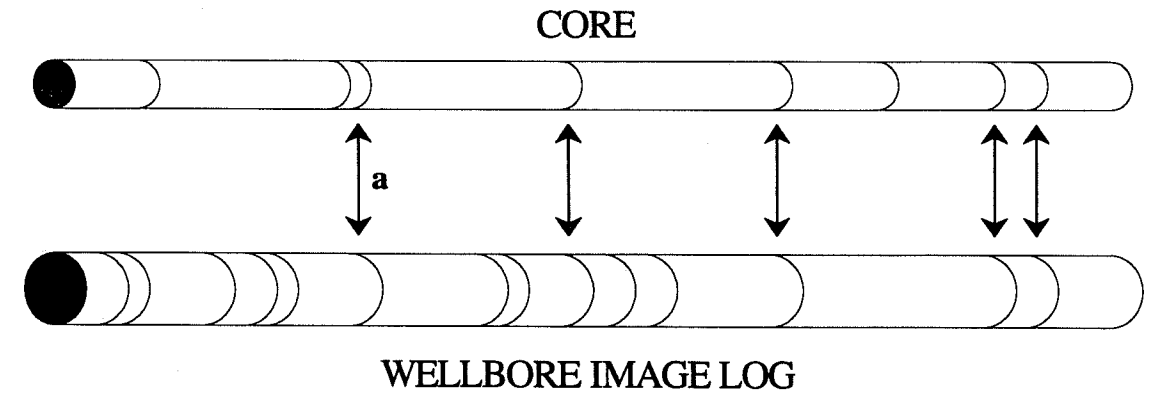

Correlative (?) Fractures

a Correlatable Fracture with unique strike in both core and log

0 5
FEET

(Log Depth 7675-7700' MD)

Figure 7

CYCLE STRATIGRAPHY AND DIAGENESIS OF THE GRAYBURG FORMATION: SOUTH COWDEN FIELD, ECTOR COUNTY, TEXAS

Stephen C. Ruppel and F. Jerry Lucia

Bureau of Economic Geology

The University of Texas at Austin

Austin, TX 78713

ABSTRACT

Permian shallow-water carbonate reservoirs in the Permian Basin are highly heterogeneous because of complex variations in depositional facies produced by high-frequency sea-level rise and fall. Accordingly, establishment of a cycle stratigraphic framework is fundamental to defining reservoir heterogeneity in these rocks. Because nearly all of these reservoirs have experienced multiple episodes of dolomitization and sulfate emplacement, however, permeability is also a function of diagenetic overprint. The extent to which diagenesis can affect permeability development is dramatically displayed in the Grayburg Formation (middle Permian) at South Cowden field, West Texas.

Three scales of cyclicity contribute to original depositional facies heterogeneity in the Grayburg; high-frequency cycles, averaging 3 meters in thickness, constitute the fundamental architectural element in the main reservoir interval. Despite original depositional heterogeneity due to this cyclicity, however, permeability development has substantially resulted from two diagenetic events: (1) dolomite alteration in vertically burrowed wackestones and packstones and (2) late alteration and removal of anhydrite.

Dolomite alteration in vertically burrowed wackestones and packstones has produced irregular vertical zones of higher permeability in mud-dominated bases of high-frequency cycles in leeward ramp-crest highstand successions. Because dolomite alteration is concentrated in burrowed highstand successions, the distribution of resultant permeability trends is partly constrained by patterns of long-term accommodation and high-frequency cyclicity. Anhydrite diagenesis, which is characterized by conversion to gypsum or by complete removal of sulfate, is developed along basinward margins of the field and crosscuts original depositional framework.

Altered dolomite in burrowed zones exhibits an average of twice the porosity and an order of magnitude greater permeability than adjacent unaltered rocks because of rock-fabric differences. Especially where sulfate removal has occurred, altered zones contain intercrystalline and touching-vug pores in contrast to intercrystalline and separate-vug pores characteristic of unaltered zones. These rock-fabric types also display distinctly different porosity-permeability relationships.

Pore types can be traced across the field by comparing acoustic and neutron-density porosity logs. Once rock-fabrics are delineated, appropriate porosity-permeability transforms can be applied to predict permeability across the reservoir. Mapping of zones of anhydrite diagenesis and associated permeability development by means of cores and acoustic log porosity signatures demonstrates that alteration and removal of sulfate and attendant permeability enhancement is highly irregular at the interwell scale.

Two cores are exhibited at this workshop. Together, they document virtually all of the depositional and diagenetic variability in the reservoir and illustrate the important controls on reservoir development.

INTRODUCTION

The South Cowden Grayburg reservoir is located on the east margin of the Central Basin Platform in eastern Ector County, southwest of Odessa, Texas (Figure 1). Oil was first discovered in the South Cowden field area (then called Addis field) in 1933 (Young and Vaughn, 1957). The field now occupies part of an essentially continuous trend of productive Grayburg rocks extending north into Foster and Johnson fields along the Grayburg platform margin. Oil production from the Grayburg in South Cowden field totaled more than 155 million barrels at the end of 1994. Most production has come from the Fina Emmons unit, the Phillips South Cowden unit, and the UNOCAL Moss unit (Figure 2). This paper deals primarily with these units, all of which are currently under waterflood.

Although previous studies have indicated that like most Permian carbonate reservoirs in the Permian Basin, the South Cowden Grayburg field contains substantial amounts of remaining mobile oil (Galloway and others, 1983), the reservoir has begun to experience significant declines in oil production rates and increases in water production. This study was initiated to develop new approaches to identifying and targeting this remaining oil resource. In this paper we summarize the results of detailed geological and petrophysical characterization studies of the reservoir and suggest some techniques for developing improved models of permeability distribution. The cores displayed at this workshop illustrate key depositional and diagentic features that contribute to reservoir development in this and other Grayburg reservoirs in the Permian Basin.

STRUCTURAL SETTING

The most productive parts of South Cowden field, including the area of this study, are developed over a southeast-trending, southeast-plunging structural nose (Figure 2). Seismic data and deep wireline log data in the South Cowden area show that this structure owes its origin to stratal drape over the underlying terminal Glorieta platform margin and a lobe-shaped, southeast-trending, progradational wedge. This wedge, which is composed of alternating sandstone and limestone, appears equivalent in both lithology and stratigraphic position to the Brushy Canyon Formation known from outcrops in the Guadalupe Mountains and the subsurface of the Delaware Basin (Ruppel and Bebout, 1996). Work by Kerans and Fitchen (1995) demonstrated that the Brushy Canyon was deposited during a major sea-level fall during middle San Andres time. Both present structure and Grayburg depositional facies distribution patterns reflect the overriding control of this lowstand-wedge geometry on subsequent deposition and subsidence (Figure 2).

STRATIGRAPHY AND FACIES

General facies characteristics and stratigraphy of the Grayburg Formation on the Central Basin Platform have been described in several field studies (Bebout and others, 1987; Longacre, 1990; Harris and Walker, 1990; Lindsay, 1991). More recently, Kerans and co-workers developed a sequence and cycle stratigraphic framework of the Grayburg and other Guadalupian strata in outcrop studies in the Guadalupe Mountains (Kerans and Nance, 1991; Kerans and Fitchen, 1995). This framework constitutes a powerful tool for correlating the Grayburg and its component facies at both regional and intrareservoir scales. Current studies of the Grayburg in outcrops of the Brokeoff Mountains by Barnaby and Ward (1995) have produced additional refinements to this framework. The results of these studies serve as an important basis for describing and

interpreting Grayburg reservoir successions in the subsurface, such as that at South Cowden field.

Like the outcropping Grayburg Formation in the Guadalupe Mountains, the section at South Cowden field constitutes a single, long-term, accommodation cycle marked by transgression and deepening at the base and shallowing and progradation at the top. Four high-frequency transgressive-regressive sequences (HFS) can be recognized within this long-term cycle, each averaging 50 to 100 ft in thickness (Figure 3). Although Kerans and Nance (1991; Kerans and Fitchen, 1995; Kerans and Ruppel, 1994) only recognized two HFS within the Grayburg (Figure 4), more recent studies of Barnaby and Ward (1994) in the Brokeoff Mountains as well as regional subsurface studies along the west margin of the Central Basin Platform by Kerans and Ruppel (unpublished) demonstrate that these four HFS are regionally recognizable. Maximum flooding of the Grayburg platform, typically reflected by widespread deposition of fusulinid wackestones at the base of HFS 3, is particularly apparent along the entire east margin of the Central Basin Platform, forming a basis for interreservoir correlation of depositional successions in other Grayburg fields, such as Dune, Foster, Johnson, Rhodes Cowden, and North Cowden, and in outcrop successions (Kerans and Nance, 1991; Barnaby and Ward, 1994).

Oil production from the Grayburg in South Cowden field is restricted to HFS 2-4 (Figure 3). Five major depositional facies can be defined within this succession: (1) fusulinid wackestone-packstone, (2) ooid-peloid, grain-dominated packstone-grainstone, (3) peloid-skeletal wackestone/mud-dominated packstone, (4) peritidal tidal-flat facies, and (5) siltstone-sandstone (Figure 3). As is typical of most Grayburg successions in the Permian Basin, all limestones have been dolomitized.

Fusulinid facies contain as much as 40 percent fusulinids and, like most rocks in the Grayburg, are generally pelleted. These deposits are mostly restricted to higher accommodation outer margins of the field except at sequence bases, where they extend well up onto the platform (Figure 3). Grain-dominated packstones are mud-free to mud-poor grain support rocks that lack evidence of cross-bedding. These rocks are abundant in updip, ramp-crest to inner-platform parts of the field (Figure 3). Most commonly, they are made up of 150- to 200-μm peloids although locally, especially at the top of HFS 2 and HFS 4, they contain larger ooids. Crossbedded grainstones are rare. Peloid-skeletal wackestone-packstones include mud-rich, mud-supported to grain-supported rocks that contain skeletal debris, principally mollusks (bivalves and snails), and peloids or pellets. These deposits are most abundant in highstand sequences (HFS 3 and 4) in inner-platform settings. Tidal-flat facies here include rocks exhibiting a variety of depositional textures and structures indicating subaerial exposure, including tubular, laminar, and irregular fenestrae, pisolites, cyano-bacterial mats, lithoclast breccias, featureless mudstone, sheet cracks, and teepee structures. Tidal-flat facies are most common at sequence tops in updip (platformward) parts of the field area (Figure 3). Sandstone-siltstone primarily comprises fine-grained quartz sandstone to coarse-grained siltstone. Beds of these clastics are most prevalent at cycle bases especially in HFS 3, which documents maximum flooding of the Grayburg platform (Figure 3).

Figure 3 depicts the eastward increase in accommodation in the Grayburg Formation across the South Cowden field area. Deeper water fusulinid wackestones-packstones generally dominate the eastern, downdip part of the area, whereas shallower water ramp-crest (grain-dominated packstones and grainstones) and inner ramp (peloidal wackestones) are abundant to the west. This relationship is especially well expressed by facies distributions at the top of HFS 2 (Figure 5). The highly

aggradational ramp crest complex that developed in the northwest part of the study area at this time is centered over the structural and thickness highs of the deeper, lower San Andres (Brushy Canyon) depositional lobe. Systematic variations in facies within the ramp-crest shoal deposits suggest that differing energy conditions may have existed around the crest. On the east side of the field, these shoals comprise amalgamated peloid/ooid grainstones and grain-dominated packstones within which cyclicity is difficult to define. In contrast, the south margin of the crest is composed of more cyclic successions that have well-developed mud-dominated facies at their bases. The contrasting energy regimes suggested by these facies-stacking differences may be wind related. Fischer and Sarntheim (1988) determined that predominant winds were northerly during much of the Guadalupian. Amalgamated grain-dominated successions on the east side of the ramp crest may reflect windward depositional conditions, whereas more cyclic, mud-dominated facies successions on the south may have accumulated in a leeward setting.

In contrast to only locally developed cyclicity in the lower Grayburg (HFS 1, 2), both HFS 3, which documents maximum flooding of the platform, and HFS 4 display well-developed, high-frequency cycles, averaging 10 to 15 ft in thickness, across the field area (Figure 6). Transgressive fusulinid-dominated high-frequency cycles in HFS 3 are defined by basal siliciclastics, reflecting the reworking of aeolian sands during maximum flooding. High-frequency cycles in HFS 4 are typically highly aggradational inner-ramp successions that are characterized by basal mud-dominated peloidal packstones and wackestones and cycle-capping grain-dominated peloidal packstones. These high-frequency cycles provide an excellent basis for high-resolution correlation and construction of a reservoir framework in the field.

Both the large-scale lateral changes in facies caused by inherited topographic relief and differential subsidence across the field and smaller scale vertical changes associated with high-frequency cycles in the upper Grayburg have the potential of exerting significant controls on reservoir development in the field. Recognition and delineation of this facies heterogeneity is an important first step in reservoir characterization of shallow-water platform carbonate reservoirs.

DIAGENESIS

As with all carbonate reservoir successions, diagenesis also plays an important role in development of porosity and permeability in the Grayburg. Virtually all Guadalupian reservoir successions in the Permian Basin have been diagenetically altered by dolomitization and sulfate precipitation. As many workers have shown, current mineralogies are the result of many episodes of diagenesis. Ruppel and Cander (1988a) and Leary and Vogt (1990) gave good overviews of these processes. Two specific elements of this diagenesis, both of which have been documented in other Guadalupian reservoirs, have exerted a strong control on porosity development in the Grayburg reservoir at South Cowden field: (1) dolomite alteration and (2) anhydrite alteration and removal.

Dolomite Alteration

As previously recognized by several Permian Basin workers (Bebout and others, 1987; Ruppel and Cander, 1988a; Leary and Vogt, 1990; Major and others, 1990), local zones of altered dolomite are common in the San Andres and Grayburg. Such altered dolomites are typically characterized by irregular zones of dolomite that contrast with the surrounding matrix in having (1) lighter color, (2) coarser crystals, (3) leached

dolomite rhomb cores, (4) higher porosity, and (5) depleted oxygen isotopes (Leary and Vogt, 1990; Major and others, 1990).

In South Cowden field, dolomite alteration and leaching are manifested by irregular, light-colored (light-brown), vertically elongate zones of altered dolomite fabric that resemble and are associated with large (1- to 3-cm X 10- to 30-cm) vertical burrows and that are stratigraphically restricted to the upper part of HFS 3 and the lower part of HFS 4 (Figure 7). Like previously reported altered fabrics, these zones typically contain abundant hollow dolomite rhombs and depleted oxygen isotopes. Analysis of $\delta^{18}O$ in 21 paired samples shows a 2.5 $^{o}/_{oo}$ to 3.0 $^{o}/_{oo}$ PDB depletion in altered dolomites compared with that of the surrounding matrix.

Although these fabrics have been described in other reservoirs, the depositional and paleotopographic controls on their development have been previously unrecognized. In South Cowden field, burrowed zones of altered dolomite are apparently largely restricted to highly cyclic, mud-dominated, inner-ramp highstand facies along the outer margins of the field (Figure 8). Burrows, most conspicuous in the mud-dominated bases of these cycles, are much less obvious in the typically more grain dominated cycle tops. The distribution of these burrowed zones of altered dolomite closely parallels both early Grayburg paleogeography and structure, being most abundant along the structural and paleotopographic margin of the field (compare Figures 5 and 8).

The association between burrowing and dolomite alteration suggests that burrows provided higher permeability pathways for the entry of diagenetic fluids. Burrowing clearly took place syndepositionally; the timing of the alteration is less obvious. Because the altered fabric is present in the interior of the field where it is

typically cemented with anhydrite, alteration apparently pre-dated the last episode of anhydrite precipitation. The timing of this event, however, is uncertain, although it probably can be tied to major evaporite precipitation and potential brine reflux in the area during the late Guadalupian (Ruppel and Cander, 1988b).

Along the margins of the field, altered dolomite displays permeabilities of as much as several orders of magnitude greater and porosities as much as five times greater than those of the surrounding matrix (Figure 9). Most production in South Cowden field has come from the Emmons and South Cowden units, where development of this fabric is greatest.

Anhydrite Alteration

Calcium sulfate in the form of anhydrite or gypsum is intimately associated with nearly all dolomitized Permian carbonates in the Permian Basin. Much of the Grayburg at South Cowden field also contains abundant, well-preserved anhydrite present as nodules, mold-fills, and poikilotopic interparticle cement. Along the east and south margins of the field, however, significant amounts of anhydrite have been altered or completely removed (Figure 10). In structurally downdip parts of the field, especially along the east margin, virtually all sulfate has been removed in much of the reservoir interval. Sulfate removal is demonstrated by total absence of sulfate and by the presence of completely open or calcite-cement-lined sulfate nodule molds. In adjacent updip areas of the field area, sulfate is locally present, but anhydrite is partly to completely altered to gypsum or the intermediate phase, bassanite.

Like the distribution of zones of altered dolomite, patterns of anhydrite diagenesis follow both Grayburg paleotopography and current structure (compare Figures 5 and 10). Greatest amounts of sulfate alteration and removal are observed along the outer,

downdip margins of the field. In these areas, sulfate diagenesis clearly crosscuts facies and stratigraphy (Figure 11).

POROSITY AND PERMEABILITY MAPPING

Maps of porosity development in the field demonstrate the key role of sulfate and dolomite diagenesis in Grayburg reservoir development. Porosity is very low in the interior of the field ,where sulfate is abundant. Highest phih is developed along the margins of the field where dolomite has been altered and where sulfate has been altered or removed (Ruppel and Bebout, 1996).

Along the margins of the field in intervals of dolomite and sulfate alteration (Figures 8 and 10), altered dolomite exhibits distinctly higher permeabilities than do other sulfate-bearing dolomite fabrics (Figure 12). Highest permeability, however, is usually developed where sulfate has been removed and especially where zones of sulfate removal and dolomite alteration coincide (Figure 13).

Comparison of porosity-permeability relationships in the reservoir demonstrates that zones of leached sulfate display a porosity-permeability transform distinctly different from that of other rocks in the reservoir. In most of the reservoir, including parts that contain abundant unaltered anhydrite (as well as those that contain both altered dolomite and altered anhydrite), permeability can be calculated from a single transform (Figure 12). Parts of the reservoir that have undergone sulfate removal, however, contain approximately an order of magnitude higher permeabilities (Figure 13). Rocks containing no sulfate define a porosity-permeability transform that differs from those that do, suggesting the presence of very different rock-fabrics.

Contrasts in porosity-permeability relationships in the reservoir can be directly attributed to pore types. Core studies show that throughout most of the reservoir

Grayburg rocks are dominated by interparticle and separate-vug pores (Ruppel and Bebout, 1996; Lucia and Ruppel, 1996). The porosity-permeability transform indicated in Figure 12, a function of a rock-fabric composed of these pore types, applies to sulfate bearing rocks throughout the reservoir. The high permeabilities observed in altered dolomite fabrics result from larger amounts of interparticle porosity relative to separate-vug pores caused by the combined effects of dolomite and sulfate alteration.

In zones where removal of sulfate has occurred, abundant touching-vug pores (Lucia, 1983; 1995) have been created by removal of poikilotopic sulfate. The development of better interconnected vuggy pores combined with the addition of new interparticle pores results in a rock-fabric having markedly higher permeability. As can be seen from Figure 13, accurate permeability calculation requires distinguishing between these two pore type groups.

Although pore types are readily identified in cores, importantly, they can also be recognized from appropriate wireline log suites (Lucia and Ruppel, 1996). Cross plots of acoustic log transit time against porosity calculated from neutron-density cross plotting provide a method of distinguishing between rocks dominated by (1) interparticle pores; (2) interparticle and separate-vug pores; and (3) interparticle, separate-vug and touching-vug pores (Figure 14). By means of this technique, it is possible to map pore-type distributions across the reservoir even where core control is unavailable (Figure 15). As predicted, log-based mapping of pore types shows a good correlation with maps of dolomite and sulfate alteration.

Using the acoustic to neutron-density cross plot technique for determine rock-fabric, and the appropriate transform to calculate permeability, it is possible to produce a detailed map of permeability of the field (Figure 16). The map shows the high permeability associated with dolomite and sulfate alteration along the downdip field

margin seen in core studies. Mapped permeability shows a very good tie to historical production trends (Lucia and Ruppel, 1996). Low-permeability zones within this area are isolated areas where sulfate has not been removed, and wells drilled in these areas have been typically poor producers. Fingerlike westward projections of more permeable rock also show the irregularity of the sulfate-dissolution process. A more complete discussion of the approaches used for characterization of porosity and permeability in the reservoir along with the results of oil saturation modeling is given by Lucia (1997).

CONTRASTS IN RESERVOIR DEVELOPMENT

Because of the competing effects of original depositional facies and diagenesis in the Grayburg at South Cowden field, the reservoir is in many ways two very different reservoirs. The structurally and depositionally updip part of the Grayburg in the interior of the field is characterized by abundant anhydrite, low porosity, and low permeability (Figure 17). Although reservoir development is limited, both porosity and permeability distribution seem to be a function of facies heterogeneity that is controlled by high-frequency cyclicity. Accordingly, in this part of the reservoir, the cycle stratigraphic framework is an important element for characterizing flow unit character. In many cases, low-permeability zones developed at cycle bases create flow baffles within this part of the reservoir.

By contrast, reservoir development in the downdip margins of the field, where overprinting dolomite and sulfate alteration are significant, shows much less association with original depositional processes, facies distributions, or cyclicity. Instead, permeability development in this part of the reservoir is controlled by dissolution fluid pathways that crosscut stratigraphy. Here, defining the distribution of diagenetic fabrics resulting from this dissolution is more important to flow unit characterization than the

cycle stratigraphy. Because of porosity and permeability enhancing sulfate dissolution, horizontally continuous, cycle-base, low-permeability zones are poorly developed in these rocks. Importantly, however, there are irregularly distributed vertical low permeability zones in this part of the reservoir. These pillars of remaining sulfate, one of which was penetrated by a cored well, have lateral dimensions of as much as hundreds of feet (Lucia and Ruppel, 1996). Although only a few of these zones are indicated by log-based mapping of permeability, it is probable that many more of these pillars exist in the reservoir and that they have an important effect on fluid flow.

CONCLUSIONS

The Grayburg reservoir at South Cowden field is a striking example of the overprinting effects of diagenesis on original depositional framework. Well-developed cyclicity in the Grayburg has produced considerable depositional facies heterogeneity at multiple scales. Both early and later diagenetic events, however, have substantially muted the impact of initial depositional architecture on reservoir development. Although definition of stratigraphic architecture is fundamental to characterization of all carbonate reservoirs, where overprinting diagenesis dominates, an alternative basis for reservoir modeling must be sought. The calibration and application of wireline logs to identification and mapping of diagenetic fabrics on the basis of their pore types, as demonstrated in this paper, represents an important step in our attempts to develop accurate models of permeability development in diagenetically altered carbonate reservoirs.

The cores on display at this workshop demonstrate the important differences in the character and distribution of depositional and diagentic rock fabrics in the South Cowden Grayburg field. These rock fabrics and their associated petrophysical

relationships are important controls of reservoir performance in Grayburg and other Permian platform carbonate reservoirs throughout the Permian Basin. Accurate characterization and modeling of these shallow platform carbonate reservoirs thus depends on the understanding and recognition of these rock fabrics.

GUIDE TO CORES ON DISPLAY AT THE WORKSHOP

Two of the 28 remaining cores in the field are on display for this core workshop. These cores (Unocal Moss Unit #9-17 and #6-20) exhibit most of the important depositional and diagenetic features of the Grayburg in the area. The cores display significantly different facies successions in the transgressive leg of the Grayburg long term accommodation cycle (HFS 2; Figure 3). The #9-17 core, which is situated both structurally and depositionally updip (Figure 2), exhibits a relatively low accommodation succession compared to the more distal, high accommodation section in the #6-20 core. Because the focus of reservoir-significant carbonate and sulfate diagenesis is along the distal, downdip margins of the field, the #6-20 core also displays a distinctly different diagenetic history. Specific elements of each of the two cores on display are summarized below.

Unocal Moss #9-17

Most of the cored interval from 4,385 ft to 4,620 ft from this well is on display. This includes parts of Grayburg HFS 2, 3, and 4 as well as the basal Queen Formation (Figure 18).

Grayburg HFS 2. The HFS 2 ramp crest is well developed in the area of #9-17. Ramp crest cycles are composed of ooid and peloid grain-dominated packstones and grainstones. Cycle bases are defined by skeletal-rich wackestones and packstones. Cyclicity here is better developed than in more windward parts of the ramp crest (Figure

5) where the succession generally comprises amalgamated, grain-dominated packstones and grainstones. The top of HFS 2 (4,589 ft) is defined by pisolitic and fenestral tidal flat facies having common interbeds of intraclast breccia. An ongoing and significant question regarding these apparent cycle- and sequence-capping exposure fabrics is whether they truly cap the underlying highstand succession or rather represent basal transgressive deposits of the ensuing sea level rise succession.

Grayburg HFS 3. The base of HFS 3 is well defined across the area by a succession of siltstone-based fusulinid-bearing cycles. This succession represents maximum flooding of the platform during the Grayburg accommodation cycle. Indicative of this are the common fusulinids despite the relatively landward position of this well. The silty cycle bases of the lower HFS 3 interval (F2 and F3 markers) are highly continuous across the area, which is typical of transgressive deposits on relatively flat-lying platforms. These depoists represent maximum flooding during the Grayburg depositional cycle.

The top of HFS 3 is weakly defined in this well. A thin peloid grain-dominated packstone is overlain by skeletal and fusulinid-bearing wackstones documenting the ensuing fllodback of HFS 4 at about 4,534 ft. Gamma ray correlations across the field demonstrate that this horizon is the surface of major basinward facies offset.

Grayburg HFS 4. Across much of the field, the middle ramp depoists of HFS 4 represent a sharp change from the outer ramp facies of the underlying HFS 3 (Figure 1). This marked basinward offset in facies tract is less apparent in the more proximal setting of the #9-17 well and in this core the contact between HFS 3 and 4 is subtle. Like HFS 4 elsewhere in the area, however, the #9-19 core displays a highly cyclic succession of peloid wackestones and packstones. Most cycles contain mud-dominated peloidal bases and grain-dominated peloidal tops although locally cycles comprise

entirely mud-dominated facies. Cycle tops tie well to gamma ray excursions, seemingly irregardless of local facies variations. The gamma ray can thus be used to correlate cycles even where cycle boundaries are lithologically cryptic. Because of this, these high frequency cycles can be used to establish a high resolution framework within HFS 4 across much of the field.

Queen Formation. Queen depositional cycles present a striking contrast in facies-stacking patterns to underlying Grayburg cycles. Queen cycles are characterized by sandstone/silstone bases and clastic-free, tidal flat carbonate facies at cycle tops (Figure 18). These depoists represent the base of Guadalupian HFS 16 (Figure 4) and the basal leg of a longer term third-order (composite) sequence (Kerans and Fitchen, 1995). The well-defined basinward offset in facies documents an overall reduction in accommodation at the beginning of Queen time. For the most part, the clastic cycle bases are not porous or permeable. However, there is some oil production from the Queen in the field along the downdip margins where impermeable tidal flat carbonate facies grade into more permeable subtidal deposits.

Diagenesis. All of the Grayburg Formation has experienced multiple episodes of dolomitization and sulfate emplacement. However, none of the particularly distinctive dolomite alteration or late sulfate diagenesis which is characteristic of the outer margins of the field and which is associated with significantly greater porosity and permeability are apparent in this core.

Unocal Moss #6-20

Core on display from this well includes a gross interval of about 240 ft (4,558 ft to 4,782 ft) (Figure 19). Representative sections from HFS 2-4 are available for comparison with equivalent intervals in the #9-17 core.

Grayburg HFS 2. The HFS 2 section in this well is composed almost entirely of outer ramp fusulinid wackestone and packstone (Figure 19). Cycles are not generally definable although vertical successions of fusulinid-rich wackestone and overlying fossil-poor peloid packstone are locally recognizable. These "cycles" can not be correlated from well to well with either cores or wireline logs, however. Compare the outer ramp, fusulinid-dominated succession seen in this core with the temporally equivalent ramp crest succession of peloid-ooid grainstones displayed in the #9-17 core.

Grayburg HFS 3. Like HFS 2, HFS 3 is dominated by outer ramp fusulinid-rich deposits. HFS 3, however, contains several silstone-based cycles (e. g., F2 and F3 markers) equivalent and correlative to those observed in the #9-17 core (Figure 19). The siltstone base of the lowermost of these cycles defines the HFS 2/HFS 3 contact. The distinctive gamma ray response to these cycle base siltstones forms the basis for field wide correlation of HFS 3 (Figure 3).

Grayburg HFS 4. As is the case elsewhere in the field, HFS 4 exhibits a major basinward offset in facies tract caused by decreasing accommodation (Figure 3). The base of HFS 4 is defined by a thin fusulinid wackestone documenting initial flooding. Note, however, that the platformward extent of these fusulinid deposits is much less than in HFS 3. As in the #9-17 core, HFS 4 here is characterized by high frequency cycles composed of basal mud-dominated peloid packstones and capping grain-dominated peloid and ooid packstones and grainstones. Note that some of these capping grain-dominated cycle caps are highly porous although the sequence-capping succession is cemented by anhydrite and non-porous.

Diagenesis. The #6-20 well is located on the downdip margins of the field in areas of significant dolomite and sulfate alteration (Figures 8 and 10). Zones of altered

dolomite are well developed in HFS 3 and 4 (Figure 19) where they are associated with vertical burrows. Note that alteration is fabric-controlled. Altered zones are most common in peloid-dominated packstones. In HFS 3 these depoists form the tops of fusulinid- dominated cycles whereas in HFS 4, they constitute the muddier bases of cycles with grain-dominated packstone caps. In all cases, porosity and permeability are substantially enhanced in altered zones relative to surrounding unaltered rocks.

Sulfate alteration, in the form of alteration to gypsum or partial or complete removal, is obvious from about 4,635 ft (F0 marker) to the bottom of the core. In the lowermost part of the core (from about 4,780 ft to TD), sulfate has been completely removed leaving open fractures, molds, and nodules. Between 4,635 ft and 4,780 ft, sulfate is partly altered. This is evidenced by the presence of gypsum rims around nodule margins and by poikilotopic gypsum. The presence of gypsum here makes determination of porosity difficult by either wireline log or core analysis means. Permeability is highest in zones of coincident sulfate and dolomite diagenesis.

ACKNOWLEDGMENTS

We thank Emily Stoudt for efforts in organizing this core workshop. The results presented in this paper are part of continuing research into the styles and causes of heterogeneity in shallow-water platform carbonate reservoirs in the Permian Basin by the Carbonate Reservoir Characterization Research Laboratory at the Bureau of Economic Geology, which is funded by the following sponsors: Amoco, Aramco, ARCO, BP International, Exxon, Fina, Japan National Oil Corporation, Marathon, Meridian, Oxy, Pennzoil, Petroleum Development Oman, Phillips, Shell Western, Shell Canada, Texaco, Total, and UNOCAL. Additional funding for the study was provided by contract no. DE-AC22-93BC14895 from the U. S. Department of Energy. UNOCAL South

Permian, Fina Oil and Gas, and Phillips Petroleum provided access to cores, wireline logs, and reservoir data on the field. Discussions with Roger Barnaby, Charlie Kerans, Jerry Dunnam, Scott Landon, Bill Dixon, Doug Bacon, Matt Gerard, and Craig Caldwell were helpful in developing our interpretations of the reservoir geology. Publication authorized by the Director, Bureau of Economic Geology.

REFERENCES

Barnaby, R. J., and Ward, W. B., 1994, Sequence stratigraphic framework, high-frequency cyclicity and 3-dimensional heterogeneity: Grayburg Formation, Brokeoff Mountains, New Mexico, *in* Pause, P. H., and Candelaria, M. P., editors, Carbonate facies and sequence stratigraphy: practical applications of carbonate models: PBS-SEPM Publication 95-36, p. 37-50.

Barnaby, R. J., and Ward, W. B., 1995, Stratigraphic hierarchy, sequence architecture, and interwell-scale heterogeneity: Grayburg Formation, Brokeoff Mountains, New Mexico: The University of Texas at Austin, Bureau of Economic Geology, Reservoir Characterization Research Laboratory Field Guide, 45 p.

Bebout, D. G., Lucia, F. J., Hocott, C. R., Fogg, G. E., and Vander Stoep, G. W., 1987, Characterization of the Grayburg reservoir, University Lands Dune field, Crane County, Texas: The University of Texas at Austin, Bureau of Economic Geology Report of Investigations No. 168, 98 p.

Fischer, A. G., and Sarntheim, M., 1988, Airborne silts and dune-derived sands in the Permian of the Delaware Basin: Journal of Sedimentary Petrology v. 58, p. 637-643.

Galloway, W. E., Ewing, T. E., Garrett, C. M., Jr., Tyler, Noel, and Bebout, D. G., 1983, Atlas of major Texas oil reservoirs: The University of Texas at Austin, Bureau of Economic Geology Special Publication, 139 p.

Harris, P. M., and Walker, S. D., 1990, McElroy Field: Development geology of a dolostone reservoir, Permian Basin, West Texas, *in* Bebout, D. G., and Harris, P. M., editors, Geologic and engineering approaches in evaluation of San Andres/Grayburg hydrocarbon reservoirs - Permian Basin: The University of Texas at Austin, Bureau of Economic Geology, p. 275-296.

Kerans, Charles, and Fitchen, W. M., 1995, Sequence hierarchy and facies architecture of a carbonate ramp system: San Andres Formation of Algerita Escarpment and Western Guadalupe Mountains, West Texas and New Mexico: The University of Texas at Austin, Bureau of Economic Geology Report of Investigations No. 235, 86 p.

Kerans, Charles, and Nance, H. S., 1991, High-frequency cyclicity and regional depositional patterns of the Grayburg Formation, Guadalupe Mountains, New Mexico, *in* Meader-Roberts, S., Candelaria, M. P., and Moore, G. E., editors, Sequence stratigraphy, facies and reservoir geometries of the San Andres, Grayburg and Queen Formations, Guadalupe Mountains, New Mexico and Texas: Permian Basin Section/SEPM Publication 91-32, p. 53-96.

Kerans, Charles., and Ruppel, S. C., 1994, San Andres sequence framework, Guadalupe Mountains: Implications for San Andres type section and subsurface reservoirs: *in* Garber, R. A, and Keller, D. R., editors, Field guide to the Paleozoic section of the San Andres Mountains, Permian Basin Section SEPM publication 94-35, p. 105-116.

Leary, D. A., and Vogt, J. N., 1990, Diagenesis of the San Andres Formation (Guadalupian) reservoirs, University Lands, Central Basin Platform, *in*Bebout, D.

G., and Harris, P. M., editors, Geologic and engineering approaches in evaluation of San Andres/Grayburg hydrocarbon reservoirs - Permian Basin: The University of Texas at Austin, Bureau of Economic Geology, p. 21-28.

Lindsay, R. F., 1991, Grayburg Formation (Permian-Guadalupian): Comparison of reservoir characteristics and sequence stratigraphy in the northwest Central Basin Platform with outcrops in the Guadalupe Mountains, New Mexico, *in* Meader-Roberts, S., Candelaria, M. P., and Moore, G. E., editors, Sequence stratigraphy, facies and reservoir geometries of the San Andres, Grayburg and Queen Formations, Guadalupe Mountains, New Mexico and Texas: Permian Basin Section/SEPM Publication 91-32, p. 111-118.

Longacre, S. A., 1990, The Grayburg reservoir, North McElroy Unit, Crane County, Texas, *in* Bebout, D. G., and Harris, P. M. editors, Geologic and engineering approaches in evaluation of San Andres/Grayburg hydrocarbon reservoirs - Permian Basin: The University of Texas at Austin, Bureau of Economic Geology, p. 239-274.

Lucia, F. J., 1983, Petrophysical parameters estimated from visual description of carbonate rocks: afield classification of carbonate pore space: Journal of Petroleum Technology, v. 35, p. 626-637.

Lucia, F. J., 1995, Rock-fabric/petrophysical classification of carbonate pore space for reservoir characterization: AAPG Bulletin v. 79, p. 1275-1300.

Lucia, F. J., and Ruppel, S. C., 1996, Characterization of diagenetically altered carbonate reservoirs, South Cowden Grayburg reservoir, West Texas: SPE Annual Technical Conference and Exhibition, Denver, CO. SPE 36650.

Lucia, F. J., 1997, Geoscience/engineering characterization of the interwell environment in carbonate reservoirs based on outcrop analogs, Permian Basin, West Texas and New Mexico - Petrophysical characterization of the South Cowden Grayburg reservoir, Ector County, Texas: Fossil Energy, DOE/BC/14895-13 (vol. II), 51 p.

Major, R. P., Vander Stoep, G. W., and Holtz, M. H., 1990, Delineation of unrecovered mobile oil in a mature dolomite reservoir: East Penwell San Andres unit, University Lands, West Texas: The University of Texas at Austin, Bureau of Economic Geology Report of Investigations No. 194, 52 p.

Ruppel, S. C., and Cander, H. S., 1988a, Effects of facies and diagenesis on reservoir heterogeneity: Emma San Andres field, West Texas: The University of Texas at Austin, Bureau of Economic Geology Report of Investigations No. 178, 67 p.

Ruppel, S. C., and Cander, H. S., 1988b, Dolomitization of shallow-water platform carbonates by sea water and seawater-derived brines: San Andres Formation (Guadalupian), West Texas, *in* Sedimentology and geochemistry of dolostones: Society of Economic Paleontologists and Mineralogists, Special Publication No. 43, p. 245-262.

Ruppel, S. C., and Bebout, D. G., 1996, Effects of stratal architecture and diagenesis on reservoir development in the Grayburg Formation: South Cowden field, Ector County, Texas: Fossil Energy, DOE/BC/14895-10, Bartlesville Project Office, 80 p.

Young, Addison, and Vaughn, J. C., 1957, Addis-Johnson-Foster-South Cowden field, *in* Herald, F. A., editor, Occurrence of oil and gas in West Texas: University of Texas, Austin, Publication 5716, p. 17-22.

LIST OF FIGURES

Figure 1. Distribution of major Guadalupian shallow-water carbonate reservoirs in West Texas and New Mexico and the paleogeography of the Permian Basin during Grayburg time. Also shown are the Guadalupe Mountains, location of reservoir-equivalent outcrops.

Figure 2. Map of South Cowden field showing structure on the top of the Grayburg Formation. Also shown are locations of cored wells and wireline log cross sections described in this report. Cores on display are those from wells #16-14 and #6-20.

Figure 3. Cross section (A-A') showing the Grayburg sequence stratigraphic framework in the South Cowden field. Four high-frequency sequences (HFS) are recognized within a longer term transgressive-regressive succession. Line of section, which approximates depositional dip, is shown in Figure 2.

Figure 4. Chronostratigraphic correlation of Guadalupian stratigraphic units in the Permian Basin. Modified after Kerans and Ruppel (1994).

Figure 5. Paleogeography of the South Cowden field area at the end of HFS 2 deposition. Depositional topography and the distribution of facies were controlled by the geometry of an underlying lower San Andres lowstand depositional wedge.

Figure 6. Cross section (B-B') showing high-frequency cyclicity in Grayburg highstand deposits (HFS 4). Cycles are correlative throughout the field and provide a basis for high resolution correlation. Line of section shown in Figure 1.

Figure 7. Cross section (A-A') showing distribution of zones of altered dolomite in HFS 3 and 4. Line of section shown in Figures 2 and 8. Data from core descriptions.

Figure 8. Map showing distribution of zones of altered dolomite along the outer, downdip parts of the South Cowden Grayburg reservoir. Data from core descriptions.

Figure 9. Comparison of porosity and permeability in altered and unaltered dolomite fabrics. Data from core plugs analyzed and provided by Phillips Petroleum.

Figure 10. Map showing extent of sulfate diagenesis along the margin of South Cowden field. Data from core descriptions.

Figure 11. Cross section (C-C') showing distribution of sulfate diagenesis in cores along a dip section through the Fina Emmons unit. Line of section shown in Figures 2 and 10. Note how sulfate diagenesis crosscuts stratigraphy and facies development.

Figure 12. Porosity-permeability relationships among diagenetic facies in the Grayburg at South Cowden field. This well is located in an area of moderate development of altered dolomite fabric and partial sulfate alteration. All rocks in the reservoir, except those that have experienced sulfate removal, display this petrographic relationship and porosity-permeability transform. UNOCAL Moss Unit #6-16.

Figure 13. Cross plot of porosity-permeability for the Grayburg reservoir in the UNOCAL Moss Unit #6-20 well, which is located on the outer margin of the field. Note that rocks in this well that have experienced sulfate removal define a porosity-permeability transform distinctly different from those that have not.

Figure 14. Distinction of Grayburg reservoir pore types using acoustic and neutron-density wireline logs. Ideal mineralogy transform lines are from Schlumberger log charts. Note breakout of sulfate diagenesis fabrics.

Figure 15. Distribution of pore types in the South Cowden Grayburg reservoir based on acoustic/neutron-density cross plots (Figure 14). Note similarity to Figure 10, which is based on core studies.

Figure 16. Distribution of Kh in the South Cowden Grayburg reservoir (HFS 2-4). Compare with Figures 8 and 10.

Figure 17. Patterns of permeability development along a dip section (D-D') in the South Cowden Grayburg reservoir. Note that stratigraphic control on permeability

distribution is progressively greater updip, where severity of overprinting sulfate diagenesis is less. Downdip, permeability generally crosscuts stratigraphy.

Figure 18. Vertical facies succession in the Unocal Moss Unit #9-17 well.

Figure 19. Vertical facies succession in the Unocal Moss Unit #6-20 well.

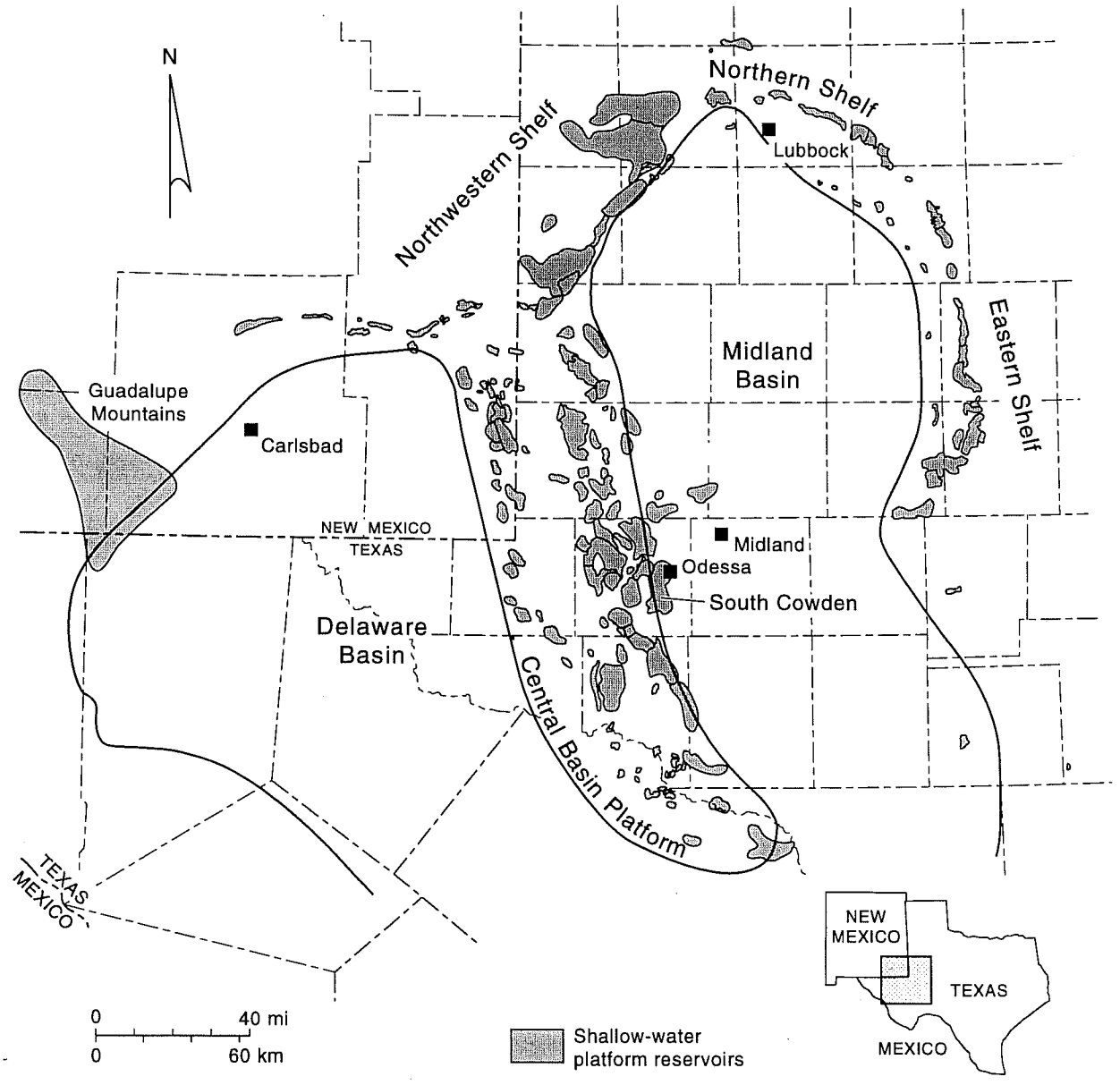
N
Northern Shelf
Lubbock
Northwestern Shelf
Midland
Basin
Eastern Shelf
Guadalupe
Mountains
Carlsbad
NEW MEXICO
TEXAS
Midland
Odessa
South Cowden
Delaware
Basin
Central Basin Platform
TEXAS
MEXICO
0
40 mi
0
60 km
Shallow-water
platform reservoirs
NEW
MEXICO
TEXAS
MEXICO

QAa7694c

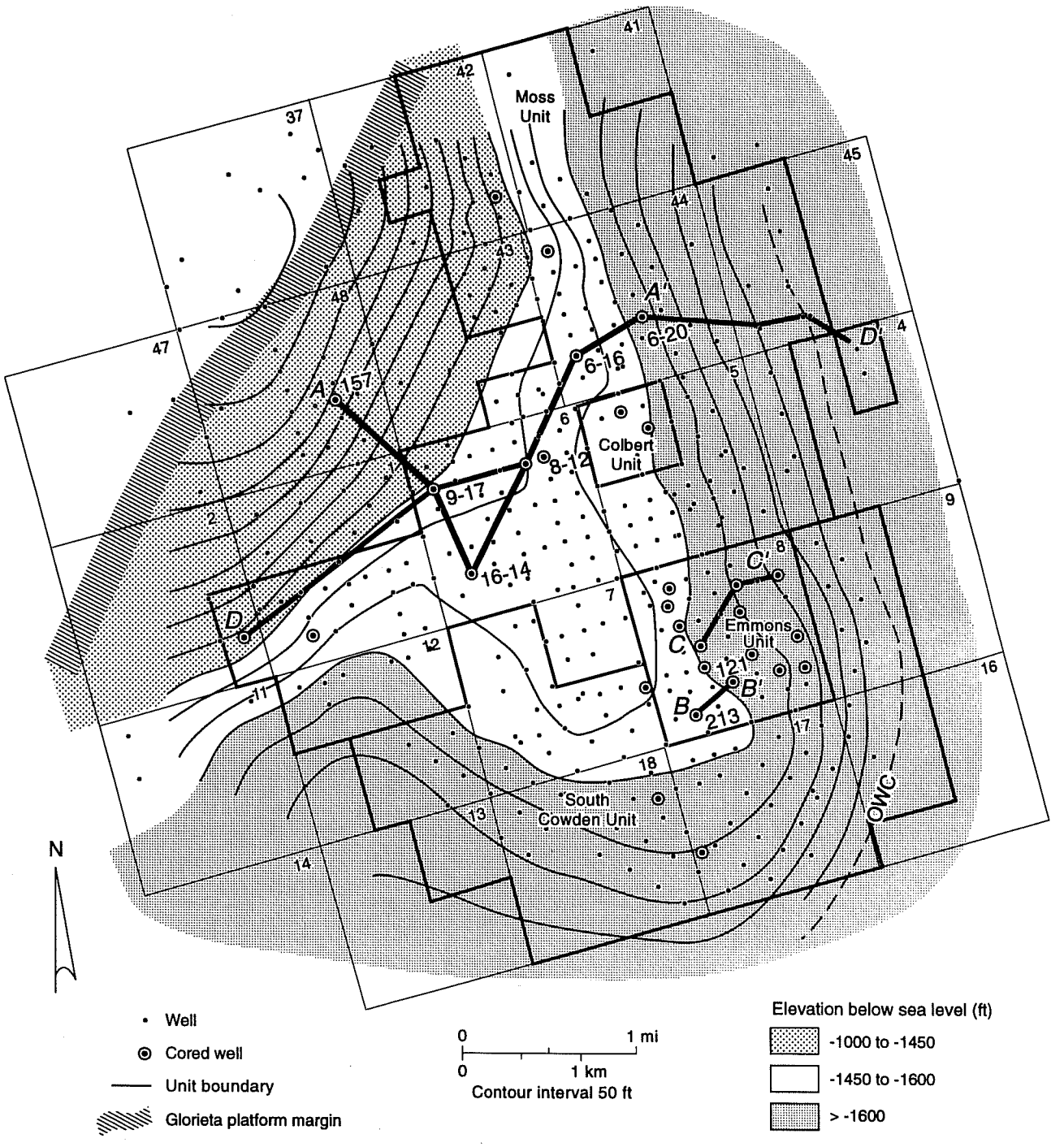
Moss Unit
Colbert Unit
Emmons Unit
South Cowden Unit
OWC
A
A'
B
B'
C
C'
D
D'
6-20
6-16
8-12
9-17
16-14
157
213
N
Well
Cored well
Unit boundary
Glorieta platform margin
0 1 mi
0 1 km
Contour interval 50 ft
Elevation below sea level (ft)
-1000 to -1450
-1450 to -1600
> -1600
QAb2979c

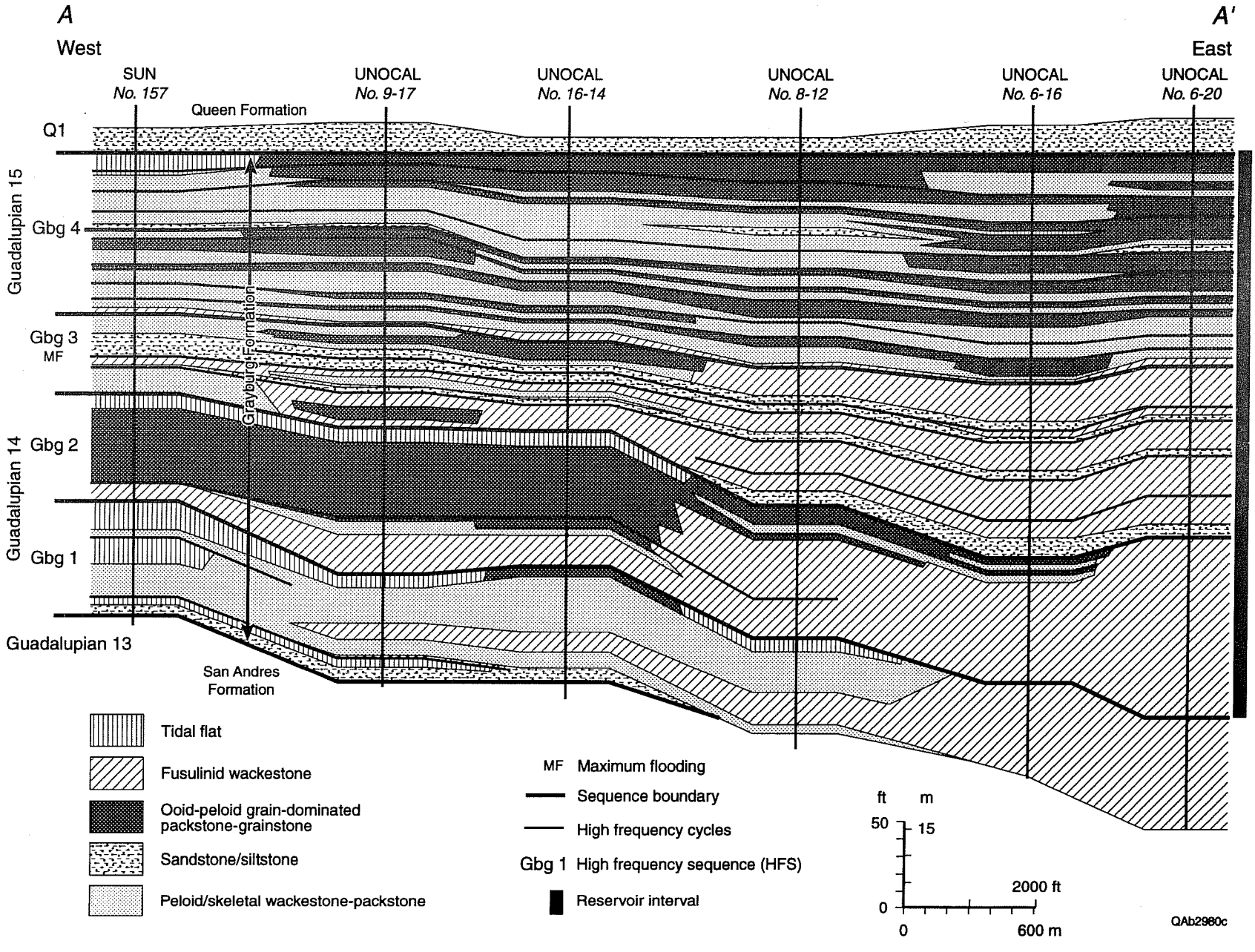
A
West
A'
East
SUN
No. 157
UNOCAL
No. 9-17
UNOCAL
No. 16-14
UNOCAL
No. 8-12
UNOCAL
No. 6-16
UNOCAL
No. 6-20
Queen Formation
Q1
Guadalupian 15
Gbg 4
Gbg 3
MF
Grayburg Formation
Guadalupian 14
Gbg 2
Gbg 1
Guadalupian 13
San Andres
Formation
Tidal flat
Fusulinid wackestone
Ooid-peloid grain-dominated
packstone-grainstone
Sandstone/siltstone
Peloid/skeletal wackestone-packstone
MF Maximum flooding
Sequence boundary
High frequency cycles
Gbg 1 High frequency sequence (HFS)
Reservoir interval
ft
m
50
15
2000 ft
0
0
600 m
QAb2980c

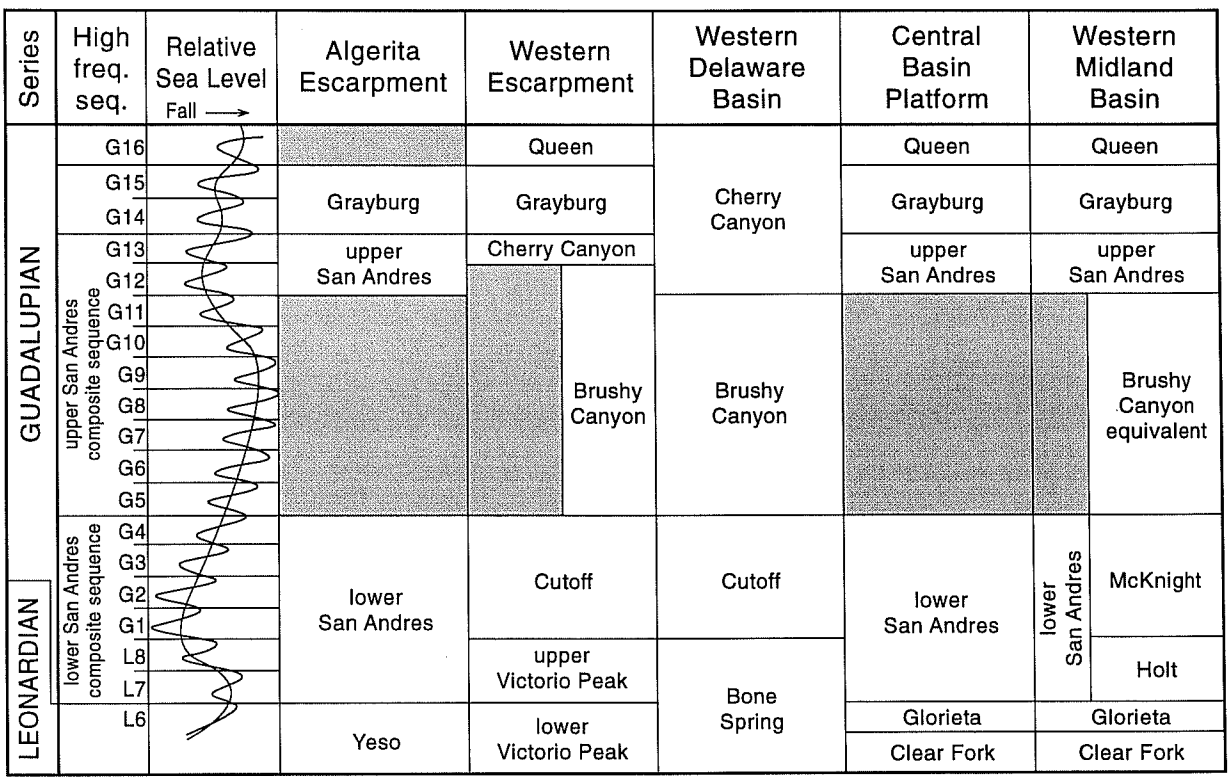
Series
High freq. seq.
Relative Sea Level
Fall
Algerita Escarpment
Western Escarpment
Western Delaware Basin
Central Basin Platform
Western Midland Basin
GUADALUPIAN
LEONARDIAN
upper San Andres composite sequence
lower San Andres composite sequence
G16
G15
G14
G13
G12
G11
G10
G9
G8
G7
G6
G5
G4
G3
G2
G1
L8
L7
L6
Queen
Grayburg
upper San Andres
Cherry Canyon
Brushy Canyon
lower San Andres
Cutoff
upper Victorio Peak
lower Victorio Peak
Yeso
Cherry Canyon
Brushy Canyon
Bone Spring
Queen
Grayburg
upper San Andres
lower San Andres
Glorieta
Clear Fork
Queen
Grayburg
upper San Andres
lower San Andres
McKnight
Holt
Brushy Canyon equivalent
Glorieta
Clear Fork

QAb3743c

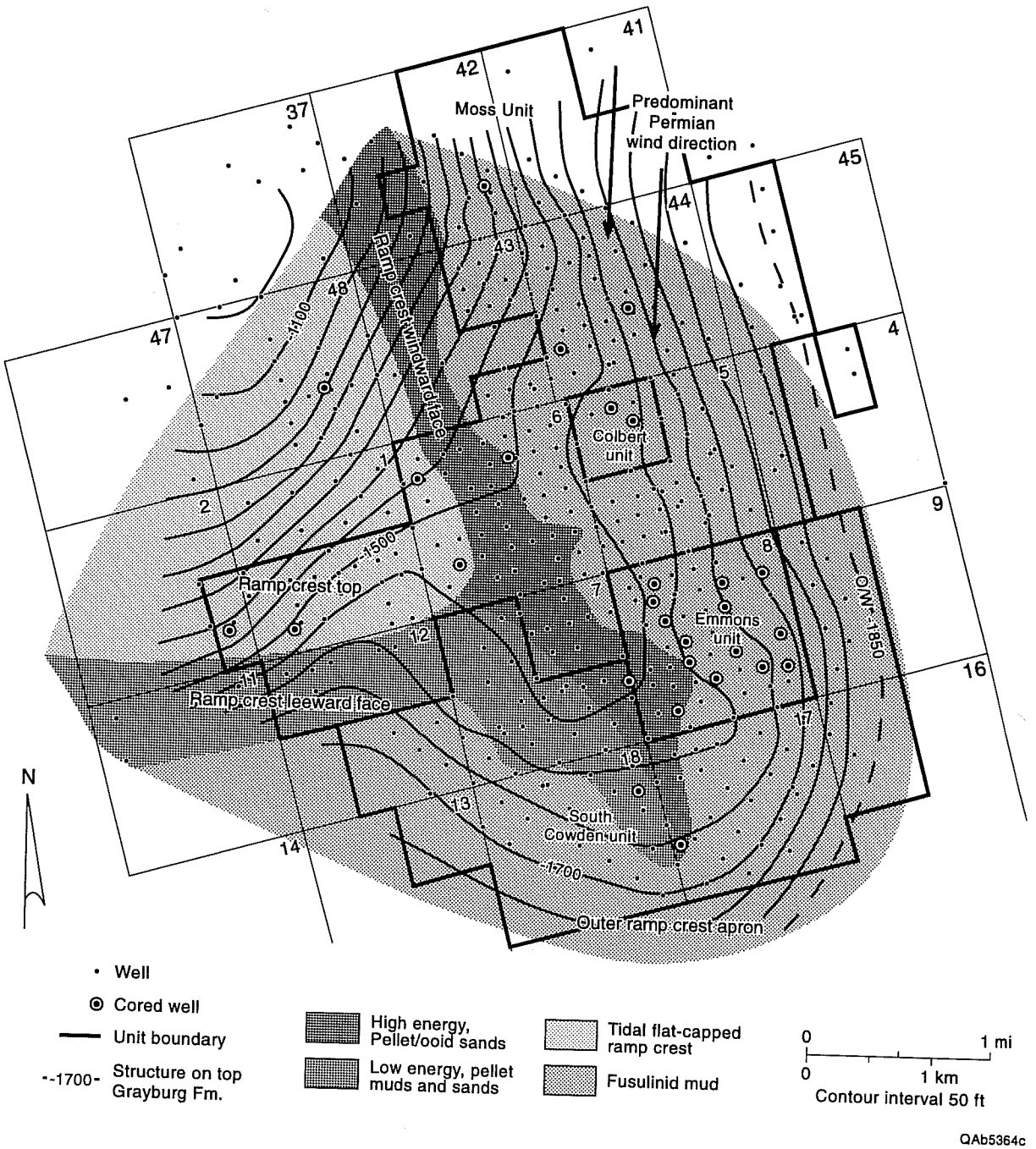

41
42
37
Moss Unit
Predominant
Permian
wind direction
45
44
43
48
47
4
5
6
Colbert
unit
1
2
9
8
7
Emmons
unit
O/W -1850
12
11
16
17
18
13
14
South
Cowden unit
-1700
Outer ramp crest apron
Ramp crest windward face
-1100
-1500
Ramp crest top
Ramp crest leeward face
N
Well
Cored well
Unit boundary
-1700- Structure on top Grayburg Fm.
High energy, Pellet/ooid sands
Low energy, pellet muds and sands
Tidal flat-capped ramp crest
Fusulinid mud
0
1 mi
0
1 km
Contour interval 50 ft
QAb5364c

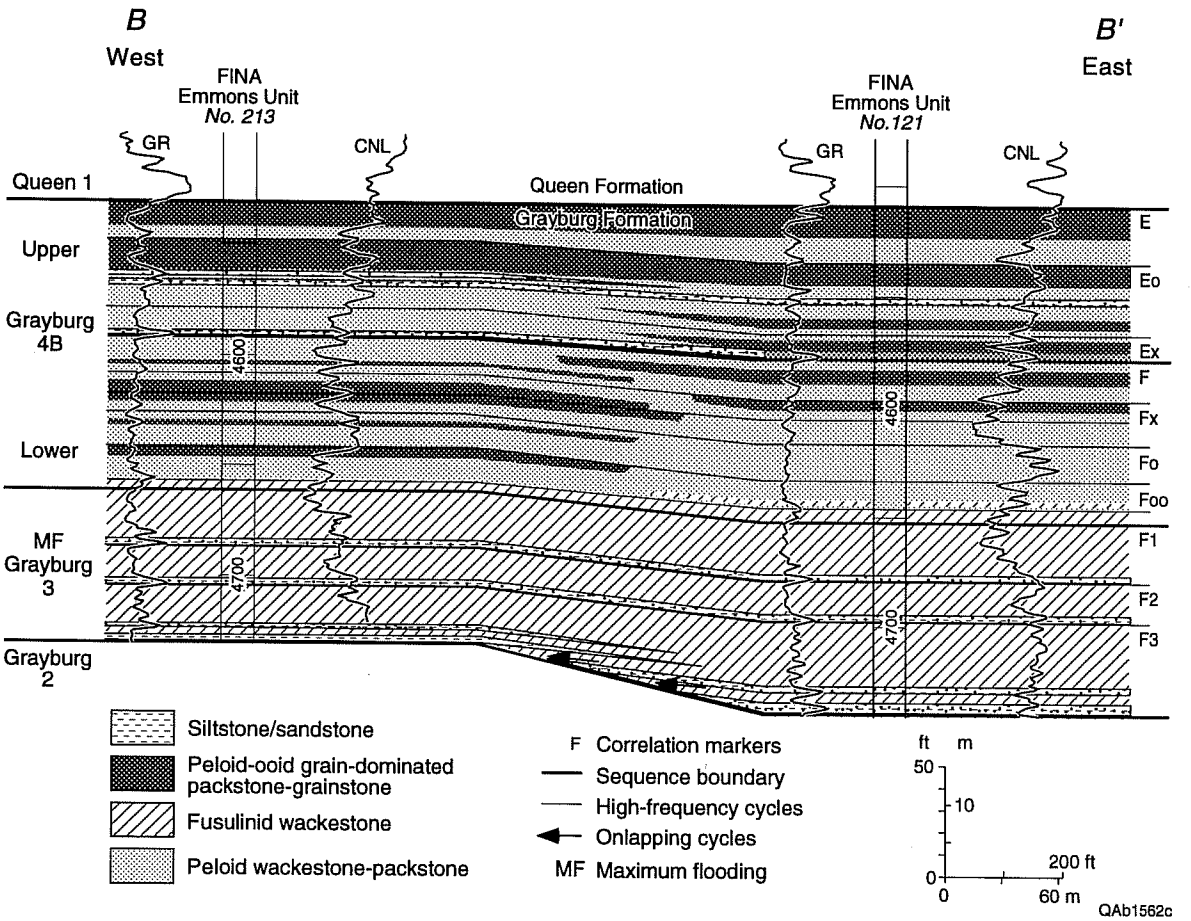
B
West
B'
East
FINA
Emmons Unit
No. 213
FINA
Emmons Unit
No.121
GR
CNL
GR
CNL
Queen 1
Queen Formation
Grayburg Formation
Upper
Grayburg
4B
Lower
MF
Grayburg
3
Grayburg
2
4600
4700
4600
4700
E
Eo
Ex
F
Fx
Fo
Foo
F1
F2
F3
Siltstone/sandstone
Peloid-ooid grain-dominated packstone-grainstone
Fusulinid wackestone
Peloid wackestone-packstone
F Correlation markers
Sequence boundary
High-frequency cycles
Onlapping cycles
MF Maximum flooding
ft m
50
10
0
200 ft
0
60 m
QAb1562c

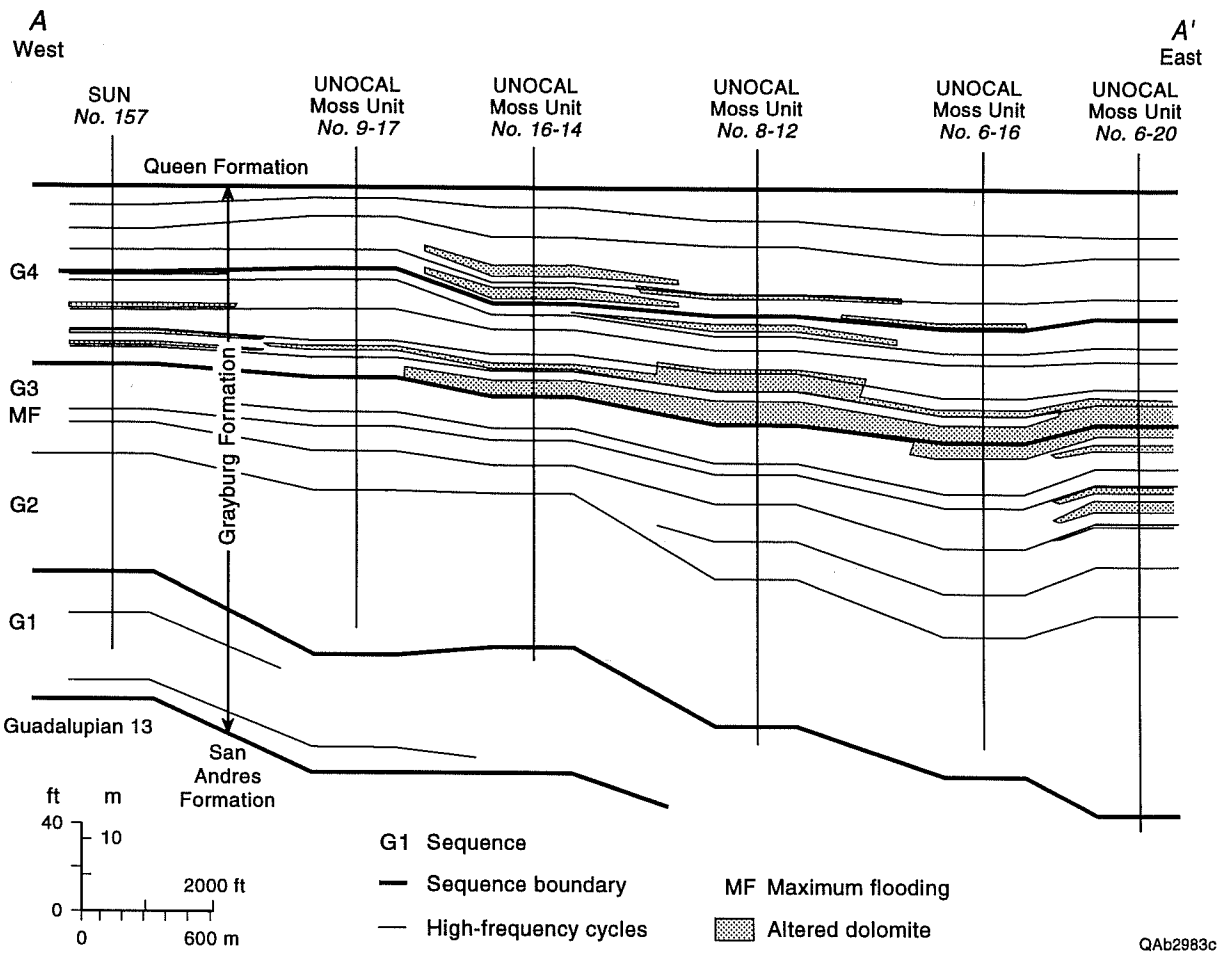
A
West
A'
East
SUN
No. 157
UNOCAL
Moss Unit
No. 9-17
UNOCAL
Moss Unit
No. 16-14
UNOCAL
Moss Unit
No. 8-12
UNOCAL
Moss Unit
No. 6-16
UNOCAL
Moss Unit
No. 6-20
Queen Formation
G4
G3
MF
G2
G1
Grayburg Formation
Guadalupian 13
San
Andres
Formation
ft
m
40
10
0
2000 ft
0
600 m
G1 Sequence
Sequence boundary
High-frequency cycles
MF Maximum flooding
Altered dolomite
QAb2983c

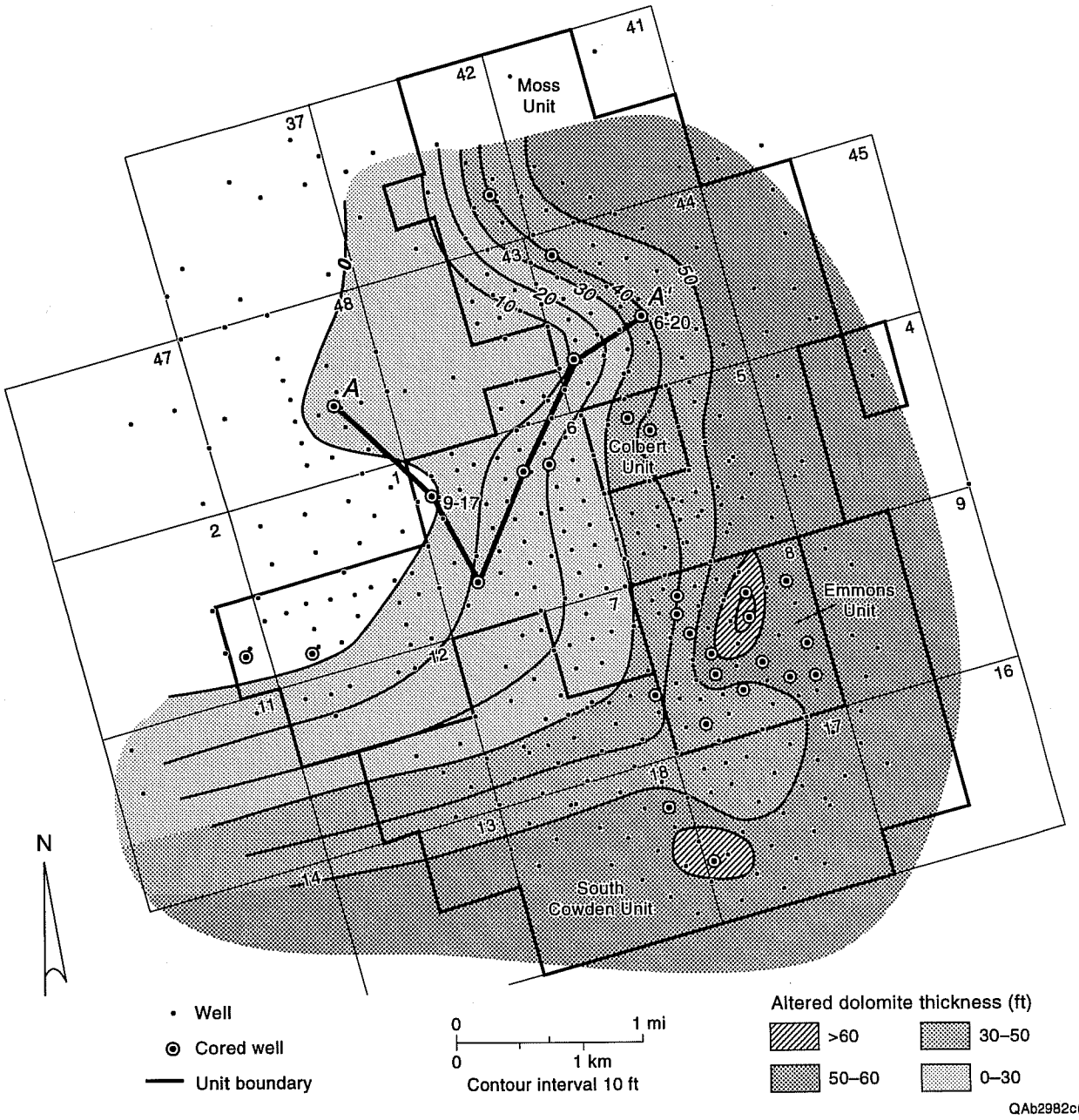
Moss Unit
Colbert Unit
Emmons Unit
South Cowden Unit
A
A'
9-17
6-20
0
10
20
30
40
50
N
Well
Cored well
Unit boundary
0 1 mi
0 1 km
Contour interval 10 ft
Altered dolomite thickness (ft)
>60
50–60
30–50
0–30
QAb2982c(a)

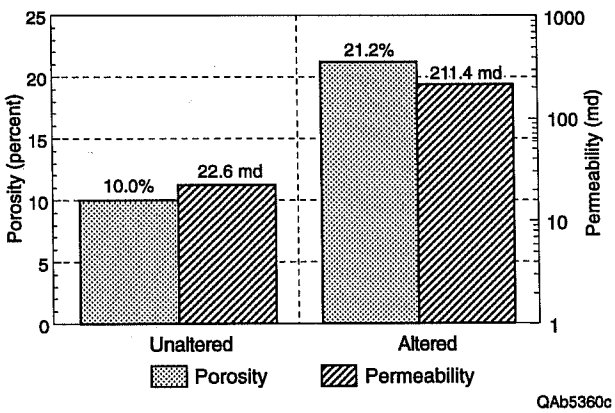
25
20
15
10
5
0
Porosity (percent)
1000
100
10
1
Permeability (md)
10.0%
22.6 md
21.2%
211.4 md
Unaltered
Altered
Porosity
Permeability
QAb5360c

41
42
37
Moss
unit
45
44
43
A
6-20
48
4
47
5
6
Colbert
unit
1
9-17'
9
2
8
C'
7
Emmons
unit
C
12
16
11
17
18
13
South
Cowden unit
14
N
Well
Cored well
Unit boundary
0
1 mi
0
1 km
Common nodular, poikilotopic and void-filling anhydrite
Altered anhydrite and gypsum
Large-scale anhydrite removal; calcite-lined vugs
QAb2984c(a)

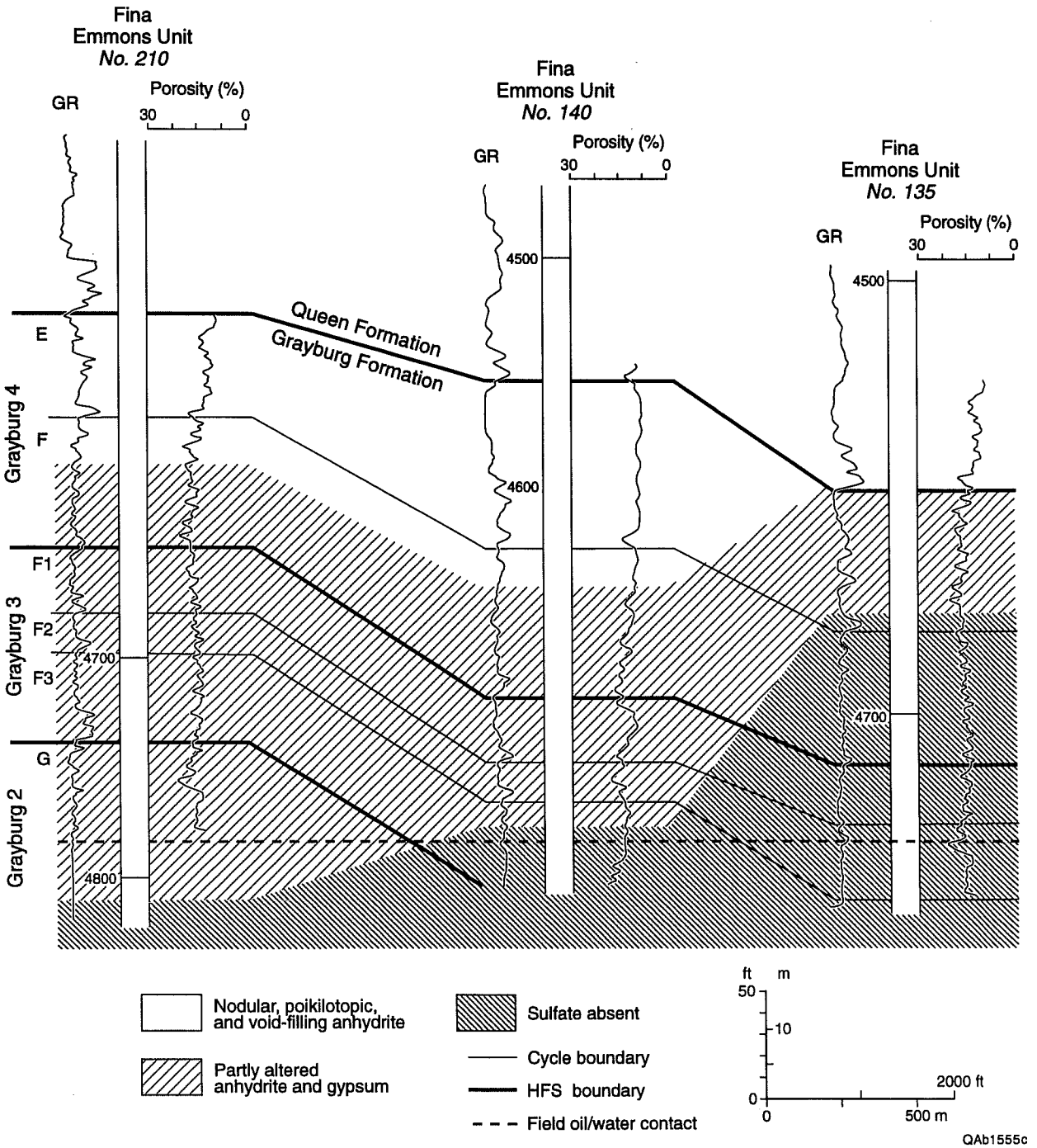
Fina
Emmons Unit
No. 210
GR
Porosity (%)
30
0
Fina
Emmons Unit
No. 140
GR
Porosity (%)
30
0
Fina
Emmons Unit
No. 135
GR
Porosity (%)
30
0
4500
4600
4700
4800
Queen Formation
Grayburg Formation
E
F
F1
F2
F3
G
Grayburg 4
Grayburg 3
Grayburg 2
Nodular, poikilotopic, and void-filling anhydrite
Partly altered anhydrite and gypsum
Sulfate absent
Cycle boundary
HFS boundary
Field oil/water contact
ft
m
50
10
0
2000 ft
0
500 m
QAb1555c

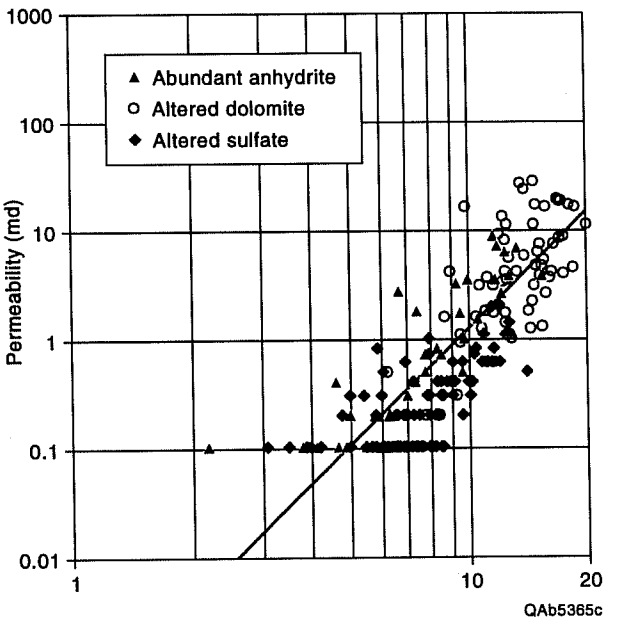
1000
100
10
1
0.1
0.01
Permeability (md)
Abundant anhydrite
Altered dolomite
Altered sulfate
1
10
20
QAb5365c

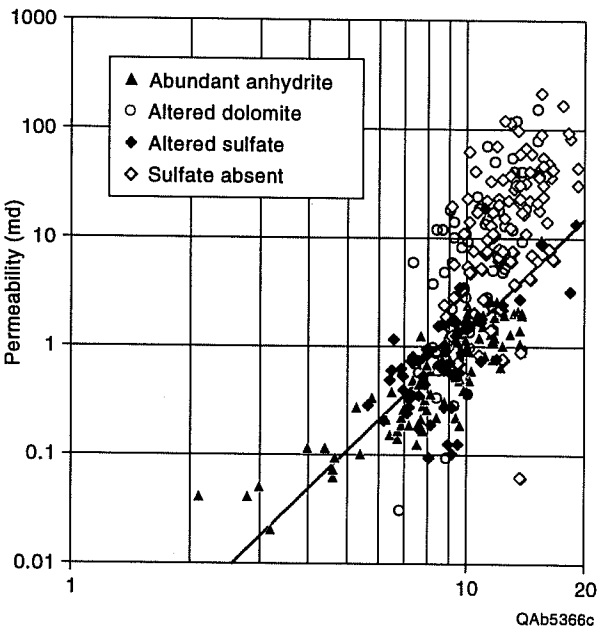
1000
100
10
1
0.1
0.01
Permeability (md)
1
10
20
Abundant anhydrite
Altered dolomite
Altered sulfate
Sulfate absent
QAb5366c

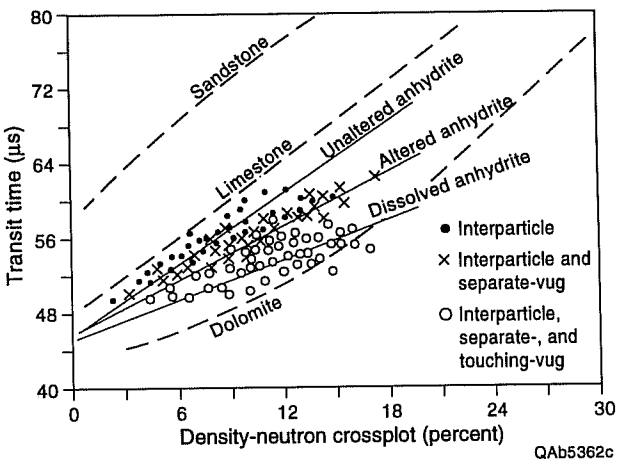
80
72
64
56
48
40
Transit time (µs)
0
6
12
18
24
30
Density-neutron crossplot (percent)
Sandstone
Limestone
Unaltered anhydrite
Altered anhydrite
Dissolved anhydrite
Dolomite
• Interparticle
× Interparticle and separate-vug
O Interparticle, separate-, and touching-vug
QAb5362c

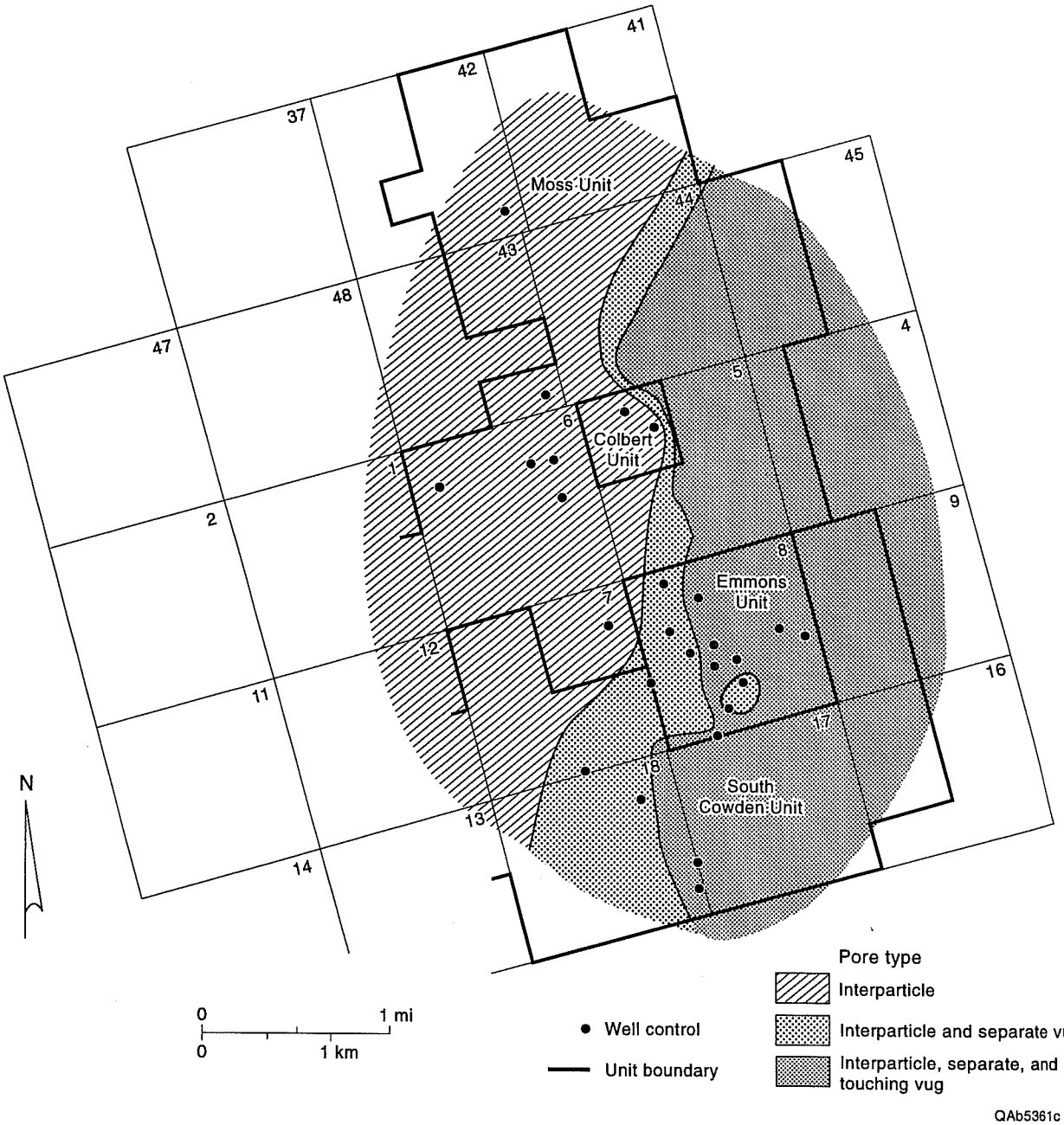
41
42
37
45
Moss Unit
44
43
48
4
47
5
6
Colbert Unit
1
9
2
8
Emmons Unit
7
12
16
11
17
18
South Cowden Unit
13
14
N
0
1 mi
0
1 km
Well control
Unit boundary
Pore type
Interparticle
Interparticle and separate vug
Interparticle, separate, and touching vug
QAb5361c

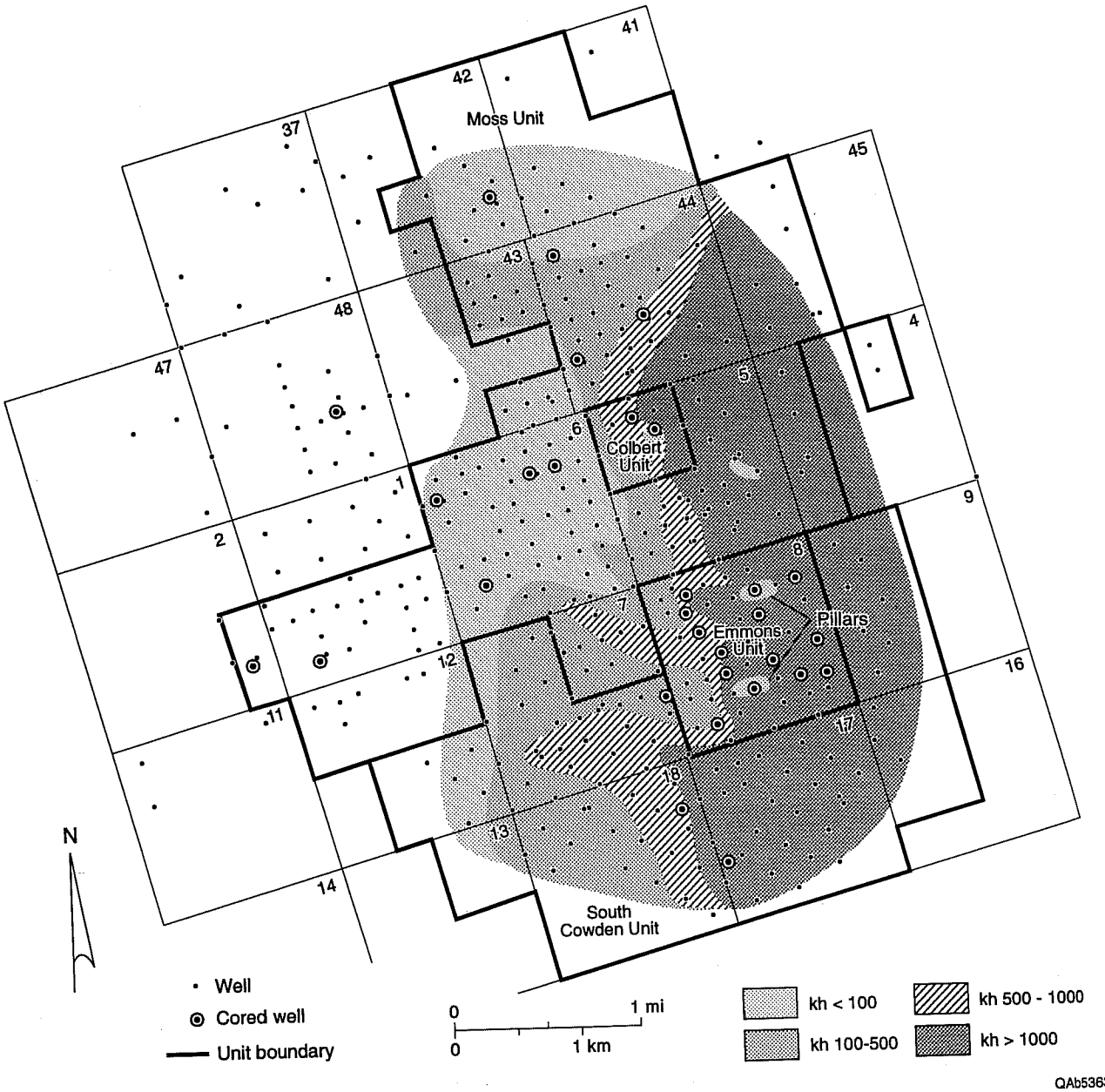
41
42
Moss Unit
37
45
44
43
48
4
47
5
6
Colbert
Unit
1
9
2
8
7
Pillars
Emmons
Unit
12
16
11
17
18
13
14
South
Cowden Unit
N
Well
Cored well
Unit boundary
0
1 mi
0
1 km
kh < 100
kh 100-500
kh 500 - 1000
kh > 1000
QAb5363c

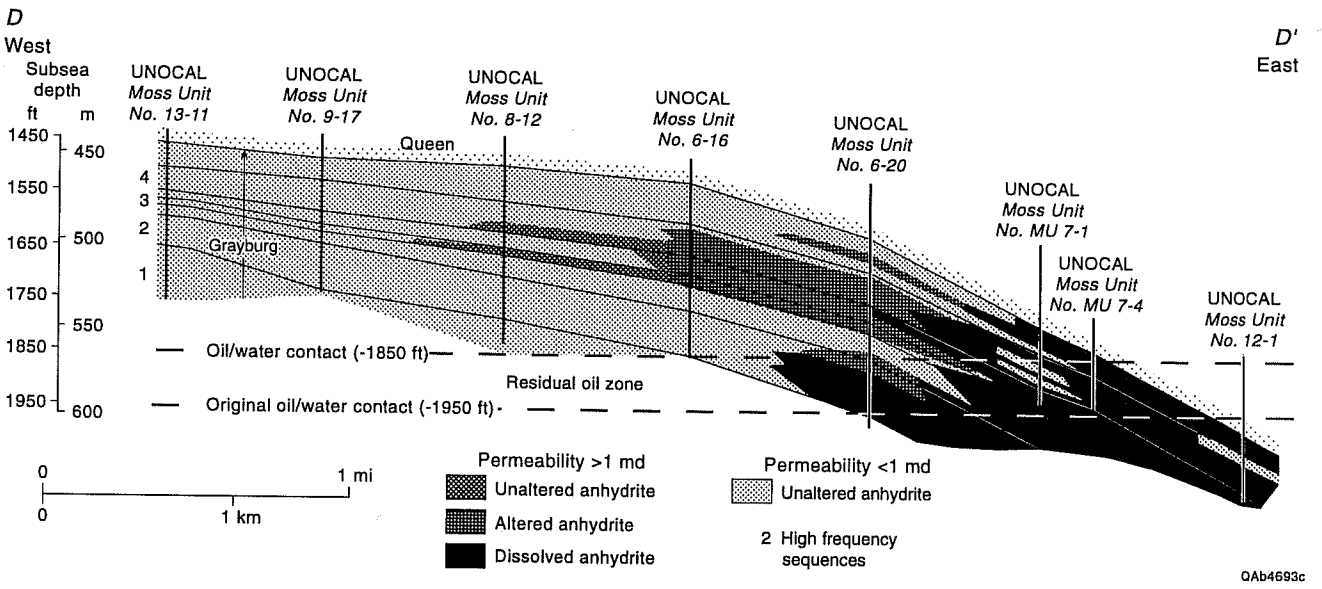
D
West
D'
East
Subsea depth
ft
m
1450
1550
1650
1750
1850
1950
450
500
550
600
UNOCAL Moss Unit No. 13-11
UNOCAL Moss Unit No. 9-17
UNOCAL Moss Unit No. 8-12
UNOCAL Moss Unit No. 6-16
UNOCAL Moss Unit No. 6-20
UNOCAL Moss Unit No. MU 7-1
UNOCAL Moss Unit No. MU 7-4
UNOCAL Moss Unit No. 12-1
Queen
Grayburg
4
3
2
1
Oil/water contact (-1850 ft)
Residual oil zone
Original oil/water contact (-1950 ft)
0
1 mi
0
1 km
Permeability >1 md
Unaltered anhydrite
Altered anhydrite
Dissolved anhydrite
Permeability <1 md
Unaltered anhydrite
2 High frequency sequences
QAb4693c

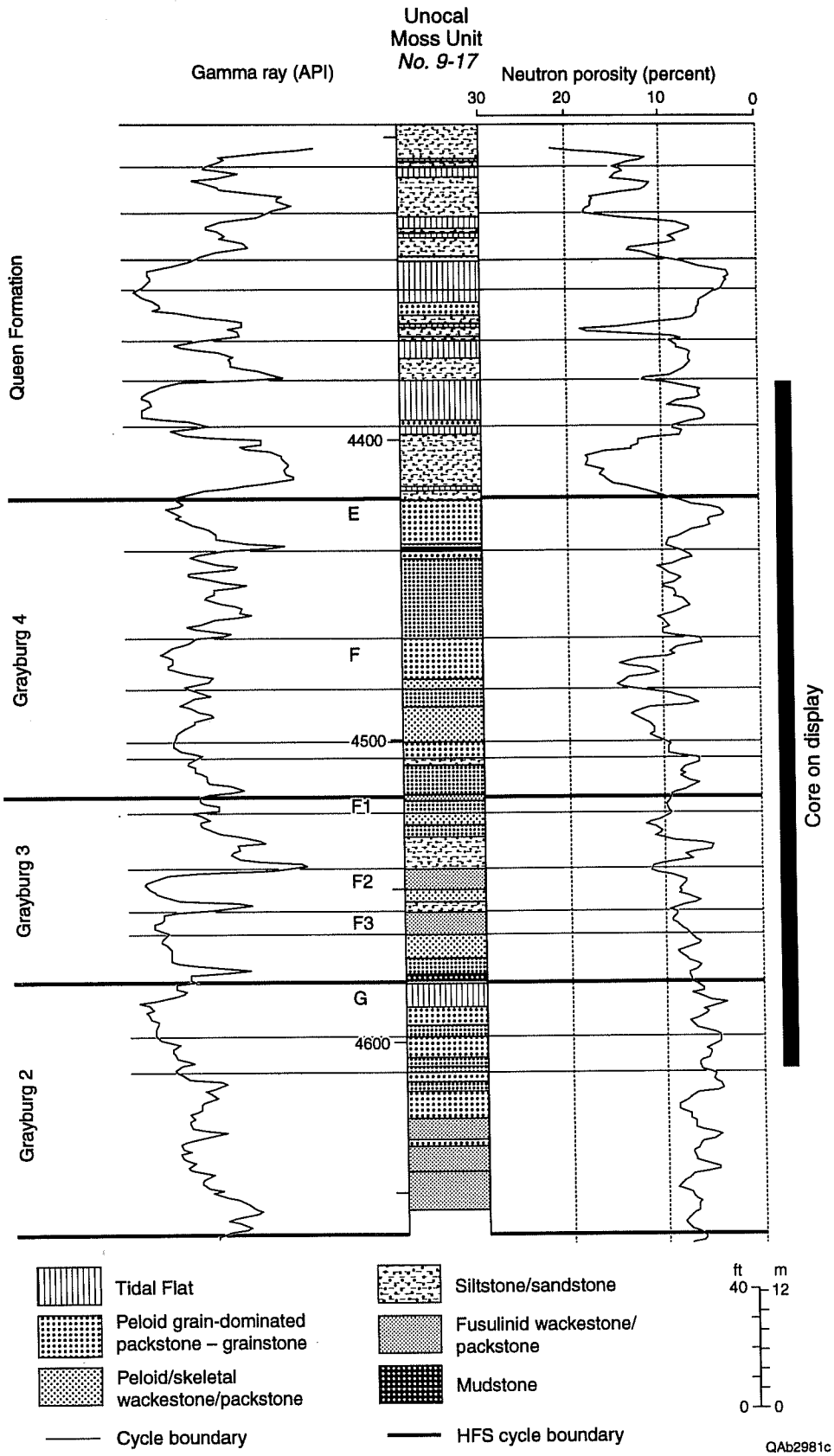
Unocal
Moss Unit
No. 9-17
Gamma ray (API)
Neutron porosity (percent)
30
20
10
0
Queen Formation
4400
E
Grayburg 4
F
4500
F1
Grayburg 3
F2
F3
G
4600
Grayburg 2
Core on display
Tidal Flat
Peloid grain-dominated packstone – grainstone
Peloid/skeletal wackestone/packstone
Cycle boundary
Siltstone/sandstone
Fusulinid wackestone/ packstone
Mudstone
HFS cycle boundary
ft
m
40
12
0
0
QAb2981c

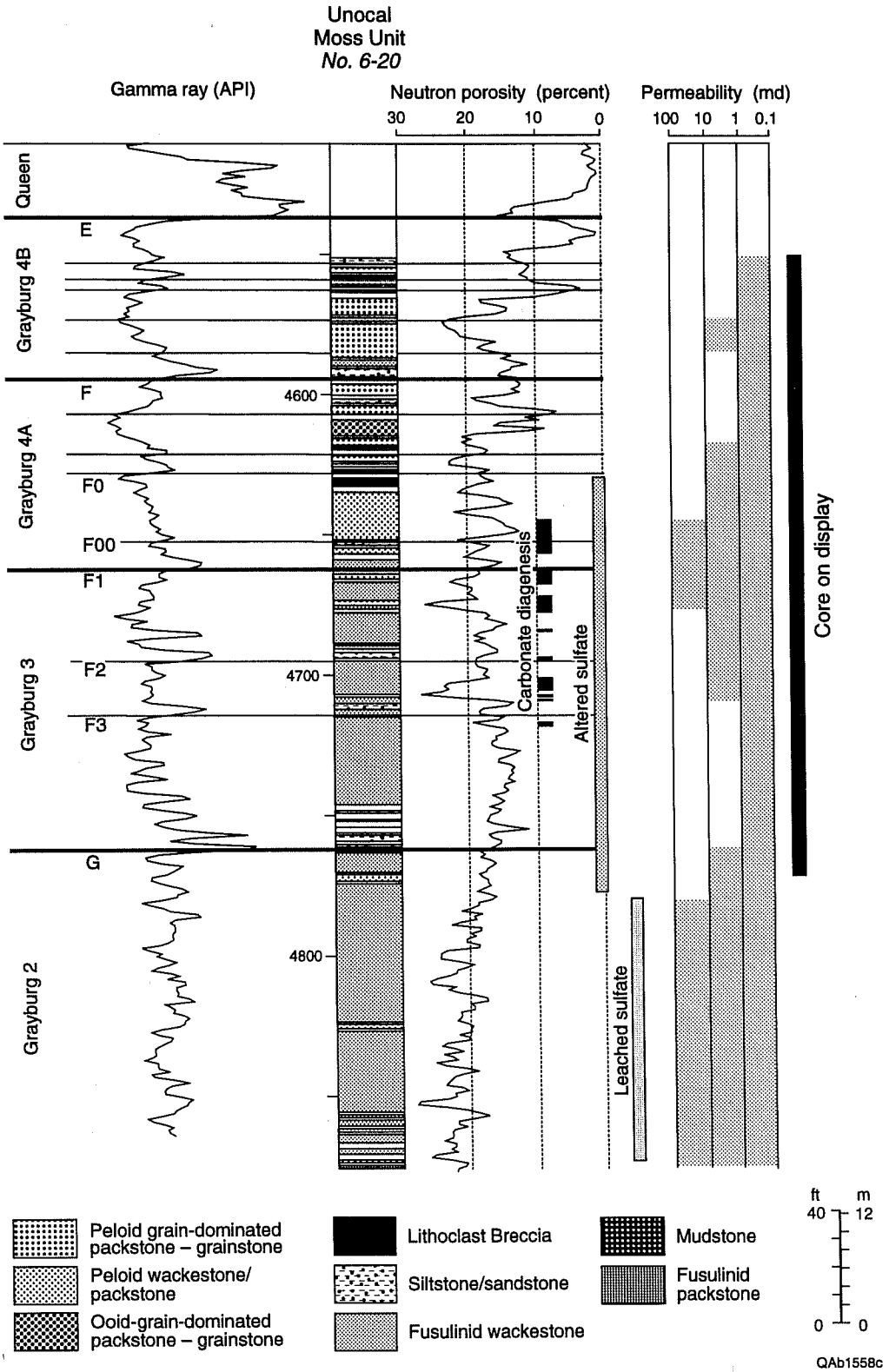
Unocal
Moss Unit
No. 6-20
Gamma ray (API)
Neutron porosity (percent)
30
20
10
0
Permeability (md)
100
10
1
0.1
Queen
E
Grayburg 4B
F
Grayburg 4A
F0
F00
F1
F2
F3
Grayburg 3
G
Grayburg 2
4600
4700
4800
Carbonate diagenesis
Altered sulfate
Leached sulfate
Core on display
Peloid grain-dominated packstone – grainstone
Peloid wackestone/ packstone
Ooid-grain-dominated packstone – grainstone
Lithoclast Breccia
Siltstone/sandstone
Fusulinid wackestone
Mudstone
Fusulinid packstone
ft
m
40
12
0
0
QAb1558c

RAMSEY SANDSTONE DEEP-WATER CHANNEL-LEVEE AND LOBE DEPOSITS, FORD GERALDINE UNIT, REEVES AND CULBERSON COUNTIES, TEXAS

SHIRLEY P. DUTTON, MARK D. BARTON, SIGRID J. CLIFT, AND JOSE I. GUZMAN,
Bureau of Economic Geology, The University of Texas at Austin, Austin, TX 78713-8924

ABSTRACT

The Ford Geraldine unit produces from the Upper Permian Ramsey sandstone in the Delaware Basin of West Texas. The Ramsey sandstone is composed of a 0- to 60-ft-thick sandstone bounded by laminated siltstones. The Ramsey sandstone has an elongate geometry in the Ford Geraldine unit; it is 5 to 6 mi long and 1 to 2 mi wide. Ramsey sandstones are interpreted as having been deposited by sandy, high- and low-density turbidity currents. The sands were deposited in a deep-water, basin-floor setting in a channel-levee system with attached lobes. Channel facies are approximately 1,200 ft wide and 15 to 35 ft thick. They consist of massive and crossbedded sandstones interpreted to have been deposited from high-density turbidity currents. Channel margins, characterized by thin-bedded, rippled and convoluted sandstones interbedded with minor siltstones, are interpreted as channel levees formed by overbanking of low-density turbidity currents. Levees have a wedge-shaped geometry and decrease in thickness away from channels. Lobe sandstones were deposited by high-density turbidity currents at the mouth of channels or in interchannel areas. They were identified by thick-bedded, massive and graded sandstones with load and dewatering structures that include flame structures, dish structures, and vertical pipes. Lobe sandstones are 3 to 30 ft thick and have a broad lens-shape or tabular geometry.

INTRODUCTION

The Ford Geraldine unit in Reeves and Culberson Counties, Texas (figs. 1, 2), produces from the Ramsey sandstone, the most prolific horizon in the Upper Permian Bell Canyon Formation. The 99 million barrels of original oil in place (Pittaway and Rosato, 1991) makes it the largest Delaware Mountain Group field in the basin. The main reservoir at Geraldine Ford field is the Ramsey sandstone, but there is also some production from the underlying Olds sandstone (fig. 3). Thirteen years of primary production and 28 years of secondary (waterflood) and tertiary (CO_2 flood) development in the Ford Geraldine unit have resulted in a recovery efficiency of only 28% (K. R. Pittaway, written communication, 1997). The Ford Geraldine unit was the focus of a DOE Class III reservoir-characterization project. Use of the abundant core control—almost 4,300 ft of core from 83 wells and nearly 8,000 core analyses from 120 wells—was critical to the characterization of this mature oil field.

Ramsey sandstone reservoirs produce oil and gas from slope and basin sandstone deposits that form long, linear trends (Williamson, 1978). Structural contours on the Lamar Limestone above the Ramsey sandstone indicate monoclinal dip to the northeast (fig. 4). The trap in Ramsey sandstone fields is formed by pinch-out of permeable sandstone into low-permeability siltstone structurally updip. Most Ramsey sandstone fields have minor structural closure because of differential compaction over the reservoir sandstone body (Ruggiero, 1985).

FIELD HISTORY

Geraldine Ford field was discovered in 1956. Well completions typically included hydraulic fracturing and acidizing. By the end of 1959 most of the field had been developed on a 20-acre spacing, and reservoir pressure had declined to bubble point (1,383 psi), resulting in a sharp increase in gas-oil ratio and water production (Ruggiero, 1985, 1993). By 1968, reservoir pressure had dropped to 300 to 500 psi. The field was unitized (into the Ford Geraldine unit) for

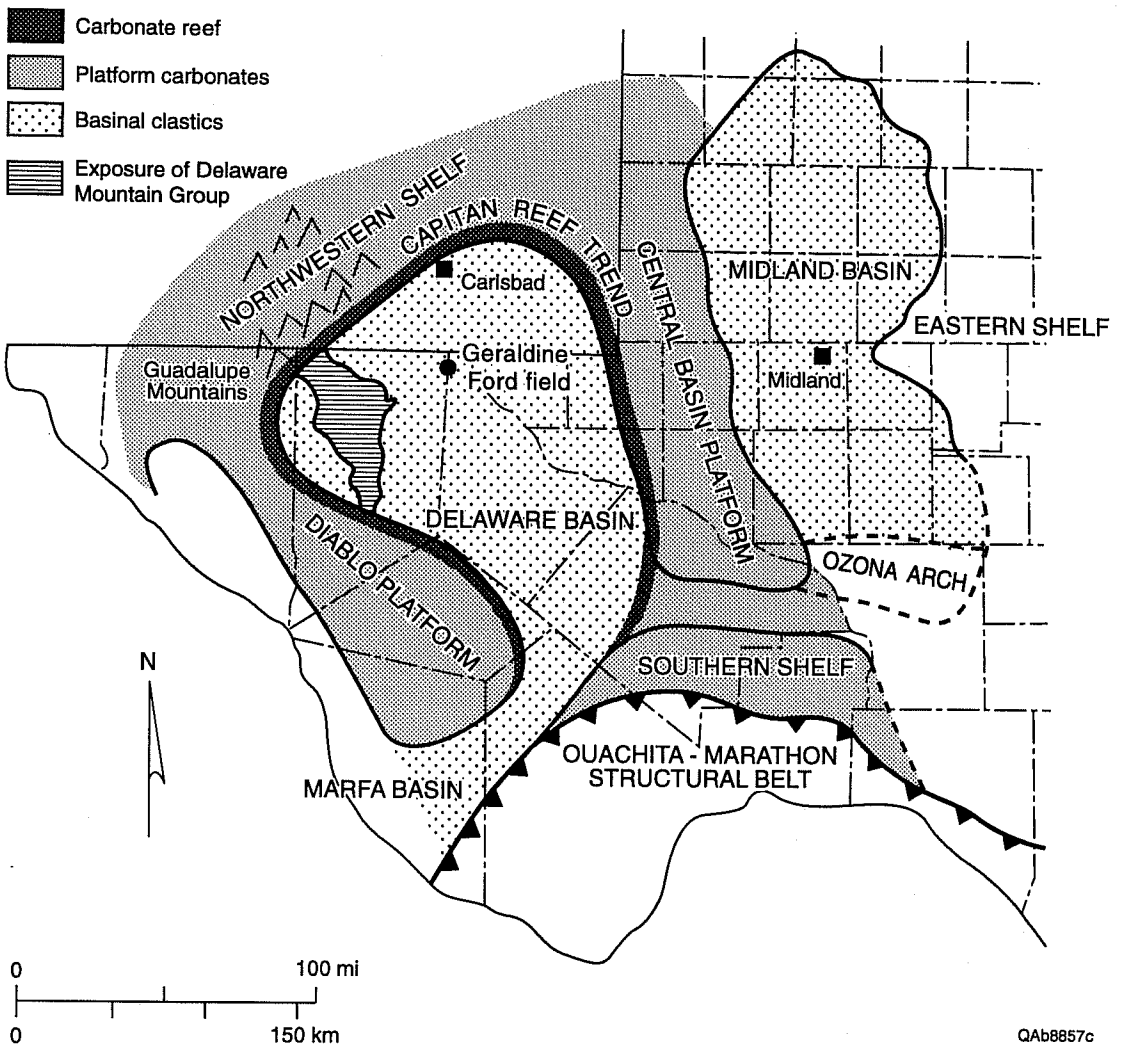
Carbonate reef
Platform carbonates
Basinal clastics
Exposure of Delaware Mountain Group
NORTHWESTERN SHELF
CAPITAN REEF TREND
CENTRAL BASIN PLATFORM
MIDLAND BASIN
EASTERN SHELF
Carlsbad
Geraldine Ford field
Midland
Guadalupe Mountains
DELAWARE BASIN
DIABLO PLATFORM
OZONA ARCH
SOUTHERN SHELF
OUACHITA - MARATHON STRUCTURAL BELT
MARFA BASIN
N
0
100 mi
0
150 km
QAb8857c

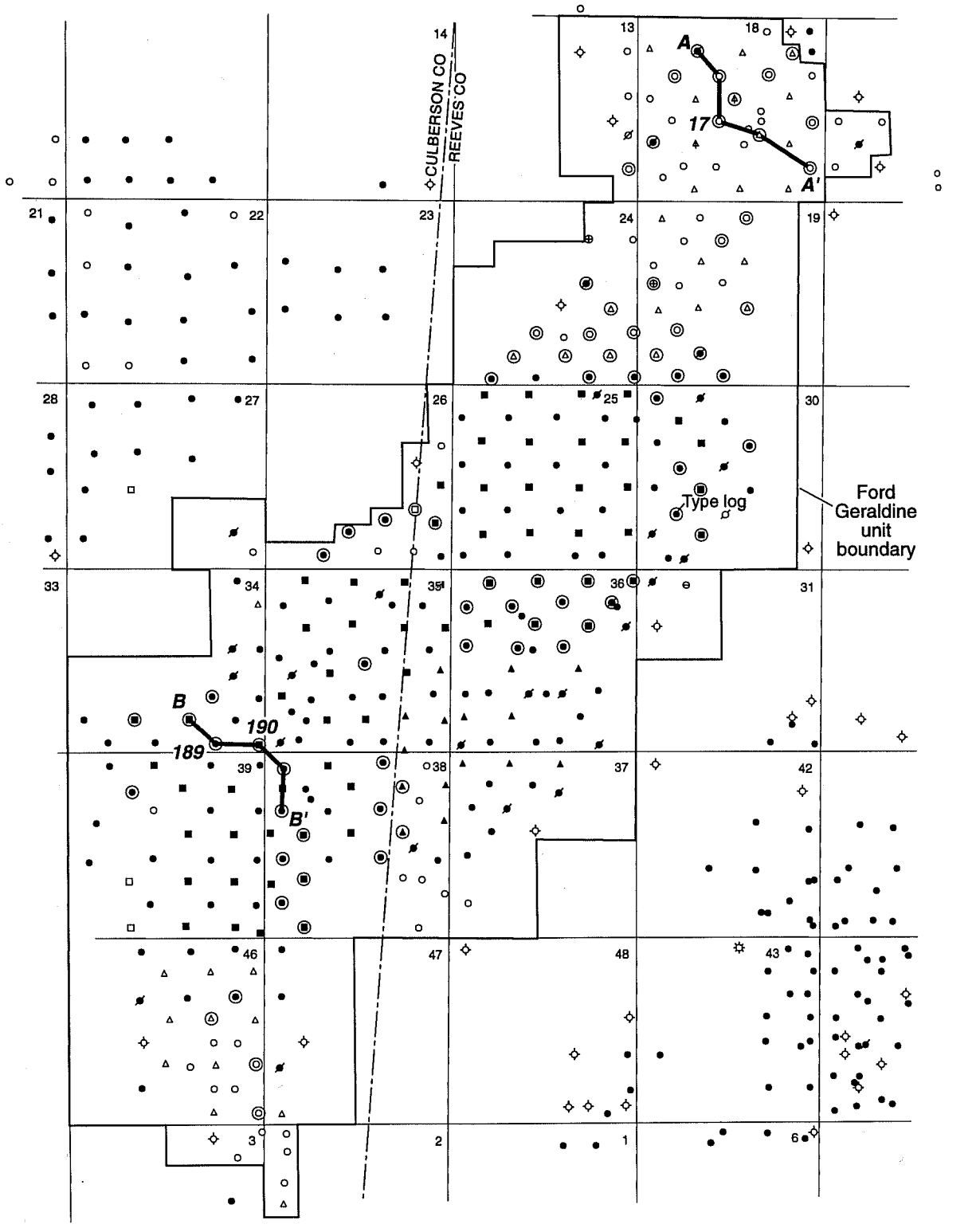
CULBERSON CO
REEVES CO
A
A'
17
B
B'
189
190
Type log
Ford Geraldine unit boundary
13
14
18
19
21
22
23
24
25
26
27
28
30
31
33
34
35
36
37
38
39
42
43
46
47
48
1
2
3
6
0
1 mi
0
1 km
◎ Cored well
• Oil producing unit
Plugged and abandoned
○ Oil, temporarily shut-in
▲ Injection, water
△ Injection, temporarily shut-in
Injection, permanently shut-in
■ Injection, CO_2
□ Injection, CO_2 shut-in
⊕ Salt-water disposal
Oil, permanently shut-in
⊖ Saltwater, temporarily shut-in
Dry hole

QAc820c

Ford Geraldine Unit No. 108

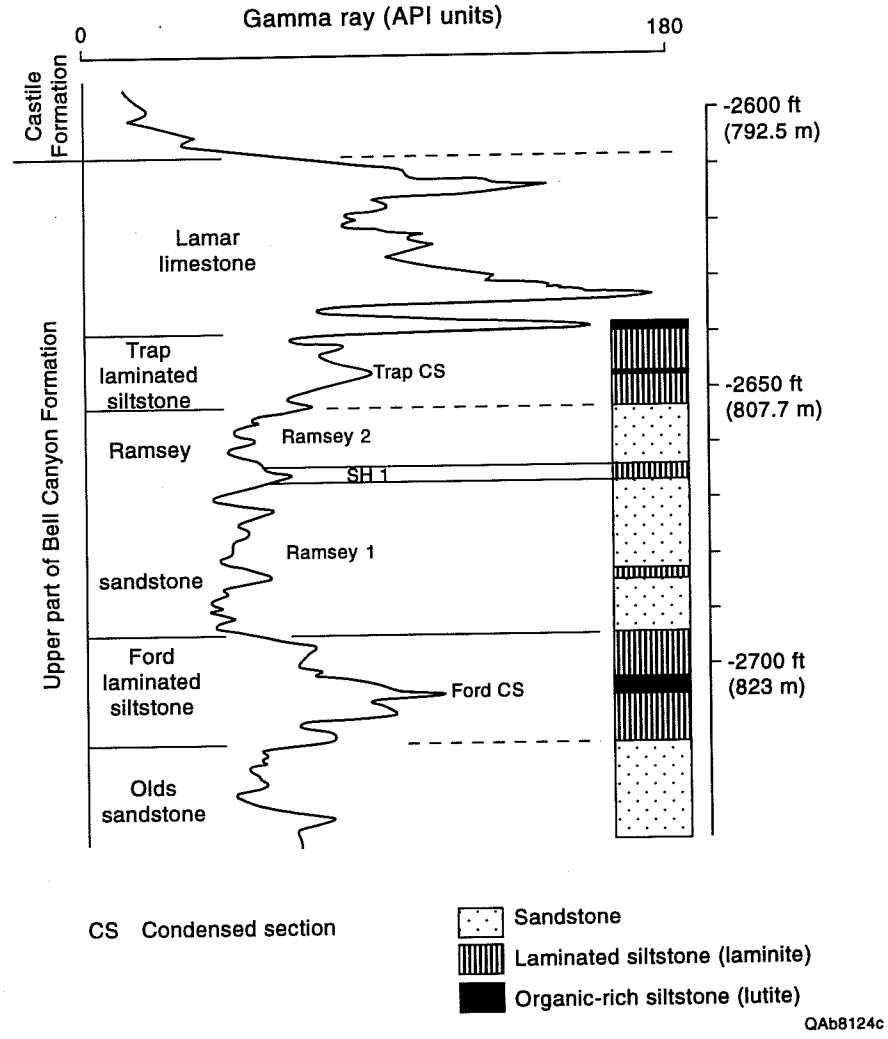

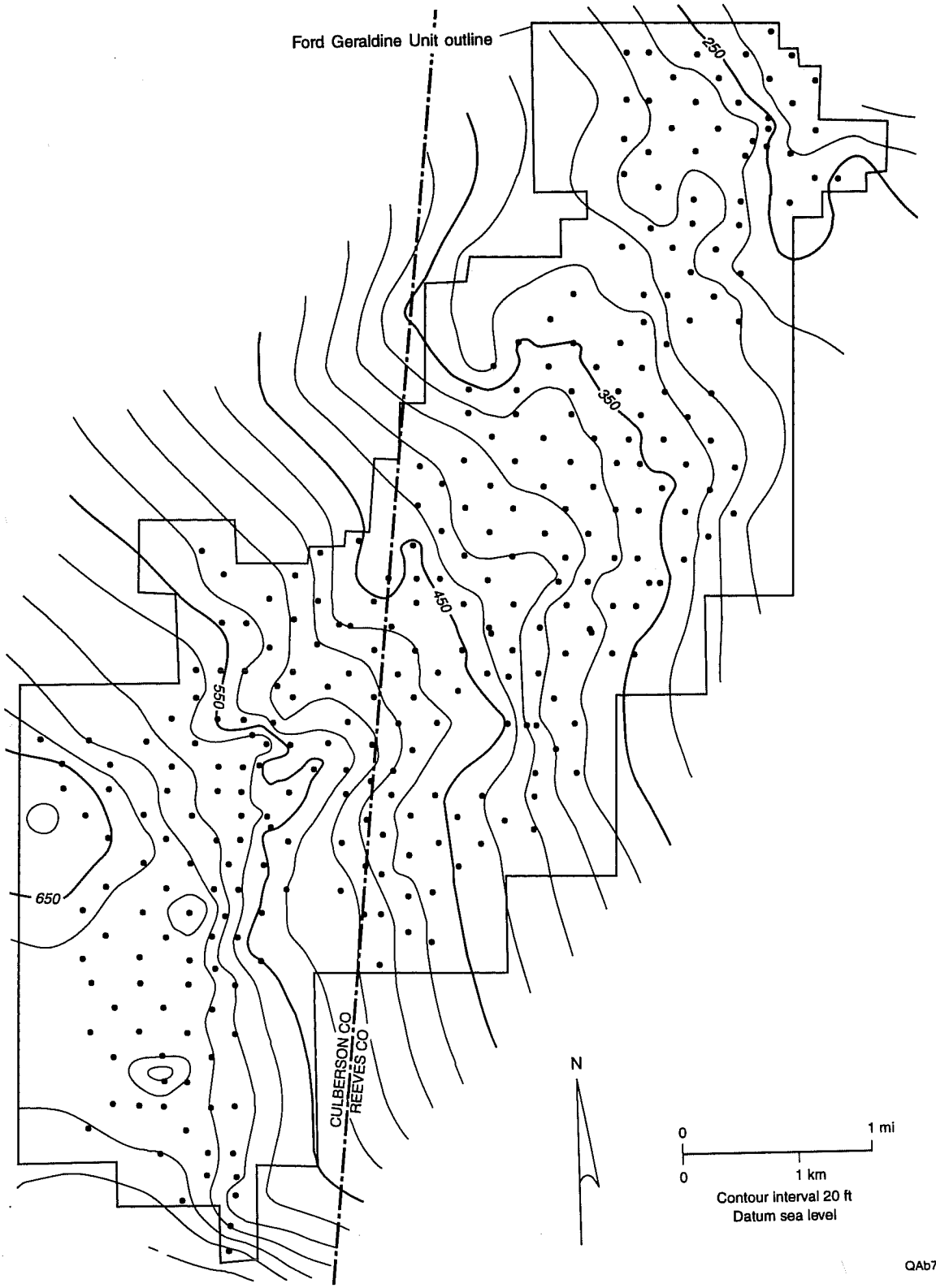
Ford Geraldine Unit outline
250
350
450
550
650
CULBERSON CO
REEVES CO
N
0
1 mi
0
1 km
Contour interval 20 ft
Datum sea level
QAb7508c

secondary development after primary cumulative production of 13.2 MMbbl (Pittaway and Rosato, 1991).

Waterflooding was initiated in 1969; injection patterns were geometric 5-spots. Secondary recovery of 2,875 bopd peaked in 1975. By 1981, recovery rates dropped to 569 bopd, and water cuts had risen to 95% of production (Pittaway and Rosato, 1991). An additional 6.8 MMbbl of oil was produced after unitization, and recovery efficiency had increased to 22.5%. Of that, 18% is attributed to primary recovery and 4.5% to secondary recovery (Pittaway and Rosato, 1991).

In 1981, tertiary recovery by CO_2 injection began in the central part of the reservoir and was gradually expanded to include most of the unit except for the northern end. The same patterns used in the waterflood were used in the CO_2 flood. Production response occurred in 1986 after higher and constant CO_2 injection began in December 1985 (Pittaway and Rosato, 1991). Before CO_2 flooding, production was down to 300 bopd; by 1991, production had increased to nearly 2,000 bopd.

Average reservoir pressure on January 1, 1997, was 1,500 psi. Cumulative tertiary production by that date was 5.7 million barrels, and tertiary recovery efficiency was 5.8% (K. R. Pittaway, written communication, 1997). Estimated ultimate tertiary recovery is 9.0%.

RESERVOIR CHARACTERIZATION OF FORD GERALDINE UNIT

Ford Geraldine unit has an excellent subsurface data base for reservoir characterization. Geophysical logs from 305 of the 340 wells in the field and 3,615 ft of Ramsey sandstone core from 70 wells were available. These data were supplemented by descriptions of 681 ft of core from 13 additional wells (Ruggiero, 1985). Information about Bell Canyon sandstones gathered from well-exposed outcrops (fig. 1) has guided interpretation of the reservoir at Ford Geraldine unit (Barton, 1997; Dutton and others, 1997a). In addition to the outcrop characterization, previous studies of Geraldine Ford field and other nearby Bell Canyon fields by Payne (1976), Williamson (1978, 1979), Berg (1979), Ruggiero (1985, 1993), and Gardner (1992, 1997) provided the foundation for this study.

Stratal relationships in outcrops about 25 mi west of Ford Geraldine unit (fig. 1) indicate that the upper Bell Canyon sandstones were deposited in channels with levees and attached lobes (Barton, 1997; Dutton and others, 1997a). This model predicts lateral heterogeneity within the reservoir sandstones caused by the juxtaposition of sandstone channel, levee, and lobe facies and their interfingering with interchannel facies composed of organic-rich siltstones. Reservoir characterization of the Ramsey sandstone at Ford Geraldine unit, summarized below, indicates that the channel-levee and lobe model best fits the data.

Ramsey Sandstone Facies

The six facies observed in Ramsey sandstone cores (figs. 5-7) were (1) organic-rich siltstone (lutite) (fig. 8); (2) laminated siltstone (laminite) (fig. 8); (3) sandstones lacking laminations but containing floating siltstone clasts, water escape features, and load structures (figs. 9-11); (4) rippled or convoluted sandstone (fig. 12); (5) cross-stratified sandstone (fig. 13), and (6) massive sandstone. Massive sandstones are volumetrically the most abundant sandstone facies in the core, although that may be in part an artifact of the narrow range of grain sizes, which makes sedimentary structures indistinct and difficult to see in the core.

The average grain size in Ramsey sandstone samples is 0.092 mm (3.44 Ø), very fine grained; the proportion of silt-sized grains in the sandstones ranges from 4 to 20%. The sandstones are mostly well sorted. Clay minerals in Ramsey sandstone are interpreted as being authigenic. Thus, as has been noted by previous workers (for example, Williamson, 1978; Berg, 1979), the Ramsey sandstones are unusual in their lack of detrital clay.

A laminated siltstone sample from the lower Trap immediately above the Ramsey 2 sandstone has an average grain size of 0.059 mm (4.09 Ø), and it contains 38% sand grains. A lutite sample near the base of the Lamar has an average grain size of 0.033 mm (4.94 Ø) and contains 46% silt, 46% organic matter, and 8% sand.

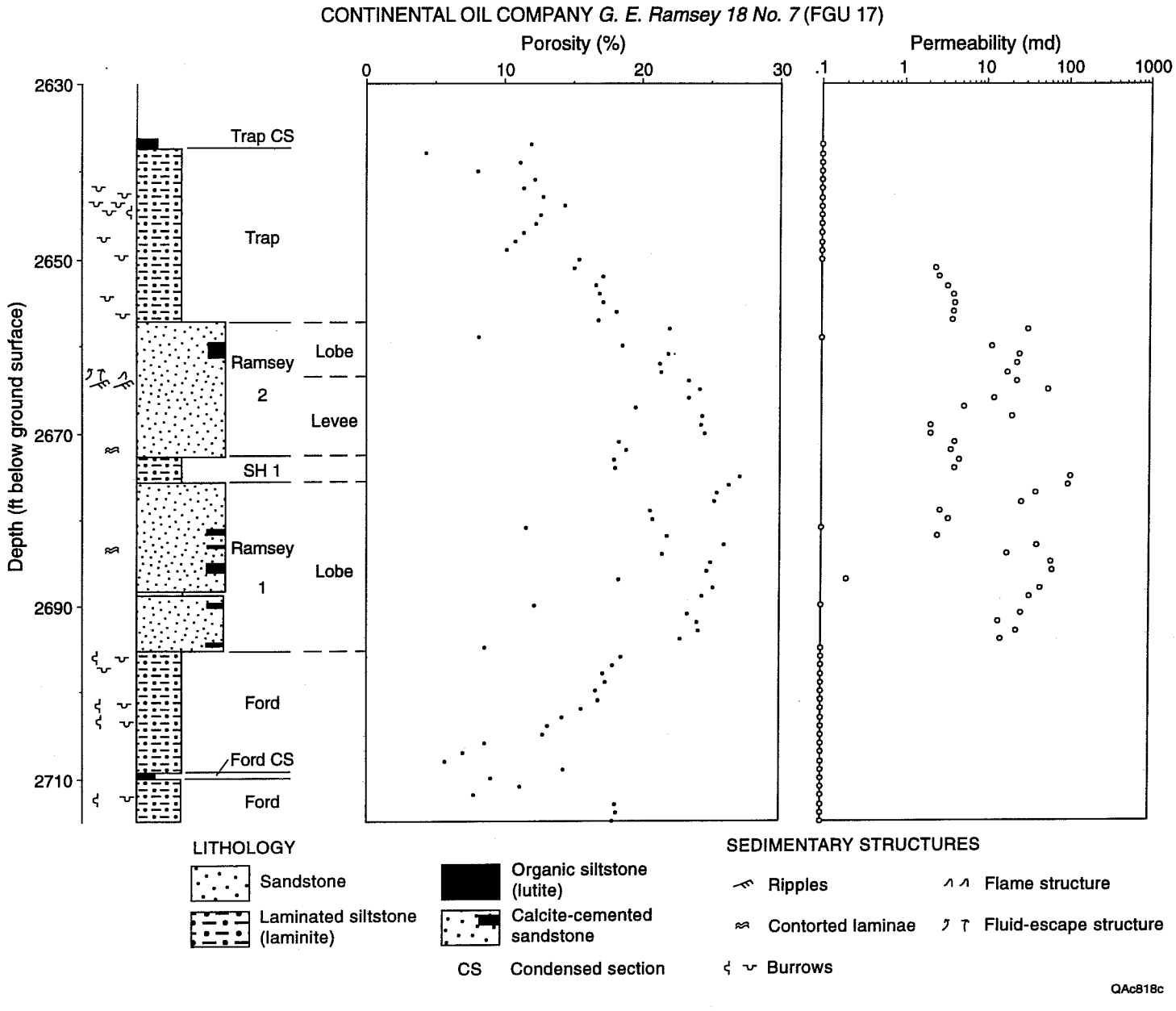
CONTINENTAL OIL COMPANY G. E. Ramsey 18 No. 7 (FGU 17)
Porosity (%)
0
10
20
30
Permeability (md)
.1
1
10
100
1000
Depth (ft below ground surface)
2630
2650
2670
2690
2710
Trap CS
Trap
Ramsey 2
Lobe
Levee
SH 1
Ramsey 1
Lobe
Ford
Ford CS
Ford
LITHOLOGY
Sandstone
Laminated siltstone (laminite)
Organic siltstone (lutite)
Calcite-cemented sandstone
CS Condensed section
SEDIMENTARY STRUCTURES
Ripples
Contorted laminae
Burrows
Flame structure
Fluid-escape structure
QAc818c

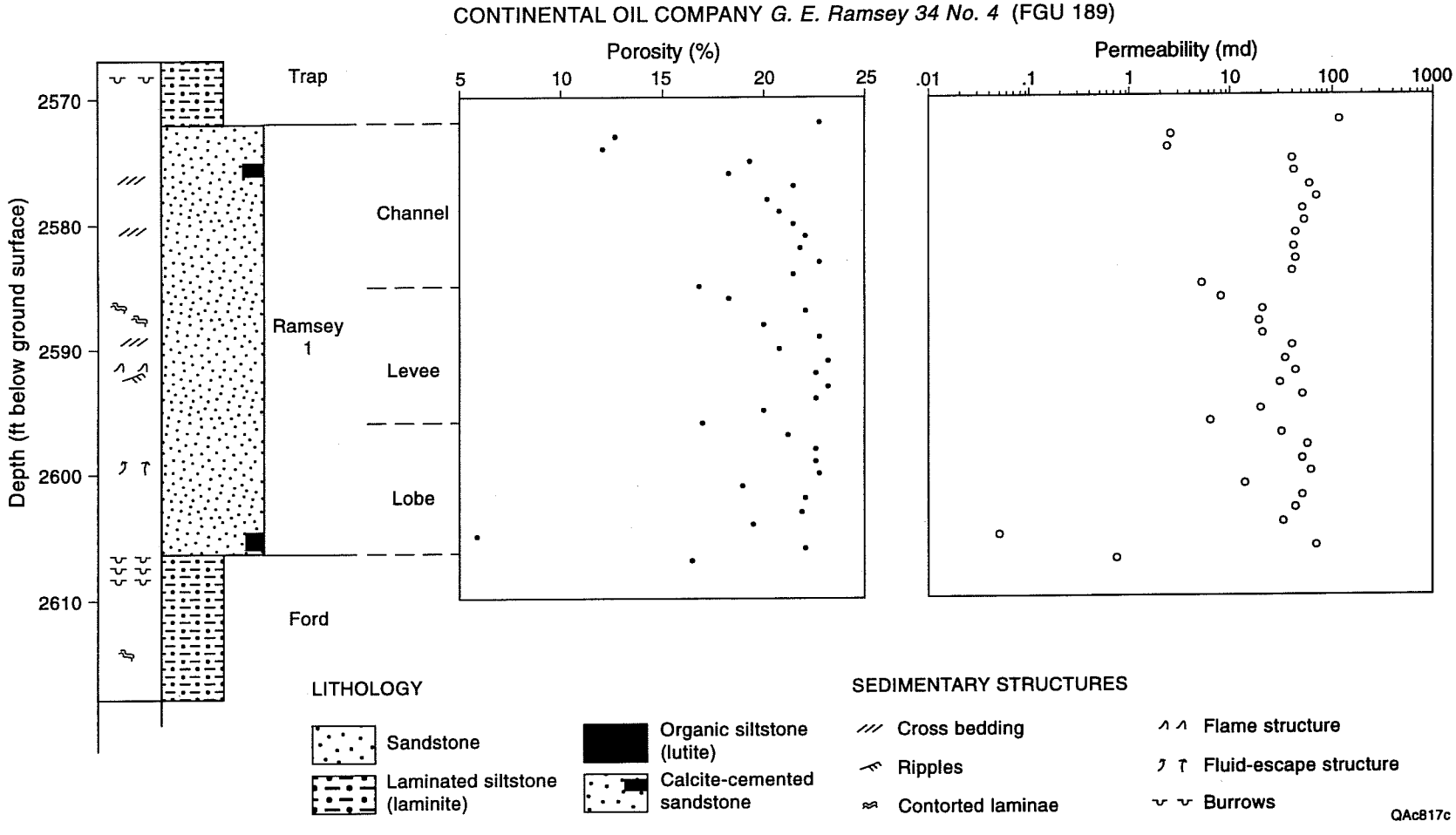
CONTINENTAL OIL COMPANY G. E. Ramsey 34 No. 4 (FGU 189)
Porosity (%)
5
10
15
20
25
Permeability (md)
.01
.1
1
10
100
1000
Depth (ft below ground surface)
2570
2580
2590
2600
2610
Trap
Channel
Ramsey 1
Levee
Lobe
Ford
LITHOLOGY
Sandstone
Laminated siltstone (laminite)
Organic siltstone (lutite)
Calcite-cemented sandstone
SEDIMENTARY STRUCTURES
Cross bedding
Ripples
Contorted laminae
Flame structure
Fluid-escape structure
Burrows
QAc817c

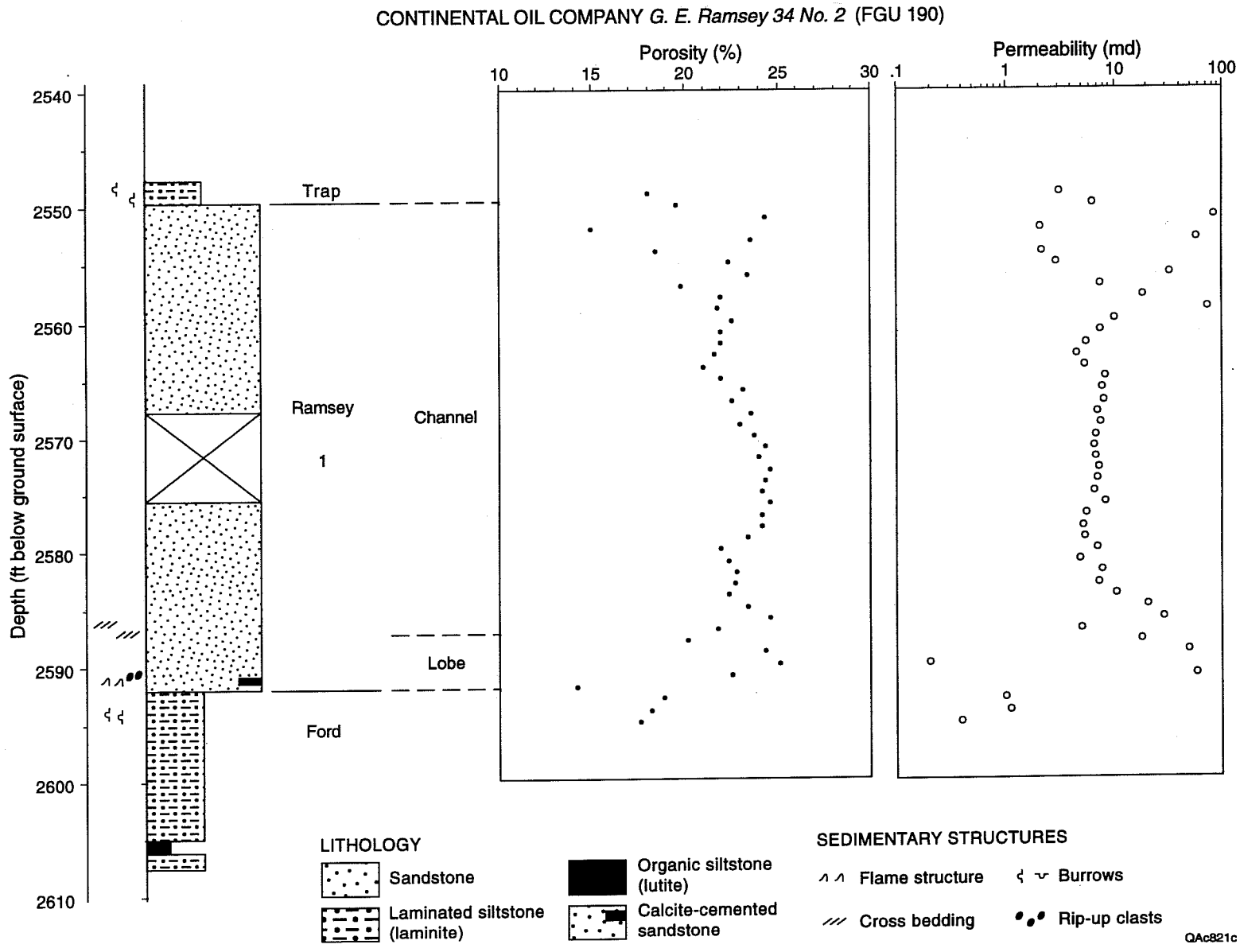
CONTINENTAL OIL COMPANY G. E. Ramsey 34 No. 2 (FGU 190)
Porosity (%)
10
15
20
25
30
Permeability (md)
.1
1
10
100
Depth (ft below ground surface)
2540
2550
2560
2570
2580
2590
2600
2610
Trap
Ramsey
1
Channel
Lobe
Ford
LITHOLOGY
Sandstone
Laminated siltstone (laminite)
Organic siltstone (lutite)
Calcite-cemented sandstone
SEDIMENTARY STRUCTURES
Flame structure
Burrows
Cross bedding
Rip-up clasts
QAc821c

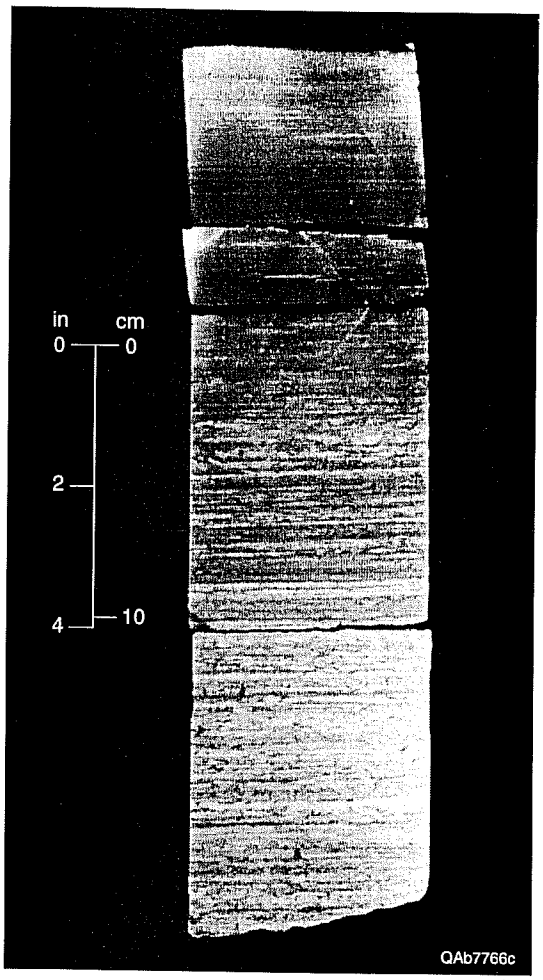
in
cm
0
0
2
4
10
QAb7766c

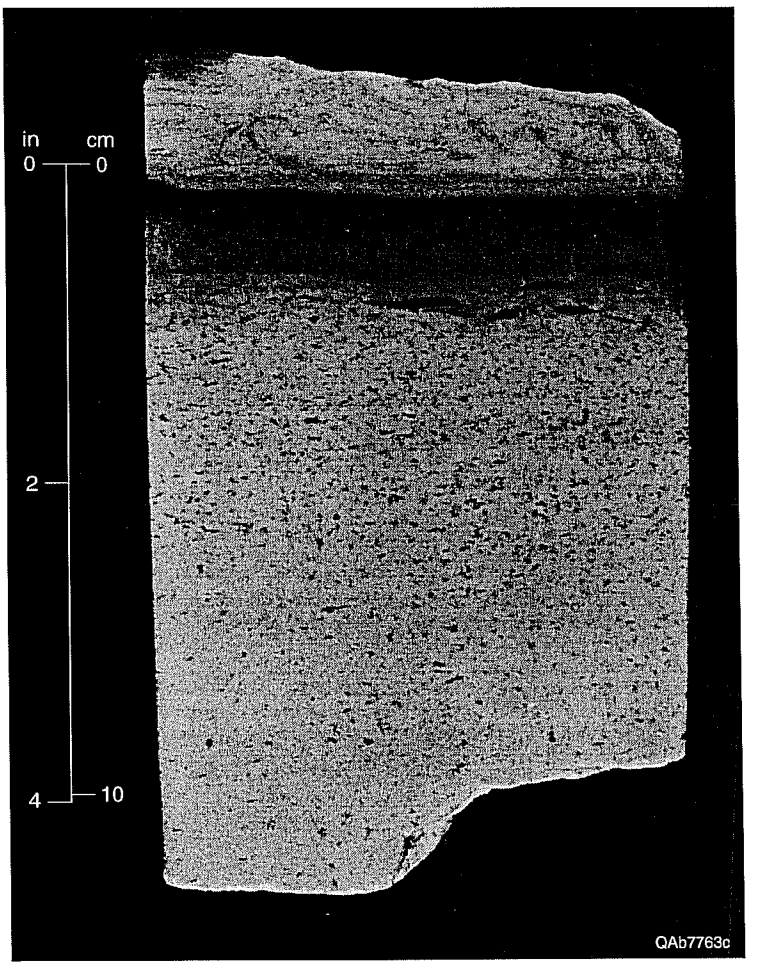
in
cm
0
0
2
4
10
QAb7763c

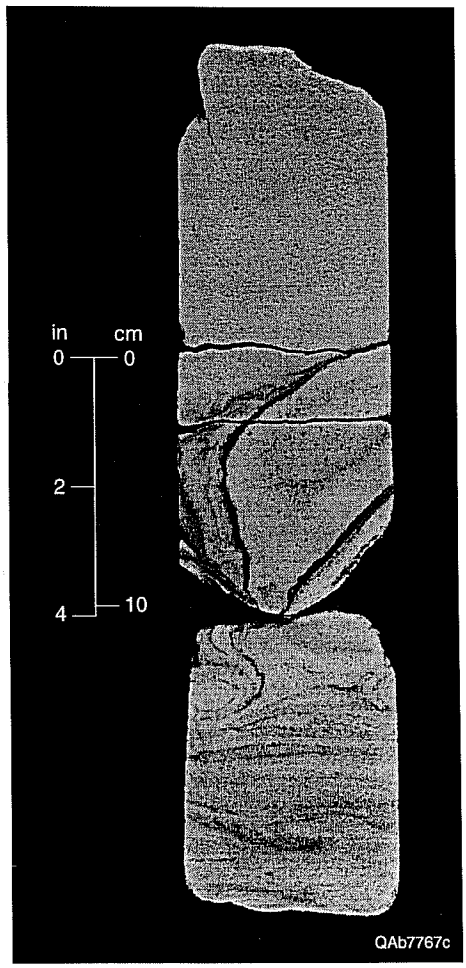
in
cm
0
0
2
4
10
QAb7767c

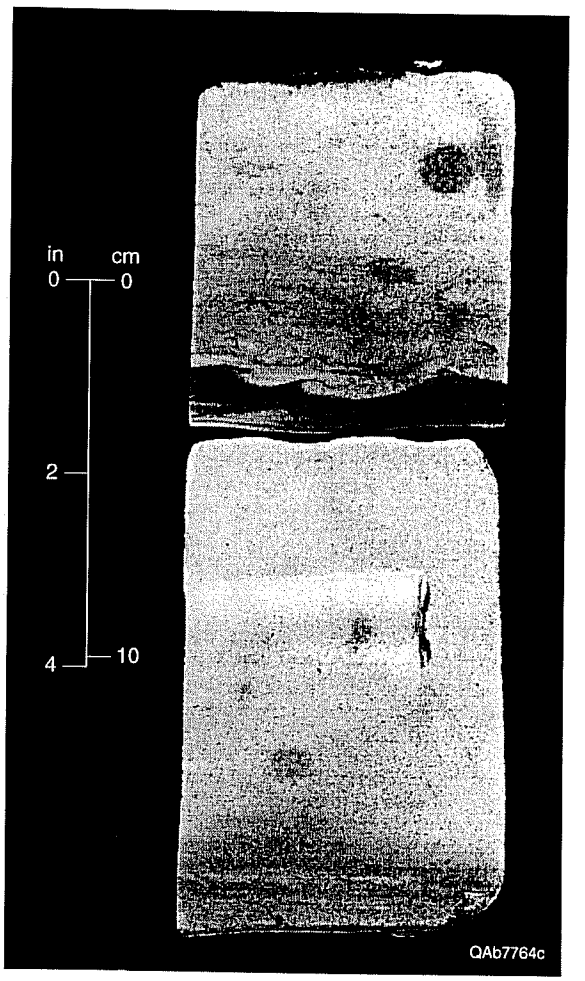
in
cm
0
0
2
4
10
QAb7764c

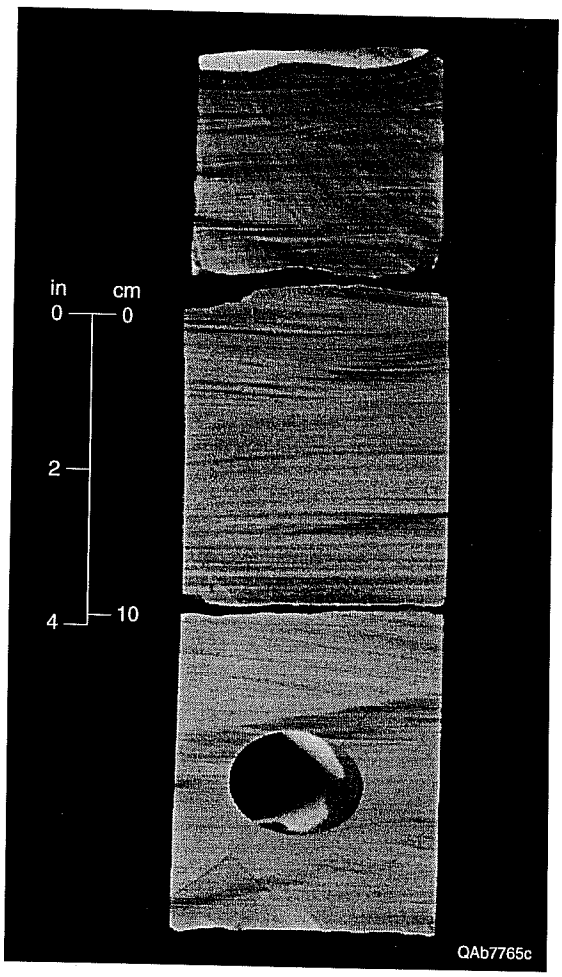
in
cm
0
0
2
4
10
QAb7765c

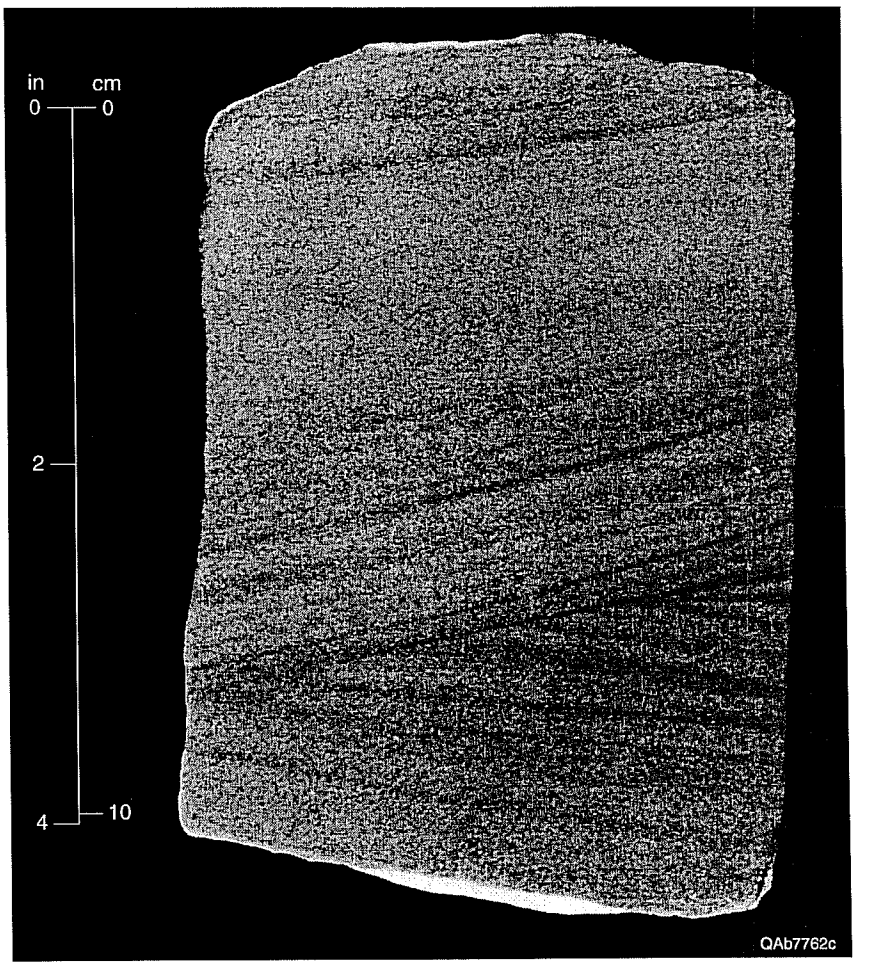
in
cm
0
0
2
4
10
QAb7762c

Mapping of Genetic Units

The Ramsey sandstone is a 0- to 60-ft-thick sandstone that is bounded by the Ford and Trap laminated siltstones. Lutites in the underlying Ford siltstone and the overlying Trap siltstone (fig. 3) are interpreted to be condensed sections that mark the top and base of a genetic unit, equivalent to a high-order cycle (Gardner, 1992; Kerans and others, 1992). In the northern part of the Geraldine Ford unit, the Ramsey is divided into two sandstones (Ramsey 1 and Ramsey 2) separated by a 1- to 3-ft-thick laminated siltstone (SH1) (Ruggiero, 1985). In the southern part of Ford Geraldine unit, only the Ramsey 1 sandstone is present. Thus, the Ramsey high-order cycle is subdivided into the following five units, from oldest to youngest: (1) upper Ford siltstone, from the Ford condensed section to the top of the Ford siltstone; (2) Ramsey 1 sandstone; (3) SH1 siltstone; (4) Ramsey 2 sandstone; and (5) lower Trap siltstone, from the base of the Trap siltstone to the Trap condensed section (fig. 3) (Dutton and others, 1997b).

The Ramsey 1 sandstone occurs across all of Ford Geraldine unit (fig. 14). It pinches out at the northwest and southeast margins of the field and reaches a maximum thickness of >35 ft along a curving northeast-southwest trend. At the southwest end of the field, the single trend of thick sandstone splits into several narrower and thinner trends (fig. 14). The Ramsey 1 sandstone interval is 83 to 100% sandstone, with some thin interbeds of laminated siltstone and lutite.

Core descriptions show that all sandstone facies occur in the Ramsey 1. Massive sandstones are common in all parts of the interval and throughout the field. Crossbedded sandstones are most common along the trend of thickest sandstone through the center of the field. Rippled sandstones and siltstone interbeds occur most commonly in the sandstone wedge that follows the margins of the thick sandstone and pinches out at the edges of the field. Massive and contorted sandstones with abundant dewatering structures occur commonly in the lower Ramsey 1 interval.

In most wells the gamma-ray response is distinctly lower in the Ramsey 1 sandstone than in the underlying Ford siltstone; in some wells the gamma-ray response continues to decrease upward in the lower Ramsey 1 interval. Porosity in the Ramsey 1 sandstone ranges from 2.9 to 29.9% and

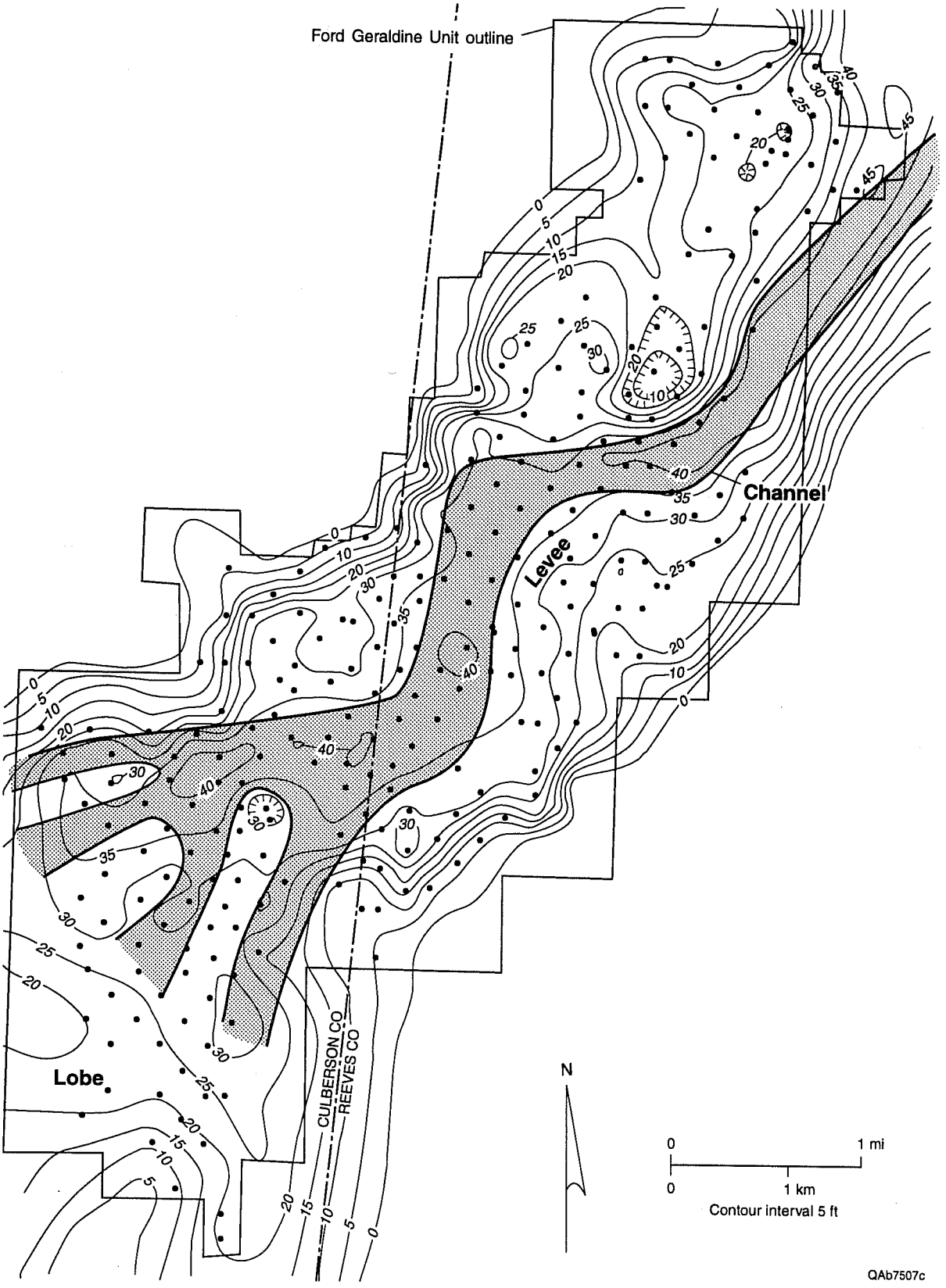
Ford Geraldine Unit outline
Channel
Levee
Lobe
CULBERSON CO
REEVES CO
N
0
1 mi
0
1 km
Contour interval 5 ft
QAb7507c

averages 21.8%. Permeability ranges from 0.01 to 400 md, and geometric mean permeability is 19 md; arithmetic average permeability is 39 md.

The younger sandstone in the Ramsey cycle, called the Ramsey 2 (Ruggiero, 1985), occurs only at the northern end of the unit (fig. 15). This sandstone is thinner than the Ramsey 1, having a maximum thickness of >14 ft along a sinuous, bifurcating northeast-southwest trend. The Ramsey 2 sandstone did not prograde as far into the basin in the Ford Geraldine area as did the Ramsey 1 sandstone. The Ramsey 2 sandstone interval is 86 to 100% sandstone, with some thin interbeds of laminated siltstone and lutite.

As was true of the Ramsey 1, core descriptions show that all sandstone facies occur in the Ramsey 2. Crossbedded sandstones are most common along the trend of thickest sandstone. Rippled sandstones and sandstones with contorted ripples occur adjacent to the margins of the thick Ramsey 2 sandstone. Massive and contorted sandstones with dewatering structures occur commonly in the areas of thinner Ramsey 2 sandstone, particularly at the northwest edge of the unit (fig. 15). Many of the thickest areas of Ramsey 2 sandstone correspond to areas of thin Ramsey 1 sandstone, suggesting that Ramsey 2 sandstones were deposited in the adjacent topographic depressions created by deposition of the preceding Ramsey 1 beds. Porosity in the Ramsey 2 sandstone ranges from 10.2 to 25.3% and averages 20.5%. Permeability ranges from 2 to 230 md, and geometric mean permeability is 17 md; arithmetic average permeability is 41 md.

Distribution of Facies

Vertical and lateral distribution of facies described in core is illustrated on representative cross sections through cored wells from the northern and central parts of Ford Geraldine unit (figs. 16, 17). On the basis of facies distribution in the widely spaced subsurface cores, combined with information on facies distribution of Bell Canyon sandstones mapped in continuous outcrops, the Ramsey sandstone at Ford Geraldine unit is interpreted as consisting of channel, levee, and lobe deposits (figs. 16, 17).

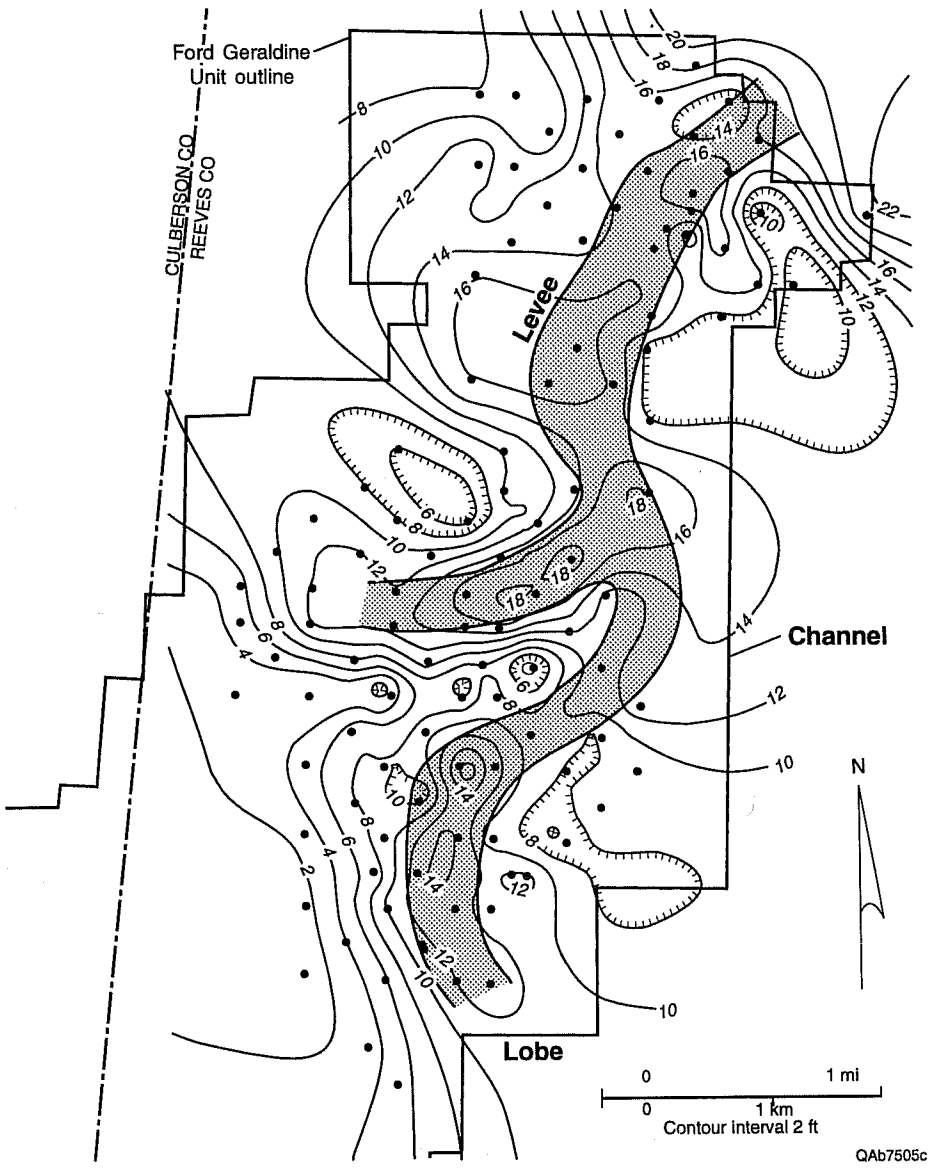
Ford Geraldine
Unit outline
CULBERSON CO
REEVES CO
Levee
Channel
Lobe
N
0
1 mi
0
1 km
Contour interval 2 ft
QAb7505c

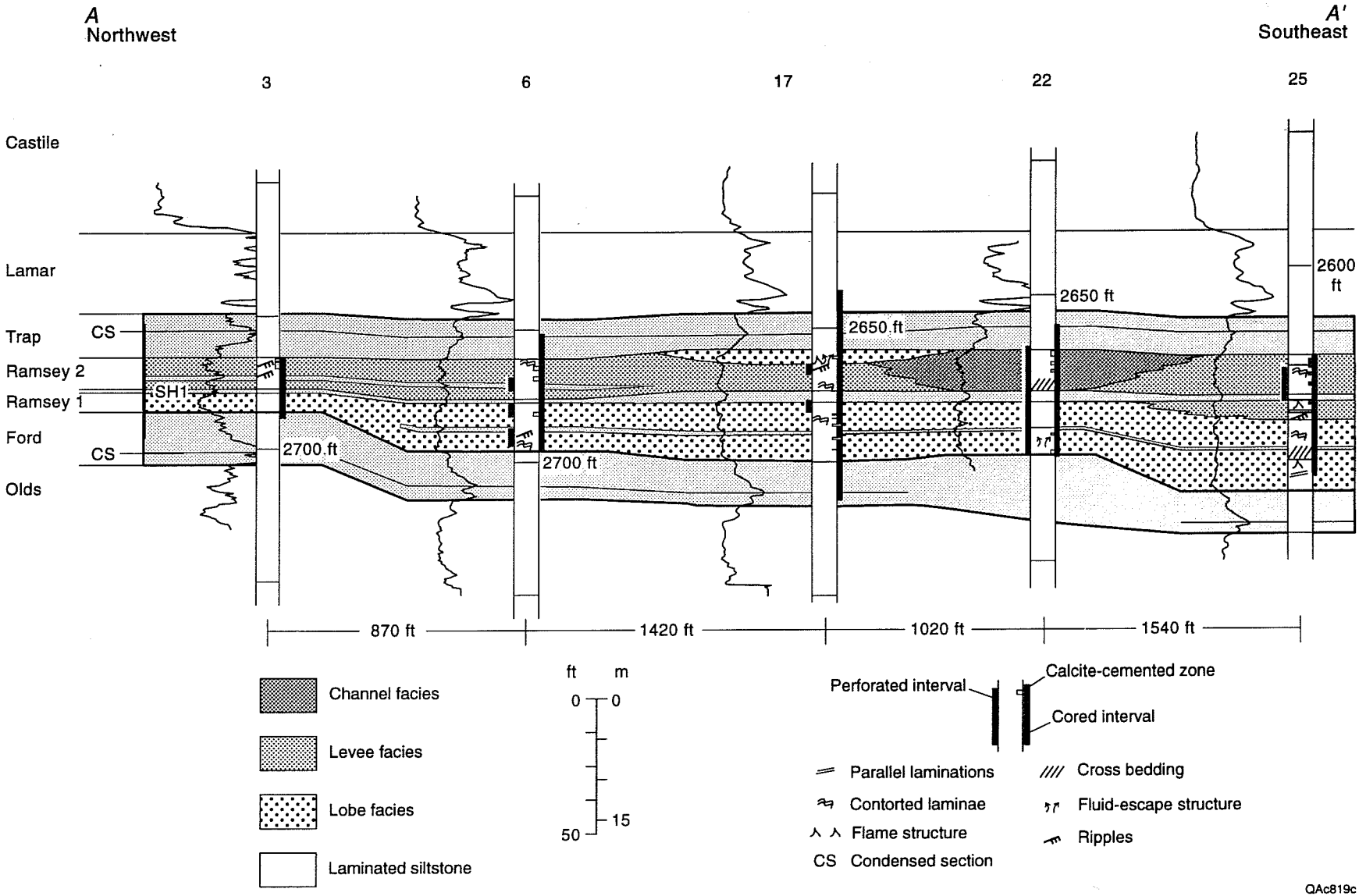
A
Northwest
A'
Southeast
3
6
17
22
25
Castile
Lamar
Trap
Ramsey 2
Ramsey 1
Ford
Olds
CS
SH1
CS
2700 ft
2700 ft
2650 ft
2650 ft
2600 ft
870 ft
1420 ft
1020 ft
1540 ft
Channel facies
Levee facies
Lobe facies
Laminated siltstone
ft
m
0
0
15
50
Perforated interval
Calcite-cemented zone
Cored interval
Parallel laminations
Contorted laminae
Flame structure
CS Condensed section
Cross bedding
Fluid-escape structure
Ripples
QAc819c

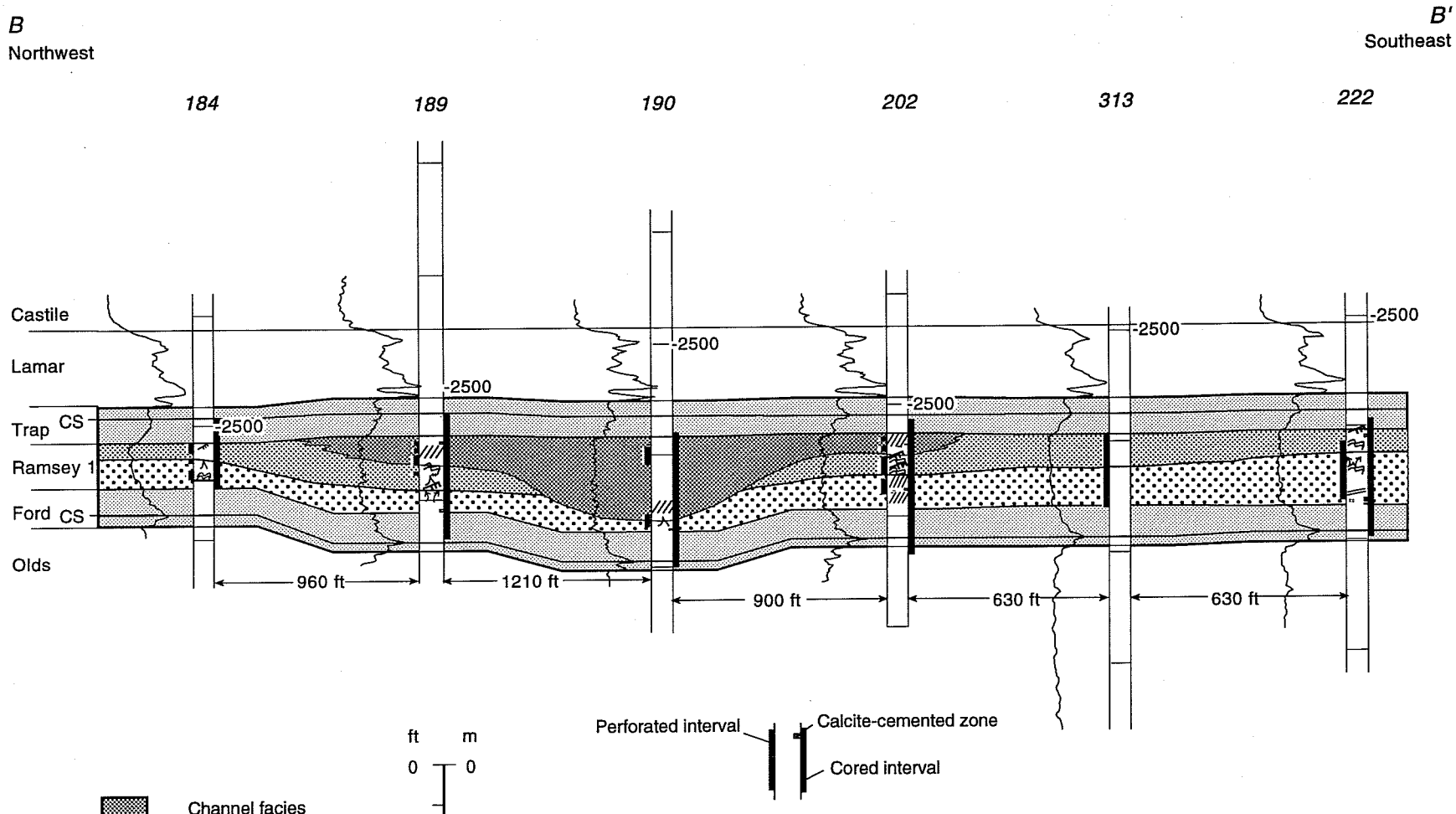
B
Northwest
B'
Southeast
184
189
190
202
313
222
Castile
Lamar
Trap CS
Ramsey 1
Ford CS
Olds
2500
960 ft
1210 ft
900 ft
630 ft
630 ft
Perforated interval
Calcite-cemented zone
Cored interval
ft
m
0
0
40
80
25
Channel facies
Levee facies
Lobe facies
Laminated siltstone
Parallel laminations
Contorted laminae
Flame structure
CS Condensed section
Cross bedding
Fluid-escape structure
Ripples
QAc816c

Channel Facies

Channels facies consist of massive and crossbedded sandstones (fig. 13) interpreted to have been deposited from high-density turbidity currents (Lowe, 1982). As interpreted from the cross sections and isopach map, channels in the Ramsey 1 sandstone are 30 to 35 ft thick and 1,200 ft across (figs. 14, 17). Ramsey 2 channels are thinner, mostly 15 to 20 ft thick, but also about 1,200 ft wide (figs. 15, 16). In outcrop, many channels were seen to be nested and laterally offset from each other. Similar nesting of multiple channels may occur in Ford Geraldine unit, but the core control is not sufficiently close to distinguish separate channels. The aspect ratio (width:thickness) of Ramsey 1 channel deposits is 40:1 to 34:1, and in Ramsey 2, 80:1 to 60:1. Log response is generally blocky. The main Ramsey 1 channel thins and bifurcates into about four channels at the southwest part of the unit (fig. 14). The Ramsey 2 channel bifurcates farther updip, at the north end of the unit (fig. 15), reflecting the backstepping of the younger sandstone in this area. The average porosity in 272 channel sandstone samples is 22.1%. Geometric mean permeability is 16 md, and median permeability is 21 md.

Levee Facies

Levee facies occur as a sediment wedge along the margins of the channels (figs. 14, 15). These channel-margin deposits consist of sandstones with partial Bouma sequences, particularly ripples (fig. 12), convoluted ripples, and interbedded siltstones. They are interpreted as channel levees formed by overbanking of low-density turbidity currents. Thickness of the levee facies decreases away from the channels, and the volume of interbedded siltstones increases. Log response is more serrated than in the channels because of the presence of interbedded siltstones. The average porosity in 318 levee sandstones is 22.3%. Geometric mean permeability is 19 md, and median permeability is 29 md.

Lobe Facies

Lobes facies occur in broad sheets at the mouths of channels and are deposited by unconfined high-density turbidity currents (figs. 14, 15). Lobe facies are characterized by massive and graded sandstones with dewatering features such as dish structures, flame structures, and vertical pipes (figs. 9-11), features that indicate rapid deposition and fluid escape. They were deposited at high suspended-load fallout rates. In a prograding system such as the Ramsey sandstone, lobe facies would have prograded into the Ford Geraldine area first, then been overlain and partly eroded by the narrower prograding channel-levee system (figs. 16, 17). Thus, lobe deposits are found at the distal ends of the Ramsey 1 and 2 sandstone channels and are also underlying and laterally adjacent to the Ramsey 1 and 2 channels and levees (figs. 14-17). Deposition of lobe sandstones was periodic, and laminated siltstones are interbedded with the lobe sandstone sheets. Some lobe deposits show an upward-coarsening log pattern, but many have a massive log response. The average porosity in 310 lobe sandstones is 21.3%. Geometric mean permeability is 13 md, and median permeability is 21 md.

Laminated Siltstone Facies

The laminated siltstone facies consists of organic-rich siltstone laminae interbedded on a millimeter scale with organic-poor siltstone laminae (fig. 8). The average porosity in 214 laminated siltstones is 15.7%, and geometric mean permeability is 0.54 md.

Lutite Facies

The organic-rich siltstones are interpreted as condensed sections that formed in the Ford and Trap intervals during times of very slow siltstone deposition. They contain abundant organic matter, including spores. The organic matter is probably derived from settling from suspension of

planktonic organisms. The average porosity in 8 lutites is 13.1%, and geometric mean permeability is 0.12 md.

Proposed Depositional Model for Ford Geraldine Unit

On the basis of core descriptions, log correlations, and study of the outcrop analog (Barton, 1997; Dutton and others, 1997a), Ramsey sandstones at Ford Geraldine unit are interpreted as having been deposited by sandy high- and low-density turbidity currents that carried a narrow range of sediment size, mostly very fine sand to coarse silt. The sands were deposited in a basin-floor setting by a channel-levee system with attached lobes. Channel facies are approximately 1,200 ft wide and 15 to 35 ft deep. They consist of massive and crossbedded sandstones interpreted to have been deposited from high-density turbidity currents (Lowe, 1982). Channel margins are characterized by rippled and convoluted sandstones interbedded with minor siltstones. Channel-margin deposits are interpreted as channel levees formed by overbanking of low-density turbidity currents. Lobe sandstones are interpreted as being deposited at the mouth of the channel by high-density turbidity currents. They were identified by massive and graded sandstones with load and dewatering structures such as dish structures, flame structures, and vertical pipes—features that indicate rapid deposition and fluid escape.

The narrow range of sediment size in the Ramsey sandstones, mostly very fine sand, supports the interpretation of Fischer and Sarnthein (1988) and Gardner (1992) of an eolian sediment source for sandstones of the Delaware Mountain Group. In their model, fine sand was transported from source areas in the ancestral Rockies by migration of eolian ergs, and silt and clay were transported as dust by the wind (Fischer and Sarnthein, 1988). Clay was carried by the wind beyond the Delaware Basin, thus accounting for the lack of clay-sized sediment in the Delaware Mountain Group deposits. Silt-sized dust was deposited in the basin by fallout from the wind and settling through the water column, forming topography-mantling laminated siltstones. During lowstands of sea level, dune sands were driven across the exposed shelf to the shelf edge, where they fed unstable, shallow-water sand wedges. Slumping of the sand wedges gave rise to turbidity

currents that carved channels and filled them with well-sorted sandstone. During highstands in sea level, the platform was flooded and the dunes were prevented from migrating to the shelf edge (Fischer and Sarnthein, 1988; Gardner, 1992).

Ramsey sandstones were probably deposited on the basin floor (Barton, 1997). Younger sandstones were deposited in topographically low areas created by deposition of the preceding bed, resulting in offset stacking of lobes, called compensation lobes by Mutti and Normark (1987). The confinement of sandstones within narrow linear trends may result in part from reef topography on the highly aggradational carbonate platform (Williamson, 1978; Gardner, 1997).

Ramsey Sandstone Diagenesis

Diagenesis is not unusually extensive in the Ramsey sandstones, but because detrital grain size is so constant in the sandstone facies, the main control on reservoir quality in these sandstones is the volume of authigenic cement. Ramsey sandstones at Geraldine Ford field are arkoses having an average composition of $Q_{63}F_{32}R_5$. Fossil fragments and carbonate rock fragments occur in several sandstone samples, particularly in the calcite-cemented zones. Cements constitute between 4 and 30% of the sandstone volume in Ramsey sandstones, with calcite and chlorite being the most abundant. Calcite cement (average = 7%, range 1 to 29%) occurs both in primary pores and in secondary pores where it has replaced feldspar grains. Chlorite (average = 3%) forms rims around detrital grains, extending into pores and pore throats.

There is a statistically significant relationship between the volume of cement and both porosity and permeability. Calcite is the most important component of total cement, and it has the greatest impact on reservoir quality. In samples with more than 10% calcite cement, geometric mean permeability is reduced to 1.3 md and average porosity to 14.4%. Sandstones having less than 10% calcite cement have a geometric mean permeability of 46 md and average porosity of 23.1%. Thus, the main controls on porosity and permeability in the Ramsey sandstones are authigenic cements, particularly calcite, and to a lesser extent, chlorite.

The distribution of calcite cement in the Ford Geraldine unit can to some extent be determined from the cores because highly calcite-cemented zones have a distinct white color. Calcite-cemented intervals were noted and described along with other sedimentary features in the core (figs. 5-7) and thus can be mapped on cross sections (figs. 16, 17). Highly calcite-cemented sandstones occur in all three sandstone facies—channel, levee, and lobe. Most cemented zones in the core are approximately 0.5 to 1 ft thick; their dimensions are unknown, but we assume they are not laterally extensive or continuous. Although they can occur anywhere within the vertical Ramsey sandstone section, they are more common near the top and base of sandstones (figs. 16, 17). The source of some of the calcite may be from the adjacent siltstones, which would explain the greater abundance of calcite near the sandstone-siltstone contacts. There may also have been at least a partial internal source of calcite in the sandstones, the detrital carbonate rock fragments and fossils.

CONCLUSIONS

Geologic heterogeneity of the Ramsey sandstone at the Ford Geraldine unit is caused by a combination of depositional and diagenetic processes. Progradation, aggradation, and retrogradation of the system resulted in lateral and vertical offset of channel, levee, and lobe facies. Laminated siltstone beds and extensively calcite-cemented sandstones are the most important causes of reservoir complexity and also reduce sweep efficiency. A laminated siltstone that is continuous across the northern part of the unit subdivides the Ramsey reservoir into two sandstones. These sandstones are in turn further subdivided by smaller siltstones that are of sufficient extent to be correlated in several wells. The calcite-cemented zones apparently are not large enough to correlate between wells, but the complexity that they add to the reservoirs probably contributes to reduced sweep efficiency.

ACKNOWLEDGMENTS

This research was funded by the U.S. Department of Energy under contract no. DE-FC22-95BC14936, by Conoco, Inc., and by the State of Texas under State Match Pool Project 4201 and as part of the State of Texas Advanced Resource Recovery project. The Bureau of Economic Geology acknowledges support of this research by Landmark Graphics Corporation via the Landmark University Grant Program. Research was assisted by Carlos Amaya, Radu Boghici, Janaka Paulus, and Mohammad Razi, whose hard work is gratefully acknowledged. Andrew Scott reviewed the manuscript. Drafting was by the Graphics staff of the Bureau of Economic Geology under the direction of Joel L. Lardon. Others contributing to this paper were Robert Sanchez, core handling and photography, Susan Lloyd, word processing, and Nina Redmond, editing. Publication was authorized by the Director, Bureau of Economic Geology, The University of Texas at Austin.

REFERENCES

Barton, M. D., 1997, Basin floor fan and channel-levee complexes, Permian Bell Canyon Formation: 1997 AAPG Annual Convention, Official Program, v. 6, Dallas, Texas, p. A9.

Berg, R. R., 1979, Reservoir sandstones of the Delaware Mountain Group, southeast New Mexico, in Sullivan, N. M., ed., Guadalupian Delaware Mountain Group of west Texas and southeast New Mexico, 1979, Symposium and Field Trip Conference Guidebook: SEPM (Permian Basin Sec.) Pub. 79-18, p. 75-95.

Dutton, S. P., Asquith, G. B., Barton, M. D., Cole, A. G., Gogas, J., Malik, M. A., Clift, S. J., and Guzman, J. I., 1997a, Application of advanced reservoir characterization, simulation, and production optimization strategies to maximize recovery in slope and basin clastic reservoirs, West Texas (Delaware Basin): The University of Texas at Austin, Bureau of Economic Geology, annual report prepared for the U.S. Department of Energy, 187 p.

Dutton, S. P., Barton, M. D., Clift, S. J., Guzman, J. I., and Cole, A. G., 1997b, Depositional history of Ramsey Sandstone channel-levee and lobe deposits, Bell Canyon Formation, Ford Geraldine Unit, West Texas (Delaware Basin): West Texas Geological Society Publication No. 97-102, p. 53-60.

Fischer, A. G., and Sarnthein, M., 1988, Airborne silts and dune-derived sands in the Permian of the Delaware Basin: Journal of Sedimentary Petrology, v. 58, p. 637-643.

Gardner, M. H., 1992, Sequence stratigraphy of eolian-derived turbidites: patterns of deep water sedimentation along an arid carbonate platform, Permian (Guadalupian) Delaware Mountain Group, West Texas, in Mruk, D. H., and Curran, B. C., eds., Permian Basin exploration and production strategies: applications of sequence stratigraphic and reservoir characterization concepts: West Texas Geological Society Publication 92-91, p. 7-12.

Gardner, M. H., 1997, Characterization of deep-water siliciclastic reservoirs in the upper Bell Canyon and Cherry Canyon Formations of the northern Delaware Basin, Culberson and Reeves Counties, Texas, in Major, R. P., ed., Oil and gas on Texas State Lands: an assessment of the resource and characterization of type reservoirs: The University of Texas at Austin, Bureau of Economic Geology Report of Investigations No. 241, p. 137-146.

Kerans, C., Fitchen, W. M., Gardner, M. H., Sonnenfeld, M. D., Tinker, S. W., and Wardlaw, B. R., 1992, Styles of sequence development within uppermost Leonardian through Guadalupian strata of the Guadalupe Mountains, Texas and New Mexico, in Mruk, D. H., and Curran, B. C., eds., Permian Basin exploration and production strategies: applications of sequence stratigraphic and reservoir characterization concepts: West Texas Geological Society Publication 92-91, p. 1-6.

Lowe, D. R., 1982, Sediment gravity flows: II. Depositional models with special reference to the deposits of high-density turbidity currents: Journal of Sedimentary Research, v. 52, p. 279-297.

Mutti, E., and Normark, W. R., 1987, Comparing examples of modern and ancient turbidite systems: problems and concepts, in Leggett, J. K., and Zuffa, G. G., eds., Marine Clastic Sedimentology: Concepts and Case Studies: London, Graham and Trotman, p. 1-38.

Payne, M. W., 1976, Basinal sandstone facies, Delaware Basin, West Texas and southeast New Mexico: American Association of Petroleum Geologists Bulletin, v. 60, p. 517-527.

Pittaway, K. R., and Rosato, R. J., 1991, The Ford Geraldine unit CO2 flood—update 1990: Society of Petroleum Engineers Reservoir Engineering, v. 6, no. 4, p. 410-414.

Ruggiero, R. W., 1985, Depositional history and performance of a Bell Canyon sandstone reservoir, Ford-Geraldine field, west Texas: The University of Texas at Austin, M. A. thesis, 242 p.

Ruggiero, R. W., 1993, Depositional history and performance of a Permian Bell Canyon sandstone reservoir, Ford-Geraldine field, West Texas, in Rhodes, E. G., and Moslow, T. F., eds., Marine Clastic Reservoirs: New York, Springer-Verlag, p. 201-229.

Williamson, C. R., 1978, Depositional processes, diagenesis and reservoir properties of Permian deep-sea sandstones. Bell Canyon Formation, Texas-New Mexico, The University of Texas at Austin, Ph.D. Dissertation, 262 p.

Williamson, C. R., 1979, Deep sea sedimentation and stratigraphic traps, Bell Canyon Formation (Permian), Delaware basin, in Sullivan, N. M., ed., Guadalupian Delaware Mountain Group of West Texas and southeast New Mexico, 1979, Symposium and Field Trip Conference Guidebook: SEPM (Permian Basin Sec.) Pub. 79-18, p. 39-74.

CAPTIONS

Figure 1. Map showing location of Delaware Basin and paleogeographic setting during the late Permian. Geraldine Ford field is on the border of Reeves and Culberson Counties, Texas.

Figure 2. Status of wells in the Ford Geraldine unit and distribution of core control. Type log is shown in figure 3, cross section A-A′ in figure 16, and B-B′ in figure 17. Core descriptions of wells identified by number (17, 189, and 190) are shown in figures 5-7.

Figure 3. Typical log from the Ford Geraldine unit well No. 108 (modified from Ruggiero, 1985). Well location is shown in figure 2.

Figure 4. Structure contours on the top of the Lamar Limestone dip to the east and northeast.

Figure 5. Core description and porosity and permeability data from the Continental Oil Company G. E. Ramsey 18 No. 7 (FGU-17) well.

Figure 6. Core description and porosity and permeability data from the Continental Oil Company G. E. Ramsey 34 No. 4 (FGU-189) well.

Figure 7. Core description and porosity and permeability data from the Continental Oil Company G. E. Ramsey 34 No. 2 (FGU-190) well.

Figure 8. Laminated siltstone (laminite) fining upward into organic-rich siltstone (lutite). From well FGU-40, 2,741.0 to 2,742.0 ft.

Figure 9. Photo of graded sandstone with floating clasts and overlying lutite. Sandstone is interpreted as having been deposited in the lobe facies. From well FGU-3, 2,685.5 to 2,685.9 ft.

Figure 10. Photo of sandstone with convoluted beds interpreted as loading and dewatering features at the base and massive sandstone above. Sandstone is interpreted as having been deposited in the lobe facies. From well FGU-22, 2,705.8 to 2,706.9 ft.

Figure 11. Photo of sandstone with flame structure, which is interpreted as a loading and dewatering feature. Sandstone is interpreted as having been deposited in the lobe facies. From well FGU-6, 2,664.8 to 2,665.5 ft.

Figure 12. Photo of climbing ripples in sandstone from well FGU-14, 2,728.2 to 2,729.1 ft. Sandstone is interpreted as having been deposited in the levee facies.

Figure 13. Photo of cross-laminated sandstone from well FGU-130, 2,670.0 to 2,670.4 ft. Sandstone is interpreted as having been deposited in the channel facies.

Figure 14. Isopach map of the Ramsey 1 sandstone, the main reservoir interval at Geraldine Ford field. It is interpreted as a channel-levee system that progrades over an elongate lobe. At the

southwestern end of the field, the channel apparently breaks up into many smaller branches with attached lobes.

Figure 15. Isopach map of the Ramsey 2 sandstone. This sandstone is also interpreted as a channel-levee system that prograded over lobe deposits, but it did not prograde as far into the basin as did the Ramsey 1 sandstone. Many of the thickest areas of Ramsey 2 sandstone correspond to thin Ramsey 1, suggesting that Ramsey 2 sandstones were deposited in the adjacent topographic depressions created by deposition of the preceding Ramsey 1 beds.

Figure 16. Cross section A-A′ through the northern end of Geraldine Ford field, where the SH1 laminated siltstone separates the reservoir into Ramsey 1 and Ramsey 2 sandstones. Deposition of Ramsey sandstones is interpreted to have occurred by sandy high- and low-density turbidity currents that carried a narrow range of sediment size, mostly very fine sand to coarse silt. On the basis of core descriptions and study of the outcrop analog, we interpret Ramsey sandstones as having been deposited on the basin floor in a sand-rich, channel-levee system with attached lobes.

Figure 17. Cross section B-B′ through the southern part of Geraldine Ford field, where only the Ramsey 1 sandstone is present. Channel, levee, and lobe facies are similar to those in cross section A-A′.

Permian Basin Section/SEPM
Core Workshop
Midland Center
105 North Main Street
Midland, Texas
February 26, 1998

Presented as part of the D.O.E. Class III project titled:

ADVANCED OIL RECOVERY TECHNOLOGIES FOR IMPROVED RECOVERY FROM SLOPE BASIN CLASTIC RESERVOIRS, NASH DRAW BRUSHY CANYON POOL, EDDY COUNTY, NM

DOE Cooperative Agreement No. DE-FC-95BC14941

Operated by:
Strata Production Company
P.O. Box 1030
Roswell, NM 88202
(505) 622-1127

Award Date:	September 25, 1995
Anticipated Completion Date:	September 24, 1998 - Budget Period I
	September 25, 2001 - Budget Period II
Name of Project Manager:	Mark B. Murphy
Contracting Officer's Representative:	Mary Beth Pearse

Introduction

A producing property operated by Strata Production Company in the Nash Draw Brushy Canyon Pool, Eddy County, New Mexico is a field demonstration site in the Department of Energy Class III program. The property is located in Sections 1, 11, 12, 13, and 14 in T23S-29E and Sections 6, 7, and 18 in T23S-R30E.

Production at Nash Draw Pool is from the basal Brushy Canyon zones of the Delaware Mountain Group of Permian, Guadalupian age. The structure trend at the Nash Draw Pool is N-S to NE-SW, and there were at least three depositional events. The reservoir consists of complex sands - a series of stacked micro-sands, vertical permeability is extremely low, and horizontal permeability is poor to good. The Brushy Canyon intervals of interest have been subdivided into four mappable stratigraphic units, designated the "J", "K", "K-2", and "L" sands. All are productive and fall within the scope of this project; however, the two main pay zones are the "K", and "L" sands.

The basic problem at the Nash Draw Pool is the low recovery typically observed in similar Delaware Basin reservoirs. By comparing a control area using standard infill drilling techniques to a similar area developed using advanced reservoir characterization methods, the goal of the project is to demonstrate that a development program based on advanced methodology can significantly improve oil recovery.

The advanced characterization effort integrates geological, geophysical, petrophysical, geostatistical, production, and reservoir engineering data. Vertical seismic profiles and a 3-D seismic survey were acquired to assist in interwell correlations and facies prediction. The stratigraphic framework is being quantified in petrophysical terms using innovative rock-fabric/petrophysical relationships calibrated to wireline logs. Geostatistical techniques are being coupled with 3-D seismic attributes to extrapolate petrophysical properties into the interwell area.

Reservoir characterization and simulation studies are being used to predict the distribution of remaining oil saturation and to optimize development drilling programs. Limited surface access at the Nash Draw Pool, caused by the proximity of underground potash mining and surface playa lakes, limits development with conventional drilling. Various combinations of vertical and horizontal wells combined with selective completions are being considered for optimizing production performance. Based on the production constraints due to high gas-oil ratios observed in similar Delaware Basin fields, pressure maintenance is a likely requirement at the Nash Draw Pool. Using the geological model that was developed, a detailed reservoir description of the pilot area has been made, and current efforts are concentrating on defining the reservoir volume which supports the pilot area wells. A preliminary evaluation of enhanced recovery options, including waterflooding, lean gas, and carbon dioxide injection, are being made for the pilot area.

Whole Core

When Well No. 23 was drilled, 203 ft of full core was cut for laboratory analysis. Normal suites of logs were obtained from this well, and a magnetic resonance tool was run in Well No. 23 for comparison to the core analysis.

A 203 ft whole core was cut from the "J" zone through the "L" zone in Well No. 23. Basic core data including porosity, permeability, oil and water saturations, grain density, show description, and lithology description were measured for each foot of core.

Generally, the rock is fine to very fine-grained, massive to very thinly laminated. There is some

evidence of turbulence as exhibited by sets of low-to-medium angle cross bedding within some of the sand units. Evidence of bioturbation occurs in some of the shaley and silty zones. There is also carbonate clastic debris present in some intervals within the core. Examination of the core under ultraviolet light shows the discontinuous character of the hydrocarbon distribution throughout the reservoir. This correlates with the erratic vertical distribution of calculated oil and water saturations seen in the log analysis.

These data were used to calibrate the logs and determine pay distribution in each zone. By performing a detailed core calibrated log analysis of S_{xo}, S_w and porosity, a detailed analysis was applied to the digitized logs to determine the productive and the water zones in each interval. The application of porosity/permeability transforms and relative permeability data to each zone yielded flow capacity data for each interval. These data were summed for each layer to be input into the reservoir simulator.

SEM Study

In the SEM study for this project, detailed petrographic, scanning electron microscopy, and x-ray diffraction analyses were performed on thin-section samples from Well No. 23. The sands were generally very fine-grained to silt-sized with variable pore geometries. The petrographic analysis of sidewall cores from Well No. 23 described the sands as follows: silty, very fine to fine grained, feldspathic to feldspathic lithic sandstones, angular to subrounded, low to moderate sphericity, and polymictic quartz. Various diagenetic effects are present including quartz and calcite overgrowths, authigenic chlorite, pore-bridging illite, mixed layer illite/smectite, and detrital kaolinite. All of these components work to influence the porosity and permeability of these reservoirs in a negative way.

A common concern in Delaware sands has always been the clays content. Fieldwide, consistently higher water saturations are calculated in the "K" sand than in the "L" sand. According to the x-ray diffraction clay analysis, there is a 1 to 2 percent by volume increase of boxwork chlorite filling the pores in the "K" sand than is present in the "L" sand. The morphology of the chlorite clays is such that they have a very high surface area upon which to bind water. A higher initial, irreducible, water saturation (Sw_{ir}) would have prohibited migration of oil into the already crowded pore spaces. If this relationship exists between the "K" and "L" sands in other wells in the field, then that could explain the low OOIP in the "K" sand.

The porosity and permeability in samples from Well No. 23 are significantly reduced due to framework grain collapse or compaction-dissolution that significantly reduces already small and asymmetrical shaped pore spaces and pore throats. Additional occlusion of the "compressed" pore throats and spaces by various clays, quartz, and carbonates cements also occurs.

Mineralogy of the "K" and "L" sands are similar. Both zones contain some clays - illite and chlorite. The "K" sand has up to 2% more chlorite which occludes permeabilties and may have influenced higher initial water saturation in the "K" sand. Overall, the "K" sand has a higher water saturation than the "L" sand.

Log Analysis

A major problem in analyzing the Nash Draw Pool reservoir is to distinguish productive pay from non-productive intervals. Therefore, a procedure for establishing net pay was developed. By using the full-core analysis to calibrate log calculations, a procedure was developed to identify the zones that are oil-productive. The procedure is based on the premise that zones with residual oil saturation have a high probability of being productive and zones with no residual oil saturation have a low probability of being productive. By calibrating the Micro Lateral Log to calculate a residual oil saturation value for each one-half foot interval from the digitized log, potential pay zones were identified. By applying porosity correction transforms, setting gamma ray and porosity limits, and calibration of resistivity values, a more accurate determination of the productive intervals was made. With corrected porosity values, water saturations, and net heights, a volumetric calculation was performed to estimate the original-oil-in-place. A comparison of volumetric analysis and decline-curve analysis indicated close agreement.

A corresponding calculation was performed to determine the zones that are water productive and the volume of water present. This analysis showed that the "L" zone has minor amounts of interbedded water, the "K-2" has many water zones, and the "K" has highly interbedded oil and water zones. The "L" has high oil saturation (greater than 50%), and the "K-2" has high oil saturations when productive zones are present. The "K" zone has lower average permeability which corresponds to higher capillary pressure and higher water saturations, with S_w in the range of 50% to 60%. Water saturations in the "L" sand average in the high 40s.

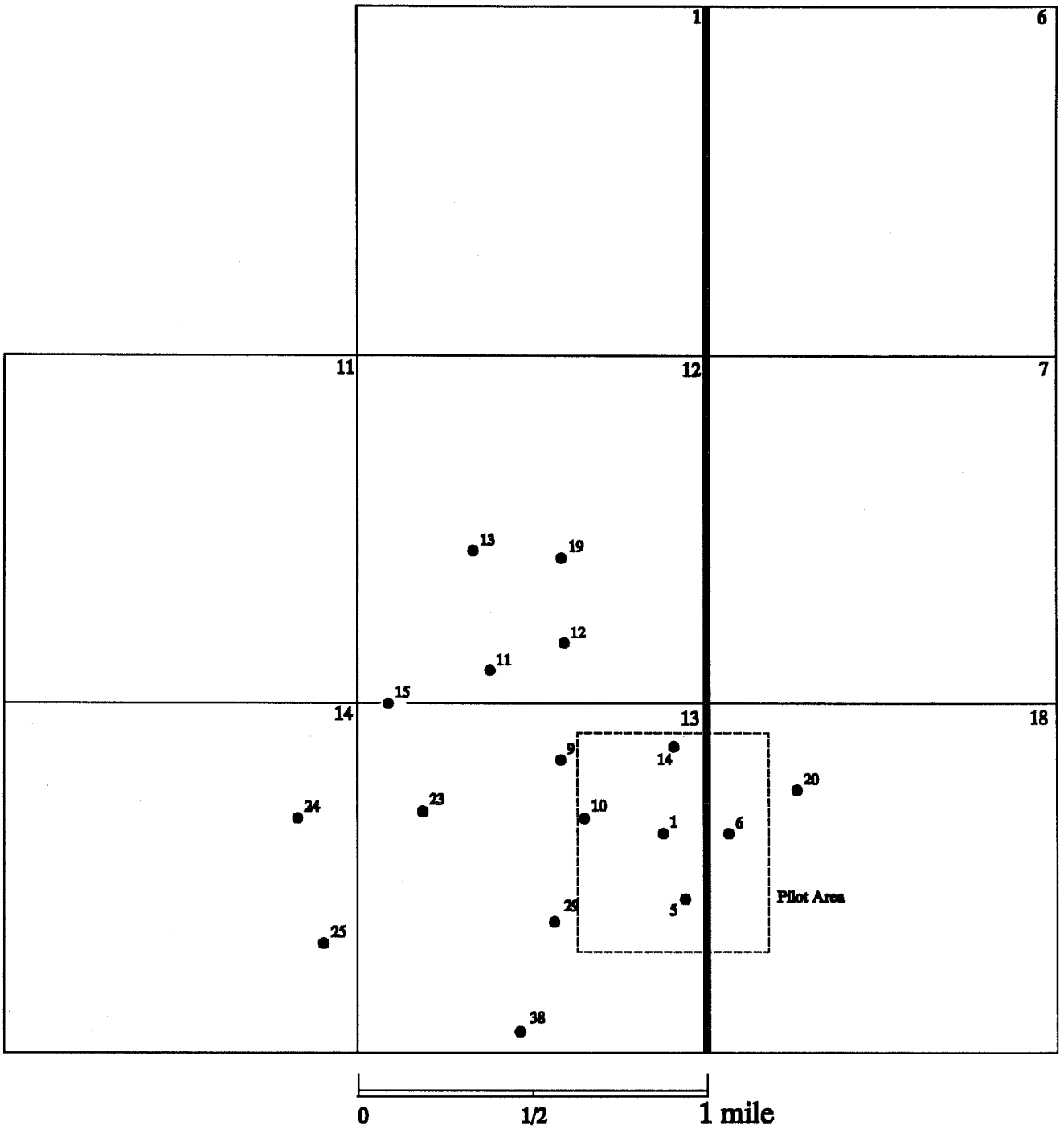

NASH DRAW UNIT

EDDY COUNTY, NM

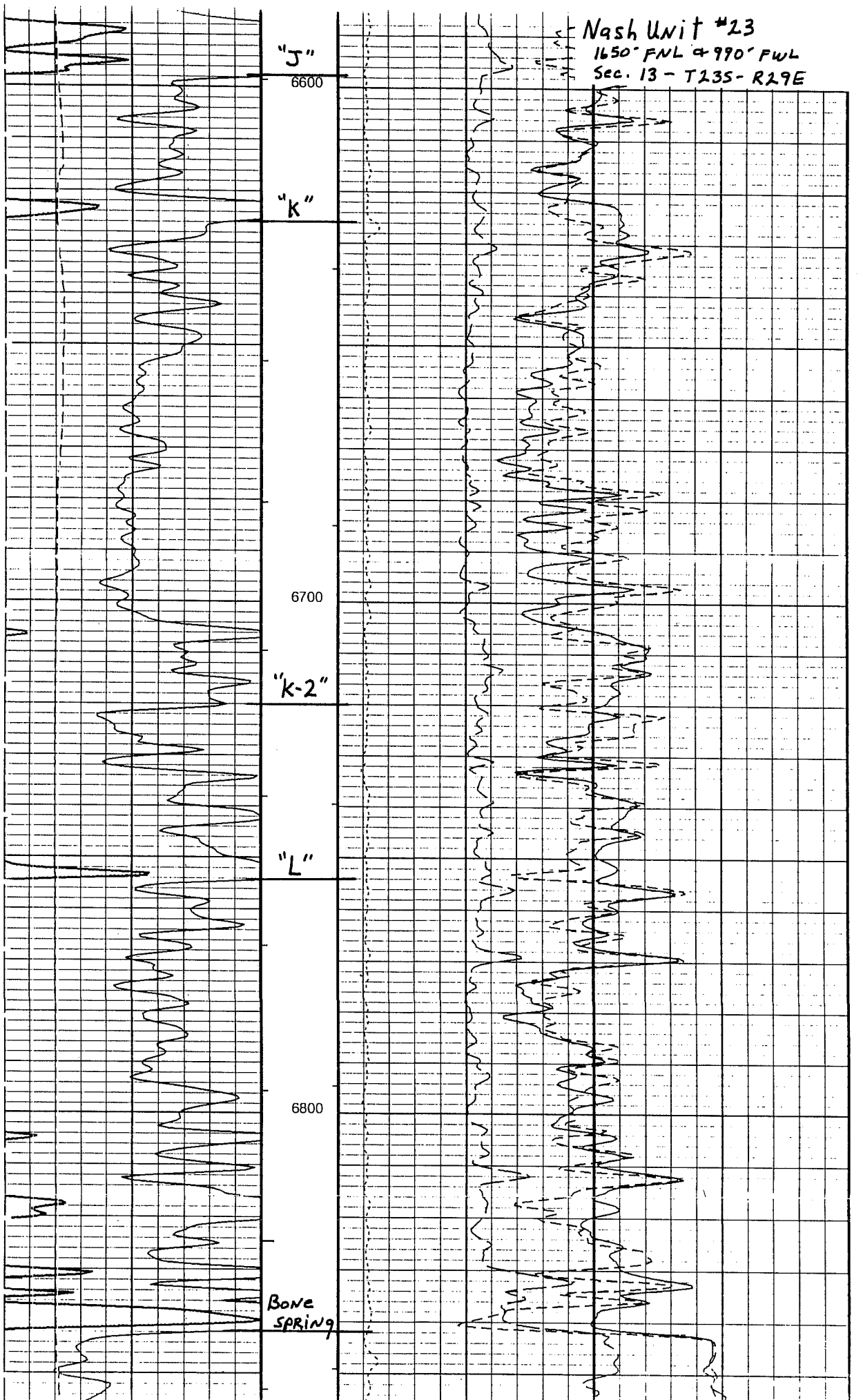
Nash Unit #23
1650' FNL & 990' FWL
Sec. 13 - T23S - R29E
"J"
6600
"K"
6700
"K-2"
"L"
6800
Bone Spring

CORELAB

PETROLEUM SERVICES

October 20, 1995

STRATA PRODUCTION COMPANY
P.O. Box 1030
Roswell, New Mexico 88201

File No.: 57181-17321
Subject: Core Analysis
Nash Unit No. 23
Nash Draw Delaware Field
Eddy County, New Mexico

Gentlemen:

The subject well was cored using diamond coring equipment and water base mud to obtain 4 inch diameter cores from 6650.0 to 6853.2 feet from the Delaware formation.

Core analysis data is presented in tabular and graphical form for your convenience. A porosity vs. permeability plot was prepared for statistical evaluation.

We trust these data will be useful in the evaluation of your property and thank you for the opportunity of serving you.

Very truly yours,

CORE LABORATORIES, INC.

Dean Olson

Dean Olson
Laboratory Supervisor

DO/ym

FULL DIAMETER CORE

Core one was cored conventionally with a water base mud system and preserved at the wellsite in CO_2 atmosphere and transported to Midland by Core Laboratories personnel.

Cores two, three and four were cored with a low invasion gel system and preserved at the wellsite in an aluminum liner then placed into a CO_2 atmosphere and transported to Midland by Core Laboratories personnel.

The aluminum liners were milled open and the low invasion gel was scraped from the surface of the core.

A Core Gamma Log was recorded for downhole E-log correlation.

The core was slabbed using fresh water as a blade lubricant.

The slabs were boxed and photographed under ultraviolet light and natural light.

Core analysis was made from selected intervals requested on one inch diameter plugs drilled with mineral oil and taken from the center of the core.

Fluid removal and saturations were determined using a Dean Stark extraction method.

Water from the Dean Stark extraction were collected from Tritium analysis. Selected samples were analyzed for tritium and the filtrate invasion was determined.

Direct grain volume measurement on plug samples was made using Boyle's law helium expansion. Bulk volume was measured by Archimedes Principle on samples after cleaning. Porosity was calculated using bulk volume and grain volume measurements.

$$\text{Porosity} = \frac{\text{Bulk Vol.} - \text{Grain Vol.}}{\text{Bulk Vol.}} \times 100$$

Steady State Air Permeability was measured in a horizontal direction while the core was confined in a Hassler rubber sleeve.

Porosity and permeability were also measured using the PSP 300 (Porosity-Sonic-Profile) and the PDPK 200 (Pressure Decay Profile Permeameter).

Fracture and bedding plane orientation was determined using data provided by Schlumberger's FMI Log.

Plugs were drilled at 6694 in the N-S, E-W and Vertical directions. Samples were cleaned and measured for porosity and permeability.

The remaining portion of the core was boxed and will remain at our Midland facility (thirty days free of charge) as we await further disposition instructions.

DRILLED SIDEWALL CORE

Sidewall Core Analysis was made on 13 drilled sidewall core samples received from Schlumberger.

Samples were photographed under both ultraviolet and natural light.

Gas expansion porosity and grain density were determined using Boyle's Law.

Gas detection was measured using a "Hot Wire Gas Detector" on gas in the sealed containers.

Air permeability was measured horizontally on drilled sidewalls.

Descriptions and fluorescence were visually determined microscopically.

The samples were returned to client.

STRATA PRODUCTION CO.
NASH UNIT NO. 23

6700.0 TO 6710.0

CORE LAB CORE PHOTO™

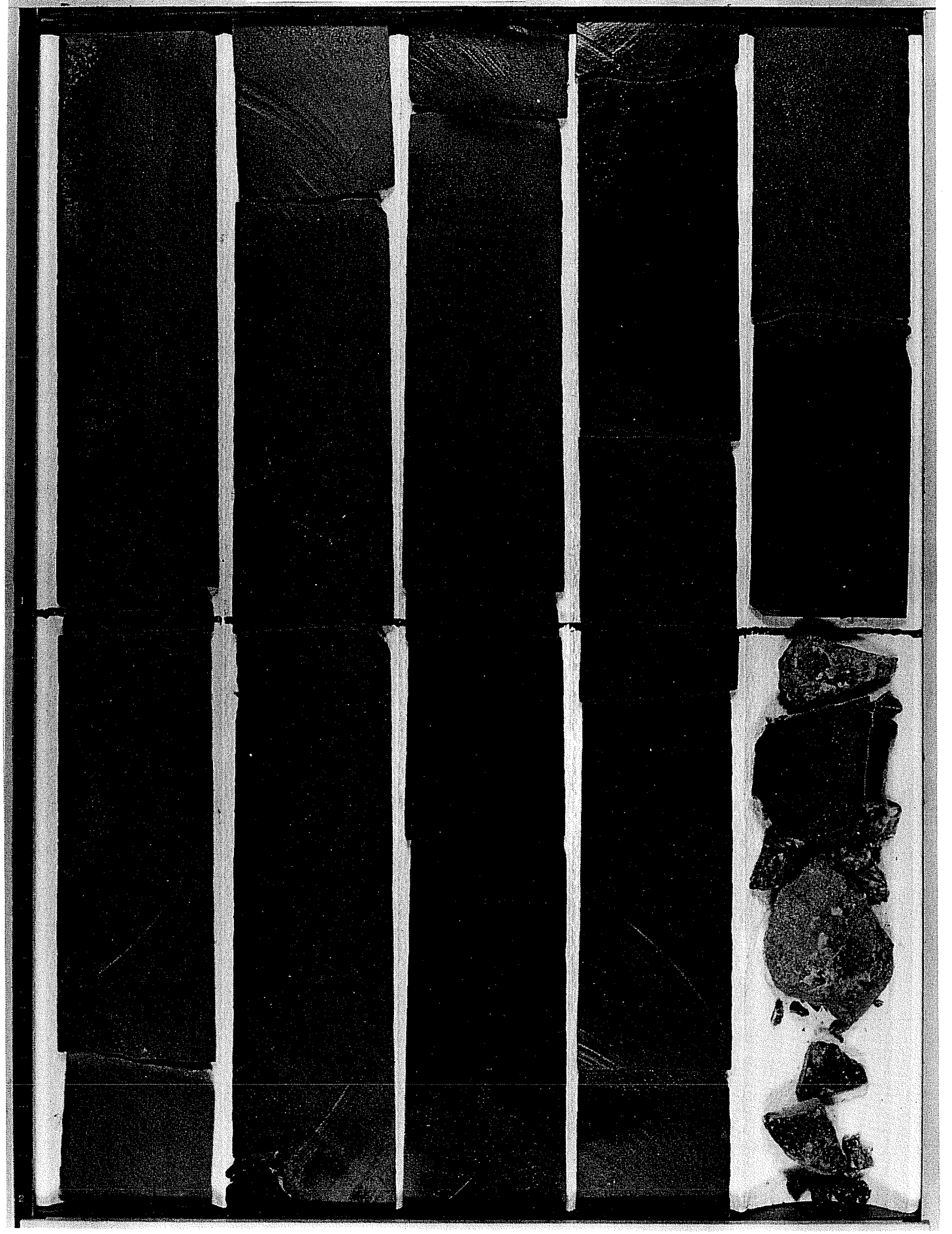

STRATA PRODUCTION
NASH UNIT NO. 23
6700.0 TO 6710.0

CORELAB CORE PHOTO™

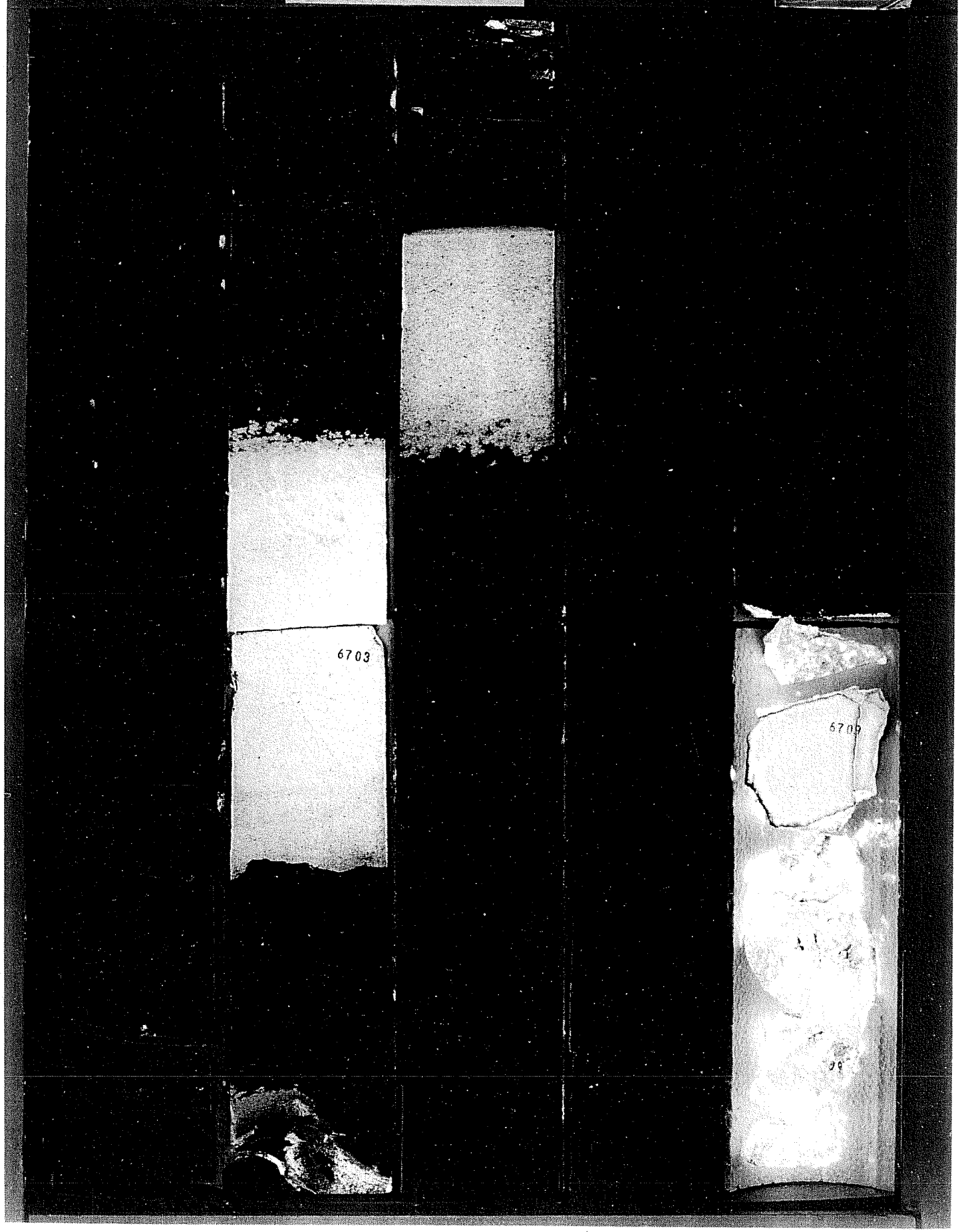

STRATA PRODUCTION CO.
NASH UNIT NO. 23

6730.0 to 6740.0

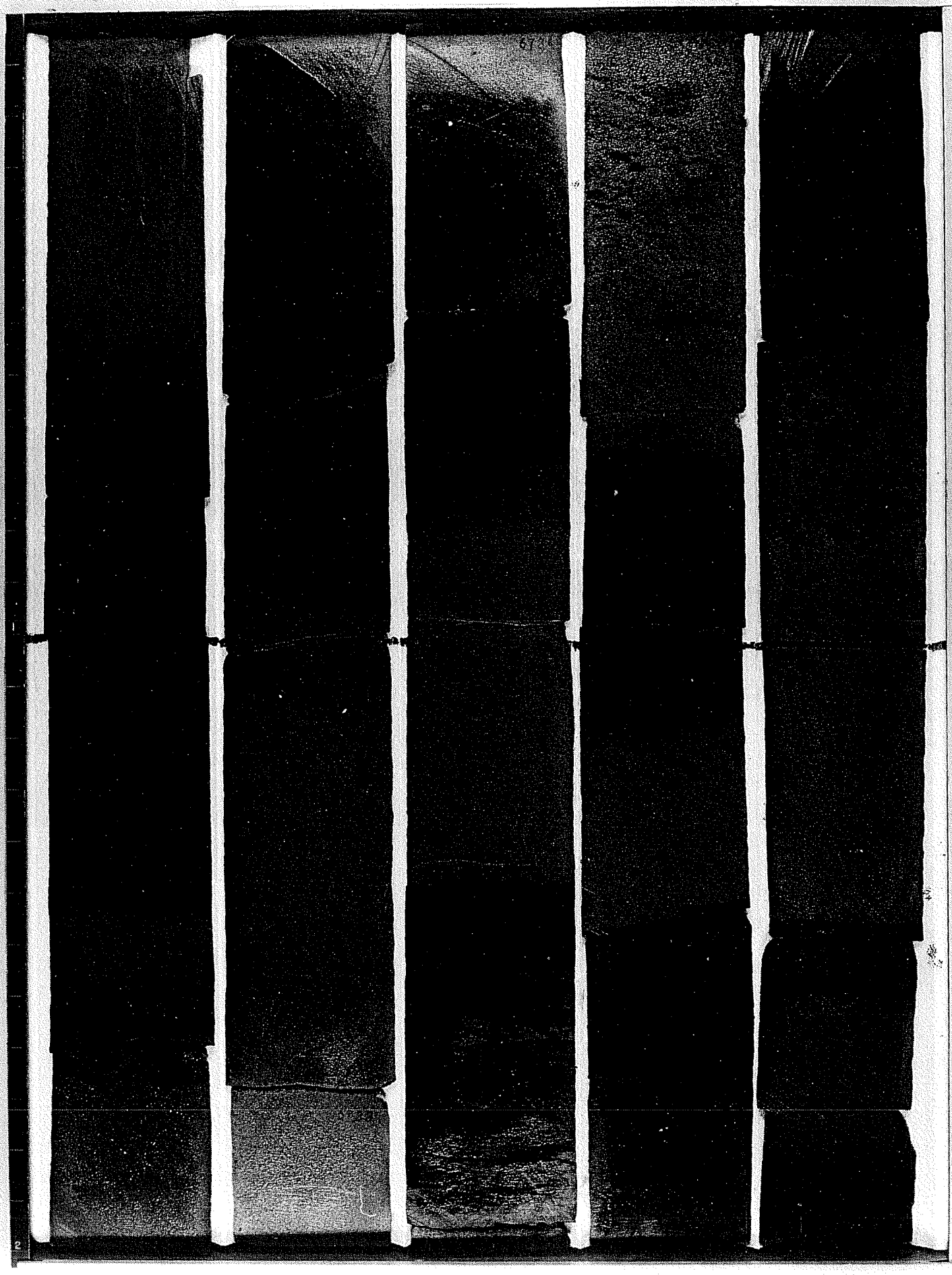

STRATA PRODUCTION
NASH UNIT NO. 23
6730.0 TO 6740.0

CORE LAB CORE PHOTO™

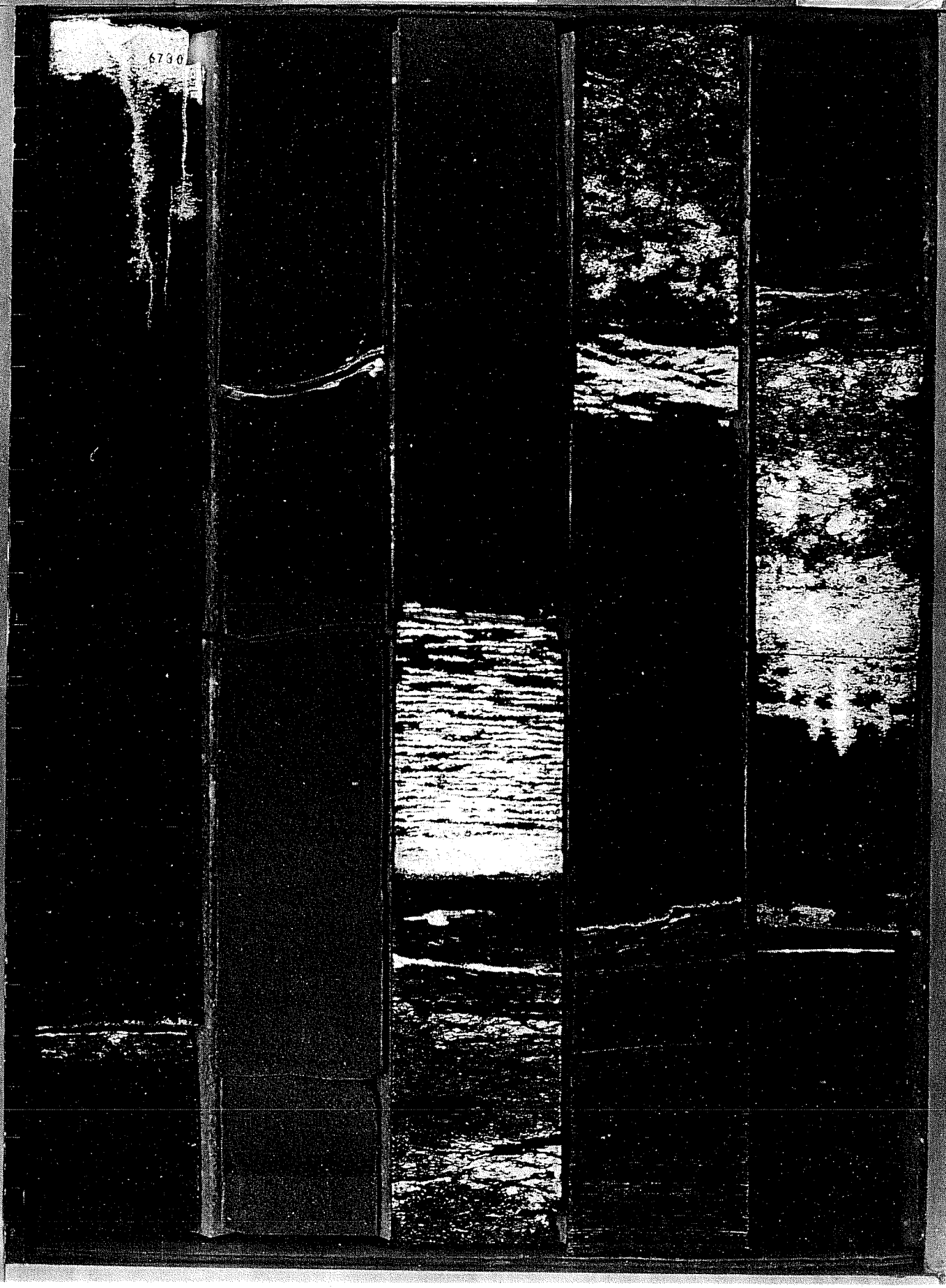

STRATA PRODUCTION CO.
NASH UNIT NO. 23

6780.0 TO 6790.0

CORELAB CORE PHOTO™

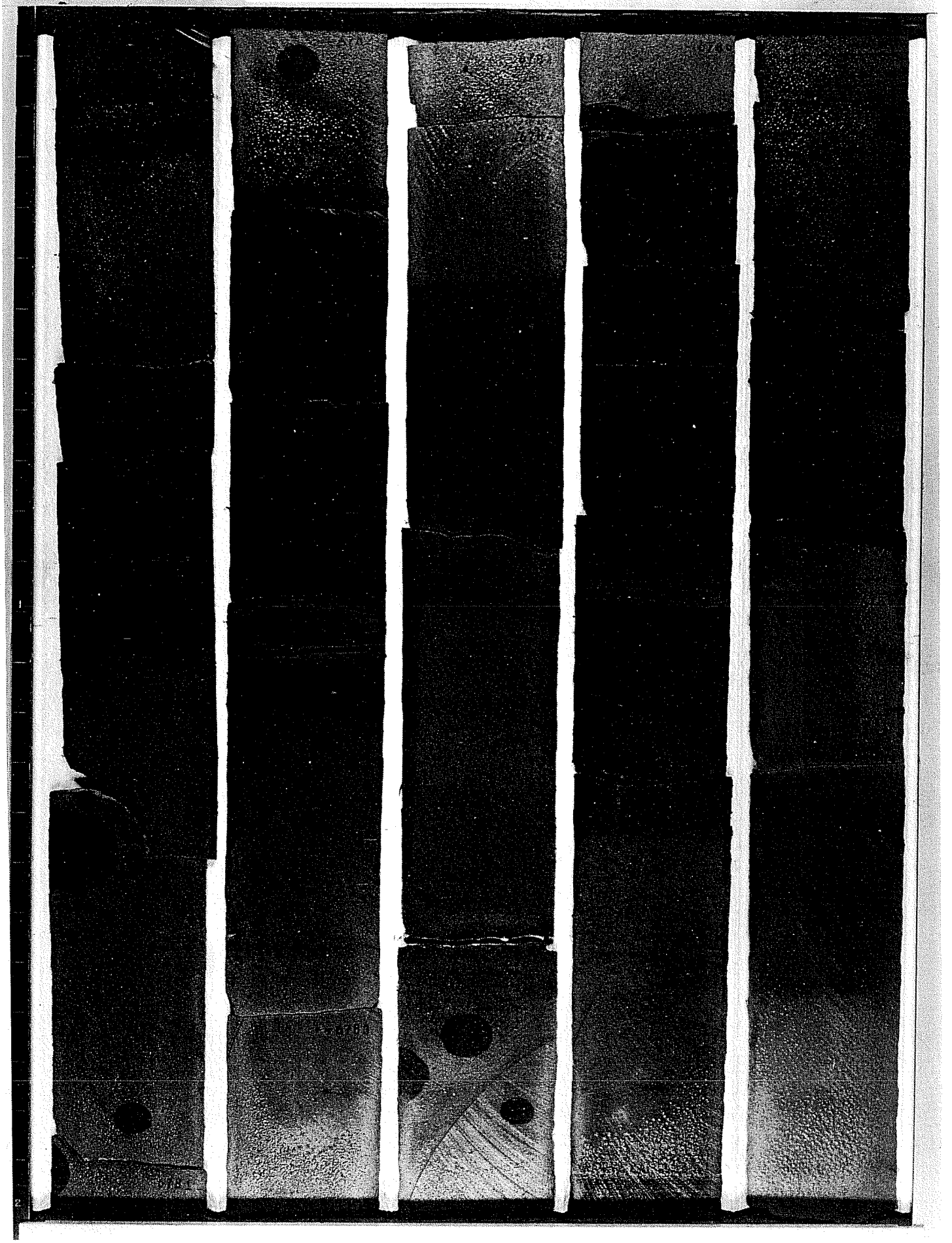

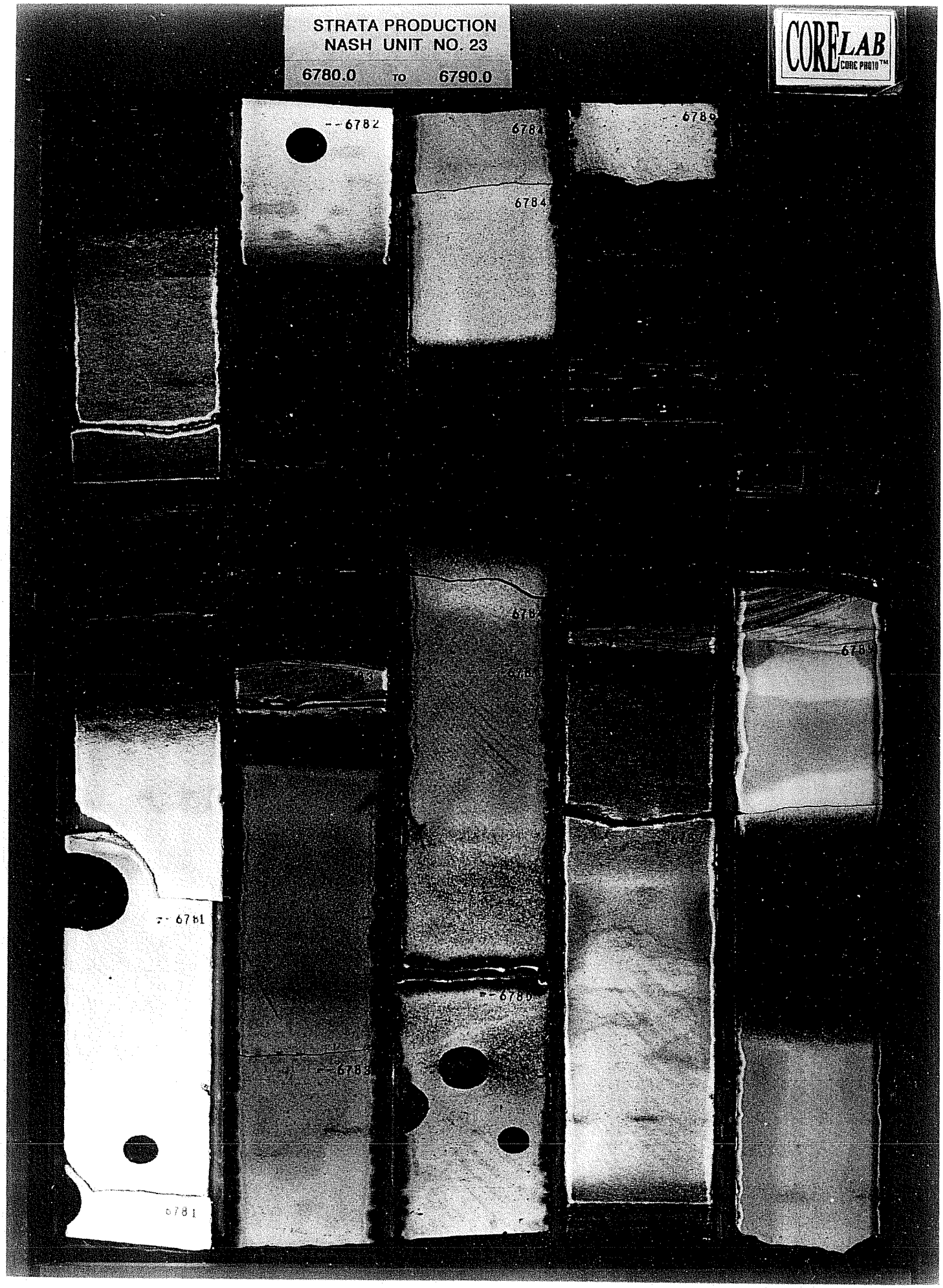
STRATA PRODUCTION
NASH UNIT NO. 23
6780.0 TO 6790.0
CORELAB
CORE PHOTO™
6782
6784
6784
6789
6781
6781

CONVENTIONAL PLUG DATA

CORE LABORATORIES

STRATA PRODUCTION COMPANY
NASH UNIT NO. 23
1650' FNL & 990' FWL, SEC. 13, T-23-S, R-29-E
EDDY COUNTY, NEW MEXICO

Field : NASH DRAW DELAWARE FIELD
Formation : DELAWARE
Coring Fluid : WATER BASE MUD
Elevation : 2986'

File No.: 57181-173
Date : 9-5-95
API No. :
Analysts: OLSON

CORE ANALYSIS RESULTS

SAMPLE NUMBER	DEPTH ft	PERMEABILITY (HORIZONTAL) Kair md	POROSITY (HELIUM) %	SATURATION (PORE VOLUME) OIL %	SATURATION (PORE VOLUME) WATER %	GRAIN DENSITY gm/cc	FLUOR %	DESCRIPTION
		CORE NO. 1 6650-6680 CUT 30' REC 31'						
1	6650.6	0.01	8.7	38.5	35.7	2.68	0.0	Sd, gry, vf gr, lam
S 2	6651.8	0.93	14.1	25.3	28.3	2.65	30.0	Sd, gry, vf gr
3	6652.7	0.61	14.1	22.8	48.5	2.64	35.0	Sd, gry, vf gr
4	6653.3	0.99	14.3	29.2	34.3	2.64	80.0	Sd, gry, vf gr
5	6653.5	0.35	10.9	23.6	41.1	2.65	0.0	Sd, gry, vf gr
6	6654.5	0.64	14.0	16.7	55.6	2.65	0.0	Sd, gry, vf gr
7	6655.4	0.02	9.1	25.1	49.9	2.67	0.0	Sd, gry, vf gr, lam
8	6656.4	0.05	9.3	25.3	50.0	2.67	0.0	Sd, gry, vf gr, lam
9	6657.6	<.01	8.9	30.2	47.2	2.65	0.0	Sd, gry, vf gr
10	6658.5	0.11	9.0	17.8	54.9	2.64	0.0	Sd, gry, vf gr
11	6659.7	0.02	10.4	15.5	59.9	2.65	0.0	Sd, gry, vf gr
12	6660.8	0.18	11.0	28.0	52.2	2.64	0.0	Sd, gry, vf gr
13	6661.4	0.42	11.1	39.1	34.4	2.64	60.0	Sd, gry, vf gr
14	6661.6	0.09	7.4	20.1	52.1	2.65	0.0	Sd, gry, vf gr
S 15	6662.4	0.65	12.6	32.7	35.2	2.64	60.0	Sd, gry, vf gr
16	6663.7	0.77	12.8	33.0	36.1	2.64	60.0	Sd, gry, vf gr
17	6664.6	0.64	12.0	41.8	28.1	2.64	60.0	Sd, gry, vf gr
18	6665.3	0.34	10.5	18.8	53.1	2.64	0.0	Sd, gry, vf gr
19	6665.8	0.53	11.9	42.1	39.5	2.64	50.0	Sd, gry, vf gr
S 20	6666.5	0.81	12.9	29.7	37.1	2.64	50.0	Sd, gry, vf gr
21	6667.7	1.40	13.9	30.1	35.0	2.64	60.0	Sd, gry, vf gr
22	6668.3	0.55	11.6	22.1	45.8	2.64	40.0	Sd, gry, vf gr
23	6669.1	0.33	13.2	20.9	57.2	2.64	0.0	Sd, gry, vf gr
24	6669.8	0.88	12.7	43.6	30.9	2.64	40.0	Sd, gry, vf gr
S 25	6670.6	1.00	12.9	33.9	32.4	2.64	40.0	Sd, gry, vf gr

CORE LABORATORIES

STRATA PRODUCTION COMPANY
NASH UNIT NO. 23

Field : NASH DRAW DELAWARE FIELD
Formation : DELAWARE

File No.: 57181-17321
Date : 9-5-95

CORE ANALYSIS RESULTS

	SAMPLE NUMBER	DEPTH ft	PERMEABILITY (HORIZONTAL) Kair md	POROSITY (HELIUM) %	SATURATION (PORE VOLUME) OIL %	SATURATION (PORE VOLUME) WATER %	GRAIN DENSITY gm/cc	FLUOR %	DESCRIPTION
	26	6671.7	0.04	6.5	34.4	45.1	2.65	0.0	Sd, gry, vf gr
	27	6672.4	0.73	12.9	22.5	44.8	2.64	30.0	Sd, gry, vf gr
	28	6673.5	0.84	13.5	22.4	45.6	2.64	80.0	Sd, gry, vf gr
	29	6674.4	<.01	1.6	10.8	57.5	2.68	0.0	Sd, gry, vf gr, calc
	30	6675.5	2.53	13.8	22.3	39.2	2.64	60.0	Sd, gry, vf gr
	31	6676.3	0.75	13.0	28.9	39.0	2.64	30.0	Sd, gry, vf gr
	32	6677.2	0.02	6.7	30.4	46.9	2.68	0.0	Sd, gry, vf gr, lam
S	33	6677.6	0.67	12.7	24.8	40.1	2.64	50.0	Sd, gry, vf gr
	34	6678.2	1.09	14.1	30.9	36.3	2.64	40.0	Sd, gry, vf gr
	35	6679.4	0.96	14.0	30.4	24.8	2.64	40.0	Sd, gry, vf gr
S	36	6680.4	1.13	12.4	39.0	22.3	2.64	40.0	Sd, gry, vf gr
			CORE NO. 2 6681-6741 CUT 60' REC 60'						
	37	6681.5	2.92	15.2	17.1	36.9	2.64	100.0	Sd, gry, vf gr
S	38	6682.9	1.43	14.2	26.8	35.0	2.64	100.0	Sd, gry, vf gr
	39	6683.5	1.01	13.4	30.6	38.8	2.64	100.0	Sd, gry, vf gr
	40	6684.6	0.15	8.8	6.4	53.3	2.64	0.0	Sd, gry, vf gr
S	41	6685.8	0.97	13.3	32.4	34.1	2.65	100.0	Sd, gry, vf gr
	42	6686.6	0.01	2.3	13.1	65.8	2.69	0.0	Sd, gry, vf gr, calc
	43	6687.4	0.01	1.8	14.9	68.5	2.67	0.0	Sd, gry, vf gr, calc
S	44	6688.2	0.81	12.4	49.5	33.6	2.64	100.0	Sd, gry, vf gr
	45	6689.3	0.91	12.5	40.0	31.6	2.64	100.0	Sd, gry, vf gr
	46	6690.2	0.01	1.8	39.5	33.6	2.67	0.0	Sd, gry, vf gr, calc
	47	6690.8	0.86	12.5	32.0	30.7	2.64	100.0	Sd, gry, vf gr
S	48	6691.4	0.87	13.1	29.1	34.7	2.64	100.0	Sd, gry, vf gr
	49	6692.6	0.98	14.5	38.7	36.4	2.65	100.0	Sd, gry, vf gr
	50	6693.4	0.14	5.1	15.2	82.5	2.70	0.0	Sd, gry, vf gr
	51	6694.4	0.23	15.4	45.4	36.5	2.63	100.0	Sd, gry, vf gr

CORE LABORATORIES

STRATA PRODUCTION COMPANY
NASH UNIT NO. 23

Field : NASH DRAW DELAWARE FIELD
Formation : DELAWARE

File No.: 57181-17321
Date : 9-5-95

C O R E A N A L Y S I S R E S U L T S

SAMPLE NUMBER	DEPTH ft	PERMEABILITY (HORIZONTAL) Kair md	POROSITY (HELIUM) %	SATURATION (PORE VOLUME) OIL %	SATURATION (PORE VOLUME) WATER %	GRAIN DENSITY gm/cc	FLUOR %	DESCRIPTION
52	6695.3	0.64	11.3	7.5	54.7	2.63	70.0	Sd, gry, vf gr
S 53	6696.1	0.67	12.4	19.6	41.7	2.63	80.0	Sd, gry, vf gr
54	6697.6	0.40	10.7	8.9	56.7	2.63	0.0	Sd, gry, vf gr
55	6698.3	0.52	12.2	7.9	54.2	2.63	0.0	Sd, gry, vf gr
56	6699.5	0.10	8.0	10.4	56.0	2.64	0.0	Sd, gry, vf gr
57	6700.4	0.32	11.4	2.8	61.5	2.63	0.0	Sd, gry, vf gr
58	6701.5	0.22	11.0	7.1	55.1	2.63	0.0	Sd, gry, vf gr
59	6702.4	0.27	11.1	10.3	52.3	2.63	0.0	Sd, gry, vf gr
60	6703.2	0.64	11.8	43.1	32.3	2.63	90.0	Sd, gry, vf gr
61	6703.6	0.31	9.7	11.1	52.5	2.63	0.0	Sd, gry, vf gr
62	6704.5	0.40	10.3	24.3	47.8	2.63	90.0	Sd, gry, vf gr
63	6705.4	0.05	2.1	15.0	53.8	2.68	0.0	Sd, gry, vf gr
64	6706.3	0.01	2.0	12.9	53.3	2.67	0.0	Sd, gry, vf gr, calc
65	6707.6	0.34	11.7	10.4	58.3	2.63	0.0	Sd, gry, vf gr
66	6708.4	0.16	9.6	9.6	57.3	2.63	0.0	Sd, gry, vf gr
	6709.0- 10.0							No Analysis
67	6710.7	0.27	12.2	8.8	53.8	2.64	0.0	Sd, gry, vf gr
68	6711.1	0.30	12.6	33.4	41.7	2.64	100.0	Sd, gry, vf gr
69	6712.7	0.18	11.2	21.1	48.8	2.63	80.0	Sd, gry, vf gr, lam
70	6713.7	0.01	2.8	12.1	50.0	2.66	0.0	Sd, gry, vf gr, calc
71	6714.4	0.03	5.2	11.2	49.5	2.67	0.0	Sd, dk gry, vf gr, lam
72	6715.4	0.10	4.8	13.4	45.3	2.65	0.0	Sltst, dk gry
73	6716.4	0.01	4.4	12.3	59.6	2.66	0.0	Sd, gry, vf gr, sl calc
74	6717.3	0.01	2.1	30.1	44.0	2.68	0.0	Sd, gry, vf gr, calc
75	6718.2	0.03	4.0	24.2	47.1	2.67	0.0	Sd, gry, vf gr, calc
76	6719.2	0.01	5.2	19.7	45.4	2.71	0.0	Sd, gry, vf gr, lam
77	6720.2	0.04	3.4	31.6	52.2	2.68	0.0	Sd, gry, vf gr, calc
78	6721.4	0.02	7.2	31.4	44.7	2.66	0.0	Sd, dk gry, vf gr, lam
79	6722.6	0.01	1.1	32.7	30.7	2.70	0.0	Sd, gry, vf gr, calc

CORE LABORATORIES

STRATA PRODUCTION COMPANY
NASH UNIT NO. 23

Field : NASH DRAW DELAWARE FIELD
Formation : DELAWARE

File No.: 57181-17321
Date : 9-5-95

CORE ANALYSIS RESULTS

SAMPLE NUMBER	DEPTH ft	PERMEABILITY (HORIZONTAL) Kair md	POROSITY (HELIUM) %	SATURATION (PORE VOLUME) OIL %	SATURATION (PORE VOLUME) WATER %	GRAIN DENSITY gm/cc	FLUOR %	DESCRIPTION
80	6723.8	0.01	4.9	26.9	41.7	2.65	0.0	Sd, dk gry, vf gr, lam
81	6724.5	0.64	3.6	5.4	58.2	2.65	0.0	Sd, dk gry, vf gr
82	6725.5	0.05	7.7	34.8	44.5	2.67	0.0	Sd, gry, vf gr
83	6726.7	0.04	7.0	29.8	51.3	2.68	0.0	Sd, gry, vf gr, lam
84	6727.5	0.01	7.0	17.3	58.4	2.67	0.0	Sd, gry, vf gr, lam
85	6728.5	0.03	6.9	32.1	47.7	2.67	0.0	Sd, gry, vf gr, lam
86	6729.5	0.09	5.7	10.3	56.9	2.65	0.0	Sd, dk gry, vf gr
87	6730.4	3.71	10.7	15.6	39.3	2.63	0.0	Sd, gry, vf gr
88	6731.3	0.01	1.2	21.3	55.3	2.68	0.0	Sd, gry, vf gr, calc
89	6732.4	0.02	2.6	21.2	50.0	2.67	0.0	Sd, gry, vf gr, calc
90	6733.6	0.26	10.1	9.1	51.2	2.64	0.0	Sd, gry, vf gr
91	6734.3	0.01	1.5	14.5	49.4	2.67	0.0	Sd, gry, vf gr, calc
92	6735.2	6.92	15.3	23.0	42.2	2.63	100.0	Sd, gry, vf gr
93	6736.3	1.41	11.4	21.8	45.5	2.63	90.0	Sd, gry, vf gr, sh incl
94	6737.3	3.54	13.9	11.7	46.1	2.63	0.0	Sd, gry, vf gr
95	6738.6	0.39	11.1	22.3	47.0	2.63	70.0	Sd, gry, vf gr, lam
96	6739.6	0.24	9.4	15.7	48.9	2.65	0.0	Sd, gry, vf gr
97	6740.6	0.01	2.1	25.1	46.1	2.67	0.0	Sd, gry, vf gr, calc
		CORE NO. 3	6741-6801	CUT 60'	REC 60'			
98	6741.3	0.82	10.7	17.2	43.5	2.64	0.0	Sd, gry, vf gr
99	6742.2	2.86	12.9	10.5	57.3	2.63	0.0	Sd, gry, vf gr
100	6743.5	0.07	3.4	18.8	50.7	2.64	0.0	Sltst, dk gry
101	6744.3	0.05	8.3	17.4	42.7	2.67	0.0	Sd, gry, vf gr, lam
102	6745.4	0.06	7.7	10.2	46.6	2.67	0.0	Sd, gry, vf gr, lam
103	6746.3	0.06	8.4	6.3	45.0	2.67	0.0	Sd, gry, vf gr, lam
104	6747.6	0.04	7.3	1.8	50.3	2.67	0.0	Sd, gry, vf gr, lam
105	6748.5	0.01	2.2	8.7	50.9	2.67	0.0	Sd, gry, vf gr, calc

CORE LABORATORIES

STRATA PRODUCTION COMPANY
NASH UNIT NO. 23

Field : NASH DRAW DELAWARE FIELD
Formation : DELAWARE

File No.: 57181-17321
Date : 9-5-95

CORE ANALYSIS RESULTS

SAMPLE NUMBER	DEPTH ft	PERMEABILITY (HORIZONTAL) Kair md	POROSITY (HELIUM) %	SATURATION (PORE VOLUME) OIL %	SATURATION (PORE VOLUME) WATER %	GRAIN DENSITY gm/cc	FLUOR %	DESCRIPTION
106	6749.6	0.01	4.5	11.2	48.7	2.64	0.0	Sd, dk gry, vf gr
107	6750.2	0.07	2.8	19.2	41.5	2.63	0.0	Sltst, dk gry, lam
108	6751.5	0.01	3.7	12.3	43.3	2.64	0.0	Sltst, dk gry, lam, sndy
109	6752.9	0.01	6.8	29.6	34.8	2.67	0.0	Sd, gry, vf gr
110	6753.4	0.01	7.8	17.3	43.2	2.67	0.0	Sd, gry, vf gr, lam
111	6754.4	0.01	1.9	18.6	66.7	2.70	0.0	Sd, gry, vf gr, calc
112	6755.3	0.05	8.0	23.2	44.1	2.67	0.0	Sd, gry, vf gr, lam
113	6756.5	0.06	7.8	15.1	51.4	2.68	0.0	Sd, gry, vf gr, lam
114	6757.5	0.05	7.8	23.1	49.2	2.67	0.0	Sd, gry, vf gr, lam
115	6758.5	0.06	8.4	27.5	41.7	2.67	0.0	Sd, gry, vf gr, lam
116	6759.5	0.09	6.6	15.8	45.5	2.68	0.0	Sd, dk gry, vf gr, lam
117	6760.5	0.01	5.3	14.1	46.9	2.66	0.0	Sd, dk gry, vf gr, lam
118	6761.7	0.01	4.3	18.1	47.3	2.63	0.0	Sltst, dk gry
119	6762.8	0.01	4.5	10.3	47.4	2.64	0.0	Sltst, dk gry
120	6763.7	0.07	8.9	23.7	31.0	2.65	100.0	Sd, gry, vf gr
121	6764.6	0.02	6.0	13.5	40.2	2.68	0.0	Sd, gry, vf gr, calc
122	6765.6	0.01	2.6	8.4	43.2	2.70	0.0	Lm, sndy
123	6766.5	0.04	2.7	8.1	43.6	2.69	0.0	Sd, gry, vf gr, calc
124	6767.4	0.05	7.4	22.1	47.8	2.68	0.0	Sd, gry, vf gr, lam
125	6768.4	0.03	5.8	20.9	48.5	2.68	0.0	Sd, gry, vf gr, lam
126	6769.4	0.01	5.2	8.9	52.7	2.67	0.0	Sd, gry, vf gr, calc
127	6770.4	0.05	8.8	6.6	53.8	2.67	0.0	Sd, gry, vf gr, lam
128	6771.6	0.06	8.6	48.1	22.7	2.66	50.0	Sd, gry, vf gr, sl calc
129	6772.7	0.12	14.3	42.5	28.4	2.64	100.0	Sd, gry, vf gr
130	6773.4	0.05	8.1	17.4	48.2	2.67	0.0	Sd, gry, vf gr, lam
131	6773.9	0.31	8.7	22.2	24.7	2.65	80.0	Sd, gry, vf gr, sl calc, lam
132	6774.6	0.03	4.0	10.3	43.5	2.67	0.0	Sd, gry, vf gr, calc
133	6774.8	0.27	8.7	27.5	36.4	2.65	100.0	Sd, gry, vf gr, calc
134	6775.2	0.58	11.3	26.3	39.8	2.65	100.0	Sd, gry, vf gr, calc

CORE LABORATORIES

STRATA PRODUCTION COMPANY
NASH UNIT NO. 23

Field : NASH DRAW DELAWARE FIELD
Formation : DELAWARE

File No.: 57181-17321
Date : 9-5-95

CORE ANALYSIS RESULTS

	SAMPLE NUMBER	DEPTH ft	PERMEABILITY (HORIZONTAL) Kair md	POROSITY (HELIUM) %	SATURATION (PORE VOLUME) OIL %	SATURATION (PORE VOLUME) WATER %	GRAIN DENSITY gm/cc	FLUOR %	DESCRIPTION
	135	6776.6	0.06	8.6	3.4	59.1	2.67	0.0	Sd, gry, vf gr, lam
	136	6777.5	0.04	7.6	9.4	58.6	2.68	0.0	Sd, gry, vf gr, lam
	137	6778.5	0.01	1.8	10.0	51.4	2.70	0.0	Sd, gry, vf gr, calc
	138	6779.5	0.01	1.0	33.7	60.2	2.70	0.0	Sd, gry, vf gr, calc
	139	6780.5	0.29	11.4	25.7	44.3	2.65	100.0	Sd, gry, vf gr
S	140	6781.2	1.90	13.4	28.3	34.4	2.65	100.0	Sd, gry, vf gr
	141	6782.2	1.25	13.2	32.2	41.2	2.64	100.0	Sd, gry, vf gr
	142	6782.5	0.07	5.4	7.0	60.2	2.69	0.0	Sd, gry, vf gr, lam
	143	6783.5	4.24	13.7	27.7	32.8	2.67	100.0	Sd, gry, vf gr, sl calc
	144	6784.3	7.46	16.0	31.8	32.0	2.65	100.0	Sd, gry, vf gr, sl calc
S	145	6785.8	9.40	15.8	36.6	30.6	2.63	100.0	Sd, gry, vf gr, sl calc
	146	6786.3	0.06	6.0	4.9	65.5	2.67	0.0	Sd, gry, vf gr, lam
S	147	6787.8	0.98	13.8	26.5	41.5	2.63	100.0	Sd, gry, vf gr
	148	6788.4	0.07	8.3	12.2	57.9	2.65	0.0	Sd, gry, vf gr, lam
	149	6789.1	3.36	16.2	28.7	30.5	2.64	100.0	Sd, gry, vf gr
	150	6790.1	3.69	15.6	23.7	31.4	2.63	80.0	Sd, gry, vf gr
S	151	6791.4	4.56	15.2	31.5	30.7	2.64	100.0	Sd, gry, vf gr, sl calc
	152	6792.4	0.35	8.0	9.9	61.9	2.66	3.0	Sd, gry, vf gr, lam
	153	6793.2	0.76	12.8	25.0	42.9	2.63	50.0	Sd, gry, vf gr
	154	6794.4	0.12	10.4	20.9	57.0	2.64	3.0	Sd, gry, vf gr, lam
	155	6795.2	9.71	10.0	23.1	53.6	2.66	3.0	Sd, gry, vf gr, lam
	156	6795.6	0.47	11.3	30.0	40.7	2.64	100.0	Sd, gry, vf gr
	157	6796.3	0.27	10.3	30.0	42.8	2.64	50.0	Sd, gry, vf gr
	158	6797.4	0.22	10.2	25.1	42.4	2.64	80.0	Sd, gry, vf gr
	159	6798.7	0.27	7.0	16.7	49.6	2.65	3.0	Sd, gry, vf gr
	160	6799.2	0.01	2.3	10.3	54.2	2.68	0.0	Sd, gry, vf gr, calc
	161	6799.8	0.26	11.5	17.5	42.1	2.65	20.0	Sd, gry, vf gr, sl calc

STRATA PRODUCTION COMPANY
NASH UNIT NO. 23

Field : NASH DRAW DELAWARE FIELD File No.: 57181-17321
Formation : DELAWARE Date : 9-5-95

C O R E A N A L Y S I S R E S U L T S

	SAMPLE NUMBER	DEPTH ft	PERMEABILITY (HORIZONTAL) Kair md	POROSITY (HELIUM) %	SATURATION (PORE VOLUME) OIL %	SATURATION (PORE VOLUME) WATER %	GRAIN DENSITY gm/cc	FLUOR %	DESCRIPTION
			CORE NO. 4 6801-6854 CUT 53' REC 53'						
	162	6800.2	0.27	11.2	14.4	44.9	2.65	50.0	Sd, gry, vf gr
	163	6801.2	2.00	14.7	37.5	24.2	2.64	80.0	Sd, gry, vf gr
	164	6801.5	0.03	4.1	17.3	54.0	2.66	0.0	Sd, gry, vf gr, sl calc
	165	6802.5	0.73	13.0	29.7	30.8	2.65	60.0	Sd, gry, vf gr
S	166	6803.6	0.46	12.1	26.5	35.8	2.65	30.0	Sd, gry, vf gr
	167	6804.4	0.01	7.3	15.1	55.9	2.66	0.0	Sd, gry, vf gr, lam
	168	6805.4	0.02	4.6	12.0	55.8	2.68	0.0	Sd, dk gry, vf gr, lam
	169	6806.4	0.01	5.1	21.2	53.3	2.66	0.0	Sd, dk gry, vf gr
	170	6807.3	0.02	7.9	20.0	49.0	2.64	0.0	Sd, gry, vf gr, lam
	171	6808.1	0.14	7.9	23.5	37.0	2.66	30.0	Sd, gry, vf gr, lam
	172	6809.3	0.03	7.0	17.7	51.8	2.66	5.0	Sd, gry, vf gr, lam
	173	6810.7	0.02	5.7	25.1	50.6	2.66	70.0	Sd, gry, vf gr, calc
	174	6811.3	0.06	5.6	11.7	60.0	2.67	2.0	Sd, gry, vf gr, lam
	175	6811.9	0.12	9.2	24.3	39.9	2.65	70.0	Sd, gry, vf gr
	176	6812.2	0.14	9.9	25.0	42.6	2.65	45.0	Sd, gry, vf gr
	177	6813.2	0.02	4.9	17.7	53.6	2.64	0.0	Sd, dk gry, vf grlam
	178	6814.3	0.02	2.8	14.2	66.7	2.64	0.0	Sd, dk gry, vf gr
	179	6815.4	0.50	10.9	46.1	27.6	2.66	90.0	Sd, gry, vf gr, sl calc
S	180	6816.1	0.72	11.1	37.5	26.8	2.65	85.0	Sd, gry, vf gr, calc, lam
	181	6816.8	0.04	8.6	27.3	45.4	2.65	15.0	Sd, gry, vf gr, lam
	182	6817.4	0.02	8.6	27.1	44.1	2.65	10.0	Sd, gry, vf gr, lam
	183	6817.9	0.02	9.7	33.3	39.5	2.65	40.0	Sd, gry, vf gr
	184	6818.4	0.08	9.9	26.4	36.9	2.66	40.0	Sd, gry, vf gr
S	185	6819.1	0.15	8.1	28.4	45.2	2.65	10.0	Sd, gry, vf gr, lam
	186	6820.7	0.01	3.7	41.7	32.0	2.68	0.0	Sd, gry, vf gr, calc
	187	6821.6	<.01	1.5	9.2	60.2	2.71	0.0	Lm
	188	6822.3	0.02	1.0	7.0	57.7	2.72	0.0	Lm, foss

CORE LABORATORIES

STRATA PRODUCTION COMPANY
NASH UNIT NO. 23

Field : NASH DRAW DELAWARE FIELD
Formation : DELAWARE

File No.: 57181-17321
Date : 9-5-95

CORE ANALYSIS RESULTS

SAMPLE NUMBER	DEPTH ft	PERMEABILITY (HORIZONTAL) Kair md	POROSITY (HELIUM) %	SATURATION (PORE VOLUME) OIL %	SATURATION (PORE VOLUME) WATER %	GRAIN DENSITY gm/cc	FLUOR %	DESCRIPTION
218	6851.6	0.02	0.8	12.6	62.5	2.71	0.0	Lm
219	6852.2	<.01	0.8	10.4	86.0	2.66	1.0	Lm, shy, frac
220	6853.2	<.01	0.4	3.0	75.0	2.69	0.0	Lm, sl shy

S INDCATES PRESERVED SAMPLE

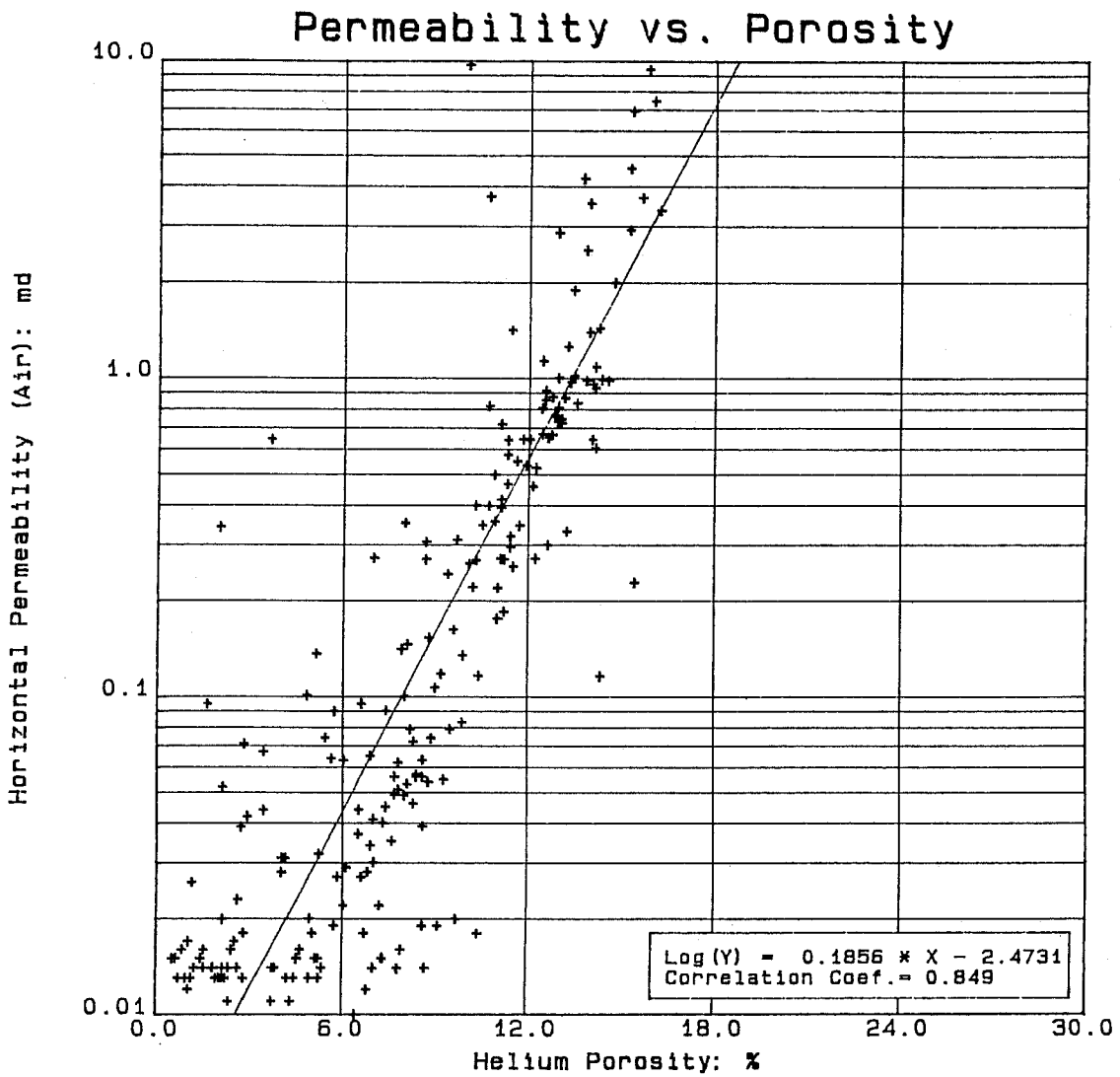

STRATA PRODUCTION COMPANY
NASH UNIT NO. 23
NASH DRAW DELAWARE FIELD

DELAWARE (6650-6854 feet)

Core Laboratories 9-5-95

- LEGEND -
DELAWARE

CORE LABORATORIES

STRATA PRODUCTION COMPANY
NASH UNIT NO. 23

Field : NASH DRAW DELAWARE FIELD
Formation : DELAWARE

File No.: 57181-17321
Date : 9-5-95

TABLE I

SUMMARY OF CORE DATA

ZONE AND CUTOFF DATA

ZONE:

Identification	DELAWARE
Top Depth	6650.0 ft
Bottom Depth	6854.0 ft
Number of Samples	221

DATA TYPE:

Porosity	(HELIUM)
Permeability	(HORIZONTAL) Kair

CUTOFFS:

Porosity (Minimum)	0.0 %
Porosity (Maximum)	100.0 %
Permeability (Minimum)	0.0100 md
Permeability (Maximum)	1000. md
Water Saturation (Maximum)	100.0 %
Oil Saturation (Minimum)	0.0 %
Grain Density (Minimum)	2.00 gm/cc
Grain Density (Maximum)	3.00 gm/cc
Lithology Excluded	NONE

CHARACTERISTICS REMAINING AFTER CUTOFFS

ZONE:

Number of Samples	211
Thickness Represented	211.0 ft

POROSITY:

Storage Capacity	1741.8 ϕ-ft
Arithmetic Average	8.3 %
Minimum	0.5 %
Maximum	16.2 %
Median	8.4 %
Standard Deviation	±4.2 %

GRAIN DENSITY:

Arithmetic Average	2.65 gm/cc
Minimum	2.52 gm/cc
Maximum	2.72 gm/cc
Median	2.65 gm/cc
Standard Deviation	±0.03 gm/cc

PERMEABILITY:

Flow Capacity	118.7 md-ft
Arithmetic Average	0.56 md
Geometric Average	0.11 md
Harmonic Average	0.04 md
Minimum	0.01 md
Maximum	9.71 md
Median	0.08 md
Standard Dev. (Geom) -- $K \cdot 10^{\pm 0.785}$	md

HETEROGENEITY (Permeability):

Dykstra-Parsons Var.	0.928
Lorenz Coefficient	0.654

AVERAGE SATURATIONS (Pore Volume):

Oil	23.6 %
Water	43.9 %

CORE LABORATORIES

LITHOLOGICAL ABBREVIATIONS

Anhy, anhy	anhydrite (-ic)
Ark, ark	arkose (-ic)
bnd	band (-ed)
Brec, brec	breccia
Calc, calctc	calcite (-ic)
carb	carbonaceous
crs gr	course grained
Chk, chky	chalk (-y)
Cht, cht	chert (-y)
Cgl, cgl	conglomerate (-ic)
crs xln	coursely crystaline
dns	dense
Dol, dol	dolomite (-ic)
F	randomly oriented fractures
f	slightly fractured
f gr	fine grained
foss	fossil (-iferous)
f xln	finely crystalline
Gil	gilsonite
Glauc, glauc	glauconite (-itic)
Grt	granite
Gyp, gyp	gypsum (-iferous)
hor frac	perdominantly horizontally fractured
incl	inclusion (-ded)
intbd	interbedded
lam	lamina (-tions, -ated)
Lim, lim	limestone
med gr	mediam grain
Mtrx	matrix
NA	interval not analyzed
Nod, nod	nodules (-ar)
Ool, ool	oolite (-itic)
Pisol, pisol	pisolite, pisolitic
p.p.	pin-point (porosity)
Ptg	parting
Pyr, pyr	pyrite (-itized, -itic)
Sd, sdy	sand (-y)
Sh, shy	shale (-ly)
SHR	solid hydrocarbon residue
sli	slightly
Slt, slty	silt (-y)
styl	stylolite (-itic)
suc	sucrosic
Su, su	sulphur, sulphurous
TBFA	TOO BROKEN FOR ANALYSIS
Trip, trip	tripoli (-itic)
v	very
vf	predominantly vertically fractured
vug	vug (-gy)
xbd	crossbedded
xln	medium crystalline
xtl	crystal

THE FIRST WORD IN THE DESCRIPTION COLUMN OF THE CORE ANALYSIS REPORT DESCRIBES THE ROCK TYPE. FOLLOWING ARE ROCK MODIFIERS IN DECREASING ABUNDANCE AND MISCELLANEOUS DESCRIPTIVE TERMS.

The analyses, opinions or interpretations contained in this report are based upon observations and material supplied by the client for whose exclusive and confidential use this report has been made. The interpretations or opinions expressed represent the best judgement of Core Laboratories. Core Laboratories assumes no responsibility and makes no warranty or representations, express or implied, as to the productivity, proper operations, or profitableness however of any oil or other mineral, property, well or sand in connection with which such report is used or relied upon for any reason whatsoever.

Chart Whole R k XRD Analysis:
Strata Prod.,
Nash Unit #23

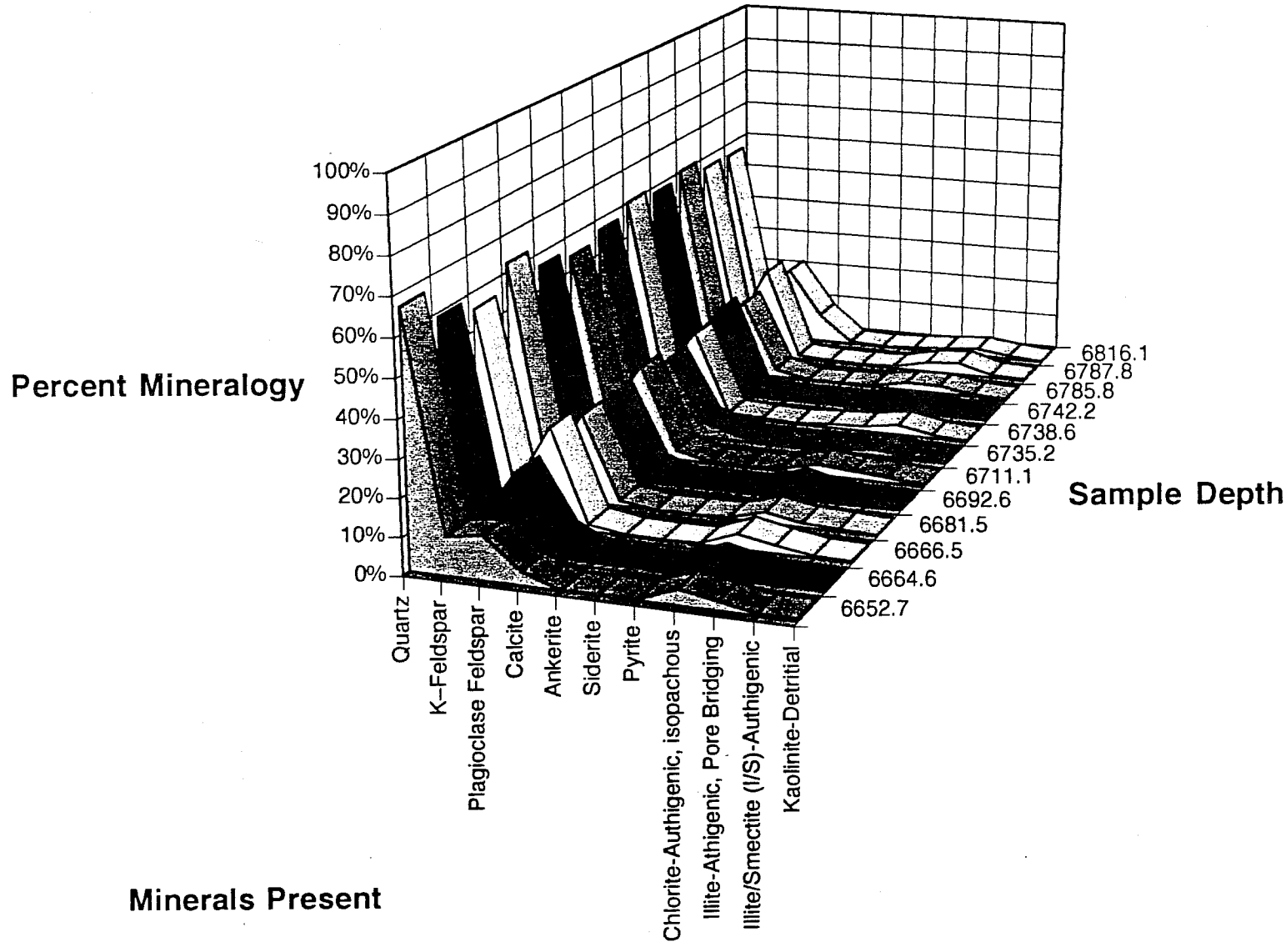

RESULTS OF ANALYSIS

Petrologic analyses are complete with thin-section petrography, scanning electron microscopy (SEM) and x-ray powder diffraction (XRD). The basis of the analyses are Brushy Canyon Formation sandstones (Upper Permian, lower Delaware Mountain Group) within the borehole of the Strata Production, Nash Unit #23, Eddy County, New Mexico. Strata Production submitted 12 conventional core permeability plugs. These samples have a relatively uniform lithology of silty, very fine to fine sand-sized, angular to subrounded, low to moderate sphericity, feldspathic to feldspathic lithic, polymictic sandstones. Because of the low sphericity (wedge to rectangular outlines) of framework grains the pore network will be characterized by high tortuosity and very high asymmetry of pore throats.

Evidence of significant reduction of initially fair to good reservoir interparticle porosity are: 1) extensively sutured and interpenetrating quartz framework grain contacts; 2) diagenetic sequence of grain-coating chlorite initially; 3) subsequent precipitation of fibrous to ligament-like pore and pore-throat bridging illite and illite/smectite on the chlorite, plus authigenic feldspars; 4) epitaxial equant quartz and syntaxial megaquartz overgrowths of detrital quartz; and, 5) diagenetic carbonate cement as tiny euhedral crystals in the pores, and on rare occasion as syntaxial multiple grain-enveloping and pore- occluding poikilitic carbonate cement nucleating on echinoderm fragments.

Where authigenic chlorite, illite and illite/smectite are less abundant, SEM microscopy reveals that lithic and quartz components have significantly greater amounts of epitaxial microcrystalline grain-coating quartz, as well as syntaxial megaquartz over growths. See The XRD Chart of clay mineralogy $\leq 4\mu$. A dramatic drop in grain-goating chloriteis noted below the sample at6,711.1 feet. Feldspars form an important framework and authigenic component of samples. The feldspathic components may show development of microporosity by framework grain feldspar dissolution, with reprecipitation of authigenic feldspar within the pore network. The initial interparticle porosity is reduced if not occluded by continued growth of the epitaxial and syntaxial quartz and common authigenic feldspar, plus the chlorite and illite, results in pore throat bridging and pore occlusion.

The silty, very fine to fine sand-sized, polymictic and low sphericity framework grains of the Brushy Canyon sandstones in this study provide opportunity for differential compaction and precipitation of authigenic mineral cements to partially or totally block the equally small-pore throats. The combination of small framework grain-size, extensive grain-coating boxwork lattice diagenetic chlorite, pore occluding fibrous illite, and microcrystalline quartz and feldspar will greatly skew log calculations for porosity and water saturation. Clay microporosity can result in high irreducible water saturations (Sw_i, bound or nonproducible). Unless some petrologic evaluation is incorporated economical hydrocarbon reserves with little or no produced water simply may be inadvertantly by-passed because log calculations indicated the interval could produce uneconomical quantities of water.

Completion planning and implementation must heed the presence of acid- sensitive (iron-rich, as well as carbonate cements) and fluid- sensitive minerals within the pore network (20% expandability in authigenic illite/smectites, plus detrital kaolinite). Drilling and completion fluids should contain at least 2% KCL to stabilize both authigenic illite/smectite and detrital kaolinite by avoiding cation exchange, resultant deflocculation and bridging of pore throats.

Iron-bearing minerals are present as grain-coating and pore-bridging chlorite, siderite, ferroan dolomite to ankerite and pyrite. Iron sequestering agents in completion fluids will maintain a low pH that buffers the solution and prevents the untimely formation of insoluble iron hydroxide gel. Completion fluids should be recovered in a timely manner to avoid exhaustion of iron sequestering agents. Surging of completion fluid injection rates has may result in migration of deflocculated illite/smectite, detrital kaolinite, as well as authigenic fibrous illite.

Plate 3--6676.5 ft.
Strata Production, Nash #15
Brushy Canyon Formation
Eddy Co., TX

All thin-sections have been impregnated with an epiflourescent solution added to the blue epoxy. Blue dye shows as porosity. Thin sections are made from rotary sidewall cores provided by Scott Exploration, Roswell, NM. Core plugs have been subjected to Dean-Stark Analysis by Core Labs. The reference grid around each photo enhances the ability to specifically reference features observed.

Figure	Footage	Description
A	6676.5	**PPL.** Subrounded, but low sphericity quartz grain at DE-3-4 is the same grain observed in Plate 2 at EF4. Note the well developed intergranular porosity shown by the blue dye. Quartz grains in this field of view are in the very fine grained sand size range. Quartz grains have a high birefringence and/or a dark brown rim that documents grain-coating authigenic clays lining pores. A microcrystalline quartz (chert) grain shows the typical light brown color under PPL at H6. SEM photos document the pore-lining clays. Clays are patchy in their distribution as dark amorphous blobs at C 2, D6, F7 and I7. The dark rhombohedron at G3 appears to be a clay "ghost" of an altered Ca rich amphibole (hornblende cleavage at 54-56 and 124 degrees). The thin light gray laths within the altered grain are most likely Na or K feldspars. A microcrystalline quartz (chert) grain at H6 shows the typical non uniform extinction. Notice the "bright points" of light observed irregularly over the photomicrograph. These are pore lining carbonate cements, either calcite, dolomite, or ankerite. 1) solution enhanced grain to grain contacts at (B1-2,C1-2, E6, F6 and H6); 2) syntaxial quart overgrowths over "dusty" rims of clay at H6, H3, F1, and C5.
B		**XPL.** The types of quartz present include reworked cryptocrystalline, metamorphic, and monocrystalline igneous types. Most of the quartz present is monocrysalline igneous quartz with a uniform extinction (K1, E1, H7, F4, B6, B7). Cryptocrystalline quartz is by multiple extinctions under XPL (H6, I2, K4). Metamorphic or "strained" quartz has an undulatory extinction under crossed nichols XPL (E5).

Strata Production, Nash # 15
Eddy Co., NM

PLATE 3

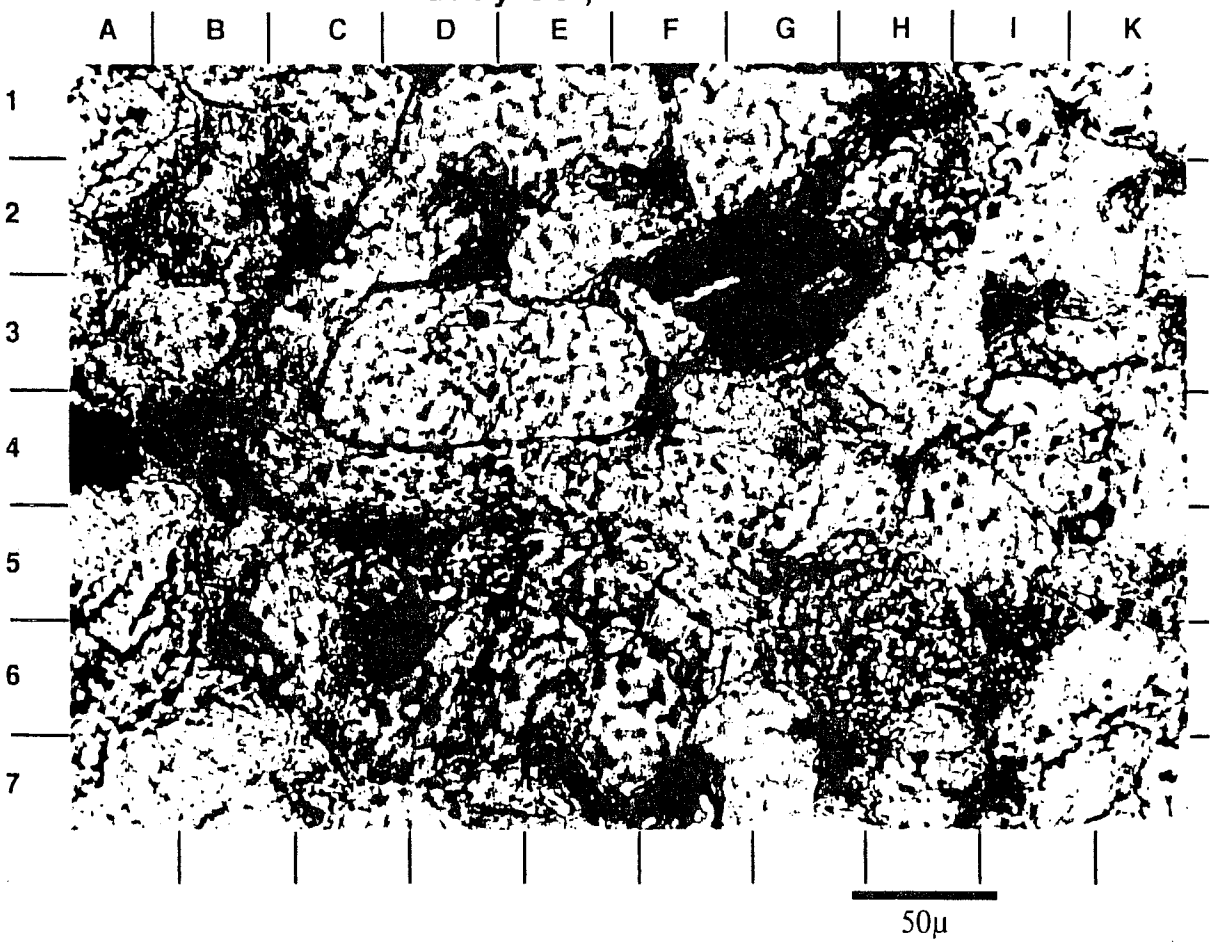

A
6676.5
PPL

B
6676.5
XPL

FHB Stratigraphic Services, Midland, TX

DESCRIPTION

Thin-Section Petrography

Core plug samples submitted span a borehole depth interval from 6652.7 to 6816.1 feet.

6652.7	6735.2
6664.6	6738.6
6666.5	6742.2
6681.5	6785.8
6692.6	6787.8
6711.1	6816.1

The XRD analyses of the same samples indicates that kaolinite is present in bulk mineralogy amounts from 0.2 to 0.6%. The peak occurrence of kaolinite is 1.5% of bulk mineralogy. The SEM and high-magnification petrography cannot corroborate the presence of "book- or vermiform" authigenic kaolinite. The kaolinite present in XRD analyses is interpreted as detrital. Examination of the clay mineral ($\leq 4\mu$) fraction shows a dramatic shift in the occurrence of chlorite with abundances of 3.0 to 4% (6652.7->6711.1 ft) dropping to less than 1.5% bulk mineralogy from 6735.2–>the lowest sample at 6816.1 feet.

The abundant authigenic, pore-filling feldspars must also be taken into account in the classification of these samples as feldspathic (subarkosic) or arkosic sandstones. The classification of sandstones noted in Pettijohn, Potter and Siever (1987, p.145) proposed that feldspathic or subarkosic be used when less than 25% of the framework grains are detrital feldspars. The term arkosic applies to sandstones with detrital feldspar content greater than 25%. I am interpreting these samples to be feldspathic lithic sandstones, with the additional percentage of feldspars exceeding 25% due to diagenetic feldspar.

Thin-section petrographic description follows and is documented by color thin-section photomicrographs. With respect to lithology, texture, fabric, diagenesis, and pore network all of the samples have marked similarities. The first few samples are described in detail.

All of the samples analyzed from the Strata Production Nash Unit #23, Eddy County, New Mexico have a similar polymictic lithology and grain size distribution. Silty, very fine to fine grained sand-sized feldspathic lithic arenites (sandstone), angular to subrounded, with very low to moderate sphericity.

The present reservoir porosity and permeability appears to be dependent upon the absence or extent of framework grain collapse and type and amount of diagenetic cements in the pore network.

Initial interparticle porosity is reduced by:

1) reduction to near collapse of grain framework by pressure solution resulting in sutured and interpenetrating quartz grains;

2) epitaxial equant grain-coating quartz and syntaxial megaquartz grain overgrowths.

3) initial diagenetic grain-coating chlorite with secondary generation filimentous pore-bridging illite, illite/smectite, as well as pore filling carbonate cements.

6652.7 feet

Silty, very fine to fine-grained feldspathic-lithic arenite[4] (sandstone), angular to subrounded with low to high sphericity, clay rims on most quartz grains, later generations of syntaxial cement overgrowths (Plate 3, coordinates G2) and grain coating dolomite and quartz cements line pores. Plagioclase feldspars dominate by less conspicuous K-feldspars. Only rarely can microcline's lattice line twinning be observed. In some cases these cements occlude or restrict pore throats. Carbonates present in XRD analysis are calcite, dolomite, ferroan dolomite to ankerite, and siderite. Framework grains have sutured to concavo-convex interpenetrating contacts. Polymictic arenite characterized by "grains" of:

1) monocrystalline quartz (Plate 2, coordinates D1-D2) with simultaneous extinction under crossed nichols, rare medium-sand size grains "floating" in finer grained fabric, most often observed with syntaxial megaquartz overgrowths;
2) aphanitic chert, with single to undulatory extinction, with relict bedding defined by inclusions or more commonly observed tiny framboids of pyrite. most often observed with microcrystalline grain coating quartz.
2) fine to medium crystalline chert (microcrystalline quartz) clasts (Plate 3, coordinates C4), most often observed with microcrystalline grain coating quartz.
3) polycrystalline quartz grain with strongly sutured and interpenetrating grain boundaries.
4) feldspars as both framework grains (Plate 2, coordinate E2) and diagenetic pore cements, plagioclase grains show dissolution, microporosity and grain collapse.

Porosity and Permeability: Best preserved interparticle porosity observed, (no framework grain collapse, as interpreted in lower samples characterized by various degrees of interpenetrating and sutured contacts are present), minimal dark brown lime micrite present, grain-coating clays seldom occlude porosity, euhedral to framboidal pyrite does occlude pore throats and reduce pore volume. There seems to be nearly equal lateral as well as vertical permeability in this core plug.

---

[4] p. 145, Figure 5-1, *in* Pettijohn, F.J. Pettijohn, P. E. Potter, R. Siever. 1987. Sand and Sandstone. Second Edition, Springer-Verlag

6664.6 feet

Same lithology as 6652.7, with greater amount of overly close grain packing, resulting in lower porosity due to sutured grain contacts; pore network significantly degraded by diagenetic carbonate and quartz cements that coat grains and in some cases occlude or restrict pore throats. Thin-section readily demonstrates a greater amount of pore occluding carbonates. XRD analysis indicates are calcite, dolomite, ferroan dolomite to ankerite, and siderite. Framework grains have sutured to concavo-convex interpenetrating contacts. Polymictic arenite with little change from 6652.7 feet.

6666.5 feet

Same lithology and rock fabric as noted for 6664.6, with overly close grain packing, resulting from grain fracture and dislocation, as well as collapsed. Tighter packing results in lower porosity due to sutured grain contacts; pore network significantly degraded by diagenetic carbonate and quartz cements that coat grains and in some cases occlude or restrict pore throats. Thin-section readily demonstrates a greater amount of pore occluding carbonates. XRD analysis indicates are calcite, dolomite, ferroan dolomite to ankerite, and siderite. Framework grains have sutured to concavo-convex interpenetrating contacts. Polymictic arenite with little change from 6652.7 feet.

6666.5 feet

Same lithology and rock fabric as noted for 6664.6, with overly close grain packing, resulting from grain fracture and dislocation, as well as collapse. Tighter packing results in lower porosity due to sutured grain contacts; pore network significantly degraded by diagenetic carbonate and quartz cements that coat grains and in some cases occlude or restrict pore throats. Thin-section petrography readily demonstrate: 1) a greater amount of pore occluding carbonates; and, 2) grain coating to pore-bridging clays. Clay bridged interparticle pores typically have very poor invasion of expoxy and result in a very pale to light blue epoxy. XRD analysis indicates calcite, dolomite, ferroan dolomite to ankerite, and siderite are present as cements. Framework grains have sutured to concavo-convex interpenetrating contacts. Polymictic arenite with little change from 6652.7 feet.

Estimated porosity is fair 10-15%, since pore network shows grain-coating clays and mineral cements. Clays serve to effectively occlude pores and pore throats.

6681.5 feet

Same lithology and rock fabric as noted previously with pervasive overly close grain packing, resulting from grain fracture, dislocation, and even collapse. This sample contains composite sand-sized grains within the upper fine- to medium sand-sized range from 177μ to 350μ. Quartz grains comprising the composite grains fall within the coarse silt to lower fine grained, sand-sized range.

Good interparticle porosity of 15-20% but separated by "tightstreaks" with 2-10% porosity ." This sample shows a bimodal pore system due of increased occlusion of interparticle pore space by quartz and carbonate cements.

Estimated porosity is fair 10-15%, since pore network shows grain-coating clays and mineral cements. Clays serve to effectively occlude pores and pore throats.

6692.6 feet

Same grain-size distribution as noted previously. Undulatory and microgranular quartz are more abundant. Rock fabric shows pervasive overly close grain packing, resulting from grain fracture, dislocation, and even collapse. Sutured and interpenetrating grain contacts significantly reduce any original interparticle porosity. Remaining interparticle pores are lined by equant carbonate cements or even occluded. Like 6681.5 this sample contains composite sand-sized grains within the upper fine- to medium sand-sized range from 177μ to 350μ. Quartz grains comprising the composite grains fall within the coarse silt to lower fine grained, sand-sized range.

Very poorly preserved interparticle porosity ≤ 5-7%. Overall.

6711.1 feet

Same grain-size distribution, polymictic quartz, and rock fabric as noted previously. Rare light tan, chalcedonic quartz fossil fragments. Pelloid-like micrite within pore spaces. Sutured and interpenetrating grain contacts reduce any original interparticle porosity. Composite quartz grains in the range of +/- 200μ (fine sand grain size). Framework grains are coated by authigenic boxlattice work chlorite.

Very poorly preserved interparticle porosity ≤ 5-7%. Overall

6735.2 feet

Same lithology, grain-size distribution, and polymictic quartz as noted previously. Discontinuous streaks of lime micrite with pervasive recrystallization to organic rich neomorphic microspar. Abundant interparticle pyrite. Very little porosity present as in 6711.1 due to sutured and interpenetrating grain contacts. Thin-sections reveal initial grain-coating chlorite, with a subsequent filimentous to short ligament-like pore bridging illite and illite/smectite.

Log calculated water saturations will be overly pessimistic, while calculated porosity will be overly optimistic. Very poorly preserved interparticle porosity ≤ 5-7%. Overall

6738.6 feet

Same lithology with visible lattice work extinction of K-feldspar (microcline), grain-size distribution, and polymictic quartz as noted previously. Discontinuous wisps of lime micrite resembling small scale flaser bedding. Organic rich micrite recrystallized to dark microspar. Abundant interparticle pyrite. Very poor porosity except in what appear to be "pockets" of original framework packing. Grain contacts are not sutured or interpenetrative, but point to point on slow sphericity grains.

Log calculated water saturations will be overly pessimistic because of microspar and authigenic clays. Very poorly preserved interparticle porosity ≤ 5% overall. Permeability will also be very poor.

6742.2 feet

Silty, very fine to fine grained, with rare medium sand-sized composite quartz grains, feldspathic, lithic sandstone, angular to subrounded, sutured to interpenetrating grain contacts, occasional brachiopod spines and shell fragments, dark pyritic and organic rich lime micrite Authigenic cements are extremely variable, so that they have "patchy" distribution. Some portions are characterized by typical first generation boxwork lattice grain-coating chlorite and second generation of fibrous illite bridging and partitioning slit-like pores, while other regions are free of authigenic clay have equant grain-coating quartz and feldspar. Interparticle porosity ranging from 10-20% in discontinuous streaks, separated by very low porosity due to overly close grain packing, organic-rich microspar and detrital clay-rich intervals.

Discontinuous porosity with low permeability characterize this interval.

6785.8 feet

Silty, very fine to fine grained, feldspathic, lithic sandstone, angular to subrounded, sutured to interpenetrating grain contacts, abundant but patchy interparticle dark pyritic and organic rich lime micrite. Feldspars dissolution indicated by relict twinning. Occasional mollusk fragments, especially tiny gastropods. Thin-section studies show typical first generation boxwork lattice grain-coating chlorite and second generation of fibrous illite bridging and partitioning slit-like pores, with carbonate cements being the last to reduce and occlude intergranular porosity. Abundant microporousity indicated by faint to pale blue epoxy typical of authigenic chlorite and illite occluding and pore throat bridging pore network.

Log calculations will be overly optimistic due to microporosity, since little effective interparticle porosity (≤5%) exists. Permeability will be low. Calculated water saturations will be extremely high, yet little may be producible water.

6787.8 feet

Same as for 6787.8, with visible pore bridging authigenic feldspars.

6816.1 feet

Silty, very fine to fine-sand-sized feldspathic lithic sandstone, angular to subrounded, low to moderate sphericity, sutured and interpenetrating grain contacts, relict twinning of feldspars with some collapse, portions of slide have thin 4-10 μ thick irregular dark brown, pyritic micritic zones. Very rare fragments of echinoderm plats that serve as low energy sites for development of syntaxial cements. Carbonate cements are present as individual authigenic crystals and as poikilitic cement encapsulating several pores and grains in one optically continuous crystal.

Irregular to streaks of porosity separated by 3-5 mm thick impermeable zones due to pore occluding epitaxial and syntaxial quartz, carbonate cements and euhedral to framboidal pyrite. Both the micritic and overly close packing with abundant diagenetic cements occluding porosity serve as discontinuous permeability barriers. Existing interparticle pore space lined with the initial authigenic chlorite and fibrous pore bridging illite.

Plate 1

Strata Production, Nash Unit #23, Eddy Co., NM

6,652.7 ft.

Core Lab prepared all thin-sections from conventional core permeability plugs. Thin sections are impregnated with blue epoxy, one half of each thin-section stained with Alizarin Red S, and finished with a cover slip. Blue dye shows as porosity.

Low magnification, scale bar beneath and to the right of photo is 100 microns or 0.1 mm (100μ). The coarse silt to very fine sand-size grains is 62μ, while the very fine to fine-grained sand boundary is 125μ.

A Silty sandstone, coarse silt-sized grains in very fine to fine sand-sized sandstone, angular to subrounded, low (rectangular to wedge) to moderate sphericity, lithic to subarkosic quartz sandstone. The Brushy Canyon Formation sandstones can be designated as polymictic because of lithic, arkosic and multiple types of quartz present. Compare the maximum grain diameter approaches 125 μ.

Note the irregular "scalloped" grain boundaries. Some framework grains (plate 3A) have a "chaotic" packing due to low sphericity of coarse silt to very fine sand grains. In other areas of the same sample the interpenetrating quartz grains form an overly close grain. A significant percentage of the quartz grains display a "cloudy to dusty" appearance under transmitted light. (B4, G4, H4), due to fluid inclusions or dissolution with subsequent diagenetic carbonate cements.

B Same view as A, with crossed nichols. Note the plagioclase feldspar twinning (G4 and B4) and the high birefringence of carbonate cements nucleated on framework grains and partially occluding some of the pore space. The carbonate cements display characteristic high birefringence ("tiny points of light" or a "rainbow" of yellow-red-blue in large crystals) readily visible (A5, B1-B2, F7, D6, H1 and K2).

Note the characteristic zebra stripe plagioclase twinning at B4 and G3-G4).

Integration of thin-section, SEM, and X-ray powder diffraction analyses indicates grain coating ("isopachous") boxwork lattices of diagenetic chlorite are present. Later diagenetic carbonate microspar rests on the grain coating chlorite, further reducing pore volume and pore throats. Pore-bridging, filamentous to ligament-like illite and illite/smectite partition already small pore throats. XRD analysis indicates that the Illite/Smectite is 20% expandible. KCl should be present in both drilling and completion fluids to stabilize the smectites. Iron-rich, pore lining minerals possess a potential for significant formation . Iron sequestering agents should be added to completion fluids to avoid untimely and irreversible precipitation of iron hydroxide gel.

Dissolution of silt to very fine, sand sized carbonates (G5, F7 and H1) could lead to loss of porosity and permeability due to selective framework collapse. The following are present siderite (Iron protocarbonate, $FeCO_3$), dolomite ($CaMg(CO_3)$ and ankerite ($2CaCO_3$),$Mg(CO_3)$, $Fe(CO_3)$ and will come into contact with completions fluids.

Interparticle porosity estimated at 18-20 %

Strata Production, Nash Unit # 23 Eddy Co., NM

A
6652.7
PPL

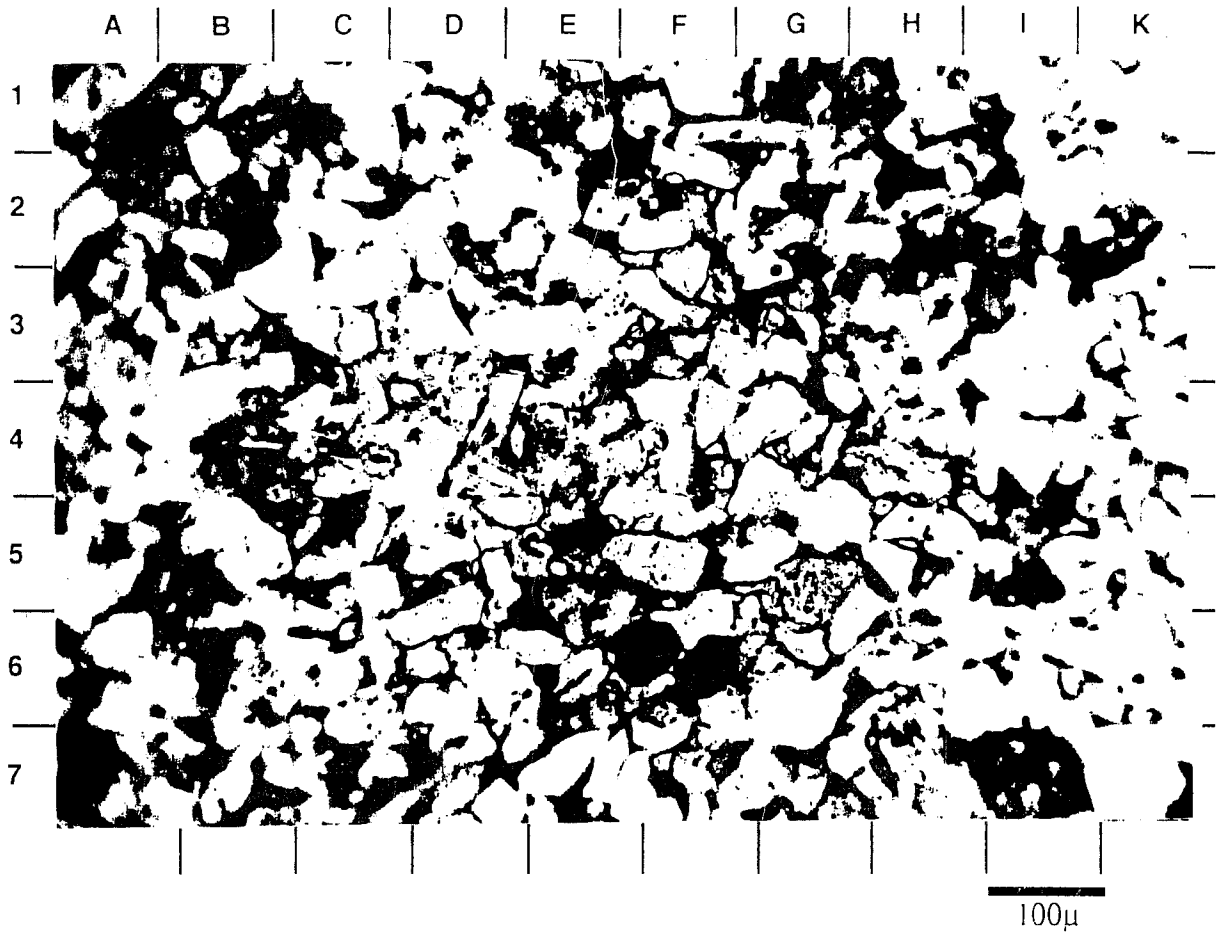

B
6652.7
XPL

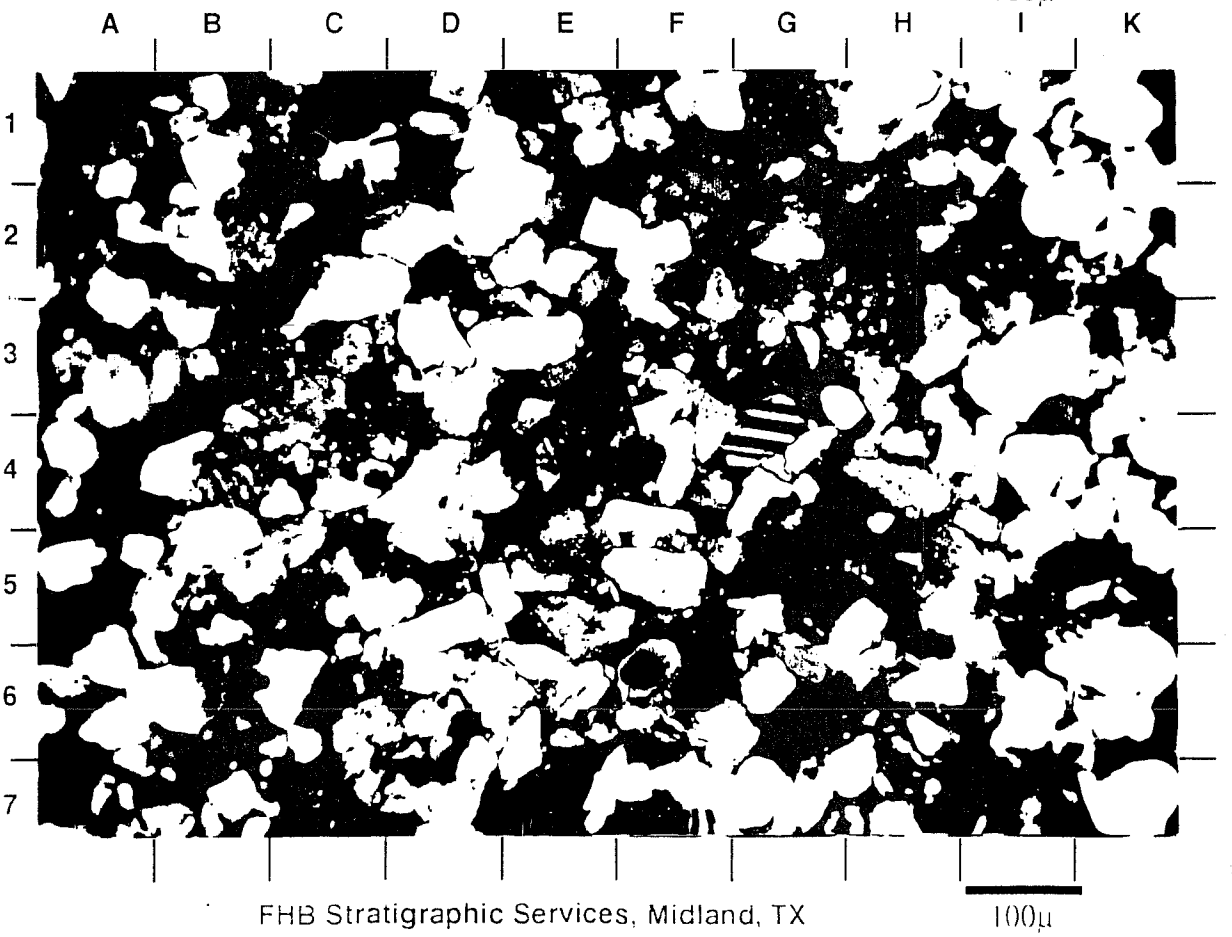

Plate 2

Strata Production, Nash Unit #23, Eddy Co., NM

6,652.7 ft.

Core Lab prepared all thin-sections from conventional core permeability plugs. Thin sections are impregnated with blue epoxy, one half of each thin-section stained with Alizarin Red S, and finished with a cover slip. Blue dye shows as porosity.

High magnification, scale bar beneath and to the right of photo is 50 microns (50μ). The coarse silt to very fine-grained sand is 62μ, while the very fine to fine-grained sand is 125μ.

A &B Note the low grain sphericity prevalent in field of view, with irregular "scalloped" grain boundaries and the overly– close grain packing. Many quartz grains display a cloudy to "dusty" appearance in plane polarized light (E6 ,G6). All grains have very thin dark brown coating of diagenetic chlorite and microcrystalline to euhedral carbonate cements. Note black opaque and translucent light to medium brown regions in **A**.

The opaque silt-sized clusters are diagenetic pyrite present as (A2, C4) under plane polarized light in **A**. The translucent light brown to "cloudy" regions display high birefringence in **B**. These regions are organic rich carbonate microspar or neomorphic carbonate whose precursor was lime. The carbonates display characteristic high birefringence ("tiny points of light" or a "rainbow" of yellow-red-blue in large crystals) readily visible in **B** (A1, B3, D3->D4, G5, I2, I5 and K5). The calcite cement at D3-D4 and I5 is poikilitic (has single crystal extinction and encloses several framework grains or completely or partially occludes several pores). Poikilitic carbonate cements form most often where echinoid fragments are present and provide a low nucleation energy for formation of optically continuous cements.

Detrital K-feldspars display rare syntaxial overgrowths and dissolution creating microporosity (E>F-1) 1). Plagioclase feldspars preserve sharply defined, as well as relict twinning. Relict twinning is seen at K5. have undergone dissolution. XRD analysis indicates that K-feldspars (10%) and Plagioclase feldspars (11.4%) confirm the thin-section designation as feldspathic-lithic-quartz sandstones. Different types of quartz present demonstrate multiple source terrains as well as immature characteristics.

This and other photos document polymictic depositional trait of the Brushy Canyon Formation-rapid deposition of arkosic, lithic and quartz rich siliciclastics. Quartz can be subdivided into: 1) grains with eroded and scalloped megaquartz syntaxial cements differentiated by a thin, but discernible boundary (D7, B3, E3); 2) undulatory extinction under crossed nichols indicate a metamorphic stress field distorted the single extinction typical megaquartz. (B&C-4&5); and, 3) microcrystalline quartz (chert) not visible in this photograph.

SEM photomicrographs (Figurel and 2) show the boxwork lattice morphology so characteristic of grain-coating and pore-lining authigenic chlorite. Later fibrous to ligament-like pore-bridging illite and illite/smectite further degrade pore throats. Authigenic chlorite, illite and illite/smectite will create overly pessimistic calculated water saturations (Sw) when most of water is "bound" or irreducible water (Swi). The clays will also provide overly optimistic porosity calculations due to contribution of microporousity in boxwork clays.

Strata Production, Nash Unit # 23 Eddy Co., NM

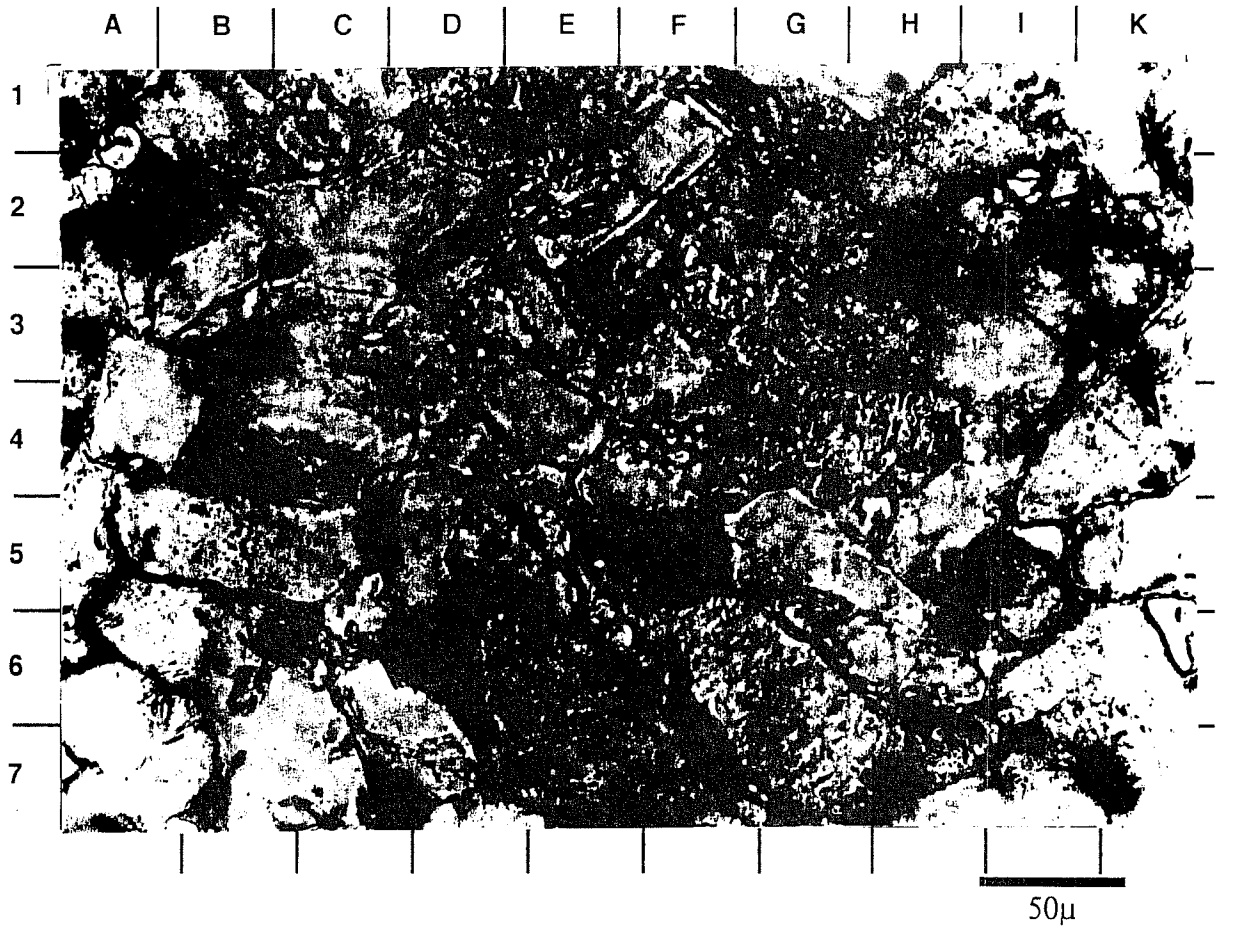

A
6652.7
PPL

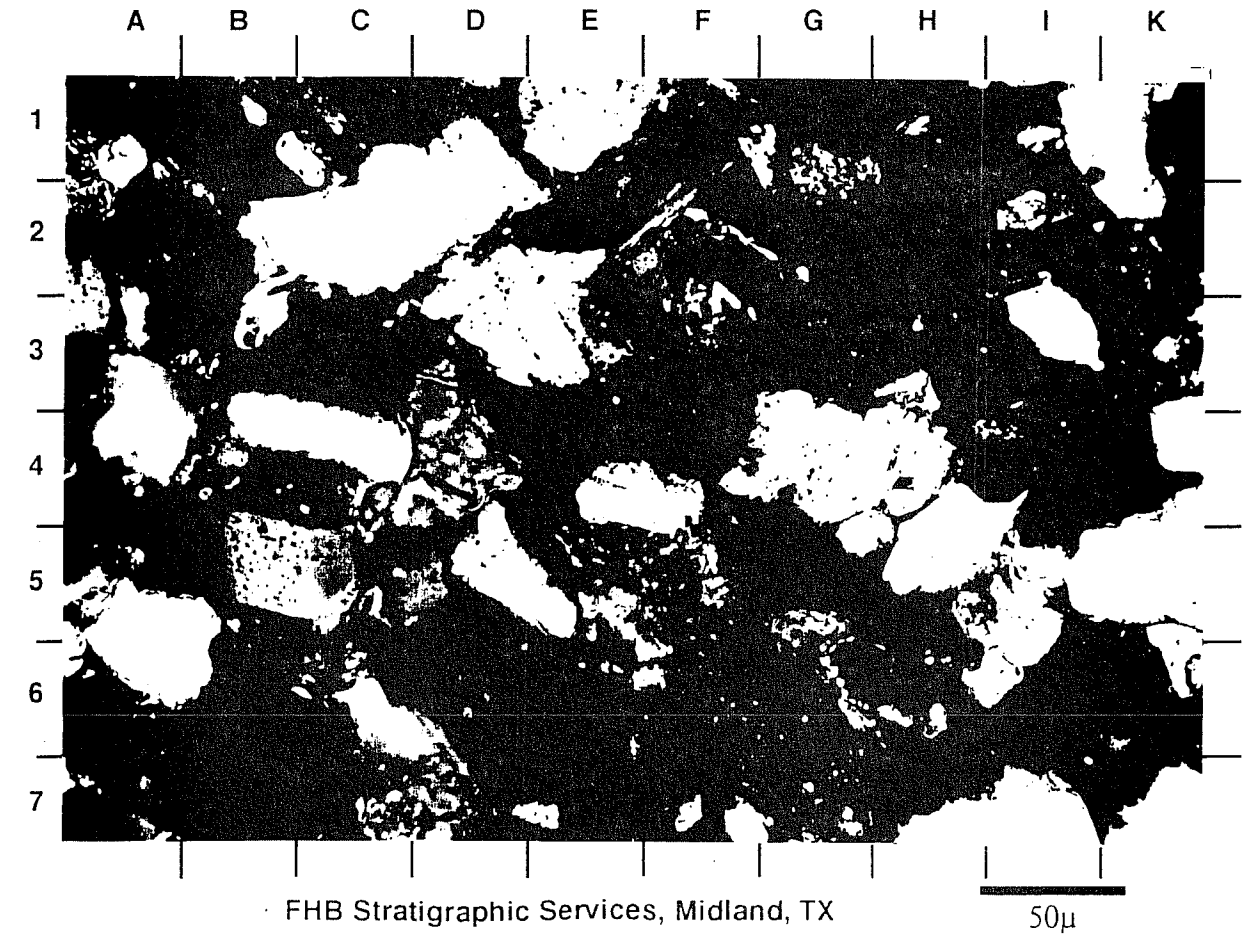

B
6652.7
XPL

FHB Stratigraphic Services, Midland, TX

Plate 3

Strata Production, Nash Unit #23, Eddy Co., NM

6,652.7 ft.

Core Lab prepared all thin-sections from conventional core permeability plugs. Thin sections are impregnated with blue epoxy, one half of each thin-section stained with Alizarin Red S, and finished with a cover slip. Blue dye shows as porosity.

High magnification, scale bar beneath and to the right of photo is 50 microns (50μ). The coarse silt to very fine-grained sand is 62μ, while the very fine to fine-grained sand is 125μ.

A Note the low grain sphericity prevalent in the field of view, with irregular "scalloped" grain boundaries and the overly– close grain packing. Many quartz grains display a cloudy to "dusty" appearance in plane polarized light (E6 ,G6). All grains have very thin dark brown coating of diagenetic boxwork lattice of chlorite with subsequent carbonate cements. Grain-coating chlorite and carbonate cement is readily discernible at E3->F3. Note black opaque and translucent light to medium brown regions in **A**.

Black and opaque, authigenic pyrite partially occludes some pores and restricts some pore throats. The pyrite ranges in size from 2 to 30μ.

B Same view as **A**, showing characteristic mixed low sphericity (C2->D4, I5) and high sphericity grains (D7 ,E5, and K4). Scalloped quartz grain boundaries, diagenetic grain coating and pore lining chlorite and later carbonates (B3, C1, C2, F7, F3, and G2). At G2 a small fragment of echinoderm plate served as a low crystallization nucleation site for syntaxial cement.

Microcrystalline quartz (chert or chalcedonies quartz; D7-D6) grains are present. Composite clasts composed of two or more grains can be seen in **A** at E5-->E6) and composite grains (E5->E7) The opaque silt-sized clusters are diagenetic pyrite present as (A2, C4) under plane polarized light in **A**. The translucent light brown to "cloudy" regions display high birefringence in **B**. These regions are organic rich carbonate microspar or neomorphic carbonate whose precursor was lime micrite The carbonates display characteristic high birefringence ("tiny points of light" or a "rainbow" of yellow-red-blue in large crystals) readily visible in **B** (A1, B3, D4, G5, I2, I5 and K5).

Detrital and highly altered feldspars show subtle relict twinning at H6 and G5-G6)

Strata Production, Nash Unit # 23 Eddy Co., NM

PLATE 3

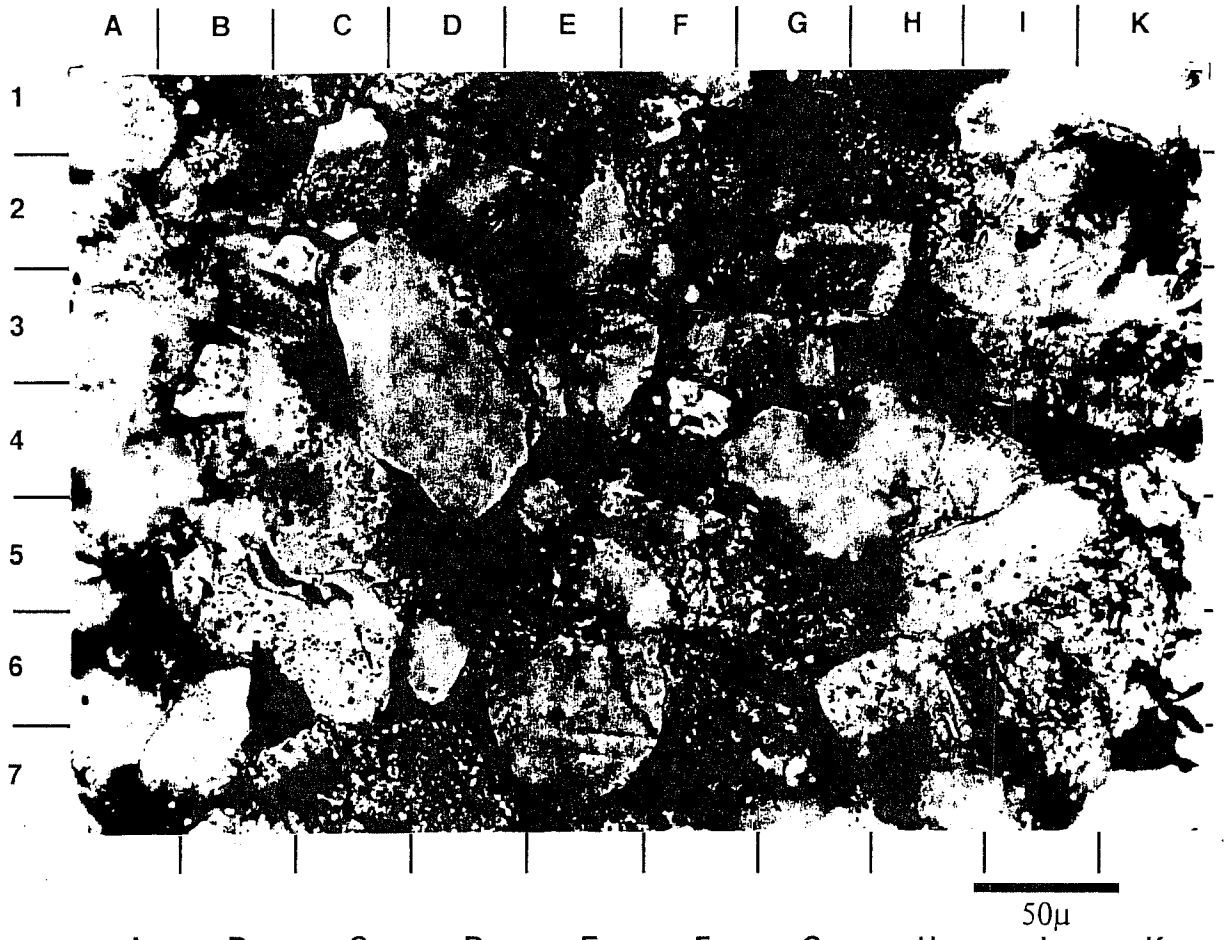

A
6652.7
PPL

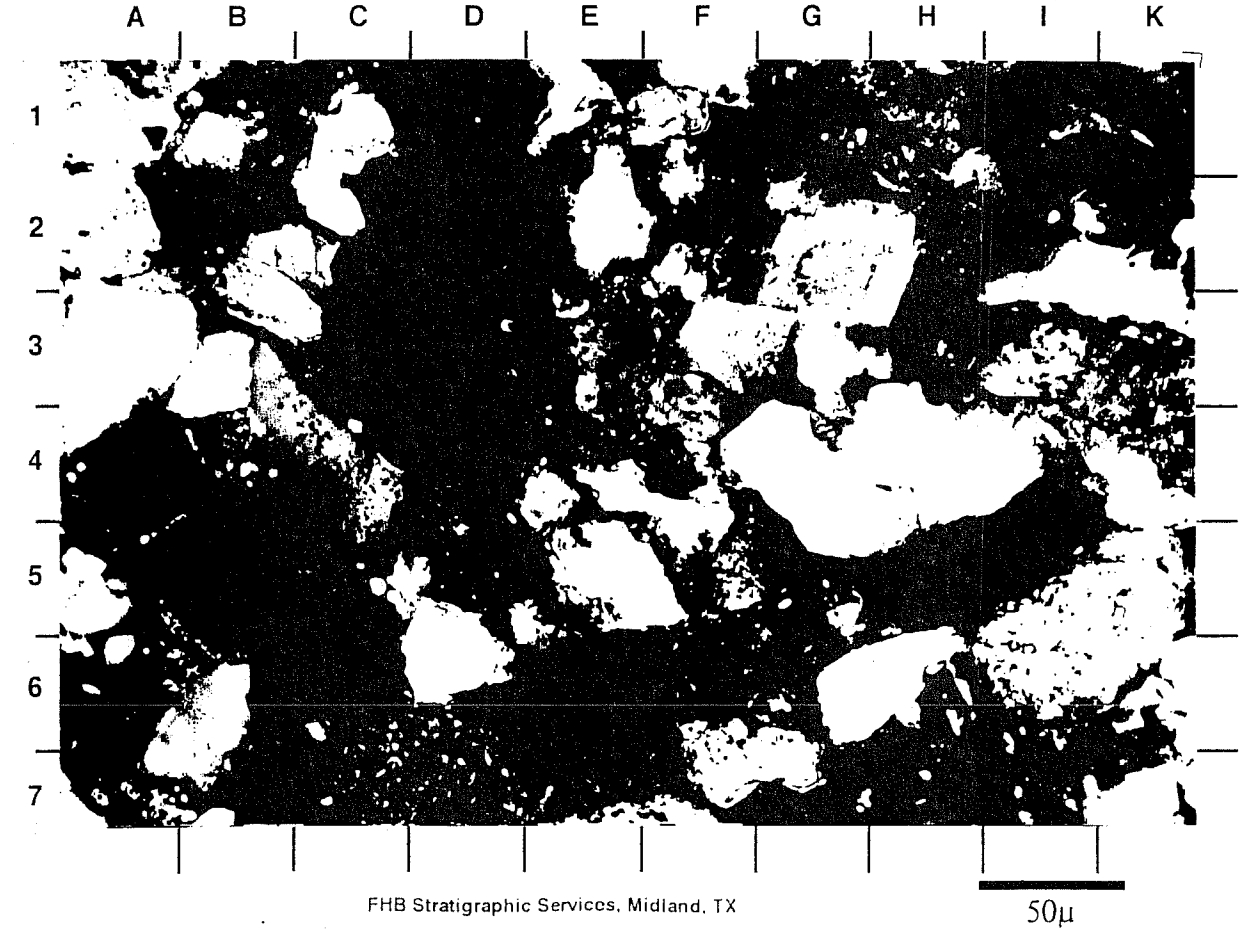

B
6652.7
XPL

Plate 4

Strata Production, Nash Unit #23, Eddy Co., NM

6,664.6 ft.

Alizarin Red S stain

Core Lab prepared all thin-sections from conventional core permeability plugs. Thin sections are impregnated with blue epoxy, one half of each thin-section stained with Alizarin Red S, and finished with a cover slip. Blue dye shows as porosity.

Low magnification, scale bar beneath and to the right of photo is 100 microns (100μ). The coarse silt to very fine-grained sand is 62μ, while the very fine to fine-grained sand is 125μ.

A Silty very fine grained sandstone, little calcite stain apparent in field of view. Stain present at H2, I7, D4->E5, as well as very small intergranular cement. Low grain sphericity prevalent in field of view, with irregular "scalloped" grain boundaries and the chaotic to overly– close grain packing. Pores are slit-like to wedge shaped, with a length:width ratio ranging from 3:1 to 10:1

Plagioclase feldspars present at G1, G2, C3, D3. Poikilitic carbonate cement at G2->H2

SEM photomicrographs (Figure 3) reveal abundant syntaxial (euhedral) quartz overgrowths. SEM (Figure 3) also shows the fibrous pore-bridging illite and grain-coating authigenic chlorite. Perhaps the presence of grain-coating chlorite inhibits quartz overgrowths. Like the Gulf Coast Wilcox Sandstone, porosity may be preserved by initial precipitation of grain coating chlorite.

Strata Production, Nash Unit# 23
Eddy Co., NM

PLATE 4

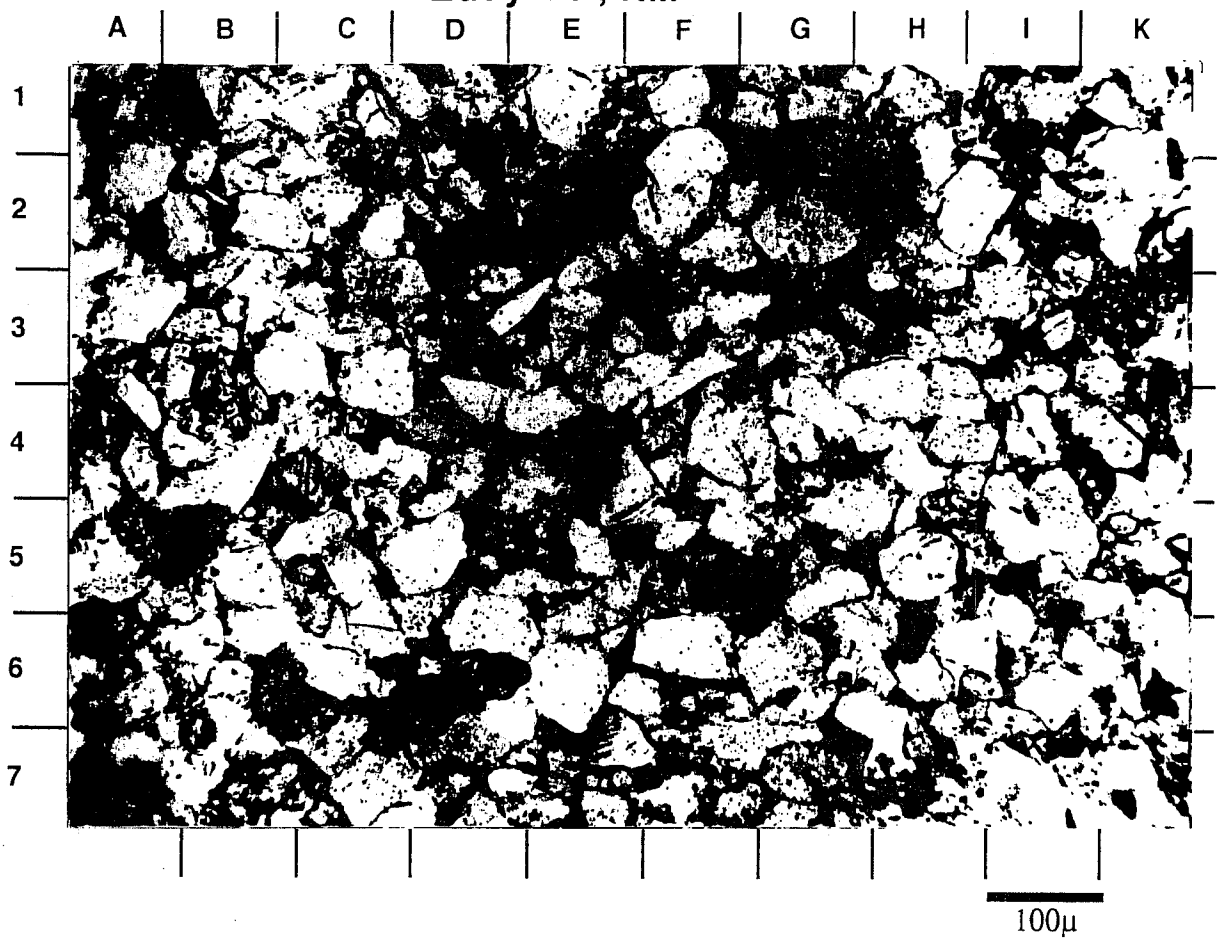

A
6664.6
PPL

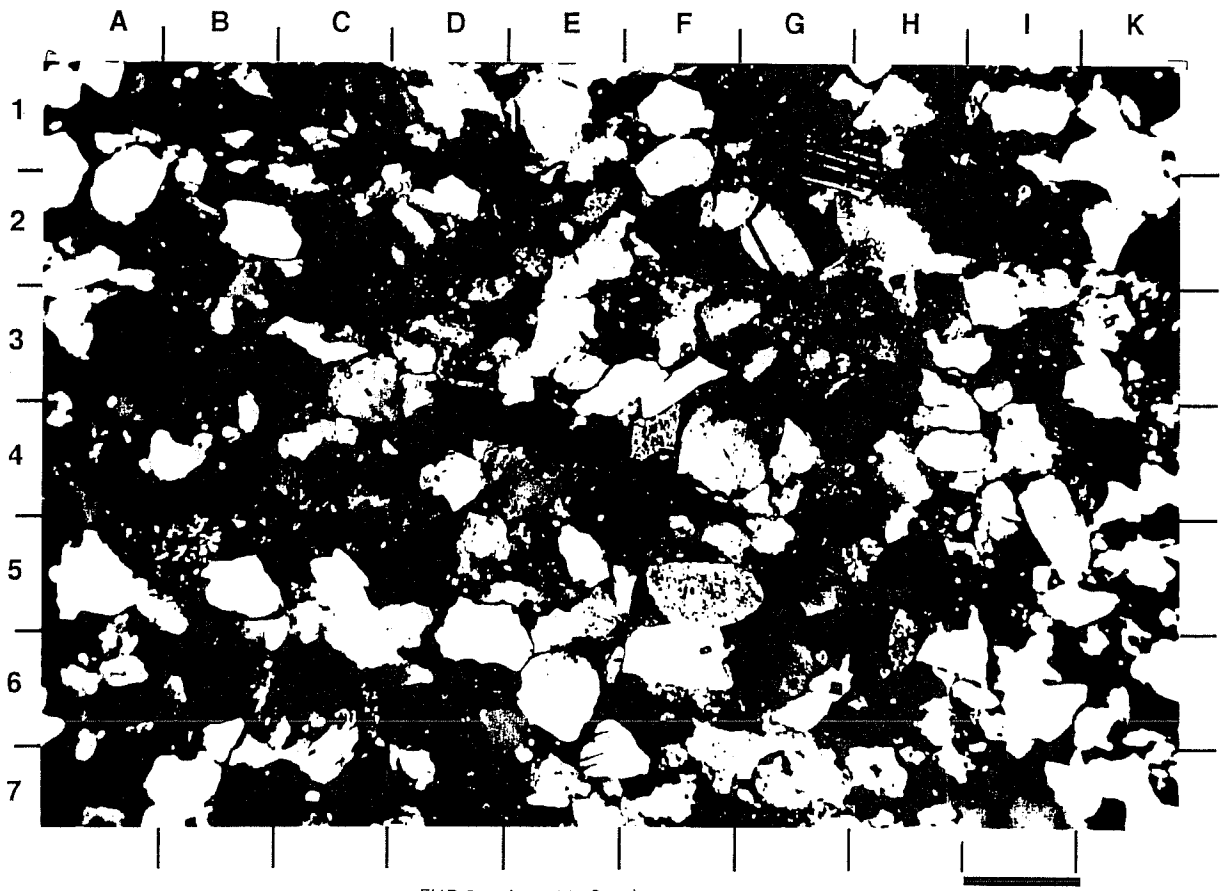

B
6664.6
XPL

FHB Stratigraphic Services, Midland, TX

Plate 5

Strata Production, Nash Unit #23, Eddy Co., NM

6,664.6 ft.

Alizarin Red S stain

Core Lab prepared all thin-sections from conventional core permeability plugs. Thin sections are impregnated with blue epoxy, one half of each thin-section stained with Alizarin Red S, and finished with a cover slip. Blue dye shows as porosity.

High magnification, scale bar beneath and to the right of photo is 50 microns (50μ). The coarse silt to very fine-grained sand is 62μ, while the very fine to fine-grained sand is 125μ.

A Silty very fine grained sandstone, minimal calcite stain apparent in field of view. Stain present at A5, B7, H4 and I2 as well as very small intergranular cement. Low grain sphericity prevalent in field of view, with irregular "scalloped" grain boundaries and the chaotic to overly– close grain packing.

Potassium feldspars show dissolution and development of microporosity at E6. Poikilitic carbonate cement at G2->H2.

A very fine-sand sized clast (D1->D3) is comprised of silt-sized quartz grains.

B Same view as **A**, but with crossed nichols permits definition of the pore occluding and pore throat blockage by authigenic clays and carbonate cements (B3 and C2 in same pore; E4->F4;B5)

The SEM photomicrograph designated as Figure 3 defines features observed in 6664.6 and 6666.5. **Figure 3**reveal abundant syntaxial (euhedral) quartz overgrowths. SEM (Figure 3) also shows the fibrous pore-bridging illite and grain-coating authigenic chlorite.

Strata Production, Nash Unit # 23 Eddy Co., NM

PLATE 5

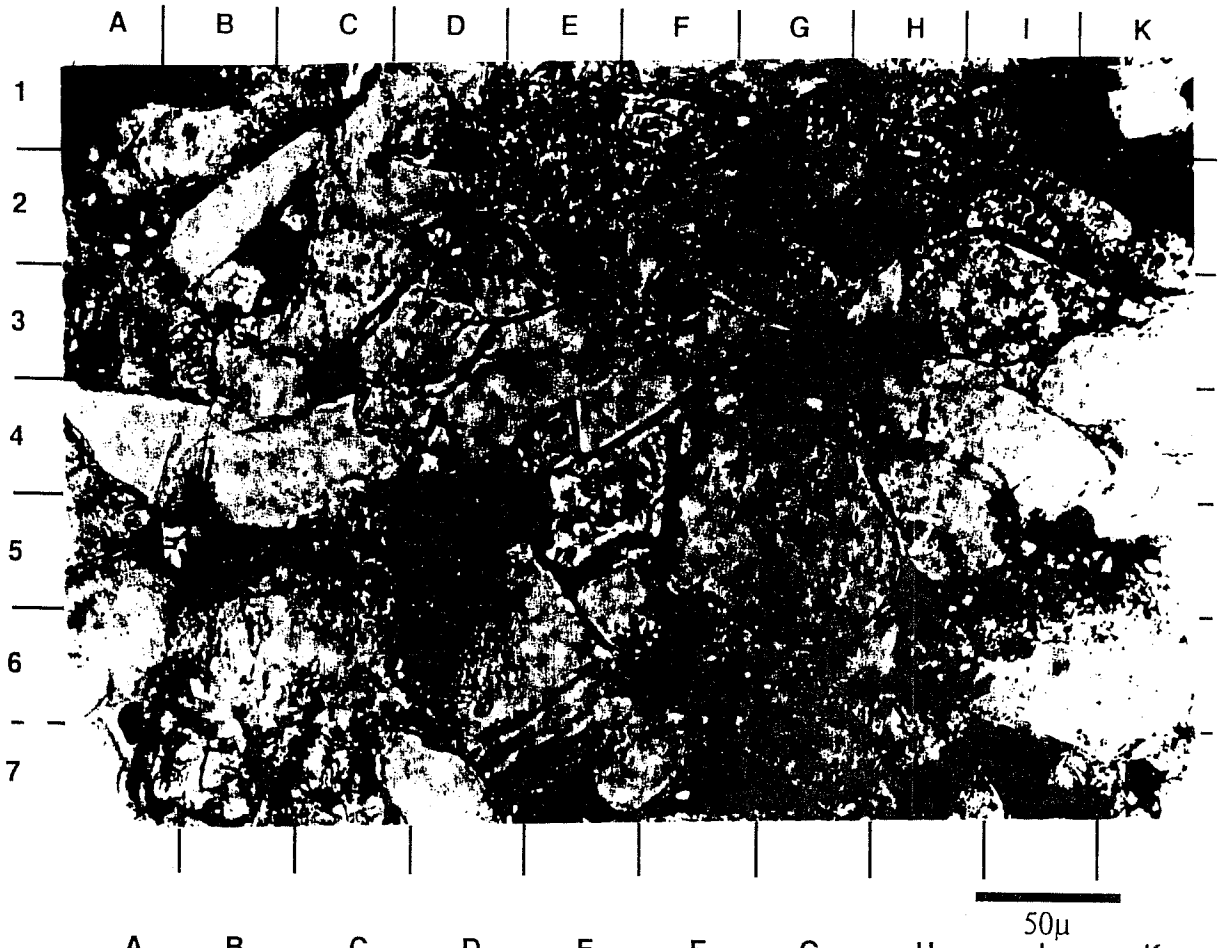

A
6664.6
PPL

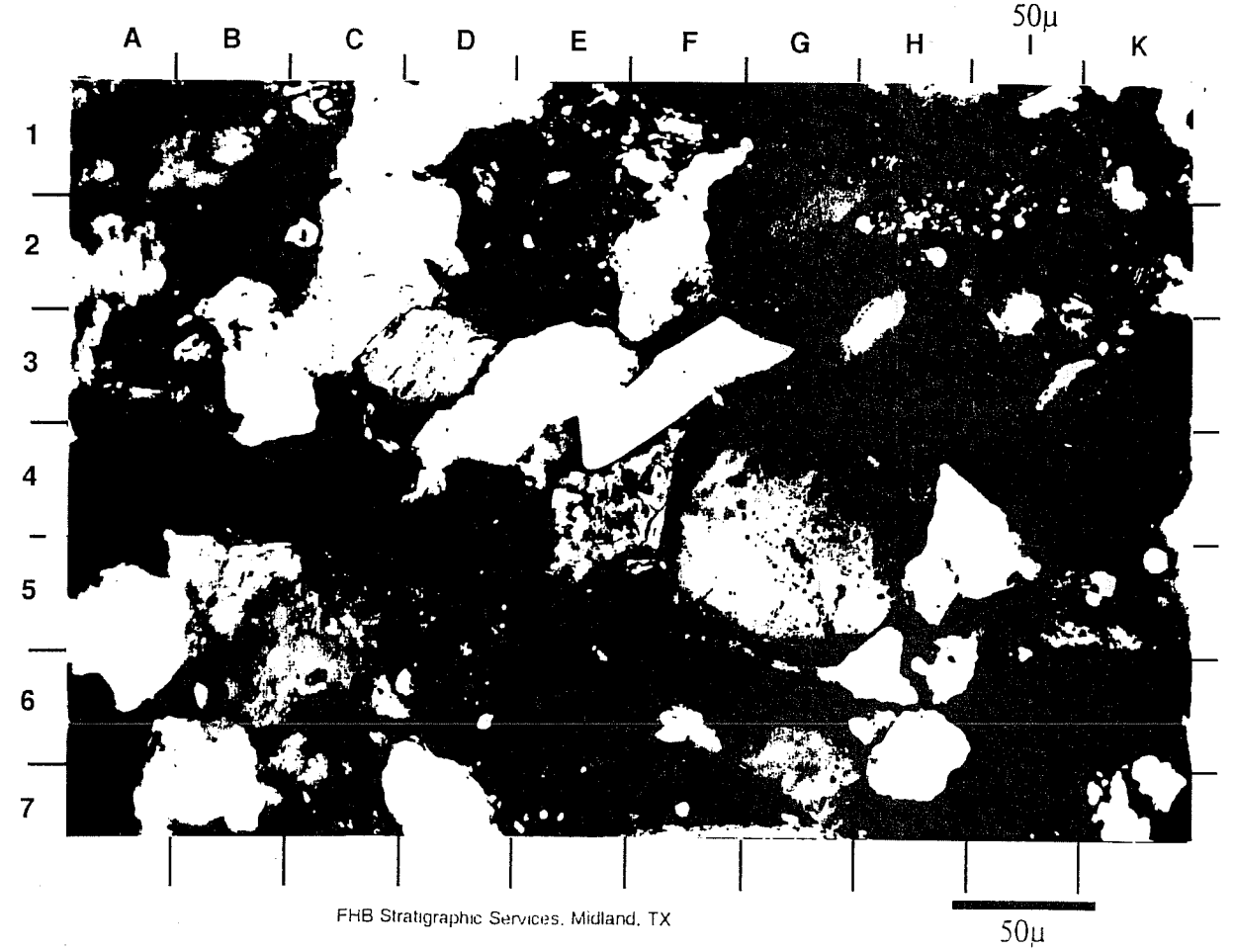

B
6664.6
XPL

FHB Stratigraphic Services, Midland, TX

Plate 6

Strata Production, Nash Unit #23, Eddy Co., NM

6,665.5 ft.

Core Lab prepared all thin-sections from conventional core permeability plugs. Thin sections are impregnated with blue epoxy, one half of each thin-section stained with Alizarin Red S, and finished with a cover slip. Blue dye shows as porosity.

Low magnification, scale bar beneath and to the right of photo is 100 microns (100μ). The coarse silt to very fine-grained sand is 62μ, while the very fine to fine-grained sand is 125μ.

A Silty, very fine grained sandstone, Low to moderate grain sphericity prevalent in field of view, with irregular "scalloped" grain boundaries and the chaotic to overly– close grain packing. Poorly preserved porosity.

Irregular dark areas are interpreted to be flattened silt free (D1, C2, D1, G1, G2) or silty fecal pellets (B5->C5).

B Plagioclase feldspars present at H6. Syntaxial quartz at F2,I3,and I5.

Strata Production, Nash Unit # 23 Eddy Co., NM

PLATE 6

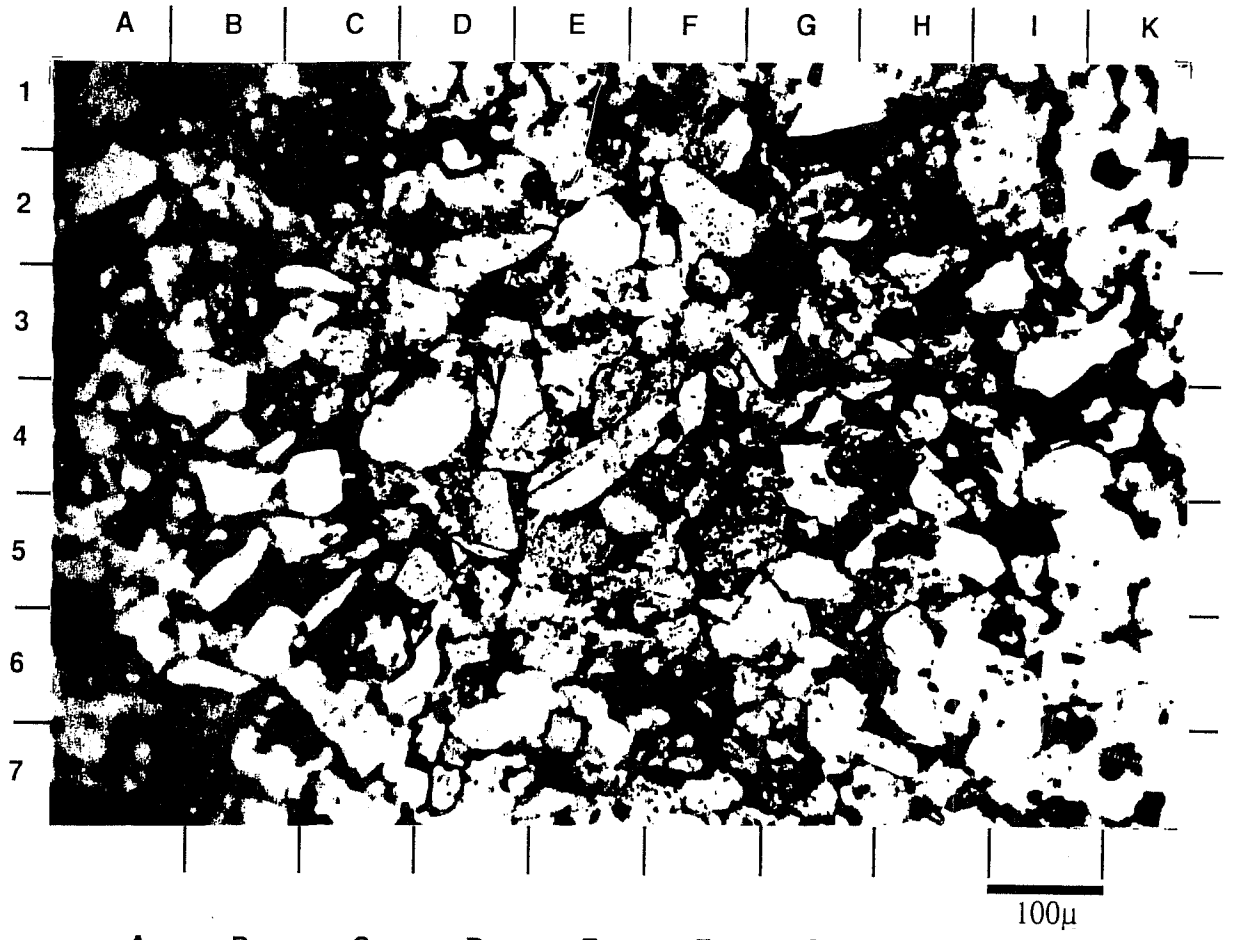

A
6665.5
PPL

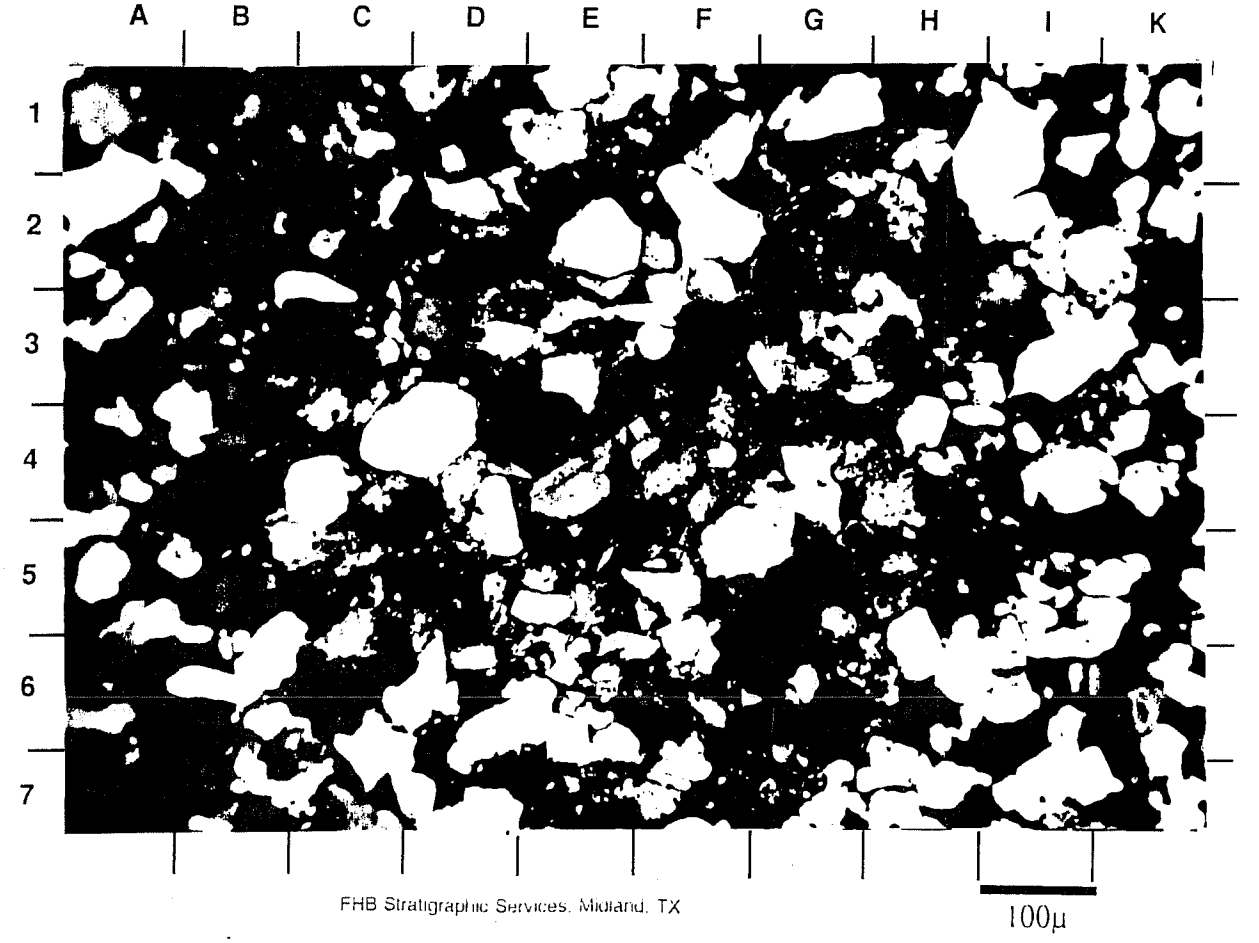

B
6665.5
XPL

FHB Stratigraphic Services, Midland, TX

Plate 7

Strata Production, Nash Unit #23, Eddy Co., NM

6,665.5 ft.

Core Lab prepared all thin-sections from conventional core permeability plugs. Thin sections are impregnated with blue epoxy, one half of each thin-section stained with Alizarin Red S, and finished with a cover slip. Blue dye shows as porosity.

High magnification, scale bar beneath and to the right of photo is 50 microns (50μ). The coarse silt to very fine-grained sand is 62μ, while the very fine to fine-grained sand is 125μ.

Plane Polarized light of region E4 in Plate 6.

Field of view only has low grain sphericity, with irregular "scalloped" grain boundaries and the chaotic to overly– close interpenetrating grain packing. The "halo" of light around framework grains are Becke lines resulting from refraction at grain-coating chlorite and the epoxy.

Rare detrital mica "banana-like" section at F4->C5. Microporous and weathered chert (?) at G3-C3.

All black opaque pyrite is grain coating and pore filling (K3, K4, I4 and others).

Irregular dark areas are interpreted to be flattened silt free (D1, C2, D1, G1, G2) or silty fecal pellets (B5->C5).

Strata Production, Nash Unit # 23 Eddy Co., NM

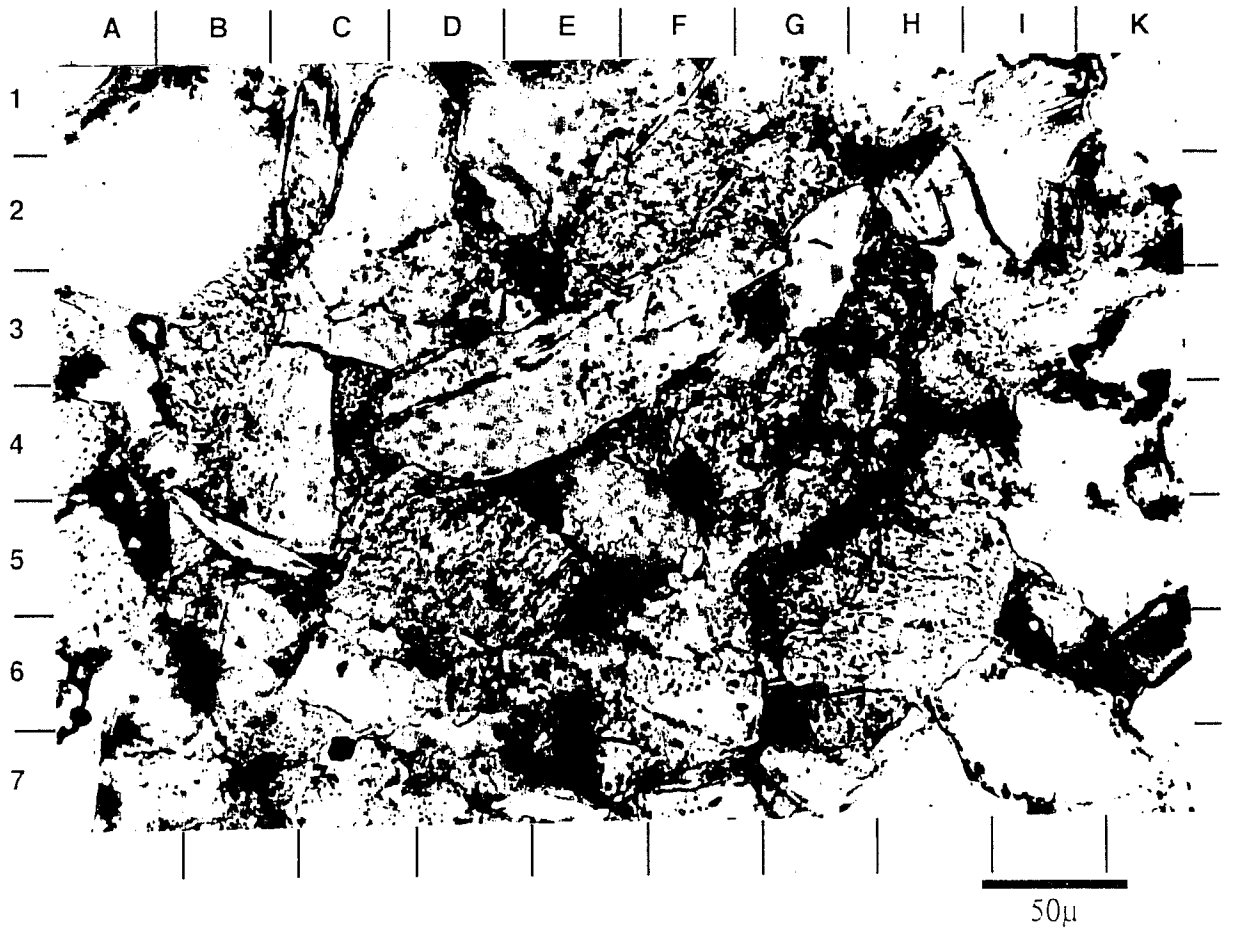

6665.5

PPL

Plate 8

Strata Production, Nash Unit #23, Eddy Co., NM

6,681.5 ft.

Core Lab prepared all thin-sections from conventional core permeability plugs. Thin sections are impregnated with blue epoxy, one half of each thin-section stained with Alizarin Red S, and finished with a cover slip. Blue dye shows as porosity.

Low magnification, scale bar beneath and to the right of photo is 100 microns (100μ). The coarse silt to very fine-grained sand is 62μ, while the very fine to fine-grained sand is 125μ.

A Silty, very fine grained sandstone, Core plug is characterized by an increase in moderate sphericity grains, with irregular "scalloped" grain boundaries and the chaotic to overly– close interpenetrating grain packing. Quartz overgrowths are not as prevalent and minor amounts of clay cement are present(grain-coating chlorite and pore bridging illite to illite /smectite.

SEM photomicrograph (Figure 4) indicates that in addition to grain-coating chlorite and pore-bridging illite and illite/smectite, pore occluding diagenetic feldspar and some carbonate cement are present.

All black opaque pyrite is grain coating and pore filling (C2, B8, E5->E6 and others).

B Same as view and magnification as in A, with crossed nichols.

Strata Production, Nash Unit # 23 Eddy Co., NM

PLATE 8

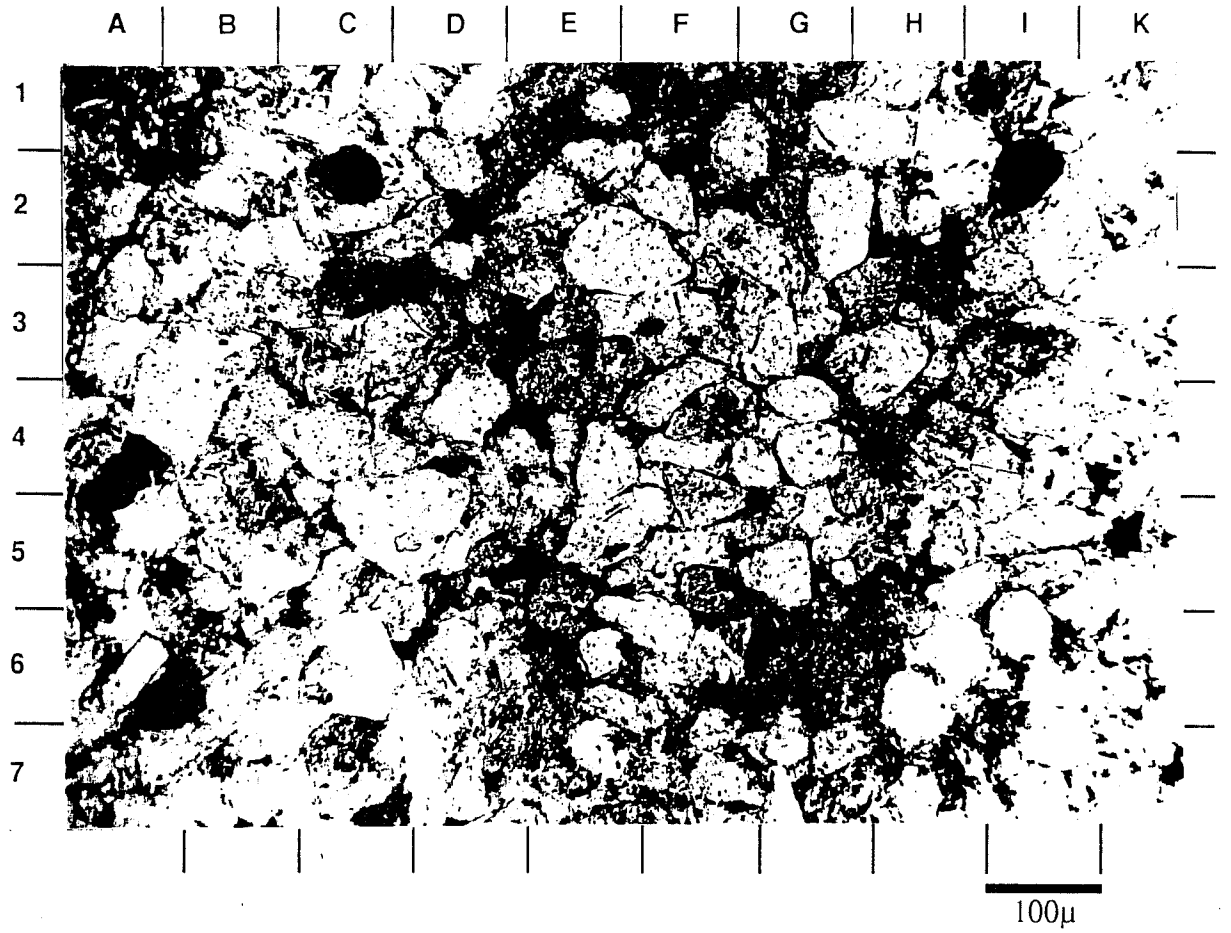

A
6681.5
PPL

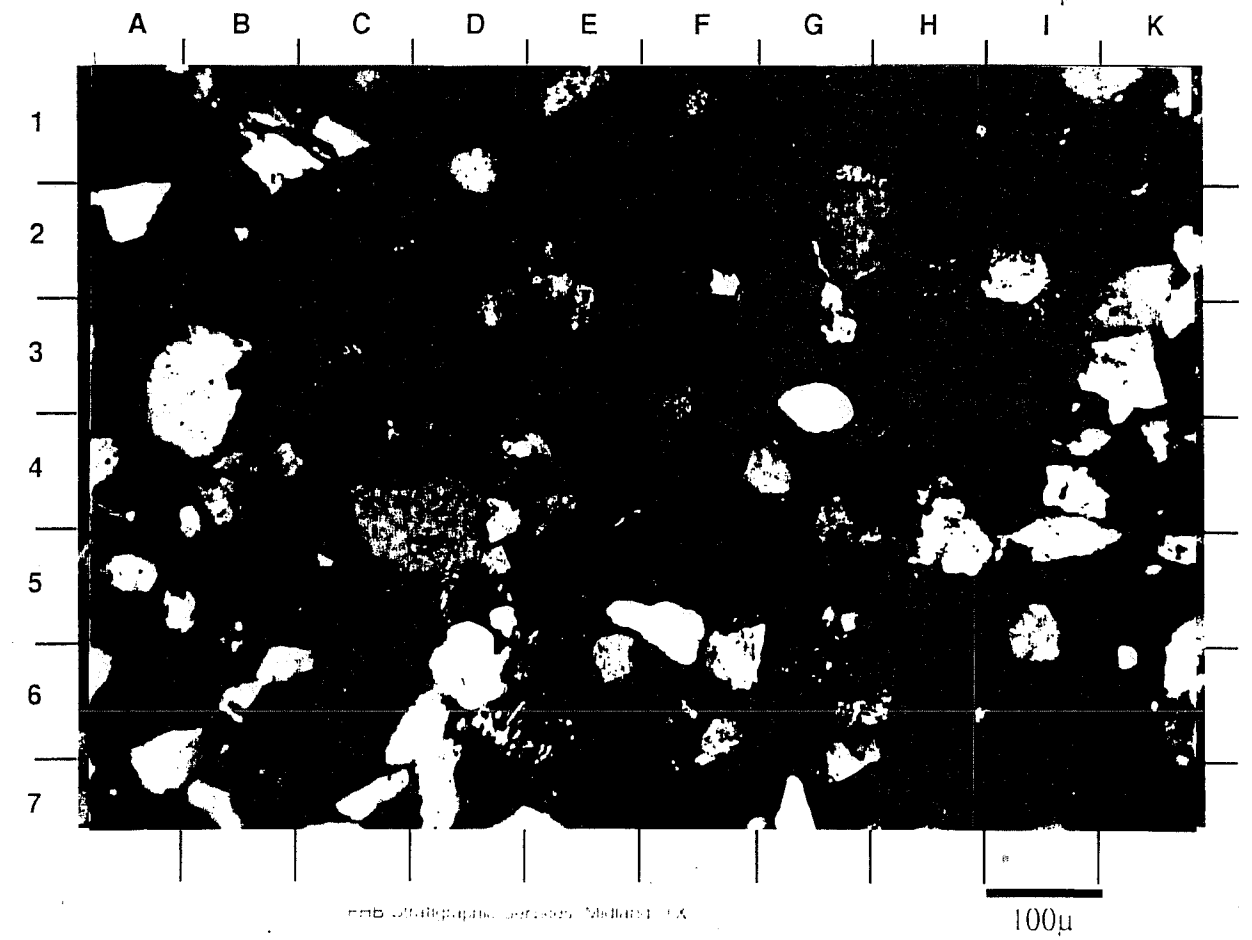

B
6681.5
XPL

Plate 9

Strata Production, Nash Unit #23, Eddy Co., NM

6,681.5 ft.

Detail of area F3->F4 in Plate 8

Core Lab prepared all thin-sections from conventional core permeability plugs. Thin sections are impregnated with blue epoxy, one half of each thin-section stained with Alizarin Red S, and finished with a cover slip. Blue dye shows as porosity.

High magnification, scale bar beneath and to the right of photo is 50 microns (50μ). The coarse silt to very fine-grained sand is 62μ, while the very fine to fine-grained sand is 125μ.

A Weathered (?) and microporous chert (?)at A1, B1, A2, B2, D2->D3, K3. Overly closed packing with spotty intergranular porosity.

Carbonate cements appear to less prevalent in this sample. SEM analysis (Figure 4) indicates that rims on the quartz grains are grain-coating chlorite, with authigenic feldspars and carbonates appears to be indicated by "thorny" aspect of grains in D4--F3-F4-F5.

B Note the elliptical quartz grain at I3 is the same grain at G3 on Plate 8B. The weathered and microporous chert (?) has some of microporousity occluded by carbonate cement (points of light within grains).

Relict (?) feldspar twinning at G7.

Strata Production, Nash Unit # 23 Eddy Co., NM

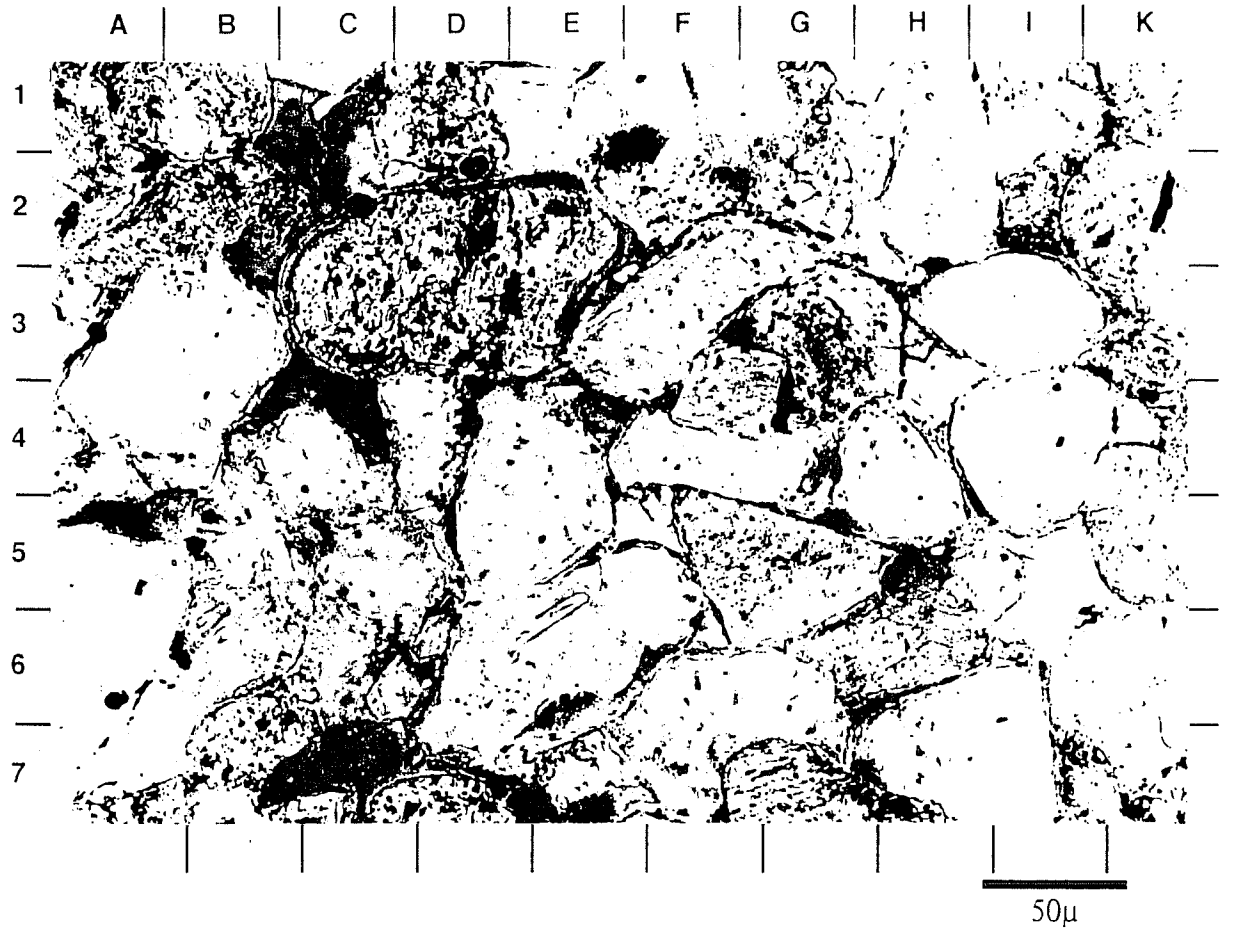

A
6681.5
PPL

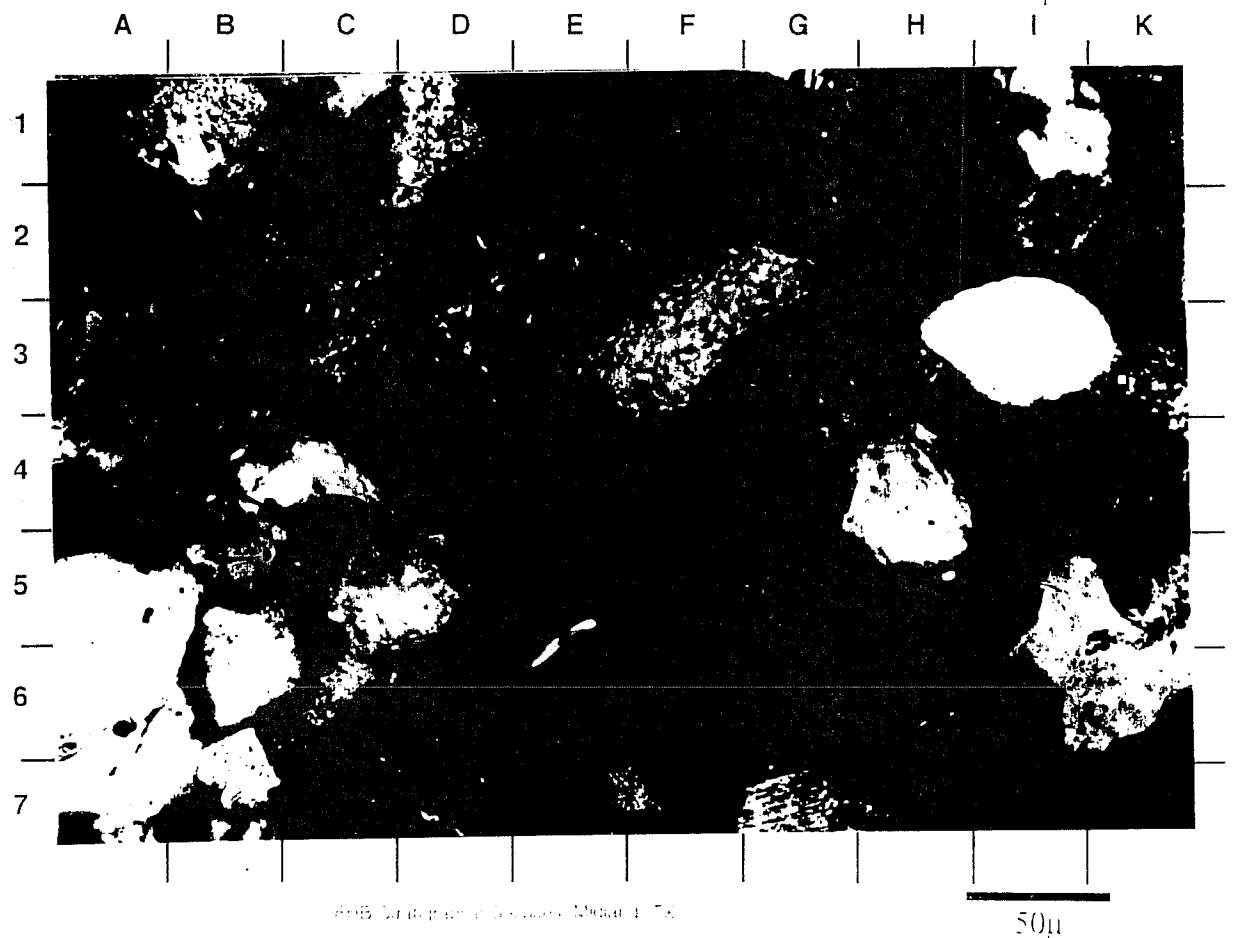

B
6681.5
XPL

Plate 10

Strata Production, Nash Unit #23, Eddy Co., NM

6,692.6 ft.

Core Lab prepared all thin-sections from conventional core permeability plugs. Thin sections are impregnated with blue epoxy, one half of each thin-section stained with Alizarin Red S, and finished with a cover slip. Blue dye shows as porosity.

Low magnification, scale bar beneath and to the right of photo is 100 microns (100μ). The coarse silt to very fine-grained sand is 62μ, while the very fine to fine-grained sand is 125μ.

A Silty and slightly fossiliferous, very fine grained sandstone. Effective porosity is estimated at less than 5% shown as deep blue epoxy at D3->H3. Very pale bluish epoxy could be overly close packing of quart grains and microporous chert or also intergranular pores now occluded by authigenic clays.

Porosity and permeability are occluded by grain-coating and pore-occluding chlorite, later pore bridging fibrous illite and illite/smectite, and quartz overgrowths.

Fossil fragments at C4, G3, I4->K4, and C5-D5.

Fair to good interparticle porosity, occluded by primary grain coating chlorite, second generation of fibrous illite, plys syntaxial quartz overgrowths. Extensive surface area provided by authigenic clays will result in very high calculated water saturation Sw, when most is Swi. Logs will appear overly optimistic with regard to effective porosity.

SEM Analysis displays theoverly close grain packing so characteristic of the thin-sections in this study and role of grain-coating to pore occluding chlorite and fibrous to ligment-like illite (**Figure 5**). Feldspar dissolution creates additonal microporosity.

B Feldspar dissolution and grain collapse are noted at C4-C5 and D2 and E3, plus A1-A2. Minor amounts of microporosity may skew calculated porosties and present very pessimistically high water satruations.The Swi will be higher were microporosity and boxwork lattice clays exponentially increase surface bound water.Grain at D3 appears to represent an older core with two "shoulders" of syntaxial megaquartz.

Strata Production, Nash Unit # 23 Eddy Co., NM

PLATE10

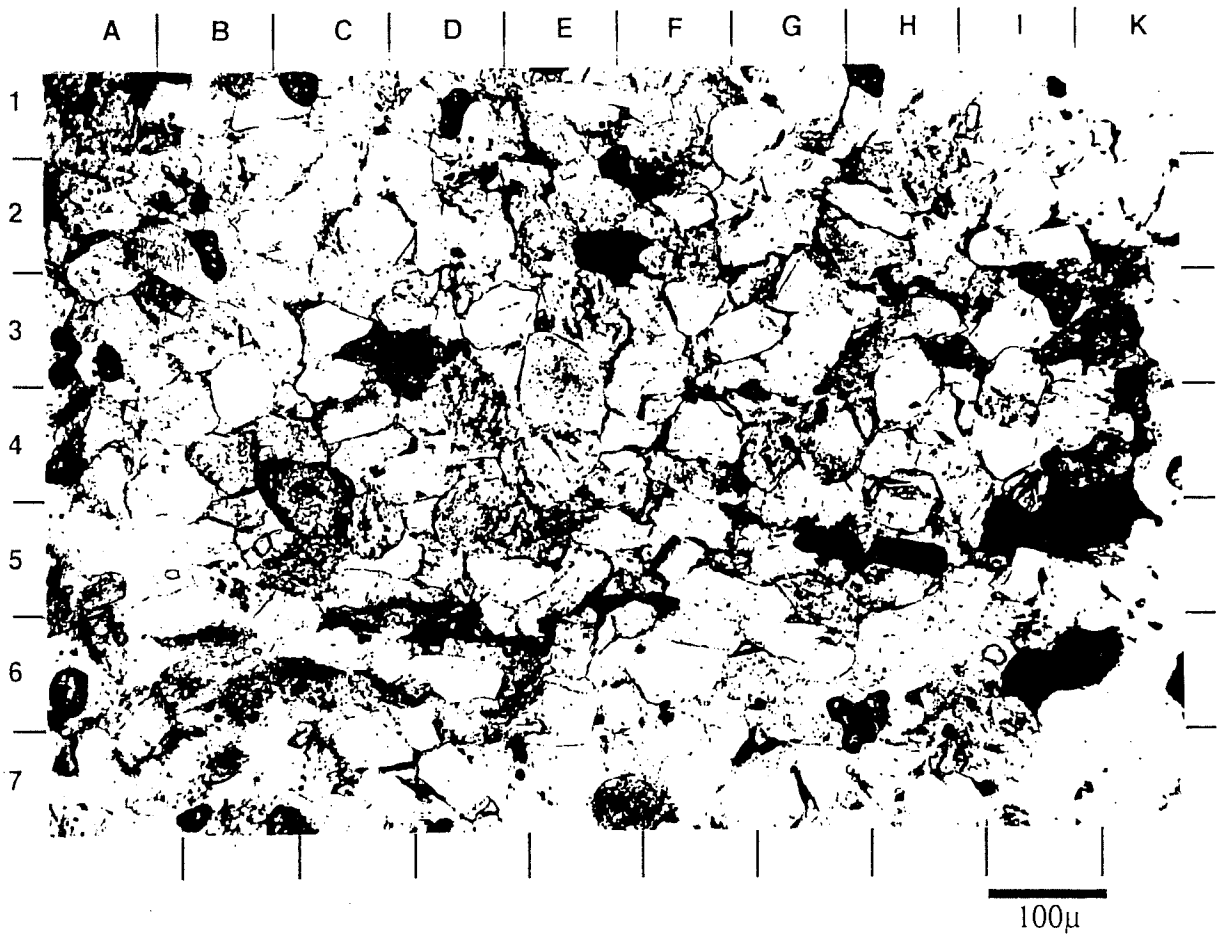

A
6692.6'
PPL

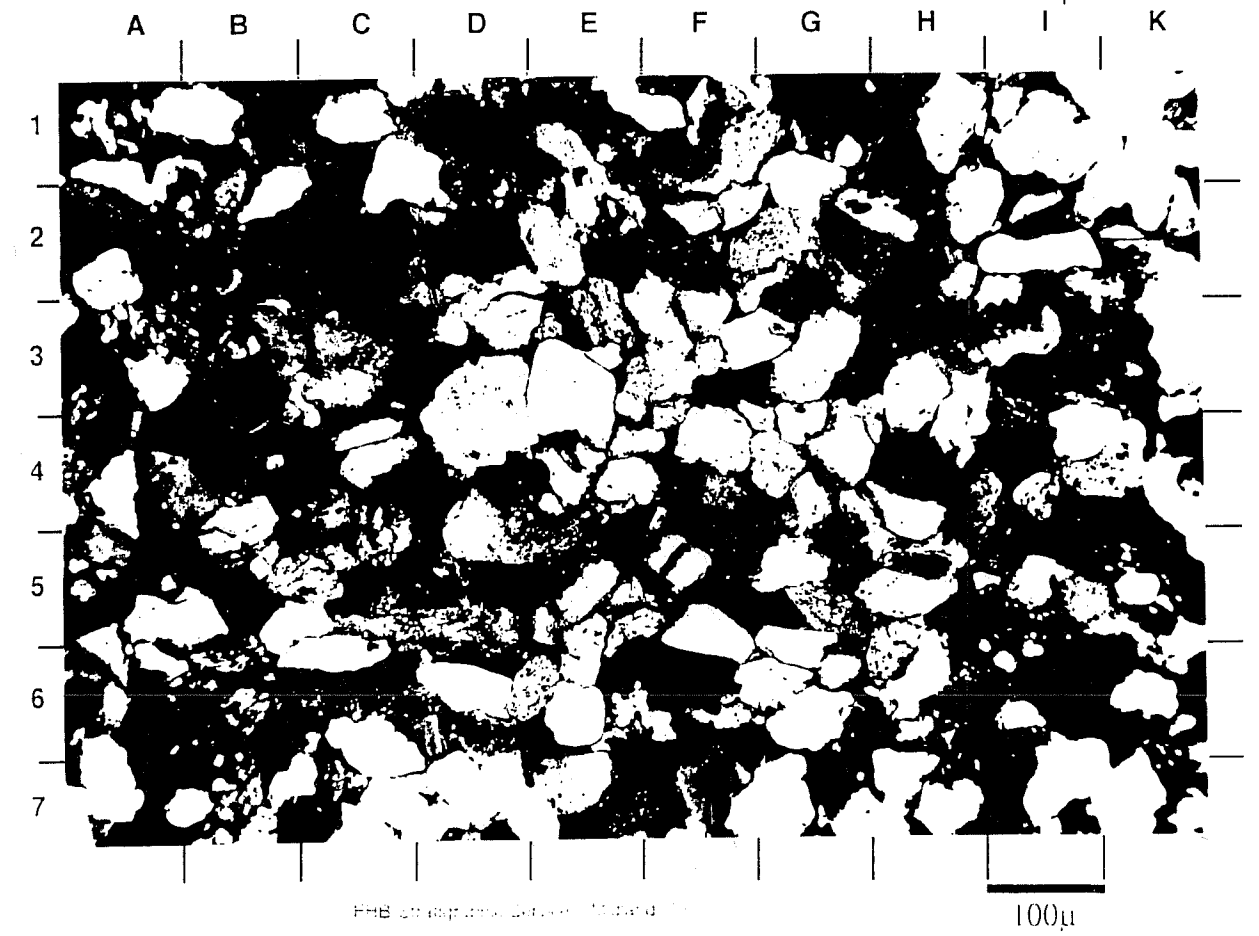

B
6692.6'
XPL

Plate 11

Strata Production, Nash Unit #23, Eddy Co., NM

6,711.1 ft.

Core Lab prepared all thin-sections from conventional core permeability plugs. Thin sections are impregnated with blue epoxy, one half of each thin-section stained with Alizarin Red S, and finished with a cover slip. Blue dye shows as porosity.

Low magnification, scale bar beneath and to the right of photo is 100 microns (100μ). The coarse silt to very fine-grained sand is 62μ, while the very fine to fine-grained sand is 125μ.

A Silty, very fine grained sandstone. Irregular and dark brown organic rich micrite (?) and interparticle cements produce erratic porosity and most likely low permeability.. Effective porosity is estimated at 5-10% shown as deep blue epoxy at E3->K2. Very pale bluish epoxy is interpreted as microporosity formed as authigenic grain-coating and pore-occluding chlorite and fibrous illite occluded primary interparticle pores. Minor amounds of porosity is lost by overly close packing of quartz grains.

Two small echinoderm plates dominating the lower left 1/4 of the photo is part of a larger "tadpole-shaped" clast that includes interpenetrating silt-sized quartz grains to shape the anterior and tail-like posterior.

B The large echinoderm plate has remnants of syntaxial carbonate cement with adjacent silt grains.

Strata Production, Nash Unit # 23 Eddy Co., NM

PLATE 11

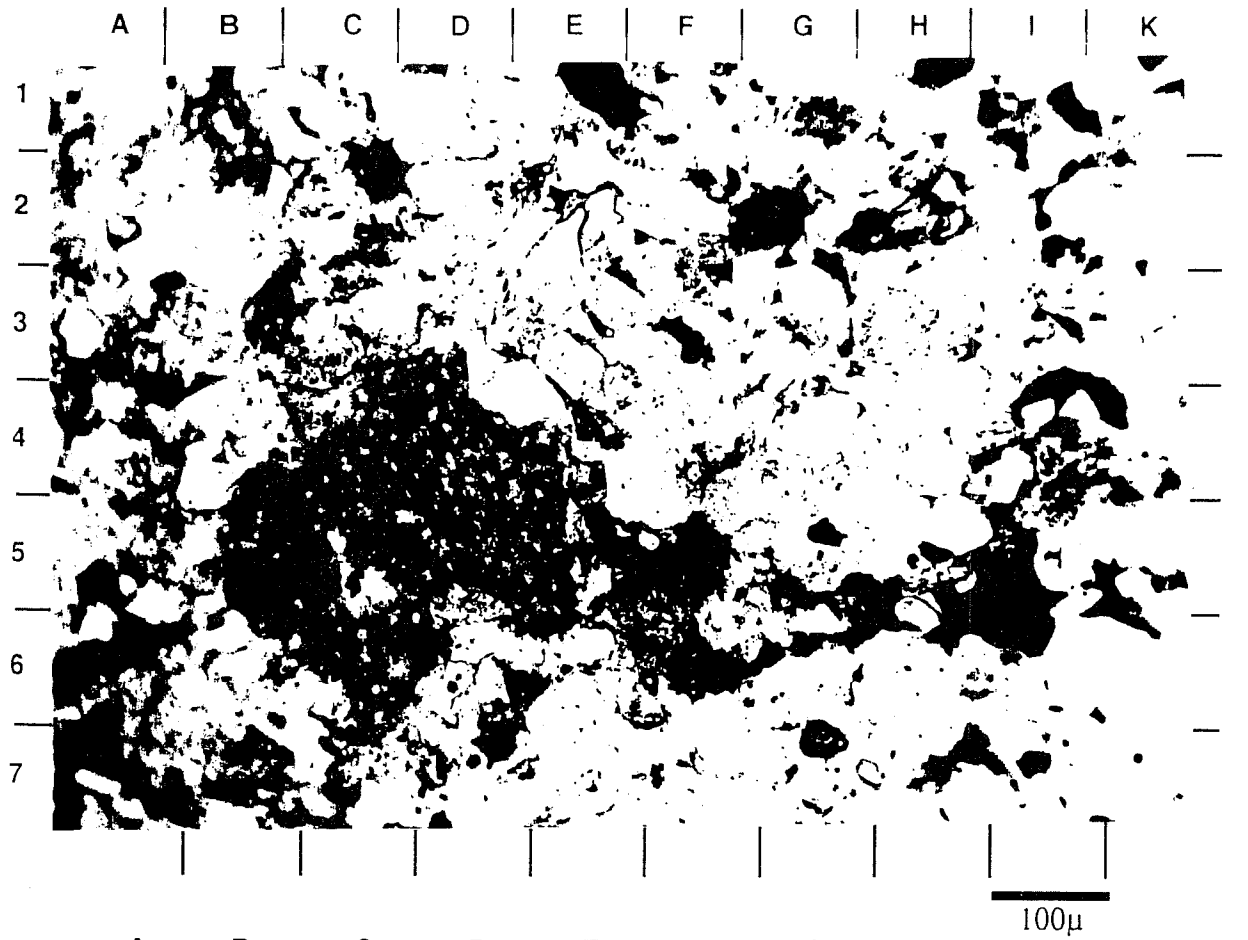

A
6711.1'
PPL

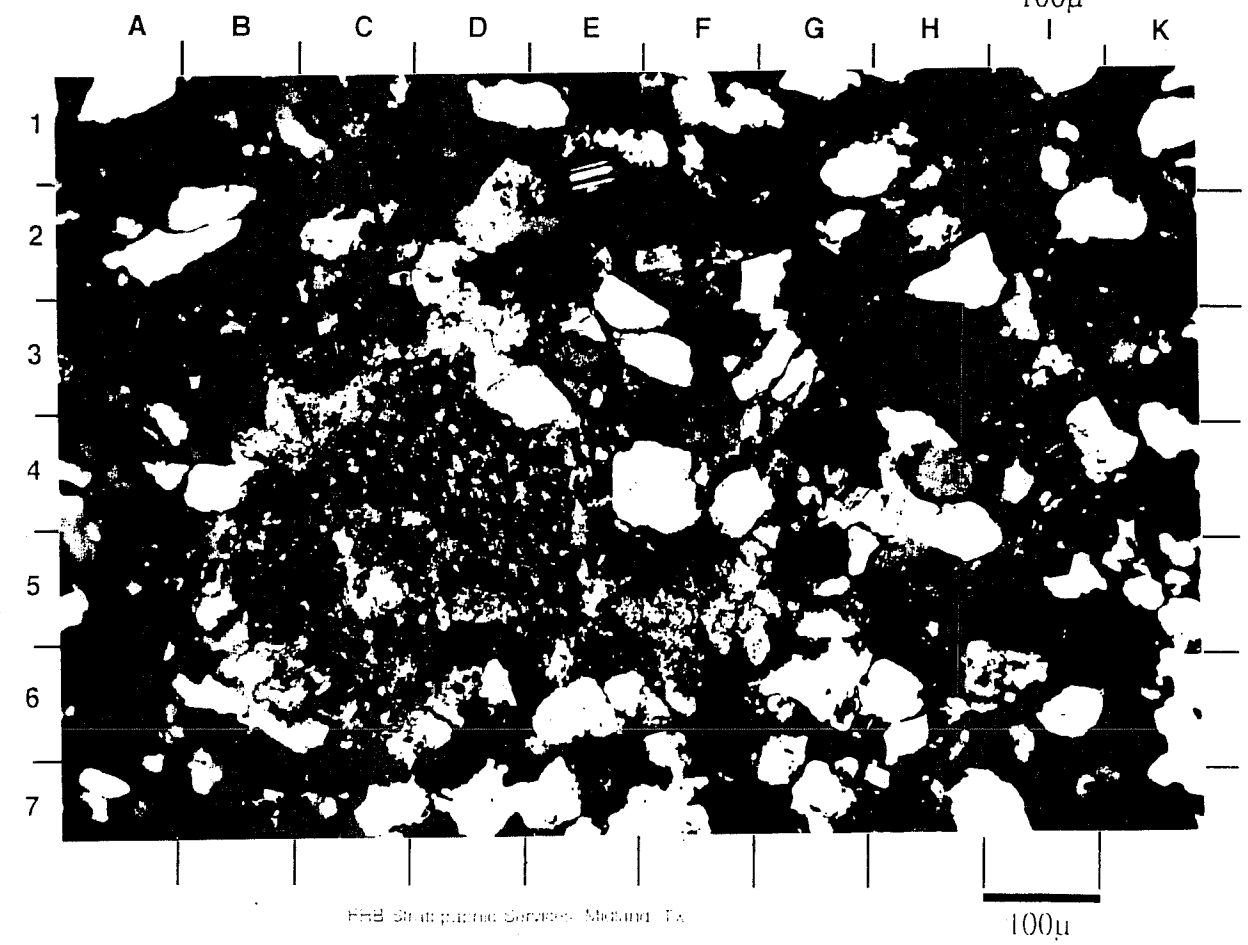

B
6711.1'
XPL

FEB Stratigraphic Services, Midland, Tx.

Plate 12

Strata Production, Nash Unit #23, Eddy Co., NM

6,711.1 ft.

Core Lab prepared all thin-sections from conventional core permeability plugs. Thin sections are impregnated with blue epoxy, one half of each thin-section stained with Alizarin Red S, and finished with a cover slip. Blue dye shows as porosity.

High magnification, scale bar beneath and to the right of photo is 50 microns (50μ). The coarse silt to very fine-grained sand is 62μ, while the very fine to fine-grained sand is 125μ.

A Same slide as Plate 11 at higher magnification of the coordinates at H4. Pore occluding pyrite at B3, K1->K2. Effective porosity is estimated at 5-10% shown by deep blue epoxy over the field of view. Very pale blue epoxy could be overly close packing of quartz grains and microporous chert or intergranular pores now occluded by authigenic clays.

"Dusty" quartz (F2-G3 and A3->B4) contains opaque, black, tiny framboidal diagenetic pyrite. This was most likely a pyritic lime micrite altered to chert by subsequent diagenesis.

Carbonate cements present as equant grain coating B1, B5 -> B6, C4, D4 and E7). Translucent medium to dark brown intergranular, organic-rich lime micrite (I5-K5, I6, A7->B7. Crossed nichols reveal some microspar.

B Crossed nichols show equant carbonate cements, pyrite in altered chert, .

Strata Production, Nash Unit # 23 Eddy Co., NM

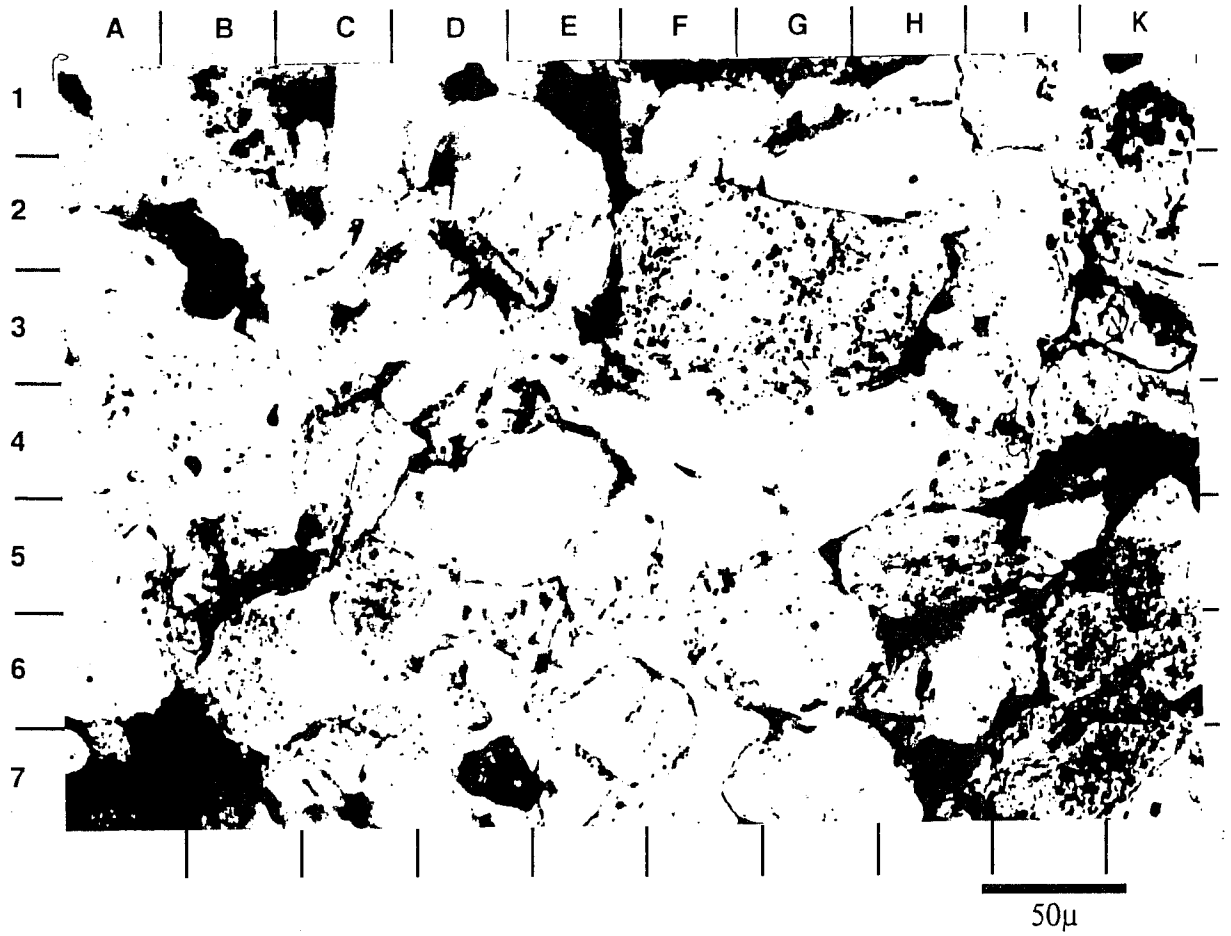

A
6711.1'
PPL

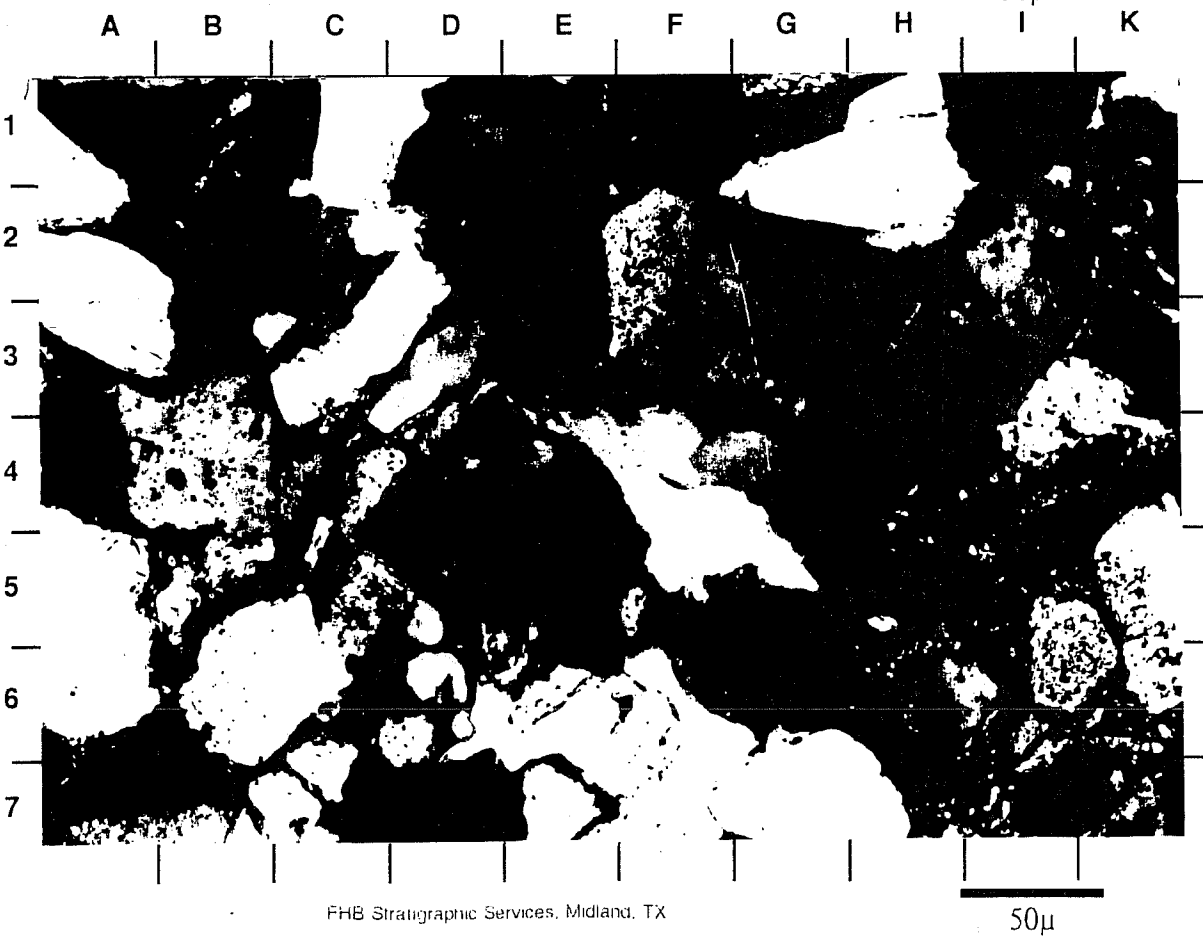

B
6711.1'
XPL

Plate 13

Strata Production, Nash Unit #23, Eddy Co., NM

6,735.2 ft.

Core Lab prepared all thin-sections from conventional core permeability plugs. Thin sections are impregnated with blue epoxy, one half of each thin-section stained with Alizarin Red S, and finished with a cover slip. Blue dye shows as porosity.

Low magnification, scale bar beneath and to the right of photo is 100 microns (100μ). The coarse silt to very fine-grained sand is 62μ, while the very fine to fine-grained sand is 125μ.

A Bubbles in the upper and lower epoxy are very troublesome in this slide. Silty, very fine grain-sandstone with higher amounts of organic rich lime micrite and overly close grain packing that significantly reduced intergranular porosity. Effective porosity over the thin-section is furter reduced by diagenetic grain-lining and pore-lining clays and subsequent carbonates. Patchy porosity is estimated at 5-7% shown by deep blue epoxy over the field of view.

Translucent medium to dark brown intergranular, organic-rich, pyritic lime micrite (B3, B6, D1->E1, F7, K2, K5).

B Crossed nichols. High birefringence of gypsum or anhydrite and carbonates visible (G1, I1, C3, G4, D7 plus orthers).

Strata Production, Nash Unit # 23 Eddy Co., NM

PLATE 13

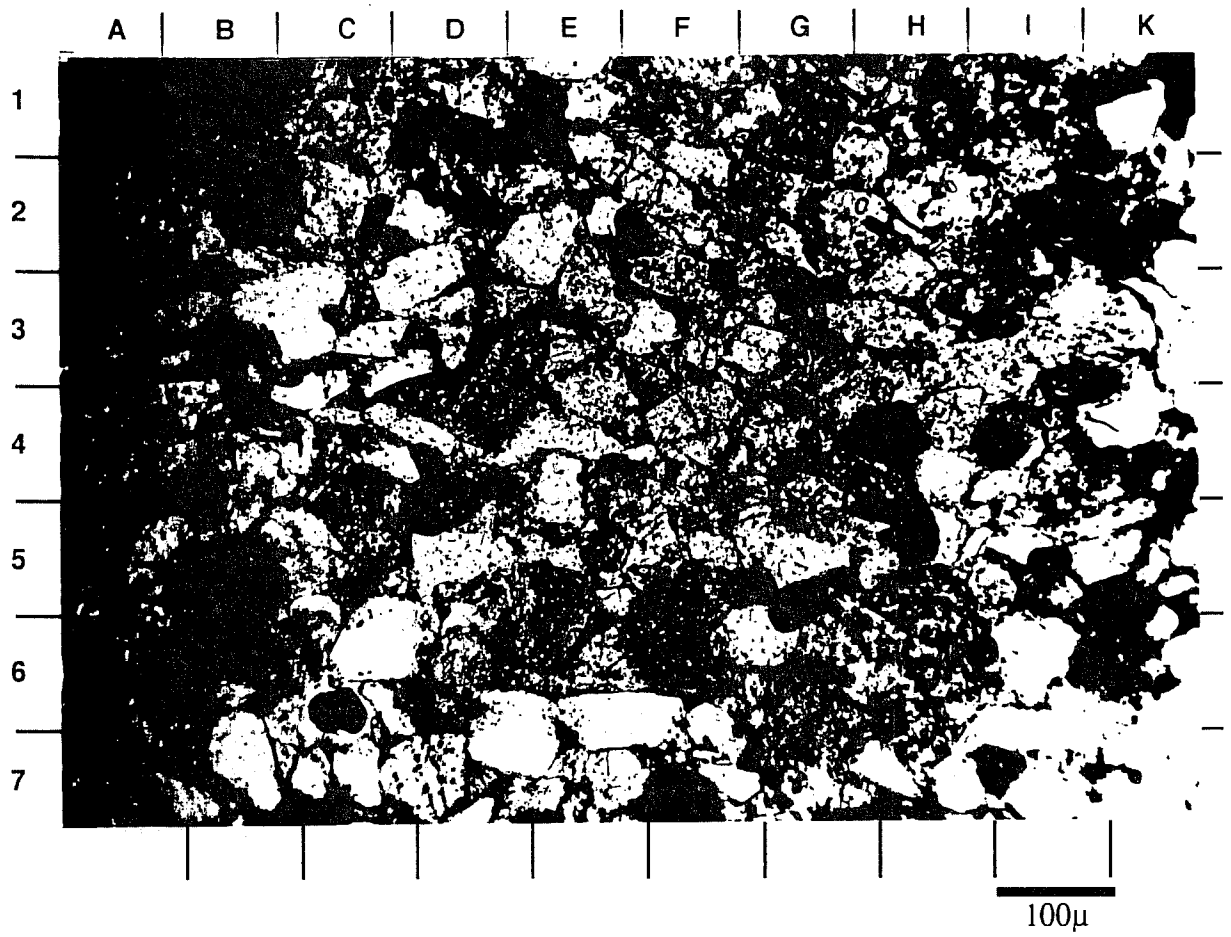

A
6735.2'
PPL

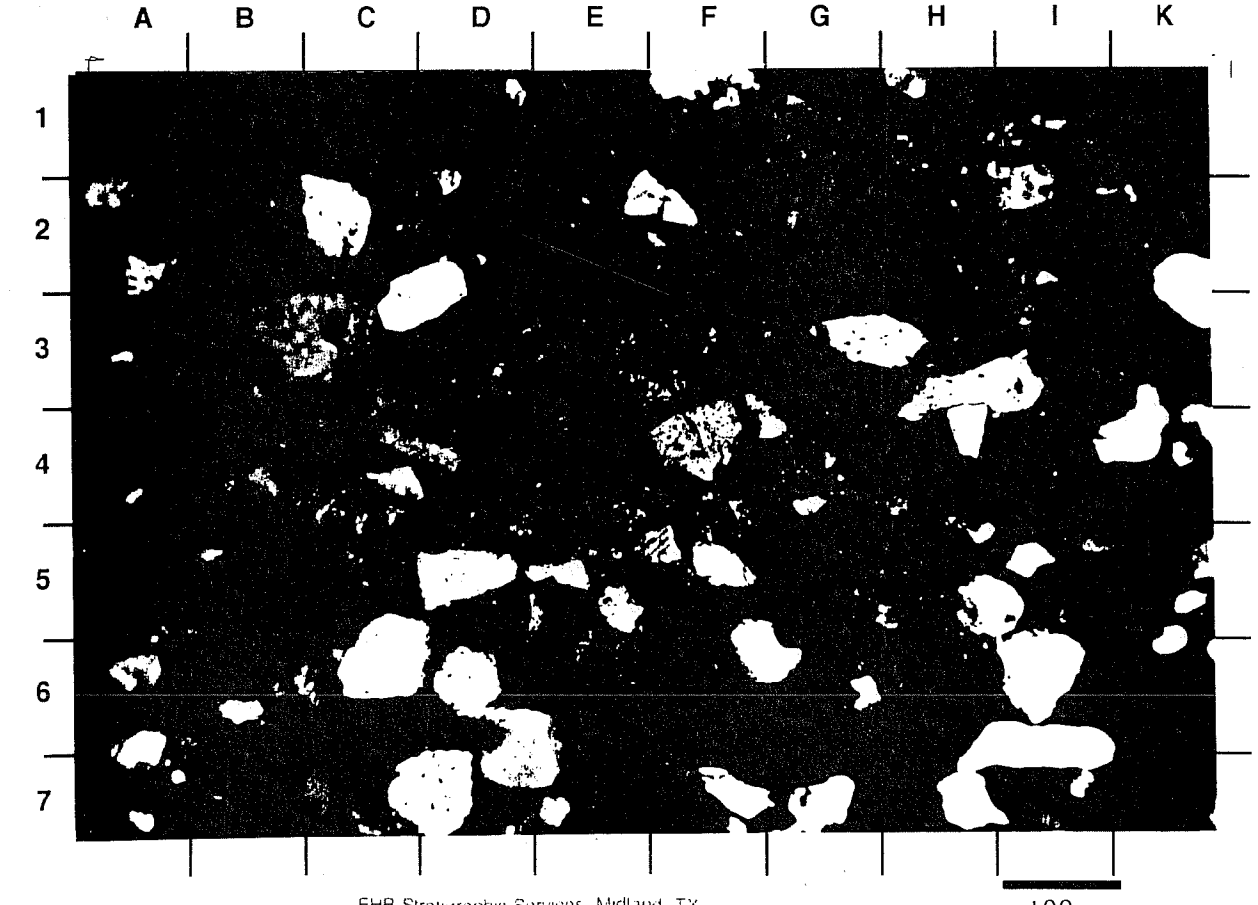

B
6735.2'
XPL

Plate 14

Strata Production, Nash Unit #23, Eddy Co., NM

6,735.2 ft.

Stained with Alizarin Red S

Core Lab prepared all thin-sections from conventional core permeability plugs. Thin sections are impregnated with blue epoxy, one half of each thin-section stained with Alizarin Red S, and finished with a cover slip. Blue dye shows as porosity.

The coarse silt size boundary with very fine-grained sand is 62μ, while the very fine to fine-grained sand is 125μ.

A High magnification, scale bar beneath and to the right of photo is 50 microns (50μ). Bubbles beneath cover slip at I3 and A1. Very tiny bright pin points of light (5-7 μ) are located at A3, C3, D2, etc.). Overly close packing and fracturing to actual breakage of framework grains common (G6, E3, E7 and others). Grains at F4->G5 appears microporous with dark framboidal pyrite. Boundaries of grain and intergranular porosity characterized by very thin reddish brown "line."

Translucent medium to dark brown intergranular, organic-rich, pyritic lime micrite (A5 and G7). Opaque black framboidal pyrite (I5->K5, H 6-H7, F4->G5, C5 and others).

B Highest magnification of photomicrograph shown in A centered at C5->D5. Scale bar beneath and to the right of photo is 0.02 mm or 20 microns (20μ) long.

Boundaries of framework quartz and grain coating cement are discernibly stained by the Alizarin Red S (C4-D4-E4--G5, H1, B2).

This photomicrograph demonstrates the presence of grain coating and pore bridging chlorite and cements (A1, B1, A2, B2 A3-A4, D,4, F5->G5) and "fibrous to ligament-like" diagenetic illite (?) or (?) illite/smectite (E6-F7, G5, and K6-K7).

Strata Production, Nash Unit # 23 Eddy Co., NM

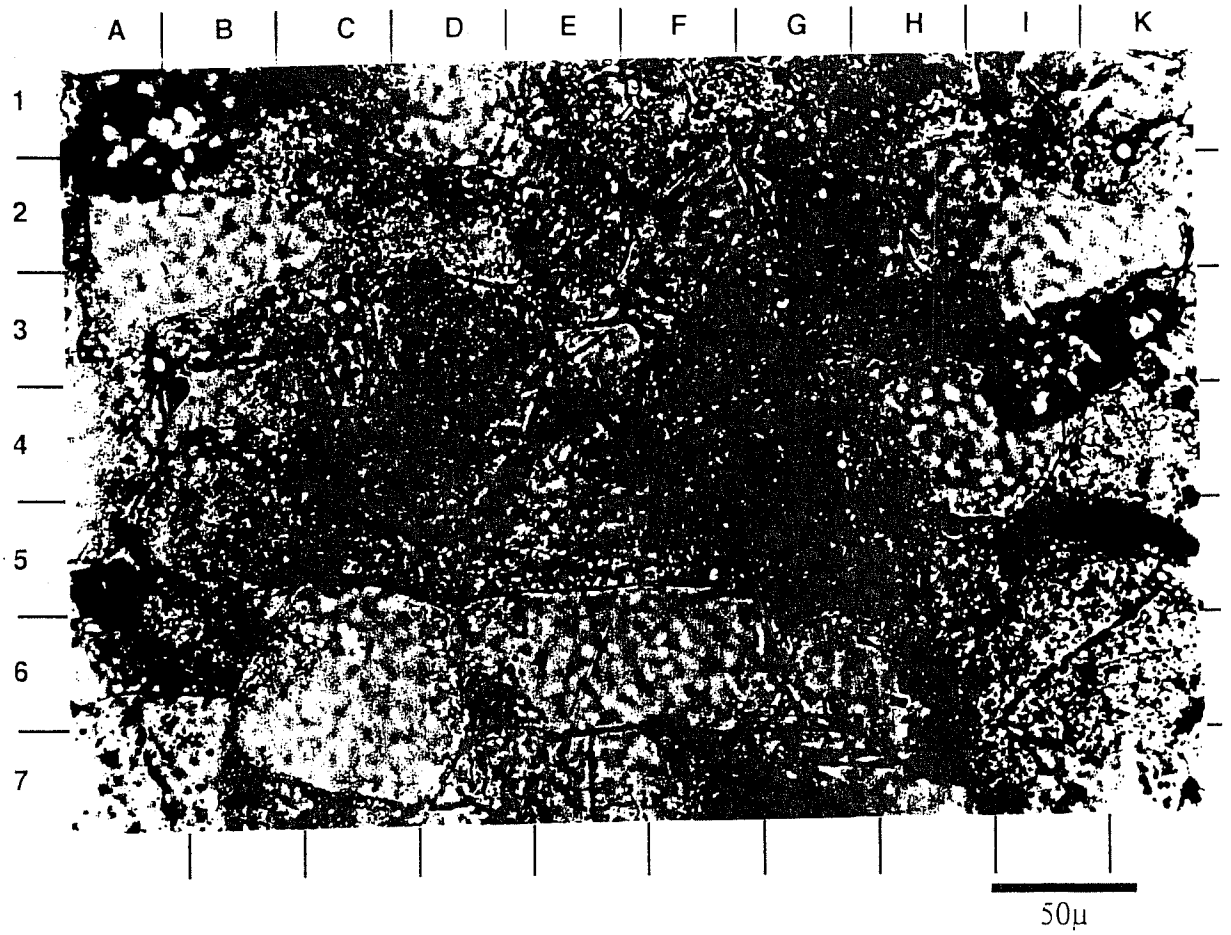

A
6735.2'
PPL

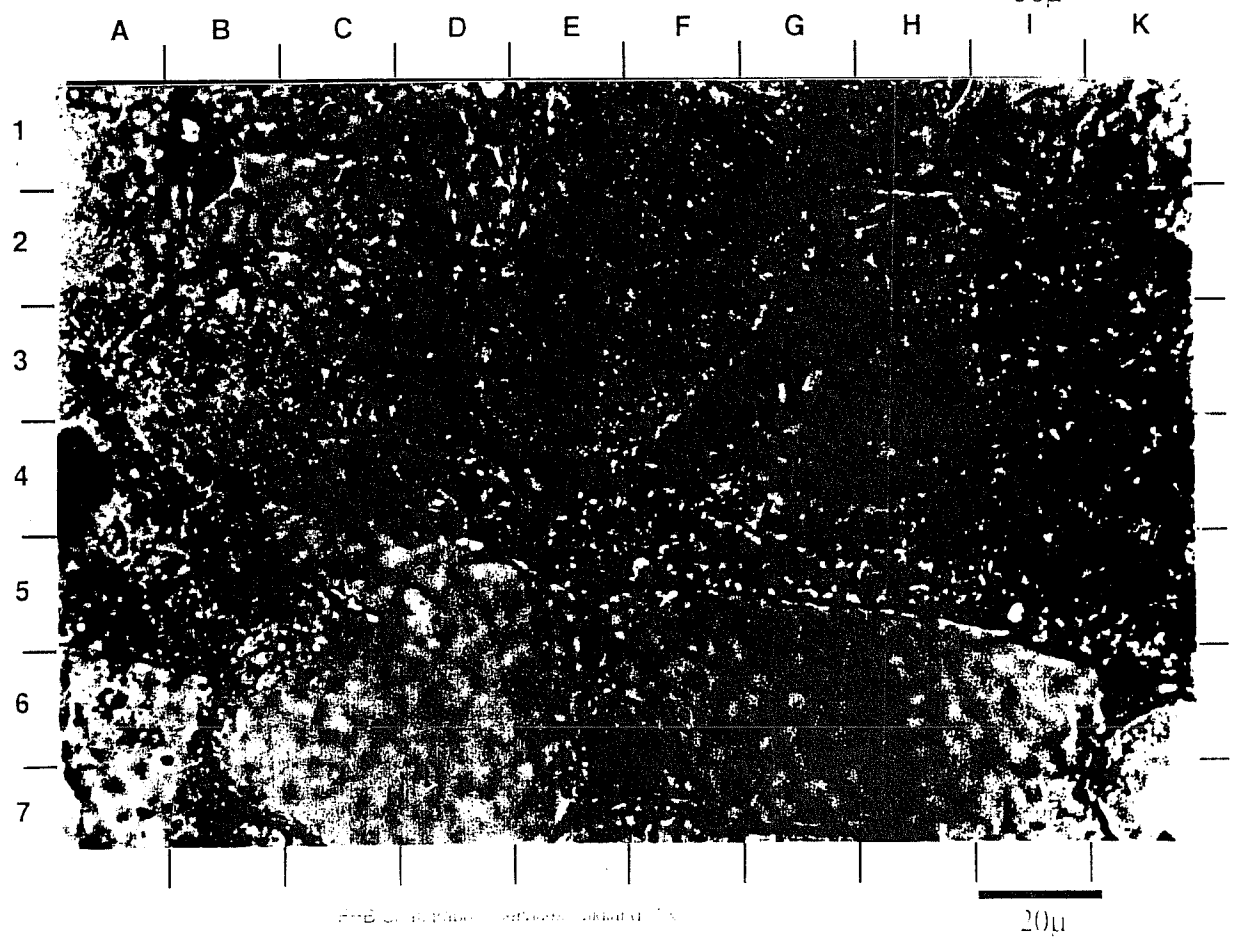

B
6735.2'

Plate 15

Strata Production, Nash Unit #23, Eddy Co., NM

6,738.6 ft.

Core Lab prepared all thin-sections from conventional core permeability plugs. Thin sections are impregnated with blue epoxy, one half of each thin-section stained with Alizarin Red S, and finished with a cover slip. Blue dye shows as porosity.

The coarse silt size boundary with very fine-grained sand-size is 62μ, while the very fine to fine-grained sand is 125μ.

Transulcent dark brown micritic to organic rich microspar beds approximately 25 to 40 μ thick produce discontinuous bedding resembling bioturbated flaser bedding. Patchy interparticle porosity, best developed in "burrows" approximating 10-20%. Vertical permeability difficult to evaluate.

Low magnification, scale bar beneath and to the right of photo is 100 microns (100μ).

A Irregular organic-rich and pyritic, microspar and micrite, overly close packing due to interpenetrating framework grains, and fracturing to breakage of framework grains significantly reduce the reservoir quality in this sample (G6, E3, E7 and others.

This core plug shows very thin and discontinuous porosity. Close examination of the fabric appears to indicate that composite grains are comprised of several coarse silt to very fine sand grains.

Overly close packing is supported by actual fracture and breakage of framework grains (B2, D1, and G6). Zig-zag grain contacts also support compression of preexisting interpartical pore space (D6)

B High birefringence typical of carbonates is rare and appears to be associate with both skeletal grains and grain coating diagenetic cements. Relict feldspar twinning is preseved in a composte grain at C4->D4.

Strata Production, Nash Unit # 23 Eddy Co., NM

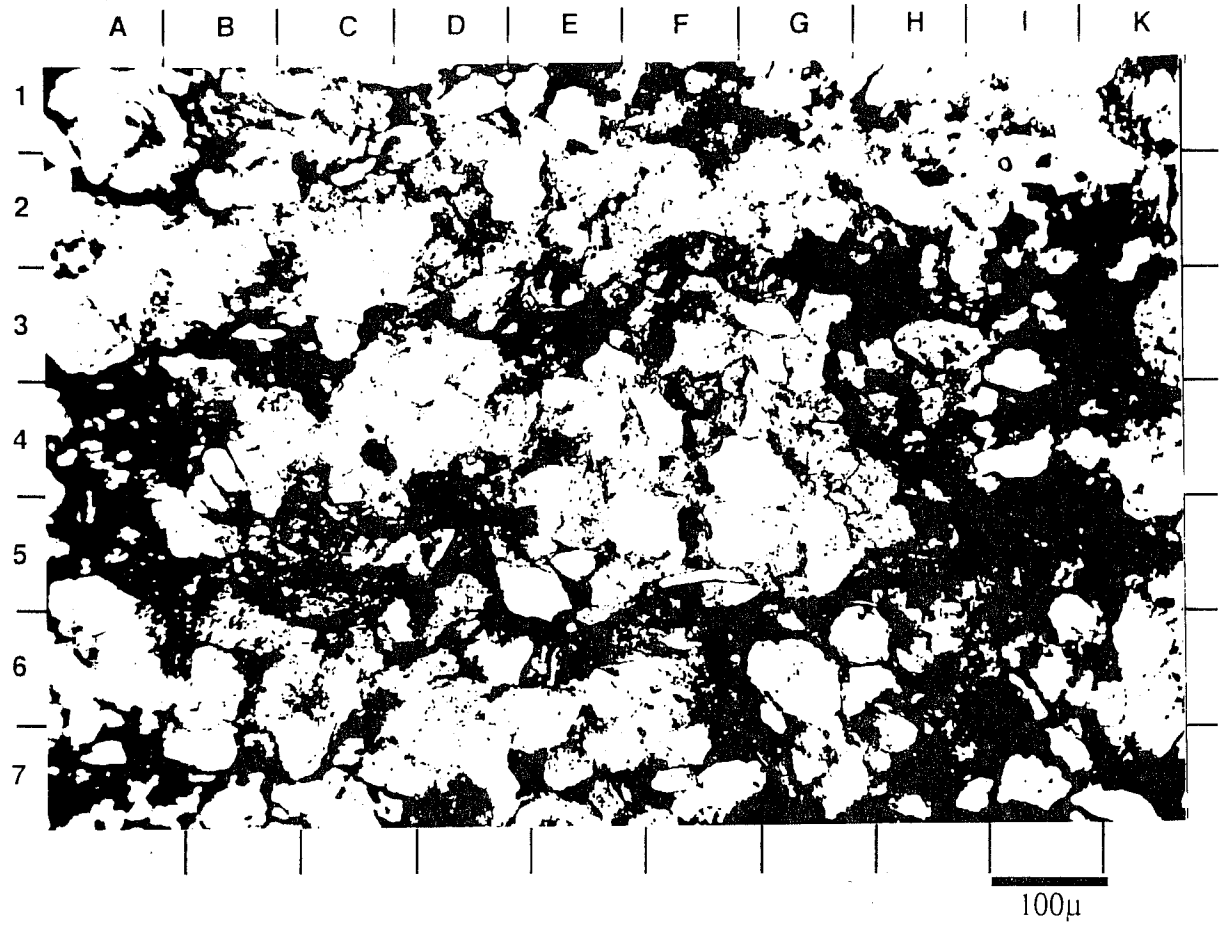

A
6738.6'
PPL

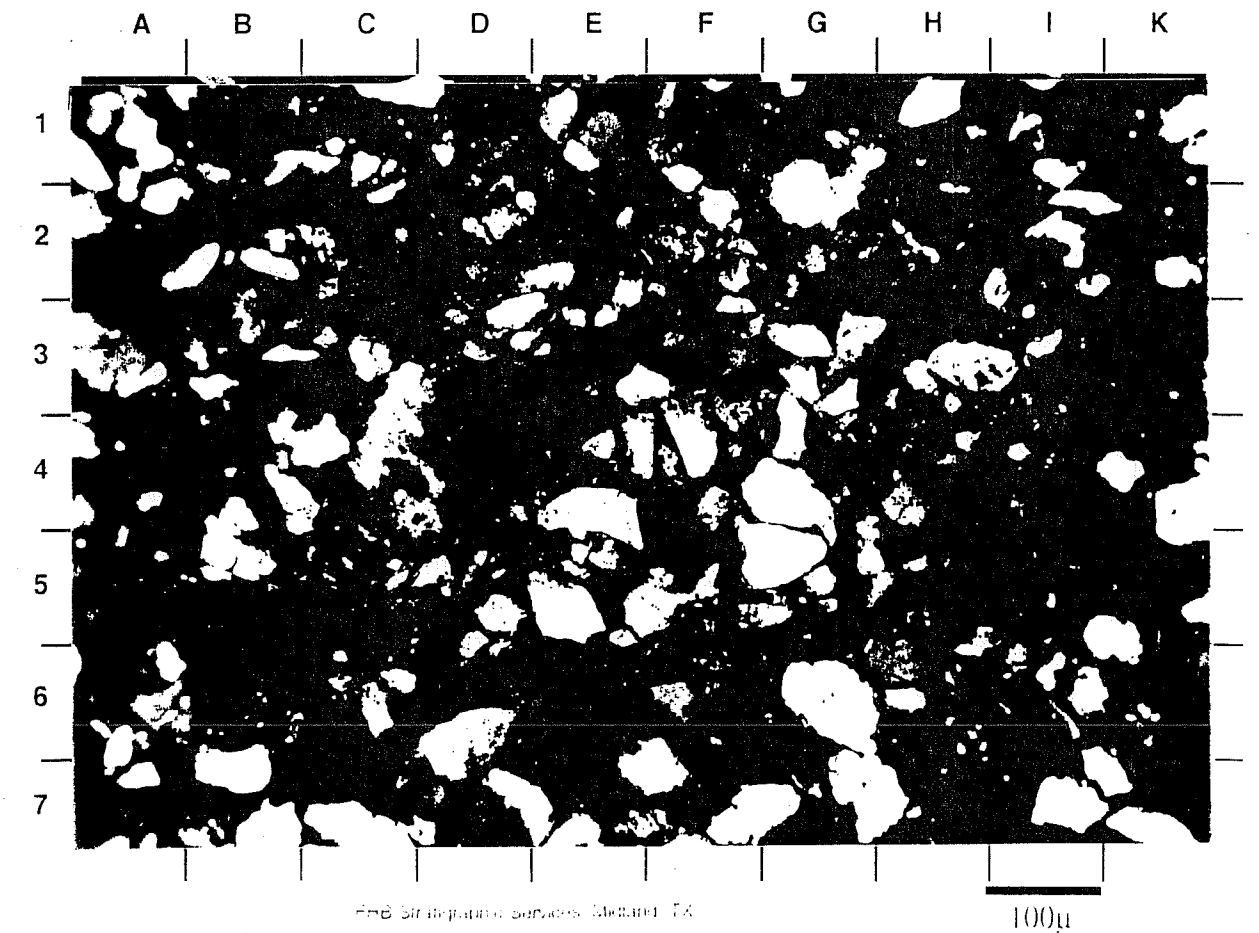

B
6738.6'
XPL

Plate 16

Strata Production, Nash Unit #23, Eddy Co., NM

6,742.2 ft.

Alizarin Red S stained

Core Lab prepared all thin-sections from conventional core permeability plugs. Thin sections are impregnated with blue epoxy, one half of each thin-section stained with Alizarin Red S, and finished with a cover slip. Blue dye shows as porosity.

The coarse silt size boundary with very fine-grained sand-size is 62μ, while the very fine to fine-grained sand is 125μ.

Low magnification, scale bar beneath and to the right of photo is 100 microns (100μ).

A Fossiliferous, silty, very fine to fine grained sandstone, mixed low and high sperical grains, angular to subrounded. Streaks of interparticle porosity from 10-18%. Permeability is discontinuous, resulting in very poor reservoir character. Several bubbles under the coverslip are at F6, G2, and C4.

Calcite stain is visible to naked eye. Laminar structure in two allochems at K3 and G4 indicate they are brachiopod shell and spine fragments, respectively. Interpenetration of silt to very fine grained quqrtz by compaction and pressure solution. The black opaque 40-50 μ bodies at G4->G5 are diagenetic pyrite. The stained grain at D3->E3 is coated by an "organic rich, pyritic micrite" rim and is likely a reworked clasts. A light tan chalcedonic fossil allochem is at G3->B4.

Very pale bluish epoxy due to microporosity (B5, H7, K7, etc.)

B High birefringence typical of carbonates is rare and appears to be associate with both skeletal grains and grain coating diagenetic cements. Relict feldspar twinning is preseved in a composte grain at C4->D4.

Strata Production, Nash Unit # 23 Eddy Co., NM

A
6742.2'
PPL

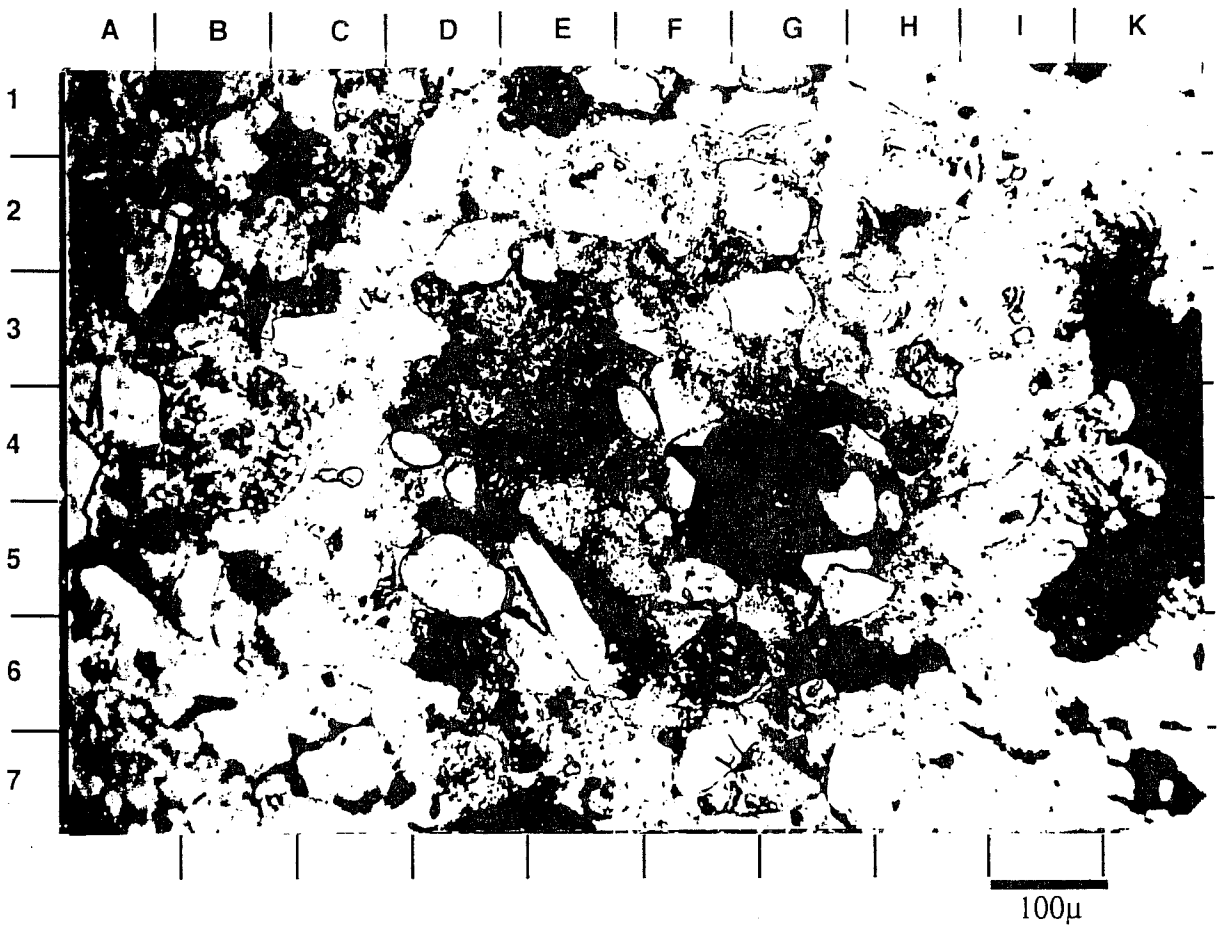

B
6742.2'
XPL

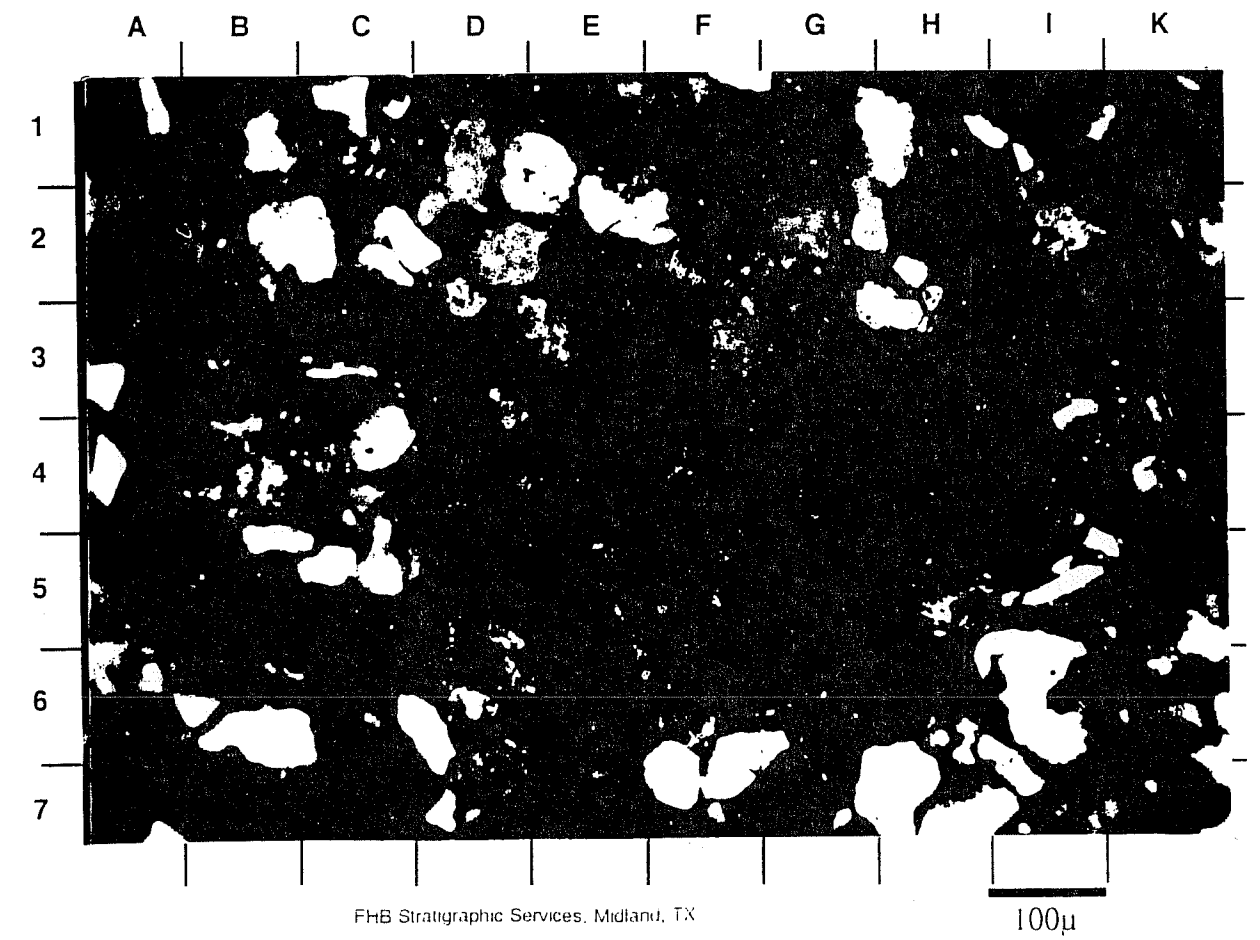

Plate 17

Strata Production, Nash Unit #23, Eddy Co., NM

6,742.2 ft.

Alizarin Red S stained

Core Lab prepared all thin-sections from conventional core permeability plugs. Thin sections are impregnated with blue epoxy, one half of each thin-section stained with Alizarin Red S, and finished with a cover slip. Blue dye shows as porosity.

The coarse silt size boundary with very fine-grained sand-size is 62μ, while the very fine to fine-grained sand is 125μ.

High magnification, scale bar beneath and to the right of photo is 50 microns (50μ).

A **Same slide as Plate 16**, different region. Calcite stain is visible to naked eye. A large dark brown to dark reddish brown micritic clast dominates the upper left 1/5 of the photomicrograph.A fractured quartz grain with an enechelon movement of fragments at E4. Grain coating equant cements are are G5->G5 and elsewhere.

Interparticle porosity present. Framework grains covered by fine quartz crystalls. No diagenetic clays observed in SEM analysis (Figure 7). SEM analysis shows diagenetic feldspars in pore network. Poikilitic calcite cements nuceating on echinoderm fragments will result in occlusion of more interparticle porosity.

Interparticle porosity fair to good, but permeability is interpreted as low.

B High birefringence typical of carbonates fossil fragments of 10-40 μ at K5, F6, and I5 did not serve as low energy nuceation sites, because of a thin micrite envelope visible with plane polarized light in **A**.

Strata Production, Nash Unit # 23 Eddy Co., NM

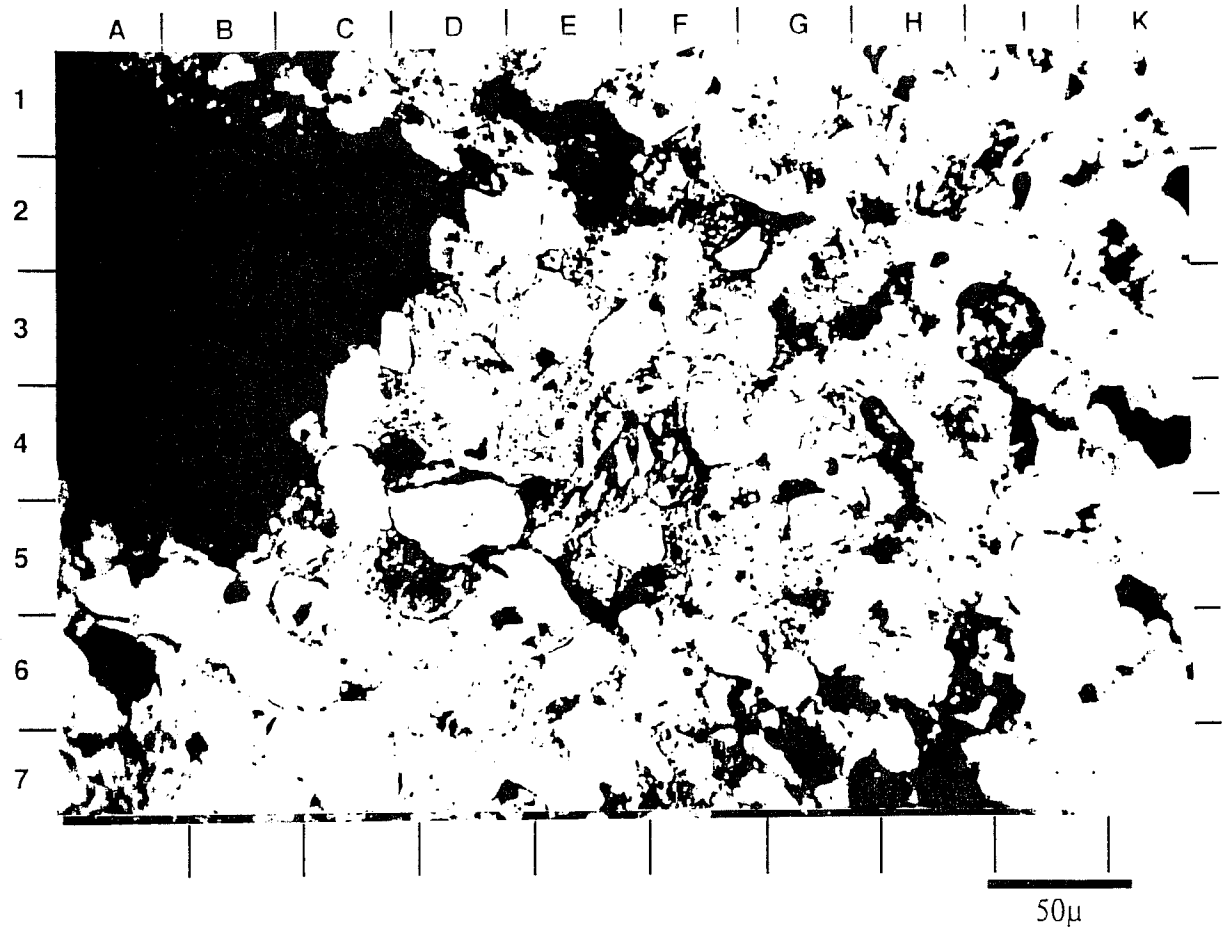

A
6742.2'
PPL

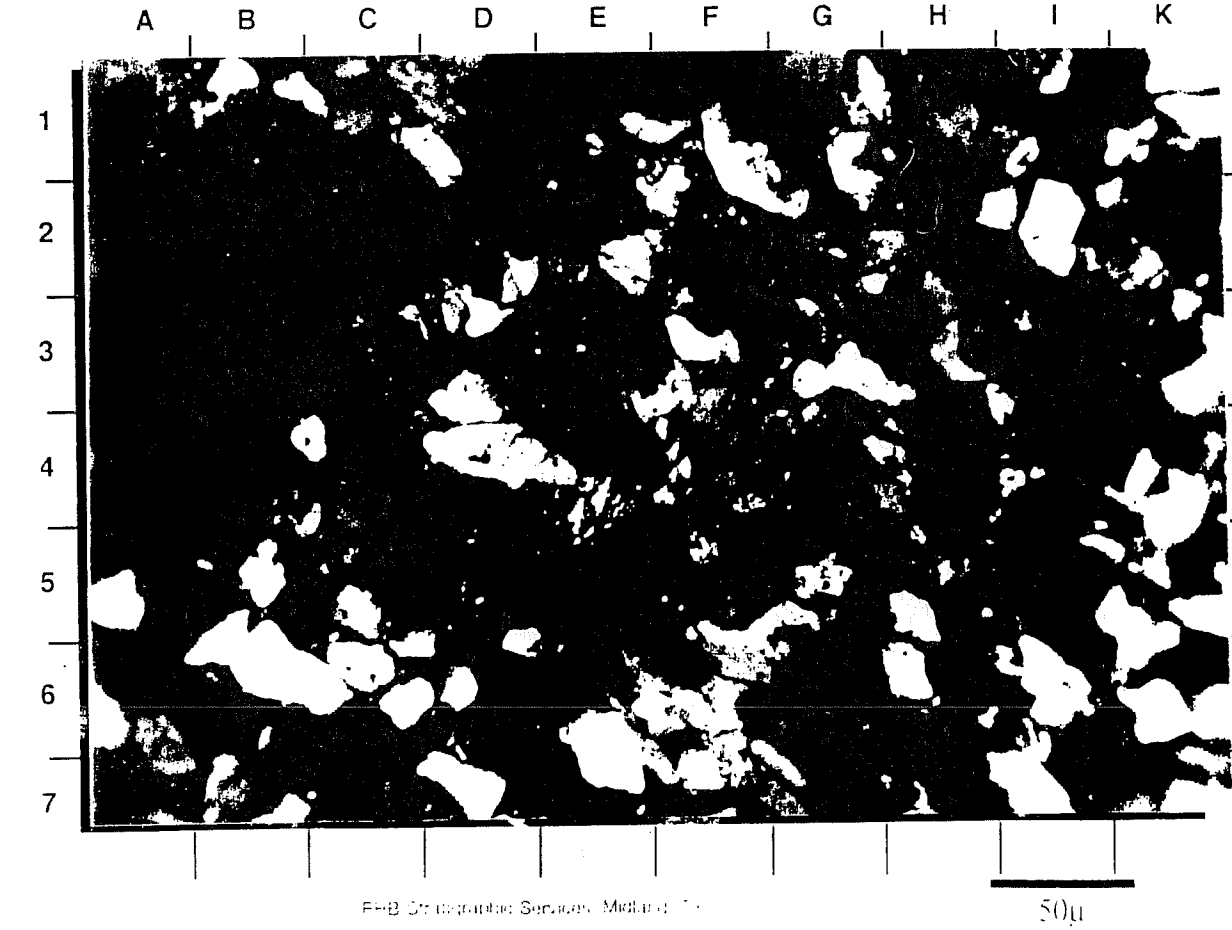

B
6742.2'
XPL

EHB Petrographic Services, Midland, TX

Plate 18

Strata Production, Nash Unit #23, Eddy Co., NM

6,742.2 ft.

Core Lab prepared all thin-sections from conventional core permeability plugs. Thin sections are impregnated with blue epoxy, one half of each thin-section stained with Alizarin Red S, and finished with a cover slip. Blue dye shows as porosity.

The coarse silt size boundary with very fine-grained sand-size is 62μ, while the very fine to fine-grained sand is 125μ.

Highest magnification, scale bar beneath and to the right of photo is 20 microns (20μ).

A **Same slide as Plate 16** with center of the region region at E4->F4. A thin zone of (?) equant carbonate cement coats framework grains, preventing the collapse of framework packing leading to preservation of greater interparticle porosity (B4->B5, F1, H5, I5, F2->G2->H3 and elseware). Pyrite is present as pore blocking cement (F5, H.6, K3, G1, and A7). Remaining pore space and pore throats bridged by fibrous to strandlike diagenetic (?) illite or illite/smectite.

Interparticle porosity estimated at 10-15%, with low permeability.

Strata Production, Nash Unit # 23 Eddy Co., NM

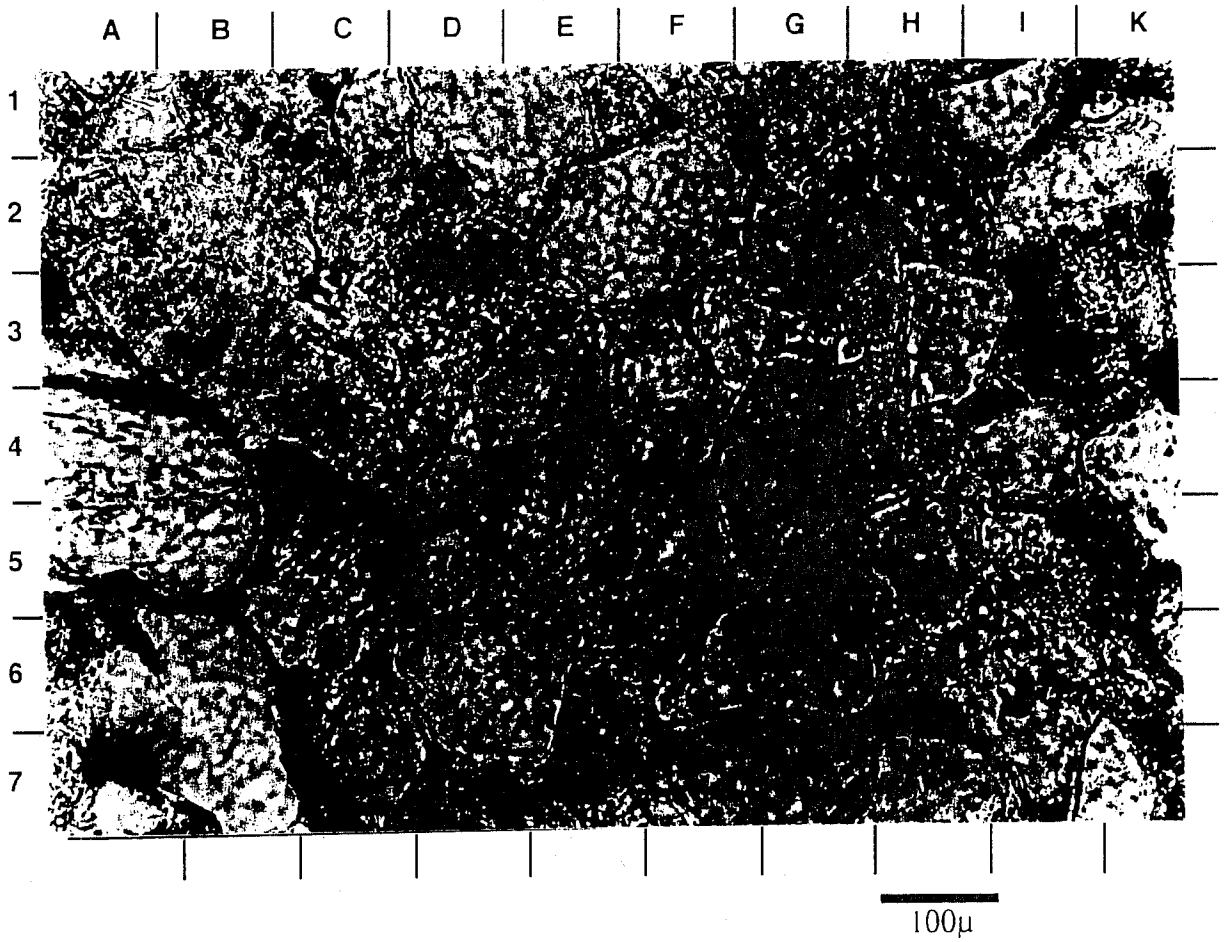

Plate 19

Strata Production, Nash Unit #23, Eddy Co., NM

6,785.8 ft.

Core Lab prepared all thin-sections from conventional core permeability plugs. Thin sections are impregnated with blue epoxy, one half of each thin-section stained with Alizarin Red S, and finished with a cover slip. Blue dye shows as porosity.

The coarse silt size boundary with very fine-grained sand-size is 62μ, while the very fine to fine-grained sand is 125μ.

Low magnification, scale bar beneath and to the right of photo is 100 microns (100μ).

A Air bubbles under cover slip at I1, K6, B1 and others.

Fossiliferous, feldspathic and silty, very fine grain sandstone, angular to subrounded grains with very low (rectangular) to moderate sphericity. Gastropod (snail) fragment in upper left hand quarter of phootomicrograph with organic rich and pyritic lime micrite. Spotty interparticle porosity, SEM analysis reveals little diagenetic clays coating grains or occluding pore space.Finely crystalline quartz and feldspar cements (Figure 7) do reduce effective porosity. Limited permeability

Quartz framework grains still reveal a polymictic aspect to the Brushy Canyon Formation sandstones. Scalloped or etching less prevalent on quartz grain boundaries. Several grains have sharp acute or right angle boundaries that are incongruent with the adjacent grains (F5-"L-shaped" and C7-"acute angle).

Pyrite present as 15-25 μ framboidal pyrite (H2->H3, D7, E1) Pyrite is also noted in chert grains at G5 and G4. Interparticle porosity estimated at 10–15%, with low permeability.

B Gastropod shell recrystallized to microgranular calcite (original thick columnar layer preserved (E1 and E3 and E4). Coarse silt and very fine sand-sized fossil fragments present (A5, A7, F1, I4, and I6).

Strata Production, Nash Unit # 23 Eddy Co., NM

A
6785.8'
PPL

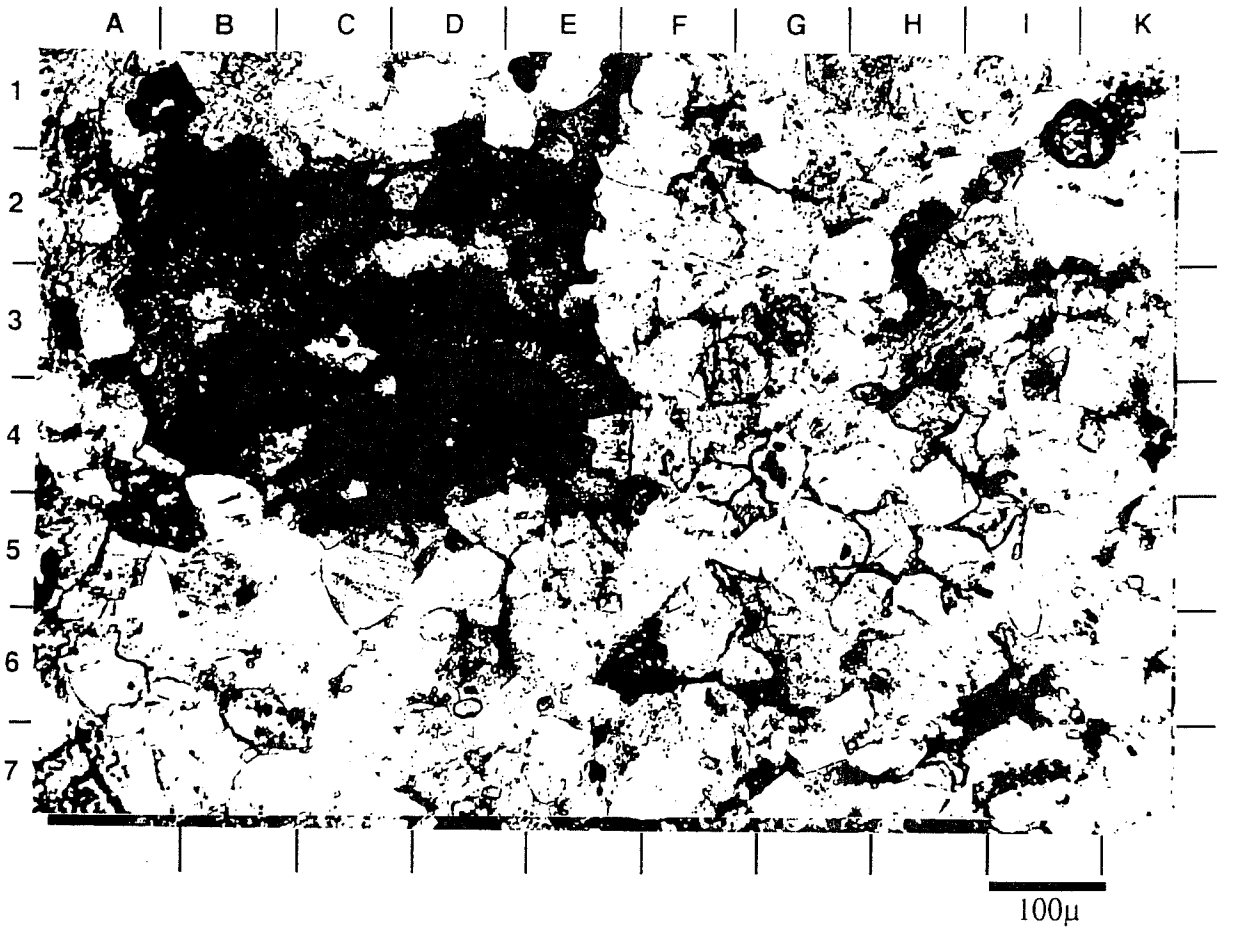

B
6785.8'
XPL

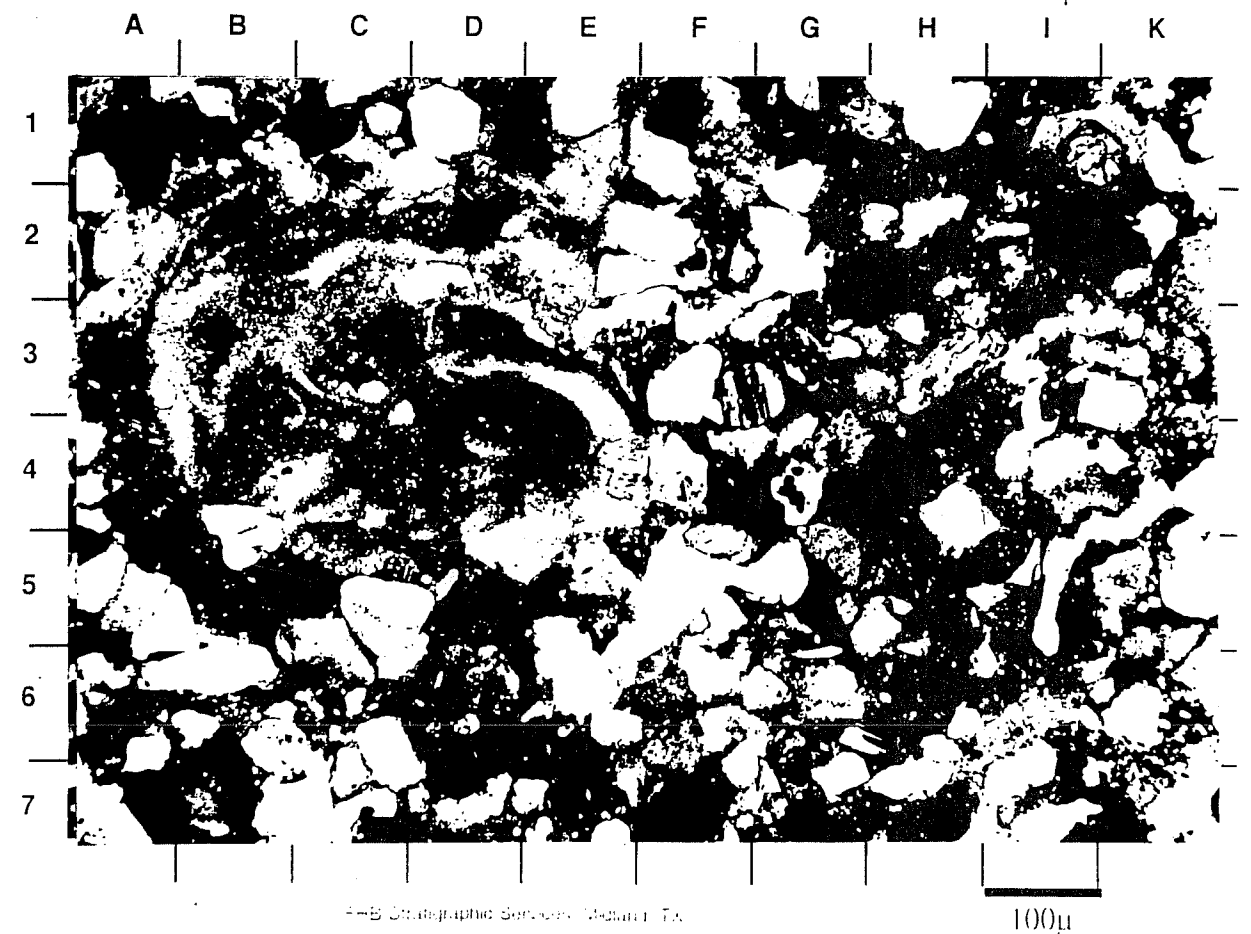

A-B Stratigraphic Services, Houston, TX

Plate 20

Strata Production, Nash Unit #23, Eddy Co., NM

6,787.8 ft.

Core Lab prepared all thin-sections from conventional core permeability plugs. Thin sections are impregnated with blue epoxy, one half of each thin-section stained with Alizarin Red S, and finished with a cover slip. Blue dye shows as porosity.

The coarse silt size boundary with very fine-grained sand-size is 62μ, while the very fine to fine-grained sand is 125μ.

High magnification, scale bar beneath and to the right of photo is 50 microns (50μ).

A A thin zone of (?) equant quartz cement coats grains, preventing the collapse of framework packing leading to preservation of greater interparticle porosity (B4->B5, F1, H5, I5, F2->G2->H3 and elseware). Pyrite is present as pore blocking cement (F5, H.6, K3, G1, and A7). Remaining pore space and pore throats bridged by megaquartz and feldspar cements.

Interparticle porosity estimated at 10-15%, with low permeability.

B Same view as A above. Gypsum or anhydrite are common interparticle cements (H2, H5 within a quartz grain and I5-I6)

Strata Production, Nash Unit # 23 Eddy Co., NM

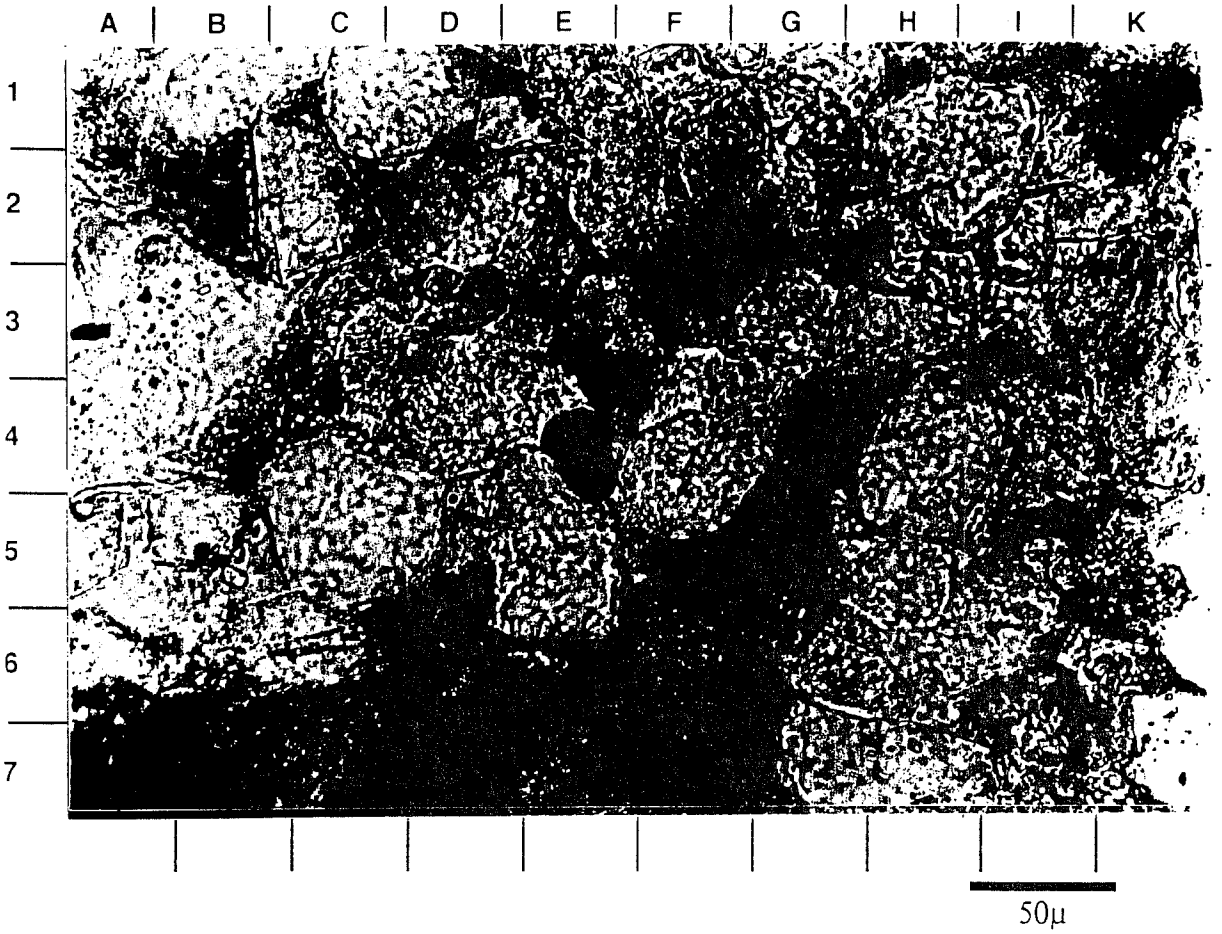

A
6785.8'
PPL

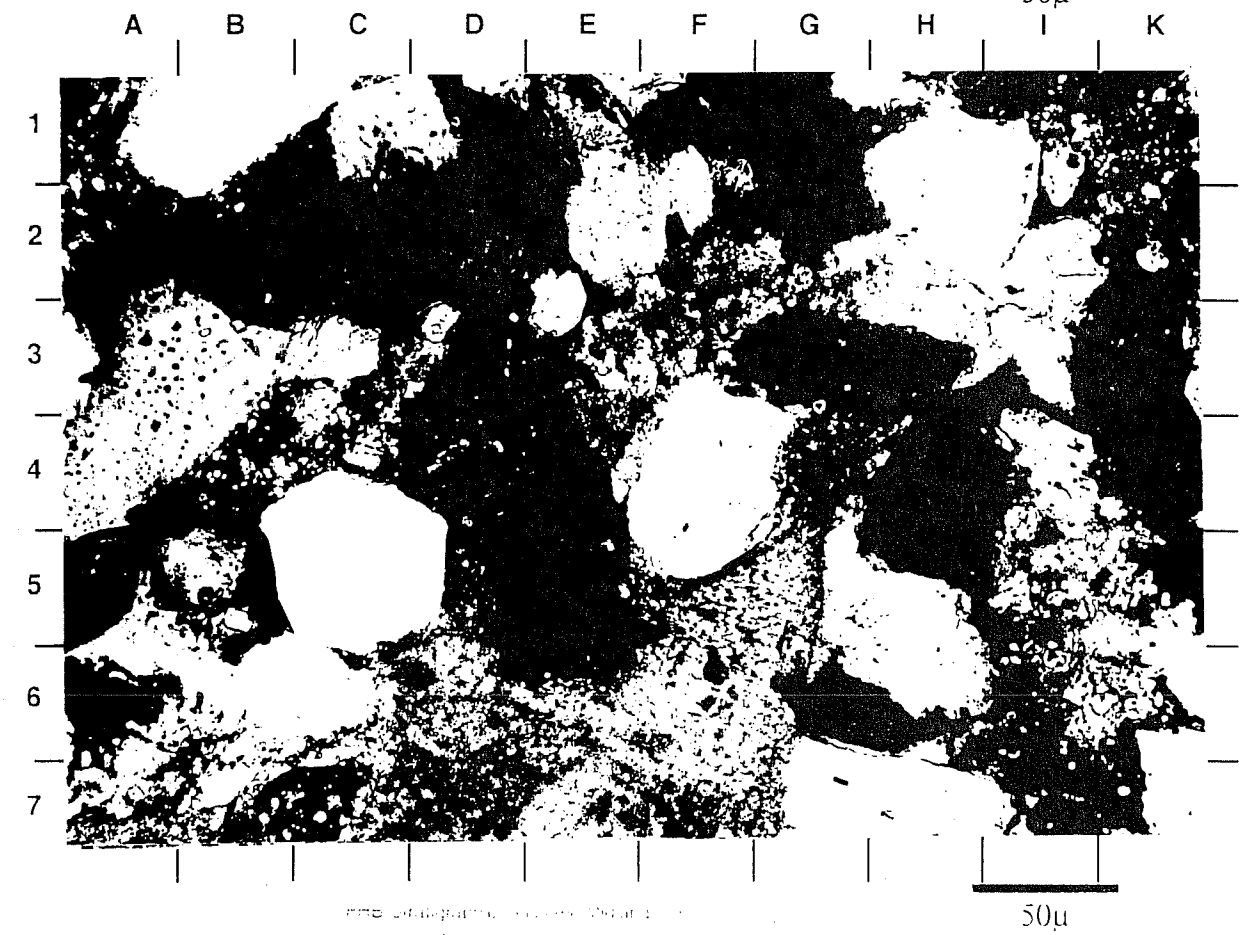

B
6785.8'
XPL

Plate 21

Strata Production, Nash Unit #23, Eddy Co., NM

6,787.8 ft.

Core Lab prepared all thin-sections from conventional core permeability plugs. Thin sections are impregnated with blue epoxy, one half of each thin-section stained with Alizarin Red S, and finished with a cover slip. Blue dye shows as porosity.

The coarse silt size boundary with very fine-grained sand-size is 62μ, while the very fine to fine-grained sand is 125μ.

Low magnification, scale bar beneath and to the right of photo is 100 microns (100μ).

A Tiny equant quartz cement coats grains while megaquartz occludes pore space. The fine quartz coating preserves isolated small pockets greater interparticle(D4. D2, I5)). Pyrite is present as pore blocking cement (F5, H.6, K3, G1, and A7). Remaining pore space reduced due to overly close packing of low sphericity gains and slit-like pore throats bridged by megaquartz and feldspar cements.

Interparticle porosity estimated at 10-15%, with low permeability.

B Same view as A above. Gypsum or anhydrite are common interparticle cements (H2, H5 within a quartz grain and I5-I6)

FHB Stratigraphic Services
P. O. Box 7648 – Midland, TX 79808-7648

Strata Production, Nash Unit # 23 Eddy Co., NM

A
6787.8
PPL

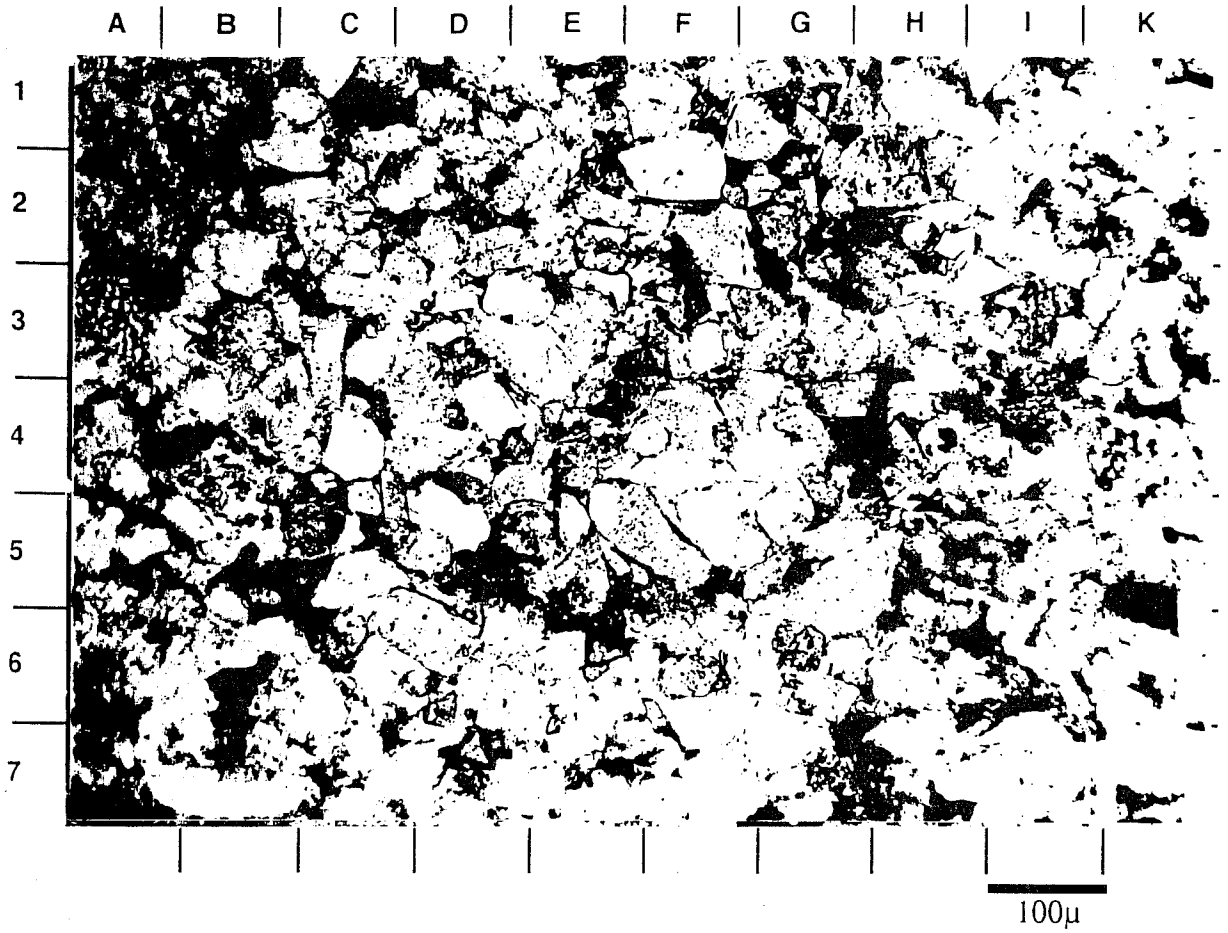

B
6787.8'
XPL

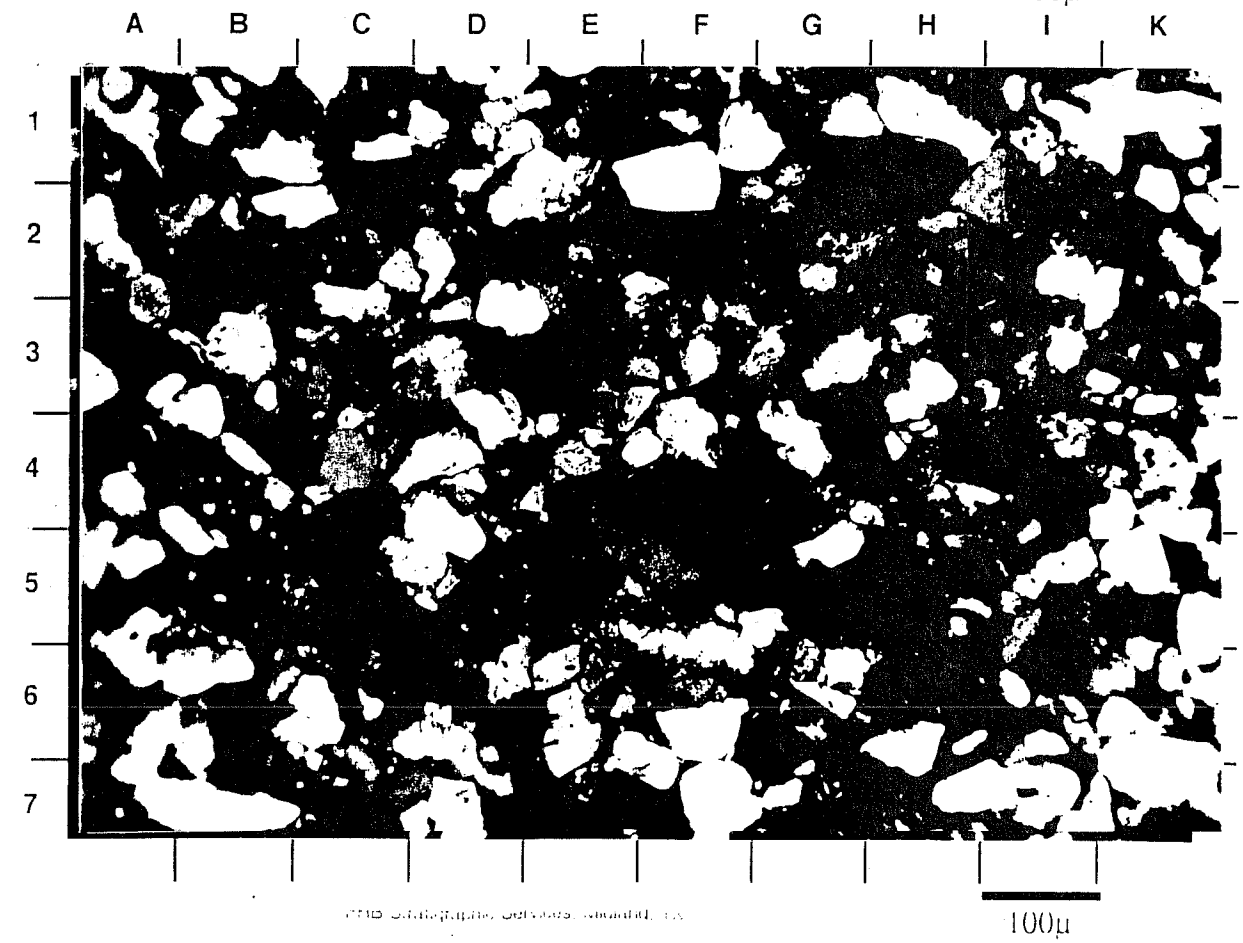

Plate 22

Strata Production, Nash Unit #23, Eddy Co., NM

6,787.8 ft.

Core Lab prepared all thin-sections from conventional core permeability plugs. Thin sections are impregnated with blue epoxy, one half of each thin-section stained with Alizarin Red S, and finished with a cover slip. Blue dye shows as porosity.

The coarse silt size boundary with very fine-grained sand-size is 62μ, while the very fine to fine-grained sand is 125μ.

High magnification with Plane Polarized Light, scale bar beneath and to the right of photo is 50 microns (50μ).

A Deposition of lime micrite (dark brown translucent organic-rich zones) filled primary space between framework grains. Tiny equant quartz cement coats grains while megaquartz occludes pore space. The fine quartz coating preserves isolated very small pockets of greater interparticle porosity (D4, D2, I5), but low and ineffective porosity. Pyrite is present as pore blocking cement (F5, H.6, K3, G1, and A7). Remaining pore space reduced due to overly close packing of low sphericity gains and slit-like pore throats bridged by megaquartz and feldspar cements.

Interparticle porosity estimated at 10-15%, with low permeability.

Strata Production, Nash Unit # 23 Eddy Co., NM

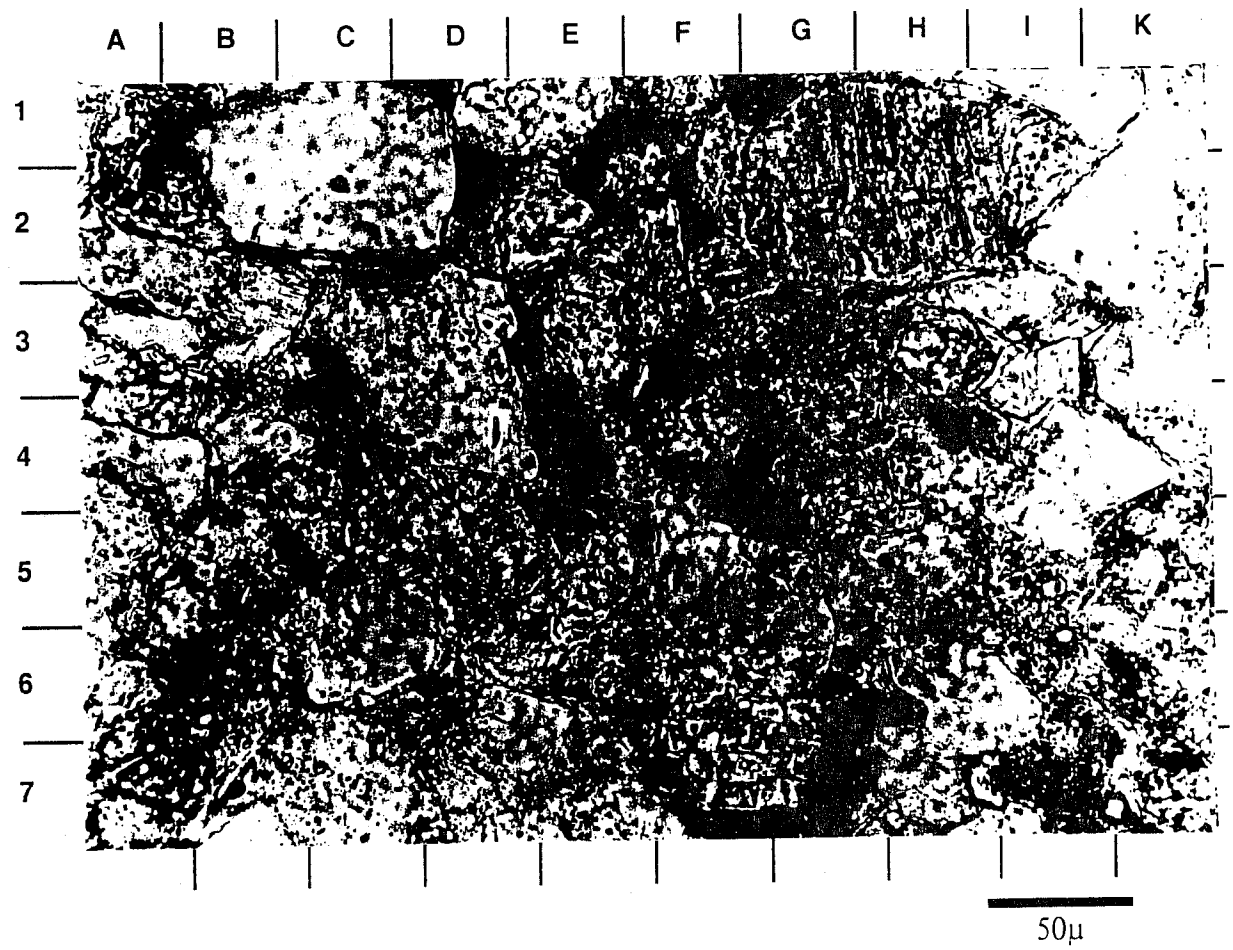

Plate 23

Strata Production, Nash Unit #23, Eddy Co., NM

6,816.1 ft.

Core Lab prepared all thin-sections from conventional core permeability plugs. Thin sections are impregnated with blue epoxy, one half of each thin-section stained with Alizarin Red S, and finished with a cover slip. Blue dye shows as porosity.

The coarse silt size boundary with very fine-grained sand-size is 62μ, while the very fine to fine-grained sand is 125μ.

Low magnification, scale bar beneath and to the right of photo 100 microns (100μ).

A Deposition of lime micrite (dark brown translucent organic-rich zones) filled primary space between framework grains. Quartz cement coats grains and occludes pore space. Fine quartz coating preserves isolated very small pockets of greater interparticle porosity, but low and ineffective porosity. Pyrite is present as pore blocking cement. Remaining pore space reduced due to overly close packing of low sphericity gains and slit-like pore throats bridged by megaquartz and feldspar cements.

Interparticle porosity estimated at 10-15%, with low permeability.

B Same view and magnification as A above. Polymictic character of sandstone, low sphericity of the majority of framework grains, and pore filling carbonate cements are very evident.

Strata Production, Nash Unit # 23 Eddy Co., NM PLATE 23

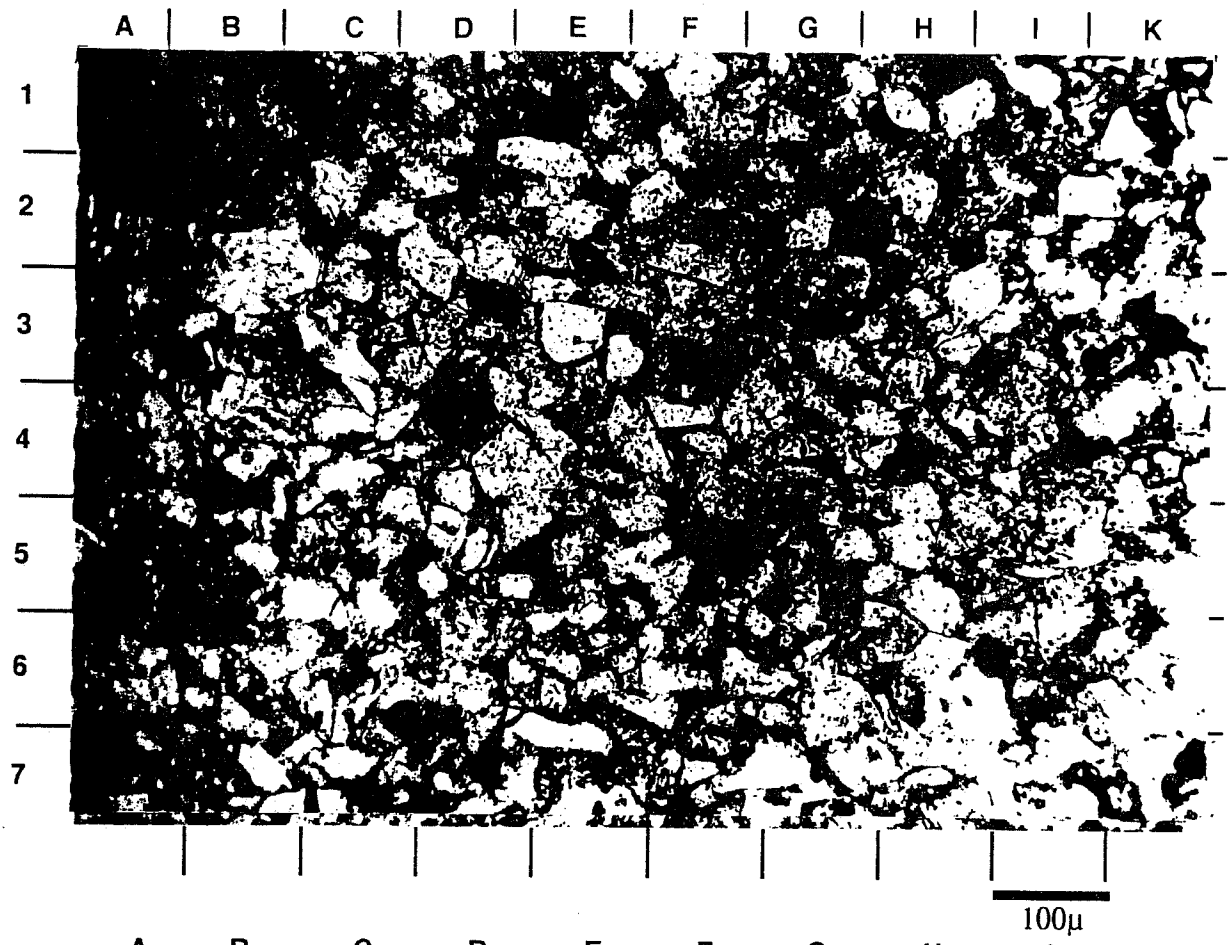

A
6816.1'
PPL

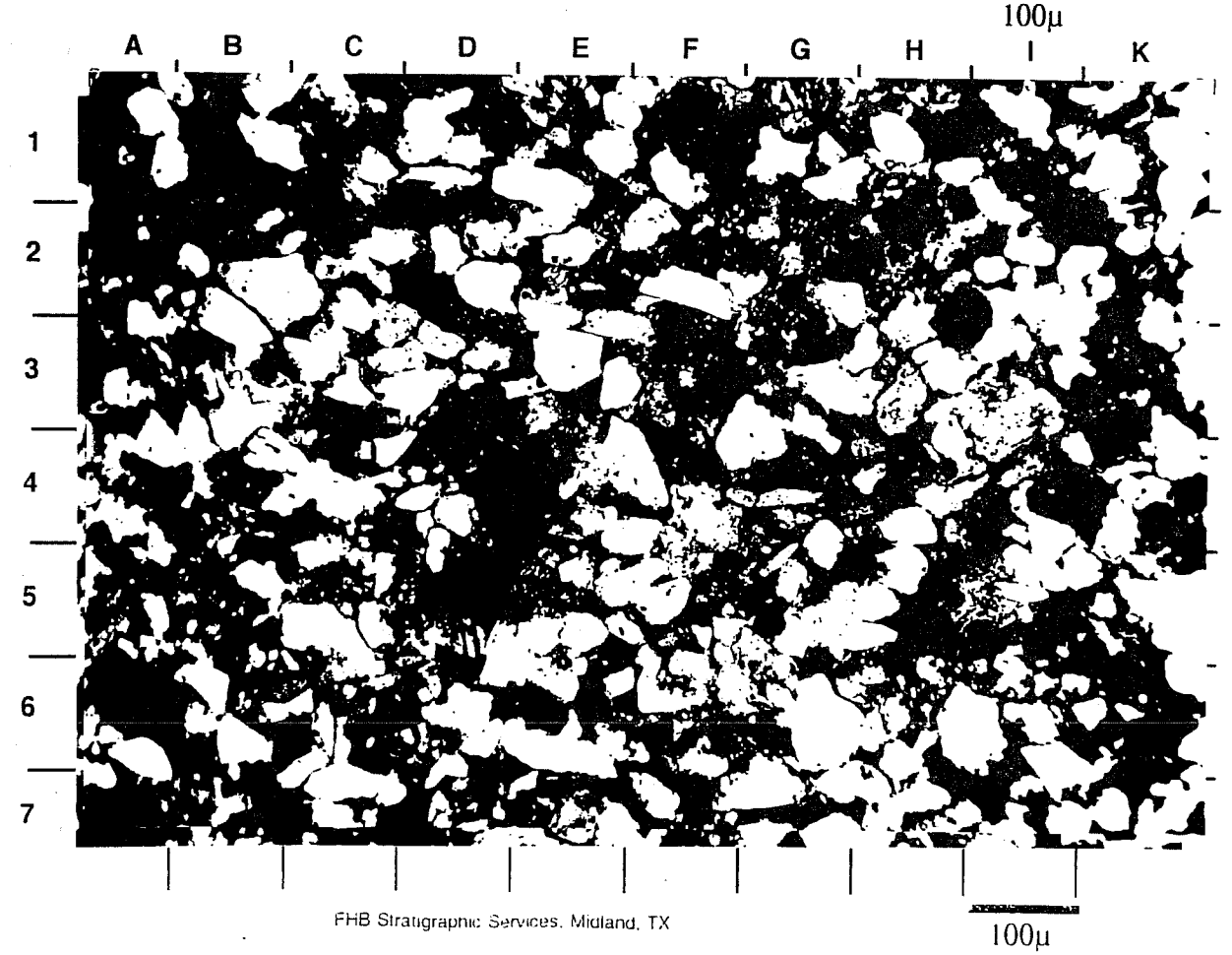

B
6816.1'
XPL

FHB Stratigraphic Services, Midland, TX

Plate 24

Strata Production, Nash Unit #23, Eddy Co., NM

6,816.1 ft.

Core Lab prepared all thin-sections from conventional core permeability plugs. Thin sections are impregnated with blue epoxy, one half of each thin-section stained with Alizarin Red S, and finished with a cover slip. Blue dye shows as porosity.

The coarse silt size boundary with very fine-grained sand-size is 62μ, while the very fine to fine-grained sand is 125μ.

Low magnification, scale bar beneath and to the right of photo 100 microns (100μ).

A Same slide as in Plate 23, but different area documenting the then micritic zones that serve as effective permeability barriers. Deposition of lime micrite (dark brown translucent organic-rich laminae. Quartz cement coats grains and occludes pore space. Fine quartz coating preserves isolated very small pockets of greater interparticle porosity, but low and ineffective porosity. Pyrite is present as pore blocking cement. Remaining pore space reduced due to overly close packing of low sphericity gains and slit-like pore throats bridged by megaquartz and feldspar cements.

Very patchy interparticle porosity estimated at 10-15%, with very low permeability.

B Same view and magnification as **A** above. Polymictic character of sandstone, low sphericity of the majority of framework grains, and pore filling carbonate cements are very evident.

Strata Production, Nash Unit # 23 Eddy Co., NM

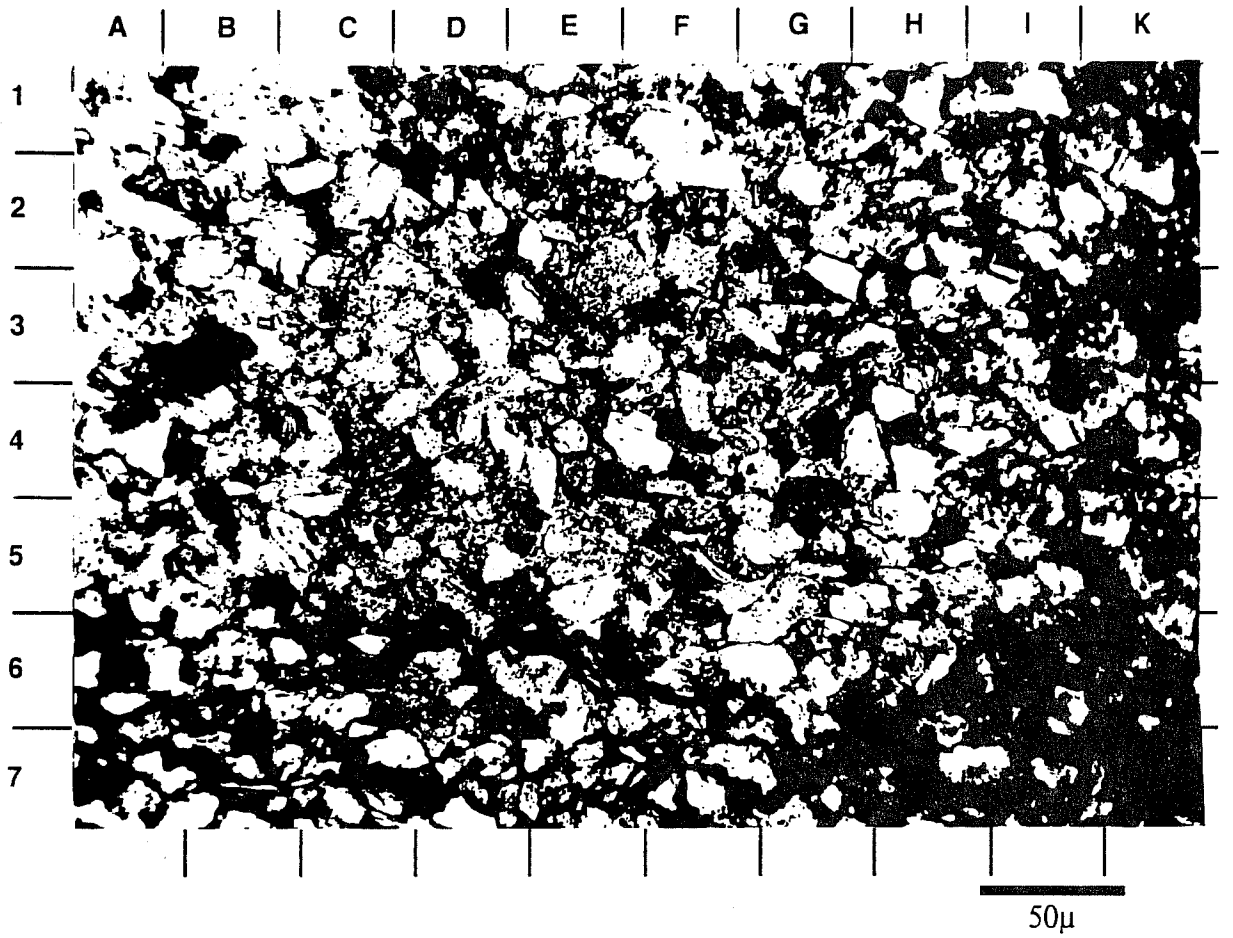

A
6816.1'
PPL

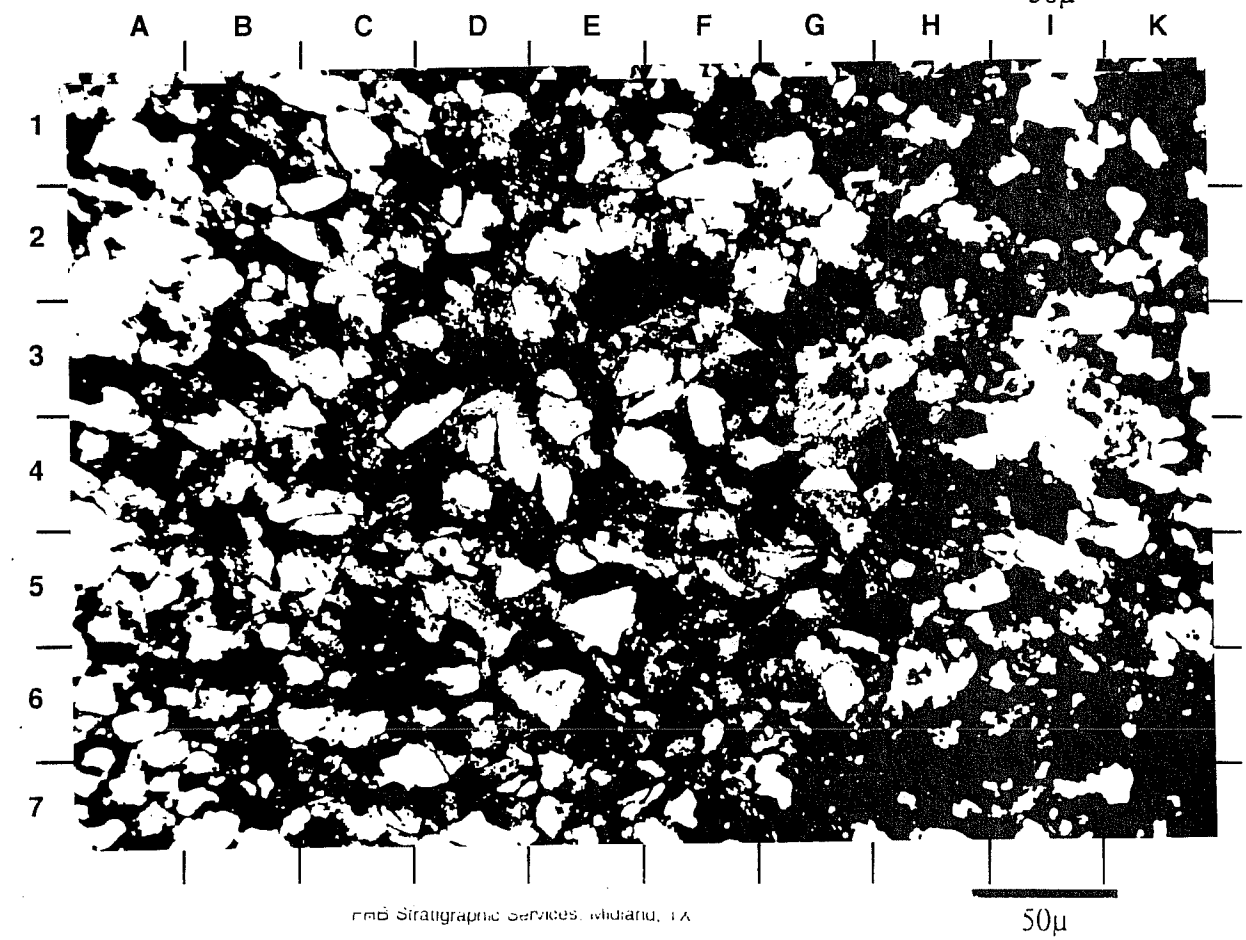

B
6816.1'
XPL

Plate 25

Strata Production, Nash Unit #23, Eddy Co., NM

6,816.1 ft.

Core Lab prepared all thin-sections from conventional core permeability plugs. Thin sections are impregnated with blue epoxy, one half of each thin-section stained with Alizarin Red S, and finished with a cover slip. Blue dye shows as porosity.

The coarse silt size boundary with very fine-grained sand-size is 62μ, while the very fine to fine-grained sand is 125μ.

HIgh magnification, scale bar beneath and to the right of photo 20 microns (20μ).

A Angular to subrounded quartz framework grains with patches of lime micrite (G1->G2, G3) Fine equant quartz cement coats grains (G2->C1, E4->G4, and elsewhere) where pores are slit-like the diagenetic quarza occludes pore space. Fine quartz coating preserves very small pockets of greater interparticle porosity, but low and ineffective porosity.

High relief euhedral pore cements at D2, F2, F5 and E7->F7) are interpreted to be diagenetic feldspars observed in SEM photomicrographs (Figure 9).

Strata Production, Nash Unit # 23 Eddy Co., NM

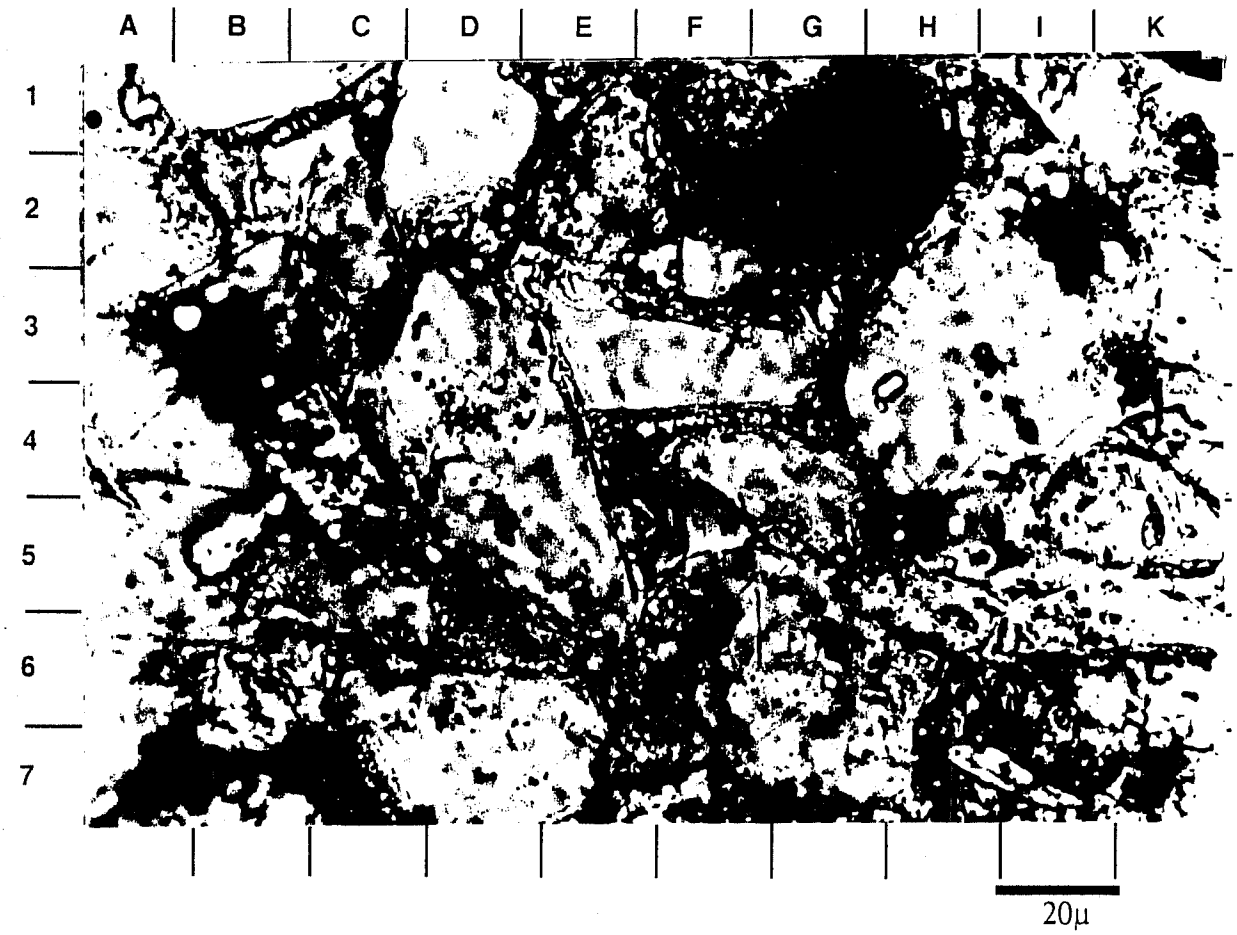

A
6816.1'
PPL

Plate 26

Strata Production, Nash Unit #23, Eddy Co., NM

6,816.1 ft.

Core Lab prepared all thin-sections from conventional core permeability plugs. Thin sections are impregnated with blue epoxy, one half of each thin-section stained with Alizarin Red S, and finished with a cover slip. Blue dye shows as porosity.

The coarse silt size boundary with very fine-grained sand-size is 62μ, while the very fine to fine-grained sand is 125μ.

HIgh magnification, scale bar beneath and to the right of photo 50 microns (50μ).

A Angular to subrounded quartz framework grains with patches of lime micrite (B1.C1D2. X6). Fine equant quartz cement coats grains (D1-D2,F2, G1).. Fine quartz coating preserves very small pockets of greater interparticle porosity, but low and ineffective porosity.

Low porosity with very poor permeability

B Similar features observed as in **A** above. Collapase grains and exceptionally low sphericity results in overly close packing in lower right hand and lower to leftmost margins of the field of view.

Low porosity with very poor permeability

Strata Production, Nash Unit # 23 Eddy Co., NM

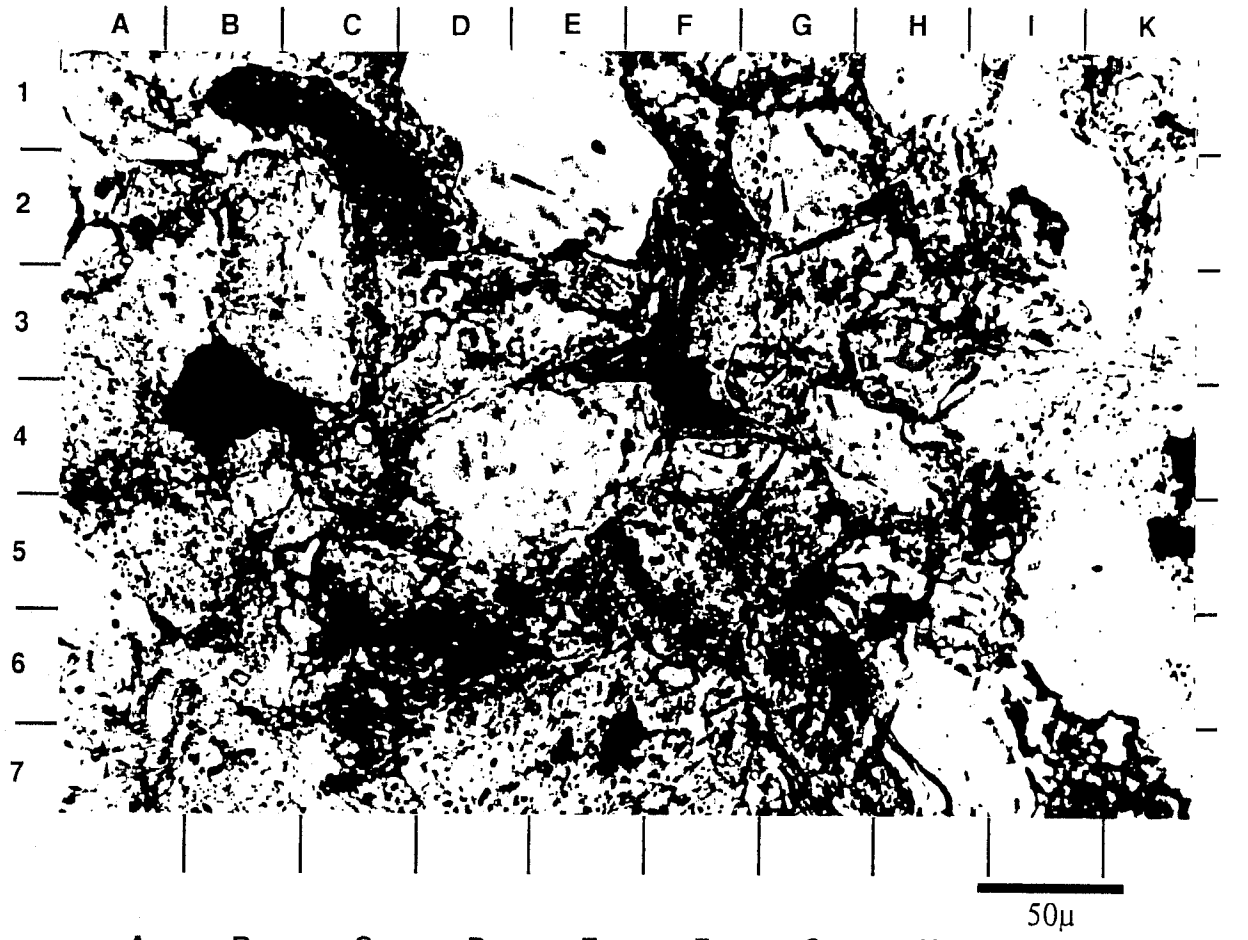

A
6816.1'
PPL

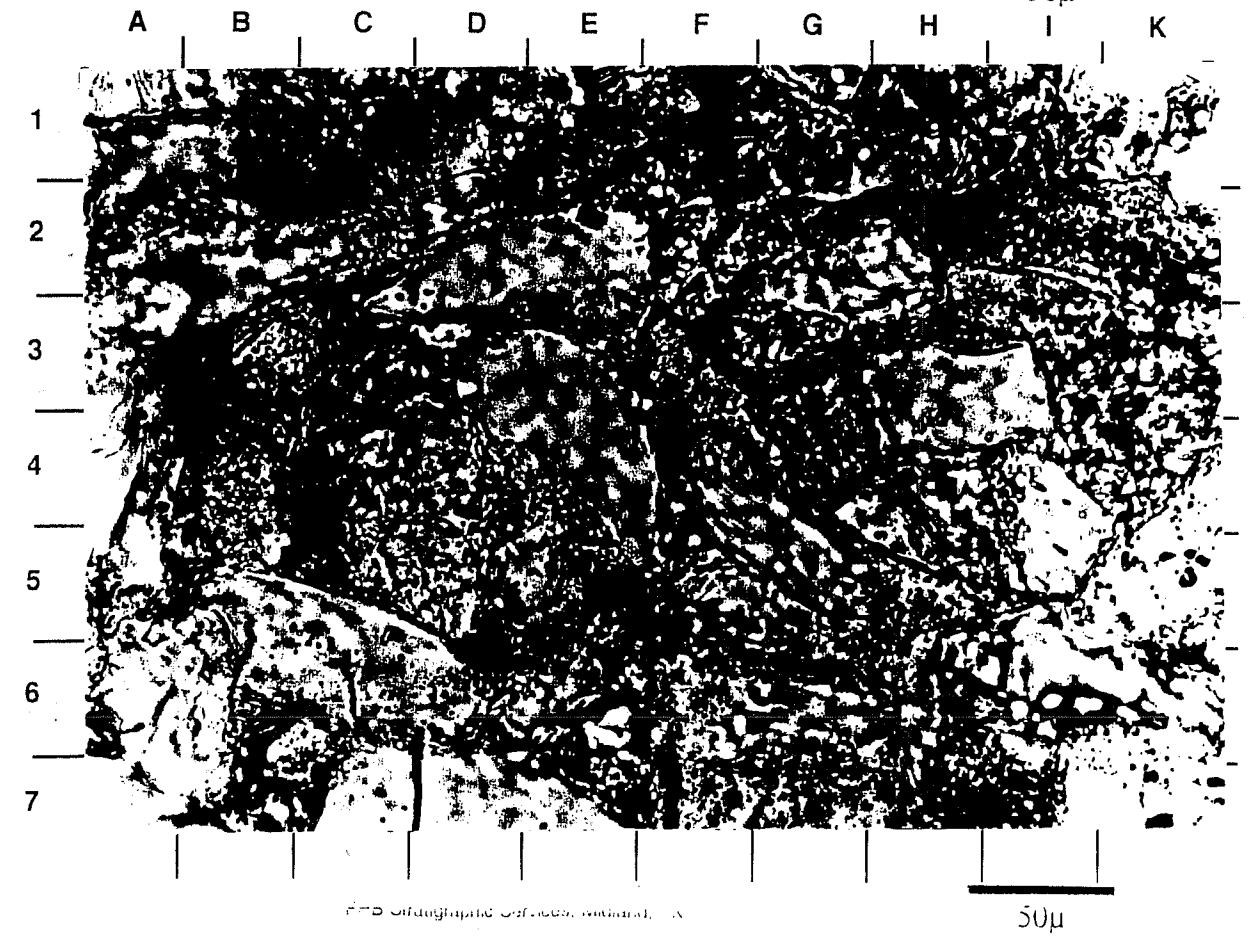

B
6816.1'
XPL

Figure 1. Sandstone with relatively abundant boxwork chlorite and fibrous illite cement lining pores and partially occluding interparticle porosity. Length of scale 100 microns. Sample 6652.7

Figure 2. Detailed view of boxwork chlorite and fibrous illite cements occluding porosity. Length of scale 50 microns. Sample 6652.7

Figure 3. Relatively abundant quartz overgrowths (top-center of photo) reducing permeability. Note some boxwork chlorite and fibrous illite around grains. Length of scale 50 microns. Sample 6664.6

Figure 4. Interparticle porosity partially occluded by boxwork chlorite (first generation cement on grains -- center of photo) and fibrous illite (possibly also some illite-smectite) in the center-right of the photo. Interparticle feldspar cement (lower left and lower right) and partially dissolved gypsum-anhydrite (bottom center of photo) also present. Length of scale 20 microns. Sample 6681.5

1

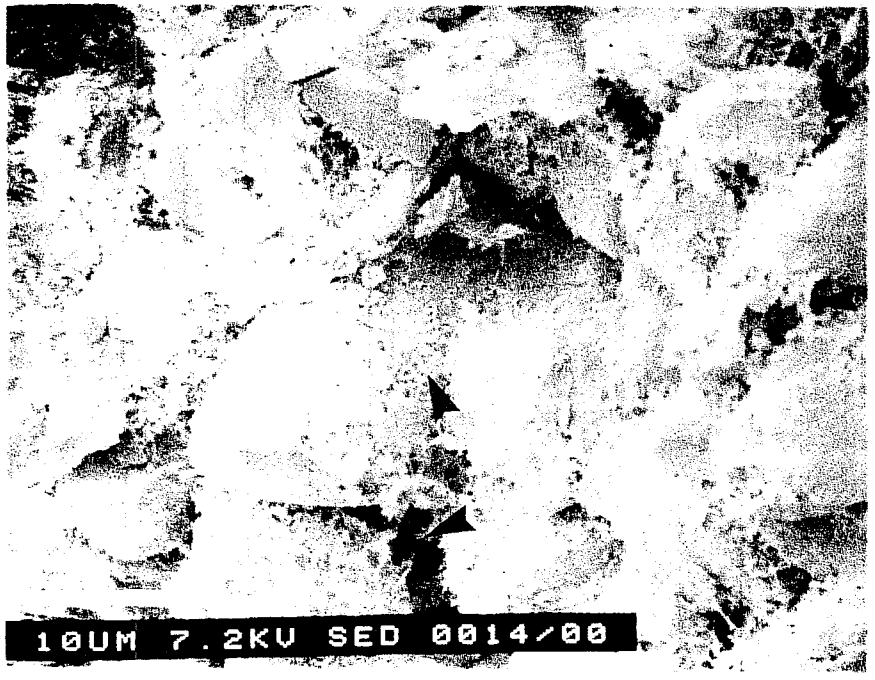
10UM 7.2KV SED 0014/00

2

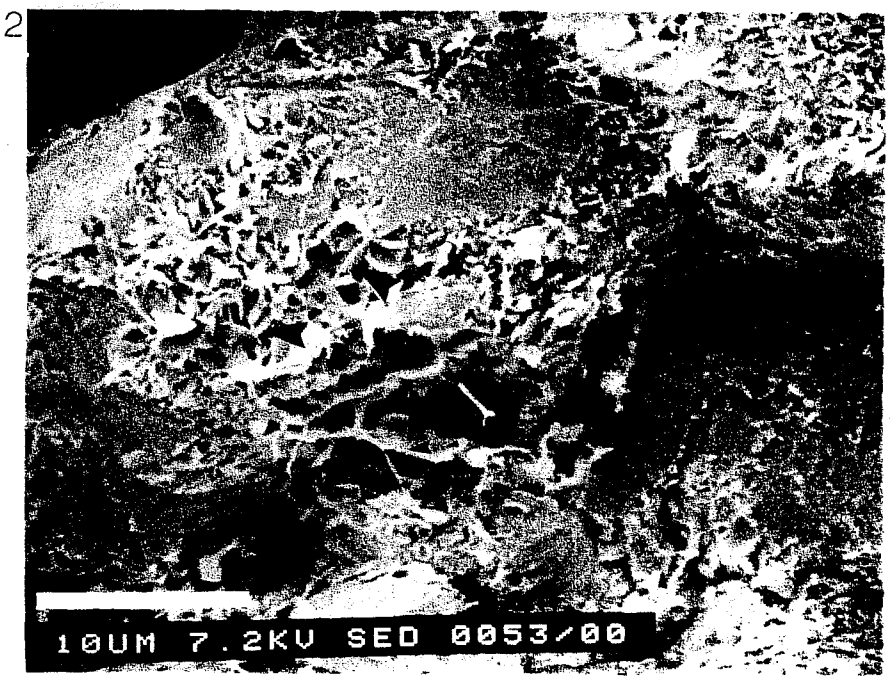
10UM 7.2KV SED 0053/00

3

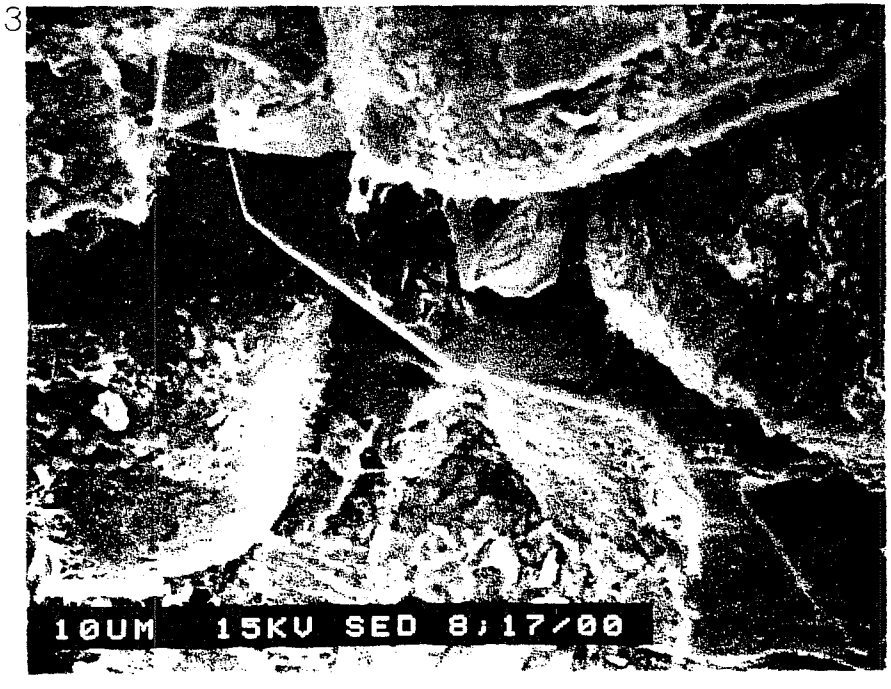
10UM 15KV SED 8;17/00

4

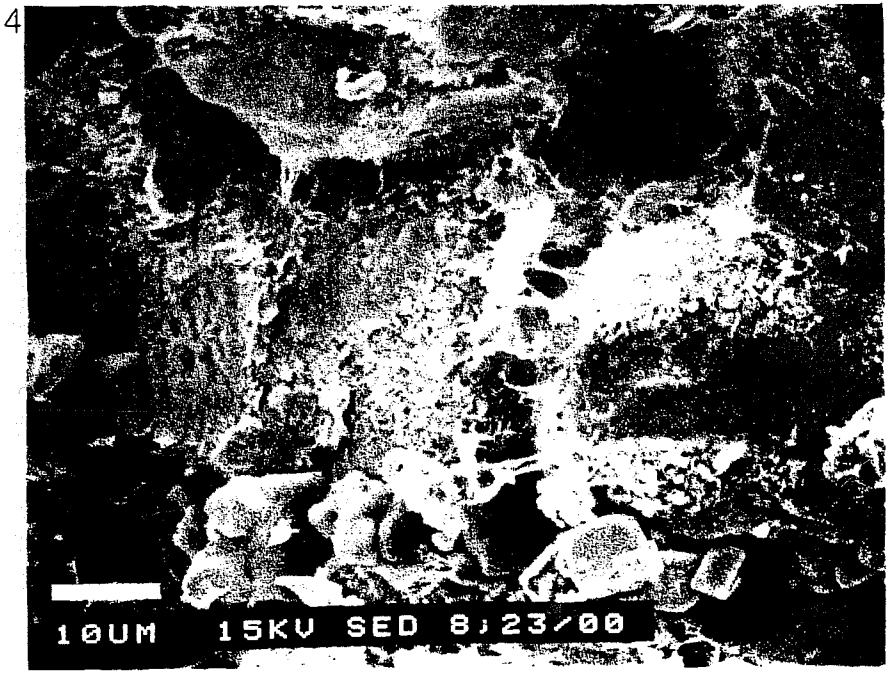
10UM 15KV SED 8;23/00

Figure 5. Interparticle porosity partially occluded by chlorite cement (center-right at top of photo). Note also the partially dissolved feldspar grains with microporosity (left-center). Length of scale 10 microns. Sample 6692.6

Figure 6. Sample with no interparticle porosity resulting from abundant mud matrix (below white line), but with some interparticle porosity (bottom right of photo and above white line). Length of scale 100 microns.Sample 6735.2

Figure 7. Interparticle porosity with no clay mineral cements, but instead, abundant fine crystalline quartz cement (center-right of photo). Note large feldspar crystals at pore throat (center-left). Length of scale 30 microns. Sample 6742.2

Figure 8. Abundant interparticle, fine crystalline quartz cement partially occluding porosity and reducing pore connections. Length of scale 100 microns. Sample 6742.2

5

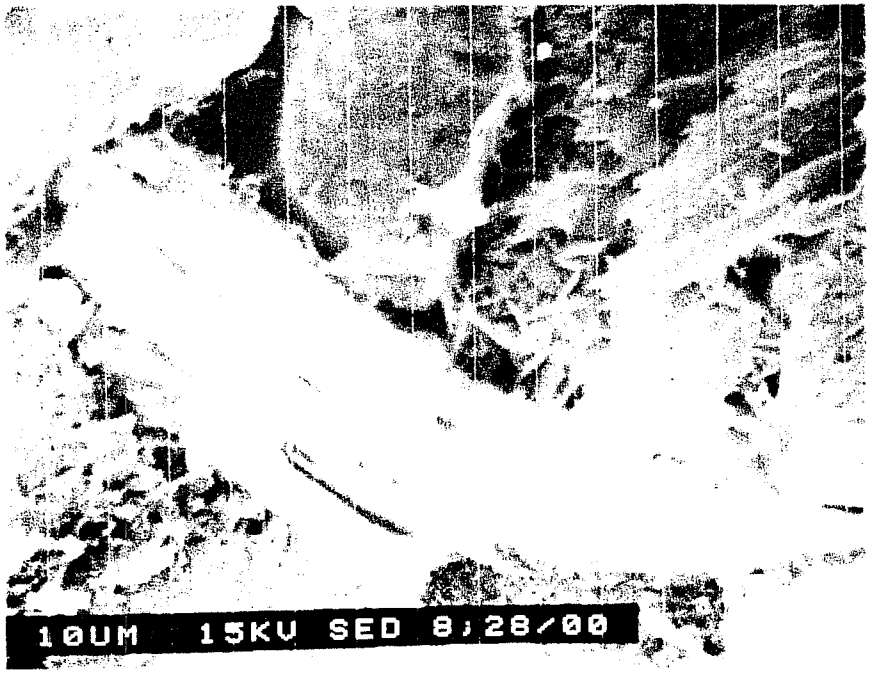
10UM 15KV SED 8:28/00

6

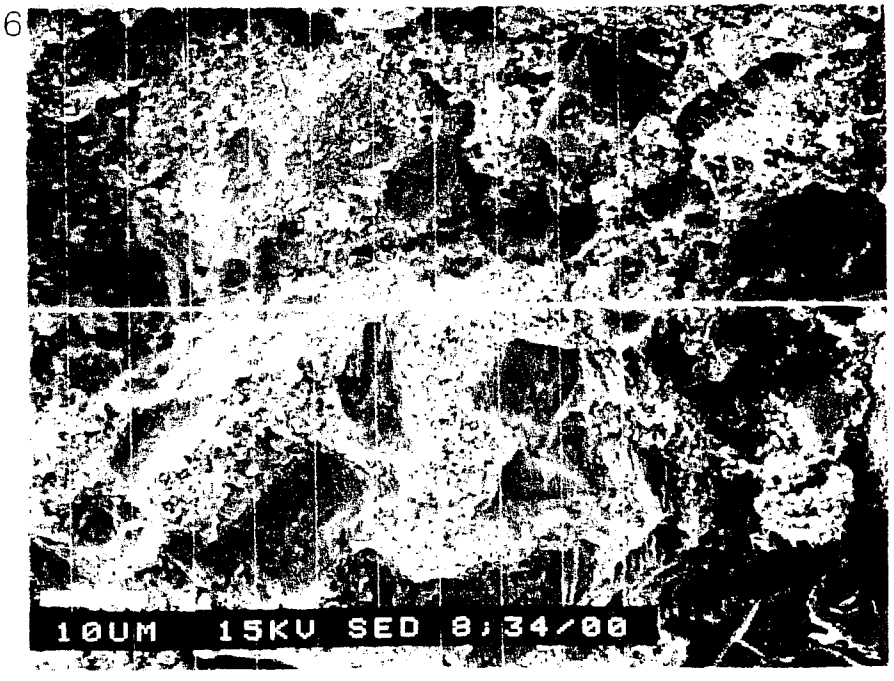
10UM 15KV SED 8:34/00

7

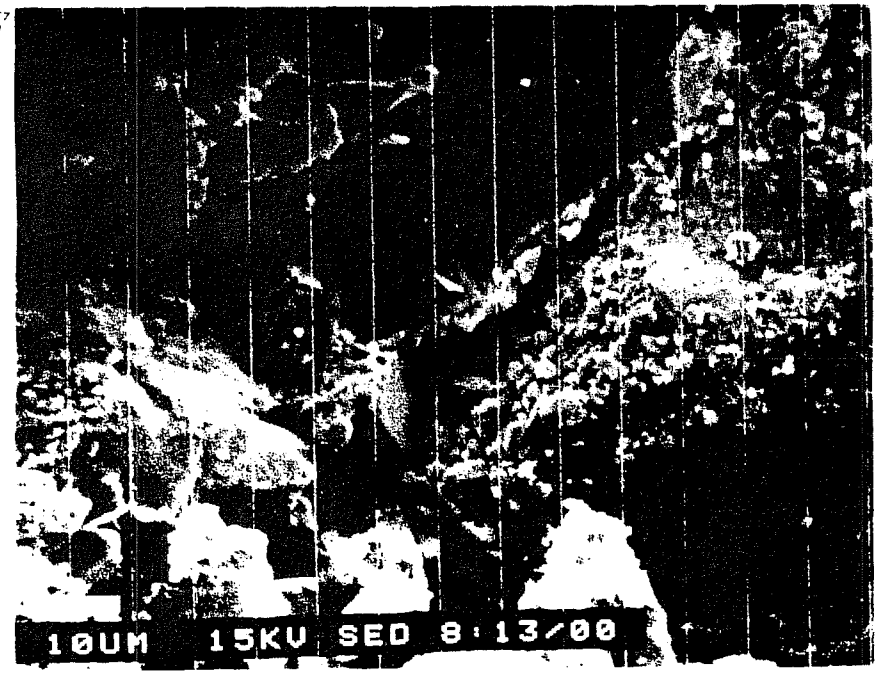
10UM 15KV SED 8:13/00

8

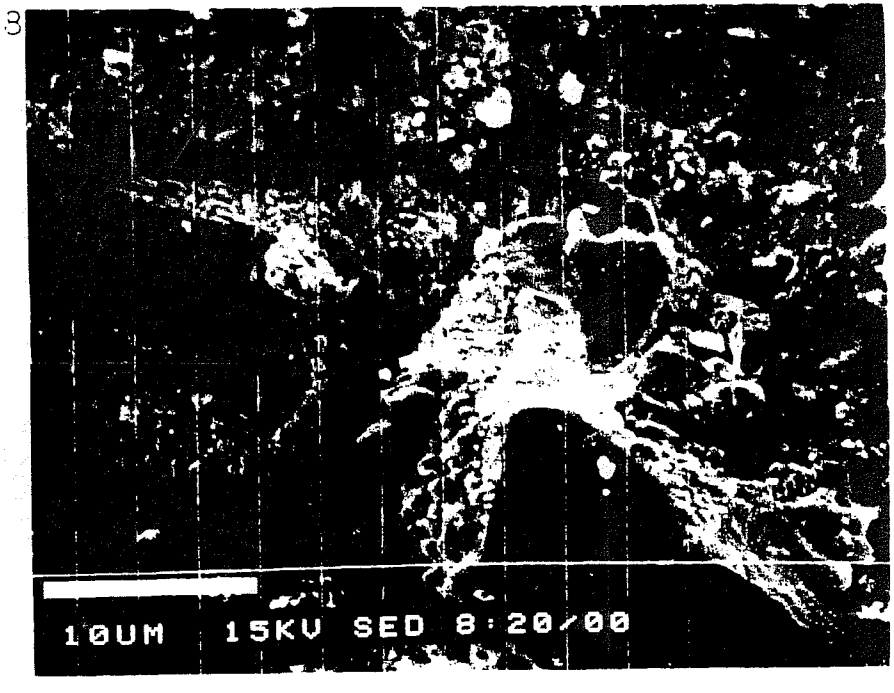
10UM 15KV SED 8:20/00

Figure 9. Small pores with abundant fine crystalline, interparticle quartz cement partially occluding pores. Length of scale 30 microns. Sample 6816.1

9

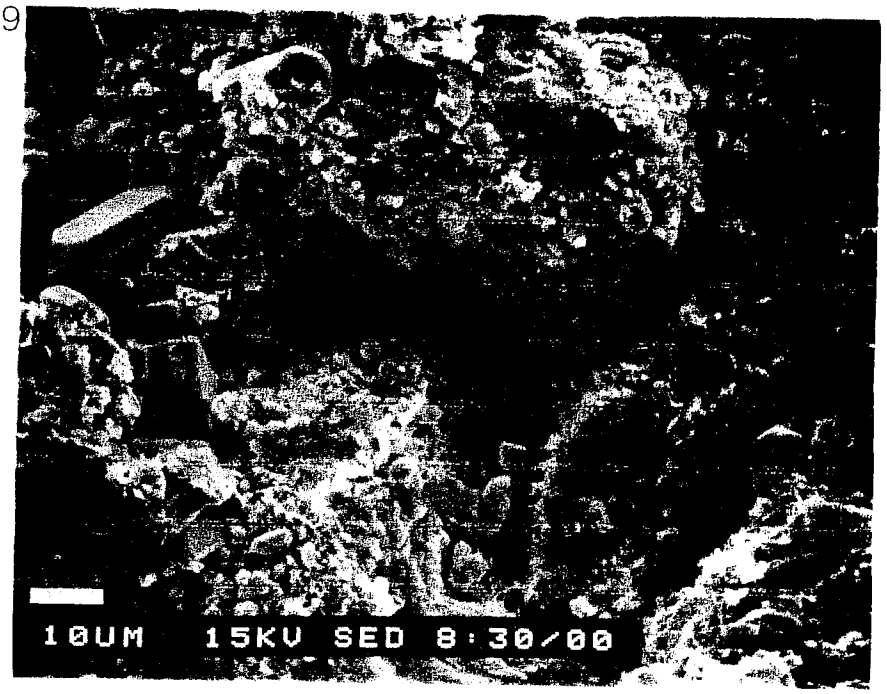

FHB Stratigraphic Services

Whole Rock XRD Analysis
Strata Production
Nash Unit #23

11/28/95

	Sample Depth											
Whole Rock Mineralogy	6652.7	6664.6	6666.5	6681.5	6692.6	6711.1	6735.2	6738.6	6742.2	6785.8	6787.8	6816.1
Quartz	66.6%	58.6%	55.2%	62.1%	56.2%	53.9%	56.6%	59.8%	57.9%	60.0%	56.5%	55.9%
K–Feldspar	10.0%	8.1%	9.3%	8.0%	9.7%	11.0%	11.2%	9.6%	9.1%	10.3%	8.4%	8.6%
Plagioclase Feldspar	11.4%	21.2%	26.4%	23.4%	22.9%	24.9%	21.4%	23.2%	25.0%	21.6%	26.0%	21.2%
Calcite	3.6%	5.1%	1.7%	1.4%	3.6%	2.6%	4.6%	1.0%	2.0%	2.3%	1.0%	8.2%
Ankerite	0.0%	0.2%	0.3%	0.0%	0.3%	0.2%	1.6%	0.6%	0.1%	0.1%	0.3%	0.6%
Siderite	0.3%	0.1%	0.1%	0.0%	0.0%	0.2%	0.2%	0.2%	0.2%	0.2%	0.2%	0.2%
Pyrite	0.4%	0.1%	0.2%	0.2%	0.2%	0.5%	0.5%	0.9%	0.5%	0.3%	0.4%	0.7%
Chlorite-Authigenic, isopachous	4.1%	3.9%	3.9%	2.9%	4.1%	3.0%	0.9%	1.3%	2.2%	2.1%	2.5%	1.4%
Illite-Athigenic, Pore Bridging	2.4%	1.7%	2.1%	1.1%	1.4%	2.0%	2.0%	2.7%	1.8%	2.2%	3.4%	2.2%
Illite/Smectite (I/S)-Authigenic	0.6%	0.6%	0.5%	0.6%	0.9%	1.3%	0.8%	0.8%	0.8%	0.6%	0.8%	0.9%
Kaolinite-Detritial	0.6%	0.3%	0.3%	0.2%	0.5%	0.3%	0.1%	0.1%	2.0%	0.2%	0.4%	0.2%
TOTAL Whole Rock %	100%	100%	100%	100%	100%	100%	100%	100%	102%	100%	100%	100%
Clay Minerals ≤ 4μ												
Sample Depth	6652.7	6664.6	6666.5	6681.5	6692.6	6711.1	6735.2	6738.6	6742.2	6785.8	6787.8	6816.1
Chlorite-Authigenic, isopachous	4.1%	3.9%	3.9%	2.9%	4.1%	3.0%	0.9%	1.3%	2.2%	2.1%	2.5%	1.4%
Illite	2.4%	1.7%	2.1%	1.1%	1.4%	2.0%	2.0%	2.7%	1.8%	2.2%	3.4%	2.2%
Illite/Smectite (I/S)	0.6%	0.6%	0.5%	0.6%	0.9%	1.3%	0.8%	0.8%	0.8%	0.6%	0.8%	0.9%
Kaolinite	0.6%	0.3%	0.3%	0.2%	0.5%	0.3%	0.1%	0.1%	2.0%	0.2%	0.4%	0.2%
TOTAL Whole Rock %	8%	7%	7%	5%	7%	7%	4%	5%	7%	5%	7%	5%

Chart Whole Rock XRD Analysis

Strata Production, Nash Unit #23 XRD Results

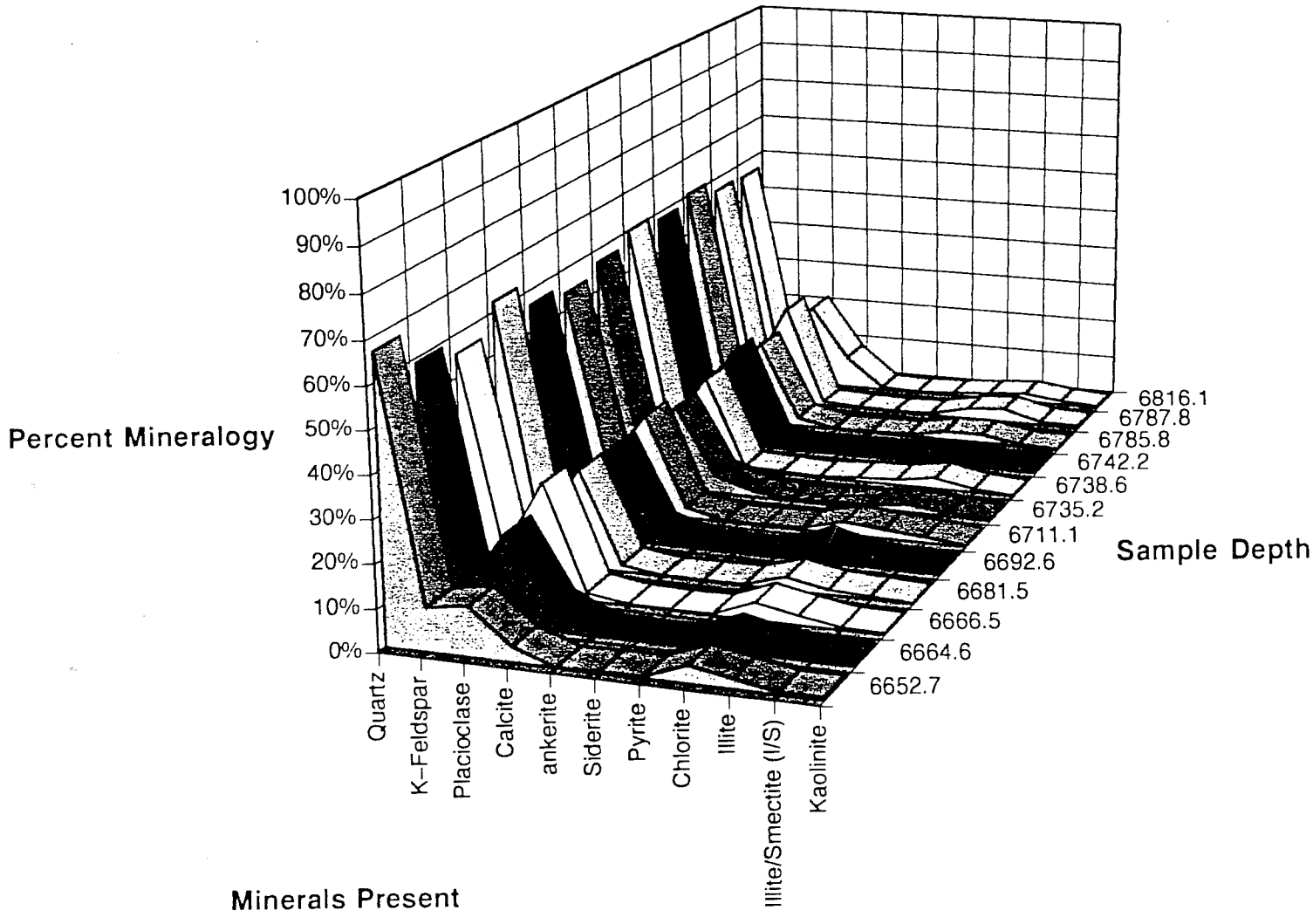

XRD Analysis by MAXRAY

Marlene Filut

Whole Rock Mineralogy												
Sample Depth	**6652.7**	**6664.6**	**6666.5**	**6681.5**	**6692.6**	**6711.1**	**6735.2**	**6738.6**	**6742.2**	**6785.8**	**6787.8**	**6816.1**
Quartz	66.6%	58.6%	55.2%	62.1%	56.2%	53.9%	56.6%	59.8%	57.9%	60.0%	56.5%	55.9%
K–Feldspar	10.0%	8.1%	9.3%	8.0%	9.7%	11.0%	11.2%	9.6%	9.1%	10.3%	8.4%	8.6%
Placioclase	11.4%	21.2%	26.4%	23.4%	22.9%	24.9%	21.4%	23.2%	25.0%	21.6%	26.0%	21.2%
Calcite	3.6%	5.1%	1.7%	1.4%	3.6%	2.6%	4.6%	1.0%	2.0%	2.3%	1.0%	8.2%
ankerite	0.0%	0.2%	0.3%	0.0%	0.3%	0.2%	1.6%	0.6%	0.1%	0.1%	0.3%	0.6%
Siderite	0.3%	0.1%	0.1%	0.0%	0.0%	0.2%	0.2%	0.2%	0.2%	0.2%	0.2%	0.2%
Pyrite	0.4%	0.1%	0.2%	0.2%	0.2%	0.5%	0.5%	0.9%	0.5%	0.3%	0.4%	0.7%
Chlorite	4.1%	3.9%	3.9%	2.9%	4.1%	3.0%	0.9%	1.3%	2.2%	2.1%	2.5%	1.4%
Illite	2.4%	1.7%	2.1%	1.1%	1.4%	2.0%	2.0%	2.7%	1.8%	2.2%	3.4%	2.2%
Illite/Smectite (I/S)	0.6%	0.6%	0.5%	0.6%	0.9%	1.3%	0.8%	0.8%	0.8%	0.6%	0.8%	0.9%
Kaolinite	0.6%	0.3%	0.3%	0.2%	0.5%	0.3%	0.1%	0.1%	2.0%	0.2%	0.4%	0.2%
TOTAL Whole Rock %	100%	100%	100%	100%	100%	100%	100%	100%	102%	100%	100%	100%

Clay Mineralogy
as
Percentage of Whole Rock

Strata Production, Nash Unit #23

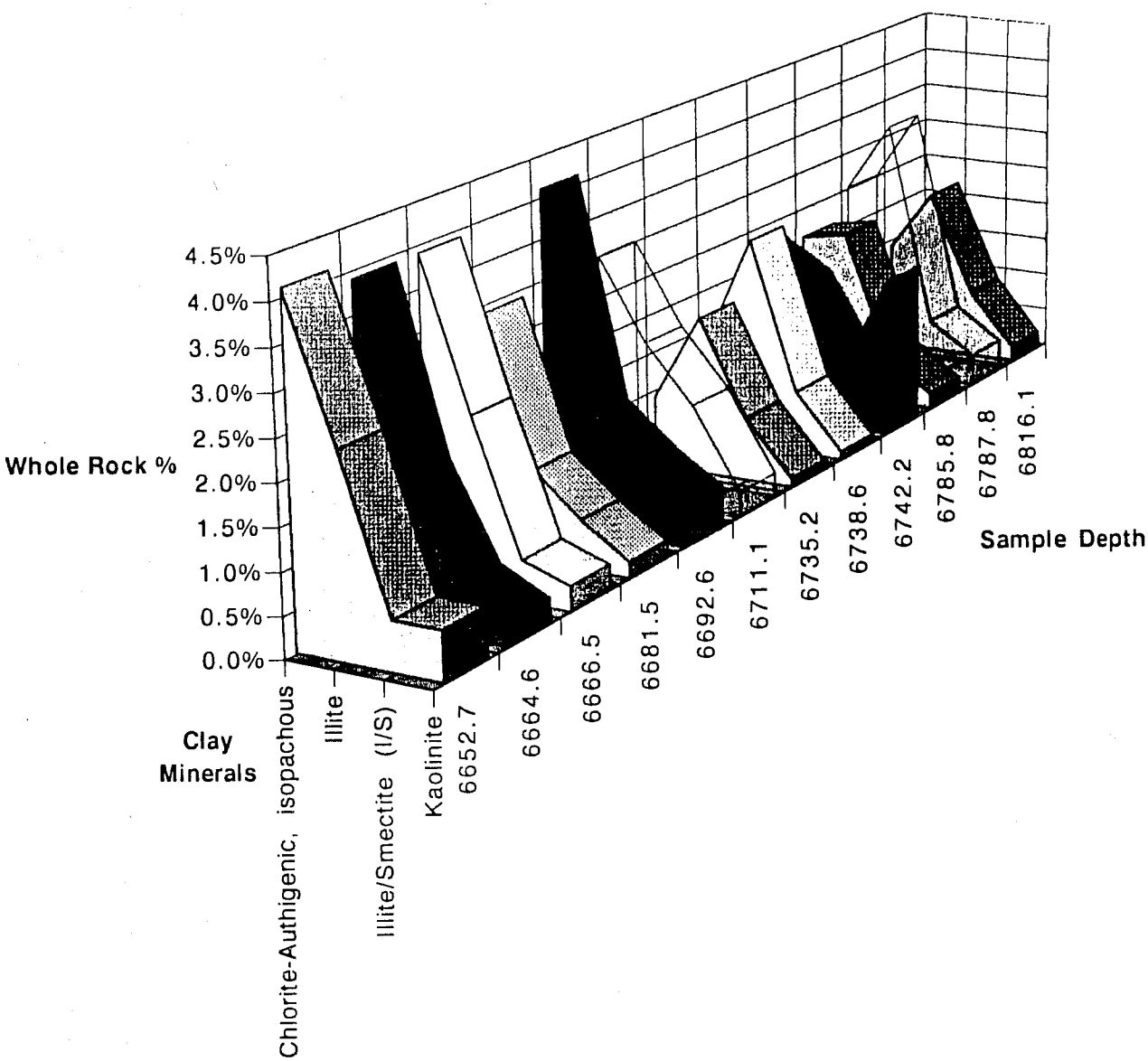

FHB Stratigraphic Services

Whole Rock XRD Analysis
Strata Production
Nash Unit #23

10/30/95

Whole Rock Mineralogy												
Sample Depth	**6652.7**	**6664.6**	**6666.5**	**6681.5**	**6692.6**	**6711.1**	**6735.2**	**6738.6**	**6742.2**	**6785.8**	**6787.8**	**6816.1**
Quartz	66.6%	58.6%	55.2%	62.1%	56.2%	53.9%	56.6%	59.8%	57.9%	60.0%	56.5%	55.9%
K–Feldspar	10.0%	8.1%	9.3%	8.0%	9.7%	11.0%	11.2%	9.6%	9.1%	10.3%	8.4%	8.6%
Plagioclase Feldspar	11.4%	21.2%	26.4%	23.4%	22.9%	24.9%	21.4%	23.2%	25.0%	21.6%	26.0%	21.2%
Calcite	3.6%	5.1%	1.7%	1.4%	3.6%	2.6%	4.6%	1.0%	2.0%	2.3%	1.0%	8.2%
ankerite	0.0%	0.2%	0.3%	0.0%	0.3%	0.2%	1.6%	0.6%	0.1%	0.1%	0.3%	0.6%
Siderite	0.3%	0.1%	0.1%	0.0%	0.0%	0.2%	0.2%	0.2%	0.2%	0.2%	0.2%	0.2%
Pyrite	0.4%	0.1%	0.2%	0.2%	0.2%	0.5%	0.5%	0.9%	0.5%	0.3%	0.4%	0.7%
Chlorite	4.1%	3.9%	3.9%	2.9%	4.1%	3.0%	0.9%	1.3%	2.2%	2.1%	2.5%	1.4%
Illite	2.4%	1.7%	2.1%	1.1%	1.4%	2.0%	2.0%	2.7%	1.8%	2.2%	3.4%	2.2%
Illite/Smectite (I/S)	0.6%	0.6%	0.5%	0.6%	0.9%	1.3%	0.8%	0.8%	0.8%	0.6%	0.8%	0.9%
Kaolinite	0.6%	0.3%	0.3%	0.2%	0.5%	0.3%	0.1%	0.1%	2.0%	0.2%	0.4%	0.2%
TOTAL Whole Rock %	100%	100%	100%	100%	100%	100%	100%	100%	102%	100%	100%	100%

Clay Mineralogy
as
Percentage of Whole Rock

Strata Production, Nash Unit #23

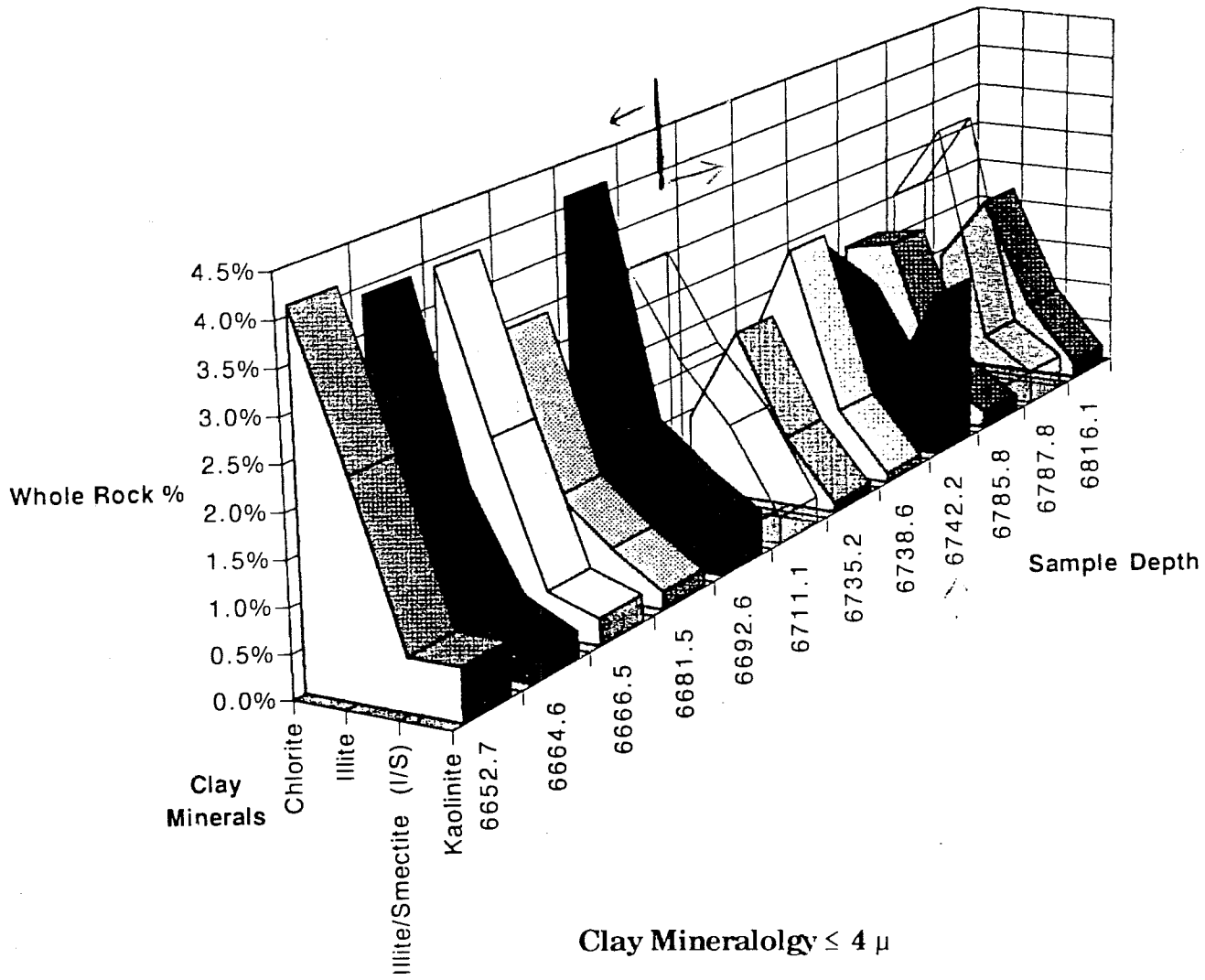

Clay Mineralolgy ≤ 4 μ

Chart Whole Rock XRD Analysis:
Strata Prod.,
Nash Unit #23

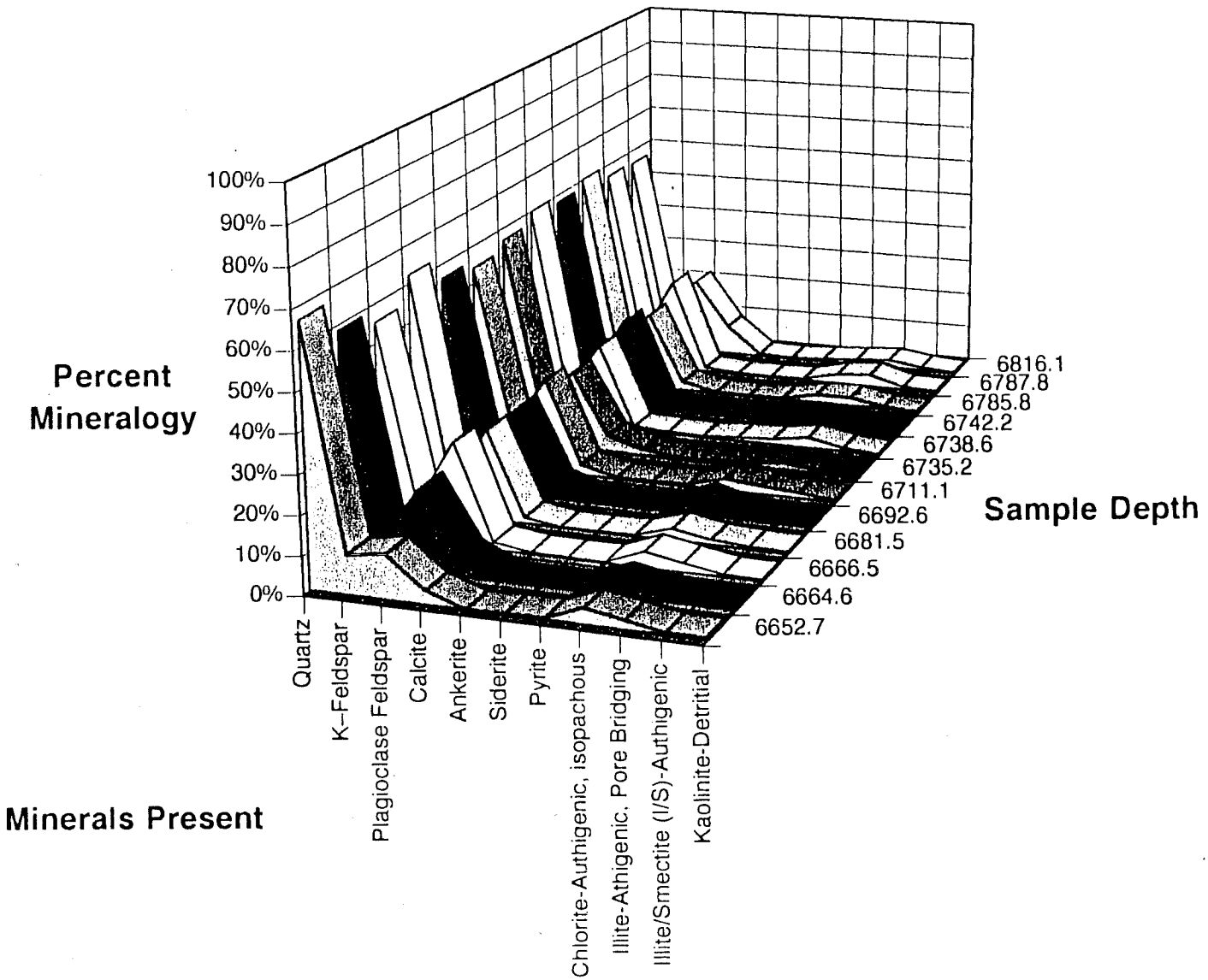

FHB Stratigraphic Services

Whole Rock XRD Analysis
Strata Production
Nash Unit #23

11/28/95

	Sample Depth											
Whole Rock Mineralogy	**6652.7**	**6664.6**	**6666.5**	**6681.5**	**6692.6**	**6711.1**	**6735.2**	**6738.6**	**6742.2**	**6785.8**	**6787.8**	**6816.1**
Quartz	66.6%	58.6%	55.2%	62.1%	56.2%	53.9%	56.6%	59.8%	57.9%	60.0%	56.5%	55.9%
K–Feldspar	10.0%	8.1%	9.3%	8.0%	9.7%	11.0%	11.2%	9.6%	9.1%	10.3%	8.4%	8.6%
Plagioclase Feldspar	11.4%	21.2%	26.4%	23.4%	22.9%	24.9%	21.4%	23.2%	25.0%	21.6%	26.0%	21.2%
Calcite	3.6%	5.1%	1.7%	1.4%	3.6%	2.6%	4.6%	1.0%	2.0%	2.3%	1.0%	8.2%
Ankerite	0.0%	0.2%	0.3%	0.0%	0.3%	0.2%	1.6%	0.6%	0.1%	0.1%	0.3%	0.6%
Siderite	0.3%	0.1%	0.1%	0.0%	0.0%	0.2%	0.2%	0.2%	0.2%	0.2%	0.2%	0.2%
Pyrite	0.4%	0.1%	0.2%	0.2%	0.2%	0.5%	0.5%	0.9%	0.5%	0.3%	0.4%	0.7%
Chlorite-Authigenic, isopachous	4.1%	3.9%	3.9%	2.9%	4.1%	3.0%	0.9%	1.3%	2.2%	2.1%	2.5%	1.4%
Illite-Athigenic, Pore Bridging	2.4%	1.7%	2.1%	1.1%	1.4%	2.0%	2.0%	2.7%	1.8%	2.2%	3.4%	2.2%
Illite/Smectite (I/S)-Authigenic	0.6%	0.6%	0.5%	0.6%	0.9%	1.3%	0.8%	0.8%	0.8%	0.6%	0.8%	0.9%
Kaolinite-Detritial	0.6%	0.3%	0.3%	0.2%	0.5%	0.3%	0.1%	0.1%	2.0%	0.2%	0.4%	0.2%
TOTAL Whole Rock %	100%	100%	100%	100%	100%	100%	100%	100%	102%	100%	100%	100%
Clay Minerals ≤ 4μ												
Sample Depth	**6652.7**	**6664.6**	**6666.5**	**6681.5**	**6692.6**	**6711.1**	**6735.2**	**6738.6**	**6742.2**	**6785.8**	**6787.8**	**6816.1**
Chlorite-Authigenic, isopachous	4.1%	3.9%	3.9%	2.9%	4.1%	3.0%	0.9%	1.3%	2.2%	2.1%	2.5%	1.4%
Illite	2.4%	1.7%	2.1%	1.1%	1.4%	2.0%	2.0%	2.7%	1.8%	2.2%	3.4%	2.2%
Illite/Smectite (I/S)	0.6%	0.6%	0.5%	0.6%	0.9%	1.3%	0.8%	0.8%	0.8%	0.6%	0.8%	0.9%
Kaolinite	0.6%	0.3%	0.3%	0.2%	0.5%	0.3%	0.1%	0.1%	2.0%	0.2%	0.4%	0.2%
TOTAL Whole Rock %	8%	7%	7%	5%	7%	7%	4%	5%	7%	5%	7%	5%